Pathogenic potential of anti-ganglioside antibodies in a murine model of axonal Guillain-Barré syndrome

KAY GREENSHIELDS MSci (Hons)

A THESIS SUBMITTED IN FULFILMENT OF THE REQUIREMENTS OF THE UNIVERSITY OF GLASGOW FOR THE DEGREE OF DOCTOR OF PHILOSOPHY

DIVISION OF CLINICAL NEUROSCIENCE

OCTOBER 2007

Abstract

Guillain- Barré Syndrome (GBS) is the world's leading cause of neuromuscular paralysis, occurring in serologically and pathogenically distinct forms. GBS is believed to have an autoimmune basis, where antibodies raised during antecedent infections (eg. *Campylobacter jejuni*) cross-react with self antigens, exemplifying the process of molecular mimicry. These self antigens are gangliosides, which are glycolipid structures enriched in peripheral nerve in specific membrane compartments termed lipid rafts. To date, successful murine models of anti-GD1a and anti-GQ1b ganglioside mediated neuropathy exist. Clinical evidence supports the involvement of anti-GM1 antibodies in nerve injury, however generation of anti-GM1 antibody mediated neuropathy models remains an enigma, and to date the only successful model is based in Japanese rabbits. This thesis aims to address the controversies surrounding anti-GM1 antibody mediated neuropathy by utilising a panel of anti-GM1 antibodies of differing specificity, and explores how the stereometric interactions of GM1 with lipid raft species underpin the pathogenic potential of these antibodies.

Dedication

I dedicate this research to all GBS patients, past and present.

Also, to my parents.

Acknowledgements

When I launched into my PhD 3 years ago, I did not know what a ganglioside was, nor could I pronounce Guillain-Barré syndrome. Since then, I have come a long way, a feat I feel would have been insurmountable without the support and friendship of, to be honest, just about everyone I know.

However, extra special thanks go to Prof Willison, for inspirational guidance, diligent mentoring and amazing ability to laugh at my many disasters. Most of all, I am indebted to you for encouraging me to pursue my experiments with DG1. From not knowing what a ganglioside was to knowing GM1 and GD1a "share a bed" is certainly quite an achievement. My deepest thanks also to Dr Sue Halstead, not only for teaching me everything I know in the lab, but for being possibly one of the best role models I will encounter, on both a professional and personal level. For technical guidance, and "patience grasshopper" wisdom (which prevented my laptop exiting via the window on many occasions), I thank Mr Peter Humphreys. I also value the support of Dr Kate Townson, another role model to whom I aspire. For my all "rafting" experiments I am grateful to Dr Luke Chamberlain - maybe one day I will be brave enough to cut my own blots!

Finally, the encouragement and friendship of Mrs Jean Veitch, Ms Dawn Nichol and Ms Pat Thomson at the Southern has been invaluable.

May there be many more fun experiments and nights out to be had.

Declaration of Authorship

All experiments are the work of the author unless specifically stated otherwise.

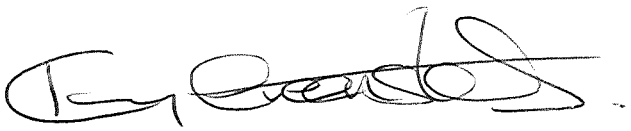

Kay Greenshields MSci (Hons)

University of Glasgow

October 2007

Contents

Chapter 4

List of Figures and Tables

Figures

Abbreviations

2^{o}	secondary
ACh	acetylcholine
AChR	acetylcholine receptor
AIDP	Acute Inflammatory Demyelinating Polyradiculoneuropathy
AMAN	Acute Motor Axonal Neuropathy
AMSAN	Acute Motor and Sensory Axonal Neuropathy
BNB	blood nerve barrier
BSA	bovine serum albumin
BTx	bungaratoxin
CFP	cyan fluorescent protein
CGT	ceramide glucosyltransferase
CST	cerebroside sulfotransferase
CSF	cerebro spinal fluid
CTb	cholera toxin, b subunit
Cy-5	cyanine 5
DAF	decay accelerating factor
DAPI	4',6-diamidino-2-phenylindole
dH_2O	distilled water
DMSO	dimethyl sulfoxide
DRG	dorsal root ganglion
DRM	detergent resistant membrane

EAN	experimental allergic neuritis
ELISA	enzyme linked immunosorbant assay
EMG	electromyograph
ER	endoplasmic reticulum
EthD-1	ethidium homodimer-1
EtOH	ethanol
FACS	fluorescence assisted cell sorter
FCS	foetal calf serum
FDB	flexor digitorum brevis
FITC	fluorescein isothiocyanate
FRET	fluorescent resonant energy transfer
GalNAc-T	GalNac transferase
GBS	Guillain Barré syndrome
GD3s	GD3 synthase
GFP	green fluorescent protein
GPI	glycosylphosphatidyl inositol
HRP	horseradish peroxidase
Ig	immunoglobulin
IgM	immunoglobulin M
IgG	immunoglobulin G
IHC	immunohistochemistry

KO or $^{-/-}$	knock out
LOS	lipo-oligosaccharide
mAb	monoclonal antibody
MAC	membrane attack complex
MAG	myelin associated glycolipid
MβCx	methyl-β-cyclodextrin
MFS	Miller Fisher syndrome
MN	motor neuron
MS	multiple sclerosis
N'Ase	neuraminidase
NF	neurofilament
NGF	nerve growth factor
NHS	normal human serum
NMJ	neuromuscular junction
NoR	node of Ranvier
OD	optical density
OEC	olfactory enhsheathing cell
PBS	phosphate buffered saline
PBST	phosphate buffered saline + 0.01% Tween-20
PFA	paraformaldehyde
PI-PLC	phosphatidylinositol specific phospholipase C
PJF	parajunctional fibroblast
PLL	poly-l-lysine

PMGS	plasma membrane ganglioside sialidase
PNS	peripheral nervous system
pSC	perisynaptic Schwann cell
RT	room temperature
ROI	region of interest
SDS	sodium dodecyl sulfate
SEM	standard error of the mean
SLI	Schmidt-Lanterman Incisure
SNARE	soluble N-ethylmaleimide-sensitive factor attachment protein receptor
TLC	thin layer chromatography
TRITC	tetramethylrhodamine isothiocyanate
TrK	receptor tyrosine kinases
TS	Triangularis Sterni
TTx	tetanus toxin
UV	ultra violet
WT	wild type
YFP	yellow fluorescent protein

Chapter 1

1.1 Introduction

Acute ascending paralytic disorders have been described for centuries, for example the clinical descriptions of Guillain Barré like disturbances in the 19th century by Auguste Francois Chomel in 1828 and James Wardrop in 1834.

However, the first modern description of a condition similar to Guillain Barré Syndrome (GBS) is credited to Landry in 1859. The report documented a patient with paresthesias and subjective weakness, with objective weakness occurring 1 month after onset of symptoms and becoming rapidly progressive until death 8 days later (Landry 1859). In 1992, Osler reported a case of acute febrile polyneuritis (Osler 1892) which was similar to GBS, however it was not until development of lumbar puncture in the 20th century that such disorders could be better characterised and distinguished from other neurological conditions such as poliomyelitis (Ropper 1992). Thus, although "Landry's ascending paralysis" is often synonymous with GBS, lack of definitive diagnostic data mean the more contemporary findings of Guillain, Barré and Strohl give rise to the term "Guillain Barré Syndrome".

In 1916, Guillain, Barré and Strohl presented comprehensive details of a clinical condition seen in 2 acutely ill soldiers with motor weakness, paresthesias and muscular pain with subsequent recovery. Examination of the cerebrospinal fluid (CSF) revealed increased CSF albumin without pleocytosis, and electrophysiological examination revealed preservation of cutaneous reflexes but pathology in the Achilles reflex and quadriceps muscle (Guillain *et al* 1916, Pritchard and Hughes 2004). Further reports of similar conditions subsequentially emerged (Marie and Chatelin

1916), and the term Guillain Barré syndrome was coined in 1927 (Draganesco and Claudian 1927) and thus GBS became a defined clinical entity.

Preceeding descriptions of GBS include Haymaker and Kernohan's autopsy study of 50 fatal cases of "Landry Guillain Barré" (Haymaker and Kernohan 1949) and the report in 1969 on 19 fatal cases by Asbury, Arnason and Adams (Asbury et al 1969). However, with the emergence of new descriptions, controversy arose over the diagnostic criteria. Thus, in 1976 following a suspected link between an increase in GBS cases and the swine influenza vaccine, the National Institute of Neurological and Communicative Disorders and Stroke (NINCDS) proposed clear, if restrictive, diagnostic criteria for GBS. These criteria were reported in 1978 (NINCDS 1978) and were 'fine tuned' further in the 1980s by Asbury (Asbury 1981, Asbury and Cornblath 1990); to date these established diagnostic criteria persist, and will be outlined briefly.

1.2 GBS Diagnosis

Required features for the diagnosis of GBS include progressive motor weakness in more than 1 extremity and areflexia. Reflex changes may be preceeded by weakness (Asbury and Cornblath 1990) which ascends rostrally to involve the upper extremities and cranial nerves (Ropper 1992, Guillain et al 1916). Eventually, muscle wastage may be present in up to 50% of patients (Winer *et al* 1988). Associated features which are highly suggestive of GBS include an acute neuropathy which reaches a nadir in 4 weeks (Loffel *et al* 1977), and notable symmetry of motor weakness. Objective sensory loss may occur (Winer *et al* 1988) tending to affect sensations relying on myelinated fibres (such as proprioception and vibration). Cranial nerve envolvement is also indicative of GBS: one study revealed facial palsy in 53% of cases (Winer *et al*

1988). At least 2-4 weeks after symptoms cease to progress, recovery begins. However, the disease leaves a legacy of paralysis or death in approximately 20% of patients, and therapies such as plasma exchange or intravenous immunoglobulin therapy serve only to half disease severity (Raphael *et al* 2001, Visser *et al* 1999). In practice, the diagnostic guidelines of GBS are not without pitfalls. Establishing the diagnosis of an acute peripheral neuropathy does not automatically rule out alternative causes. Furthermore, it is not always easy to rule out chronic inflammatory demyelinating polyradiculoneuropathy (CIDP), in which the onset phase of 4-8 weeks (Hughes *et al* 1992, Oh *et al* 2003) may overlap with that of GBS. This is particularly true of patients with recurring episodes of GBS (Odaka *et al* 2003, Mori *et al* 2002). In order to definitively confirm a diagnosis, other investigations are useful and have also aided an understanding of the pathological mechanism of GBS.

1.2.1 *Lumbar Puncture*

This is traditionally performed to examine the CSF. Although no correlation exists between CSF protein values and the progression of the disease (Beghi *et al* 1985, Loffel *et al* 1977, Arnason and Soliven 1993) it is a useful tool in aiding the initial diagnosis of GBS. CSF protein levels are normal at the beginning of illness (Paradiso *et al* 1999) but increase approximately 1 week after symptom onset and reach peak levels at the 4 week nadir and onwards (Congia *et al* 1989, Ropper *et al* 1992). However, while lumbar puncture remains a useful diagnostic tool, normal CSF protein values may be present in 20% of cases up to 10 weeks after onset of symptoms (Beghi *et al* 1985, Congia *et al* 1989). As the timeframe for therapeutic intervention is narrow (1-4 weeks), early diagnostic accuracy is essential and now greatly aided by modern advances in neurophysiological testing.

1.2.2 *Neurophysiological Testing*

Although the clinical criteria outlined in 1978 (NINCDS 1978) document normal nerve conduction in 20% of patients, recent advances in electrodiagnostic testing have increased the sensitivity and technique of such investigations, with reports of electrophysiologic abnormalities in up to 90% of cases (Winer *et* al 1988, Olney and Aminoff 1990, Ropper *et al* 1990, Bradshaw *et al* 1992, Vajsar *et al* 1992). Such techniques have allowed classification of GBS into its distinct clinical subtypes (as shall be detailed in forthcoming sections). Abnormal motor and/or sensory nerve conduction and late motor responses are typical in GBS, either alone or in combination (Oh 1993).

1.2.2.1 *Abnormal Nerve Conduction*

Motor nerve conduction is measured by recording the compound muscle action potential (CMAP) produced in a muscle following supramaximal stimulation (proximally to give proximal CMAP and distally to give distal CMAP) of a motor nerve. Terminal motor latency (TML) represents the duration required to produce distal CMAP after distal stimulation, and subtracting this value from time taken to achieve proximal CMAP after proximal stimulation yields the motor conduction time. From this, overall conduction velocity is determined. A similar protocol is used for sensory nerve conduction (Oh 1993). An abnormal CMAP duration indicates that lesioned nerve fibres within a given nerve bundle may be affected to different degrees, resulting in abnormal temporal dispersion by the consequential asynchronous firing of motor units (Cornblath *et al* 1991). If the amplitude of the proximal CMAP is significantly lower than the distal, this indicates conduction block. Conduction block is a sensitive method of indicating segmental demyelination, a process involving

preservation of the axon but degradation of the myelin sheath. Evidence of demyelination is present in approximately 60% of GBS patients within 2 weeks of illness onset (Olney *et al* 1990, Bradshaw *et al* 1992, Brown and Feasby 1984), but successful remyelination means recovery can be rapid. If conduction velocity is normal but a striking reduction in CMAP amplitude is noted, this indicates axonal degeneration from which recovery is slow and often incomplete (Asbury 1994).

1.2.2.2 *Abnormal Late Motor Responses*

F wave latency is also informative. Following stimulation of a nerve, the stimuli travels anterograde to elicit a CMAP, but also travels retrograde to the spinal cord, where it then travels back down the nerve to produce a late motor response termed the "F wave" (ie. a miniature CMAP). A prolonged F-wave latency (or absent F-wave) is indicative of abnormal conduction in the proximal nerve, and in some GBS patients may be the only electrophysiological abnormality detected (Kiers *et al* 1994). As the next section shall outline, such advances in the diagnosis of GBS have allowed classification of patients into one of the three main subtypes: AIDP, AMAN and AMSAN (Hadden *et al* 1998, Ho *et al* 1995).

1.3 GBS – A Heterogenous Syndrome

Initial elecrophysiological observations of GBS were consistent with demyelination, and pathological changes typically included inflammatory demyelination of roots and nerves (Asbury *et al* 1969, Prineas 1981). Thus, owing to its status as a demyelinating condition, classic GBS was believed to be a homogenous syndrome, synonymous with acute inflammatory demyelinating polyneuropathy (AIDP). However, improved

electrophysiological testing and advancing immunological techniques (Albers *et al* 1985) have highlighted anomalies within the seemingly homogenous entity of GBS.

1.3.1 *AIDP*

This is the most frequent form of GBS encountered in Europe and North America (Peterman *et al* 1959, Asbury *et al* 1969). AIDP patients present with flaccid paralysis and areflexia, and upon physical examination display mild sensory loss. Macrophage mediated destruction of the myelin sheath results in segmental demyelination of the peripheral nerve (Hafer-Macko *et al* 1996). Myelinating axons supplying the extra ocular muscles are spared, with demyelination affecting myelinated limb, axial and lower cranial nerves (motor and sensory). Injury is predominant in areas lacking a blood nerve barrier, including proximal nerve roots and distal intramuscular nerve segments (Olsson 1968). Electrophysiological testing can pinpoint the likely site of pathology: absent/delayed F wave latencies or prolonged distal motor latencies are respective indicators of proximal or distal involvement. Recovery of segmental demyelination can be rapid, as resting Schwann cells remyelinate the lesion site (Cornblath *et al* 1991, Parry and Sumner 1992). Axonal injury does not form part of the primary injury, although may occur as "bystander" injury (Hadden and Hughes 2003).

1.3.2 *AMAN and AMSAN*

In 1985, a pivotal electromyography (EMG) study by Albers (Albers *et al* 1985) highlighted a subpopulation of GBS patients with suspected primary axonal degeneration. One year later, Feasby noted that in a small group of AIDP patients, EMG studies revealed rapid fall in compound motor action potential (CMAP) and

sensory nerve conduction potential (SNAP) with no conduction block and normal distal latency. This led to the hypothesis of axonal degeneration, a theory later confirmed upon autopsy of similar patients (Feasby *et al* 1993). However, limited inferences can be drawn from such a small study sample. Further insight was gained in 1991 (McKhann *et al* 1991), where the term "Chinese Paralytic Syndrome" was coined to describe a GBS like condition found in rural China. Further investigation of these patients (McKhann *et al* 1993), who presented with acute onset flaccid paralysis, revealed normal sensory function, rapidly ascending quadraparesis, involvement of lower cranial nerves and respiratory failure. Conduction velocities and distal latency were normal, and upon autopsy Wallerian like motor nerve degeneration, in the absence of inflammation, was commonly observed. Since this study, reports of similar cases have emerged, with the majority being from Chinese and Japanese locale. Thus, the GBS subtype "acute motor axonal neuropathy" (AMAN) was created. This body of evidence is in agreement with the initial observations of Feasby, with the exception that the latter cases had sensory and motor involvement and therefore this condition is classed as "acute motor and sensory neuropathy" (AMSAN).

Further support of primary axonal degeneration was heralded by a long term collaborative study between John Hopkins University, University of Pennsylvania and the Second Teaching Hospital, Shijiazhuang, China (McKhann *et al* 1993). Wallerian degeneration of peripheral nerves, minimal lymphocytic involvement, no inflammation or demyelination and macrophage infiltration between the axolemma and the Schwann cell (Griffin *et al* 1995) were the prominent findings. Later studies (Griffin *et al* 1996) focussed on the sequale of events preceding the advanced pathology often seen at autopsy. Early changes involved the nodes of Ranvier,

followed by macrophage migration into the periaxonal space of the paranode, leading to separation of the axon and ad-axonal plasmalemma. Wallerian degeneration then followed. These findings were similar to AMSAN pathological studies (Griffin *et al* 1996), where clearance of myelin debris from fibres undergoing Wallerian degeneration (as the primary insult) was characterised by "foamy" macrophages.

1.3.3 *MFS*

Regional variants of GBS also exist, which paralyse specific anatomical sites (Ropper 1994). The most widely recognised and studied variant (Fisher 1956, Chiba *et al* 1992, Willison and O'Hanlon 1999), Miller Fisher Syndrome, was first described in 1956 (Fisher 1956). Clinical signs were believed to reflect GBS, although the symptoms of mild ptosis, opthalmoplegia, areflexia and cerebellar type ataxia were suggestive of a central lesion. However, EMG and nerve conduction studies lend support to its classification as a peripheral neuropathy, as opposed to a central syndrome (Guiloff 1977). Respiratory and limb involvement mean cases of MFS often 'overlap' with confluent GBS.

1.3.4 *GBS subtypes: summary*

Table 1 provides an overview of the GBS subtypes discussed, their associated anti-ganglioside antibodies and clinical features.

GBS Subtypes: an overview			
Subtype	**Acronym**	**Associated anti-ganglioside antibodies**	**Clinical features**
Acute inflammatory demyelinating polyradiculoneuropathy	AIDP	unknown	Autonomic involvement, segmental demyelination, "bystander" axonal injury
Acute motor and sensory axonal neuropathy	AMSAN	GM1, GM1b, GD1a	Axonal subtype: motor and sensory fibres. Affects limbs and respiration.
Acute motor axonal neuropathy	AMAN	GM1, GM1b, GD1a, GalNAc-GD1a	Axonal subtype: motor fibres only. Affects limbs and respiration.
Miller Fisher syndrome	MFS	GQ1b, GT1a	Triad of opthalmoplegia, ataxia and areflexia. Facial and lower cranial nerve involvement.

Table 1. Summary of the main GBS subtypes, common acronyms, associated anti-ganglioside antibodies and clinical features specific to each subtype.

1.4 GBS - An Immune Mediated Disorder

The early pathologic findings of GBS cite the presence of a perivenular mononuclear cell infiltrate as the pathologic hallmark (Oh 1990). Asbury and co-workers (Asbury *et al* 1969) reported perivenular mononuclear cell infiltration of motor, sensory, cranial and autonomic nerves, where the accumulation of inflammatory cells was mostly in the vasculature surrounding the endoneurium. Early cells were small and medium sized lymphocytes, with more advanced lesions displaying a predominance of macrophages, and there was evidence of active phagocytosis of the myelin. Electron microscopy (EM) studies of GBS specimens have expanded the original

observations of Asbury, by describing two distinct populations of macrophages in areas of demyelination (Hughes *et al* 1992, Brechenmacher *et al* 1987, Carpenter 1972, Arstila *et al* 1971, Vallat *et al* 1994). One population cause focal destruction of the myelin, allowing macrophage processes to invade the gaps and strip the innermost layers of myelin from the axon. These active macrophages express major histocompatability class II antigens (Honavar *et al* 1991, Feasby *et al* 1993, Hartung *et al* 1995) and contain no organelles (Brechenmacher *et al* 1987). The second type of macrophage (the "foamy macrophage") is not active, and contains debris from the phagocytosed nerve components (Griffin *et al* 1990). These early findings were suggestive of a primary inflammatory and demyelinating attack on the myelin, which subsequently led to Wallerian degeneration of the axon as a secondary event. While this theory fits with the model of AIDP, it does not explain pathogenesis of AMAN, where axonal degeneration is present in the absence of severe demyelination. A report by McKhann (McKhann *et al* 1993) detailed a group of patients with acute flaccid paralysis, where axons undergoing Wallerian degeneration had macrophages located within the endoneurium and the axon itself (McKhann *et al* 1993, Brechenmacher *et al* 1987).

The observations of demyelination or axonal damage in association with inflammatory cell infiltration led to the theory that GBS is an immune mediated disorder, and the development of an animal model (EAN) was the next major development in elucidating the pathogenesis of the disease.

1.4.1 *EAN*

Experimental autoimmune neuritis (EAN) was devised in 1955 by Waksman and Adams (Waksman and Adams 1955) by injecting homogonates of whole peripheral nerve into rabbits. It is widely used as a model of human demyelinating GBS, as it

recapitulates many of the electrophysiological and immunological traits of the human condition (Hartung 1993). It is now known that the peripheral nerve homogenate used in the early development of EAN contains autoantigens responsible for the induction of the disease (Astrom and Waksman 1962, Linington *et al* 1986, Szymanska *et al* 1983). In 1979 (Kadlubowski and Hughes 1979), it was reported that Lewis rats were susceptible to EAN induced by P2 protein, which comprises approximately 5% of the myelin membrane and is thought to be involved in assembly and maintenance of peripheral nerve myelin (Whitaker 1981, Khalili-Shirazi *et al* 1993). P0 protein, specific to peripheral nerve myelin and accounting for approximately half of the total protein content (Kaldor and Speed 1984) can induce EAN in the Lewis rat to give an effect similar to that of P2 immunisation.

EAN introduced the possibility that myelin reactive T lymphocytes exist in the natural immune repertoire, and upon infection with a structure bearing an epitope similar to a myelin protein, immune tolerance is broken and autoimmune attack proceeds to the effector phase (myelin destruction). Lymph node cells from animals immunized with myelin or P2 protein (Hughes *et al* 1981) were transferred to naïve animals and this resulted in development of EAN; the absence of antibodies to P2 protein in the sera of the recipient animals was suggestive of a T cell mediated immune response. Furthermore, EAN can be blocked by T-cell suppression or elimination (Brosnan *et al* 1987). The role of macrophages is also emphasised by EAN: they have been identified by immunocytochemistry in the lesion site (Hartung *et al* 1988). These macrophages also express MHC class II antigens, and may therefore function as antigen presenting cells. Antibodies against MHC class II antigens inhibit the development of EAN (Strigard et al 1988), and macrophage depletion (Craggs *et al* 1984), Hartung *et al* 1988, Heininger *et al* 1988, Tansey and Brosnan 1982) prevents

the clinical and histologic signs of EAN. Thus, the role of macrophages in EAN appears to be critical, either through their role as antigen presenting cells or through disruption of their metabolic pathways which mediate inflammation (Hartung *et al* 1991).

While it seems evident that T-cells play a major role in the development of EAN, a potential area of conflict was highlighted when it was shown that plasmapheresis is protective against EAN (Arnason and Soliven 1993). While this may be partly due to the removal of inflammatory mediators, such as cytokines (Exley *at al* 1994) it would be foolish to rule out a possible role of antibodies. For example, in EAN induced by inoculation with whole peripheral nerve, disease severity correlates with antibodies against P0 (Archelos *et al* 1993). Thus it became increasingly evident that the humoral immune response may play a role in the pathogenesis of EAN, perhaps by acting synergistically with the T-cell mediated response.

In 1979, emphasis shifted to the humoral response in GBS when an experimental demyelinating neuropathy was induced in rabbits (Saida *et al* 1979) by sensetization with galactocerebroside. This glycolipid has poor immunogenic properties, thus requires direct injection into the myelin to elicit an antibody response. However, galactocerebroside acts as a hapten, so injection with a carrier protein and complete Freund's adjuvant will also induce an antibody response. Using this approach, repeated injection of galactocerebrocide resulted in over 50% of rabbits showing demyelinating lesions, with typical symptoms including flaccid quadrapareisis, limb hypoesthesia and respiratory paralysis – i.e. symptoms comparable to EAN (Saida *et al* 1979, Saida *et al* 1981). Upon autopsy, animals displayed no pathology in the CNS, and PNS changes included early demyelination around venules, with adjacent fibres displaying early vesiculation of the outer sheath which later progressed to a full

lesion. Perivenular cuffing of small lymphocytes in early lesions suggests the process is antibody, as opposed to cell mediated (Saida *et al* 1981). Furthermore, a correlation was noted between the location of lesions and "leaky" areas of the blood nerve barrier, indicating a possible route for migration of serum antibodies. Deposition of complement component C5b9 has been demonstrated on Schwann cells and myelin before the initiation of demyelination (Stoll *et al* 1991), and *in-vitro* studies have shown that deactivation of complement abolished demyelinating activity, giving weight to the idea that the pathogenesis is antibody and complement mediated (Sumner *et al* 1982). However, while this model seemingly contradicts the major findings of EAN, there are significant overlaps. Rabbits immunized with Freund complete adjuvant develop subclinical demyelinating PNS lesions, suggesting that the action of a pathogenic antibody in the galactocerebrocide inoculated animals is not the sole event, and may in part be aided by an inflammatory response perhaps to further enhance dysfunction of the blood nerve barrier (Powell *et al* 1987). On the same note, rats treated with cobra venom factor to deplete complement component C3 had delayed onset and milder symptoms of EAN (Feasby *et al* 1987) again hinting at a possible synergy between the humoral and inflammatory response.

Shortly after the thought provoking experiments of Saida, a report emerged of a patient with a severe demyelinating neuropathy which was associated with increased titres of IgM. It was subsequentially demonstrated that the target of this immunoglobulin was the peripheral nerve protein myelin associated glycolipid (MAG) (Braun *et al* 1982), and the reactive epitope was shared by two other peripheral nerve glycolipids, sulphated glucoronyl paragloboside (SGPG) and sulfate-3-glucoronyl lactosaminyl paragloboside (SGLPG) (Chou *et al* 1986, Ariga *et al* 1987). It is therefore reasonable to accept the assumption that there is a direct link

between the presence of anti-MAG antibodies and neuropathy, as biopsy studies revealed marked demyelination often accompanied by axonal degeneration, and deposition of IgM and complement components at the lesion site (Trojaborg *et al* 1995, Hays *et al* 1988, Monaco *et al* 1990). Perhaps the most conclusive evidence however, was the demonstration that passive transfer of human IgM anti-MAG antibodies to chicks resulted in a successful reproduction of the lesion (Tatum 1993). As interest in the pathogenic properties of anti-myelin antibodies began to grow, it was soon realised that other potential autoantigens may exist. The notion that gangliosides may also act as autoantigens was raised by Freddo (Freddo *et al* 1986): monoclonal antibodies from a patient with progressive limb weakness and absent reflexes had specificity for GM1, GD1b and asialo-GM1 gangliosides. Thus the association of anti-ganglioside antibodies and para-proteinaemic neuropathies was established (Latov 1994), and the implications of these findings became relevant in the pathogenesis of GBS when antibodies raised against glycolipid epitopes (gangliosides) were identified in association with GBS (Ilyas *et al* 1988). Although emerging evidence of antibody and complement dependent attack on the PNS is increasingly accepted, the theory is not consistent with early biopsy studies (for example, Asbury *et al* 1969) which placed little emphasis on complement. However, more recent pathological studies such as that of Hafer-Macko (Hafer-Macko *et al* 1996) show activated complement components around the axon, serving to further the probability that the disease is largely antibody mediated.

1.5 GBS and Anti-Ganglioside Antibodies

1.5.1 *Anti-GM1 antibodies.*

In 1986 Freddo and co-workers (Freddo *et al* 1986) described a patient with lower motor neuron disease who had anti-GM1 serum IgM paraprotein, and it was proposed that these antibodies induced pathology by targeting peripheral nerve regions enriched in GM1, such as motor nerve terminals, nodes of Ranvier and motor neuron cell bodies (Ganser *et al* 1983). Since this early report, numerous examples of patients with motor neuron disease and elevated titres of anti-GM1 antibodies have been presented (Pestronk *et al* 1988, Lewis *et al* 1982, Pestronk 1991, Pestronk *et al* 1990, Lange *et al* 1992, Feldman *et al* 1991, Pestronk *et al* 1989, Salazar-Grueso *et al* 1990, Sadiq *et al* 1990, Adams *et al* 1991, Nobile-Orazio *et al* 1990). Interestingly, the presence of anti-GM1 antibodies appear to define a clinical subtype of patients with motor neuron disease, as those patients with anti-GM1 antibodies have lower motor neuropathy or conduction block characteristic of AMAN (Pestronk 1991, Sadiq *et al* 1990, Lamb and Patten 1991). Evidence of patients developing motor neuropathies following parenteral therapy with ganglioside mixtures including GM1 (Yuki *et al* 1991, Figueras *et al* 1992, Nobile-Orazio *et al* 1992) lend support to the argument that anti-GM1 antibodies are associated with motor neuropathies, a finding which is becoming increasingly relevant to the association of anti-GM1 antibodies and AMAN pathology. In cases of GBS, 10-20% of patients have elevated anti-GM1 antibodies (Yuki *et al* 1991, Walsh *et al* 1991, Ilyas *et al* 1992, van den Berg *et al* 1992) and clinical symptoms of AMAN which include pronounced motor involvement often with axonal degeneration, from which recovery is poor.

1.5.2 *Anti-GD1a antibodies*

AMAN is also associated with anti-GD1a antibodies, and it has been suggested that they are also elevated in AMSAN (Yuki *et al* 1999). Anti-GD1a antibodies are likely to mediate an attack on the axolemma (Hafer-Macko *et al* 1996) leading to electrophysiological disturbance (Kuwabara *et al* 2002). A successful murine model of AMAN has recently been generated using an anti-GD1a monoclonal antibody (Goodfellow *et al* 2005), lending further support to the involvement of anti-GD1a antibodies in AMAN. Anti-GD1a IgG antibodies are correlated with worse clinical outcomes (Yuki *et al* 1993), while anti-GD1a antibodies of the IgM isotype are thought to peak after the acute phase of AMAN, and may play a role in either regeneration or further pathology in the recovery phase of AMAN (Press *et al* 2001).

1.5.3 *Anti-GD1b Antibodies*

Anti-GD1b antibodies bind to sensory neurons and dorsal root ganglion cells (Kusunoki *et al* 1993), implicating their role in GBS with sensory involvement. Although not strictly a GBS subtype, ASAN (acute sensory axonal neuropathy) has been linked to anti-GD1a antibodies (Pan *et al* 2001), while monospecific anti-GD1b IgG antibodies have been linked to GBS associated sensory ataxia (Wicklein *et al* 1997). It has been suggested that anti-GD1b antibodies can cause cereballar ataxia by targeting the granular layer of the cerebellum or sensory fibres of the spinocereballar tract (Sugimoto *et al* 2002).

1.5.4 *Anti-GQ1b Antibodies*

Anti-GQ1b antibodies are present in up to 95% of MFS patients (Carpo *et al* 1998), and are the definitive serological diagnosis of MFS (Chiba *et al* 1992). Titres of anti-

GQ1b antibodies correlate with disease severity, peaking upon the most acute phase of the disease, and specifically affect the cranial nerves where ganglioside GQ1b is known to be enriched (Chiba *et al* 1997). MFS has also been demonstrated in a mouse model using an anti-GQ1b antibody (Halstead *et al* 2004). Taken together, this evidence supports the direct role of anti-GQ1b antibodies in MFS.

1.6 Gangliosides

In the Golgi apparatus, stepwise addition of sugar and sialic acid moieties to a glucose ceramide core is catalysed by specific glycosyltransferases and sialytransferases (Lloyd and Furukawa 1998, Maccioni *et al* 1999, Riboni *et al* 1997) (Figure 1). The resultant molecules (gangliosides), constitute a family of sialic acid containing glycoshingolipids (Marks *et al* 1996, Voet and Voet 1995, Svennerholm 1963, Svennerholm 1994), which are amphipathic components of vertebrate cell plasma and intracellular membranes associated with secretory and endocytotic pathways (Marks *et al* 1996, Voet and Voet 1995). Sialic acid is the generic term for N-acetylneuraminic acid (NeuNAc), and is linked to the internal or terminal galactose of the oligosaccharide core via α2-3 linkage (Svennerholm 1994, Svennerholm 1956, Svennerholm and Raal 1961), forming a carbohydrate moiety. The oligosaccharide core is composed of up to 4 sugars with the sequence glucose-galactose-N-acetylgalactosamine-galactose (Ledeen 1985). Ceramide is a fatty acid linked to a sphingosine chain, and forms the lipid moiety of the ganglioside. The synthesis of gangliosides begins in the endoplasmic reticulum, where the ceramide moiety is produced, and in the lumen of the Golgi complex specific glycosyltransferases (multi-enzyme complexes in the Golgi membrane) act to build the oligosaccharide moiety (Giraudo *et al* 2001, Bieberich *et al* 2002, Giraudo and Maccioni 2003).

The ampipathic character of gangliosides is due to the polar nature of their components: enveloped within the membrane is the hydrophobic lipid moiety, serving as an anchor to the hydrophilic carbohydrate moiety (possible antigenic target) on the outer surface. The *a*, *b* and *c* ganglioside series are based on the "simple" gangliosides GM3, GD3 and GT3, where the stepwise addition of sugars and sialic acids form the more complex gangliosides. Figure 1 shows a simple diagram of ganglioside synthesis. The *c* series has been omitted for clarity, as *c* series gangliosides are not included in the experiments within this thesis.

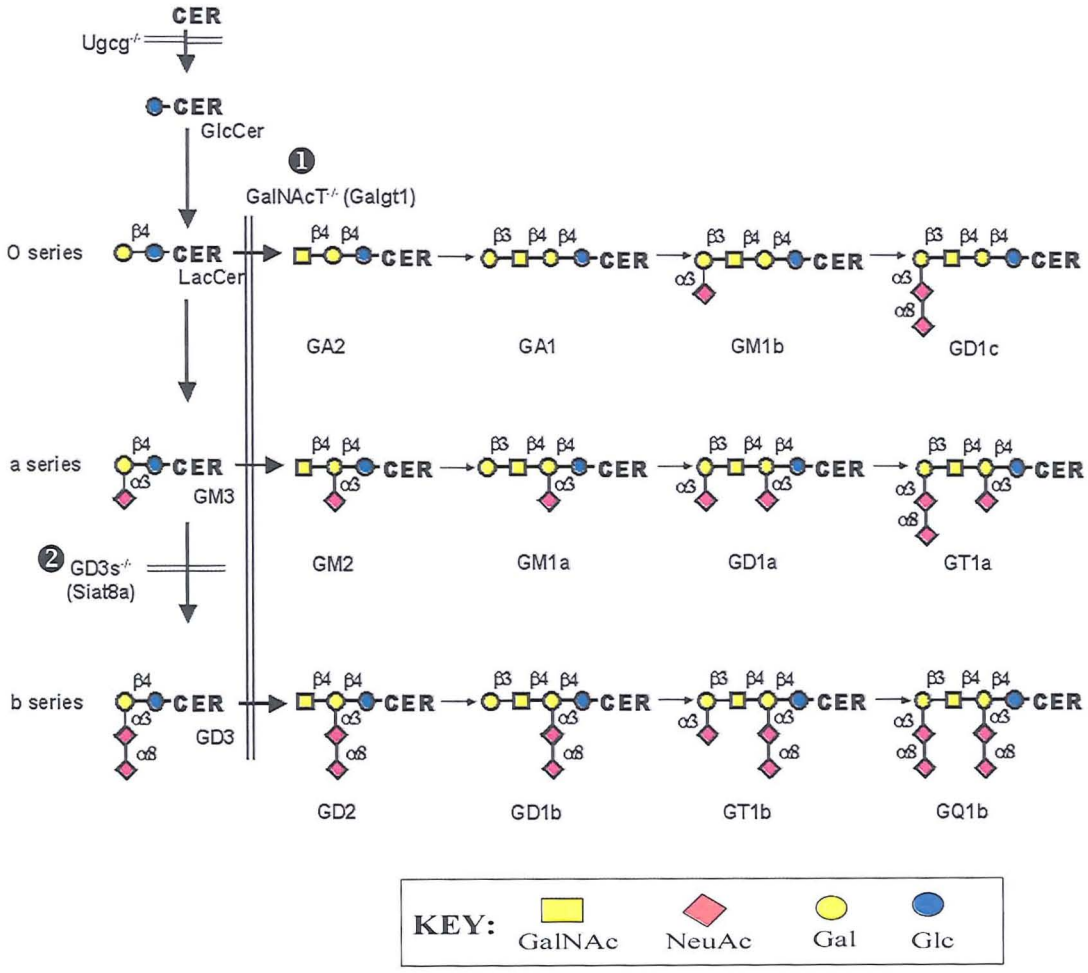

Figure 1. Schematic representation of GD3 synthase and GalNAc (GM2) transferase enzymes in the ganglioside biosynthesis pathway. ❶Removal of GM2 synthase results in expression of simple gangliosides. ❷Removal of GD3 synthase results in no *b* series gangliosides and upregulation of the *a* series.

Thin layer chromatography (TLC) allows the separation of gangliosides based upon the size of their oligosaccharide core and the number of attached sialic acids. This is the basis of their terminology, devised by Svennerholm (Svennerholm 1963, Svennerholm 1994) and in agreement with IUPAC-IUB Commission on Biochemical Nomenclature, (IUPAC 1977). For simplicity, Svennerholm proposed a code system: **G** refers to *ganglio*, and the *number of sialic acid residues* is represented by **M** (mono), **D** (di-), **T** (tri-) and **Q** (quad-). The sequence of migration in TLC is represented by Arabic numerals and lower case letters.

1.6.1 *Gangliosides: Neurobiological Function*

Investigating the pathogenesis of anti-ganglioside mediated disease has not only important clinical considerations, but is also relevant to furthering the scientific understanding of ganglioside function. Gangliosides function as receptors for toxins (Willison and Kennedy 1993), meaning it makes evolutionary sense for their expression to be minimal yet sufficient to carry out essential physiological function. The high expression of gangliosides, particularly in the nervous system, therefore indicates they may have crucial biological roles. Indeed, gangliosides are believed to have an array of neurobiological functions (Nagai 1995). Exogenous administration of gangliosides can enhance neurite outgrowth and recovery from injury (Karpiak 1984, Tsuji *et al* 1988, Roisen *et al* 1984, Riggot and Matthew 1997). Cholera toxin, the natural ligand for GM1, is a known mitogen in the proliferation of Schwann cells (Moss and Vaughn 1979), while GM1 induces morphological changes (characteristic of differentiation) in rat astroglial cells (Facci *et al* 1988). Furthermore, oligodendrocyte progenator cells in culture express different gangliosides during different stages in development, suggesting a link between ganglioside expression and

developmental regulation (Schnaar *et al* 1996). The role of gangliosides in development may also be linked to their role in regeneration of the adult nervous system. For example, in the developing and adult rat nervous system acetylated GD3 (9-O-acetyl GD3) is expressed in areas of cell migration and neurite outgrowth (Mendez-Otero and Ramon-Cueto 1994). In development, acetylated GD3 staining is observed in association with an abundance of growth cones on extending axons, which upon reaching their target cease to express acetylated GD3. The role of acetylated GD3 in development and regeneration is furthered by observations in the olfactory system. This is unique from the CNS in that it continues to replenish ("turnover") neurons throughout life, including in response to injury (Graziadei *et al* 1979, Farbman *et al* 1990). The expression of acetylated GD3 does not resemble that of other systems, in that axons maintain it's expression, suggesting the regenerative properties of the olfactory system may be, in part, due to the presence of acetylated GD3 (Mendez-Otero 1988, Mendez-Otero and Ramon-Cueto 1994). Furthermore, the expression of acetylated GD3 is upregulated in the regenerating sciatic nerve (Mendez-Otero and Santiago 2003). Other gangliosides including GD1b, GD1a, GQ1b and GM1, but most notably GT1b, promote neuronal regeneration of the rat hypoglossal nerve (Itoh *et al* 2001). The role of gangliosides in regeneration may be related to potential neurotropic ability: gangliosides can protect cells from glutamate and kainate neurotoxicity (Favaron *et al* 1988). Furthermore, bath application of gangliosides modulate synaptic plasticity of *in- vitro* brain preparations (Egorushkina *et al* 1993, Furuse *et al* 1998, Ramirez *et al* 1990, Wieraszko and Seifert 1985). The exact function of gangliosides in development and regeneration is currently unknown, although it may result from their involvement in transmembrane signalling (Hakomori 1990). For example, cholera toxin binding to GM1 triggers intracellular

signalling and cell proliferation (Bukley *et al* 1995) while it is proposed that fibroblast growth factor 2 (FGF2) interacts with membrane bound GM1 to activate signal transduction pathways which complement those of the activated FGF2 receptor (Rusnati *et al* 2002). GM1 is closely associated with the nerve growth factor (NGF) receptor TrK, which enhances the cellular response to NGF (Mutoh *et al* 1995). Interestingly, free gangliosides sequester growth factors and thus can inhibit proliferation (Rusnati *et al* 1999), indicating their direct association with the cell membrane is integral to their role in modulating the cellular responses. Although these observations are not based specifically on neuronal culture conditions, it is not unreasonable to apply such findings to the nervous system, where neuronal membranes are particularly enriched in gangliosides.

Mutant mice which lack GM3 synthase (α 2,3-sialyltransferase) are viable, but display increased sensitivity to insulin, thought to be as a result of an altered phosphorylation of the insulin receptor (Yamashita *et al* 2003). Mice lacking both GM2/GD2 synthase (β1,4 GalNAc-transferase) and GD3 synthase (α 2,8-sialyltransferase) have reduced skin integrity (Inoue *et al* 2002).

Mice lacking the gene encoding the glycosyltransferase β1,4 GalNAc-transferase (GM2/GD2 synthase) lack complex gangliosides, and consequently upregulate the simple gangliosides GM3 and GD3. These mice (GalNAc-$T^{-/-}$) display only mild defects of the nervous system (Takamiya *et al* 1996, Sheikh *et al* 1999), while 12-16 week old mice display signs of axonopathy, suggesting a role for complex gangliosides in myelination and axonal maintenance (Takamiya *et al* 1996). This notion is furthered by the progressive motor deficits observed in 12 month old mice (Chiavegatto *et al* 2000). The observations that gangliosides are integral in development, function and maintenance of the nervous system are noteworthy

(Ledeen 1985, Lloyd and Furukawa 1998, Nagai 1995), although the underlying molecular mechanism is unknown. The role of complex gangliosides and Ca^{2+} interaction may be a plausible route of exploration, as altered Ca^{2+} binding properties of GalNAc-$T^{-/-}$ neurons has been observed, and may explain the pathology of these mice (Wu *et al* 2001). Although the role of gangliosides in the human nervous system is difficult to study, identification of individuals carrying a mutation leading to a defect in the synthesis of GM3 synthase is interesting (Simpson *et al* 2004). Individuals bearing the mutation suffer early onset epilepsy, which may correlate with the disrupted ganglioside biosynthetic pathway (i.e. lack of complex *a* and *b* series gangliosides and increased levels of lactosylceramide). Although ethical considerations mean genetically modified animals will remain fundamental research tools, humans who inherently lack complex gangliosides may in future be able to lend valuable insight into the biological role of complex gangliosides, bridging the knowledge gap between murine and human studies.

Existence of gangliosides alongside proteins critical to exocytosis (syntaxin and SNAP 25: members of the soluble N-ethylmaleimide-sensetive factor attachment protein receptor (SNARE) family) indicate that gangliosides also may play a critical role in exocytosis (Chamberlain *et al* 2001, Lang *et al* 2001), while the presence of gangliosides in both post and pre synaptic membranes suggests a role in synaptic transmission (Thomas and Brewer 1990). Bath application of gangliosides (GM1 and GQ1b) to synaptosomes increases K^+ evoked neurotransmitter release (Ando *et al* 1998, Tanaka *et al* 1997). However *in vivo*, GalNAc-$T^{-/-}$ mice display normal ACh release at the NMJ under physiological conditions (Bullens *et al* 2002) indicating the role of gangliosides may not be critical in normal synaptic function. Interestingly, the role of complex gangliosides may be of critical importance in synapse function at low

temperatures (Raman *et al* 1998, Bullens *et al* 2002), although this is a finding less germaine to mammalian studies.

1.7 Autoimmunity

Horror autotoxicus: the possibility that the body can potentially raise antibodies to itself, was first raised as a hypothetical concept by Ehrlich in 1885. However, it was much neglected by experimentalists until 1956, when rabbits immunised with rabbit thyroid extract developed thyroid autoantibodies. Thus, the belief that "for many years only foreign proteins were considered true antigens" (Witebsky *et al* 1957) was challenged by achieving the first experimental model of autoimmunity. Autoimmunity arises in the context of an inappropriate immune response mounted against an exogenous or endogenous antigen that inadvertently targets an endogenous tissue component, thereby causing pathology in the absence of persistent infection.

1.7.1 Molecular Mimicry

Up to 75% of GBS cases arise preceeding respiratory or gastrointestinal infection (Mishu and Blaser 1993). Antecedant infection by a range of causative agents (Hankey 1987, Hart *et al* 1994, Winner and Evans 1993, Boucquey *et al* 1991, Ravi *et al* 1994, Merelli *et al* 1992, Dowling and Cook 1981) have been implicated in triggering GBS, but evidence of cytomegalovirus and *Campylobacter jejuni* (*C. jejuni*) infection are the most convincing (Winer *et al* 1988). The first documented report of GBS following *C.jejuni* infection was in 1982 (Rhodes and Tattersfield 1982), and GBS patients who are serologically positive for *C. jejuni* display mainly axonal forms (McKhann *et al* 1993, Blaser *et al* 1991 and tend towards poorer clinical outcome (Winer *et al* 1988, Rhodes and Tattersfield 1982 , Vriesendorp *et al* 1993,

Kaldor and Speed 1984). It has been suggested that *C.jejuni* may sensitise an individual by producing a ganglioside binding protein (Rees *et al* 1995) however molecular mimicry is widely suspected to be the main underlying process.

C.jejuni strains isolated from Japanese GBS patients were serotyped by analysis of heat-stable antigens (Penner method) (Hartung *et al* 1995), and revealed prevalence of serotype O:19, which is uncommon in general gastroenteritis cases (Fujimoto *et al* 1992, Kuroki *et al* 1993). The outer membrane of gram negative bacteria (such as *C.jejuni*) contain lipopolysaccharides , of which the saccharide moiety may mimic host structures : while this may camouflage the pathogen from the host, the molecular mimicry may also induce antibodies in the host, which unfortuitously cross react with host structures (ie. autoimmunity) (Moran *et al* 1996, Moran 1996). The first host structure implicated in GBS related molecular mimicry was GM1 (Yuki *et al* 2004) and it has since been shown that homology exists between the core oligosaccharide (OS) of *C.jejuni* O:19 and the saccharide moiety (Gal(β1-3)GalNAc) of GM1 and GD1a (Yuki *et al* 1993, Aspinall *et al* 1994) (Figure 2).

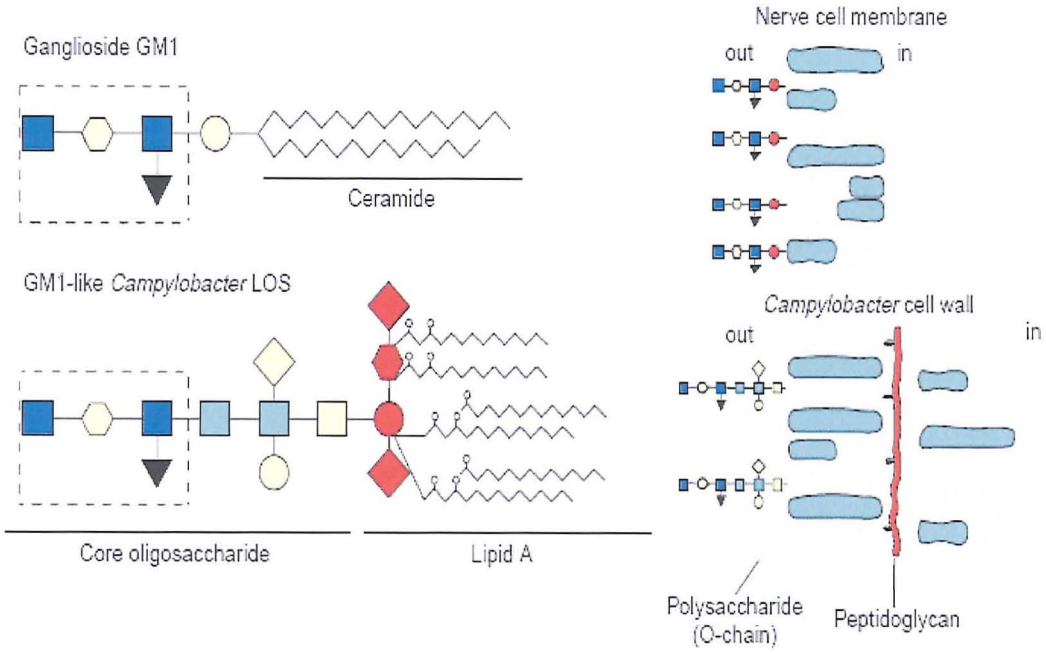

Fig 2. Schematic comparison of GM1 presentation in the cell membrane and the GM1 like oliogsaccharide (LOS) presentation on the outer wall of *C. jejuni.* Diagram extracted from Ang et al 2004.

In cases of Miller Fisher Syndrome, antibodies against GQ1b in patients sera were shown to cross react with GQ1b like antigens of the LPS of *C.jejuni*, isolated from these patients (Yuki *et al* 1993). Thus it can be hypothesised that the antigenic structure of the preceding infection determines the resultant form of GBS. At present, no clear model exists to categorically prove this hypothesis over other possible explanations, such as greater immunogenicity of certain *C.jejuni* strains (as opposed to expression of specific surface antigens) or differing immunogenic backgrounds of the hosts. However, a putative model of AMAN has been developed by feeding *C.jejuni* isolated from an AMAN patient to chickens, which went on to develop symptoms indicative of Wallerian degeneration (Li *et al* 1996).

Regardless of how the antiganglioside antibody is induced, its effect may be direct (Raphael *et al* 2001, Visser *et al* 1999), but evidence exists to support the notion that the action of antiganglioside antibodies is complement dependent (Sumner *et al* 1982,

Hays *et al* 1987, Hays *et al* 1988, Monaco *et al* 1995). Peripheral nerve biopsies of GBS patients have shown deposition of activated complement components in close approximation to antibody (Hafer-Macko *et al* 1996, Koski *et al* 1987, Luijten and Baart de la Faille-Kuyp 1972, Nyland *et al* 1981), and *in-vitro* effects of anti-GQ1b antibodies have been shown to be complement dependent (Plomp *et al* 1999).

1.8 Complement

Invading pathogens encounter a first line defence mechanism of approximately 20 proteins which are enzymatically activated and act in an ordered cascade (reviewed in Morgan 2000). Serum protein C3 is activated by the classical, alternative and mannose binding pathways (Lyons and Liebowitz 1998), all of which culminate in formation of a MAC pore in the cell membrane (summarised in Fig 2). The classical pathway is activated by antibody bound pathogens, immune complexes containing antigen, and IgM or complement fixing IgG isotopes. The alternative pathway (Pillemar *et al* 1955) is activated by C3b on activated pathogens, either as a result of the natural "tickover" of C3 or via the "amplification loop", where C3b deposited by the classical or mannose binding pathway propagates activation of the alternative pathway (reviewed by Muller-Eberhard 1988). It has been suggested that complement activation via the classical pathway requires contribution from the alternative pathway to induce injury (Girardi *et al* 2003, Haas *et a*l 2002). Furthermore, activation of the alternative pathway does not depend on the presence of a specific antibody (Trowbridge and Emiling 1997) and may be initiated by foreign proteins such as bacterial lipopolysaccharides (Trowbridge and Emiling 1997). The mannose binding pathway (Vorup-Jensen *et al* 2000) begins with the binding of mannose binding lectin (MBL) to carbohydrate structures, and the resultant complex

binds to MBL associated serine proteases (MASPS) which hydrolyse C4 and follow a similar route to the classical pathway.

A number of factors mediate the activation of complement, including human and mouse decay accelerating factor (DAF), CD59, complement receptor 1 (CR1) and mouse CR1-related gene y (Crry) (Mizuno and Morgan 2004, Morgan and Harris 2003, Turnberg and Botto 2003). CD59 inhibits MAC formation, and the decay of C3/C5 convertases is accelerated by DAF (Harris *et al* 2004, Mizuno and Morgan 2004, Lukacik *et al* 2004).

MAC assembly is a result of the terminal sequence of the complement cascade, and following the cleavage of C5 to release C5a into solution, and C5b which is membrane bound. Following these enzymatic steps, the constituents of the MAC pore give rise to a hydrophobic structure, which inserts into the lipid bilayer and completes the MAC pore by polymerising C9 (Law and Reid 1995). The polymerisation of C9 results in a cylindrical pore allowing uncontrolled Ca^{2+} influx into the cell (Halstead *et al* 2004). This results in calpain induced cytoskeletal degradation (O'Hanlon *et al* 2003), while the influx of electrolytes and water (Hesketh *et al* 1971) disturb osmotic balance and lead to lysis (B.P. Morgan 1989). The pathway is shown diagrammatically in Figure 3:

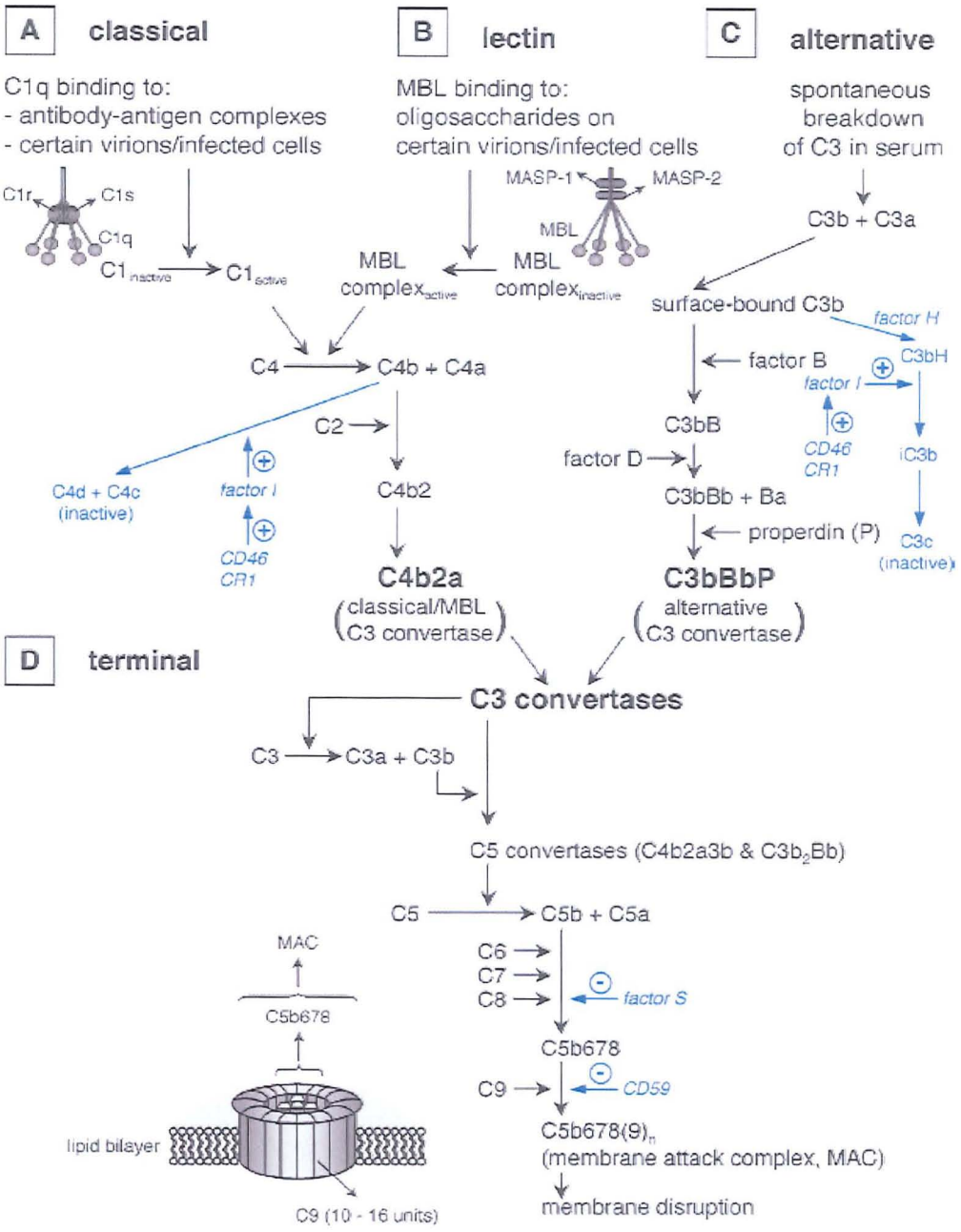

Figure 3. Overview of the main components of the complement cascade, with regulatory proteins shown in blue. Activation of the classical, alternative or lectin binding pathway converge to ultimately cause deposition of a MAC pore in the cell membrane and subsequent lysis. Image extracted from Favoreel *et al* 2003.

1.9 The Peripheral Nervous System

This section will outline briefly the modern understanding of the gross anatomy of the peripheral nerve, before focussing on the interactions of its individual components

and molecular organisation, with specific emphasis on gangliosides. The interaction of axonal and glial compartments in peripheral nerve is a potential target of anti-ganglioside antibody mediated disruption, and therefore a more detailed understanding of antibody mediated dysfunction of the peripheral nerve may be gained by exploring the cellular and molecular mechanisms underlying the process, while also addressing the role of gangliosides in the peripheral nervous system.

1.9.1 Gross Anatomy

"The medullated nerve fibre, then, consists of an external solid membrane – sheath of Schwann – of a tubular cell – Schwann cell – of a fatty sheath, and of an axon" (Cajal 1928). Although the discoveries of early researchers are now somewhat eclipsed by the knowledge gathered from more contemporary investigative techniques, a fascinating review charting the milestones of discovery, both past and present, is reviewed by Rosenbluth (Rosenbluth 1999). Often, general anatomy texts will assume the terms axon, nerve fibre and nerve to be synonymous. However, this is not the case, as a single peripheral nerve consists of a collection of nerve fibres bound by connective tissue. Each nerve fibre is comprised of an axon and its sheath

1.9.1.1 *Axon*

The axon is a single continuous process which develops as a continuation of cytoplasm from the cell body. The cytoplasm of very large axons, such as that of the great squid, behave as a viscous fluid, while the axons of mammals is a relatively gelatinous cord. Classical histological investigations, such as silver "staining" of the axon, revealed that the axoplasm comprised of many thread like processes, named neurofibrils, running through its length (Hoerr 2005). More detailed investigations

using electron microscopy suggested that these were more likely to be artefacts of the tissue processing, and that the thread like fibres comprised of two populations: neurotubules and neurofilaments. Neurotubules resemble the microtubles found in other cell types, and are the route of fast axonal transport taken by membranous organelles (Weiss *et al* 1971). Neurofilaments do not run as continual tracts owing to interruptions to the axon diameter at the nodes of Ranvier, and their absolute function is unknown. In the PNS there are 3 types of axon fibre: somatic motor, somatic sensory and autonomic (Kiernan and Barr 2005).

1.9.1.2 *Internodes*

Internodal segments represent the territory of the axon which a Schwann cell ensheaths in a multilameller spiral membrane. The sheath cell wraps the axon in a spiralling double layer of plasma membrane to give a layer of compact myelin, observed by electron microscopy to display a pattern of alternating electron dense and lucent lines (Norton 1977). The outer protein layers of the apposed plasma membranes become fused, forming the intraperiod line. While it is commonly accepted that the intraperiod line is continual with the extracellular space, it should be noted that the "line" is in fact 2 lines divided by a narrow gap which communicates with the extracellular space (Robertson 1958). The major dense line of compact myelin is a consequence of the cytoplasmic component of the Schwann being reduced as the spirals become more tightly wrapped. Thus, the inner protein layers of the closely apposed membranes fuse.

1.9.1.3 *Node of Ranvier*

The node of Ranvier, first described in 1875 (Ranvier 1875) is visible as the 'naked' segment of axon, or 'gap', between the terminations of internodal myelin lamellae. Overlapping extensions, or 'nodal collars' of the two internodes project finger like extensions of Schwann cell cytoplasm into the gap, where they are in close proximity with the axon (Berthold and Rydmark 1983). The nodal collar diameter increases with increasing axon diameter, although the actual diameter of the axon at the nodal gap is consistent for all diameters of fibre (Robertson 1959).

Since the early descriptions and models of the node of Ranvier, such as the demonstration of the nodal region using a plasticine model (Robertson 1959), more contemporary studies have revealed the node to be a more complex structure comprising well organised domains. The detailed 3D model of the node of Ranvier, created by Sosinsky (Sosinsky *et al* 2005) using serial electron tomography (Fig 4), is particularly useful in allowing the visualisation of the individual components of the node, and appreciating their spatial organisation with respect to one another.

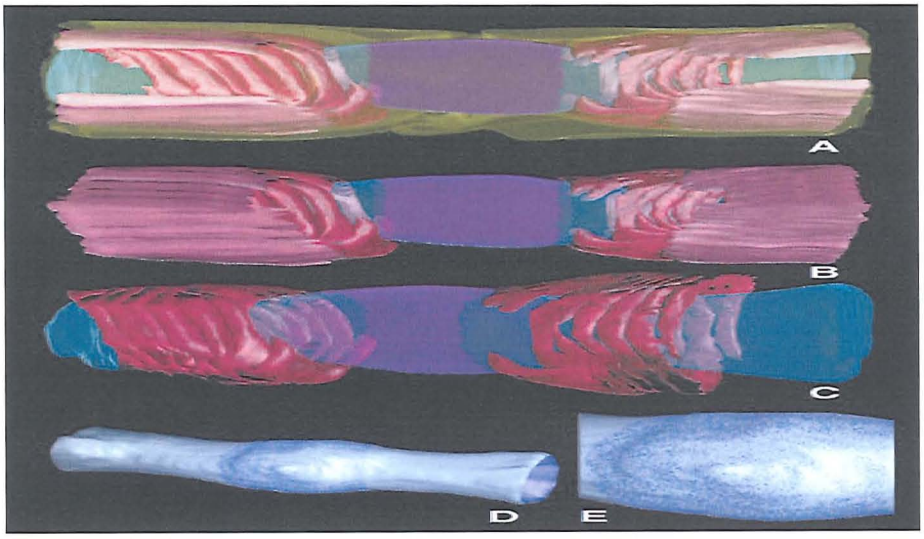

Fig 4. **A:**Illustration of the entire nodal structure. *Transparent yellow*=Schwann cell membrane, *pink*=compact myelin, *magenta*=paranodal loops, *turquoise*=axonal membrane. *Dark blue* delineates the nodal axolemma. **B** and **C** show sequential

removal of the Schwann cell and compact myelin to allow a more detailed view of the paranodal loops. **D:** Axon reconstruction demonstrating location and density of sodium channels at the node, magnified in **E**. Illustration exerted and text modified from Sosinsky *et al* 2005.

The node of Ranvier is a structure frequently involved in peripheral neuropathies (Griffin *et al* 1996, Sima *et al* 1993), and an insight into these highly organised structures may lend to an understanding of disease processes. For example, disruption of the highly compartmentalised proteins and ion channels of the node may lead to disturbance of the normal physiological function of the peripheral nerve. A novel form of ankyrin (Kordeli and Bennet 1991), a cytoskeletal protein, is abundant at the node (Kordeli *et al* 1990), while the proteins ezrin, radixin and moesisn are present in the microvilli extending into the nodal gap (Gatto *et al* 2003, Scherer *et al* 2001). NrNCAM is co-expresed with neurofascin at the node (Davis *et al* 1996), while several extra-cellular matrix proteins are present (Apostolski *et al* 1994, Rieger *et al* 1986, Martini *et al* 1990). One such protein, dystroglycan, is expressed on the Schwann abaxonal membrane and when deleted impairs nerve conduction, possibly through a concomitant reduction in nodal sodium channels (Saito *et al* 2003). The stabilisation and formation of the axoglial junction is thought to involve Caspr and contactin, both proteins specific to the nodal axoglial junction (Boyle *et al* 2001). While this overview does not provide an exhaustive list of nodal proteins, it serves to highlight how antibody mediated disruption of the membrane could potentially disrupt a number of functions reliant on nodal proteins.

The node of Ranvier has long been established to have an important role in action potential generation in myelinated fibres (Chiu *et al* 1979). During development, K^+ channels become specifically clustered under juxtanodal compact myelin (Vabnick *et al* 1999, Wang *et al* 1993), and upon demyelination are exposed leading to a reduction

in excitability (Rasaband *et al* 1998). It is also thought that voltage-independent K^+ channels are present at the node (Roper and Schwarz 1989).

The high density of adhesion molecules on the nodal axon is thought to be related to the clustering of Na^+ channels at the node (Davis *et al* 1996), which houses an abundance of voltage gated Na^+ channels (Ritchie and Rogart 1977, Ellisman and Levinson 1982). The density of Na^+ channels at the node is approximately 25 times greater than internodal regions (Shrager 1989), suggesting they play an important role in the propagation of the action potential. Thus, it is reasonable to assume that any disruption to Na^+ channel clusters may have a detrimental effect on function – for example, resulting in conduction block. Figure 5 gives a detailed schematic overview of the nodal region.

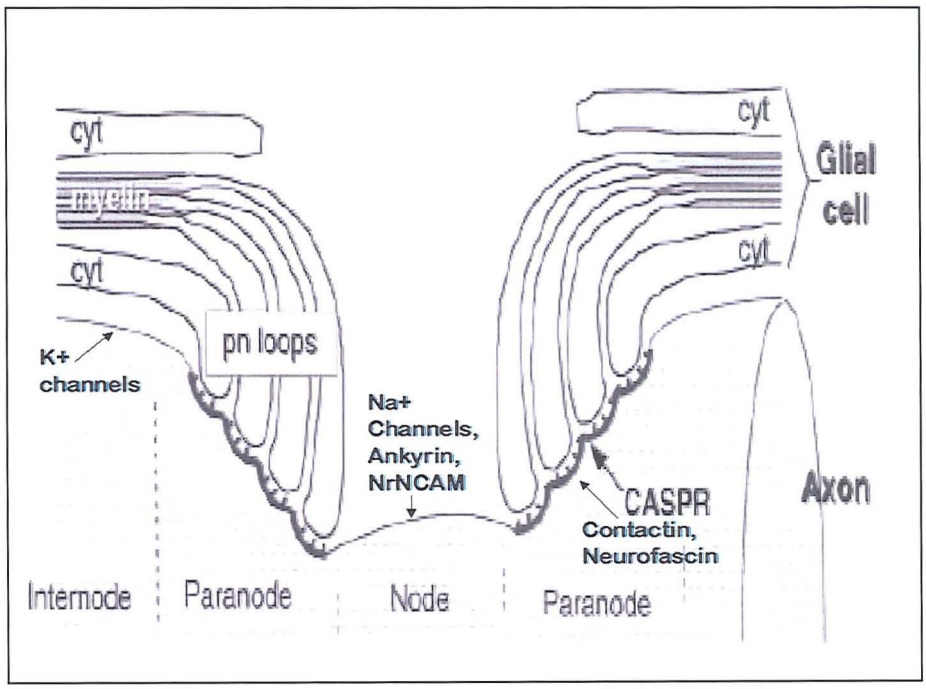

Fig 5. Schematic overview of the node of Ranvier showing an overview of the main components in each domain. *Cyt* = cytoplasm and *pn* = paranodal. Modified from Einheber *et al* 1997.

1.9.1.4 *Schmidt-Lanterman incisure*

These cleft like structures in the myelin were first described in 1874 and 1877 by Schmidt and Lanterman respectively (Lanterman 1877, Schmidt 1874) and to date remain a contemporary area of investigation. Although once regarded as artefacts (Young 1944), more recent studies using electron microscopy have confirmed their presence. A detailed ultrastructural study by Hall and Williams (Hall and Williams 1970) reveals that incisures typically show separation of the myelin lamellae with the position of the dense line being occupied with Schwann cell cytoplasm, which contains microtubules and vesicles. Interestingly, this organisation bears a resemblance to developing myelin, before the lamellae are compacted, leading to the theory that the incisures may play a role in myelin growth (Celio 1976). However, absence of Golgi apparatus and rough endoplasmic reticulum (Hall and, Williams 1970) mean they are unlikely to play a role in protein synthesis, thus perhaps are more involved in metabolic support for maintenance, or plasticity of the myelin. Interestingly, Gould and coworkers (Gould *et al* 1995) show mutant mice lacking or underexpressing myelin basic protein (MBP) have an increased density of Schmidt-Lanterman incisures when compared to wild type mice. From this, it is logical to assume that the increased number of SLI is to compensate the function of MBP in axon-Schwann cell communication. During Wallerian degeneration, SLI are the foci of myelin segmentation (Webster 1965, Williams and Hall 1971, Ghabriel and Allt 1979), and also represent an important area to study when considering the pathology of immune mediated peripheral nerve disorders. For example, intraneural injection of EAN serum has been shown to cause vesiculation of the myelin at the site of SLI (Saida *et al* 1978, Saida *et al* 1979) and sural nerve biopsies of IgM paraproteinaemic neuropathy cases have shown widening of the myelin in the region

of the SLI (Jacobs and Scadding 1990). As the authors of the latter report discuss their findings, they point out that the IgM antibody may be binding to myelin associated glycolipid (MAG) or other glycoproteins, including gangliosides. In a later study (Schroder and Himmelmann 1992), it was shown that there was a link between inflammatory neuropathies and increased accumulation of immunoglobulin deposits, inferred from an observed accumulation of granular material in SLI. From these studies, it may be reasonable to assume that an anti-ganglioside antibody may cause a similar pathology (ie. demyelination); granular immunoglobulin deposits in the SLI may perturb the interaction of axon-Schwann cell communication, although as yet no data exists to support this.

1.9.1.5 *The Neuromuscular Junction*

A motor unit is the interface between a muscle fibre and its innervating motor axon. In the muscle, the terminal end of the axon loses its myelin sheath, and branches to form the characteristic "pretzel" like structure where the terminal axon branches and boutons contact the muscle fibre, shown in Figure 6.

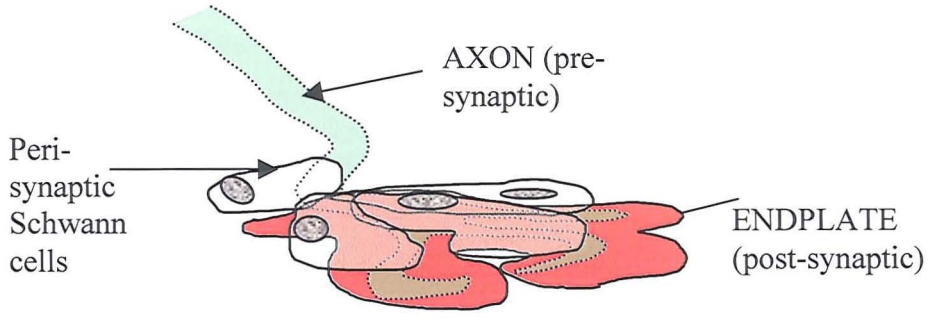

Figure 6. Simplified diagram: gross anatomy of the NMJ. The post-synaptic endplate in shown in red, in reference to the use of TRITC-BTx, which in this manuscript is frequently used to deliniate the endplate by binding to the nAChR on the muscle surface. The pre-synaptic axon and PSC overly the BTx positive area of the muscle fibre surface.

Within the motor nerve ending are active zones, containing an accumulation of vesicles. These vesicles contain a "quantum" (5000-10000 molecules) of acetylcholine (ACh), which is released across the synaptic cleft and is converted to an action potential at the post synaptic site. The synaptic cleft houses the basal lamina, which covers the muscle fibre and myelinated nerve fibre, and serves to anchor the enzyme acetylcholinesterase (AChE). The post-synaptic membrane consists of numerous infoldings with wide longitudinal crests and narrower interfolds. The active zones of the pre-synaptic axon correspond to the post-synaptic crests, which express a high density of Ach receptors, while the bottom of the folds contain voltage gated Na^+ channels (Figure 7). α-bungarotoxin (BTx) is commonly as a marker of the post-synaptic endplate, as it recognises the ACh receptor (AChR).

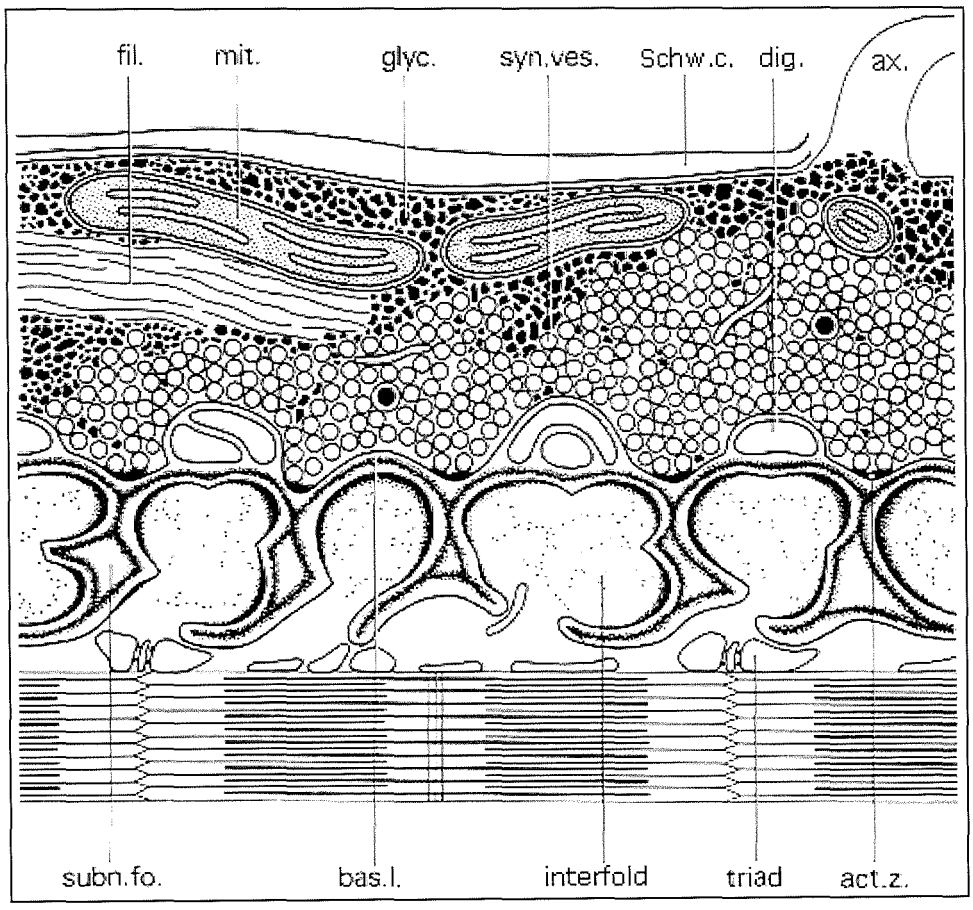

Figure 7. ultrastructure of the NMJ, modified from Couteaux and Spacek 1988. *ax* – axon, *fil* – neurofilament, *mit* – mitochondrion , *glyc* – glycogen, *syn.ves* – synaptic

vesicles, *Schw c.* – Schwann cell, *dig* – terminal digitations of Schwann, *subn. fo.* – subneural fold, *bas. l.*- basal lamina, *act. z.* – synaptic active zone.

When an action potential depolarizes the nerve terminal, voltage-gated calcium channels (VGCCs) are opened allowing a small localised influx of calcium that activates the soluble N-ethylmaleimide sensitive factor attachment protein receptor (SNARE) machinery involved in vesicle fusion. ACh is released by exocytosis into the synaptic cleft. Most is broken down by AChE and the breakdown product recycled by the nerve terminal. However, release of excess ACh as a "safety factor" (Wood and Slater 2001) ensures enough ACh reaches the post synaptic membrane to open the nicotinic AChR pore and cause Na^+ and K^+ influx. This depolarizes the membrane to cause an endplate potential (EPP): if of enough magnitude, voltage gated Na^+ channels will open and generate an action potential resulting in muscle contraction.

It is widely accepted that there are variations in morphology of NMJs depending on muscle fibre type (Sieck *et al* 1989, Larsson 1991). A study by Prakash *et al* (Prakash *et al* 1996) showed that the morphometric properties of both pre- and post-synaptic NMJs differed depending on the muscle fibre type which they innervated. By creating 2D reconstructions of NMJs, the authors show for the pre-synaptic aspect, that type I and IIa fibres had axon terminals with smaller areas and fewer but longer branches than type IIx and IIb fibres.

The NMJ can be viewed as a tripartite synapse, owing to the presence of not only post- and pre- synaptic compartments, but also the presence of specialised peri-synaptic cells which are likely to be integral in maintenance and repair of the NMJ.

1.9.1.6 *The Peri-Synaptic Schwann Cell (pSC)*

In addition to the well characterised pre- and post-synaptic elements of the NMJ, the tripartite nature of the synapse is largely owed to the presence of the peri-synaptic Schwann cell (pSC). Although the pSC expresses several proteins common to myelinating Schwann cells, such as P0, MAG and galactocerebroside (Georgiou and Charlton 1999), it can be uniquely distinguished by specific markers (Astrow *et al* 1998) and does not myelinate the nerve terminal.

It is widely accepted that the pSC has an active role in synaptic transmission at the NMJ (Auld and Robitaille 2003). The specific functional differences of the mammalian pSC in comparison to the amphibian indicate that the mammalian pSC has become specially tailored to facilitate its role in synaptic modulation (Rochon *et al* 2001), a role which to date is not fully understood. The interaction of the pSC and nerve terminal is complex, and damage to the pSC may interfere with the normal neurotransmission on which the integrity of the NMJ depends (Auld *et al* 2003).

The expression of agrin by the pSC is upregulated upon regeneration of a damaged axon, and may be related to the aggregation of AChRs at the regenerating NMJ (Yang *et al* 2001), implicating the pSC in regeneration and repair of the NMJ. The role of the pSC in nerve regeneration mean it remains a contemporary and important area of investigation. The pSC has successfully been labelled and visualised, for example using dyes such as calcein blue (O'Malley *et al* 1999). Upon re-innervation of a damaged NMJ, pSC cell bodies were shown to develop and act as a substrate for which the early axon sprout could navigate over. More impressive is the development of a transgenic mouse expressing green fluorescent protein (GFP) in the Schwann cells and cyan fluorescent protein (CFP) in the motor neuron. This has facilitated direct visualisation of the pSC in the living mouse and monitoring of its response

following partial denervation of muscle (Kang and Thompson 2002). At denervated sites, elongated pSC processes were shown to form, along which the regenerating axon then developed. Longer term monitoring revealed several new observations. Firstly, the pSC processes often vacated the denervated synaptic site, and such regions were not targeted by the regenerating axon. Secondly, the formation of "Schwann cell bridges" was observed, highlighting the ability of the Schwann processes to grow from a denervated site and make contact with another. Based on these observations, future research will hopefully unveil some of the key signalling molecules and receptors involved in this fascinating response to denervation, and perhaps in the distant future new therapeutic advances may result. On the same note, identification of the pSC as a disease target associated with anti-disialosyl antibodies and neuromuscular paralysis (Halstead *et al* 2004) reinforces the clinical significance of the pSC. For example, anti-disialosyl antibodies which selectively ablate the pSC provide a useful tool to study the response of the NMJ to loss of the pSC and perhaps provide new insight into its function in maintaining and supporting the synapse.

1.9.1.7 *The Parajunctional Fibroblast (PJF)*

In addition to the pSC, the tripartite nature of the NMJ relies on the presence of a third cell type, likely to be a fibroblast (Fig 8). In comparison to the pSC, the parajunctional fibroblast is little understood, yet deserves equal attention as it may be as functionally significant as the pSC.

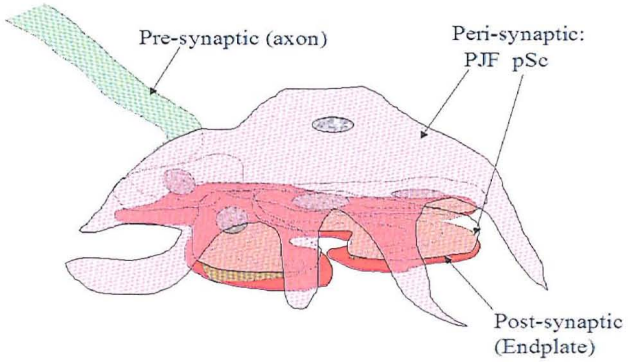

Fig 8. The NMJ, comprising the post synaptic endplate, and pre-synaptic axon and pSCs is enveloped by the processes of the PJF, as shown in translucent red.

A recent study suggests that the cell (termed the *kranocyte (*or *helmet cell)* as described by Court *et al*, in process) is located at the majority of unlesioned NMJs. This suggests that upon denervation, the cell may become activated and play a role in the recovery of the synapse, as proposed by earlier works which originally observed the influx of fibroblast like cells to denervated NMJs (Connor and McMahan 1987). Following denervation of muscles these authors determined a marked increase in refractivity of areas of the muscle which corresponded to the overall appearance of junctional zones. The authors demonstrated that these cells are the products of cell division, and distinct from other cell types which undergo mitosis following denervation, such as muscle satellite cells. Owing to their morphology, they are unlikely to be perisynaptic Schwann cells, and following denervation their accumulation resulted in a "diaphanous veil of cell processes" enclosing a region "centered around the synaptic site". Immediate, as opposed to delayed, re-innervation halted their accumulation, suggesting that absence of the axon maintains the population of cells perhaps via a signal originating from the degenerating junctional region. This is suggestive that the fibroblasts mediate a role in regeneration. In

accordance with the study of Connor and McMahan, Gatchalian *et al* found denervated endplates to be targeted selectively by proliferating interstitial cells which displayed the characteristics of fibroblasts (Gatchalian *et al* 1989). These authors provide further insight into the possible function of the cells by showing their presence is closely correlated with the upregulation of adhesive molecules: N-CAM was deposited on the surface of the accumulated cells while tenascin(J1) was associated with fibrils in close contact with the fibroblasts. *In vitro*, fibroblasts from denervated muscle were shown to synthesise N-CAM, tenascin(J1), fibronectan and M-HSPG (a matrix associated heparin sulfate proteoglycan). The expression of tanascin(J1) is likely to be associated with proliferating cells, leading the authors to postulate that following denervation, proliferation of the perisynaptic fibroblasts is induced resulting in an increase of adhesive molecules which enhances axon migration over the perisynaptic connective tissue to the original site of innervation. To date, it remains unclear whether peri-synaptic cells, including the parajunctional fibroblast, have a lineage distinct from that of their extra-junctional counterparts, or whether their proximity to the junctional region affords them the unique ability to respond to signals form the NMJ. The expression of the transgene LacZ by cells within close proximity to the synaptic region indicates that peri-synaptic cells share a pattern of gene expression (Weis *et al* 1991), and it has also been suggested that the accumulating cells associated with the damaged NMJ are not of the fibroblast lineage, but are bone marrow derived cells of the monocyte macrophage cell line. Upon denervation, it is proposed that the pSC release chemokines which attract an influx of bone marrow derived cells to the junctional region: these cells then release growth factors which stimulate local cells to produce extracellular matrix molecules to aid the regeneration of the axon, as summarised in Figure 9 (Mochizuki *et al* 2005).

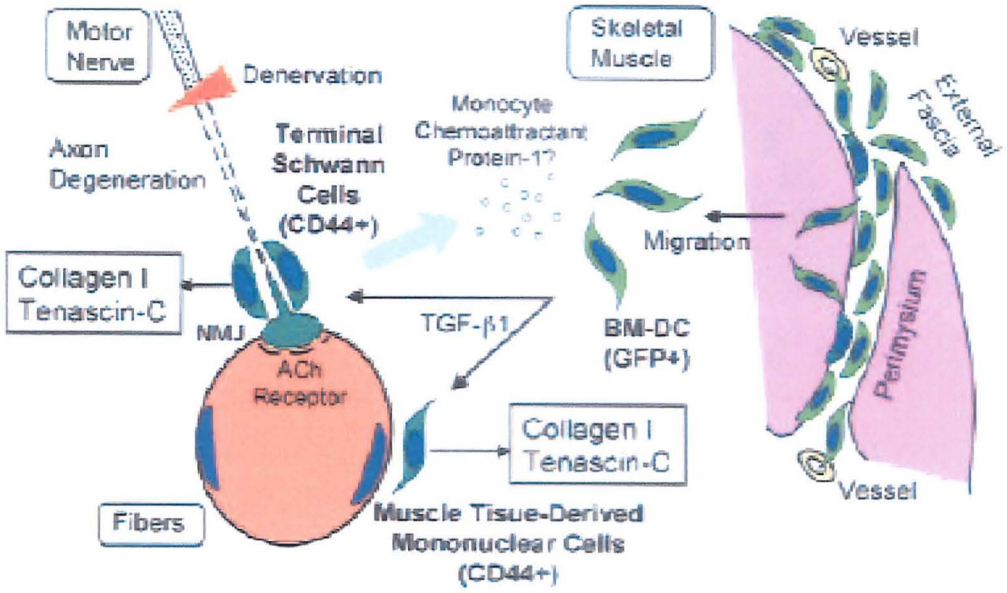

Fig 9. Sequence of events following denervation and subsequent activation of bone-marrow derived fibroblast like cells to the synaptic region (figure exerted from Mochizuki *et al* 2005).

However, this model does not address the presence of the existing fibroblasts at the uninjured NMJ, as described by Court *et al*. These seemingly senescent cells may become activated upon denervation and release cytokines and growth factors, perhaps further aided by the infiltration of the bone marrow derived cells as shown in the above model. Future research will hopefully lead to a more detailed understanding of this comparatively "novel" cell type, and lend insight into its role at the NMJ in both maintenance and repair.

1.9.2 Gangliosides and the PNS

Gangliosides account for 1-2% of the total lipid content of non-neuronal cell membranes, with a significantly higher abundance (10-20%) in neuronal cell membranes (Ledeen 1985). The division of GBS phenotypes and their association with specific anti-ganaglioside antibodies is consistent with the fact that

gangliosides expression follows a tissue (and species) specific pattern (Yamakawa and Nagai 1978).

1.9.2.1 *GM1*

In human motor and sensory nerve, GM1 is more enriched in the axonal fraction when compared to the myelin fraction, in which ganglioside LM1 is the major ganglioside (Ogawa-Goto *et al* 1990). Analysis of the ventral and dorsal roots of the second lumbar nerve by the same authors (Ogawa-Goto *et al* 1992) demonstrated that motor nerve myelin contained significant GM1, while the content for sensory nerve was much less (15% and 2% respectively). This is suggestive that the composition of GM1 in sensory nerve myelin is too low to be antigenic. However, an alternative explanation may be that the sensory GM1 is presented in a different manner, and may thus be inaccessible as a potential target to circulating autoantibodies. This study focussed on the ventral and dorsal roots of the lumbar and sacral nerves: there is a differential expression of gangliosides along the rostro-caudal axis, for example the enrichment of GQ1b in the cranial nerves (Chiba *et al* 1993, Chiba *et al* 1997), and it would be interesting to determine if the GM1 levels between motor and sensory nerves is perhaps regulated in differential manner along this axis. It would also be interesting to determine the significance of GM1 in the motor nerve myelin: not all components of the myelin membrane are synthesised by Schwann but are derived from axonally transported materials (Brunetti *et al* 1981). It could perhaps be that gangliosides are transported from axon to myelin in the PNS.

GM1 has been located at nodes of Ranvier in myelinated peripheral nerve fibres (Ganser *et al* 1983, Corbo *et al* 1993, Kusunoki *et al* 1993, Molander *et al* 1997), but these studies did not distinguish whether the Gal(β 1-3)GalNac moieties were in the axon or surrounding structure. To address this issue, Sheikh *et al* (Sheikh *et al* 1999)

investigated the distribution of Gal(β1-3)GalNAc binding sites in mice, humans and rats, where it was shown that staining was similar in all species. In teased fibres of normal mice CTb stained the nodal gap and paranodal region of Schwann cell, and also the Schmidt-Lantermann incisure. Electron microscopy revealed CTb binding to nodal axolemma, paranodal and internodal axolemma with no binding to Schwann cell basemant membrane overlying the nodal gap. The failure of these authors to detect GM1 in compact myelin seemingly contradicts the chemical studies of Ogawa-Goto (Ogawa-Goto *et al* 1992. Immunocytochemical (ICC) studies with IgG mouse monoclonal antibodies (Gong *et al* 2002) showed no staining of compact myelin of rat, mouse or human tissue, indicating that the gangliosides are inaccessible to the mAb using the present techniques. A possible explanation for this may be that in the context of the living membrane, GM1 is sterically hidden in the compact myelin and thus failure to detect it via laboratory methods indicates that *in-vivo*, it is probably also inaccessible to circulating antibodies.

In immunofluorescence studies of tissue from rabbits immunised with Gal(β1-3)GalNAc epitope or GM1, approximately 70% of nodes of Ranvier were stained, with immunoreactive IgM or IgG extending from the nodal gap and along the edge of paranodal myelin (Thomas 1991). These observations suggest that GM1 associated with the node of Ranvier (as opposed to compact myelin) is accessible in the *in-vivo* situation, and therefore represents a possible target of anti-GM1 antibodies, either through GM1 itself, or the Gal(β1-3)GalNAc epitope.

While the use of monoclonal antibodies has been useful, a more clinically relevant approach was introduced by O'Hanlon *et al* (O'Hanlon *et al* 1996), who used antibodies cloned from neuropathy patients. These authors noted "substantial" differences in the binding of each mAb to PNS structures. Sm1, a GM1 monoclonal

antibody stained a population of mouse dorsal root ganglia (DRG) neurons, representing the population which were most strongly stained by CTb. In contrast, DRG cells which were weakly stained by CTb were stained by Do1 (which recognises the Gal(β1-3)GalNAc epitope). In teased fibre preparations, Sm1 was shown to weakly label the fibre surface, and bind to exposed areas of compact myelin. Paranodal staining was not observed, and Sm1 did not stain rat sciatic nerves. In both cases, Do1 was negative. At the mouse NMJ, Sm1 stained intramuscular nerve structures, but none overlying the NMJ, while no Do1 staining could be detected. This study is important in that it highlights the fine specificities of anti-ganglioside antibodies. The subtle differences noted between mice and rats serves to illustrate that there may be differences in GM1 expression between species, or it may simply be that the presentation of the ganglioside in the membrane is different. It is of particular interest to note that the study of O'Hanlon *et al* was performed on the NIH mouse strain. The peri-synaptic Schwann cell of this mouse has been shown to be resistant anti-disialosyl antibody mediated injury compared to Balb/C and C57Bl/6 strains (Halstead *et al* 2005) suggesting possible differences in profile or presentation of disialosyl gangliosides may exist in certain strains for certain cell types. The CTb and Sm1 staining of compact myelin of the NIH mouse is in contrast to the findings of other studies (Thomas 1991, Sheikh *et al* 1999) and thus would be interesting to determine if the profile of GM1 expression in this mouse is also altered.

Studies of human tissue further support the notion that the presence of GM1 may often be "missed" when a monoclonal antibody fails to detect it. A monoclonal anti-GM1 antibody failed to stain human peripheral nerve (Kusinoki *et al* 1993). Similar results were shown in a later study (Kusunoki *et al* 1997), however following neuraminidase treatment to convert GD1b to GM1, the same antibody bound to DRG

neurons and paranodal myelin. This suggests that in order for the antibody to bind GM1, the GM1 must be densely localised and accessible. There are several possible scenarios: firstly, simply increasing the amount of GM1 on the membrane is allowing the mAb to bind, alternatively, GD1b is located in a more accessible manner within lipid rafts, and thus following neuraminidase treatment the "new" GM1 is also more accessible when compared to the native GM1. Of course, a combination of these factors may come into play, with binding to native GM1 enhanced by the new epitope created from GD1b. Finally, it is also possible that GD1b may be masking GM1, and the removal of GD1b is facilitating GM1 to be detected by the antibody.

1.9.2.2 *GD1b*

Defining the exact staining profile of GD1b is often confounded by the fact that many anti-GD1b antibodies recognise the Gal(β1-3)GalNAc epitope shared with GM1. CTb is commonly used to unequivocally detect GM1, and although tetanus toxin (TTx) can be used to localise GD1b, it is not an "acid test" as TTx also detects other *b*-series gangliosides including GQ1b and GT1b (Angstrom *et al* 1994). GD1b has been shown to be present in motor and sensory nerve (Ogawa-Goto *et al* 992) in comparable amounts, with a greater proportion in the myelin when compared to the axon (Svennerholm 1994) in sensory and motor nerve myelin. Monospecific anti-GD1b antibody stained nerve cells in the human DRG and paranodal myelin of the ventral and dorsal roots (Kusunoki *et al* 1993), with a later study confirming that the staining could be abolished with chloroform:methanol and neuraminidase treatment, proving the antibody was recognising a specific carbohydrate structure specific to a glycolipid (Kusunoki *et al* 1997). In the same study, a Gal(β1-3)GalNAc antibody gave the same profile of staining as the GD1b antibody indicating the Gal(β1-

3)GalNAc epitope of GD1b is more accessible than that of GM1. The binding of peanut agglutinin (PNA) in the paranodal myelin (Corbo *et al* 1993) may thus be recognising the Gal(β1-3)GalNAc of GD1b as opposed to GM1, although the results of PNA studies must be interpreted with caution as PNA also recognises this epitope on glycoproteins (Apostolski *et al* 1994).

A monoclonal anti-GD1b antibody has been shown to give similar staining profiles in human, rat and mouse tissue, staining both motor and sensory axons in the spinal roots in addition to the abaxonal Schwann cell membrane and node of Ranvier of the sciatic nerve (Gong *et al* 2002). Interestingly, this study also lends support to the possibility that anti-GD1b antibodies selectively injure large sensory neurons (Kusunoki *et al* 1996). The monoclonal antibody specifically stained medium and large DRG neurons, with no staining observed in small diameter DRG neurons or Remak bundles (Gong *et al* 2002). Although this does not exclude the presence of GD1b in the small diameter neurons (as these were shown to be GT1b positive and must therefore synthesise GD1b), it highlights the fact that GD1b may be displayed differently in small neurons and thus is not a potential antibody target. In support of this study, the binding of a human antibody which recognises GD1b and GM1 with similar affinity via the Gal(β1-3)GalNAc epitope was shown to bind a population of DRG neurons which were labelled only weakly by CTb (O'Hanlon *et al* 1996), suggesting the antibody may be recognising GD1b in this specific subset of DRG neurons.

1.9.2.3 *GD1a*

GD1a is present in human motor and sensory nerves and has a higher concentration in motor than sensory myelin from human roots. In both cases, GD1a is most enriched

in the axonal fraction when compared to the myelin. Differences in the ceramide portion of ventral and dorsal GD1a have been suggested, as it shows different migration patterns in extracts from motor and sensory roots (Ogawa- Goto *et al* 1990), a finding confirmed by TLC, where the mobilities of GD1a from the ventral and dorsal roots were distinct from each other (Gong *et al* 2002). An antibody showing high affinity for GD1a was shown to bind preferentially to rat and human motor nerves, although low level binding to DRG neurons was not ruled out and the difference between mouse sensory and motor nerve was less striking (Gong *et al* 2002). The same authors show that antibodies reacting GD1a and GT1a preferentially bind unmyelinated fibres, but again display greater binding in motor fibres. In teased fibre studies, nodes of Ranvier and abaxonal Schwann cell membranes were stained, with no staining in the paranodal region. One factor which may account for the differences in staining profiles may be cross reactivity of anti-GD1a antibodies with Gal(β1-3)GalNAc GD1a. This is a minor ganglioside expressed in the peripheral nerve, and the first description of GalNAc GD1a was in 1988 (Ilyas 1988), when a human IgM reactive with the Gal(β1-3)GalNAc was shown to bind bovine, human and rabbit peripheral nerves. No staining was observed in the myelin, although Gal(β1-3)GalNAc GD1a may be present in amounts which were undetectable to the antibody used. Further studies using patient sera have been useful, such as that of de Angelis (de Angelis *et al* 2001). High titre anti-GD1a IgG was shown by immunofluorescence microscopy to bind to the nodal region of human motor roots but not sensory, and serum preadsorbed with GD1a failed to bind, proving specificity of the antibody for GD1a in tissue. However, colocalization using botulinum toxin A (BTA, to bind the sialic acid of GD1a) provided slightly contradictory results, as BTA bound nodal and paranodal region of motor and *sensory* roots. BTA also recognises

the sialic acid of other gangliosides such as GT1a , so this may explain the discrepancies, or as the authors note, the antibody may be recognising N-acetlygalactoseaminyl-GD1a and binding may thus be influenced by steric hindrance, while the smaller toxin is unaffected. However, it seems more plausible that the antibody and toxin are binding different epitopes, as in the double labelling procedure one would have expected the toxin to bind preferentially to the ganglioside and abolish or significantly decrease the antibody binding. In mouse tissue, a GD1a specific IgG monoclonal antibody was shown to be exclusive to the axolemma, including the distal portion overlying the synaptic gutters of the NMJ with no presence on the pSC cell (Goodfellow *et al* 2005). Although localisation studies were done in the GD3s$^{-/-}$ mouse which overexpresses the *a* series gangliosides, the overall pattern of staining appeared similar compared to WT mice (Goodfellow – unpublished observations) and thus this study is useful for determining the anatomical distribution of GD1a, but less informative regarding absolute levels of expression. The same authors also showed that human anti-GD1a AMAN sera displays same pathogenisis as the monoclonal antibody, suggesting it is probably binding the same target as the monoclonal antibody.

1.9.2.4 *GQ1b*

Biochemical analysis has shown that compared to dorsal and ventral roots of the human spinal cord, the cranial nerves contain a greater amount of GQ1b, with the highest expression in the trochear, abducens and oculomotor nerves (Chiba *et al* 1993, Chiba *et al* 1997). The same authors have shown that these nerves have dense location of GQ1b in the paranodal regions, as inferred from the binding of a monoclonal anti-GQ1b antibody (Chiba *et al* 1993). An immunohistochemical study of the human

DRG (using the same monoclonal antibody) displayed immunoreactivity in a minor population (10%) of large DRG neurons, with weak binding to other structures, including grey matter of the brain stem and spinal cord, and both deep and granular layer neurons of the cerebellum (Kusunoki *et al* 1999). Further details on the localisation of GQ1b can be obtained using sera from MFS patients, in which autoantibodies reactive with disialosyl epitiopes are present. For example, fluorescence microscopy studies have shown IgG fractions of MFS sera, shown to be reactive with GQ1b, specifically label NMJ regions and intramuscular nerve branches (Wessig *et al* 2001). This finding is supportive of the "alpha-latrotoxin" like effect seen at the distal motor nerve, a likely result of antibody binding to GQ1b (Plomp *et al* 1999), and the immunohistochemical and ultrastructural damage of the nerve terminal induced by anti-GQ1b antibodies (O'Hanlon *et al* 2001, Jacobs *et al* 2003). A monoclonal anti-GQ1b antibody cloned from CANOMAD* sera and displaying similar specificity to the anti-ganglioside antibodies of MFS patients was shown to bind specific neuronal structures in the rodent PNS (Willison *et al* 1996). *Ex-vivo*, neurons of the DRG were immunopositive, as were nerve fibre bundles, spinal nerve roots and trunks and intramuscular nerve bundles. Sensory neurons were also stained, as were motor end plates. *In-vivo* antibody binding (via passive transfer) revealed a similar pattern of staining, suggesting that anti-GQ1b antibodies are able to bind both DRG and nerve terminals and as a consequence, exert a pathological effect. The similar abilities of a monoclonal mouse antibody and MFS sera to exert complement mediated damage to the nerve terminal (O'Hanlon *et al* 2001) is indicative that both are binding to the same target antigen at the same site. The mouse monoclonal antibody, termed CGM3, is an IgM antibody reactive with GQ1b, GD3 and GT1a (Goodyear *et al* 1999). Application of the antibody to *ex-vivo* mouse muscle

preparations (Halstead *et al* 2004) confirmed, at the level of light microscopy, antibody binding to the NMJ with presence of "nuclear shadows", interpreted as evidence of pSC membrane labelling. Immuno-electron microscopy by the same authors confirmed uniform staining of the presynaptic neuronal and pSC membranes, a novel finding which implicates the pSC, in addition to the distal motor nerve, as a potential target in MFS owing to a high density of disialosyl gangliosides.

*CANOMAD: chronic ataxic neuropathy with opthalmoplegia, M-protein, agglutination, and disialosyl antibodies). Disialosyl epitopes present on gangliosides including GQ1b, serve as IgM autoantibody targets.

1.10 AMAN : Finding the Definitive Animal Model

While there is increasing acceptance of GBS as an autoimmune disease, confirmation that its classification as an autoimmune disease is more than circumstantial relies on the fulfilment of Witebsky's Postulates (Witebsky's Postulates revisited, Rose and Bona 1993):

Witebsky's Postulates:

Presence of autoantibody or self reactive T-cell, which

Corresponds to a "self" antigen

Analogous response must be induced in animal models, which manifest a similar disease.

Following early reports of GM1 immunized rabbits displaying pathology (Nagai *et al* 1976), a more successful model of AMAN (fulfilling Whitebskys postulates) has been developed. Sensitising rabbits with bovine brain ganglioside mixture (BBG) or GM1 resuled in elevated anti-GM1 antibody titres corresponding to AMAN like flaccid paralysis (Yuki *et al* 2001). Furthermore, sensitising rabbits with *C.jejuni* LOS

resulted in generation of anti-GM1 antibodies and subsequent Wallerian-like nerve fibre degeneration and associated limb weakness was observed (Susuki *et al* 2003). This AMAN model proves the molecular mimicry hypothesis, and to date is the most successful experimental model on which to gain an insight into the human pathology of AMAN.

Thus, to date, GM1 has been identified as an autoantigen (Yuki *et al* 2001), its expression has been shown on human peripheral nerve (Ogawa-Goto *et al* 1990) and antibodies have been raised in experimental animals which go on to develop pathology similar to AMAN (Susuki *et al* 2003). However, while the rabbit model offers a valuable insight into the immunopathology of AMAN, there are several criticisms. For example, the authors describe the phenotype of the animals as severe, leaving animals unable to lift their head or body (Fig 10).

Fig 10. Modified from Yuki *et al* 2001. 14 days after disease onset the rabbit could not stand or raise its head. Forelimbs and extremities were weak.

One would assume that the majority of axons from these animals would have IgG deposition, with a significant proportion of these axons being damaged. However, peroxidase conjugated Protein G staining of the sectioned sciatic nerve showed few axons to have abundant IgG deposition, and overall the peroxidase staining appeared weak. Similar illustrations were presented in a later paper using the same immunisation protocol on a different batch of Japanese White rabbits (Fig 11).

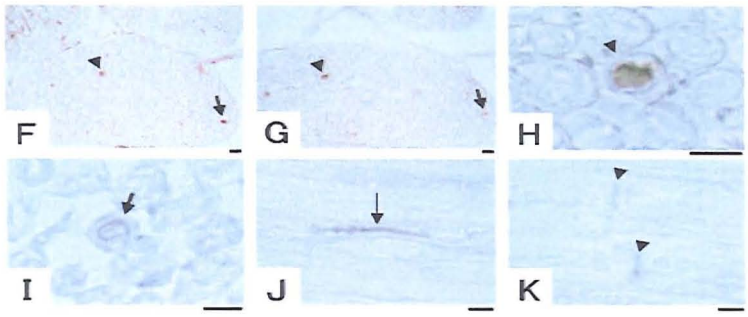

Fig 11. Modified from Susuki *et al* 2003 Peroxidase staining showing IgG deposits on axons of immunized rabbits. Arrows show areas of strong staining of axons and axonal membranes (panel j).

While the authors state that the rabbit model is a faithful model of human AMAN, they do not formally address the relationship between IgG deposition, complement activation and fibre damage (Hafer- Macko *et al* 1996). Demonstration of activated complement components along the injured axons would more conclusively prove the role of complement in mediating the lesion. Furthermore, the deposition of activated complement is likely to infer IgG deposition, so may be a more sensitive method (than Protein G staining) for detecting even low levels of IgG binding.

The authors demonstrate the presence of macrophages in the periaxonal space, where myelin is spared and the axon is damaged. However, there is no indication as to whether the macrophage activation occurs as a result of complement activation, where they are recruited to "mop up" the debris (Stuart and Ezekowitz 2005), or whether deposition of IgG opsonises the axon, and macrophages bearing the FC receptor (FcR) are recruited and induce cytotoxicity (van Sorge *et al* 2003) causing axonal damage. This alternative scenario would happen in the acute phase of the lesion. While it is commonly accepted that the acute lesion is largely complement mediated (Hafer- Macko *et al* 1996), it opens up an interesting question surrounding the role of macrophages. If the axon has been opsonised by IgG deposition, does macrophage infiltration via the FcR occur? It would also be interesting to investigate the

accumulation of other inflammatory cell types during the acute phase, such as chemokine responsive neutrophils (Graves and Jiang 1995).

Illustrations of the sciatic nerves from paralysed animals reveal axonal damage (Fig 12).

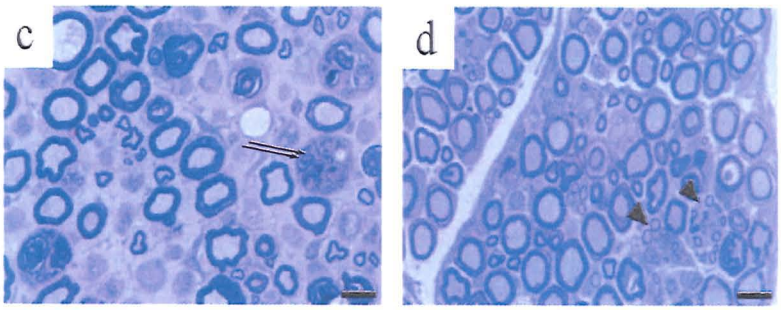

Fig 12. Modified from Yuki *et al* 2001. c) transverse sciatic nerve section from paralysed rabbit showing myelin ovoids (indicating myelin collapse, shown by double arrow) in the myelinated fibres. d) arrowheads show regenerating fibres in the transversely sectioned anterior root.

However, only a minority of axons appear to be damaged. This does not sufficiently explain why the rabbits displayed pronounced paralysis: severe cases of AMAN are associated with axonal transection, which was not demonstrated in the paralysed rabbits. However, re-examination of the rabbit sciatic nerve may reveal a "sampling issue": in other words, sampling more distal sites may have revealed a higher proportion of damaged axons, due to the retrograde process of Wallerian degeneration. Additional insight may have been gained from analysis of the intramuscular nerve bundles, where damaged axons may have been abundant. However, without this data, it is not possible to conclude that the muscle wasteage seen in these rabbits is due to axonal transection, as would be the case in severe human AMAN. It would therefore be useful to investigate other sites such as the node of Ranvier (eg. where complement mediated sodium channel destruction may occur (Susuki *et al* 2007)) and subsequentially block action potential conduction, or

at the NMJ, where interruption of synaptic transmission, such as that demonstrated in anti- GD1a antibody associated AMAN (Goodfellow *et al* 2005) may cause muscle fibre degeneration.

1.10.1 *Problems In Elucidating the Pathogenesis of AMAN*

So far, the contemporary model of AMAN does not fully elucidate the immunopathogenesis of the condition. For example, there are considerations relating to the interaction of antibody and epitope, and also the consequences of this interaction:

1) GM1 may be tightly regulated by complement regulator proteins in lipid rafts, so a potentially pathogenic anti-GM1 antibody may not cause a complement mediated lesion. However rafts are heterogenous (Pike 2006), and antibody interaction with GM1 located in a raft lacking complement regulators may lead to activation of the complement cascade and a subsequent lesion. Thus, an anti-GM1 antibody may be high affinity and able to bind GM1, but it's pathogenic potential is dictated by the constituents of the lipid raft in which GM1 lies.
2) Anti-ganglioside antibody causes neuropathy by binding to target (eg. axon/Schwann cell/glycosynapse) and disturbing ion flow, leading to conduction block (Buchwald *et al* 1998, Weber *et al* 2000).
3) Anti-ganglioside antibody binds to target, activates complement and MAC formation results in calpain mediated lysis of the target membrane (O'Hanlon *et al* 2003).

4) Anti-ganglioside antibody activates complement, and the chemotactic properties of complement trigger an inflammatory response (Stuart and Ezekowitz 2005), leading to nerve damage
5) Leukocytes activated by anti –ganglioside antibodies (via interaction of antibody and leukocyte immunoglobulin receptor (FcR)) mediate toxicity and phagocytosis (van Sorge *et al* 2003)
6) Antibody is raised against *C.jejuni* LOS which "mimics" GM1. The resultant antibody may not, however, bind to GM1. Instead, it may bind another epitope which, to the antibody, is "masquerading" as GM1. In other words, anti-ganglioside antibodies raised against *C.jejuni* LOS are misnomers. Instead, the "anti-oligosaccharide antibodies" are binding a non-GM1 epitope via "molecular masquarade".

Thus, development of murine models of AMAN, utilising a number of GM1 antibodies with varying affinities and specificities, would afford a robust system on which to fully assess the pathology induced by these antibodies, and perhaps resolve some of the main possibilities underlying the AMAN pathogenesis

Aside from the aforementioned effector functions of anti-GM1 antibodies, the specific interaction of anti-GM1 antibodies and GM1 is not straightforward.

AMAN patients' sera is unlikely to contain a homogenous population of anti-GM1 antibody. Instead, the overall anti-GM1 titre may comprise of clonally distinct antibodies with different specificities, although all reactive with GM1. This complication gives rise to several possible scenarios where antibody may react with:

*GM1 alone (Latov *et al* 1988, Pestronk 1991)

*the terminal Gal(β1-3)GalNAc of GM1, GD1b and asialo-GM1 (Pestronk 1991, Sadiq *et al* 1990)

*asialo-GM1 (Weng *et al* 1992) or GD1b alone (Fishman *et al* 1991)

*GM1 and GM2 via a common internal epitope (Ilyas *et al* 1988)

Furthermore, serum may comprise of different combinations of these antibodies, and the ability of any given population to mediate the disease process depends on the both the concentration and affinity of the antibody. To further complicate, while an anti-GM1 antibody may be of high affinity, its ability to induce pathology depends upon the antibody-antigen interaction. This is largely influenced by presentation of the antigen in the lipid bilayer (Marcus *et al* 1989, Ishii and Watanabe 1992), which determines the availability of the epitope to be "seen" and bound by the antibody. The latter issue is of particular relevance, as gangliosides are situated within lipid rafts, meaning the presentation of the ganglioside may be influenced by the constituent proteins of the raft, which may serve to mask the ganglioside or its antigenic region. Furthermore, it is possible that there are tissue specific variations in ganglioside containing rafts, rendering some tissue more susceptible to anti-ganglioside antibody mediated attack.

1.11 The Lipid Raft

Perhaps one of the most intriguing aspects of gangliosides, in particular GM1, is their association with cell surface microdomains known as rafts (Simons and Ikonen 1997). The recent characterisation of lipid rafts is relatively contemporary, however indications of their existence within physiological membranes have long been established. For example, anatomical studies in the 1950s describing cholesterol molecules forming complexes with phospholipids (Finean 1953) may have been one of the earliest indications that rafts exist. Despite this, in the 1970s the popular Singer-

Nicholson model was accepted as the bone fide description of the lipid bilayer; a model which points to a system whereby membrane molecules are randomly distributed and free to move within the membrane (Singer and Nicolson 1972). However, observations that upon phagocytosis, proteins can be selectively included or excluded from the internalised membrane (Oliver *et al* 1974) contradict the Singer-Nicolson model of random distribution, and provide evidence that proteins can segregate. Taken together with the complexes observed in the early 50s, this suggests the organisation of proteins and lipids in the membrane is of a complexity beyond that of the Singer-Nicolson model. Lipid rafts themselves now represent an increasing area of research, opening up the expanding science of "membranomics".

Lipid rafts can be viewed as small islands or platforms floating in a sea formed by the greater membrane. On the exoplasmic side of the bilayer, lipid rafts are composed of cholesterol and sphingolipids (Fridriksson *et al* 1999). Inner leaflet rafts also exist, however when comparing the composition of rafts to the non-raft areas of the plasma membrane, outer leaflet rafts are more compositionally different than inner, suggesting there is a more specific selection procedure for inclusion of species into outer leaflet rafts (Pike *et al* 2005). This finding may be related to the stability of the rafts, where cholesterol interacts via van der Waals forces, prefentially with sphingolipids (Boggs *et al* 1987), to induce a "liquid ordered state" of lipids (Ipsen *et al* 1987). The inner leaflet rafts are less stable (Niu and Litman 2002), a fact perhaps related to the depletion of sphingolipids in the inner leaflet, and a 6 fold enrichment of sphingloipids differentiating into the outer leaflet (Edidin 2003). This is suggestive that the interaction of cholesterol and phospholipids confers less stability on the raft when compared to the interaction of cholesterol and sphingolipids. The stabilising effects of cholesterol in the outer leaflet are perhaps counteracted to a degree by

presence of polyunsaturated species, allowing maintenance of the liquid ordered state (Blom *et al* 2001). Interestingly, transmembrane proteins can interact with both inner and outer leaflet rafts, and this may be of functional significance in colocalising signalling molecules from each leaflet (Pike *et al* 2005).

The liquid ordered phase induced by cholesterol (Ahmed *et al* 1997), is an intermediate phase between fluid liquid crystalline and gel phase (Brown and London 1998) and thus distinct from the more fluid, "liquid disordered" bulk membrane (Fig 13), which consists mainly of unsaturated fatty acids (Schroeder *et al* 1994). The "incomplete dissolution" of rafts following cholesterol depletion (Fujita *et al* 2007) suggests that cholesterol is not the sole mediator of raft stability. It has been suggested that the cellular cytoskeleton (Fujiwara *et al* 2002) and glycosphingolipids (Sheets *et al* 1997) contribute to the properties of rafts.

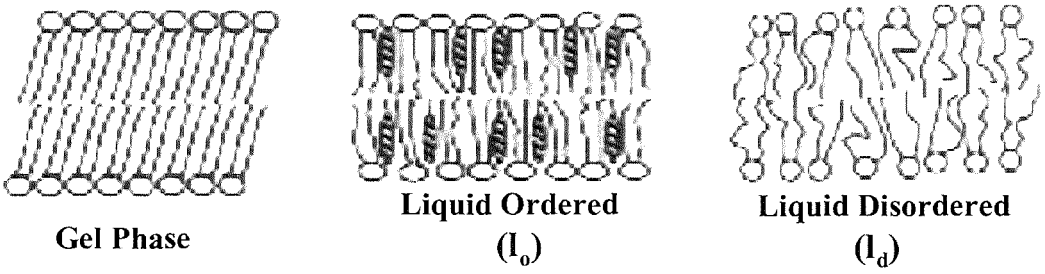

Fig 13. Modified from Munro 2003. The gel phase has tightly ordered acyl chains and is tightly packed (left diagram). This phase is not physiologically relevant owing to the low melting point of the gel phase: above the melting point of the gel phase, the molecules become liquid disordered (right diagram), which represents the nature of the bulk plasma membrane at physiological temperatures. In rafts, presence of cholesterol orders the acyl chains of the liquid disordered phase to create a liquid ordered phase, which is intermediate between the gel and liquid disordered phases (Munro 2003).

A schematic representation of their presence in the membrane is shown in Fig 14.

.

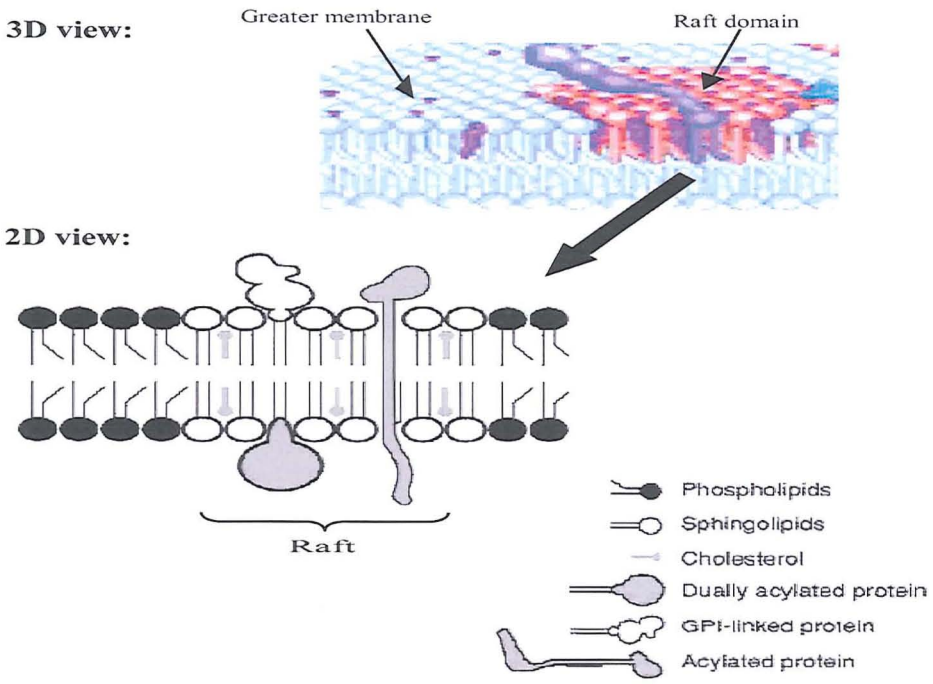

Fig 14. 3D representation (modified from Mayor and Rao 2004) of a portion of the membrane bilayer, showing the inclusion of a raft domain within the liquid disordered greater membrane. Inset image shows a 2D translation (modified from Dykstra *et al* 2003) of this, illustrating the presence and relative scaling of the constituent proteins, lipids and cholesterol in the raft domain.

To summarise, small domains of highly ordered molecules exist within the bilayer, and their stability is mediated by the influence of cholesterol. However, while this simple statement adequately defines a raft, it does not divulge the complexity of the different proteins and lipids in rafts, how they are targeted to rafts, nor the functional relevance of their presence.

Lipid rafts, much like islands, are heterogenous (Schade and Levine 2002, Drobnik *et al* 2002), with each comprising of different proteins and lipids. Furthermore, rafts comprise of a specific subset termed cavaeoli (a term which is often, and somewhat confusingly, interchanged with "raft"). While cavaeoli share many of the defining features of rafts (Rothberg *et al* 1990), they are defined by presence of the protein caveolin (Rothberg *et al* 1992), a protein which interacts strongly with cholesterol and polymerises to form the raft (Murata *et al* 1995). In the absence of caveolin, lipid

rafts can still be isolated, further confirming that lipid rafts and caveoli represent 2 independent subtypes (Parton and Simons 1995). GPI anchored proteins were amongst the first demonstrated to be raft associated (Brown and Rose 1992, Cinek and Horejsi 1992), and rafts can be viewed as cellular signalling stations due to their 10 fold enrichment in signalling molecules (Foster et al 2003). Signalling proteins such as acylated Src kinases (Song *et al* 1997), cytokine receptors (Resh *et al* 1999), growth factor receptors (Waugh *et al* 1999) and integrins (Baron *et al* 2003) are all enriched in rafts. Proteins involved in exocytosis, such as SNARE proteins, are also enriched in rafts (Chamberlain *et al* 2001), while gangliosides and cerebrosides form a significant proportion of raft lipids (Prietti *et al* 2000).

One of the most confounding issues surrounding the study of lipid rafts is their somewhat elusive nature. The role of rafts in signalling means it is logical for their formation to occur rapidly, perhaps in response to certain cues. This is of functional significance: the turning of growth cones in response to chemotactic cues is thought to be mediated by redistribution of chemotactic receptors into lipid rafts (Guirland *et al* 2004). This means rafts are believed to be transient structures, and it has been shown that GPI anchored proteins become transiently located within small "transient confinement zones", which rely on the glycosphingolipid content of the membrane (Sheets *et al* 1997). Based on such observations, it is accepted that rafts have an average lifespan of seconds (Dietrich *et al* 2002) (Fig 15).

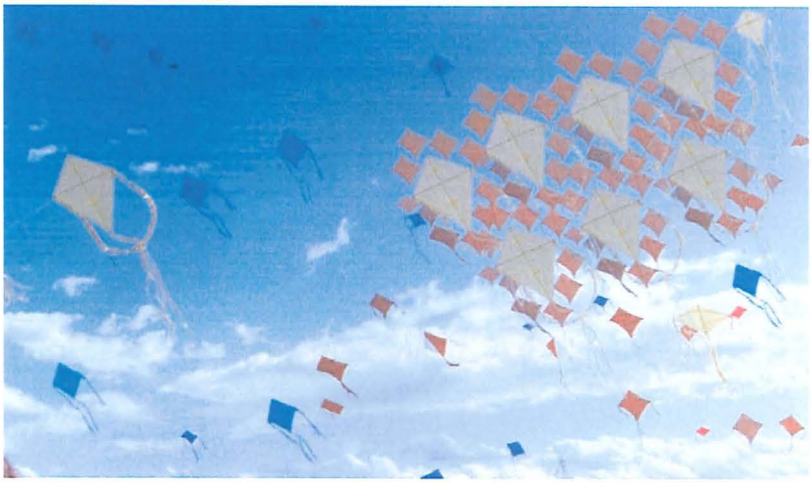

Fig 15. Small brown kites represent the transient rafts, which can coalesce upon certain cues and form a larger functional raft, to which proteins (large pale kites) can become targeted to. Modified from Mayor *et al* 2006.

On a similar note, the transient nature and small size of rafts makes them difficult to visualise, and therefore accurately measure. The use of sensitive techniques to study such micro-scale clusters predicts that rafts range between 30-200nm in diameter (Yuan and Johnston 2001).

The selection of specific species for inclusion into these nanoscale, transient domains indicates that there are criteria for inclusion into the raft. Fatty acylation is one such criterion for targeting lipids to rafts (Zacharias *et al* 2002). Unsaturated acyl chains have large cross sectional areas, and hinder the ability of lipids to pack into rafts, meaning the presence of a saturated acyl chains is a pre-requisite for packing lipids into the liquid ordered phase (Moffett *et al* 2000, Panasiewicz *et al* 2003). Transmembrane proteins such as hemaglutinin are also raft associated (Lin *et al* 1998), and it is believed that their 'packing requirements' depend on palmytolation (Melkonian *et al* 1999). On the contrary, the unpalmytolated protein neuraminidase is able to associate with rafts (Barman *et al* 2000) suggesting there are other possible interactions involved (Zhang *et al* 2000), perhaps related to the length of the transmembrane domain (Munro 1995). Aside from the complexities surrounding the

formation of lipid rafts, there is increasing evidence that they are recycled in a continual pathway from the cell membrane to the Golgi, and back to the cell membrane. Internalisation of raft proteins into recycling endosomes in a clathrin independent pathway has been demonstrated for the folate receptor (Nichols *et al* 2001) and the GPI anchored protein DAF (Sabharanjak *et al* 2000). However it is possible that the recycling of rafts also relies on an, as yet, uncharacterised pathway. For example, CD59 and transgenic GPI-GFP are present in 2 major pools: the plasma membrane and the Golgi complex, and a continual cycling of these proteins between the 2 locations was shown to rely on a clathrin independent endosomal pathway of untraced origin (Nichols *et al* 2001).

Clearly, our knowledge of lipid raft biology is continually expanding, and advances in the approaches used to study rafts have been fundamental in their study. The dynamics of rafts have been studied using techniques such as single particle tracking to follow the path of gold-tagged membrane proteins (Simson and Sheets 1995), combined electron and scanning force microscopy to determine the distribution of immunogold receptors (Damjanovich *et al* 1995) and trapping with laser optical tweezers (Edidin *et al* 1994). A more common method used in the study of rafts is fluorescence resonant energy transfer (FRET). FRET was first developed in the 1970s in the study of cell surface lectins (Fernandez *et al* 1976), and is used to determine the colocalisation of 2 species (for example, fluorescently tagged receptors) if their association is within approximately 60 angstroms (Å). FRET relies on the presence of 2 fluorophores (a "FRET pair"), one of which is termed a 'donor' and one an 'acceptor'. The donor is excited at its specific wavelength, and upon absorbing the energy, transfers it resonantly (i.e. without energy conversion) to the acceptor fluorophore. In turn, the subsequent increase in acceptor fluorescence can be

measured. There are several different methods of detecting FRET, and the specific technical understanding of each is beyond the scope of this introduction (for review see Sekar and Periasamy 2003 and references within). Overall, the technique of FRET has inherent failings, and failure to detect FRET between 2 molecules does not necessarily exclude the possibility that they are, or can become, raft associated. To illustrate this point, Damjanovich (Damjanovich *et al* 1995) failed to detect FRET when analysing the clustering of MHC molecules at the angstrom level. However use of transmission electron microscopy and scanning force microscopy revealed "macroclustering" of the receptor. Thus, failure to detect FRET should not lead to the assumption that a molecule is not raft associated: when one considers that rafts are dynamic and transient structures, the observation of such macroclusters is of importance. Upon receptor stimulation, the macroclusters may coalesce into more tightly packed raft domains to facilitate receptor clustering and signalling, in which case the molecules would become transiently confined to lipid rafts. In order to identify species with weaker affinities for rafts, membrane species can be cross-linked with antibodies leading to a stabilisation of the membrane which causes the "co-patching" of membrane species with similar lipid affinities, which contrasts to the remainder of the unpatched membrane species (ie. those with no raft affinity) (Harder *et al* 1998). On a more technical note, when binding fluorescent antibodies to antigens of interest, the presence or absence of FRET is influenced by the orientation of the fluorophore on the bound antibody, a problem not encountered when detecting FRET with fluorescing target proteins.

Biochemical techniques are also commonly used in the study of rafts, hence the common description of lipid rafts as "detergent resistant membranes" (DRMs). Lipid rafts are insoluble at 4°C in detergents (such as Triton X-100), and the detergent

insolubility of raft lipids and GPI anchored proteins may be as a result of saturated acyl chain interactions (Schroeder *at al* 1994). Furthermore, the DRM fraction is of light buoyant density and can be floated out on a sucrose gradient. Both the detergent insolubility at 4°C and light buoyant density are the hallmark of lipid rafts (Brown and Rose 1992). Much like FRET, the isolation of DRMs has failings. Cellular structures other than the membrane (eg. endosomes) also contain proteins and lipids which may have affinity for rafts, and during the preparation of the cellular DRMs, these may contribute. It is therefore accepted that the DRM does not represent the inherent membrane organisation, and presence of a species in a DRM is taken more as evidence of its affinity for rafts (Shogomori and Brown 2003). Furthermore, proteins may have a "weak but significant raft interaction which is not detectable by the DIG criterion" (Harder *et al* 1998), meaning they are not represented in the DRM (note that DIG stands for detergent-insoluble glycolipid-enriched fraction, another acronym for lipid raft).

In this brief overview, the main points and considerations of raft biology and how they are studied have been discussed, but to review such highly organised and complex structures in full detail would be outwith the scope of this introduction (for review see Allen *et al* 2007). However, one important aspect of raft biology which cannot be ignored is their possible involvement in pathological processes. The association of GBS associated auto-antibody targets (ie. gangliosides) with rafts is one such example.

1.11.1 *Gangliosides and Lipid Rafts.*

The association of gangliosides with lipid rafts confers stability to the lipid raft. The specific packing of gangliosides within the membrane relies on complex chemical and

structural interactions, and an in-depth review by Sonnino (Sonnino *et al* 2006) provides a detailed depiction of H-bonding at the lipid-water interface, geometry of individual hydrophilic headgroups (determined by the molecular structures of each ganglioside species) and as a result of these "physico-chemical" properties, how individual gangliosides have differential packing properties and contribute to the overall stabilisation of the lipid raft. GM1 is particularly enriched in cavaeoli (Parton 1994), and the overall curvature of the caveolar invagination depends on the number of sugars present in the head group of a ganglioside – the larger the headgroup, the more pronounced the curvature (Sonnino *et al* 2006) and Fig 16:

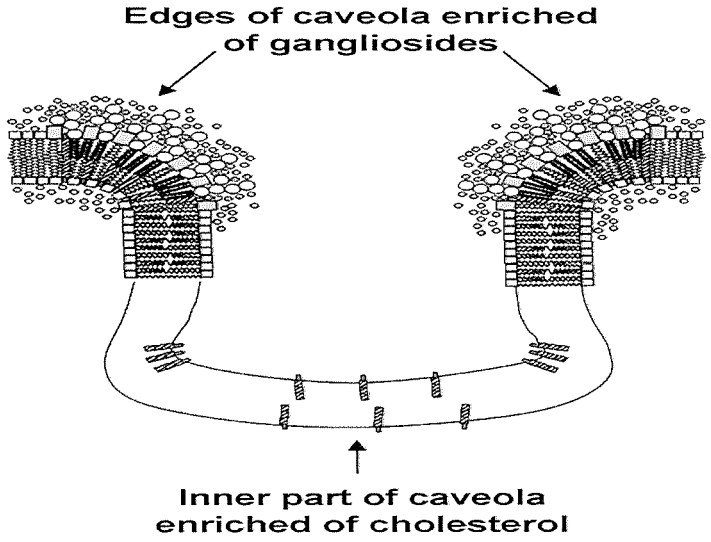

Fig 16. Exerted from Sonnino *et al* 2006. Ganglioside concentration at the caveolar edges, by nature of their space occupying head groups, lead to curvature of the membrane and an invagination.

The function of gangliosides in rafts extends beyond their role in structural maintenance. For example, GM1 is closely associated with the nerve growth factor (NGF) receptor TrK, and is believed to enhance the autophosphorylation of this receptor and thus enhance the response to NGF (Mutoh *et al* 1995). Increased expression of raft associated GM1 by human blood monocytes correlates with an

increase in their endocytotic ability, and also susceptibility to raft mediated pathogen invasion (Moreno-Altamirano *et al* 2007). While these are examples of endogenous gangliosides enhancing signalling functions, it is of interest to note that gangliosides can also disrupt such raft mediated signalling events. Gangliosides shed by tumour cells inhibit T cell activation (Lu and Sharom 1996), which is a raft mediated process relying on antibody induced cross linking of GPI anchored proteins (Lanzavecchia *et al* 1999). This suggests that the shed gangliosides are directly interfering with raft mediated signalling events. A possible route of this interference may be related to overall disruption of the raft, as addition of exogenous GM1 is capable of displacing GPI anchored proteins from rafts (Crespo *et al* 2002).

A further function of gangliosides and lipid rafts is endocytosis (Parton and Richards 2003). This is particularly relevant to the NMJ, which owing to its location outside the blood nerve barrier (BNB) allows any endocytosed substance to cross the BNB. In the motorneuron, CTb binds to GM1 and the GM1-CTb complex is internalised via a clathrin independent pathways (Roux *et al* 2005). Furthermore, tetanus toxin binding (TTx) relies on the presence of the gangliosides GT1b and GD1b (Kitamura *et al* 1999) and its uptake into motor neurons (MNs) is dependent on cholesterol and GPI anchored proteins (Herreros *et al* 2001) indicating it is raft mediated. Interestingly, however unlike the GM1-CTb complex, the TTx-ganglioside complex is not internalised: instead the toxin is shunted from GD1a in the raft and into clathrin coated pits, where it is internalised (Deinhardt *et al* 2005), providing novel evidence of an endocytotic pathway which relies on the synergy of raft-mediated and clathrin-mediated pathways. Rafts can perhaps therefore be regarded as another dimension of the BNB, owing to the functional role of gangliosides in allowing toxin binding and internalisation.

Although not strictly a "function" of gangliosides, they are important autoantibody targets in GBS. Recent advances in the specificity of GBS patients' sera for ganglioside complexes as opposed to individual species (Kaida *et al* 2004) strongly points towards the notion that this is a raft based phenomenon, where one can envisage the close approximation of 2 gangliosides within the raft. On a similar note, potentially diverse glycoclusters, such as the "glycosynapse" (reviewed by Hakomori 2004) may also exist: antibodies to ganglioside complexes ("glycoepitopes") may induce neuropathy by altering the function of the glycodomain (Kaida *et al* 2004). If such a mechanism does operate, it could yield valuable understanding into the pathogenesis of GBS. For example, it has been postulated that myelin-axonal communication is facilitated through a glycosynapse containing galactosylceramide (GalC) and its sulphated form galactosylceramide-I3-sulfate (SGC) (Boggs *et al* 2004). Disruption of such a glycosynapse could result in breakdown of the axon-myelin communication, and subsequent neurodegeneration. Thus, it is not unrealistic to assume that GBS associated gangliosides may exist in similar pathways:(eg. GM1 containing glycosynapses between paranodal myelin and axon) and associated neuropathy is a result of autoantibody mediated disruption.

1.12 Aims of Thesis

There is a wealth of clinical evidence to suggest a role for anti-GM1 antibodies peripheral nerve injury (Ilyas *et al* 1988, Nardelli *et al* 1988, Shy *et al* 1989, Nobile-Orazio *et al* 1990). This has been confirmed in the Japanese rabbit model already discussed (Yuki *et al* 2001), although the immunogenicity of this immunisation paradigm failed to induce EAN in earlier studies in the Lewis rat (Zielasek *et al* 1993), and neurological symptoms in New Zealand strain rabbits (Dasgupta *et al* 2004) are not apparent. On a similar note, the results of other studies have yielded

conflicting data, with some studies supporting a pathogenic role for anti-GM1 antibodies (Arasaki *et al* 1993, Takigawa *et al* 1995, Santoro *et al* 1992, Susuki *et al* 2003), and others concluding anti-GM1 antibodies have no effect (Harvey *et al* 1995, Takigawa *et al* 1995). Owing to the discrepancies in the understanding of anti-GM1 antibody mediated neuropathy, there is no unifying understanding of the pathogenesis induced by anti-GM1 antibodies.

This thesis generates the broad hypothesis that many of the lacunae which explain anti-GM1 mediated pathology are related to the association of gangliosides with lipid rafts (Simons and Ikonen 1997), where stereometric interactions with raft species may influence their presentation to circulating antibodies and directly influence the ability of these antibodies to induce pathology. Furthermore, the unveiling of ganglioside complexes within the membrane (Kaida *et al* 2004) supports the rationale that ganglioside species are able to *cis* interact, and the potential masking of epitopes from antibodies may underpin the apparent lack of pathogenicity of such antibodies.

In order to address the enigma of anti-GM1 antibodies and neuropathy, the aims of this thesis were to:

*Profile the distribution of GM1 in the peripheral nerve

*Identify and characterise a suitable murine model on which to base anti-GM1 studies

*Rationalise the presentation of the GM1 antigen in the membrane based on the ability of anti-GM1 antibodies with differing specificities to bind and cause a complement mediated lesion.

Materials and Methods:

2.1 Commonly Used Solutions

2.1.1 *Reagents, Abbreviations, Suppliers (and Stock Concentrations if required)*

*Texas Red labelled alpha-bungaratoxin (TRITC-BTx), (Molecular Probes, Leiden, The Netherlands) *(stock concentration 1mg/ml)*

*Citifluor antifade (Citifluor, Canterbury, UK)

*FITC-Goat anti-human C3 (Dako, Ely, UK)

*Mouse anti-human C5b-9 (Dako, Ely, UK)

*FITC and TRITC Goat anti-mouse secondary antibodies: IgG2a, IgG2b, IgG3, IgG, IgM. (Southern Biotech, Birmingham, USA) *(stock concentration 1mg/ml)*

*FITC and TRITC Goat anti-human secondary antibodies: IgM, IgG, (Southern Biotech, Birmingham, USA) *(stock concentration 1mg/ml)*

*Alexafluor-488 alpha-bungaratoxin (Alx-BTx) (Molecular Probes) *(stock concentration 1mg/ml)*

*Cholera-toxin B subunit –FITC (CTb-FITC), (Sigma, Poole, Dorset) *(stock concentration 1mg/ml)*

*Cholera-toxin B subunit-TRITC (CTb-TRITC), (List Biological Laboratories, Campbell, CA) *(stock concentration 1mg/ml)*

*Ethidium homodimer-1 (EthD-1), (Molecular Probes)

*Aminopropyltriethoxysilane (APES), (Sigma)

*Vectashield (with DAPI), (Vector Laboratories, Burlington, CA)

*Tissue-Tek, (Sakura Finetek, Torrance, USA)

2.1.2 *Recipies*

*Ringer (Stock X10 solution)

NaCl	67.79g	
KCl	3.35g	
$NaHCO_3$	19.32g	
NaH_2PO_4	1.19g	or ($NaH_2PO_4.2H_2O$ 1.56g)
Glucose	19.82g	
1M $MgCl_2$	10ml	

Make up to 1000ml with dH_2O.

Dilute 1 in 10 to use, bubble with O_2 and add 2ml 1M $CaCl_2$ per 1000ml

*PBS (Stock X10 xolution)

NaCl	80g
KH_2PO_4	2g
$Na_2HPO_4.12H_2O$	29g
KCl	2g

Make up to 1000ml with dH_2O.

Dilute 1 in 10 to use.

2.2 *Ex-Vivo* Muscle Nerve Preparations

2.2.1 *Triangularis Sterni (TS) Preparation*

The TS muscle is a thin sheet of muscle fibres (several fibres thick), which lines the interior surface of the ribs. The muscle is innervated in segments by the intercostal nerves, and has an abundance of easily visualised NMJs (McArdle *et al* 1981). Because of this, and the fact the muscle can be stained and imaged whole mount (ie. without sectioning), it is the ideal muscle for illustrative purposes.

2.2.1.1 *TS Dissection*

To expose the TS, mice were killed by a rising concentration of CO_2 in accordance with UK Home Office guidelines. Mice were pinned in the supine position, and the

skin reflected to reveal the upper thoracic region. The pectoral muscles and tissue overlying the ribcage was cleared, as was the diaphragm. Viscera within the thoracic cavity were carefully removed in order to avoid tearing the TS, and the ribcage removed. The ribcage was pinned pectoral side up, in a Sylgard (Dow Corning, Michigan, USA) lined Petri dish filled with Ringer. Using a dissecting microscope with transverse illumination, the TS muscles were exposed by cutting away the overlying layers of intercostals muscles. Ribs were carefully cut and peeled off, and any overlying tissue debris removed leaving the intact TS. The sternum was then cut up the midline to leave 2 TS preparations, each of which retained the support of the sternum. Each TS was pinned in a Sylgard lined staining chamber for staining or treatment. Staining chambers were prepared by lining a 12 well tissue culture plate (BD Biosciences) with Sylgard, and pinning muscles in individual wells.

2.2.1.2 *TS Staining Procedure (2 colour staining)*

Unlesioned Tissue: BTx + CTb *or* BTx + anti-ganglioside mAb

TRITC-BTx (2μg/ml) was applied with anti-ganglioside mAbs (100μg/ml) or CTb (2μg/ml) in Ringer for 2 hours at 32°C, followed by 30 minutes at 4°C. Tissue was rinsed 3X in Ringer and fixed for 20 minutes at RT in 4% PFA (Sigma). Tissue was rinsed 3X in PBS, and 0.1M glycine/PBS applied for 10 min at RT to quench endogenous aldehydes resulting from the fixation, and thus reduce non-specific background fluorescence. To detect anti-ganglioside mAbs, subtype specific FITC-conjugated secondary antibodies (3.3μg/ml) were applied overnight in PBS at 4°C. TS was rinsed 3X in PBS, unpinned and the muscle removed from the sternum and bordering tissue. TS was mounted in Citifluor on glass slides, coverslipped and sealed with nail polish.

Lesioned Tissue: BTx + C3 *or* BTx + MAC *or* BTx + IgG

To illustrate the pathogenic effects of anti-ganglioside mAbs, they were applied as described above (with TRITC-BTx), rinsed off 3X in Ringer and 40% NHS applied to the preparation for 1 hour at RT. Tissue was rinsed 3X in Ringer. To detect C3 deposition, FITC-goat anti-human C3 (50μg/ml) was applied for 1.5 hrs at 4°C before fixation and mounting as detailed above. For MAC detection, tissue was fixed, incubated in 0.1M glycine and mouse anti-human C5b-9 applied overnight at 4°C in PBS (363μg/ml), followed by 3X rinses in PBS and detection with FITC anti-mouse IgG2a (5μg/ml) overnight at 4°C. To detect anti-ganglioside mAb deposition, fixed tissue was incubated in the relevant FITC-anti-mouse secondary (5μg/ml) overnight, as already described.

Imaging

Dual colour images were acquired with a Zeiss LSM 5 Pascal microscope (Carl Zeiss, Hertforshire, UK), and 3D images generated from z-stacks using the softaware package Voxx2 (available from http://www.nephrology.iupui.edu/imaging/voxx).

Multi-Colour Staining (FITC, TRITC and Cy-5)

**BTx, CTb and either S100, Neurofilament (1217) or Synaptophysin*

Tissue was incubated in TRITC-BTx (2μg/ml) and CTb (2μg/ml) in Ringer for 1 hr at 32°C, rinsed 3X in Ringer, fixed for 15 min at RT in 4% PFA, rinsed 3X in PBS and incubated for 10 min in 0.1M glycine for 10 min at RT. S100 (22.5μg/ml, Dako, Ely, UK) or Synaptophysin (30.5μg/ml, Affinity BioReagents, Cambridge, UK) or 1217 (rabbit polyclonal, diluted 1 in 200, Affinity BioReagents, Cambridge, UK) were applied to fixed tissue overnight in 0.5% Triton in PBS at 4oC, rinsed 3X in PBS and detected overnight with Cy-5 conjugated anti-rabbit IgG (5μg/ml, Southern

Biotech, Birmingham, USA). Images were obtained using a BioRad MRC 1024 Confocal laser scanning microscope (BioRad, Hemel Hempsted, UK).

Further staining protocols for multi-colour images were developed upon introduction of the Zeiss Axio-Imager Z1 microscope (with Apotome optical sectioning). These methods do not apply to the results of this thesis, however represented a significant input into a study submitted for publication. Details and examples of optimised triple colour staining are outlined in Appendix 2. Images were reconstructed by generating a maximal intensity projection (MIP) using AxioVision Release 4.6 software.

2.2.2 *Hemi-Diaphragm Procedure*

Mice (5-10 weeks old, male) were killed by a rising concentration of CO_2 in accordance with UK Home Office guidelines. Mice were immediately pinned in the supine position and the skin reflected from thorax to pubis. A window was cut in the thorax to expose the heart and lungs, and each phrenic nerve cleared of connective tissue and carefully tied off (as near to the thyroid as possible) with fine thread. The liver was exposed by cutting the abdominal peritoneum to the xiphisternum, and the diaphragm freed from surrounding viscera by cutting through the ligamentum teres, aorta, vena cava and oesophagus while avoiding damage to the diaphragm. The muscle nerve preparation was removed by cutting the spine above the diaphragm and through the ribs at the back of the chest. The preparation, comprising the diaphragm, attached ribs and phrenic nerves was pinned carefully in a Sylgard lined petri dish to preserve muscle tension. Excess muscle tissue and membranes were cleared, and the diaphragm halved up the midline to leave left and right hemi-diaphragms with an intact nerve supply. The dorsal most portion of each was removed and immediately

snap frozen to give quantitative"baseline" measurements for IgG, NF, C3 and MAC. Remaining tissue was used for incubations. From each mouse, one hemi-diaphragm was incubated with mAb, while the other was incubated in Ringer under identical conditions to serve as a control.

Anti-ganglioside mAb was diluted in Ringer to a final concentration of 100μg/ml (unless otherwise stated). Normal human serum was diluted to 40% in Ringer, and each were dialysed overnight against Ringer at 4°C. Calculations allowed for at least 1.5ml of solution to be applied per hemi-diaphragm to ensure adequate coverage.

*Anti-ganglioside antibody (or Ringer) for 2hrs at 32°C, followed by 30min at 4°C and finally, 10min at ambient room temperature.

*Remove and retain antibody sample. Rinse tissue 3X in Ringer.

*Add 40% NHS for 1 hour at room temperature and observe tissue under dissecting microscope for muscle fibre fibrillations.

*Rinse 3X in Ringer

*Remove attached ribs to free diaphragm with phrenic nerve insertion and snap freeze.

2.2.2.1 *Hemi-Diaphragm Analysis*

Following the hemi-diaphragm preparations, tissue for immunohistochemical analysis was snap frozen and maintained at –70°C until cut onto slides.

Tissue was mounted onto Tissue-Tek and cut using a cryostat onto APES coated slides and left to air dry before being stored at –20 °C or processed immediately for IHC. Tissue was cut at 8μm, with every 5th section at 20μm.

8μm sections were processed for IgG/IgM , C3 and MAC staining. For each condition, 3 unstained slides were selected (encompassing sections from start, middle and end of the cut tissue series) and stained in one staining run with adequate positive and negative controls. NMJs were localized using TRITC-BTx, (1.3μg/ml). All reagents were diluted (if required) in PBS. Slides were mounted in Citifluor antifade and the coverslip sealed with nail varnish. All other reagents and dilutions were as follows:

C3

Sections were treated with TRITC -BTx and FITC-Goat anti-human C3 (33μg/ml) for at least 2 hours at 4°C. Slides were rinsed in PBS and mounted.

IgG/IgM

Sections were incubated in TRITC -BTx and FITC-Goat anti-mouse IgG2b/IgG3 (3.3μg/ml) at 4°C for a minimum of 3.5 hours. For human IgM detection, slides were incubated overnight in goat anti-human IgM (3.3μg/ml) and TRITC -BTx (1.3μg/ml) at 4°C. A positive control (if available) was included in the staining run. Slides were rinsed in PBS and mounted.

MAC

Mouse anti-human C5b-9 (363μg/ml) and TRITC -BTx was applied to slides for 2 hours at 4°C. Slides were then rinsed in PBS and FITC-goat anti-mouse IgG2a applied at 5μg/ml for 3.5 hours. For experiments where the anti-ganglioside mAb was IgM, MAC could also be detected using a pan-IgG secondary (FITC-goat anti-mouse IgG, 5μg/ml).

2.3 Enzymatic Treatments at the *Ex- vivo* NMJ

2.3.1 *Neuraminidase (N'ase) from Clostridium perfringens* (Sigma, Poole, UK)

(This enzyme cleaves terminal sialic acid residues from gangliosides; the sialic acid residue of GM1 is resistant to the enzyme).

For TS preparations, N'ase was used at 2 units/ml, diluted in Ringer, and tissue incubated for 1.5hrs at 32°C. In the hemi-diaphragm, N'ase was used at 5 units/ml under the same conditions.

2.3.2 *Phosphatidylinositol-specific Phospholipase-C (PI-PLC) from Bacillus cereus* (Sigma, Poole, UK)

(This enzyme removes GPI anchored proteins from the membrane).

PI-PLC was used at 3.5 units/ml (diluted in Ringer) for 1.5hrs at 32°C.

2.4.Topical Staining

2.4.1 *Tissue Harvest*

Mice (5-10 weeks old, male) were killed by a rising concentration of CO_2 in accordance with UK Home Office guidelines. Sciatic nerves or muscles (gastrocnemius, soleus, diaphragm, flexor digitorum brevis (FDB)) were dissected out, placed in Eppendorfs and snap- frozen on dry ice. Tissue was stored for up to 1 month at –70°C prior to use. Muscle tissue was mounted onto Tissue-Tek and cut at 8μm using a cryostat (Bright Instruments) onto APES coated slides. Nerves (except those for teased fibre preparations) were carefully placed in semi-frozen Tissue- Tek in the required orientation and frozen before cryo-sectioning at 15μm.

2.4.2 *Muscle Tissue Staining*:

2.4.2.1 *Immunoglobulin Binding Assay*

Optimal concentrations for primary mAbs were firstly determined by performing a dilution series, typically ranging from 5μg/ml and increasing to 50μg/ml. The optimal staining concentration represented the dilution giving immunoglobulin deposition over the endplate at a detectable level in wild type mice, but which was not overly saturating if applied to the relevant KO strains (eg. anti *a* series ganglioside mAbs in the *a* series ganglioside overexpressing GD3s$^{-/-}$). Primary mAbs were diluted to the required concentration in PBS along with TRITC -BTx (1.3μg/ml) and applied to the slides for 2.5 hours at 4°C. Negative controls were also included by incubating one slide per staining run in TxR-BTx and PBS alone. Slides were rinsed in cold PBS and secondary antibody (FITCconjugated) applied at 1.3μg/ml in PBS for 3.5hrs at 4°C. Slides were rinsed again and mounted in Citifluor.

2.4.2.2 *Complement Activation Assay*

Primary mAbs and TRITC-BTx were applied to the tissue as before, rinsed, and incubated at 32°C in 4% NHS (diluted in Ringer) for 1hr. Slides were rinsed and FITC-Goat anti-human C3 applied at 33μg/ml for at least 2 hours at 4°C. Slides were rinsed in PBS and mounted. Negative controls were included by either omitting addition of primary mAb or substituting 4% human serum for Ringer alone.

2.4.3 *Nerve Staining*

2.4.3.1 *Sectioned Nerve*

Nerves were removed, embedded immediately in semi-frozen Tissue- Tek and mounted onto a cryostat chuck for sectioning onto APES coated slides. Cryostat cut sections of nerve were immunostained using the same method as muscle tissue. BTx was not used and all mAbs were used 10μg/ml.

2.4.3.2 *Teased Fibres*

Sciatic nerves were removed and immediately placed into oxygenated Ringer. For teasing, they were cut into sections of 3-4mm and placed onto an APES coated slide with a small volume of PBS. Using 2 fine needles, nerves were desheathed by removing the epineurium and carefully teasing out the individual fibres with the needle, under a dissecting light microscope. Nerves were adhered to the slides by air drying for approximately 3 hours. Staining was performed by applying primary antibody diluted in PBS to a concentration of 15μg/ml, or CTb at 1μg/ml. After 1.5 hours at 4°C, slides were carefully rinsed by dipping into PBS, and if required secondary antibody (anti-mouse IgG FITC) applied at a dilution of 3.3μg/ml in PBS for 3 hours at 4°C. Nerves were mounted in Citifluor or Vectashield with DAPI, coverslipped and sealed with nail varnish.

2.5 Fluorescence Analysis at the NMJ

C3, MAC and Ig deposition were analysed by measuring the intensity of the signal overlying the TRITC-BTx area (i.e. the NMJ). In order to do this, the BTx image was thresholded to delineate the NMJ, and used to define a region of interest (ROI) which was applied to the FITC image. The mean intensity of the FITC signal within this ROI was measured. To analyse percent coverage of the NMJ (as done in the topical

mAb staining, and for all NF analysis) the TRITC and FITC channels were thresholded, and the area of the FITC signal expressed as a percentage of the TRITC-BTx area. Figure 17 shows a diagram outlining the procedure for measuring FITC intensity.

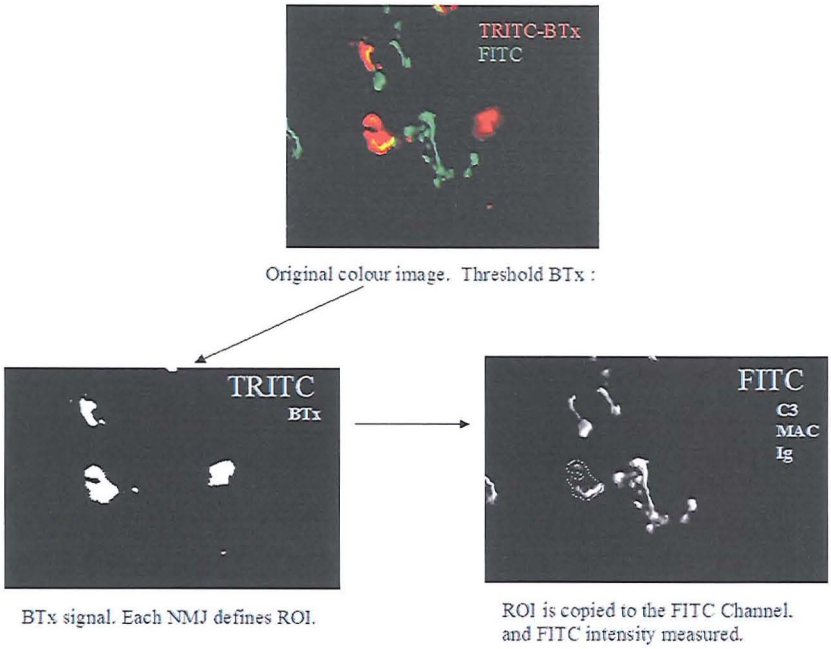

Fig 17. Example of the analysis procedure for measuring FITC fluorescence intensity (eg. of C3, Ig or MAC) over the NMJ, as delineated by TRITC-BTx. In the TRITC image (black and white), the white areas correspond to the BTx signal (ie. an NMJ). One NMJ is selected, and this ROI copied to the FITC channel where the mean intensity is measured within the ROI.

2.6 Antibody Culture

All tissue culture work was done in a sterile Class II hood using standard sterile practice. All incubations were done in a Class II incubator, at 32°C in 95%O_2, 5% CO_2.

Media were prepared several days prior to use, and an aliquot placed in the incubator to confirm sterility prior to use. If required, media were warmed to 32°C prior to use.

2.6.1 *Hybridoma Culture*

Media:

Growth media = Complete RPMI 1640 media with 20% FCS and 1% L-glutamine

Integra media = Complete RPPMI 1640 with 1% L-glutamine

Freezing media= 10% dimethyl sulfoxide (DMSO), 90% FCS

All media and supplements were purchased from Sigma (Poole, UK) unless otherwise stated. All culture flasks and sterile containers were purchased from BD Biosciences (Oxford, UK).

2.6.1.1 *Thawing of Cell Lines*

Hybridoma cell lines were placed in freezing media and stored in liquid nitrogen until required for mAb production. Upon removal from liquid nitrogen, cells were rapidly thawed and placed in Falcon T75 sterile flasks (with 35ml growth media). Flasks were incubated overnight, then contents removed into sterile 50ml tubes (Falcon) and spun at 1000RPM for 5 minutes in a Beckman GS-6R centrifuge to pellet the cells. The supernatant (containing DMSO from the freezing medium) was discarded, and the pellet resuspended in approximately 2ml of growth media and split between 2 new T175 flasks containing 35ml growth media each.

2.6.1.2 *mAb Production*

*Cell Cuture Flasks

Each hybridoma line displayed different optimal growth conditions, so flasks were monitored every 2-3 days to determine the optimal density at which they could be maintained and continue to produce antibody. Once this was established, cells were spun down as before, and supernatant retained at -20°C until purification. Samples of supernatant were regularly run on standard ganglioside enzyme linked

immunosorbent assay ((ELISA), section 2.7) to check the cells were continuing to produce antibody. The cells were returned to T175 flasks with fresh growth media and replaced in the incubator until ready to be split again. It had been observed that cells left to become highly confluent do not survive long, but tend to produce more antibody. Thus, several flasks were left to become over-confluent, before the supernatant was removed and the cells discarded.

*Integra (Integra Biosciences, Switzerland)

Integra Celline flasks (Fig 18) were found to be a convenient method of antibody production, giving a yield of antibody in excess of that easily achievable in culture flasks. Cells are grown in the cell compartment at up to $1x10^7$/ml, and the separation of the cell and nutrient compartments by a dialysis membrane allows the free exchange of nutrients but not secreted antibody. Secreted antibody is retained in the cell compartment, and service ports allow regular harvest of secreted product and media exchange.

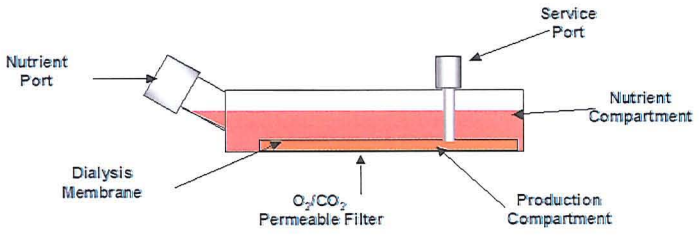

Fig 18. Schematic diagram of the Integra flasks used for hybridoma culture.

Prior to initiating a new Celline, 6 T175 flasks were maintained until approximately confluent, and spun down in individual Falcon tubes. Supernatant was retained, while pellets were resuspended in growth meduim to give a cell suspension of 5ml, ready for inoculation into Celline.

Intergra Celline flasks were set up as per manufacturer's instructions. Briefly, 15ml of growth medium was added to the cell compartment and 50ml of Integra media to the nutrient compartment and left for 5 minutes to equilibriate the system. 5ml of cell inocculum was then added to the cell compartment and the nutrient compartment topped up to a final volume of 1L.

Media was exchanged twice weekly (500ml per exchange) and antibody harvested once weekly by removing 7.5ml of cell suspension from the cell compartment and replacing with 7.5ml growth medium. Once monthly, cells were added to a T75 flask and cultured for 1 week to ensure no contamination

2.6.1.3 *Freezing Down*

A 175ml flask was maintained until cells were confluent, and cells spun down as before. Supernatant was retained, the pellet resuspended in freezing media, and 1ml aliquots of the single cell suspension placed into cryovials. Cryovials were then rapidly frozen overnight at –70°C before being placed in liquid nitrogen.

2.6.1.4 *Antibody Purification*

DG1 and MOG 35 (IgG 2b) cell culture supernatants were purified by protein G sepharose chromatography, on HiTrap Protein G affinity columns (Amersham Biosciences). DG2 and MOG 1 (IgG3 supernatants) were purified using HiTrap Protein A affinity columns (Amersham Biosciences). On application to the column, the antibodies bind to the protein and the flow-through material, containing the impurities, can be discarded. The bound antibody is then eluted in acidic solution (pH 2-3). Tissue culture supernatants were defrosted at RT and centrifuged (Sorval RC5C) at 10000 RPM for 30 minutes, 4°C. Prior to application to the Protein G or

Protein A column, supernatants were adjusted to the composition of the binding buffer (0.1M Phosphate Buffer: 0.2M $NaH_2PO_42H_2O$ and 0.2M $Na2HPO_4$, pH 7.4) by overnight dialysis against binding buffer at 4°C (binding buffer volume was at least 10X that of supernatant volume). The supernatant was then filtered using a 0.45μm membrane bottle top filter (Nalgene Nunc, New York) and stored on ice for the duration of the purification. All solutions for application to the column were filtered using a 0.45μm single use syringe top filter unit (Sartorious Minisart, Germany). The column was firstly equilibriated to pH 7.4 by application of 10 column volumes of binding buffer. Flow speed was noted by calculating time taken to collect 10 column volumes, thus allowing the peristaltic pump to be set at a rate of no more than 1 column volume per minute. Supernatant was then run through the column, and flow-through retained. Once the sample was loaded onto the column, it was washed with at least 10 column volumes of binding buffer, and 10 fractions collected until the absorbance at 280nm (A_{280nm}) was < 0.03 with a binding buffer blank. 10 column volumes of filtered elution buffer (0.1M Glycine- HCl, pH2.7 for Protein G columns, or 0.1M Citric acid, pH 3 for Protein A columns) were loaded and 10 fractions collected into bijoux bottles containing the required volume of neutralizing buffer (Tris-HCl, pH 9). A280nm were recorded per fraction to ensure IgG peaked on the early elute fractions and late fractions contained <0.05 with a blank of neutralised elution buffer. The column was washed with 10 volumes of binding buffer followed by 5 column volumes of 20% ethanol prior to storage at 4°C.

A standard "plus minus" ganglioside ELISA (section 2.7) was performed using samples of pre-purified supernatant, the wash fractions, elution fractions and the flow through. Anti-ganglioside antibody activity in the flow through indicates the column may have become saturated and not all IgG was able to bind. Similarly, IgG in the

wash fractions indicates unbound antibody had been removed along with impurities from the tissue culture growth supernatant. High A280nm values for the elution fractions should correlate with high OD490nm from the ganglioside ELISA, thus confirming the protein contained in the sample is functional antibody (Figure 19)

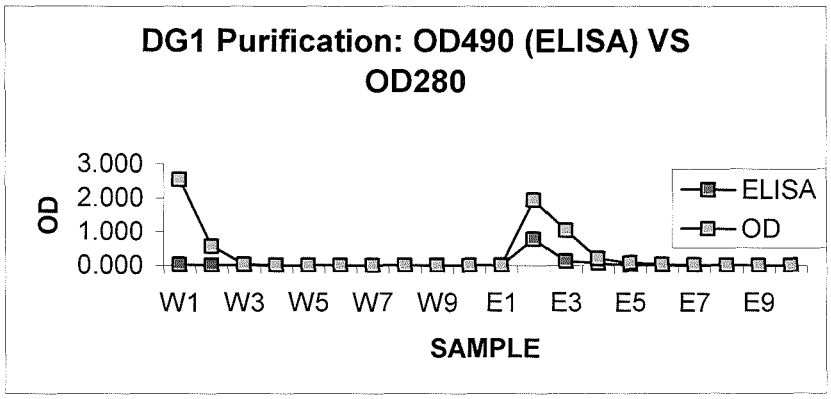

Fig 19. Comparison of A280nm (spectrophotometer) and OD490nm (ELISA) readings for Wash (W) and Elution (E) fractions. High A280nm readings in the Wash fractions 1 and 2 do not give similar ELISA readings, indicating the protein present in these fractions is FCS impurities as opposed to antibody. The high A280nm readings of the Elution fractions correlates with the ELISA data, indicating functional antibody has been eluted.

Fractions containing purified antibody were pooled and the A280nm recorded. The final sample was then desalted using PD10 desalting columns (Amersham Biosciences) following manufacturers instructions. The A280nm of the final sample recorded (against a blank of PBS) to ensure no IgG had been retained in the PD10 column, and to give a final concentration of the sample in mg/ml (A280nm/1.43). Purified antibody was aliquoted and stored at –70°C.

2.7 ELISA ("plus minus")

Immulon 2 microtiter plates (Dynatech, Chantilly, Va.) were designated alternate positive and minus rows. Positive wells were coated with 200ng of ganglioside

(Sigma) per well, in methanol, while minus rows received 100µl of 100% methanol to control for background optical density readings. Plates were left to dry by evaporation overnight, and stored at 4°C for at least 1 hour before use. Wells were then blocked with 200µl of 2% BSA solution (Sigma) diluted in PBS. After at least 1 hour at 4°C, the block was discarded by flicking the plate and patting dry on tissue. 100µl of sample was added to respective positive and minus wells and serially diluted across the plate in 0.1% BSA solution. Incubations were left for a minimum of 4 hours at 4°C, and after discarding the sample, wells were washed 5 times in cold PBS and the plate patted dry. 100µl of horseradish-peroxidase (HRP) conjugated secondary antibody (Sigma) was added per well: secondary antibodies were diluted in 0.1% BSA (0.25µg/ml for rabbit-anti mouse IgG, 0.76µg/ml for rabbit-anti human IgM) and incubated for a minimum of 1 hour at RT. The plate was then washed 3X in cold PBS and developed by adding 100µl of substrate solution (30ml dH_20, 16ml 0.2M Na_2HPO_4, 14ml 0.1M $C_6H_8O_7$, 1 OPD tablet and 20µl H_2O_2) per well for 20 minutes in the dark (prior to addition of substrate solution, a drop was added to any remaining, unused secondary antibody solution to confirm colour change). The reaction was halted using 50µl per well of 4M H_2SO_4 and optical densities read at 490nm (OD 490nm) using an automated plate reader.

2.8 PC12 Cell Culture

2.8.1 *Preparation of Flasks and Coverslips*

All solutions were added to flasks in the following volumes:

T25 = 1.25ml

T75 = 5ml

T175= 30ml

PBS and dH_20 were autoclaved and stored at 4°C to ensure sterility.

Poly-L-Lysine (PLL, Sigma, Poole UK) coated flasks were prepared by addition of PLL diluted to a concentration of 13.3µg/ml in dH_2O to tissue culture flasks. PLL was left in flasks with loosened lids for 10 minutes, and discarded before rinsing flasks in PBS. Excess PBS was pipetted out and flasks incubated overnight at 37°C and stored at RT for up to 2 weeks. Sterile Petri dishes (5mm diameter) were also coated, using the same method for flasks. Cells were grown overnight in dishes prior to treatments followed by FACS analysis (Section 2.8.6).

To coat coverslips, PLL solution was prepared as before and 20ml placed in a Petri dish. To this, autoclaved 13mm coverslips were added and left overnight at 37°C. Curved forceps were then used to remove coverslips to a 24 well tissue culture plate (1 per well). Excess PLL was removed by tipping the plate and pipetting off excess and allowing the plate to air dry for 10 minutes before a final overnight incubation at 37°C.

2.8.2 Cell Maintenance

Cells' doubling times were approximately 4 days (Walton *et al* 1988), upon which cells were split and subcultured at a third of the initial density. To split the cells, growth media (DMEM (Invitrogen, Paisley, UK) plus 7.5.% FCS and 7.5% Horse Serum (HS), (both Sigma)) was discarded from the flasks and residual media removed by rinsing the cells once in PBS and discarding. PBS containing 0.25% of Trypsin (bovine pancreas, Sigma) was added to the flasks and incubated for 2 minutes at 37°C. The cell suspension was transferred to 50ml Falcon tubes and an equal volume of media added to neutralise trypsin activity. Cells were centrifuged at 1000rpm for 5

minutes, and the media discarded. The pellet was dissociated by gently flicking the Falcon, and resuspended in 3ml of fresh growth media. 1ml was then added to a fresh flask containing 30ml of growth media.

2.8.3 *Seeding Coverslips*

Cells were split as described, and the pellet resuspended in 2ml of media. Cell density was determined using a hemocytometer. Taking into account the number of coverslips to be coated (500µl cell suspension/well), cells were diluted in media to an average density of $3x10^4$/ml. Following addition of 500µl to each well, plates were incubated overnight at 37°C prior to coverslip removal and staining.

2.8.4 *Cell Staining*

Coverslips were removed from wells using curved forceps, and rinsed twice in PBS and blotted on tissue before being placed in staining trays, cell covered surface facing upwards. Primary antibody was diluted in PBS (to a final concentration of 12.5 µg/ml) and 100µl added to each coverslip. Staining trays were incubated at RT for 30 minutes, before coverslips were rinsed 3X in PBS and incubated in darkness with secondary antibody (anti-mouse IgG) at 3.3µg/ml for 45 minutes, at RT. Coverslips were rinsed 3X in PBS and fixed by application of 100µl of 4%PFA for 15 min at RT. Coverslips were finally rinsed 3X in PBS, blotted and placed face down in Vectashield-DAPI and sealed with nail varnish.

2.8.4.1 *Live/Dead Staining*

The "Live/Dead Assay" (Molecular Probes Inc, Leiden, The Netherlands) containing Calcein Green and EthD-1 was used. A mixture of Calcein green (2µM/ml) and EthD-1 (2µM/ml) diluted in PBS, was applied to cells for 30min (37°C). After

staining, coverslips were rinsed 3X in PBS, mounted (unfixed) in PBS and imaged immediately.

2.8.5 *Cell Treatments*

For immunofluorescence studies of treated cells using a microscope, cells were seeded onto coverslips as already described. For analysis of staining intensities using flow cytometry, cells were plated in 5ml PLL coated Petri dishes 24 hours prior to enzymatic treatment.

2.8.5.1 *Neuraminidase (N'ase)*

Cells were rinsed in PBS 3X. N'ase was used at 2 units/ml in serum free DMEM). Coverslips were incubated in this solution for 1 hour at 37°C, and Petri dishes for 1.5hrs at 37°C, then rinsed 3X in PBS.

2.8.5.2 *Phosphatidylinositol-Specific Phospholipase C (PI-PLC)*

Cells were rinsed 3X in PBS. PI-PLC was used at 2 units/ml diluted in PBS. Cells were incubated for 1 hr at 37°C.

2.8.5.3 *Exogenous Addition of Gangliosides*

GT1a, GD1b or GD1a were added to the cells at 20μg/ml. 100μl of ganglioside was removed from the stock solutions, at 1mg/ml (Sigma), and dried under a stream of nitrogen. 500μl dH_2O was added to the dried gangliosides, and sonicated for 30min. As a "placebo", 500μl of dH_2O containing no ganglioside was treated under the same protocol. Solutions were warmed to 37°C (Facci *et al* 1984) for 1 hour and added to 4500μl of warmed SFM and vortexed. Rinsed and pelleted PC12 cells were

resuspended in the solutions and incubated overnight at 37°C in PLL coated Petri dishes.

2.8.5.4 *Methyl-β-Cyclodextrin (MβCx)*

Cells were trypsinised, pelleted and resuspended in 50ml of serum free media (SFM) containing 50mM MβCx, for 45 minutes at 37°C. Cells were rinsed by pelleting and resuspending in PBS. Cholesterol depletion was confirmed by expressing cholesterol content of treated and untreated cells as a ratio of cholesterol:protein, using the method as described below.

2.8.5.4.1 *Cholesterol Assay*

Pelleted cells (control and MβCx treated) were freeze/thawed by storing at –80°C for 20 min to lyse. Pellet was resuspended in 200µl of 0.1M potassium phosphate buffer (0.2M KH_2PO_4, 0.2M K_2HPO_4) containing protease inhibitors (PI) (Roche Applied Biosciences) and sonicated on ice for 10 sec with a probe sonicator. 10µl of the sample was removed to fresh Eppendorfs (in duplicate) and stored on ice, while the remainder was discarded. Cholesterol standards (Alpha Laboratories, Hampshire, UK) of 1, 2, 5 and 10µg/ml were prepared in phospahate buffer (including PI as before), along with a blank containing only phosphate buffer and PI. To all samples, 2µl of 1% Triton X-100/20mM sodium cholate (in Phosphate buffer), 2.5µl of 95% EtOH and 1ml Infinity Reagent (Alpha Laboratories) was added and incubated for 20 min at 37°C. Samples were spun at 12000rpm to pellet any debris which may interfere with optical density readings, the supernatants transferred to cuvettes and read at 500nm after blanking the BioPhotometer (Eppendorf) with the phosphate buffer only sample.

2.8.5.4.2 *Protein Assay*

Protein estimation was done using the BCA Protein Reagent Assay (Pierce Chemical Co., Rockford, IL), following manufacturer's instructions. Standard curves were generated using Albumin standard controls (supplied with the kit). Assay was performed in a 96 well ELISA plate, and read at 562nm.

2.8.6 *PC12 FACS Analysis*

Adherent cells were rinsed 3X in serum free media (SFM) and trypsinised. For cells grown in PLL coated Petri dishes, remaining adherent cells were dislodged using a cell scraper (BD Biosciences). Cells were then added to 50ml Falcon tubes containing 5ml of FACS buffer (2% FCS in PBS) to neutralise the trypsin, and spun at 1500rpm for 5 minutes at RT, to pellet the cells. Media was discarded and the cell pellet resuspended in 1ml of FACS buffer. Cells were counted using a hemocytometer. Based on the number of sample tubes to be analysed, cells were diluted in FACS buffer to allow for $1x10^5$ cells/100µl to be added per tube. Cells were initially placed in 1.5ml Eppendorf tubes for staining and rinsing steps before final transfer to FACS tubes. 100µl of primary antibody, anti-ganglioside mAbs at 10µg/ml or Thy-1 at 7.752µg/ml (CD90, AbCam, Cambridge, UK) diluted in FACS buffer, was then added per tube, triturated using a pipette and incubated on ice for 30 mins. CTb-FITC was incubated at 1µg/ml for 1 hr, omitting the secondary detection step below. During all incubations, tubes were frequently agitated to ensure cells remained suspended in antibody solution. To rinse cells, 1ml of FACS buffer was added per tube, mixed with a pipette and tubes spun at 1500rpm for 5 min (RT). Supernatant was carefully pipetted off, and 100µl of secondary antibody (anti-mouse IgG at

3.3μg/ml, diluted in FACS buffer) added to each tube and triturated. The samples were incubated in darkness for 30 min on ice, and rinsed as before. The pellet was finally resuspended in 600μl of FACS buffer, transferred to FACS tubes and analysed using a FACScan flow cytometer (Becton Dickinson, USA). FACS settings remained constant for each experimental repeat.

2.8.7 *Purification of DRMs from PC12*

PC12 cells were washed and pelleted in an Eppendorf tube by spinning at 1500rpm for 5 minutes. Approximately 10 million cells per preparation was used. Cells were resuspended in 475μl MES (2-(N-morpholino)ethanesulphonic acid) buffered saline (MBS) (25mM MES, 150mM NaCl, pH6.5) plus protease inhibitors (Roche Applied Science) and cells retained on ice for all subsequent steps. 25μl of 10% detergent (Triton X-100 (Sigma) or Brij-96 (Sigma)) in MBS was added to the cells to give a final concentration of 0.5% detergent, and following a 20 min incubation (on ice, and in the cold room at 4°C) the solution was homogenised with 10 strokes of a Dounce homogeniser. 0.4ml of lysate was mixed with 80% sucrose (in MBS) in a centrifuge tube (BD Biosciences) and bubbles removed from the surface. This was overlaid successively with 2.2ml of 30% sucrose and approximately 1.4ml of 5% sucrose. Tubes were spun for 18-24hrs at 50,000rpm (Beckman SW60 rotor). 390μl fractions from the top of the gradient (designated fraction 1), through to bottom, designated fraction 12 were collected. If a pellet formed at bottom of tube, it was resuspended in 1ml MBS and collected as fraction 12. Figure 20 shows a schematic diagram of the procedure. Following collection of fractions from the gradients, fractions (in labelled Eppendorfs) were stored at –20°C or if used in magnetic bead separation experiments, stored on ice and used immediately.

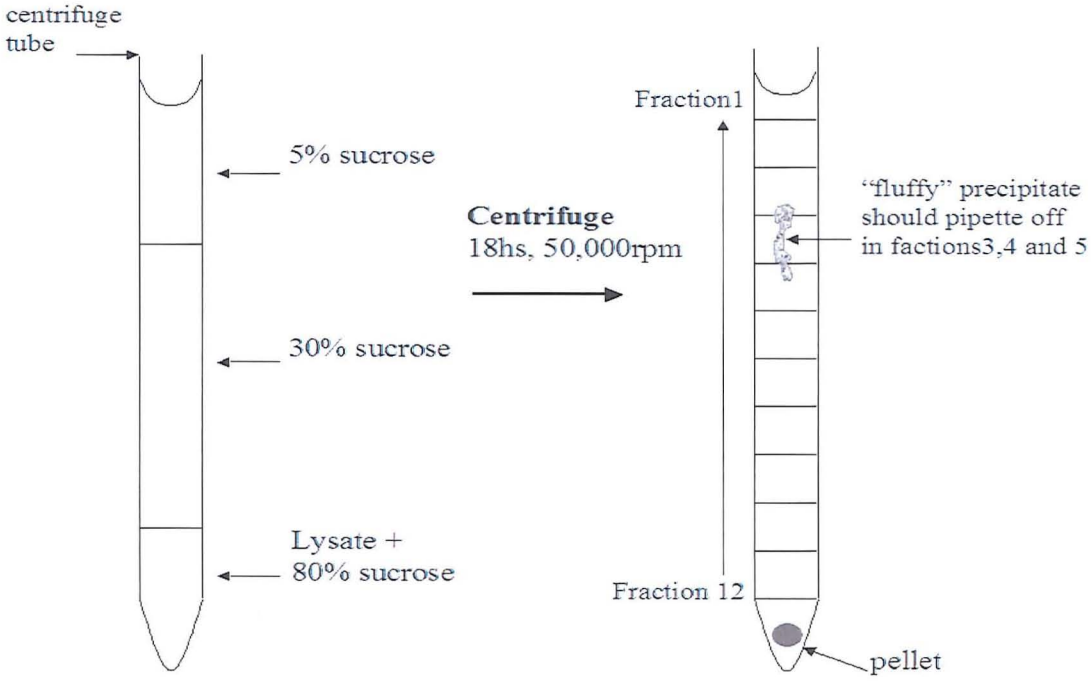

Fig 20: pictorial representation of the sucrose gradient profile and fraction collection.

2.8.7.1 *Magnetic Bead Separation*

*Indirect Isolation

A confluent T175 was trypsinised and cells resuspended in PBS. Cells were stained in suspension in Eppendorfs, in either MOG 35 or EG1 at 15µg/ml diluted in PBS. Cells were triturated with a pipette every 15 min to avoid settling out of suspension and were rinsed by pelleting and resuspending in PBS 3X.

Raft preparations were set up as above, using the detergent Brij-96. 12 fractions were collected, and an equal aliquot of fractions 3, 4 and 5 retained to be electrophoresed alongside the non-raft fractions. The remaining fractions 3-5 were pooled and stored on ice while anti-mouse IgG coated Dynabeads (Invitrogen) were prepared. 300µl of both the EG1 and MOG 35 incubated cells was removed and retained in a separate

tube (on ice) and designated "starting material", and 300µl used for Dynabead incubation.

Dynabeads were inverted resuspended in the storage container, and 100µl removed into an Eppendorf. To this, 1ml of PBS was added and the tube placed against a magnet while the PBS was removed and discarded. 1ml of fresh PBS was added, and the tube removed from the magnet to redistribute the beads. A total of 5 rinses were performed in this manner. After the final rinse, the beads were resuspended in 100µl of PBS and divided into 2 Eppendorfs (50µl each) to be used for either the EG1 or MOG 35 incubated cells. The PBS was removed as before and the 300µl raft samples added to the Eppendorfs and gently inverted. Eppendorfs were placed on a tilting/rotating mixer at 4°C for 30 min. Tubes were then placed against a magnet and unbound fraction retained and stored on ice. Beads were then rinsed 4X in PBS (as before) to remove any non-specifically bound proteins/lipids. Novex loading buffer (Invitrogen) was added to the rinsed beads, and the samples boiled for 1 minute to release the bound rafts fractions in preparation for gel loading. "Starting material", "unbound" and fractions 1-12 were mixed with reducing loading buffer and boiled in the same way.

*Direct Isolation

Raft fractions were prepared from untreated PC12 cells, and fractions 1-12 removed. Before fractions 3-5 were pooled, aliquots were removed. Remaining fractions 3-5 were then pooled, and 300µl dedicated to the control incubated beads, and 300µl dedicated to the MOG 35 incubated beads. A sample of starting material was also retained. Beads were aliquoted and rinsed as before, then resuspended in either MOG 35 or control antibody (EG1 or mouse-IgG (Sigma)) at 50µg/ml for 1hr on a tilting/rotating mixer at 4°C. Beads were rinsed 5X in PBS, and the raft sample added

for 30min at 4°C on a tilting/rotating mixer. The unbound sample was removed, and beads rinsed in PBS 5X, and samples prepared as before.

2.8.7.2 *Western Blotting*

Prior to electrophoresis, all samples were reduced by addition of 25mM dithiothreitol (DTT, Amersham). 10µl of sample was loaded with a Hamilton syringe onto Novex 16% Tricene gels (1.0mm well, (Invitrogen)) and gels run at 125V for 1hr 45 min. Gels were blotted overnight in a transfer cell according to manufacturer's instructions (Bio-Rad, Hemel Hempstead UK) onto nitrocellulose membranes (Whatman, Schleicher & Schuell, Dassel, Germany). Membranes were washed briefly in PBS-T (0.02% Tween-20 (Sigma) in PBS) and incubated in 5% non-fat Marvel (Premier International Foods, Lincs, UK) in PBS-T for 45 minutes at RT on a rocking platform, then drained off. Primary antibody (anti-ganglioside mAb at 20µg/ml, Horseradish Peroxidase conjucated CTb (HRP-CTb, Invitrogen) at 0.1µg/ml). Raft protein markers: anti-Transferrin receptor (Invitrogen), anti-Flotillin (BD Biosciences), anti-SNAP 25 (provided by Dr L. Chamberlain, (Chamberlain *et al* 2001)) all at 10µg/ml were added in PBS-T for 1 hour at RT on the rocker, then drained off and membranes washed 5X in PBS-T over 30 min. With the exception of membranes incubated in HRP-CTb, membranes were incubated in secondary-HRP conjugated anti-mouse IgG antibody (0.38µg/ml, Sigma) in 1% Marvel/PBS-T for 45 min at RT on rocker, drained and washed as before. Membranes then developed using ECL (Amersham Buckinghamshire, UK), according to manufacturer's instructions. Membranes were exposed to film (Kodak, Rochester, NY, USA) under red light and developed using an X Omat (Kodak) processor.

2.9 Statistical Analysis

One-way analysis of variance (1-way ANOVA) was used to determine statistical significance, with a p value of <0.05 considered significant. Where graphs are displayed as "box and whisker plots", 1-way ANOVA was not appropriate, owing to non-parametric data. Therefore, significance was determined using the non-parametric Mann-Whitney mean ranks test, and again, a p value of <0.05 was considered significant. The "box and whisker plots" are not interpreted as standard bar graphs. The horizontal line shows the median. The data in the box below the median represents one quarter of the data which lies below the median, while the upper box represents one quarter of the data which lies above the median. This forms the interquartile range. The "whiskers" on either side show the quarter of the data which lies above the interquartile range, and the quarter of the data which lies below the interquartile range. Outliers have not been shown on the plots, but were included in the Mann-Whitney statistical test.

Chapter 3

3.1 Introduction

The overall aim of this chapter was to focus on the mouse NMJ and systematically analyse the expression levels and distribution of GM1. The hypothesis is that the GD3s$^{-/-}$ mouse, which has increased levels of GM1, will represent the ideal model on which to base both *in-vivo* and *ex-vivo* injury paradigms using anti-GM1 antibodies. However, use of this genetically modified strain is beneficial only if there is a significant enhancement in GM1 levels when compared to the wild type mouse. Furthermore, while the levels of GM1 may be increased, confirmation is needed that an existing panel of anti-GM1 antibodies is able to bind to the upregulated GM1 and cause a subsequent complement mediated lesion, as already demonstrated for an anti-GD1a antibody (Goodfellow *et al* 2005). It is also important to consider the profile of GM1 expression: increased levels of expression in the GD3s$^{-/-}$ mouse should optimise the model by increasing the pre-existing antigenic target, but ectopic expression of GM1 in this mouse would represent a contraindication to its use, as the subsequent pathology induced by anti-GM1 antibodies may not be physiologically relevant. The profile of GM1 expression was examined at the NMJ with specific reference to the pre-synaptic axon, pSC and PJF (as described in Sections 1.9.1.5 - 1.9.1.7 of Chapter 1).

3.2 Results

3.2.1 Topical CTb staining of WT and GD3s$^{-/-}$ diaphragm

Diaphragm muscle sections from the GD3s$^{-/-}$ and WT mouse were directly compared in a topical staining assay using CTb. CTb is specific for GM1, and the increased expression of GM1 by the GD3s$^{-/-}$ should result in an obvious increase in CTb

binding.

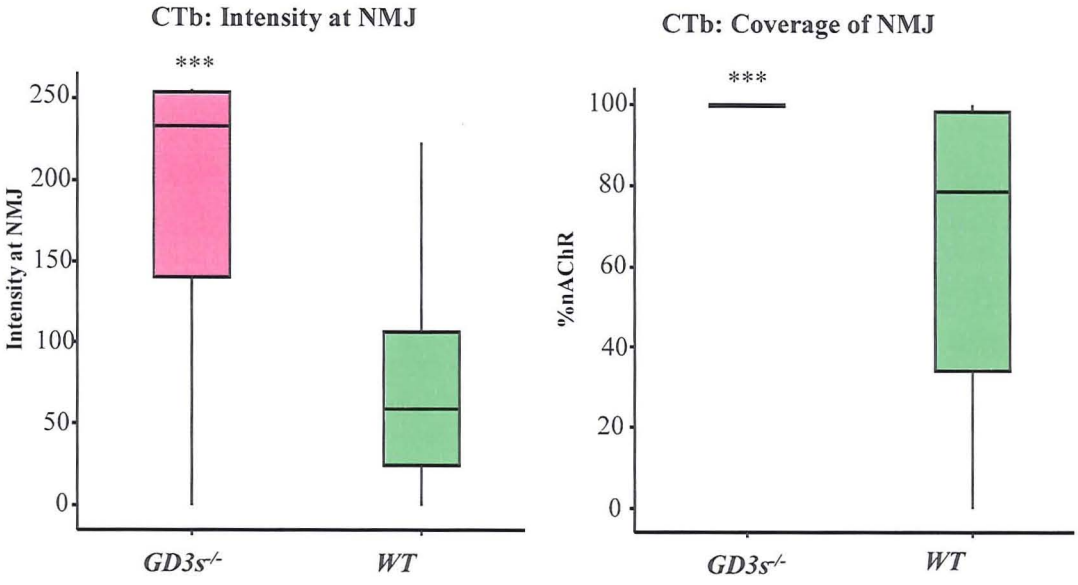

Fig 21. Topical staining of WT and GD3s$^{-/-}$ tissue with CTb. Astrices indicate significant difference when compared to WT tissue ($p<0.05$).

As shown in Fig 21, the intensity of CTb in the GD3s$^{-/-}$ is significantly greater ($p<0.0001$) than in the WT mouse. CTb coverage of the NMJ in the GD3s$^{-/-}$ mouse is also significantly greater ($p<0.0001$) when compared to the WT. Taken together these findings indicate that in the diaphragm, GM1 levels are increased at the NMJ, and are detected by CTb binding.

3.2.2 Topical CTb staining in other muscle groups

Different muscles from the GD3s$^{-/-}$ mouse and WT were compared directly to determine the uniformity of the upreguled GM1 expression. As a negative control to confirm the specificity of CTb for GM1, the GalNAc-T$^{-/-}$ was included (as it lacks the enzyme to synthesise complex gangliosides including GM1). As shown in Fig 22, for each GalNAc-T$^{-/-}$ muscle group analysed, CTb did not bind confirming its specificity for GM1. In the GD3s$^{-/-}$, each muscle has a significantly increased level

of GM1 when compared to the WT ($p<0.0001$). For the WT muscles, it is apparent that the GM1 expression in the FDB, gastrocnemius and soleus are comparable, while the diaphragm has a lower level of expression. In the GD3s$^{-/-}$ mouse the increase in GM1 expression is not uniform although expression in the diaphragm remains the lowest. It is impossible to comment on the significance of this trend: the aim of the study was to analyse GM1 expression in each muscle with regard to mouse strain, so valid statistical comparisons cannot be made between different muscle groups due to separate staining runs.

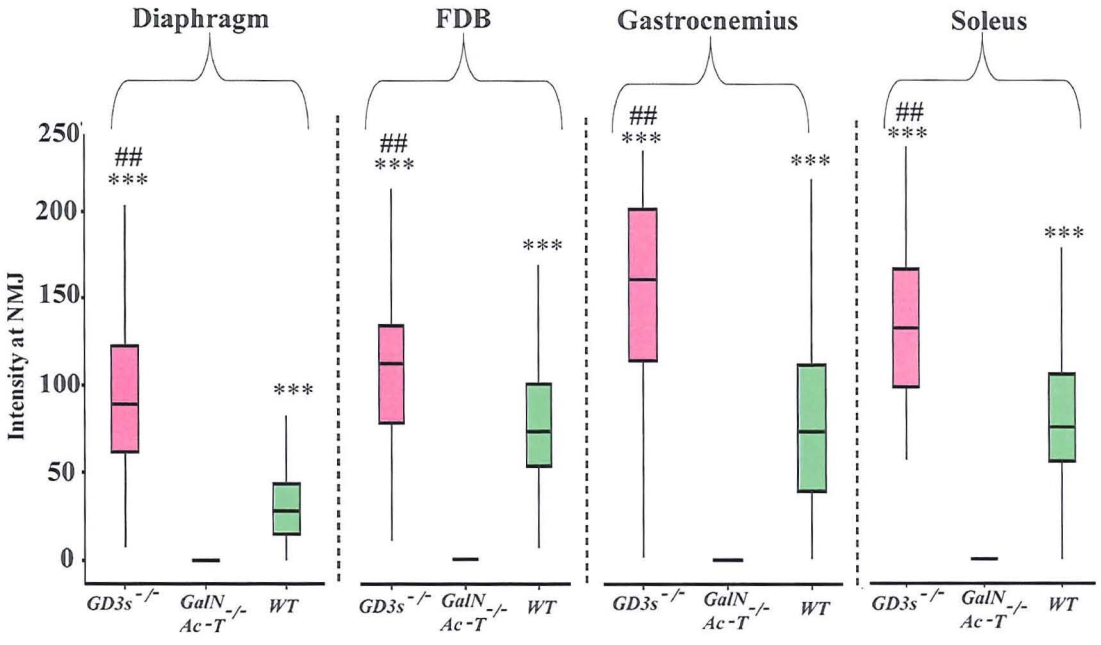

Fig 22. Comparison of CTb binding in different muscles. Note the use of the GalNAc-T$^{-/-}$ to act as a negative control. Astrices indicate significant ($p<0.05$) difference when compared to GalNAc-T$^{-/-}$. In all cases, CTb intensity was higher in GD3s$^{-/-}$ muscle tissue compared to WT ($p<0.05$) (indicated by hash symbols).

3.2.3 *Ex-vivo* demonstration of increased GM1 in the GD3s$^{-/-}$

As shown in the topical assays, the GD3s$^{-/-}$ has an increased level of GM1 when compared to the WT ($p<0.0001$). In order confirm the results of topical tissue

staining to living tissue, *ex-vivo* TS muscle was stained with CTb and the data was quantified (Fig 23) using the same method as for topical staining.

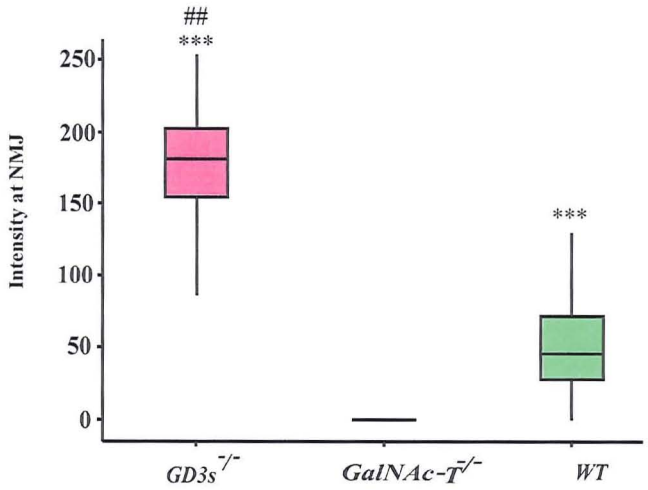

Fig 23. *Ex-vivo* TS preparation. CTb at the NMJ. Astrices indicate significant increase in intensity ($p<0.05$) compared to the GalNAc-$T^{-/-}$. GD3$s^{-/-}$staining is significantly higher ($p<0.05$) compared to the WT (indicated by hash symbols).

As seen in Fig 23, CTb staining was negative in the GalNAc-$T^{-/-}$ mouse, and the intensity significantly increased in the GD3$s^{-/-}$ when compared to the WT ($p<0.0001$).

3.2.4 GM1 Expression profile: Teased Sciatic nerve fibres

From topical staining data, the specific profile of the GM1 upregulation cannot be distinguished, and the possibility of ectopic GM1 expression by the GD3$s^{-/-}$ mouse cannot be ruled out from this data alone. Teased fibres were stained with CTb to determine the distribution of GM1 in the peripheral nerve, at sites upstream of the NMJ. No obvious difference is detectable by eye indicating the macro-distribution of GM1 is not altered. Again, staining of the GalNAc-$T^{-/-}$ mouse was negative and the use of DAPI confirms the presence of GM1 negative fibres by highlighting the presence of the Schwann cell nuclei surrounding the axon. Without the use of specific markers it is impossible to comment on the exact structures stained, but the

intense staining of the area surrounding the node of Ranvier suggests that both the node and paranode are CTb positive. There appears to be no staining on the myelin, although occasional intense patches of staining along the length of the fibre (resembling areas of damage, perhaps due to the teasing process) suggest that the underlying axon is exposed and therefore intensely stained, or that GM1 within the wraps of compact myelin is being exposed to CTb.

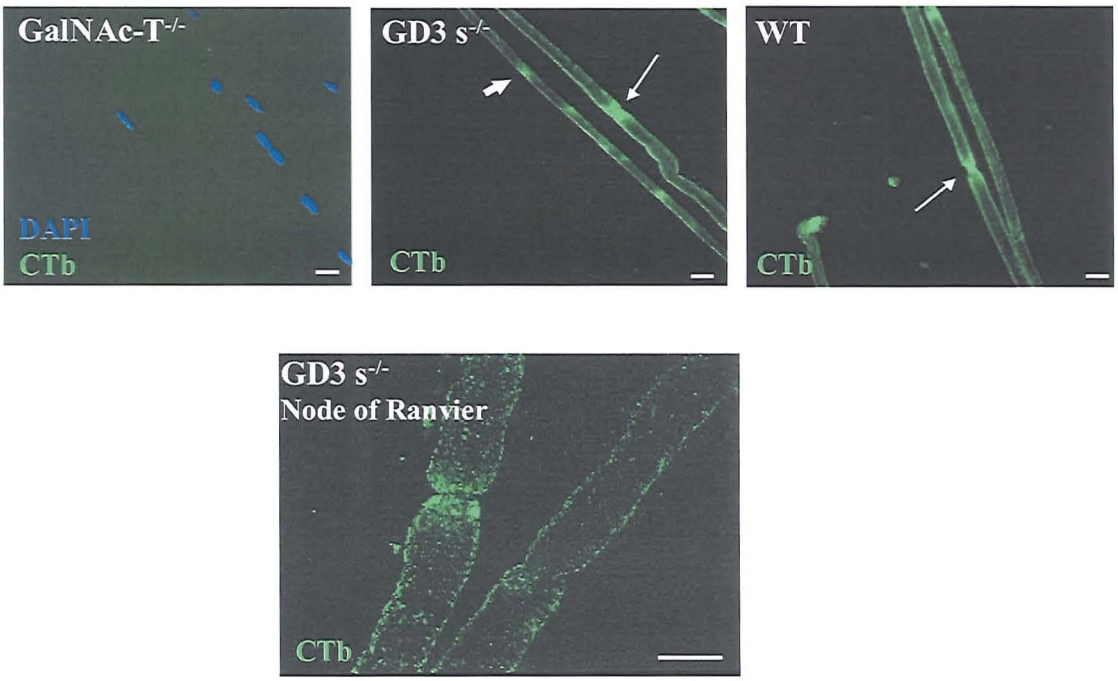

Fig 24. CTb staining of teased sciatic nerve fibres. GalNAc-$T^{-/-}$ nerves were not stained, and presence of the negative fibres is shown by uptake of DAPI in the myelinating Schwann cells surrounding the axon. In both the $GD3s^{-/-}$ and WT, staining is intense at the nodes of Ranvier (fine arrows), and uniform over the length of the fibre. Intense patches of staining are likely to be areas of damage (heavy arrow). Detailed reconstruction in the bottom panel shows detail of the nodal staining in the $GD3s^{-/-}$ mouse. Scalebar=10μm.

3.2.5 GM1 Expression profile: *Ex-Vivo* Triangularis Sterni of different mouse strains

The staining profile of CTb was studied in *ex-vivo* triangularis sterni (TS) muscle preparations. Different strains of mice were compared (Fig 25) to get a broad

overview of the distribution of GM1: any differences observed between mouse strains may be indicative that not all humans have identical GM1 expression patterns

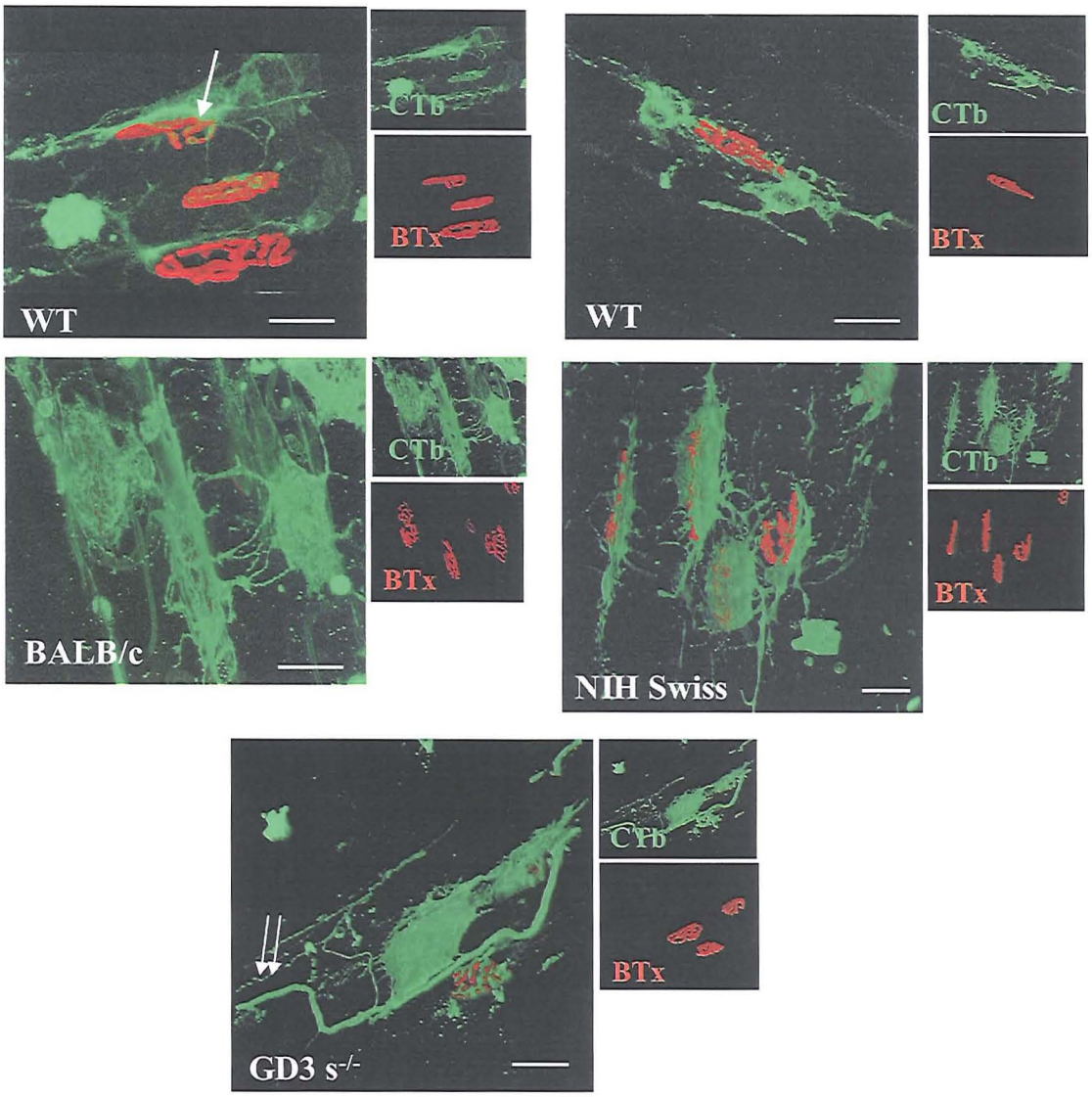

Fig 25. CTb staining to reveal GM1 profile in different mouse strains. Single arrow highlights CTb positive parajunctional fibroblast (PJF) processes networking between adjacent PJFs. Double arrow indicates axonal staining. The NMJ is shown by BTx staining, in red. Scalebar=20μm

BALB/c

Staining is intense and specific for the PJF cell body and associated processes, some of which appear to extend to and contact neighbouring PJF cells. Axonal staining is difficult to characterise due to the almost complete coverage by the CTb positive PJF.

WT

Compared to the Balb/c, staining of the PJF is less obvious in the cellular processes, appearing more sparsely distributed, and is located more on the cell body. There is little evidence of pre-synaptic axonal CTb staining.

NIH Swiss

Staining of the PJF cell body and network of processes is strong. The profile of GM1 distribution appears similar to the Balb/c.

GD3s$^{-/-}$

The PJF cell body and proximal processes are intensly stained, with less evidence of the web like network of CTb positive processes extending away from the NMJ (as seen in the Balb/c and NIH Swiss). Axonal staining over the NMJ is strong, with upstream axonal staining indicative that the GD3s$^{-/-}$ mouse has a high level of GM1 on the axon when compared to the other strains.

3.2.6 GD3s$^{-/-}$: Detailed GM1 localisation in *ex-vivo* TS

Detailing the specific location of GM1 in a WT mouse is influenced by the inherent problem that structures bearing only a small amount of GM1 may not be easily distinguished, even with the use of CTb. To this end, the GD3s$^{-/-}$ was advantageous in that all GM1 bearing structures had enhanced GM1 levels. Multi-colour staining using CTb with BTx and either S100 (Schwann cell specific marker) or neurofilament (axonal marker) and synaptophysin (synaptic vesicle marker) provided confirmation of the structure stained by CTb (Fig 26).

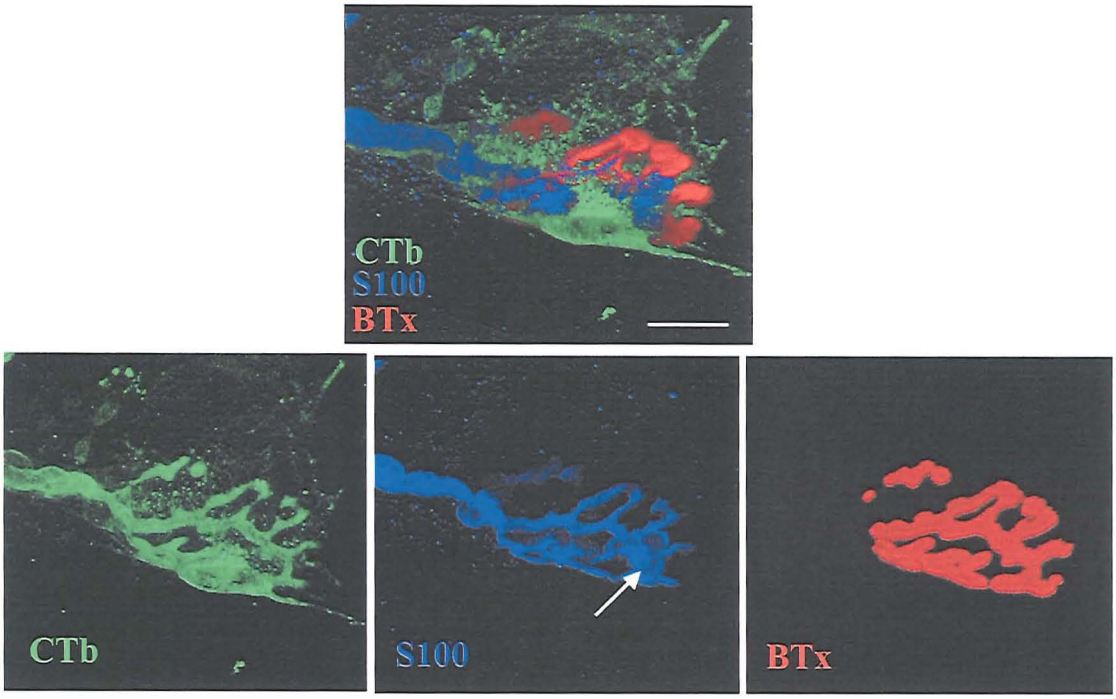

Fig 26. CTb and S100 staining. Bottom left panel shows the PJF cell body and processes stained with FITC-CTb. Upstream of this, the axon is also stained. Bottom middle panel shows S100 staining, which is Schwann cell specific. The pSC cell body and processes are stained over the NMJ region, and the last myelinating Schwann cell of the axon is also stained. The staining profile does not mirror the FITC-CTb staining, indicating the Schwann cells are not stained by CTb. Bottom left shows BTx to delineate the NMJ. Top panel shows a merged image of each channel, to show the complete staining profile. Scalebar=20μm

S100 staining over the NMJ is specific for the arborisations of the pSC, and a pSC cell body can be seen. There is no CTb staining on the pSC cell body, and over the NMJ the staining profile of the S100 and CTb differs. The CTb staining appears to be on the axon underlying the processes of the pSC. As shown in the bottom panel, there is strong staining of cell body adjacent to the pSC. This is likely to be the PJF cell body, and staining of the processes is weak when compared to the cell body. Therefore it can be concluded that GM1 expression is strongly axonal, and the PJF is GM1 positive.

Lower power images, as shown in Figure 27, display a more general landscape of the GM1 distribution. Figure 27a) shows CTb strongly staining the axon directly over the NMJ, and also upstream of the NMJ. A strongly decorated plexus of what is likely to be parasympathetic fibres wrapping a blood vessel can also be seen, proving the expression of GM1 in the GD3s$^{-/-}$ is on other fibre types. Further evidence of this is seen in Figure 27b), where neurofilament (1217) and synaptophysin (SF) specifically stain the axon and pre-synaptic vesicles in the terminal portion of the axon. Here, GM1 can be seen along the length of the axon, and on a blood vessel and surrounding fibres.

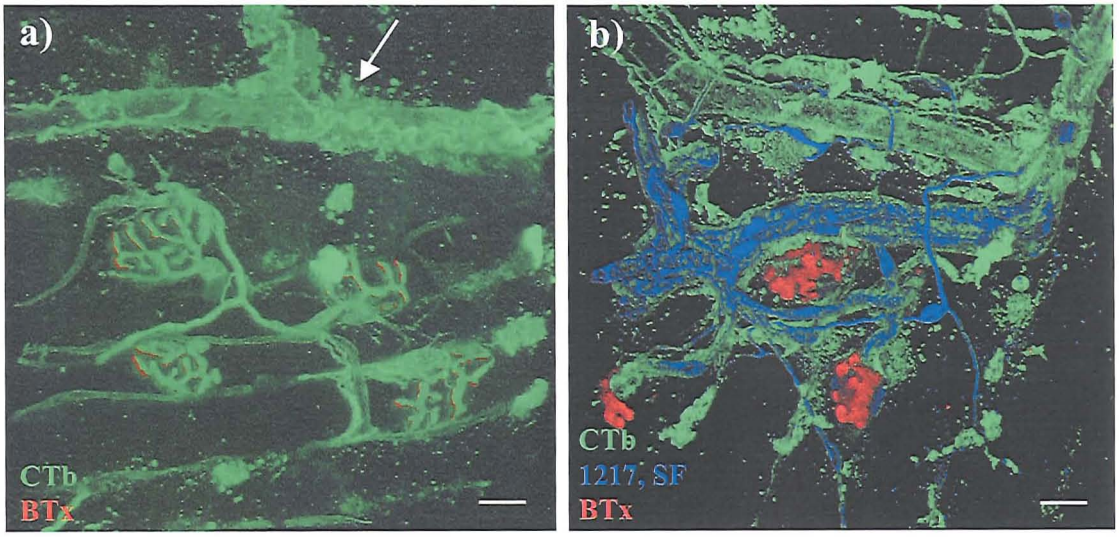

Fig 27. BTx (Bungaratoxin), CTb (Cholera toxin), 1217 (Neurofilament) and SF (synaptophysin) staining. a) Localisation of GM1. Blood vessels and sympathetic fibres are strongly stained (arrow) with CTb-FITC. Also, axons over and adjacent to the NMJ (BTx (red)) are stained. b) Blood vessel staining. Axons distinguished with neurofilament and synaptophysin staining, shown in blue. CTb staining (green) can be seen wrapping the axons. Scalebar=20μm

3.2.7 Anti-GM1 Antibodies (mAbs) in the Peripheral Nerve

Having established where the antigen is distributed in the peripheral nerve, the next stage of the study was to determine whether anti-GM1 antibodies bind to the target. Topical staining was used to determine whether the mAbs bind to diaphragm sections. The three anti-GM1 antibodies tested had differing specificities:

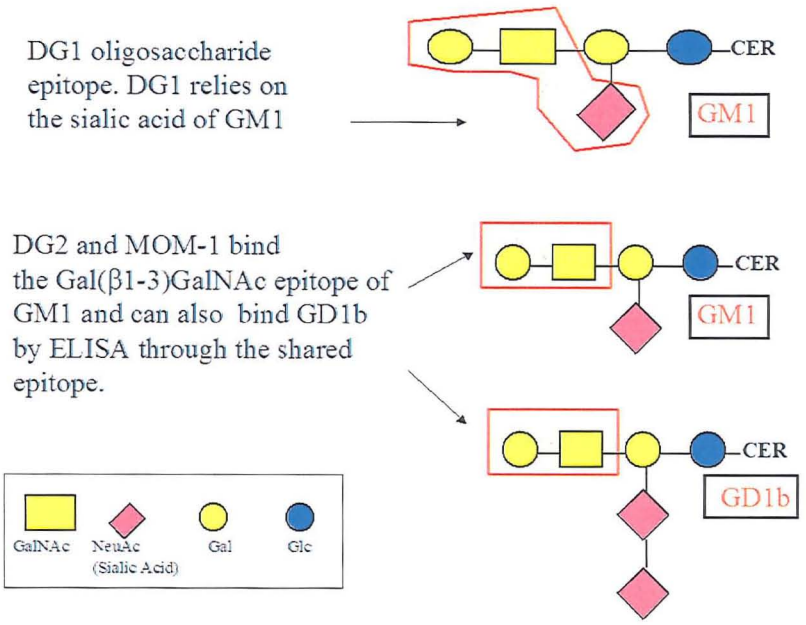

Fig 28. Schematic diagram showing the oligosaccharide epitopes recognised by DG1, DG2 and MOM-1. Note that while DG2 and MOM-1 also bind the Gal(β1-3)GalNAc epitope of GA1, this ganglioside is not relevant to the mouse model as mice lack GA1 in neural tissue (Seyfried *et al* 1996).

While the antibodies are able to bind GM1 via the epitopes shown in Fig 28, this gives no information on the strength of the interaction between antibody and antigen. The affinity of an antibody-antigen interaction can be determined by competition ELISA, by pre-incubating the antibody with various concentrations of antigen and assessing its subsequent ability to bind to antigen when coated to ELISA plates. The half-maximal binding concentration (half-max) can be calculated from a standard ELISA, to give an approximate value of the binding strength of the antibody for the antigen. For DG1 and DG2, these data are known, and their binding strength for GM1

epitiopes has been demonstrated by ELISA (Townson *et al* 2007) (Fig 29). The same authors demonstrate the affinity of each mAb for GM1 is also similar (using BiaCore).

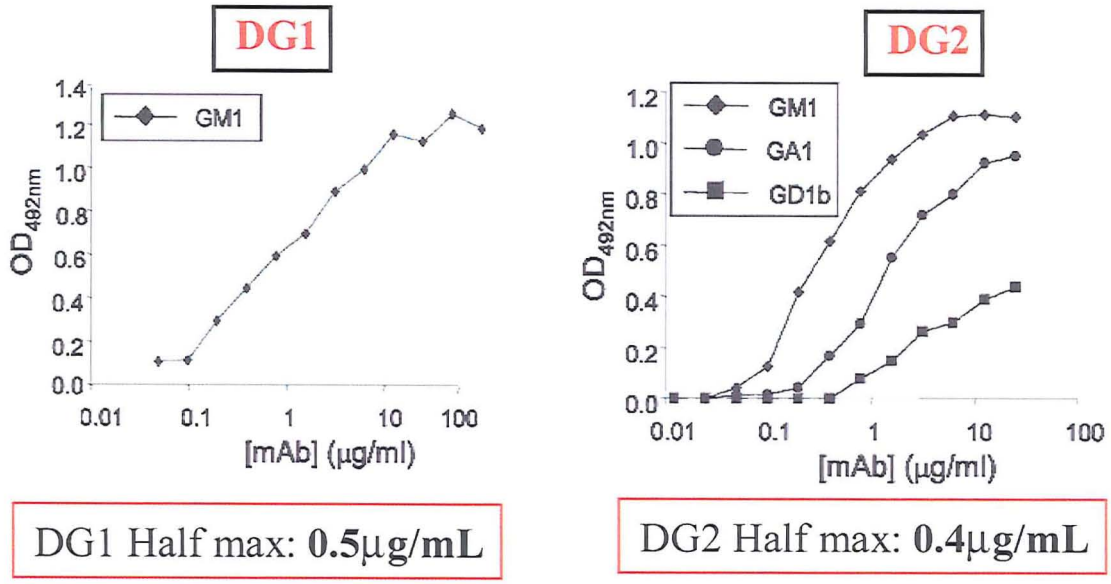

Fig 29. Data from Townson *et al* 2007. ELISA data showing DG1 is monospecific for GM1, while DG2 binds, in order of binding strength, GM1, GA1 and GD1b by the common Gal(β1-3)GalNAc epitope. The half max values for mAbs binding to GM1 are similar.

DG1 Binding:

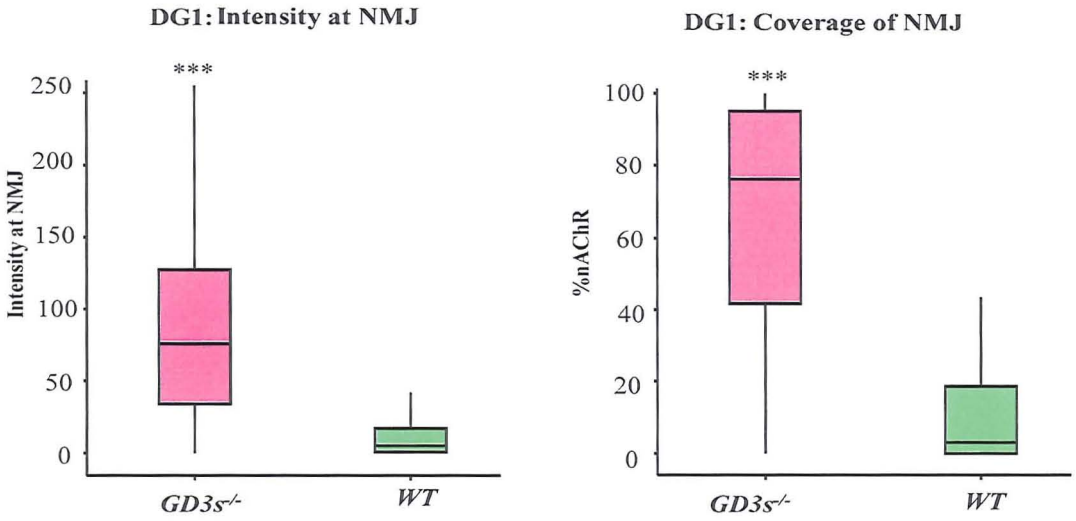

Fig 30. The binding of DG1 to diaphragm sections. Intensity of IgG fluorescence at the NMJ is increased in GD3s$^{-/-}$ compared to WT, and IgG area coverage of NMJ indicates the relative increase in IgG deposition relative to the increased expression of GM1. Astrices indicate significant increase in GD3s$^{-/-}$ compared to WT ($p<0.05$).

DG1 bound to diaphragm sections of the WT mouse, and in the GD3s$^{-/-}$ binding intensity and area coverage at the NMJ was significantly greater ($p<0.0001$). This result infers that, like CTb, the antibody is recognising the increased levels of GM1 in the GD3s$^{-/-}$ mouse, as depicted by enhanced antibody deposition when compared to the WT (Fig 30).

MOM 1 Binding

MOM 1: MOM 1 bound strongly to GM1 in the WT mouse, and although there was a detectable increase in the intensity of binding over the NMJ in the GD3s$^{-/-}$ when compared to the WT, this increase was not statistically significant ($p=0.25$). Similarly, there was no significant increase in the area coverage of the GD3s$^{-/-}$ when compared to the control ($p=0.21$) (Fig 31):

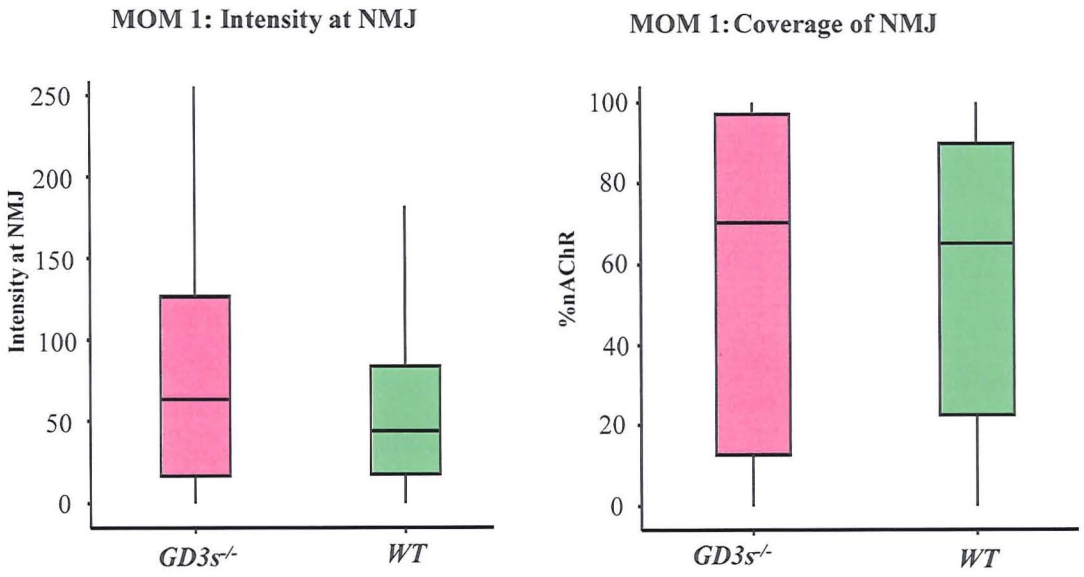

Fig 31: The binding of MOM 1 to diaphragm sections: intensity at NMJ and coverage of NMJ. There is no significant difference in either the intensity of binding at the NMJ, or the area of IgG deposition over the NMJ with MOM-1 when comparing the WT and GD3s$^{-/-}$.

DG2 Binding:

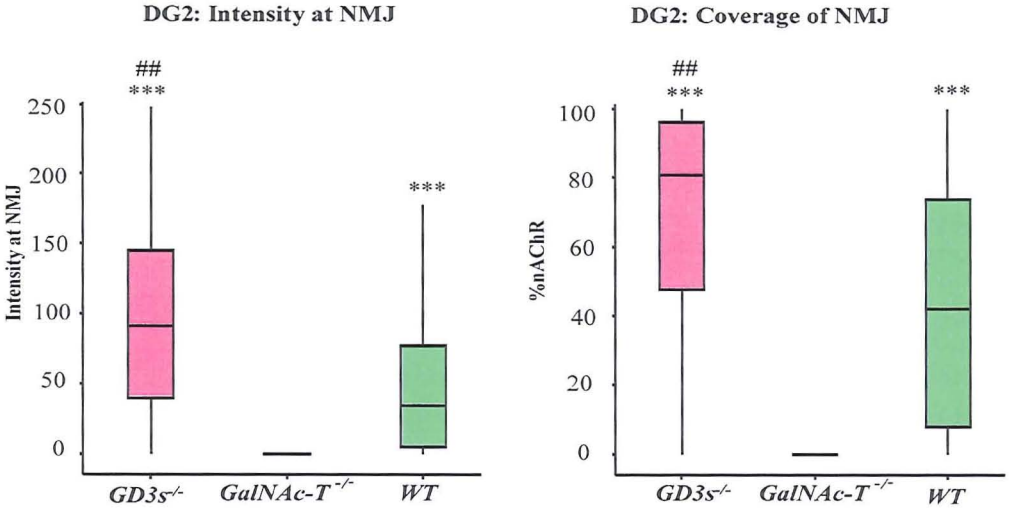

Fig 32 The binding of DG2 to diaphragm sections: intensity at NMJ and coverage of NMJ. Astrices indicate increase compared to GalNAc-$T^{-/-}$ ($p<0.05$). $GD3s^{-/-}$ mAb intensity and area coverage are significantly increased compared to WT (shown by hash symbol).

DG2 bound over the endplate in the WT and $GD3s^{-/-}$, with a significant increase in antibody intensity and area coverage of the NMJ in the $GD3s^{-/-}$ mouse compared to the WT ($p<0.0001$) (Fig 32). The GalNAc-$T^{-/-}$, used as a negative control, shows no antibody deposition over the NMJ, or in any other area of the tissue (such as the intramuscular nerve bundles). This indicates that the binding of DG2 is via the Gal(β1-3)GalNAc epitope of GM1 as opposed to glycoproteins or any other species bearing the Gal(β1-3)GalNAc epitope.

3.2.8 Ability of anti-GM1 mAbs to activate complement: Topical assay

Confirmation that the antibodies are able to bind does not directly indicate their pathogenic ability. In order to establish suitability in the model system, ie. to induce a complement mediated attack on the peripheral nerve, the ability of the antibodies to

activate and fix complement was addressed. Diaphragm tissue from the GalNAc-T$^{-/-}$, GD3s$^{-/-}$ and WT mouse were compared, and as a negative control, PBS applied as opposed to antibody, to rule out any non-specific deposition of activated complement components. The disialosyl antibody CGM3 causes a complement mediated destruction of the peripheral nerve (O'Hanlon *et al* 2001) so was applied to tissue as a positive control to confirm the viability of the complement source used and the ability to detect the activated complement components (Fig 33). CGM3 binds to disialosyl gangliosides (eg. GD3 and GQ1b), and should only therefore bind in the WT mouse (which has GM3 and GQ1b) and the GalNAc-T$^{-/-}$ (which had GD3). CGM3 will not bind in the GD3s$^{-/-}$.

Anti-GM1 IgG Antibodies (DG1 and DG2)

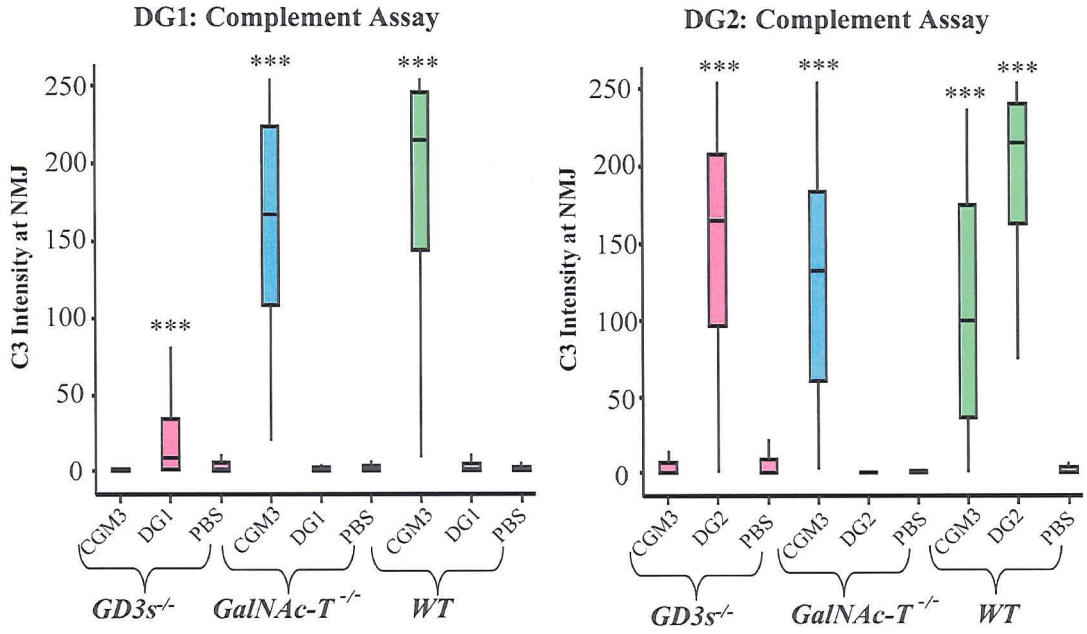

Fig 33. Ability of DG1 and DG2 IgG antibodies to bind to GM1 and activate complement. Positive control mAb CGM3 activates complement in the GalNAc-T$^{-/-}$ and WT. Astrices indicate significant difference in C3 deposition at NMJ ($p<0.05$) when compared to PBS control of the same strain.

DG1:

In the GalNAc-$T^{-/-}$ and WT, CGM3 incubation led to a strong activation of complement, detectable over the endplate. The C3 signal over the endplate in the WT was significantly greater than in the GalNAc-$T^{-/-}$ ($p<0.0001$). PBS control treated tissue for all strains had no detectable complement activation specifically over the NMJ or other area of the tissue. In the WT mouse, DG1 and PBS treated tissue had no significant difference in C3 intensity over the NMJ ($p=0.53$). In the $GD3s^{-/-}$ diaphragm, DG1 complement activation was significantly increased when compared to PBS treated tissue ($p<0.0001$) and CGM3 treated tissue ($p<0.0001$), and also to DG1 treated tissue in the WT mouse ($p<0.0001$). These results suggest that the use of the $GD3s^{-/-}$ mouse should be beneficial in causing both an *ex-vivo* and *in-vivo* anti-GM1 antibody mediated lesion. However, the activation of complement by CGM3 in both the GalNAc-$T^{-/-}$ and WT was significantly greater than the activation of complement by DG1 in the $GD3s^{-/-}$ ($p<0.0001$), indicating that the IgG 2b DG1 is less potent in its ability to activate complement than the IgM, CGM3.

DG2:

In the GalNAc-$T^{-/-}$ and WT, the positive control antibody CGM3 led to a significant increase in C3 deposition at the NMJ when compared to PBS treated tissue ($p<0.0001$) and to CGM3 treated tissue in the $GD3s^{-/-}$ ($p<0.0001$). The level of C3 intensity in the CGM3 treated GalNAc-$T^{-/-}$ and WT was similar ($p=0.28$). In the $GD3s^{-/-}$ mouse, the C3 intensity of the CGM3 treated and PBS tissue was similar ($p=0.86$), representing non- specific deposition of C3 which was detectable as "background" under the microscope analysis settings. DG2 activation of complement was not evident in the GalNAc-$T^{-/-}$ tissue, with C3 levels comparable to

that of PBS treated tissue (p=0.01), indicating DG2 was not binding to any epitopes in the GalNAc-$T^{-/-}$ tissue. In both the $GD3s^{-/-}$ and WT, the activation of complement was significantly increased when compared to PBS treated tissue (p<0.0001). Surprisingly, the C3 deposition in the WT mouse was significantly greater than that in the $GD3s^{-/-}$ mouse (p<0.0001). C3 deposition resulting from DG2 binding in the $GD3s^{-/-}$ and WT diaphragm is significantly greater than that resulting from CGM3 binding in the GalNAc-$T^{-/-}$ and WT (p<0.0001 in each case), suggesting DG2 is equally able (if not better) at activating complement when directly compared to CGM3.

MOM 1:

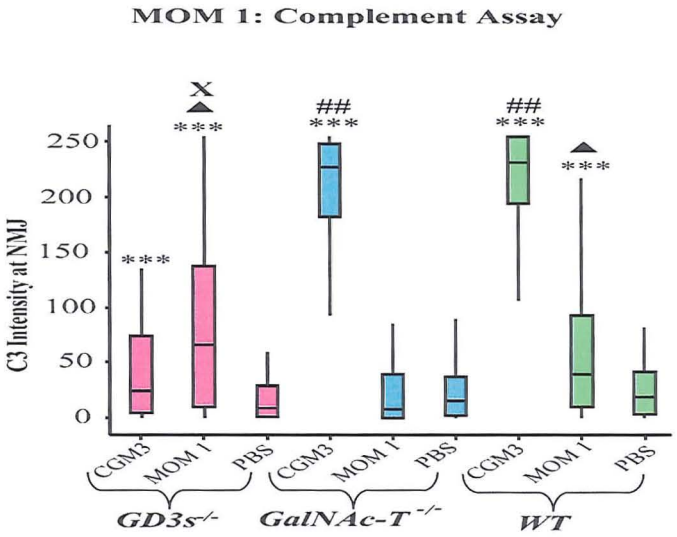

Fig 34. Ability of MOM-1 to activate complement. CGM3 positive control activates complement in the GalNAc-$T^{-/-}$ and WT. MOM-1 activates complement in the $GD3s^{-/-}$ and WT. Astrices indicate significant increase in C3 deposition (p<0.05) compared to PBS control of the same strain. Hash symbols indicate increased CGM3 mediated C3 deposition compared to $GD3s^{-/-}$, triangles indicate increased MOM-1 mediated C3 deposition compared to GalNAc-$T^{-/-}$ and cross indicates increased MOM-1 mediated C3 deposition compared to WT.

CGM3 in both the GalNAc-$T^{-/-}$ and WT increased the C3 intensity when compared to respective PBS treated control tissue (p<0.0001), with CGM3 induced complement

activation being similar for both strains (p=0.48). In the GD3s$^{-/-}$, CGM3 C3 level was not significantly higher than that of the PBS treated tissue (p=0.02). However, it remained lower than the MOM 1 induced C3 intensity (p<0.0001), suggesting that the CGM3 treated tissue C3 levels were due to background. In the WT, CGM3 caused significantly greater complement activation than MOM 1 (p<0.0001).

MOM- 1 treated tissue in the GalNAc-T$^{-/-}$ was not significantly different in C3 intensity when compared to PBS treated (p=0.25), in the GD3s$^{-/-}$ it was higher than PBS treated tissue (p<0.0001) and also in the WT was higher than PBS treated tissue (p=0.03). Comparing the C3 intensity in the GD3s$^{-/-}$ and WT MOM- 1 treated tissue shows the increased C3 levels on the GD3s$^{-/-}$ is significant (p=0.04) (Fig 34).

3.2.9 Ability of DG1 and DG2 to bind sulfatide

DG1 and DG2 are both able to bind sulfatide in ELISA. It was therefore logical to address the assumption that they could also bind it in tissue. Provision of tissue from mice either lacking or overexpressing sulfatide was ideal in providing both positive and negative control tissue for the topical application of the mAbs. CTb was used to block any possible binding to GM1 in the nerve sections and O4 antibody was used to confirm the presence or absence of sulfatide. O4 antibody is a well characterised oligodendrocyte marker, relying on the sulfatide epitope (Pfeiffer *et al* 1993)

To establish the ability of the mAbs to bind to GM1 in the NMJ of these mice, DG2 was selected for topical staining of diaphragm muscle to these mice.

Nerve Tissue:

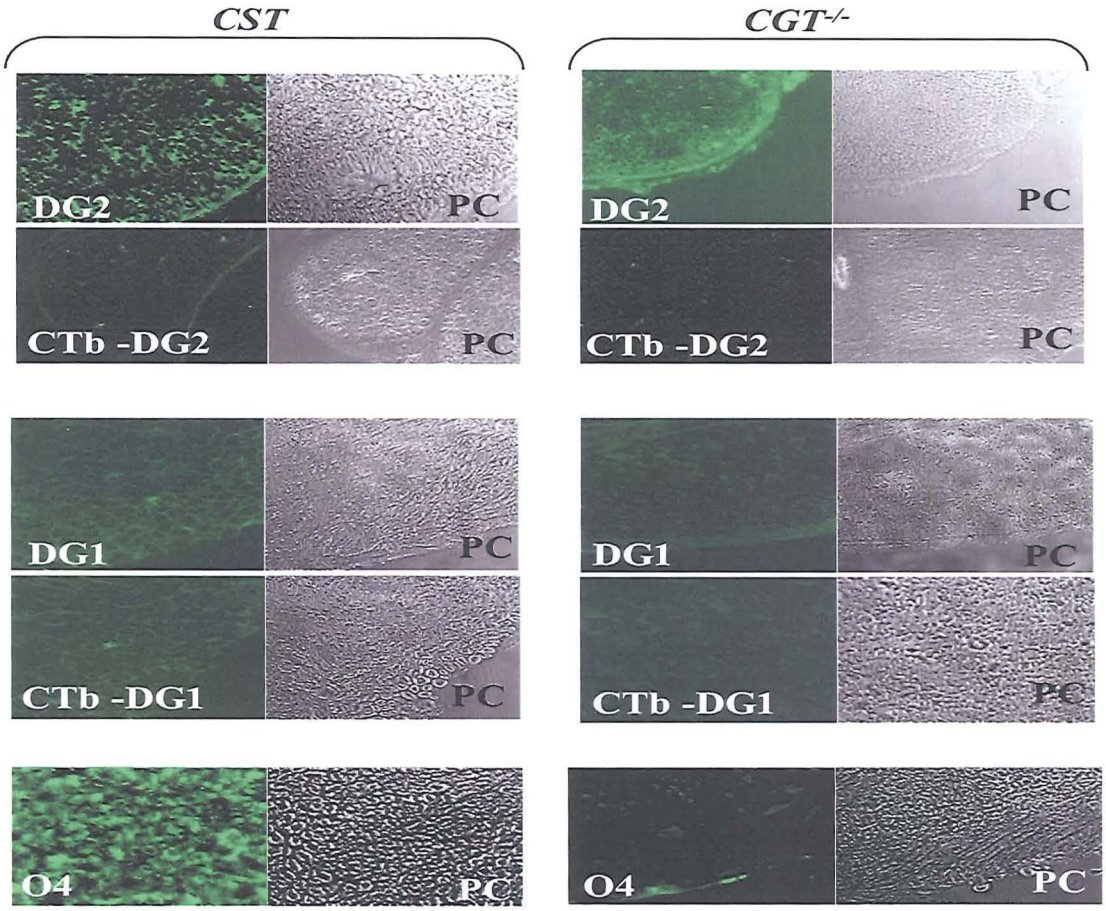

Fig 35. Sulfatide overexpressing (CST) and sulfatide deficient ($CGT^{-/-}$) nerves. Nerves were sectioned in the transverse plane. Fluorescent FITC images (left panels) show mAb binding following PBS or CTb pre-incubation. Phase contrast (PC) images show nerve outline.

As shown in Fig 35, the upper panel for both $CGT^{-/-}$ and CST nerves show DG2 binding (to GM1), and this staining is abolished upon pre-incubation of the tissue with unlabelled CTb. In the middle panel, the same can be said for DG1, although prior to the CTb block the DG1 staining was much weaker than the DG2 (all pictures were taken under the same microscope levels). In the CTb blocked tissue, levels were comparable to that of negative controls, ie. CTb blocked tissue followed by PBS as opposed to mAb, and finally incubated in secondary FITC antibody (not shown). O4 staining confirms the presence of sulfatide in the CST tissue, with absence of staining

in the $CGT^{-/-}$ (staining comparable to PBS incubated tissue followed by secondary, not shown).

Diaphragm

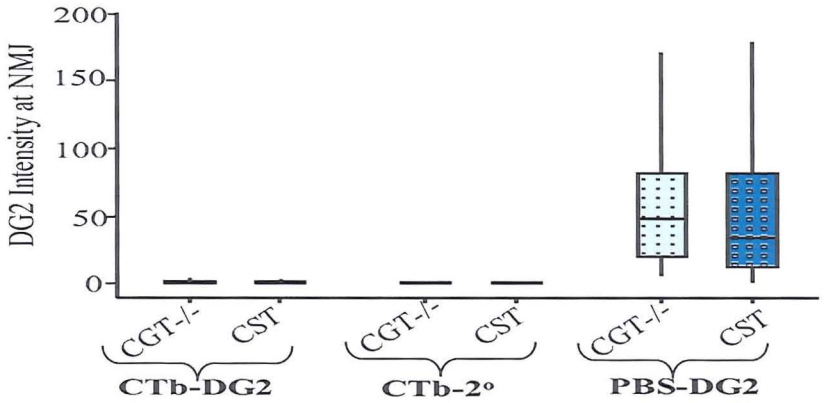

Fig 36. Topical staining of the diaphragm from the CST (sulfatide overexpressing) and $CGT^{-/-}$ (sulfatide null) mice. CTb abolishes DG2 binding, while PBS alone has no effect on DG2 binding at the NMJ of each strain.

DG2 binds over the NMJ in both the CST and $CGT^{-/-}$ mouse ($p=0.12$). The binding of DG2 is specific for GM1, as in both strains of mouse it can be blocked with CTb to give a comparable intensity to that of CTb blocked tissue followed by PBS alone then secondary antibody ($p<0.0001$) (Fig 36).

3.2.10 Discussion

Analysis of antibody or toxin staining intensity and area of coverage of the NMJ (ie. area directly overlying the BTx signal) are ideal ways in which to semi-quantify the differences in staining observed between different tissue sections, provided all are stained together in 1 staining run, and that the microscope detection settings are held constant throughout. The image analysis method is also of use when analysing the differences in complement deposition. Details of the analysis method are in Materials and Methods.

Ex-vivo staining results with CTb confirm that GM1 is over-expressed in the $GD3s^{-/-}$ mouse and is present in the WT mouse. Use of the GalNAc-$T^{-/-}$ proves that CTb-FITC

is not binding either non-specifically, or to another ganglioside in the tissue (Blank *et al* 2007). All anti-GM1 antibodies tested are able to bind GM1 in the WT and GD3s$^{-/-}$ sectioned tissue. From this data, it can be inferred that the GM1 presentation in the tissue is displaying the epitope on which the antibody binding relies.

The disadvantage of topical staining lies with the poor morphology of the tissue, meaning teased nerves and whole mount imaging was required to profile GM1 distribution. With teased fibre staining, differences in CTb intensity were not detectable by eye, suggesting similar levels of GM1. This leads to the hypothesis that in the sciatic nerve there may be a rate limiting step in the synthesis of GM1, such as a low expression of the enzyme Gal Transferase ((Tettamanti 2004) and see appendix 1). Future development of imaging software would allow more formal quantification of the CTb levels. For example, the intensity of signal over an axonal marker could be used, much in the same way as the NMJ intensity and area analysis.

Whole mount *ex-vivo* staining of TS tissue is an unequivocal way of demonstrating GM1 distribution. An important technical point to note is that after fixation with aldehydes, molecules are still mobile in the membrane (Chandler 1984, Jost *et al* 1973), meaning the binding of multivalent ligands such as CTb can laterally displace membrane proteins and lipids. Thus, with staining, primary mAbs and most importantly CTb, were applied to the tissue prior to fixation in order to maintain the best depiction of their in-situ profile. Whole mount TS staining with CTb in the various strains of mice also revealed a surprising variability in the GM1 profile. While the axonal presence of GM1 was uniform throughout the strains, there was obvious variability in GM1 expression by the PJF. Again this could be related to several factors, including strain differences in the levels of enzymes required to synthesise GM1 at this site. Another interesting possibility is based on observations in the

olfactory bulb, where the expression of the O4 antigen by olfactory ensheathing cells (OECs) is thought to be due to the phagocytosis of O4 positive axonal fragments, and not due to the actual synthesis of O4 antigen by the OECs (Wewetzer *et al* 2005). This interpretation could translate to the expression of GM1 by the PJF, where uptake of axonal fragments leads to introduction of axonal glycolipids (namely GM1) to the PJF, which in turn becomes GM1 immunoreactive. Why such a mechanism would display strain specific differences is difficult to reconcile, but GM1 is strongly associated with axonal regeneration (Lainetti and Da-Silva 1993), so it may be interesting to look at the regenerative properties of the axon in the different mice to determine if there is a correlation of GM1 expression by the PJF and regenerative ability. The PJF staining profiles are reminiscent of the demonstrated anomaly of ganglioside expression on the pSC of different mouse strains. The NIH Swiss pSC is resistant to anti-disialosyl antibody mediated injury, in contrast to that of the Balb/c (Halstead *et al* 2005), indicating gangliosides are expressed in different profiles, or perhaps lie in cryptic domains in certain strains of mouse.

This chapter demonstrated a lack of GM1 on the pSC. It would be interesting to determine if there is a difference in GM1 expression between myelinating and non-myelinating Schwann cells. The use of primary cultured Schwann cells would allow alteration of the phenotype from non-myelinating to myelinating (Guenard *et al* 1994), which would be a dynamic way of addressing the GM1 expression. PCR would be a useful tool in determining the presence of enzymes involved in ganglioside biosyntheis (shown in Appendix 1), as these may fluctuate depending on phenotype, or under certain culture conditions. For example, addition of inflammatory cytokines to simulate axonal stress may result in a non-myelinating pSC to express GM1 and aid in axonal regeneration. However, the use of PCR is limited by the fact

that the detection of DNA confirms the presence of the biosynthetic enzyme, however gives no information on the levels of final product (i.e. ganglioside). For example, while there may be an abundance of a specific enzyme, a lack of substrate would affect the synthesis of the final product, meaning it is inherently difficult to determine at which point in the biosynthetic pathway a synthesis limiting situation occurs.

IgG from different species (including mouse) is able to react with human C1q (Hoffken *et al* 1978), thus the topical complement assay used was ideal in demonstrating that binding by the mAbs to GM1 was functional, owing to their ability to initiate the complement cascasde. Activation of complement is an indication that an antibody has bound stably to its epitope. Initiation of the cascade occurs upon activation of the C1 complex, via the C1q molecule, which comprises 6 globular head groups (Law and Reid 1983). For activation, at least 2 C1q head groups must interact with a binding site on the Fc region of an antibody: this requires an aggregation of IgG molecules (Hughes-Jones *et al* 1983) or the binding of a single pentameric IgM molecule to a cluster of antigens to expose the C1q binding sites which are already close within the structure of the molecule (Poon *et al* 1985). The binding of Ig to a specific epitope induces a conformational change to expose the C1q binding site on the Fc region of the Ig molecule, which increases the affinity of the C1q binding site by 10,000 fold (Burton 1985) (with the exception of IgG4 subclass, which does not bind C1q (Garred *et al* 1989)). Thus, the ability of the anti-ganglioside mAbs to activate complement indicates that they have bound to their epitope in a stable conformation, as opposed to a non-specific or weak attraction.

Surprisingly, DG2 demonstrated greatest complement activation in the WT mouse, which does not seem logical as more antibody was deposited in GD3s$^{-/-}$ tissue. DG2 bound better in the WT than DG1, and the low level of binding demonstrated by the

latter mAb appeared to be insufficient to activate complement. However, the high IgG deposition with DG2 was enough to activate the cascade, and a possible explanation for the high C3 detected in the WT when compared to the GD3s$^{-/-}$ may be that sectioning tissue in a freezing cryostat may have altered the spatial relationship between GM1 and complement regulators, and once initiated the complement cascade in the WT mouse was not under control by complement regulator proteins. An alternative possibility is that DG2 has aggregated (a feature of IgG3 subtype antibodies) (Kaminski *et al* 1999), and resultant "piggyback" binding of DG2 to GM1 in the GD3s$^{-/-}$gives a high IgG signal, but does not represent functional binding.

Chapter 4

4.1 Introduction

Chapter 3 demonstrated that anti-GM1 antibodies are able to bind GM1, and the increase in antibody deposition in the GD3s$^{-/-}$ mouse when compared to the WT. This establishes the GD3s$^{-/-}$ as the ideal disease model to further characterise these mAbs, and other anti-GM1 antibodies.

The aim of the next stage of the study was move to more physiologically relevant (ie. living) tissue, and ascertain the ability of anti-GM1 antibodies to induce a complement mediated lesion. *Ex-vivo* nerve muscle preparations were used, in this case the hemi-diaphragm. The mouse mAbs DG1 and DG2 were used, followed by the human antibodies Do1 and Sm1 to reinforce the clinical aspect of this work. Sm1 was cloned from a patient with multifocal motor neuropathy (MMN), while Do1 was cloned from a GBS patient (Paterson et al 1995). Sm1 has a similar specificity to DG1 (i.e. GM1 monospecific), while Do1 has a similar binding profile to DG2 (i.e. Gal(β1-3)GalNAc epitope dependent).

4.2 Results

42.2.1 DG2 Ex-Vivo: GD3s$^{-/-}$, GalNAc-T$^{-/-}$, WT

The first antibody investigated was DG2, the Gal(β1-3)GalNAc dependent anti-GM1 mAb.

4.2.1.1 *DG2: IgG, C3, MAC, NF*

*IgG intensity (Fig 37A)

In the GalNAc-T$^{-/-}$mouse, there was no difference between IgG deposition in Ringer and mAb treated tissue (p=0.05), indicating no DG2 had bound. In the WT, the IgG

deposition was significantly greater when compared to the Ringer control ($p<0.0001$), and the mAb treated GD3s$^{-/-}$ tissue also displayed greater IgG deposition than its Ringer control ($p<0.0001$). Comparison of the IgG deposition in the GD3s$^{-/-}$ and WT shows the mAb binding in the GD3s$^{-/-}$ is higher ($p<0.0001$).

*C3 Intensity (Fig 37B)

No difference in C3 intensity was detected in the mAb and Ringer control tissue from the GalNAc-T$^{-/-}$ ($p=0.05$). For both the WT and GD3s$^{-/-}$ tissue, mAb treated tissue had increased C3 deposition when compared to their respective Ringer control ($p<0.0001$). The C3 intensity in the GD3s$^{-/-}$ was greater than that of the WT ($p=0.01$).

*MAC Intensity (Fig 37C)

MAC deposition was not evident in the mAb treated GalNAc-T$^{-/-}$ tissue ($p=0.51$ compared to control). Both the GD3s$^{-/-}$ and WT had an increase in MAC intensity when mAb treated tissue was compared to Ringer treated ($p<0.0001$), and the GD3s$^{-/-}$ had the greatest MAC deposition at the NMJ compared to the WT ($p<0.0001$).

*NF Coverage (Fig 37D)

Neurofilament coverage of Ringer and mAb treated tissue in the GalNAc-T$^{-/-}$ was different ($p=0.01$), however the data does not point to NF destruction in the mAb treated tissue, as there was an increase in intensity when compared to the control. This represents natural biological variability in one GalNAc-T$^{-/-}$ mouse preparation. In the WT mouse, the mAb treated tissue has less NF over the NMJ compared to its Ringer control ($p<0.0001$), and the GD3s$^{-/-}$had less NF compared to the Ringer control ($p<0.0001$).

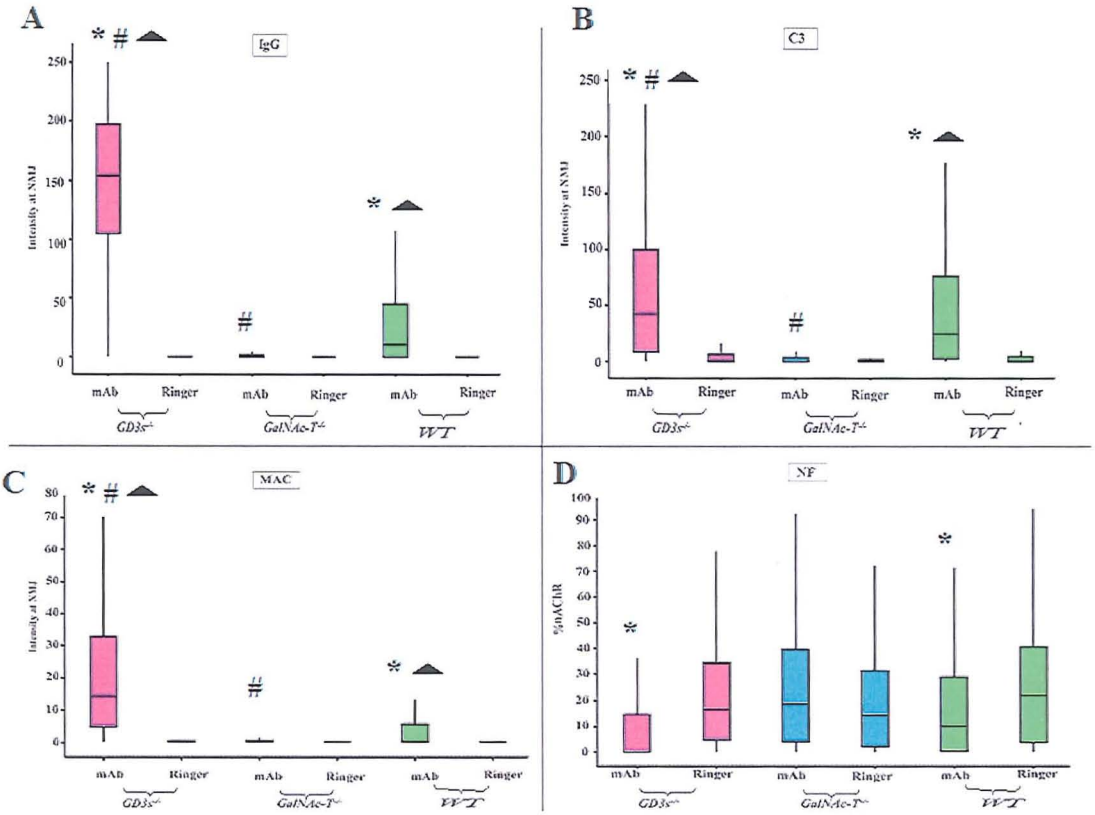

Fig 37. *Ex-Vivo* effect of DG2 showing IgG, C3 and MAC intensity over NMJ, and NF coverage. In all cases the GD3s$^{-/-}$ mAb treated tissue was significantly different compared to WT mAb treated tissue ($p<0.05$). Astrices indicate significant difference compared to Ringer control ($p<0.05$), hash symbols indicate significant difference compared to WT and triangles show significance compared to GalNAc-T$^{-/-}$.

From the data (Fig 37) it is shown that in both the WT and GD3s$^{-/-}$ diaphragms, DG2 is able to bind and cause a complement mediated lesion of the NF. Antibody binding, complement activation and subsequent axonal injury are greatest in the GD3s$^{-/-}$ mouse.

4.2.1.2 *Antibody viability*

As shown in Fig 38, the antibody from each incubation bound with similar affinity to a GM1 coated ELISA plate. This confirms that the differences in response from each mouse strain was not due to variability in the applied antibody.

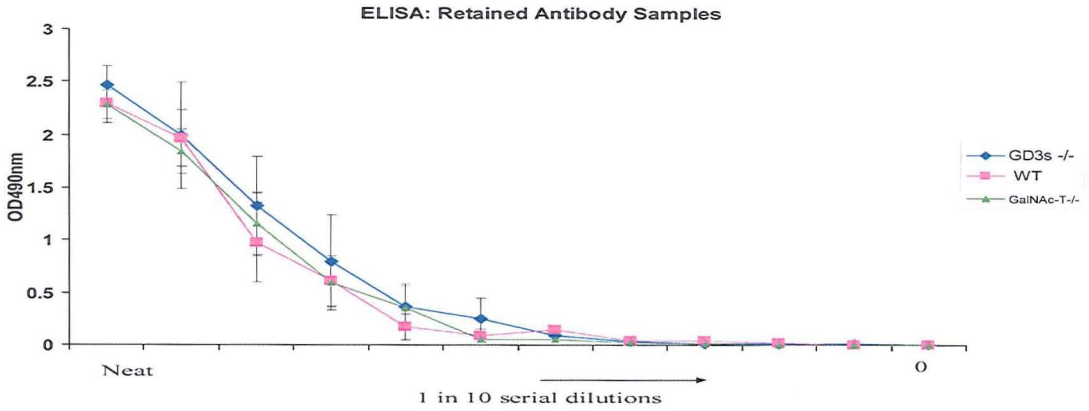

Fig 38: Retained antibody samples from each hemi-diaphragm incubation. n=3 for each strain, and error bars represent SEM.

4.2.1.3 *Ex-vivo antibody binding profile: sectioned tissue*

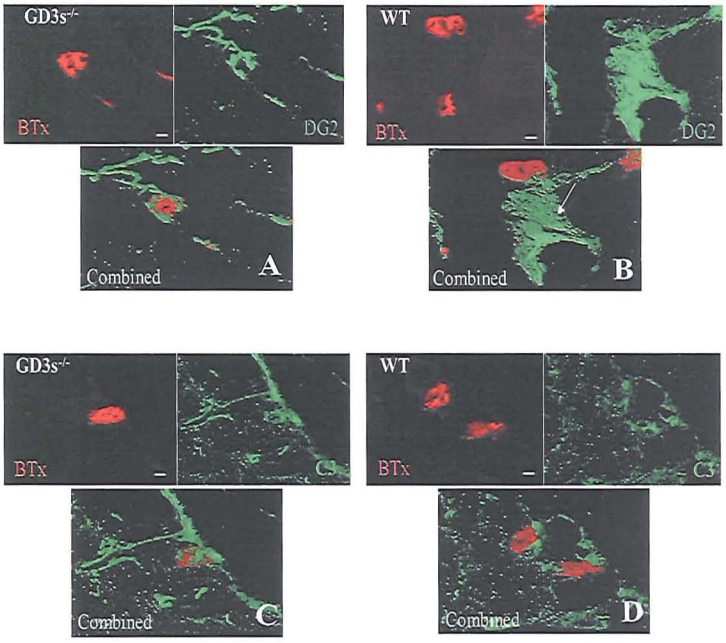

Fig 39. Immunostaining of 20µm sections of diaphragm from GD3s$^{-/-}$ and WT diaphragm. A and B: DG2 deposition in GD3s$^{-/-}$ is strongly axonal, and overlies the NMJ. In the WT, intramuscular nerve bundles (arrow) are intensly stained, but staining at the NMJ is less obvious compared to the GD3s$^{-/-}$. C and D: C3 deposition is similar in profile to DG2 staining, and most intense in the GD3s$^{-/-}$.

Following incubation of live tissue with mAb and NHS, 20μm sections of tissue were gathered and anti-mouse IgG or anti-C3 applied to profile mAb and C3 deposition overlying the NMJ. Overall staining pattern resembled that seen in Chapter 3, with obvious deposition of IgG and C3 over the endplate, and in the intramuscular nerve bundles. This indicates the distribution of the GM1 recognised by DG2 is similar to that as would have been predicted from the topical data. However the tissue morphology did not facilitate enough structural detail to comment on more discrete staining profiles (Fig 39).

4.2.1.4 *Ex-vivo antibody binding profile: TS preparation*

A more detailed profile of DG2 staining was examined in a TS prep, which is a thinner muscle than the diaphragm particularly useful for viewing staining profiles in *ex-vivo* muscle.

* $GD3s^{-/-}$:

In the $GD3s^{-/-}$ TS muscle, DG2 bound in a strong neuronal profile, with pre-synaptic axonal staining intense over the BTx delineated endplate, and also upstream of the NMJ. The PJF cell body and branching processes were also bound strongly by DG2 forming an umbrella like veil over the entire NMJ (Fig 40).

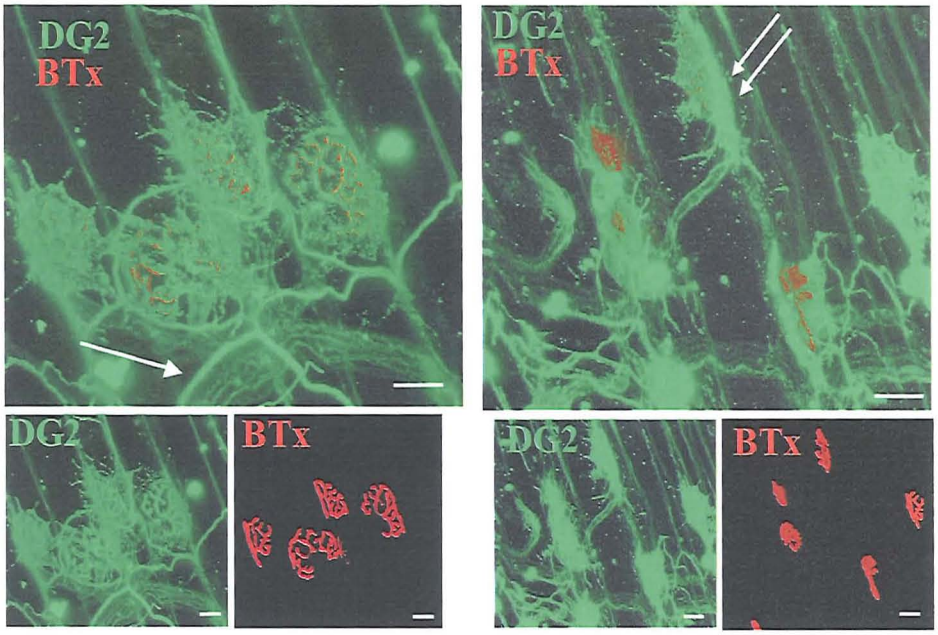

Fig 40. DG2 staining in the GD3s$^{-/-}$mouse. Arrow shows axonal staining upstream of the NMJ, and double arrow shows DG2 deposition on the PJF cell body directly over the NMJ. NMJs are stained with BTx (red). Scalebar = 20μm

*WT

In the WT (Fig 41), the PJF staining was evident, although the profile of DG2 deposition over the cell body and processes appeared more punctate than in the GD3s$^{-/-}$. Staining of the axon leading to the NMJ was positive, although the intensity of the axonal staining overlying the endplate was notably less intense (sometimes absent) than seen on the GD3s$^{-/-}$.

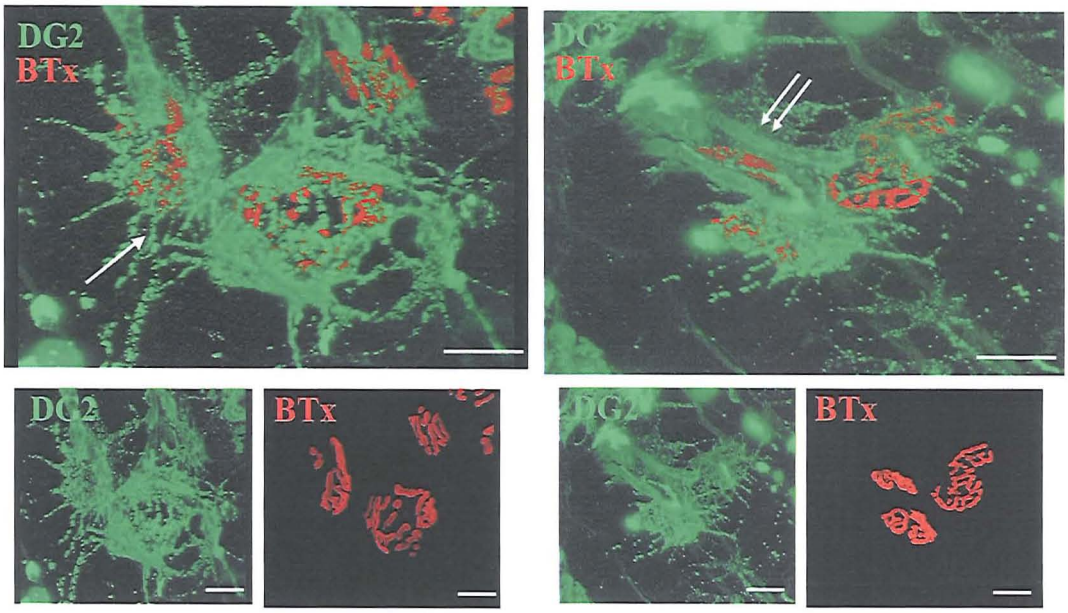

Fig 41. DG2 staining in the WT mouse. Single arrow indicates the punctate staining of the PJF processes, and double arrow shows the DG2 stained axon leading to the NMJ. NMJs are stained with BTx (red). Scalebar = 20μm

* GalNAc-$T^{-/-}$:

There was no detectable DG2 binding in the GalNAc-$T^{-/-}$ mouse, either at the NMJ or in other regions, such as intramuscular nerve bundles or blood vessels (Fig 42).

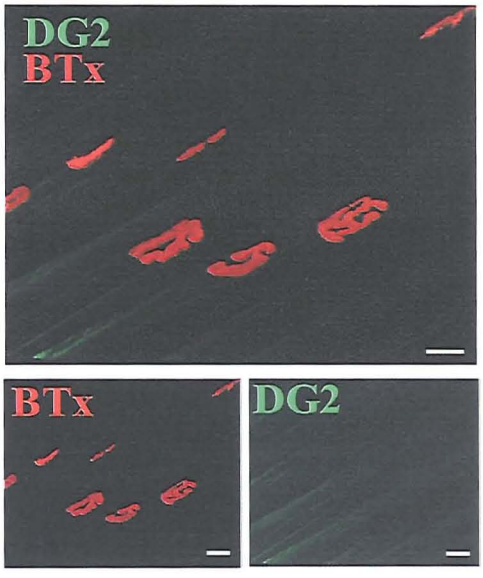

Fig 42. DG2 staining in the GalNAc-$T^{-/-}$ mouse. DG2 did not bind, as indicated by absence of FITC signal. NMJs are shown by BTx staining (red). Scalebar = 20μm

*C3 deposition in the GD3s$^{-/-}$ mouse:

The ability of DG2 to bind in the GD3s$^{-/-}$ led to the assumption that it would be able to induce a complement mediated lesion. To demonstrate the ability of the mAb to fix complement (Fig 43), it was applied to the TS followed by NHS, and the tissue stained to determine the profile of C3 deposition (i.e. *ex-vivo* complement assay- Materials and Methods).

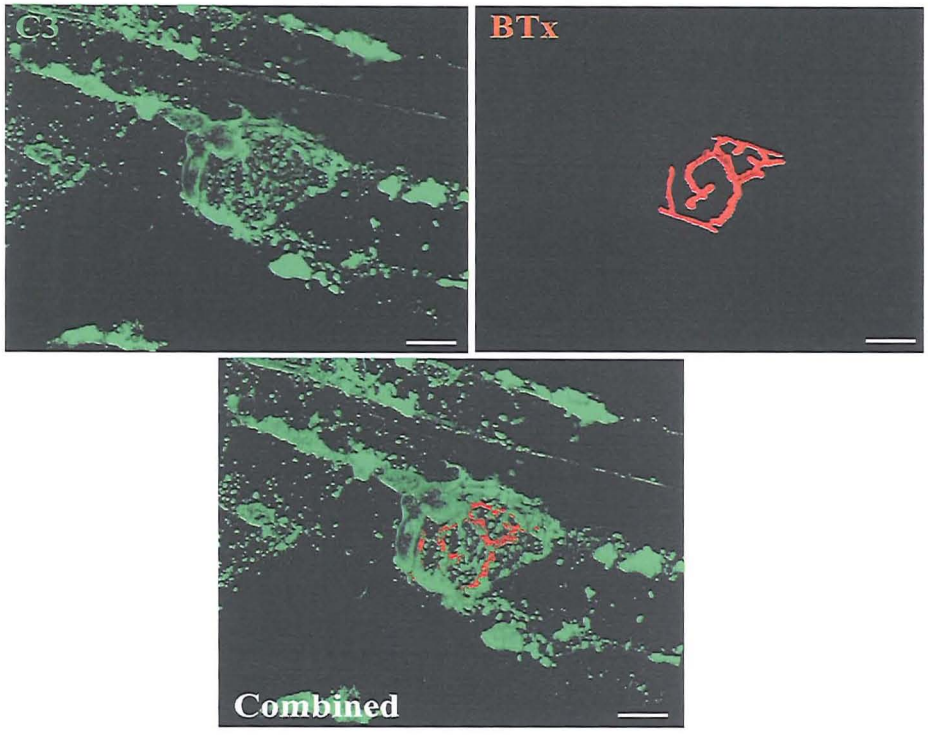

Fig 43: complement activation profile in the GD3s$^{-/-}$ following incubation in DG2 and NHS. C3 is present along the axon, and the halo of C3 around the NMJ (shown with BTx (red)) is suggestive of C3 deposition on the PJF. Scalebar = 20μm

*Double labelling: structural characterisation of DG2 Binding

Following the demonstration of the DG2 antibody and complement deposition, double staining techniques were used to identify the key structures susceptible to DG2 mediated damage. As shown in Fig 44, DG2 binds to the PJF and axon over the NMJ, but in a profile distinct from the body and processes of the pSC (stained with S100).

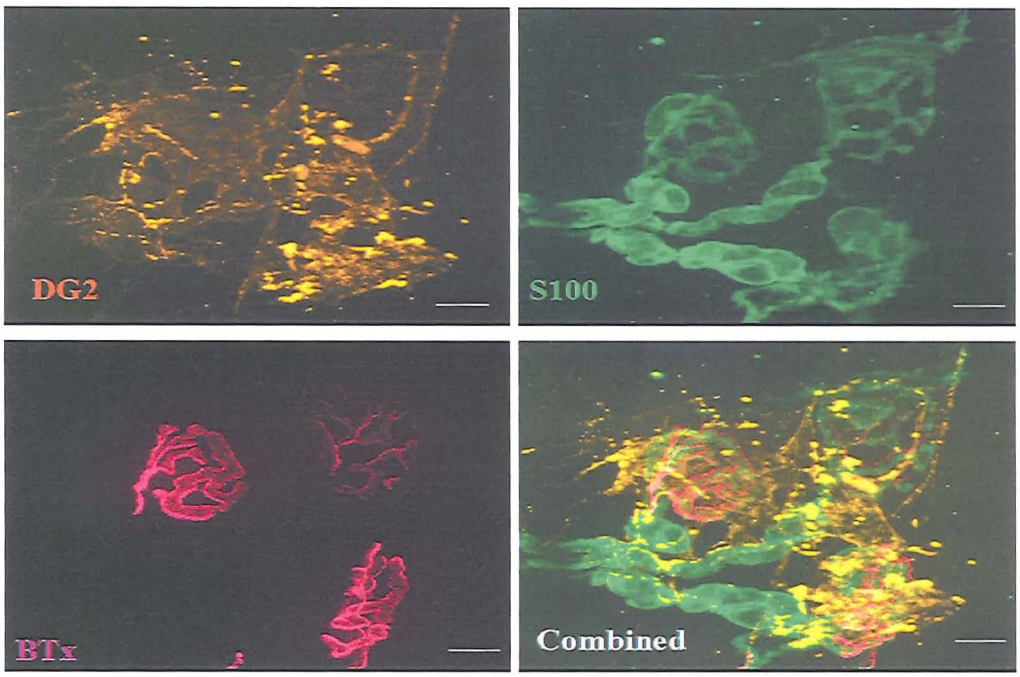

Fig 44. Triple staining: S100 (FITC (green)), DG2 (TRITC (orange)) and BTx (Cy-5 (pink)). DG2 binds to the NMJ in a veil like profile (orange). This is distinct from the profile of S100, which is shown in green and is specific for the myelinating Schwann cells of the axon, and also the pSC, the cell body and processes of which lie directly above the NMJ (shown with BTx (pink)). Scalebar = 20μm

4.2.2 *Do1 Ex-Vivo*

4.2.2.1 *Do1: IgM, C3, MAC, NF*

Following the success of DG2, a human monoclonal antibody was tested in the *ex-vivo* muscle nerve preparations to see if a similar lesion was produced. Do1 was applied to the GD3s$^{-/-}$and the GalNAc-T$^{-/-}$ used as a control to confirm pathology was a result of interaction with GM1 (Fig 45).

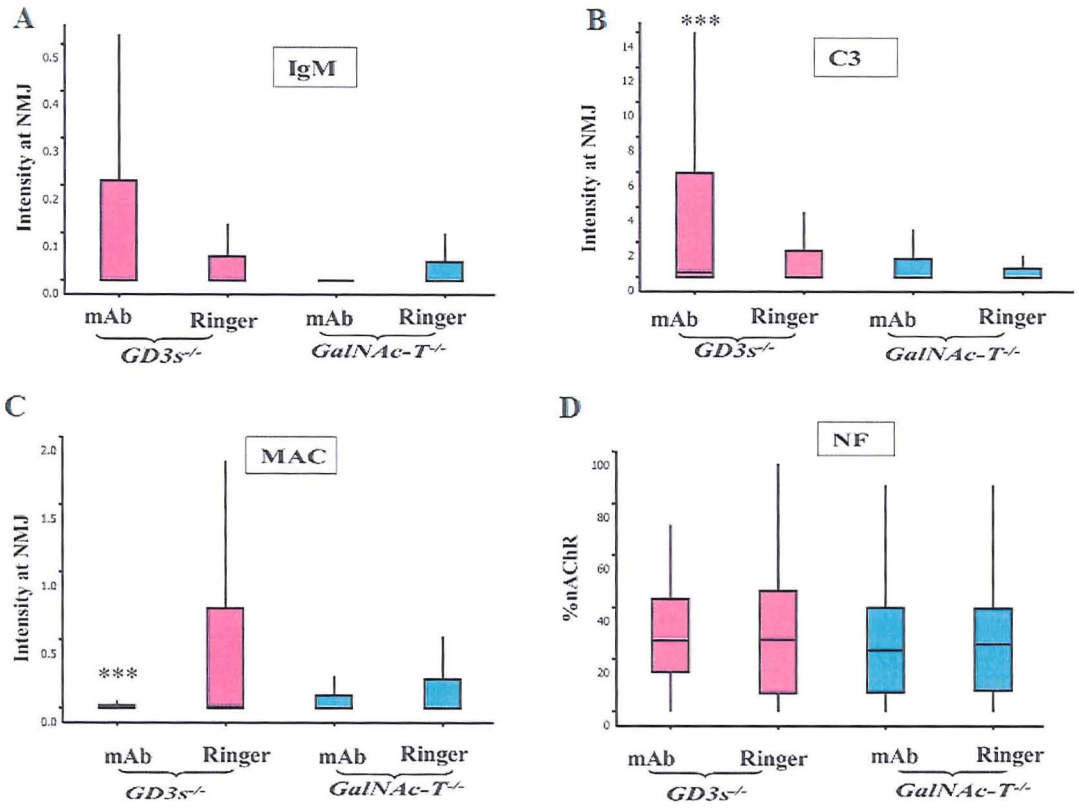

Fig 45. Do1 hemi-diaphragms showing IgM, C3 and MAC intensity over the NMJ, and percentage coverage of the NMJ by NF. Astrices indicate significance ($p<0.05$) compared to Ringer control. Note: the Intensity signal scale (for IgM, MAC and C3) is from 0 (baseline) to 255(saturation), and the axes of the graphs have been adjusted for clarity.

*IgM intensity (Fig 45A)

There was no significant difference in IgM deposition between mAb and Ringer treated tissue of either the GD3s$^{-/-}$or GalNAc-T$^{-/-}$ ($p=0.52$ and $p=0.18$ respectively).

*C3 Intensity (Fig 45B)

C3 deposition in the GD3s$^{-/-}$mAb treated tissue was significantly increased compared to Ringer control ($p<0.0001$), however these levels were only marginally above baseline. There was no significant difference between the mAb and Ringer treated tissue of the GalNAc-T$^{-/-}$ ($p=0.17$).

*MAC Intensity (Fig 45C)

Ringer treated tissue in the GD3s$^{-/-}$ had more MAC deposition than the mAb incubated ($p<0.0001$), indicating endogenous mouse IgG had been detected by the secondary antibody to MAC (anti-mouse IgG). It is also possible that there was a low level of endogenous MAC present in the tissue. There was no evidence of MAC deposition in the mAb treated tissue. In the GalNAc-T$^{-/-}$, Ringer and mAb incubated tissue did not differ significantly ($p=0.23$), indicating the signal represented endogenous mouse IgG.

*NF Coverage (Fig 45D)

There was no significant difference in NF signal between the Ringer treated and mAb treated tissue of the GalNAc-T$^{-/-}$or the GD3s$^{-/-}$ ($p=0.71$ and $p=0.68$ respectively), indicative of no axonal lesion.

Summary: Although there was significant C3 deposition in the GD3s$^{-/-}$ mAb treated tissue, the level was barely detectable above baseline with the microscope levels adjusted for maximal detection. No IgM or MAC was detected and there was no NF loss. Taken together, this indicates that Do1 does not bind the NMJ to cause a NF lesion.

4.2.2.2 Antibody Viability

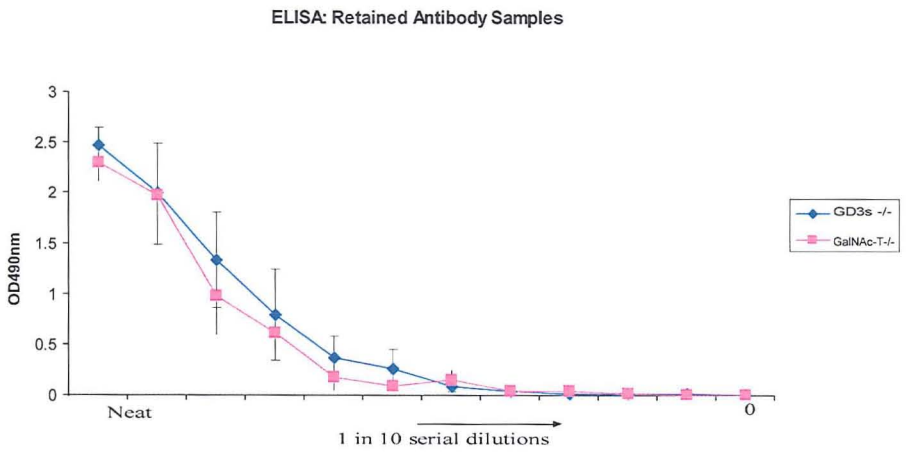

Fig 46. Retained Do1 samples.

4.2.2.3 *Do1 Ex-Vivo (TS)*

The hemi-diaphragm data indicated that Do1 was not binding to the epitope, yet the retained antibody bound well to GM1 on ELISA. To investigate this anomaly, Do1 was applied to the TS muscle of the GD3s$^{-/-}$ to localise antibody deposition (Fig 47 a). The TS muscle is thinner than the diaphragm, and facilitates better antibody accessibility.

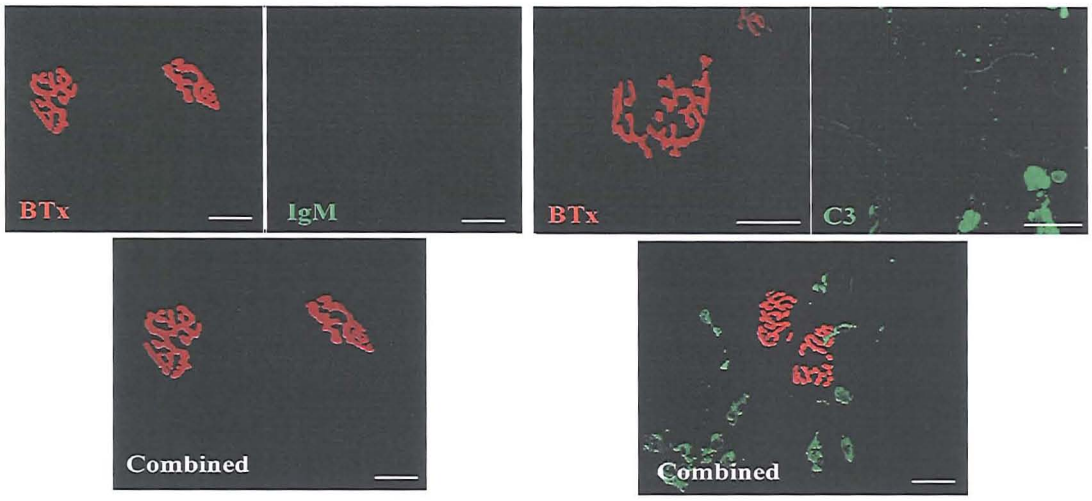

Fig 47 a), B) Fig 47b) Do1 did not bind to the NMJ in the GD3s$^{-/-}$ TS preparation. Fig 47 b) Do1 does not activate complement over the NMJ. Scalebar = 20μm

Do1 deposition was not detected over the NMJ, or in any other areas of the tissue such as the intramuscular nerve bundles and blood vessels. After antibody incubation, application of complement and staining for C3 revealed no C3 deposition over the endplate. As shown in Fig 47 b), scattered C3 positive cells were present throughout the tissue, although not specific for the NMJ. These are likely to be inflammatory cells, such as neutrophils, perhaps responding to inflammatory mediators in the complement source or chemokines (Kieseier *et al* 2002) This proves that the failure to detect bound mAb is not a failure of secondary antibody approach, as even weak levels of the IgM Do1 would fix complement.

4.2.3 Sm1 *Ex-vivo*

4.2.3.1 *Ex-Vivo :TS*

Sm1, like Do1, is an antibody cloned from human neuropathy sera. It was applied to the TS preparation of the GD3s$^{-/-}$to analyse IgM and C3 deposition over the NMJ (Fig 48).

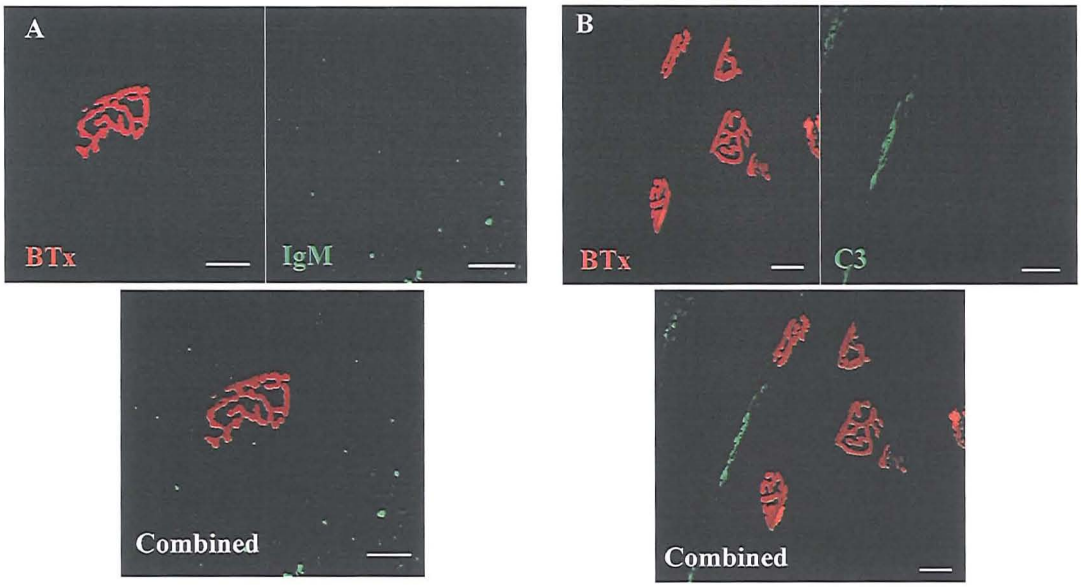

Fig 48. Sm1. A) IgM deposition is not detected over the NMJ, and B), SM1 does not activate complement in the *ex-vivo* GD3s$^{-/-}$ TS. Scalebar = 20μm

Results of the TS preparation were suggestive that SM1, much like Do1, was not binding to any area of the tissue, and not activating complement.

4.2.3.2 *IgM, C3, MAC, NF*

A pilot experiment (n=1) was done in the hemi-diaphragm of the GD3s$^{-/-}$ and its control, the GalNAc-T$^{-/-}$ (Fig 49).

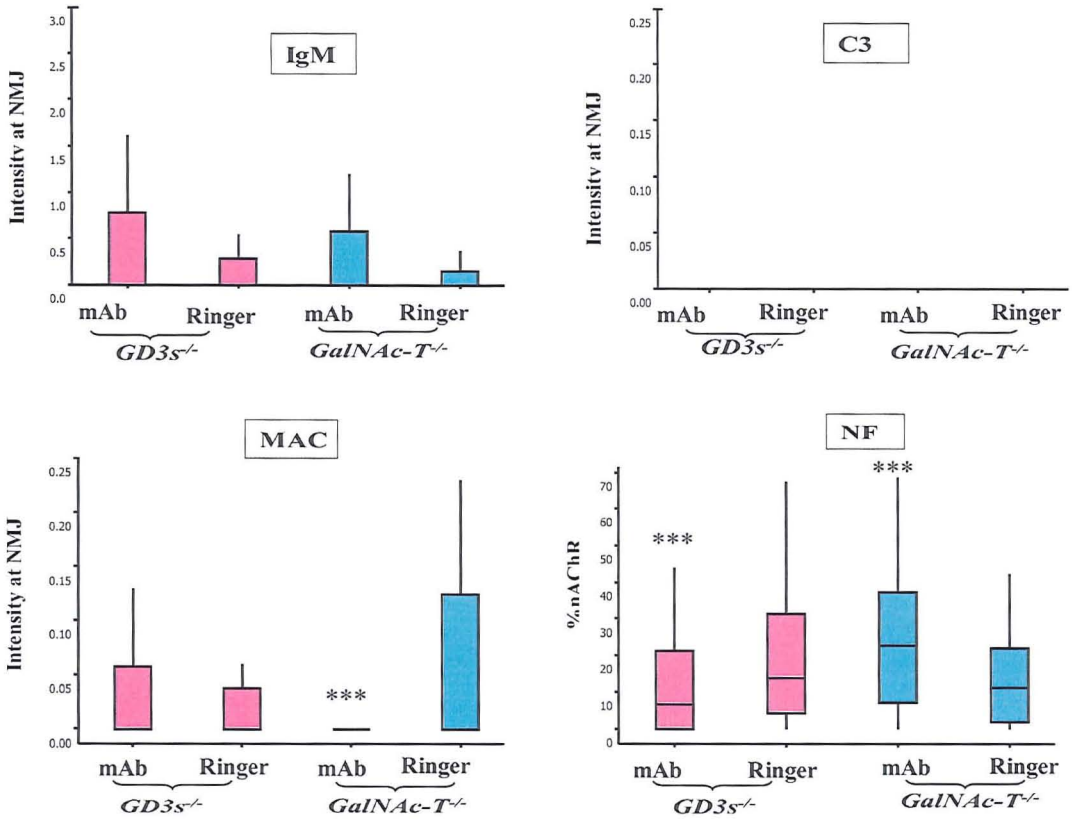

Fig 49. Sm1 hemi-diaphragms. Pilot study, n=1. Astrices indicate significance ($p<0.05$) compared to Ringer control. Note: the Intensity signal scale is from 0(baseline) to 255 (saturation), and the axes of the graphs have been adjusted for clarity.

*IgM intensity (Fig 49A)

For both the GD3s$^{-/-}$and GalNAc-T$^{-/-}$, there was no significant difference in IgM intensity between mAb and Ringer treated tissue ($p=0.33$, $p=0.40$ respectively).

*C3 Intensity (Fig 49B)

C3 intensity was below the level of detection, with no deposition in the GD3s$^{-/-}$ or GalNAc-T$^{-/-}$ mAb treated tissue compared to Ringer control ($p=0.79$ and $p=0.11$ respectively).

*MAC Intensity (Fig 49C)

There was no difference in MAC intensity between mAb and Ringer tissue of the GD3s$^{-/-}$ ($p=0.60$). Ringer control tissue of the GalNAc-T$^{-/-}$ had a greater MAC signal

than mAb treated ($p=0.03$), most likely as a result of background mouse IgG. It is important to note that this background signal, although significant, is negligible, as it is below 1 unit of fluorescence intensity on a scale of 0 to 255 units.

*NF Coverage (Fig 49D)

In the GD3s$^{-/-}$, there was a significant reduction in NF in mAb treated tissue compared to control ($p<0.0001$) with mAb treated tissue showing a reduction compared to control. The Ringer treated tissue of the GalNAc-T$^{-/-}$ had a significant loss of NF compared to the mAb treated ($p<0.0001$)

Summary: There was no evidence of IgM, C3 or MAC in the mAb treated tissue of the GD3s$^{-/-}$mouse. The loss of NF compared to the Ringer control can be attributed to degradation due to damage during manipulation of the diaphragm during the incubations and pinning out under tension. This is the most likely observation, as the Ringer treated tissue of the GalNAc-T$^{-/-}$had a similar NF loss, unlikely to be attributable to mAb mediated damage (as an anti-GM1 antibody should not bind in a mouse with no GM1).

4.2.3.3 *Antibody Viability*

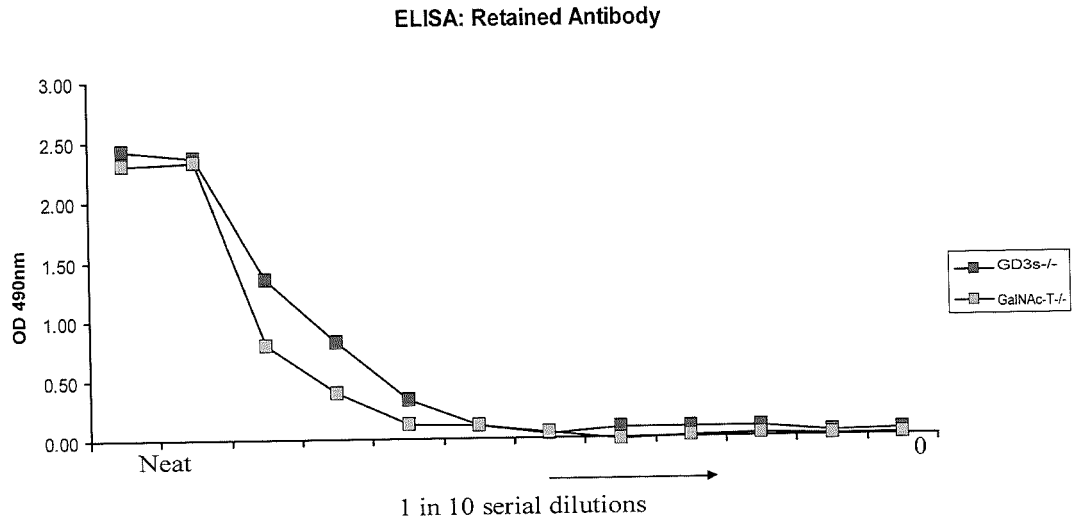

Fig 50. Sm1 from each incubation was equally viable.

4.2.4 *DG1*

The results of Do1 and Sm1 show an apparent discrepancy between the ability of the mAb to bind to GM1 in ELISA, compared to the living membrane. In order to address this, another mouse monoclonal antibody was utilised. DG1 is a mouse monoclonal monospecific for GM1, and should therefore bind specifically to GM1 in tissue, in a similar profile to CTb. DG1 binding can be detected topically (Chapter 3), and should represent the ideal candidate to induce an anti-GM1 antibody mediated attack on the peripheral nerve.

4.2.4.1 *CTb saturation of GM1: dilution curve*

DG1 is monospecific for GM1 on ELISA, and this was confirmed in tissue sections by blocking GM1 with CTb, i.e. inhibiting DG1 binding to confirm its specificity for GM1. An adequate amount of CTb was calculated by performing a dilution series in the GD3s$^{-/-}$, WT and GalNAc-T$^{-/-}$ (as a control). Using FITC conjugated CTb,

increasing doses were applied to the tissue until no difference in intensity over the endplate could be detected, indicating saturation.

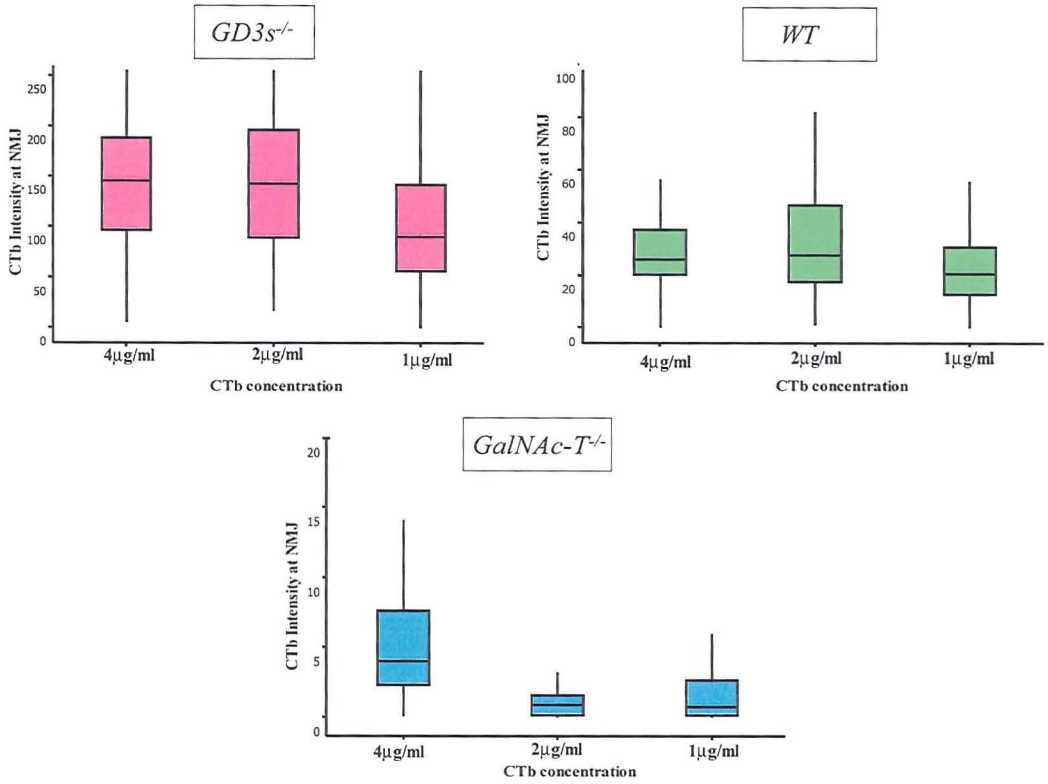

Fig 51. Calculating the saturating dose of CTb (FITC labelled, concentrations as indicated, diluted in PBS). Saturation was taken as the point where no significant difference ($p<0.05$) in CTb intensity could be detected between 2 concentrations.

In the GalNAcT$^{-/-}$, CTb did not bind and only background levels were detected by the microscope. At a dilution of 4µg/ml, the background was significantly higher than for the lower dilutions ($p<0.0001$), however there was no specific localisation in any area of the tissue, proving the background levels did not represent specific binding. In the WT and GD3s$^{-/-}$, a dilution of 2µg/ml gave a higher signal than 1µg/ml ($p<0.0001$). However, when comparing 2µg/ml and 4µg/ml no difference in signal intensity was evident ($p<0.0001$), indicating that saturation of GM1 by CTb had occurred at 2µg/ml. Thus the saturating dose of CTb in the GD3s$^{-/-}$ and WT was established at 2µg/ml (Fig 51).

4.2.4.2 *CTb inhibition of GM1*

Unlabelled CTb at the saturating dilution, or PBS alone, was applied to cryostat sectioned GD3s$^{-/-}$ and WT tissue at 4°C for 1.5 hrs. Following 3 rinses in PBS, DG1 was applied following the normal protocol, and detected with anti-mouse IgG2b.

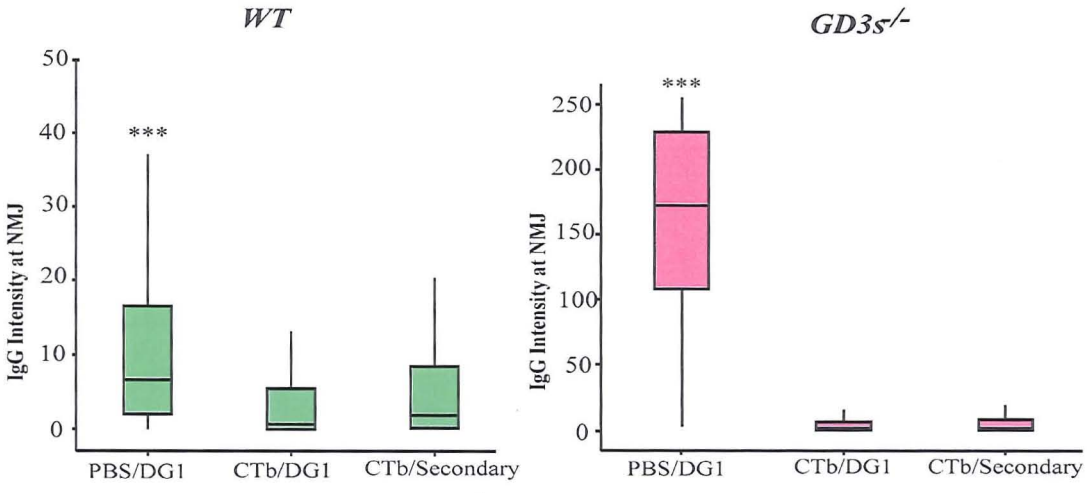

Fig 52. Application of the saturating dose of CTb and demonstration that it blocks DG1 binding. In both the WT and GD3s$^{-/-}$, DG1 binding was inhibited by CTb ($p<0.05$) and binding levels diminished to that of the negative control ($p<0.05$).

In the WT, the binding of DG1 to tissue pre-incubated in PBS alone was significantly higher that that of CTb blocked tissue ($p<0.0001$). For tissue incubated in CTb followed by PBS (as opposed to DG1) and secondary antibody, the IgG intensity overlying the endplate was higher that that of the CTb inhibited tissue ($p=0.01$), proving that any weak signal detected in the CTb blocked and DG1 incubated tissue was due to background. In the GD3s$^{-/-}$, DG1 in control (PBS) incubated tissue bound strongly compared to CTb blocked tissue ($p<0.0001$). CTb and DG1 incubated tissue had similar background levels to CTb tissue incubated in PBS and then secondary ($p=0.89$) (Fig 52). These data prove that the binding of DG1 can be inhibited by saturating endogenous GM1 with CTb.

4.2.4.3 *DG1 in the ex-vivo hemi-diaphragm*

The next question addressed was whether DG1 gives a similar biological readout in the *ex-vivo* hemi-diaphragm preparation as DG2 (ie. IgG deposition, complement activation and neurofilament loss) (Fig 53).

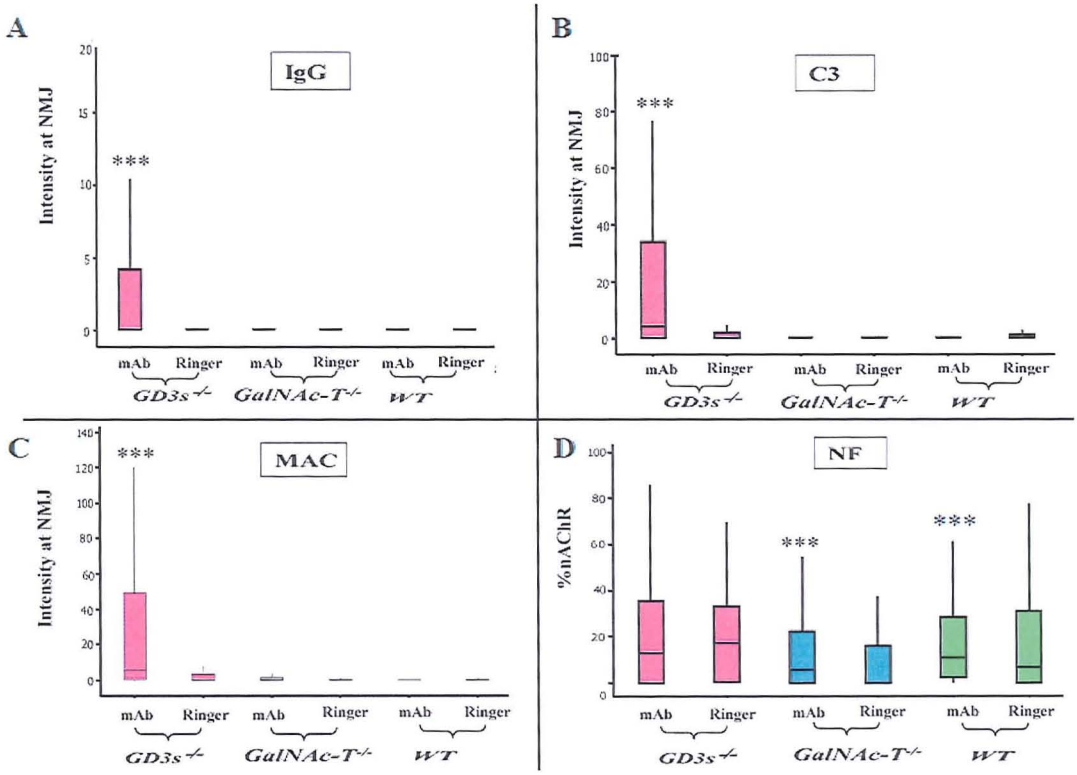

Fig 53. DG1 hemi-diaphragm preparations. Astrices indicate significance ($p<0.05$) compared to Ringer control. Note: the Intensity signal scale (for IgG, MAC and C3) is from 0 (baseline) to 255(saturation), and the axes of the graphs have been adjusted for clarity.

*IgG Intensity (Fig 53A)

There was no difference in DG1 deposition between mAb and Ringer treated tissue in the WT or GalNAc-$T^{-/-}$ ($p=0.05$, $p=0.26$ respectively). There was a significant increase in IgG in mAb treated tissue of the GD3$s^{-/-}$compared to Ringer control ($p<0.0001$).

*C3 Intensity (Fig 53B)

Only the GD3s$^{-/-}$ mAb treated tissue had a significant increase in C3 compared to Ringer control ($p<0.0001$). mAb and Ringer treated tissue of the WT and GalNAc-T$^{-/-}$ had no difference in C3 intensity ($p=0.05$, $p=0.17$ respectively).

*MAC Intensity (Fig 53C)

Again, only the GD3s$^{-/-}$ mAb treated tissue had a significant increase in MAC intensity compared to Ringer treated tissue ($p<0.0001$).

*NF Coverage (Fig 53D)

The GD3s$^{-/-}$ mAb and Ringer treated tissue had no significant difference in percentage coverage of the NMJ by NF ($p=0.37$). The WT mAb treated and Ringer treated tissue were not significantly different ($p=0.12$). The NF coverage of the mAb treated GalNAc-T$^{-/-}$ tissue was greater than the Ringer control, which was a significant difference ($p=0.02$).

Summary: In the GD3s$^{-/-}$ mAb treated tissue, IgG, MAC and C3 was significantly greater than in the Ringer tissue, indicating DG1 is binding. However, the detection settings of the microscope were maximal, and as shown in the graphs, the medians are all below 10 arbitary units (on a fluorescence intensity scale of 0 to 255). The lack of NF loss proves that DG1 is not binding to a biologically significant level, and is not able to induce a complement mediated lesion in the GD3s$^{-/-}$ hemi-diaphragm.

4.2.4.4 *Antibody Viability*

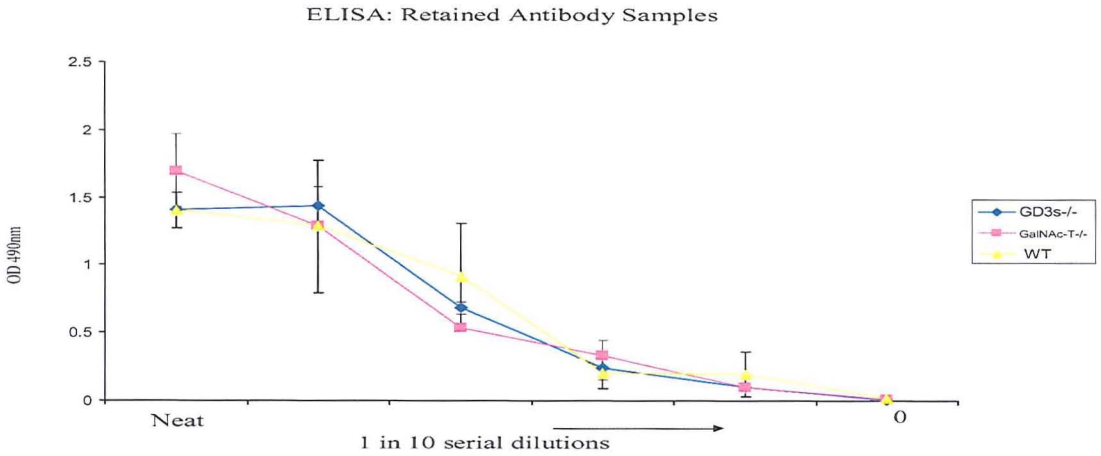

Fig 54. ELISA of retained DG1 samples

From the data, it is clear that DG1 is able to bind GM1 on ELISA, but not capable of inducing a complement mediated lesion in the murine peripheral nerve.

4.2.5 *Summary*

To summarise, out of 4 anti-GM1 antibodies tested in *ex-vivo* muscle preparations, only DG2 was shown to bind and induce a lesion. DG2 relies on the Gal(β1-3)GalNAc epitope of GM1, and this epitope is also available on the ganglioside GD1b. Thus, with specific emphasis on DG2, it was decided to investigate the possibility that DG2 may be cross-reacting with the Gal(β1-3)GalNAc epitope of GD1b.

4.2.5.1 *GD1b in the peripheral nerve: topical staining*

Before the binding of DG2 to GD1b can be hypothesised, the first point to clarify was the presence of GD1b in the peripheral nerve. Initially topical staining was done on 8μm cryostat sections of diaphragm, using the anti-GD1b antibody termed MOG 1.

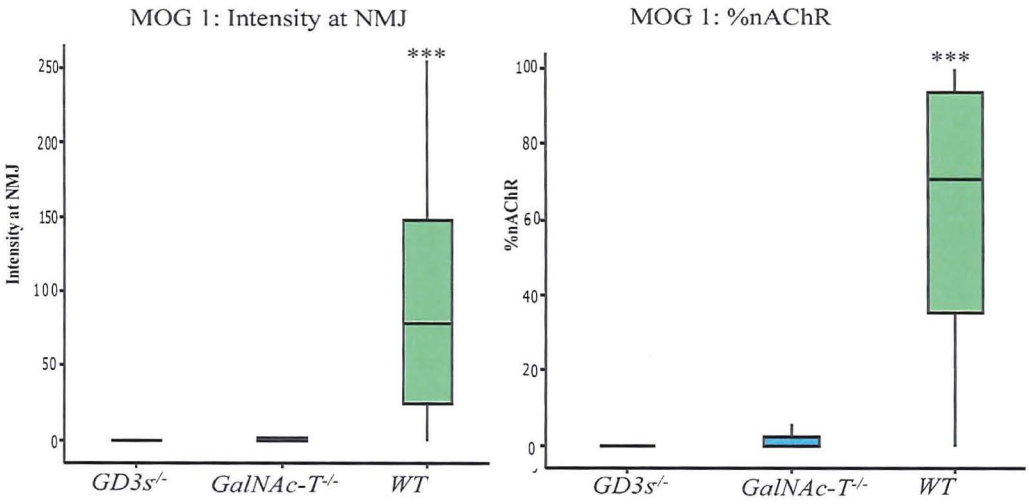

Fig 55. Topical staining of GD3s$^{-/-}$, GalNAc-T$^{-/-}$ and WT diaphragm sections with MOG 1. Astrices indicate significance ($p<0.05$) compared to GalNAc-T$^{-/-}$.

As shown in Figure 55, MOG 1 does not bind in the GalNAc-T$^{-/-}$ or GD3s$^{-/-}$ mouse. The binding intensity and area coverage of the NMJ is significantly greater in the WT when compared to the GalNAc-T$^{-/-}$ and GD3s$^{-/-}$ ($p<0.0001$). This data shows that in topical sections, GD1b in the WT mouse is available to MOG 1, and the lack of staining in the GalNAc-T$^{-/-}$ and GD3s$^{-/-}$ (which lack GD1b) proves MOG 1 is unlikely to be binding to another epitope.

4.2.5.2 *GD1b in the peripheral nerve: ex-vivo TS*

MOG 1 was applied to the living membrane in the TS preparation to profile the antibody distribution.

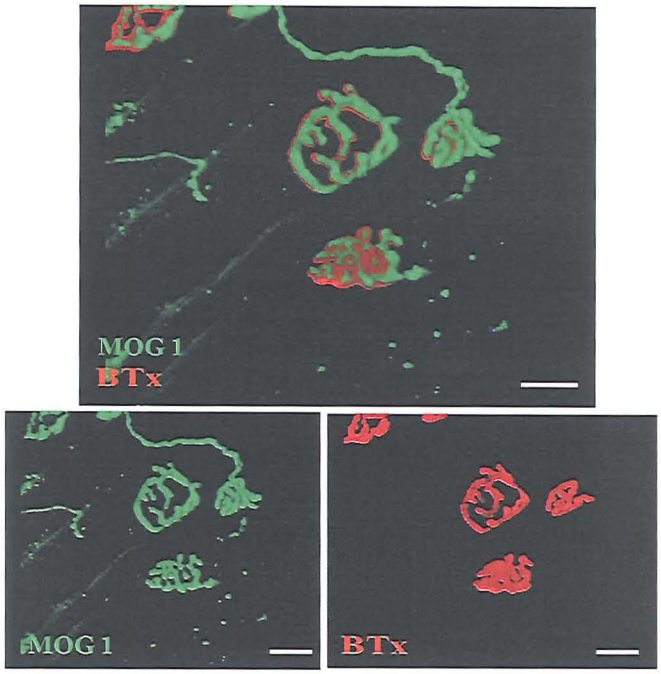

Fig 56. MOG 1 applied at 100μg/ml to the TS muscle in the WT mouse. FITC staining represents the MOG 1 profile, and over the NMJ, shown by BTx (red) and along the axon, MOG 1 staining is intense and uniform.

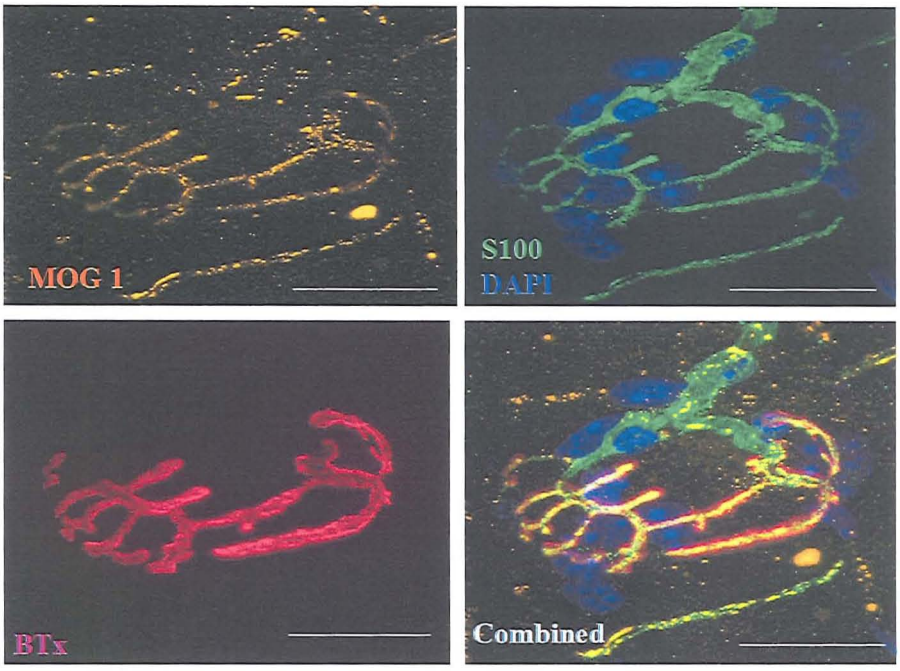

Fig 57. S100 staining (green) shows the pSC body and processes over the NMJ, which is stained with BTx (pink). Myelinating Schwann cells around the axon leading away from the NMJ are also stained with S100. Cell nuclei of the pSC and myelinating Schwann cell are shown with DAPI. MOG 1 staining profile (orange) appears specific to the axon and the staining profile does not overlap that of the pSC, indicating MOG 1 does not bind Schwann cells.

As shown in Figs 56 and 57, MOG 1 has a strongly neuronal staining profile, with staining of the axon over the NMJ and upstream of the NMJ. No staining of the PJF or pSC was apparent.

The intense staining of MOG 1 infers high levels of GD1b expression. However, MOG 1 is an IgG3 subtype, and these antibodies are known to aggregate (Kaminski *et al* 1999). Such aggregation can lead to "piggyback" binding (ie. non-specific and non functional binding of more than 1 IgG to the epitope). It cannot therefore be ruled out in the case of MOG 1, and such strong staining may be a result of piggyback binding. To address this, MOG 1 concentration was adjusted to 25μg/ml and applied in the same way to a TS preparation

As shown in Fig 58, the staining profile remained the same, suggesting that the intense signal seen with 100μg/ml is not due to aggregation of the antibody, and thus suggests GD1b is abundant in the mouse peripheral nerve.

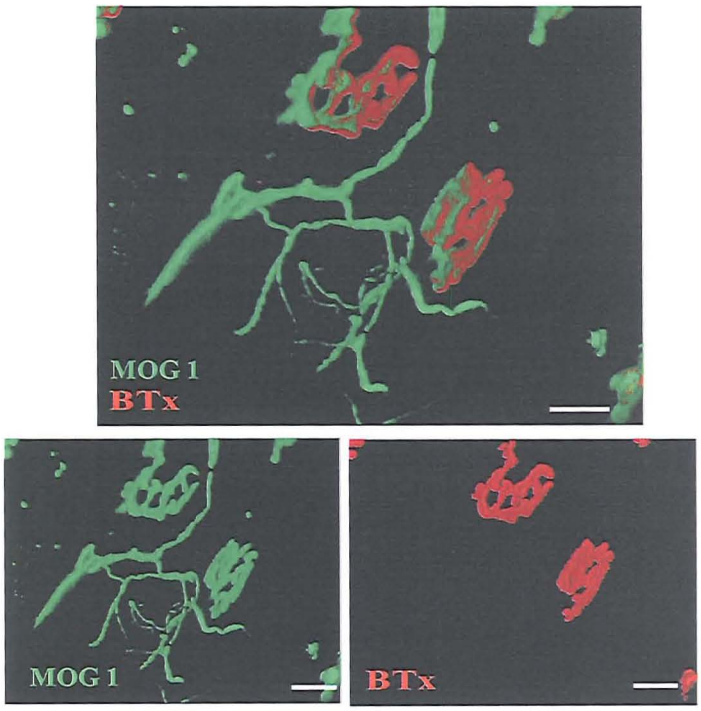

Fig 58. MOG 1 applied to the TS at 25μg/ml in the WT. Staining of the axon remained intense, ruling out the possibility that at higher concentrations the MOG 1 intensity is due to homophilic binding.

MOG 1 was also applied to the TS of the GD3s$^{-/-}$as a negative control. No binding was detected, again inferring that in live tissue MOG 1 is specific for GD1b. In WT hemi-diaphragm preparations, MOG 1 is able to induce a significant complement mediated lesion, data generated by J. Roxburgh.

4.2.5.3 *CTb inhibition of DG2: topical staining*

In a similar protocol to the DG1 inhibition, saturating CTb, or PBS, followed by the mAbs DG1, DG2 or MOG 1was applied to topical diaphragm sections from the GD3s$^{-/-}$, GalNAc-T$^{-/-}$ and WT mice. MAb or secondary antibody alone intensity was then analysed.

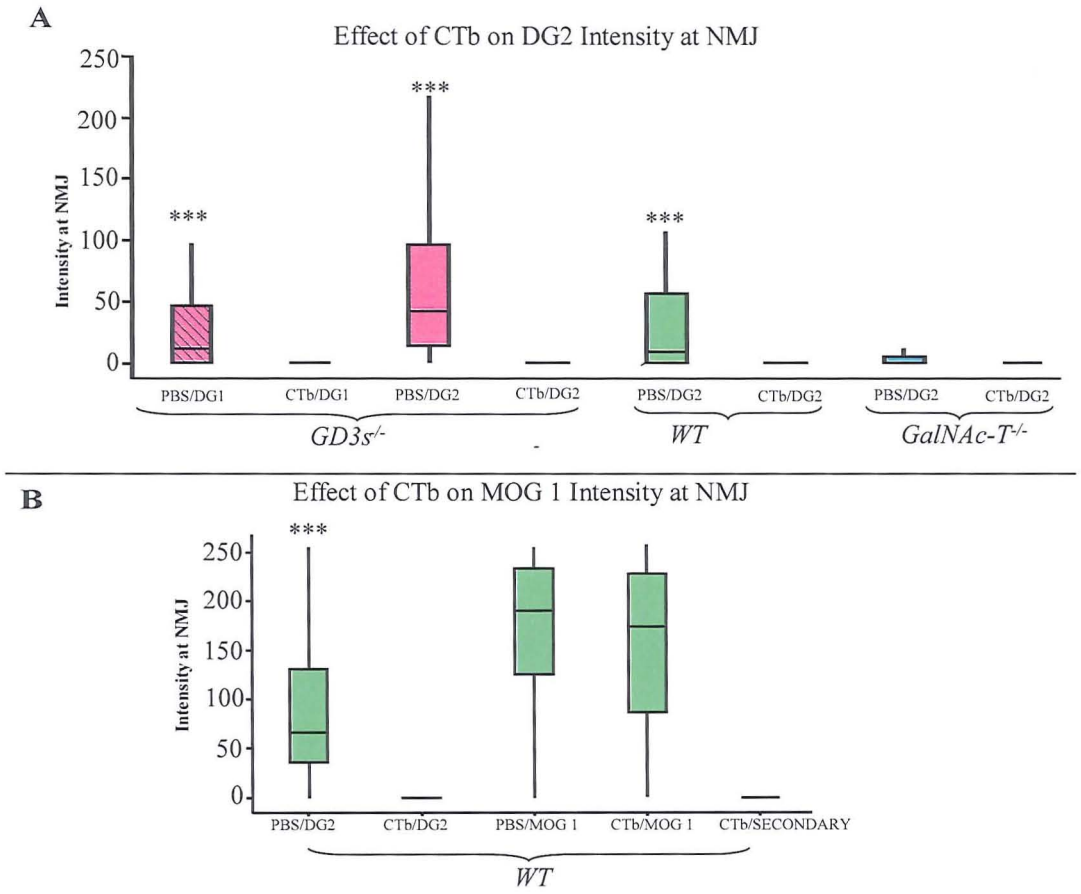

Fig 59 Effect of CTb block on MOG 1 and DG2 intensity at NMJs of topically stained diaphragm sections of GD3s$^{-/-}$, GalNAc-T$^{-/-}$ and WT mice. Astrices indicate significance compared to CTb blocked tissue ($p<0.05$).
A) DG1 (as a positive control) and DG2 binding in CTb incubated tissue was inhibited compared to control tissue ($p<0.05$). DG2 was also inhibited in the WT and

did not bind the GalNAc-T$^{-/-}$. B) DG2 was inhibited by CTb. CTb had no significant effect on MOG 1 binding intensity compared to control MOG 1 tissue ($p>0.05$).

As shown in Fig 59 (top panel), DG2 bound in GD3s$^{-/-}$ and WT tissue, with increased intensity in the GD3s$^{-/-}$ ($p<0.0001$). In both the GD3s$^{-/-}$ and WT, pre-incubation of the tissue with CTb inhibited binding when compared to PBS pre-incubated tissue ($p<0.0001$ for each strain). To confirm the CTb specificity for GM1, DG1 was applied to GD3s$^{-/-}$ tissue and was significantly inhibited by CTb compared to the control ($p<0.05$).

It is possible that CTb may bind other gangliosides in tissue (Blank *et al* 2007), an important consideration to address especially when using saturating amounts. To address this, the effect of CTb on MOG 1 binding was analysed. As shown in Fig 59 (bottom panel), CTb pre-incubation did not lead to a significant decrease in MOG 1 binding when compared to PBS pre-incubated control tissue ($p=0.08$). Again, control staining was done, this time using DG2, to confirm the success of the CTb block in this staining run. From these experiments it can be concluded that CTb does not inhibit the binding of DG2 by blocking the Gal(β1-3)GalNAc epitope on GM1 and GD1b, as CTb pre-incubation of the tissue allows MOG 1 to bind. From this, it can also be inferred that the binding of CTb to GM1 is not interfering with the ability of antibodies to access other epitopes, in this case GD1b.

4.2.5.4 *CTb inhibition of DG2: ex-vivo*

The above topical data was next demonstrated in the living membrane, with Fig 60 showing illustratively the ability of CTb to block DG1 binding. Microscope threshold levels were reduced to increase the ability to detect any weak DG2 binding. No

residual DG2 binding could be detected on the axon or PJF, indicating CTb had effectively saturated all GM1 and abolished DG2 from accessing the epitope.

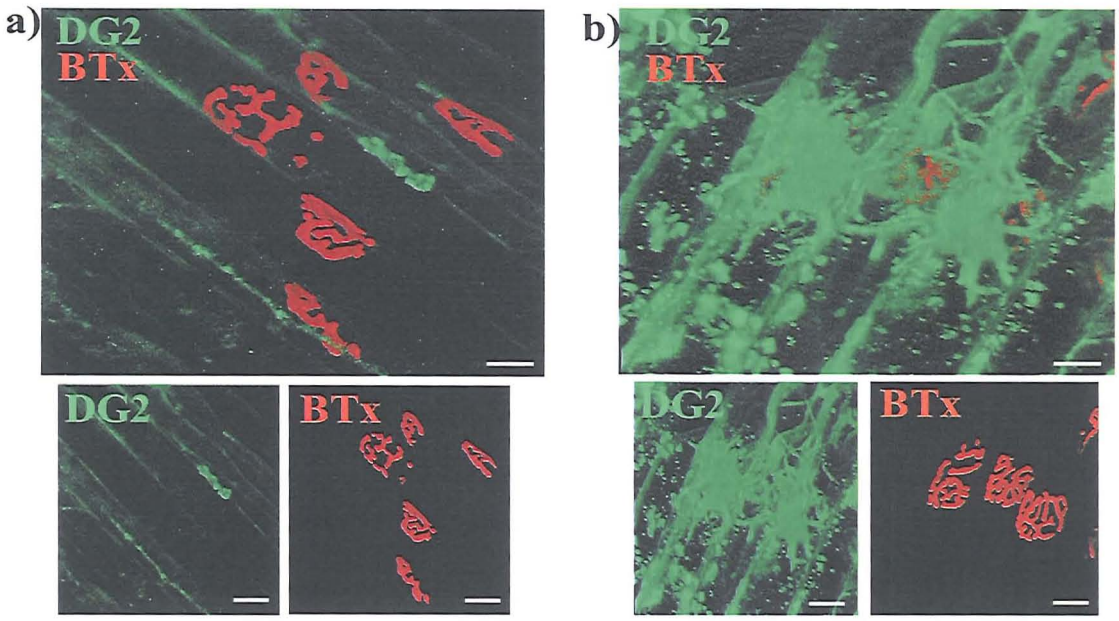

Fig 60. Effect of unlabelled CTb on the ability of DG2 to bind in the living membrane. a) unlabelled CTb abolishes the binding of DG2: note the absence of the FITC signal. b) Control (Ringer treated) tissue followed by incubation of DG2 results in a strong FITC signal representing strong binding of DG2 to GM1 to the axon and PJF.

4.3 Discussion

This chapter demonstrates the viability of the *ex-vivo* hemi-diaphragm muscle nerve preparation in modelling the pathological changes induced by anti-GM1 antibodies. Tissue can be kept viable during the duration of the incubations, and tissue conveniently cryostat sectioned to look in parallel at IgG deposition, complement activation and NF destruction. Furthermore, the use of NHS is an ideal method of "humanising" the system, and relating it to the clinical condition.

The success of DG2 in causing complement mediated destruction of the peripheral nerve proves that the GD3s$^{-/-}$mouse optimises the lesion when antibodies are applied

to live tissue. Thus, the GD3s$^{-/-}$ is the ideal mouse in which to design an *in-vivo* model of anti-GM1 mediated neuropathy.

DG2 binding to GM1 expressed on the axon leads to the deposition of MAC pores, and subsequent calpain induced destruction of the NF which leads to paralysis, most likely in a manner similar to that of other anti-ganglioside antibodies with a known alpha-latrotoxin like effect at the NMJ (O'Hanlon et al 2001, Goodfellow *et al* 2005). An interesting and somewhat novel feature of this antibody is its ability to kill the PJF (Goodfellow, unpublished observations). Loss of NF is likely to be the main feature in AMAN, where paralysis is a result of axonal destruction, and it is thus difficult to determine how loss of the PJF can contribute to the direct pathology of AMAN. Instead, it is attractive to speculate that its loss may hinder recovery and regeneration of the axon, where in its normal state it may provide trophic support or guidance to regenerating axons. Little is known about this cell type, and while a potential role in regeneration is a highly topical subject, the timescale of this thesis does not lend itself to a thorough investigation of the cell. Proof that DG2 is not binding to GD1b via the common Gal(β1-3)GalNAc epitope confirms that it is binding GM1 on both the axon and the PJF.

It was of interest that GD1b could be detected in the peripheral motor nerve, and an anti-GD1b antibody could cause a lesion. Anti-GD1b human neuropathies spare the motor fibres and are specific for the sensory nerves (Willison and Yuki 2002), and it is logical to assume that this is due to absence or low levels of GD1b in the motor system. Data from this chapter highlights that there is an enrichment of GD1b in the murine peripheral nerve, which is open to antibody mediated attack via anti-GD1b antibodies. This finding suggests there may be a difference in the GD1b expression

profile between human and mouse nerves, or that in humans, GD1b in the motor system is cryptically masked from antibodies.

Having demonstrated the ability of an anti-GM1 antibody (DG2) to bind and cause a lesion, it was surprising that 2 antibodies cloned from human neuropathy sera did not have an effect. It is, of course, possible that these antibodies were not responsible for pathogenesis, but still lies the conundrum that they bind to GM1 strongly by ELISA, yet do not bind it when applied to tissue (*ex-vivo* TS). This phenomenon was reproduced by the mouse monoclonal, DG1. The DG1 characterisation experiments add a new dimension however, as Chapter 3 proves they are able to bind well topically (ie. to dead tissue) and on ELISA, but not to live tissue. One possible explanation is that certain anti-GM1 antibodies such as DG1 are internalised and cause pathology upstream of the NMJ. For example, in AMAN they may be taken into the ventral horn and exert a cytotoxic effect. To test this, the antibodies could be injected (passive transfer) to the mouse, and the ventral horn removed to determine if the antibody had been internalised (Fabian and Petroff 1987, Fabian 1988). The second possibility is that the antibodies are simply not able to bind GM1 in the living membrane. This links to the observation that anti-GD1b antibodies are specific for human sensory nerves, yet in the mouse GD1b is abundant in the motor nerves. As mentioned previously, it is also possible that GD1b in the human motor nerve cannot be bound by human anti-GD1b antibodies, similar to the DG1 and GM1 observation in this chapter.

Chapter 5

5.1 Introduction

The results of chapter 4 demonstrated that the ability of antibodies, such as DG1, to bind their epitope (in this case GM1) on an ELISA plate does not infer that they are able to bind it in the living membrane. DG1 can bind GM1 in topical (ie. dead, cryostat cut tissue), but its inability to bind it in living tissue indicates that there are differences in the presentation of the epitope. On the same note, DG1 and DG2 both bind well to sulfatide on ELISA (Townson *et al* 2007) yet not in tissue (whether cryostat cut or living tissue). It has been suggested that fixation of tissue allows antibodies to bind (Quattrini *et al* 1992). It is an interesting notion that fixations can allow an antibody to bind: fixation must somehow disrupt the membrane structure and exposing an otherwise unavailable epitope. The sulfatide binding antibody DG2 was analysed to determine if it could be induced to bind sulfatide via fixation, and in the case of DG1, to see if GM1 binding could be established.

5.2 Results

5.2.1 *Effect of Tissue Fixation on Sulfatide Binding (DG1 and DG2)*

Sulfatide over-expressing (CST) and sulfatide deficient ($CGT^{-/-}$) nerves were cut onto slides (as described in materials and methods) and various fixation techniques tried (based on Quattrini *et al* 1992), with 3 slides analysed per fixation:

- Freezing ethanol (EtOH) (-20°C) for 10 minutes
- EtOH at RT for 10 minutes
- 4% PFA (RT) for 10 minutes

Fix was rinsed off 3X in PBS, and the GM1 epitope blocked using unlabelled CTb for 1.5 hrs at 4°C, then rinsed off in PBS. DG2 was applied for 2 hours at 4°C prior to rinsing and application of anti-mouse IgG3 secondary for 3 hours at 4°C. Negative

controls were performed by substituting DG2 for PBS, and adding secondary as normal. The $CGT^{-/-}$ mouse was a negative control: any increase in DG2 binding in this mouse indicates DG2 is binding to another epitope (and not sulfatide) after fixation.

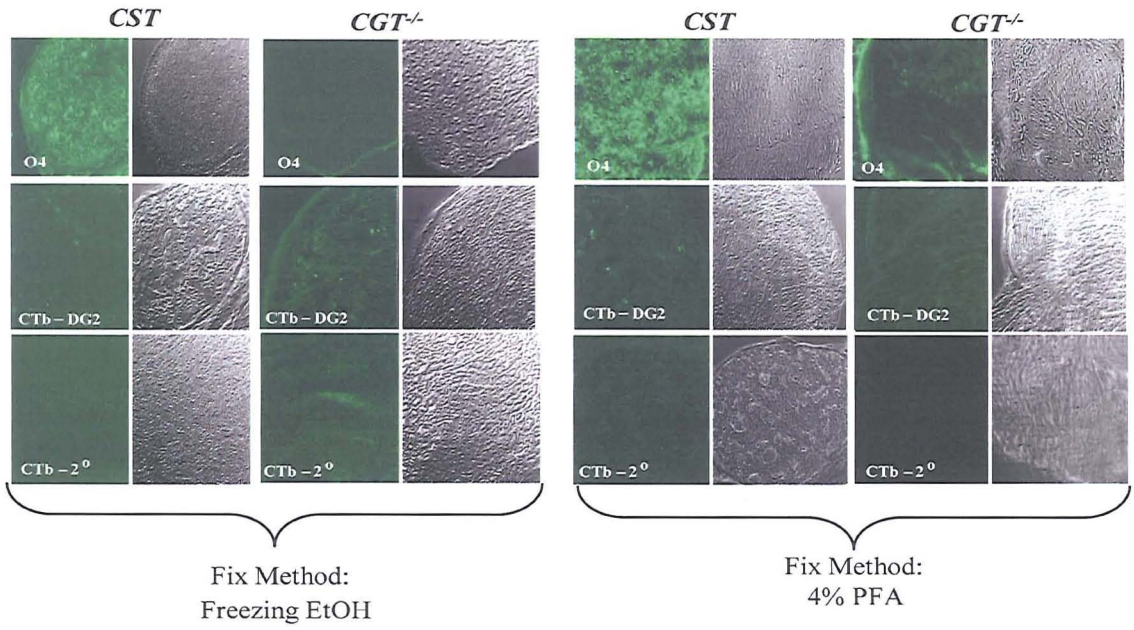

Fig 61: Effect of tissue fixation on epitope presentation. O4 (top panel) bound to sulfatide under both conditions of fixation in the CST nerve. Freezing EtOH and 4%PFA fixation did not result in DG2 binding to sulfatide. EtOH = ethanol and PFA = paraformaldehyde.

None of the tested fixation methods affected the binding of the anti-sulfatide antibody O4 (Fig 61), indicating the fixations had not altered the antigenic properties of sulfatide to antibody binding. DG2 remained unable to bind sulfatide in the CST nerve, where background FITC staining was comparable to that of the negative control tissue (PBS followed by anti-mouse IgG3). Fixing the tissue in EtOH at RT gave the same result as freezing cold EtOH. The $CGT^{-/-}$ tissue remained negative for both O4 and DG2 binding throughout, due to no sulfatide expression in this strain.

5.2.2 *Effect of fixation on GM1 availability to DG1 (Pilot study, n=1)*

Whole mount TS was incubated firstly in BTx, then fixed in a variety of ways for 20 min:

*Freezing EtOH
*Freezing Acetone
*4% PFA at RT
*PBS (ie. control unfixed)

DG1 was applied (to rinsed tissue) at 4°C for 2 hours and rinsed, followed by detection with anti-mouse IgG2b overnight.

Analysis of the tissue showed 4% PFA and freezing EtOH did not facilitate DG1 binding. Acetone treatment resulted in a neuronal, but patchy pattern of DG1 binding over the NMJ, which was not apparent in the PBS incubated (ie.unfixed) tissue ($p<0.0001$). Omitting addition of DG1 to acetone fixation prior to incubation in anti-mouse IgG2b did not result in any staining, ruling out possible non-specific binding of the secondary antibody (Fig 62).

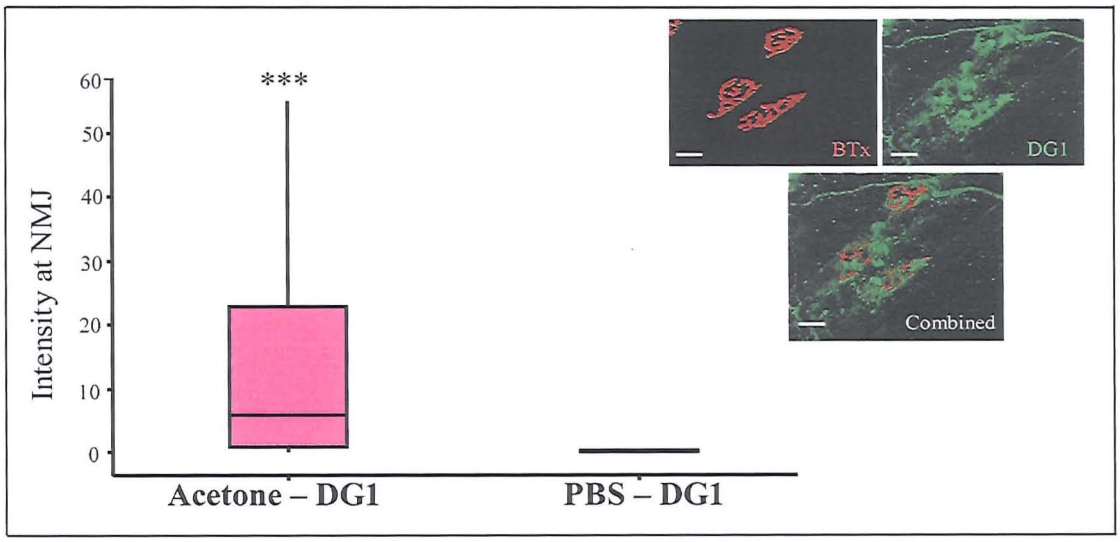

Fig 62. Effect of acetone treatment on DG1 binding. n=1 animal. Graph shows semi-quantitative analysis of DG1 deposition in acetone treated tissue compared to control. Astrices indicate significance compared to control ($p<0.0001$). Inset: DG1 binding profile following acetone treatment appears neuronal and over the NMJ.

This pilot study demonstrates that agents such as acetone are able to expose epitopes – possibly resulting from removal of membrane components which may be 'hiding' GM1.

5.2.3 *Demonstation of GPI anchored proteins masking gangliosides*

Gangliosides reside in lipid rafts, so it was hypothesised that any potential masking may be due to another raft component. The first line of investigation was GPI anchored proteins, which may act as "umbrellas" in shielding gangliosides. Phosphatidylinositol-specific phospholipase C (PI-PLC) is an enzyme commonly used to release GPI anchored proteins from the cell surface by cleaving the GPI anchor. For example, PI-PLC releases the GPI anchored glycoprotein Thy 1 from the membrane (Kukulansky *et al* 1999), which is abundant in neuronal cells (Campbell *et al* 1981).

PI-PLC treatment was firstly established in the PC12 cell line: this neuronal cell line expresses gangliosides (Walton *et al* 1988), and is known to have GPI anchored proteins such as Thy 1 (Kukulansky *et al* 1999). Use of a cell line was chosen to increase the efficiency of the study: cells were easy to treat, and analysed via FACS to give high sample numbers in a relatively short space of time. To establish the PI-PLC protocol at the NMJ for a variety of antibodies would have used a considerable quantity of reagents and animals to achieve significant *n* numbers.

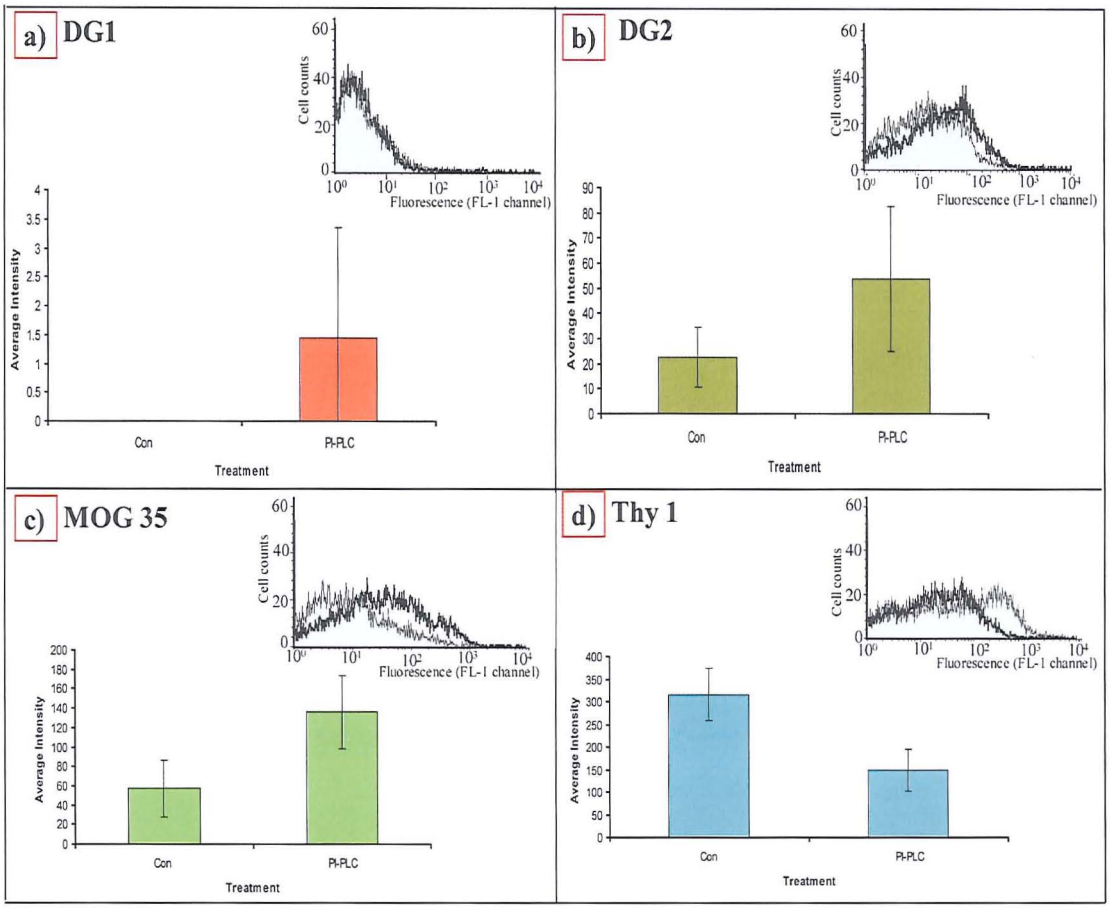

Fig 63. The effect of PI-PLC on antibody intensity in PC12 cells. Inset are representative examples of the FACS histogram plots, with the shaded curve showing the fluorescence of the untreated cells and the heavy dark line showing the shift in fluorescence for the PI-PLC treated cells.

DG2, MOG 35 (anti-GD1a mAb) and Thy 1 PI-PLC treated cells are all significantly different compared to control cells ($p<0.05$), but no significant difference was detected for DG1 ($p>0.05$).

Results are shown in Fig 63. Confirmation that PI-PLC removed a significant proportion of GPI anchored proteins is shown by the decrease in antibody binding to Thy 1. Further abolition of Thy 1 required increased concentrations or incubations of the PI-PLC enzyme, which led to death of the majority of cells. As inferred from the ability of DG1 to bind dead as opposed to live tissue, dead cells would have added an unfair variable to the experiment and it would not have been conclusive whether differences in mAb binding were due to disrupted membranes as a result of death, or

due to specific removal of GPI anchored proteins. Both MOG 35 and DG2 binding were increased in PI-PLC treated cells when compared to control, indicating that removing GPI anchored proteins from rafts is exposing more ganglioside or allowing better antibody accessibility.

5.2.4 *GPI anchored protein removal at the NMJ*

GPI anchored proteins are present at the NMJ, for example the complement regulator CD59, as shown in Fig 64.

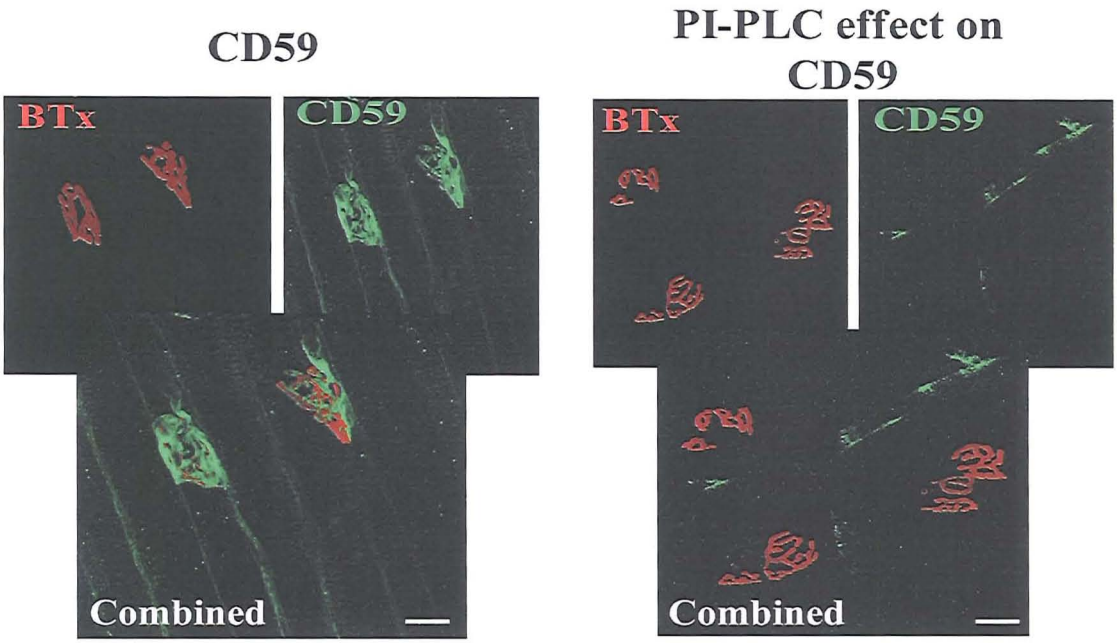

Fig 64. CD59 staining in the WT TS. Left panel shows the normal profile of CD59 at the NMJ. Staining is strongly associated with the NMJ. As seen on the right, pre-treatment of the tissue with PI-PLC abolished CD59 immunostaining, indicating the enzyme has cleaved the GPI anchor of CD59 and released it from the neuronal membrane. Anti-CD59 mAb was used at 1:750 in Ringer for 1 hour at 32°C. The secondary antibody is anti-mouse IgG1-FITC, used at 1:300. mAb is courtesy of Dr BP Morgan, University of Cardiff.

It is hypothesised that removal of GPI anchored proteins from the NMJ will have a similar effect as that demonstrated in the PC12 cell: i.e. GPI anchored protein removal may enhance the binding of certain mAbs to gangliosides.

A useful point to consider is the "nodal staining" observations of an earlier PhD student, John Goodfellow. Mice lacking in complement regulators (the DAF1$^{-/-}$, CD59a$^{-/-}$ and CD59a$^{-/-}$/DAF1$^{-/-}$) had differences in nodal staining profiles using MOG 35 (unpublished results). The following hypothesis was generated: differences in the profile of MOG 35 staining may be due to the removal of GPI anchored proteins, such as DAF1 and CD59a. This would lend weight to the theory that gangliosides can be sterically hidden by other membrane components. The complement regulator KO mice are ideal candidates to further advance this study at the NMJ, as it allows analysis of the removal of specific proteins and the subsequent effect on antibody binding at the NMJ. Antibodies were applied to the *ex-vivo* hemi diaphragm preparation, followed by a source of complement, and the differences in antibody deposition at the NMJ analysed. Activation of complement leading to MAC and NF loss were taken as evidence that the enhanced binding was contributing to a pathological lesion.

5.2.5 *MOG 35 binding to mice lacking GPI anchored complement regulators*

Initial experiments were done in complement regulator KO mice with normal ganglioside profile to firstly address the effect of the GPI protein removal. In these mice it is also more likely that their lipid rafts are normal, as the increased ganglioside content of the membrane in the GD3s$^{-/-}$ may have a detrimental effect on the structure of the raft (Crespo *et al* 2002). Experiments were then performed on GD3s$^{-/-}$ to determine whether the combination of GPI anchored protein removal and increased ganglioside expression can enhance epitope availability.

5.2.5.1 *MOG 35 Optimal Concentration*

MOG 35 is a potent antibody in the induction of complement mediated NF loss in the $GD3s^{-/-}$ (Goodfellow *et al* 2005). A dilution series was performed to establish a concentration adequate to produce an effect, but not causing total destruction of NF, as this would render it impossible to distinguish differences between each strain tested (refer to Fig 65):

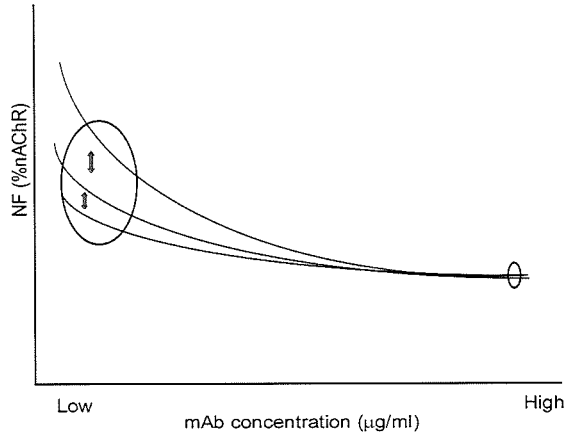

Fig 65: Concentration of MOG 35 should be adequate to produce a lesion, but at the end of the scale where varying severities of lesion are distinguishable.

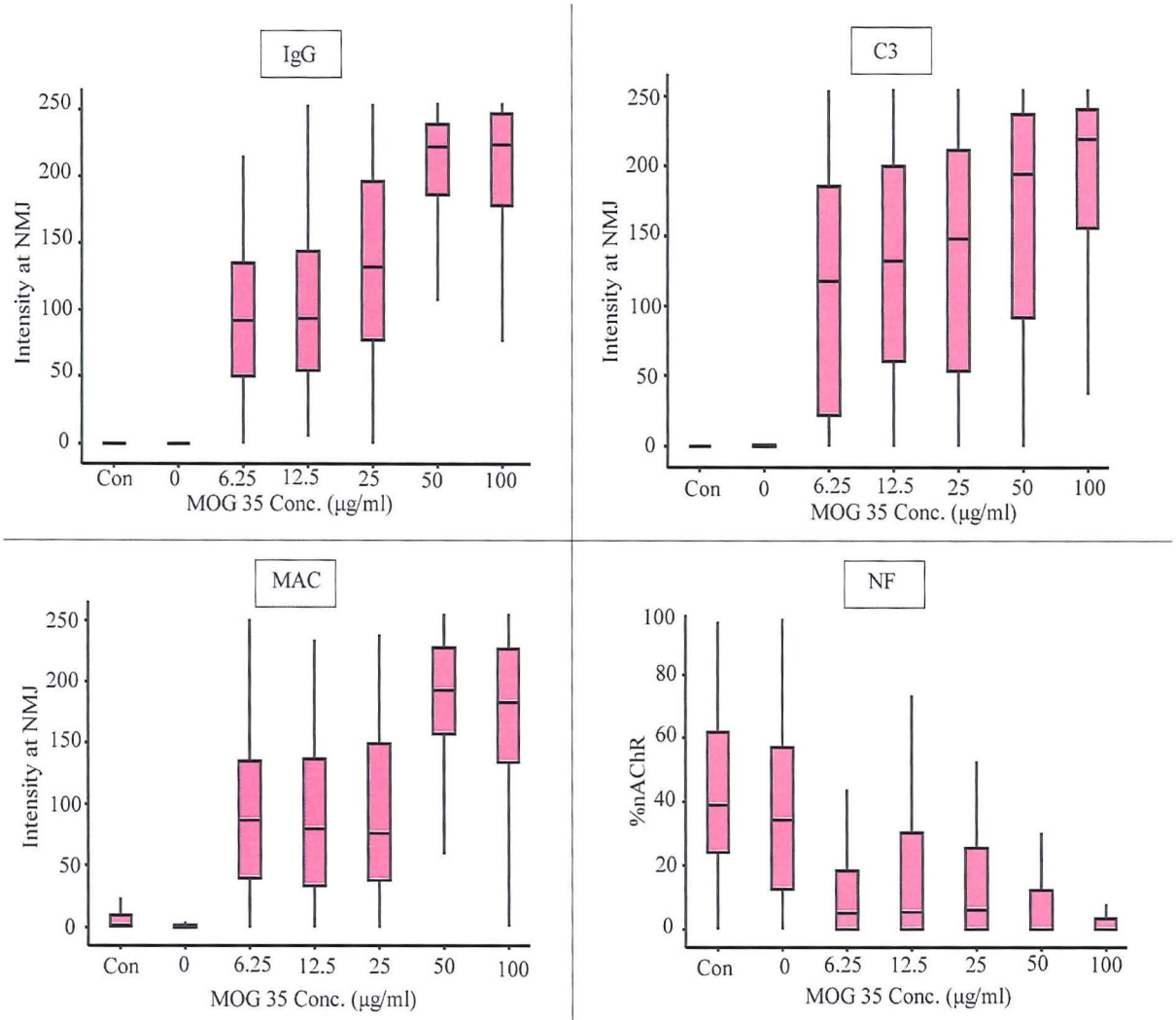

Fig 66. MOG 35 dilution series in GD3s$^{-/-}$ hemi-diaphragm. n=1. Differing dilutions of mAb were used, and IgG, C3 and MAC intensity over the NMJ analysed. Axonal integrity was analysed based on NF coverage of the endplate.

Analysis of the dilution series tissue compared the IgG, C3 and MAC deposition in addition to NF loss, for doubling dilutions of antibody, ranging from 6.25µg/ml to 100µg/ml and including a Ringer control. 3 GD3s$^{-/-}$ mice in total were used, with each mouse providing 2 hemi-diaphragms: a different dilution was tested per hemi-diaphragm. For each mouse, a portion of diaphragm was immediately removed and snap frozen, and tissue analysed to ensure that the baseline levels (ie. endogenous levels of IgG, C3, MAC and NF) from each mouse did not vary and affect the results of the dilution series.

As shown in each graph, the baseline levels (ie. untreated tissue) were comparable to Ringer control tissue ($p<0.0001$), indicating that the "starting point" of analysis for each dilution was equal.

NF levels were calculated as a percentage of the untreated control. Ringer control tissue showed no significant loss of NF ($p<0.0001$), with all other dilutions showing significant NF loss compared to the untreated control ($p<0.0001$). mAb concentrations of 50 and 100μg/ml showed a similar level of damage ($p=0.10$). At more dilute doses of 12.5 and 6.25μg/ml the lesion was less severe. 6.25μg/ml of mAb is the ideal dilution at which to cause a significant but milder lesion when compared to all other dilutions except 12.5μg/ml where the lesion is milder than at 6.25μg/ml. However the NF loss at 12.5μg/ml does not fit the overall linear trend (shown in Fig 66), and is possibly due to natural "wobble" which would be eliminated with further experimental repeats.

Based on the NF data, analysis of the IgG, C3 and MAC intensity for 6.25μg/ml was compared to the baseline control and 100μg/ml of mAb (where intensity is assumed maximal). For IgG, C3 and MAC, at 6.25μg/ml the intensity is higher than that of the untreated (and Ringer treated) controls ($p<0.0001$) and less than that of 100μg/ml ($p<0.0001$).

In summary, 6.25μg/ml is sufficient to cause a lesion, but the mild nature of the lesion compared to that induced by the higher concentrations means any enhancement caused by the removal of complement regulators should be detectable.

5.2.5.2 *MOG 35 @ 6.25µg/ml: CD59a$^{-/-}$ /DAF1$^{-/-}$ and WT*

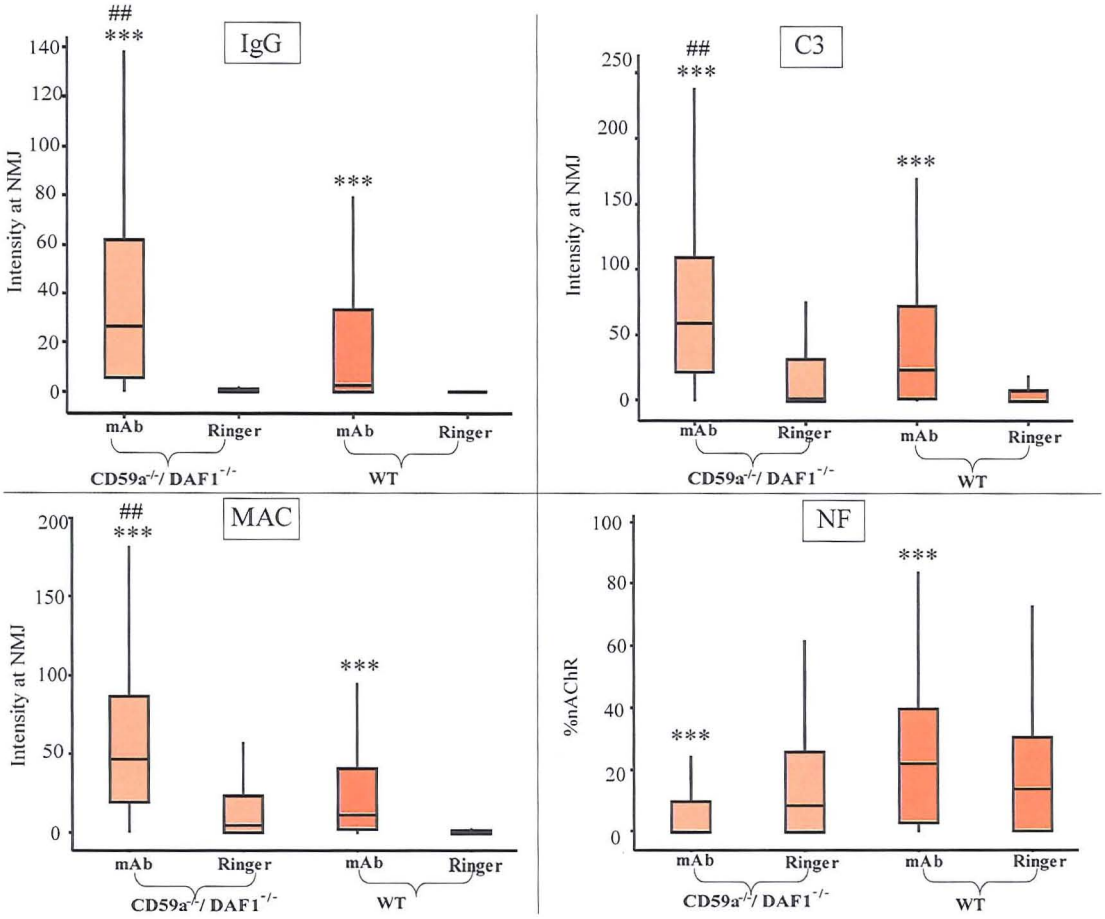

Fig 67. Graphical overview of MOG 35 in the CD59a$^{-/-}$/DAF1$^{-/-}$ and WT. Astrices indicate significance compared to Ringer control ($p<0.05$) and hash symbols indicate significance compared to WT.

IgG Intensity

Both strains had significantly greater IgG deposition compared to the Ringer control ($p<0.0001$). The CD59a$^{-/-}$/DAF1$^{-/-}$ mAb treated tissue had more IgG deposition at the NMJ compared to the WT ($p<0.0001$).

C3 Intensity

C3 deposition was increased when compared to Ringer control ($p<0.0001$) for both strains, and again the C3 intensity was greater for the mAb treated tissue of the CD59a$^{-/-}$/DAF1$^{-/-}$ when compared to the WT ($p<0.0001$).

MAC Intensity

MAC intensity was significant ($p<0.0001$ compared to Ringer control), and again MAC was strongest in the mAb treated tissue between the CD59a$^{-/-}$/DAF1$^{-/-}$ and WT ($p<0.0001$).

NF Coverage

No NF lesion was detected in the WT mAb treated tissue: in fact the mAb treated tissue had more NF coverage of the NMJ when compared to Ringer treated tissue ($p<0.0001$). In the CD59a$^{-/-}$/DAF1$^{-/-}$ however, there was a reduction in NF coverage, which is significant when compared to the CD59a$^{-/-}$/DAF1$^{-/-}$ Ringer treated tissue ($p<0.0001$) and also the WT mAb treated tissue ($p<0.0001$).

Summary

IgG, C3 and MAC intensity are increased in the CD59a$^{-/-}$/DAF1$^{-/-}$, which also has the most apparent NF lesion when compared to the WT. For all incubations, the viability of the antibody was comparable (Fig 68).

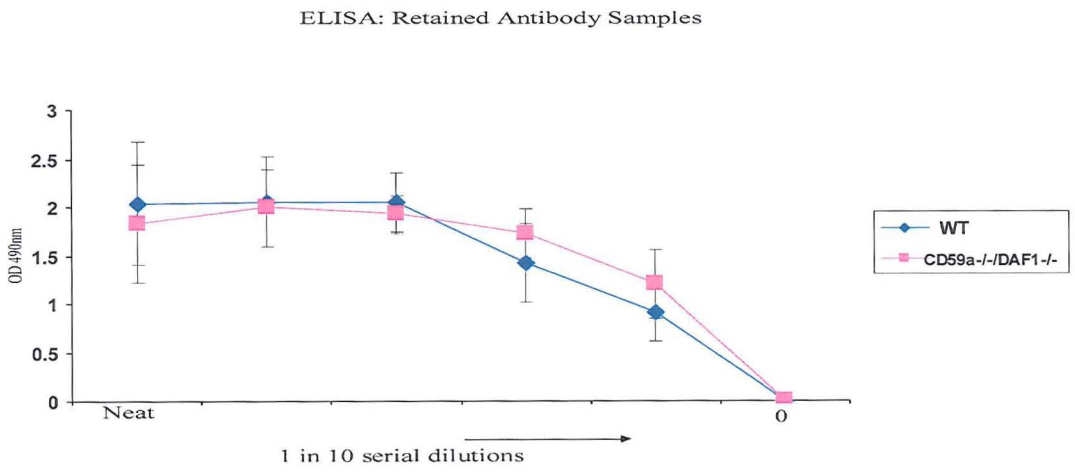

Fig 68: Antibody viability

5.2.5.3 *MOG 35 @ 6.25μg/ml: CD59a$^{-/-}$, DAF1$^{-/-}$ and WT*

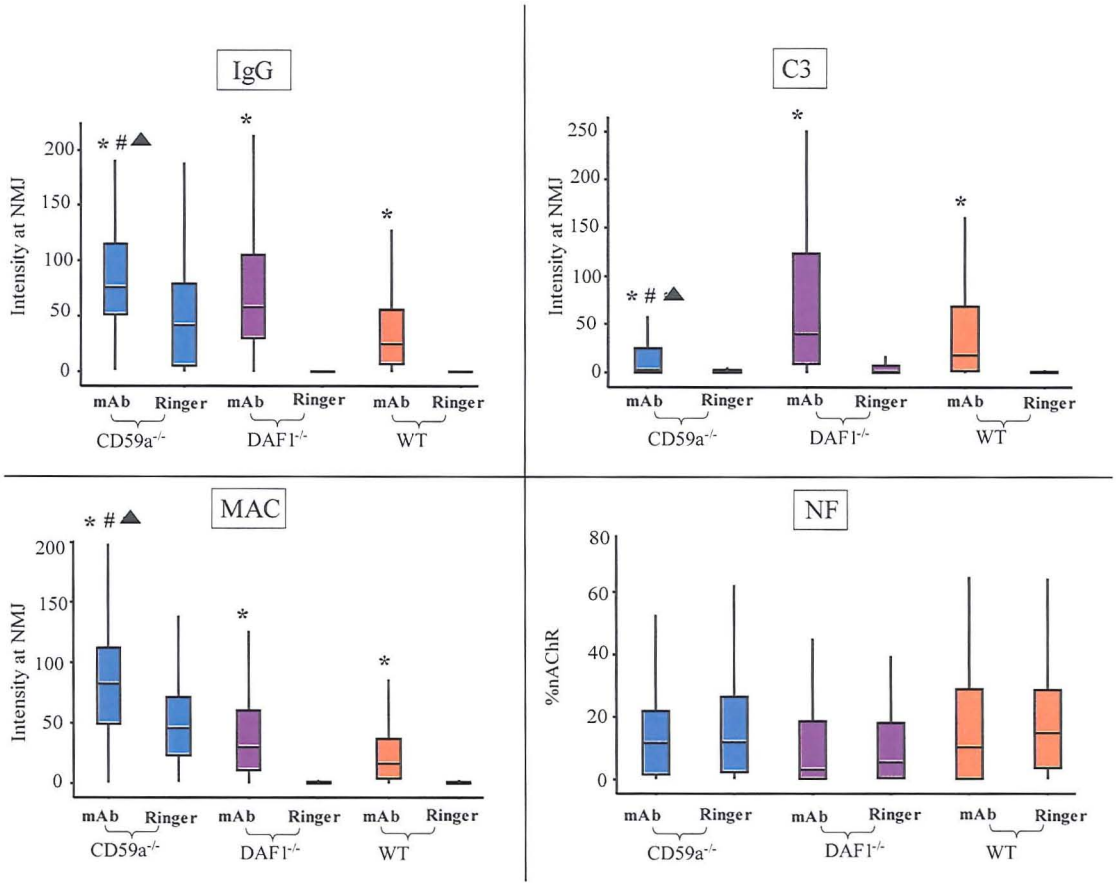

Fig 69. Graphical overview of MOG 35 in the CD59a$^{-/-}$, DAF1$^{-/-}$ and WT. Astrices indicate significnce compared to Ringer control ($p<0.05$), hash symbol indicates significance compared to WT and triangle indicates significance compared to DAF1$^{-/-}$.

IgG Intensity

For all strains, the IgG deposition at the NMJ was greater in the mAb treated hemi-diaphragm than for the Ringer treated half ($p<0.0001$). Both the CD59a$^{-/-}$ and DAF1$^{-/-}$ had greater IgG deposition compared to the WT ($p<0.0001$), with the CD59a$^{-/-}$ mAb treated tissue having higher IgG intensity than the DAF1$^{-/-}$ ($p<0.0001$), although it should be noted that the baseline in the CD59a$^{-/-}$ is greater.

C3 Intensity

C3 intensity over the NMJ was increased in mAb treated tissue when compared to respective Ringer control tissue for all strains ($p<0.0001$). The DAF1$^{-/-}$ mAb treated tissue had greatest C3 intensity when compared to both the CD59a$^{-/-}$ and WT ($p<0.0001$), while the CD59a$^{-/-}$ had less C3 than the WT ($p<0.0001$).

MAC Intensity

MAC deposition was significant in the mAb treated tissue of all strains, compared to Ringer tissue ($p<0.0001$). MAC in the WT mAb treated tissue was lower compared to the DAF1$^{-/-}$ and CD59a$^{-/-}$ mAb treated tissue ($p<0.0001$), with the CD59a$^{-/-}$ having the most significant MAC deposition in mAb treated tissue compared to the other strains ($p<0.0001$).

NF Coverage

No statistically significant difference was shown for any strain when comparing the Ringer control and mAb treated tissue.

Summary

Initially it appears that the CD59a$^{-/-}$ has greater MOG 35 deposition and MAC intensity. However, although levels in the mAb treated tissue are greater than in the Ringer tissue, the Ringer control tissue of this mouse is significantly different when compared to the Ringer control tissue of the other strains ($p<0.0001$). This indicates that this mouse has an endogenous deposition of IgG over the endplate, which are detected when analysing MAC and IgG and thus contributing to the intensity. When the cut and stained baseline tissue (ie. immediately snap frozen portion of diaphragm) from the CD59a$^{-/-}$ was analysed, the IgG intensity and MAC intensity showed similar staining to the Ringer treated tissue ($p<0.0001$), confirming that this batch of mice

had endogenous IgG deposition over the endplate, a phenomenon which is difficult to explain. To eliminate this "background" would have been detrimental to the detection of MAC and MOG 35 deposition in the WT mouse. Thus from the experiment the only definite conclusion which can be drawn is that IgG, C3 and MAC intensities are greater in the DAF1$^{-/-}$ compared to the WT. It is also difficult to explain why, in the presence of MAC, no significant lesion of the NF was detected. The retained antibody samples for each incubation were similar (Fig 70).

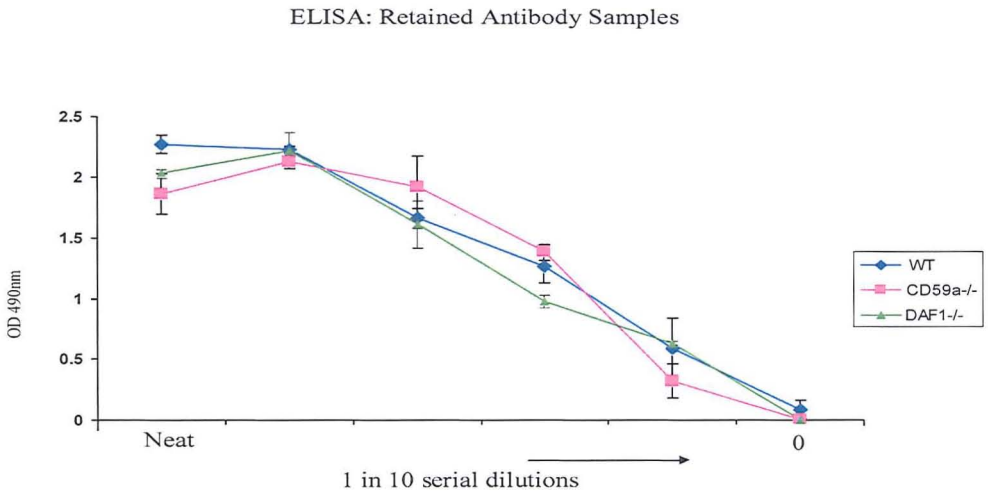

Fig 70. Retained antibody samples were equally viable.

5.2.5.4 *MOG 35 @ 6.25µg/ml: GD3s$^{-/-}$, GD3s$^{-/-}$/CD59a$^{-/-}$, GD3s$^{-/-}$/DAF1$^{-/-}$*

IgG Intensity

For each strain, IgG deposition in the Ringer tissue is negligible when compared to the mAb treated tissue ($p<0.0001$). There is a similar IgG intensity in the GD3s$^{-/-}$/CD59a$^{-/-}$and GD3s$^{-/-}$ mAb treated tissue ($p=0.96$), with the highest IgG intensity in the GD3s$^{-/-}$/DAF1$^{-/-}$ when compared to the other strains ($p<0.0001$).

C3 Intensity

The trend described for IgG intensity is replicated for C3 deposition, with greatest C3 detected in the GD3s$^{-/-}$/DAF1$^{-/-}$ mAb treated tissue ($p<0.0001$) compared to the other strains.

MAC Intensity

Again, for each strain Ringer treated tissue showed no significant staining intensity compared to mAb treated tissue ($p<0.0001$). The GD3s$^{-/-}$/CD59a$^{-/-}$ had lower MAC intensity than the GD3s$^{-/-}$ ($p<0.0001$) and GD3s$^{-/-}$/DAF1$^{-/-}$($p=0.08$), and the GD3s$^{-/-}$ had similar MAC intensity to the GD3s$^{-/-}$/DAF1$^{-/-}$($p=0.01$).

NF Coverage

All strains had significant NF loss when compared to the Ringer control treated tissue ($p<0.0001$).

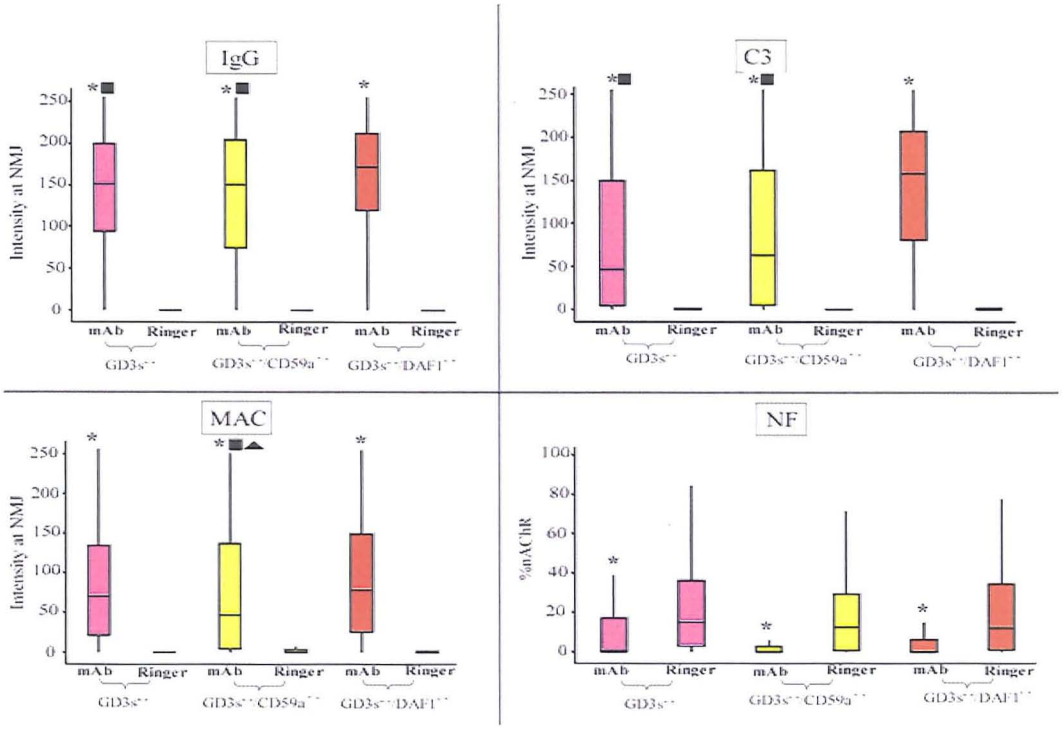

Fig 71. Graphical overview of MOG 35 in the GD3s$^{-/-}$, GD3s$^{-/-}$/CD59a$^{-/-}$ and GD3s$^{-/-}$/DAF1$^{-/-}$. Astrices indicate significance compared to Ringer control ($p<0.05$), squares indicate significance compared to GD3s$^{-/-}$/DAF1$^{-/-}$ and triangles indicate significance compared to GD3s$^{-/-}$.

ELISA of Retained mAb Samples

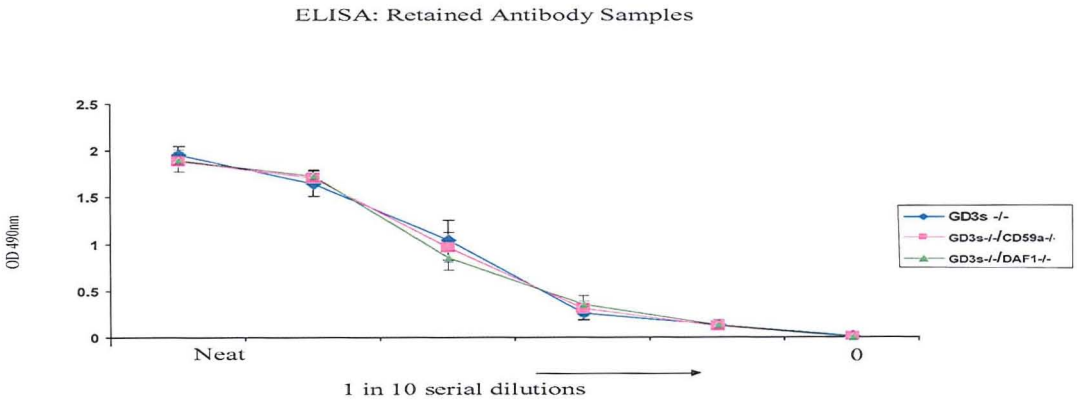

Fig 72. Antibody viability by ELISA.

5.2.6 *DG1: GalNAc-T$^{-/-}$, GD3s$^{-/-}$, GD3s$^{-/-}$/CD59a$^{-/-}$/DAF1$^{-/-}$, WT*

In summary, the above findings suggest that removal of GPI anchored proteins can increase antibody deposition at the NMJ. It was hypothesised that GPI anchored protein removal would enable the binding of DG1. To test the hypothesis, DG1 hemi diaphragms from the GD3s$^{-/-}$/CD59a$^{-/-}$/DAF1$^{-/-}$ and GD3s$^{-/-}$ were incubated in DG1 to directly analyse the effect of GPI anchored protein removal. The GalNAc-T$^{-/-}$ was used as the negative control, and the WT as a baseline control.

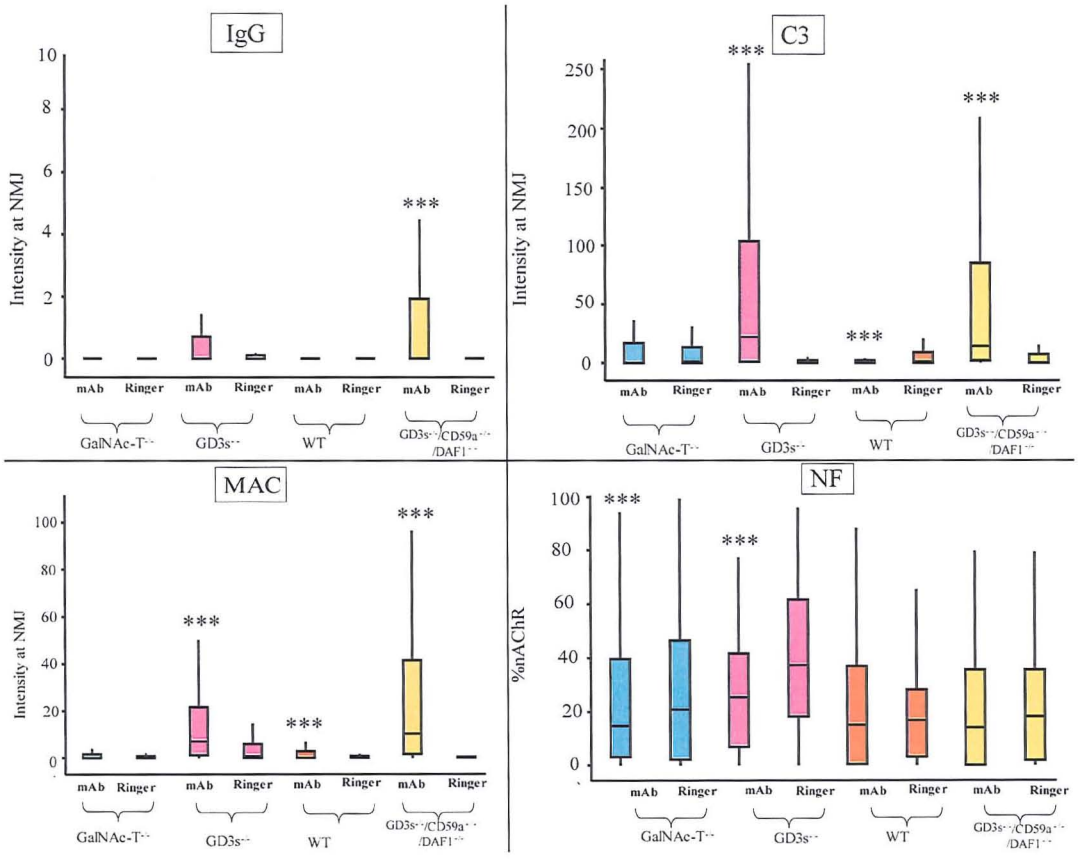

Fig 73. Graphical overview of DG1 in the GD3s$^{-/-}$, GD3s$^{-/-}$/CD59a$^{-/-}$/DAF1$^{-/-}$ and respective controls (GalNAc-T$^{-/-}$ and WT). Astrices indicate significance compared to Ringer control ($p<0.05$).

IgG Intensity

The GD3s$^{-/-}$/CD59a$^{-/-}$/DAF1$^{-/-}$ had a significant increase in DG1 binding compared to Ringer control tissue ($p<0.05$). The GD3s$^{-/-}$, WT and GalNAc-T$^{-/-}$ had no significant difference between mAb and Ringer treated tissue ($p=0.16$, $p=0.2$, $p=0.66$ respectively). Comparison of the DG1 intensity in the mAb treated tissue of the GD3s$^{-/-}$/CD59a$^{-/-}$/DAF$^{-/-}$ and the GD3s$^{-/-}$shows no difference ($p=0.40$).

C3 Intensity

The GD3s$^{-/-}$/CD59a$^{-/-}$/DAF1$^{-/-}$ and GD3s$^{-/-}$ both show a significant increase in C3 intensity in DG1 treated tissue compared to Ringer treated tissue ($p<0.0001$). WT mAb treated tissue has a lower C3 intensity than Ringer treated tissue ($p<0.0001$), indicating non-specific adherence of activated complement components in the NHS to the Ringer tissue. The GalNAc-T$^{-/-}$ has no difference between Ringer and mAb treated tissue ($p=0.78$). There is no significant difference between the C3 intensity of the mAb treated GD3s$^{-/-}$ and GD3s$^{-/-}$/CD59a$^{-/-}$/DAF1$^{-/-}$ tissue ($p=0.89$).

MAC Intensity

MAC intensity is significantly increased in mAb treated compared to Ringer treated tissue in the WT ($p=0.02$), GD3s$^{-/-}$($p<0.0001$) and GD3s$^{-/-}$/CD59a$^{-/-}$/DAF1$^{-/-}$ ($p<0.0001$). Ringer treated and mAb treated tissue of the GalNAc-T$^{-/-}$ shows no statistical difference ($p=0.51$). The mAb treated tissue of the GD3s$^{-/-}$ and GD3s$^{-/-}$ /CD59a$^{-/-}$/DAF1$^{-/-}$ is not significantly different ($p=0.51$).

NF Coverage

The WT mAb treated tissue has no significant alteration in NF coverage over the NMJ compared to the control ($p<0.0001$). The GD3s$^{-/-}$ mAb treated tissue has significantly

less ($p<0.0001$) NF coverage than Ringer control tissue, and the GalNAc-$T^{-/-}$ shows a significant NF lesion ($p=0.02$) in mAb treated tissue compared to the Ringer control. Only the $GD3s^{-/-}/CD59a^{-/-}/DAF1^{-/-}$ has no significant difference between the Ringer and mAb treated tissue NF levels ($p=0.33$).

Summary: MAC, C3 and IgG levels in both the $GD3s^{-/-}$ and $GD3s^{-/-}/CD59a^{-/-}/DAF1^{-/-}$ mAb treated tissue are not significantly different, indicating the absence of CD59a and DAF1 are not enhancing the ability of DG1 to bind to GM1. Although only the $GD3s^{-/-}/CD59a^{-/-}/DAF1^{-/-}$ displays an increase in IgG intensity in mAb treated tissue compared to Ringer control, the median intensity lies on zero (in other words, 50% of the NMJs were negative), indicating binding of IgG (in the 50% of positive) NMJs is just below the threshold of detection and does not represent a biologically relevant mAb deposition. The NF analysis indicates a significant lesion in the $GD3s^{-/-}$ mouse, however the apparent lesion in the GalNAc-$T^{-/-}$ (which had no MAC, IgG or C3 deposition in mAb treated tissue) indicates the NF of each strain may have been damaged during the hemi-diaphragm incubations or due to natural variability in the tissue. This could be overcome by increasing the number of experimental repeats.

5.2.7 Discussion

DG2 is able to bind sulfatide strongly on ELISA, but not in tissue. The effect of tissue fixation in EtOH and PFA have shown to be effective in epitope exposue (Quattrini *et al* 1992), however this was ineffective in facilitating sulfatide recognition for DG2. It is possible that the mAbs which are capable of binding sulfatide on ELISA, but not in tissue, are not able to recognise the epitope when in the membrane. This could be a direct result of the epitope being shielded (or "masked") by something in the membrane, or it could be due to the way sulfatide is orientated in the membrane,

whereby its antigenic domain is not freely accessible to the mAbs. The anti-sulfatide antibody O4 is able to bind membrane associated sulfatide, indicating it relies on a different epitope or presentation than the mAbs in our panel. Overall, from the data there is evidence that something is able to interact with sulfatide and inhibit the ability of mAbs to bind, especially in the context of the membrane.

The notion of epitope shielding was expanded in attempt to explain why DG1 cannot bind GM1 in living membranes. There is evidence that acetone fixation enhances the ability of some anti-ganglioside antibodies to bind (Urmacher *et al* 1989), and as shown in the results, treatment of the tissue in acetone resulted in a significant DG1 signal over the NMJ. Organic solvents such as acetone can significantly reduce the level of membrane associated gangliosides (Schwartz and Futerman 1997) and thus DG1 binding following acetone treatment supports the theory that GM1 is "masked": acetone may remove any lipids or proteins masking GM1, but more importantly, probably also solubilises a percentage of GM1 and therefore the ability of DG1 to bind is suggestive that binding is not dependent on the GM1 density, but rather the availability. However, the possibility that DG1 may be binding non-specifically following acetone treatment cannot be ignored, although it is highly unlikely that acetone is able to dissolve glycolipids in a way which results in the creation of more GM1 like epitopes. This experiment is indirect evidence that GM1 is being masked from DG1, and from this more specific experiments were designed to identify the "culprit".

The first line of investigation involving removal of GPI anchored proteins led to an increased ability of DG2 and MOG 35 to bind. This is evidence that a new population of gangliosides have been made available to the mAbs, and provides direct evidence of the clustering of gangliosides and GPI anchored proteins. Observations in PC12

cells are relevant to the NMJ, due to the existence of GPI proteins (eg. CD59) at this site which are likely to exert a similar raft mediated masking effect. If an antibody is able to bind better in the absence of GPI anchored proteins, then the inference is that they will result in an enhanced lesion. The hemi-diaphragm data is highly suggestive that removal of GPI anchored DAF1 enhances MOG 35 binding at the NMJ. This could be due to direct epitope exposure whereby DAF1 is directly hiding the ganglioside, or a knock on effect, where GPI anchored protein removal alters raft architecture and molecules which normally associate with gangliosides are "moved" and thus expose the ganglioside. However, the correlation between increased antibody binding and enhancement of the lesion is difficult to interpret from the current data. The increased C3 and MAC levels may be due to the increased levels of antibody, or as a result of the decreased complement regulation, or a combination of the two factors. In order to address this, a KO mouse with normal complement regulators but loss of another NMJ associated GPI anchored protein would need to be studied.

Chapter 6

6.1 Introduction

In Chapter 5, the removal of GPI anchored proteins did not facilitate the binding of DG1. However rafts are diverse, and the association of GM1 with other potential "masking" structures is addressed in the context of lipid rafts, forming the basis of this chapter.

6.2 Results

6.2.1 *DG1 Binding*

The first hypothesis generated was that GM1 (or at least the sialic acid of GM1) can be masked by other gangliosides, in this case GD1b, GD1a and GT1b which represent the most abundant neuronal gangliosides (Willison and Yuki 2002). This would explain why DG1 is unable to "see" GM1 in the living membrane, although it can clearly bind GM1 alone.

The hypothesis was tested by ELISA, to determine the ability of anti-GM1 antibodies to bind GM1 in the presence of other gangliosides. DG1 binding to GM1 alone or when mixed in a 1:1 ratio with another ganglioside was tested (Fig 74). All antibody binding curves are the mean of 3 repeats, with SEM indicated.

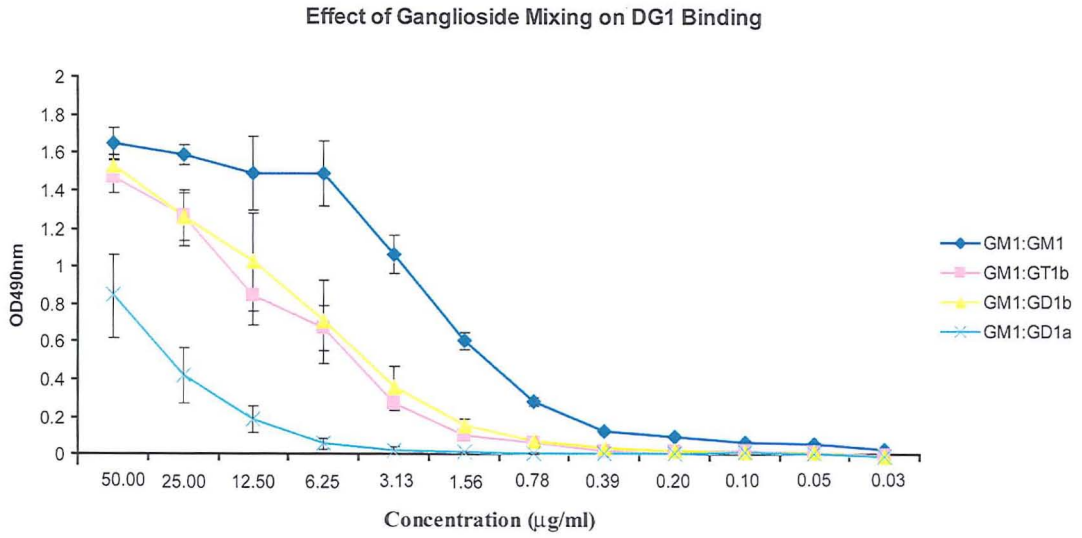

Fig 74. Binding curves showing the $OD490_{nm}$ of DG1 binding to GM1 alone, or GM1 mixed with gangliosides. Neat sample is 50µg/ml.

Mixing GM1 in a 50:50 ratio is theoretically reducing the amount of GM1 on the plate, but GM1:methanol (MeOH) (50:50) did not have lower OD 490nm compared to GM1 alone. Thus, it was concluded any alterations in antibody binding due to mixing GM1 with gangliosides is not due to reducing the quantity of GM1.

When comparing DG1 binding to GM1 alone, mixing GM1 50:50 with GD1b or GT1b caused a decrease in the binding of DG1. GD1a had a more pronounced decrease on the binding, indicating that on the ELISA plate, GD1a is the most effective ganglioside at obscuring GM1 from DG1.

6.2.2 *DG2*

The masking effects of gangliosides, as inferred from the DG1 data above, were tested using DG2. The Gal(β1-3)GalNAc epitope is shared with GD1b, and DG2 binds GD1b on ELISA, although the binding to GM1 is much stronger (Townson *et al* 2007).

DG2 bound strongly to GM1 with a weak signal also detected for both GD1b and GD1a. In order to determine the inhibitory effect of these gangliosides when mixed with GM1, the $OD490_{nm}$ values of the mixed wells were adjusted by subtracting the values of DG2 binding to either GD1a or GD1b alone, thus giving a more accurate comparison of antibody binding to either GM1 alone or GM1 in a mixed well without the added interference from weak binding to the other ganglioside species (Fig 75 a, 75b).

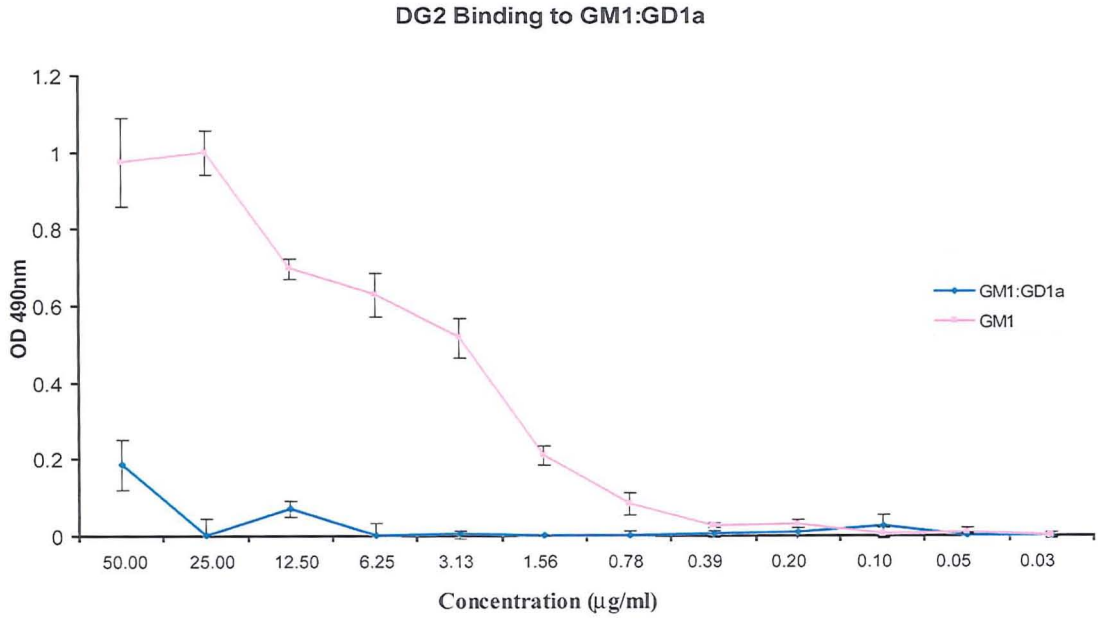

Fig 75 a) Comparison of DG2 binding GM1 alone and DG2 binding GM1:GD1a (subtracted value). Neat sample is 50µg/ml.

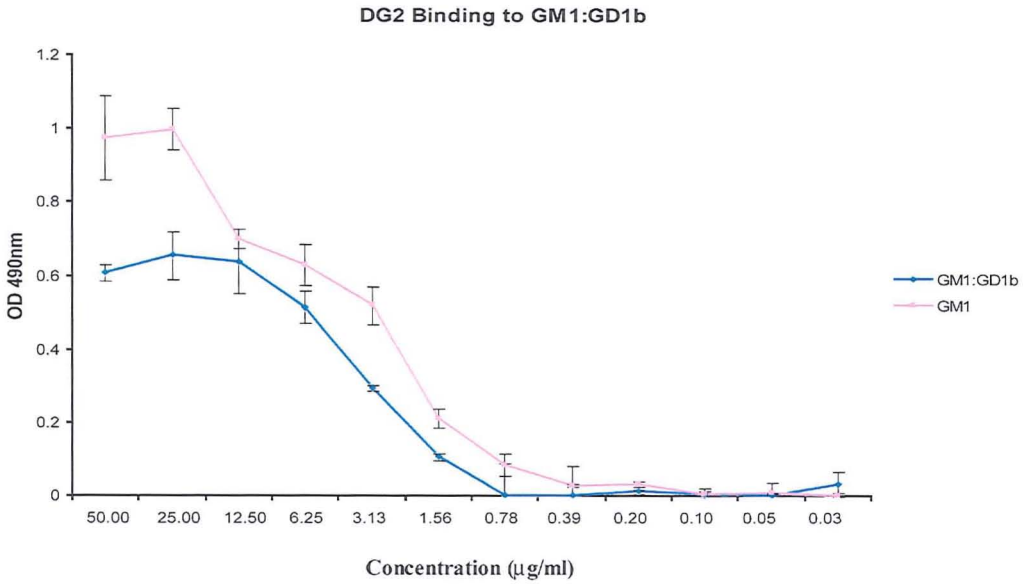

Fig 75 b) Comparison of DG2 binding GM1 alone and DG2 binding GM1:GD1b (subtracted value). Neat sample is 50µg/ml.

As shown in Fig 75b, mixing GM1:GD1b appears to have a minor inhibitory effect on the binding of DG2 to GM1. However, mixing of GM1:GD1a (Fig 75a) results in an almost complete inhibition of DG2 binding to GM1.

6.2.3 *CTb*

Before conclusions were drawn from the antibody binding data, it was important to account for the possibility that mixing GM1 with other gangliosides may displace GM1 and prevent it from binding to the plate. This would mean the inability of antibodies to bind GM1 in the presence of GD1a may be misinterpreted as a "masking" effect which may instead be an artefact of the experimental design. CTb binding to GM1 is of much higher affinity than mAbs binding to GM1, as the CTb interaction with GM1 oligosaccharide is one of the highest affinity protein-carbohydrate interactions recognised to date (Turnbull *et al* 2004). Thus any alteration of CTb binding to GM1 is a good indicator that GM1 has not bound to the

plate. It has been suggested that in certain assay conditions, CTb is not specific for GM1 (Kuziemko *et al* 1996) and thus the first consideration of this experiment was therefore to establish which gangliosides CTb binds to by ELISA.

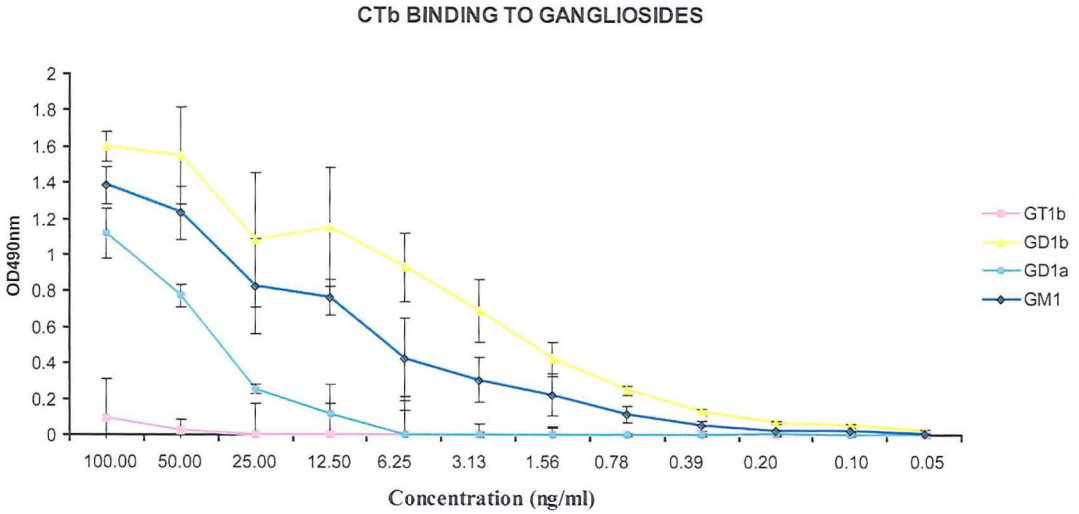

Fig 76. Binding curves of CTb to gangliosides GT1b, GD1b, GD1a and GM1. Neat sample of CTb is 100ng/ml.

As shown in Fig 76, by ELISA CTb is not specific for GM1, and bound strongly to GD1b and with lower affinity to GD1a and GT1b. For all concentrations of CTb tested, CTb binding to gangliosides GD1a, GT1b and GD1b gave a similar profile (graphs not shown) indicating the specificity of the toxin was not influenced by concentration.

6.2.3.1 *CTb and Mixed Gangliosides*

The high affinity of CTb for GM1 when compared to GD1a and GT1b was demonstrated in Fig 76, and from this it was hypothesised that *in vitro*, CTb binding to GM1 alone or GM1 mixed with GD1a or GT1b should give comparable $OD490_{nm}$.

To account for the binding of CTb to other gangliosides, it was assumed that in a mixed well, CTb will preferentially bind GM1 over the lower affinity gangliosides (GT1b and GD1a).

Therefore, for these gangliosides, the binding of CTb in mixed wells was adjusted by subtracting the value of CTb binding either GT1b or GD1a alone (Fig 77 a, Fig 77b) and the results depicted graphically.

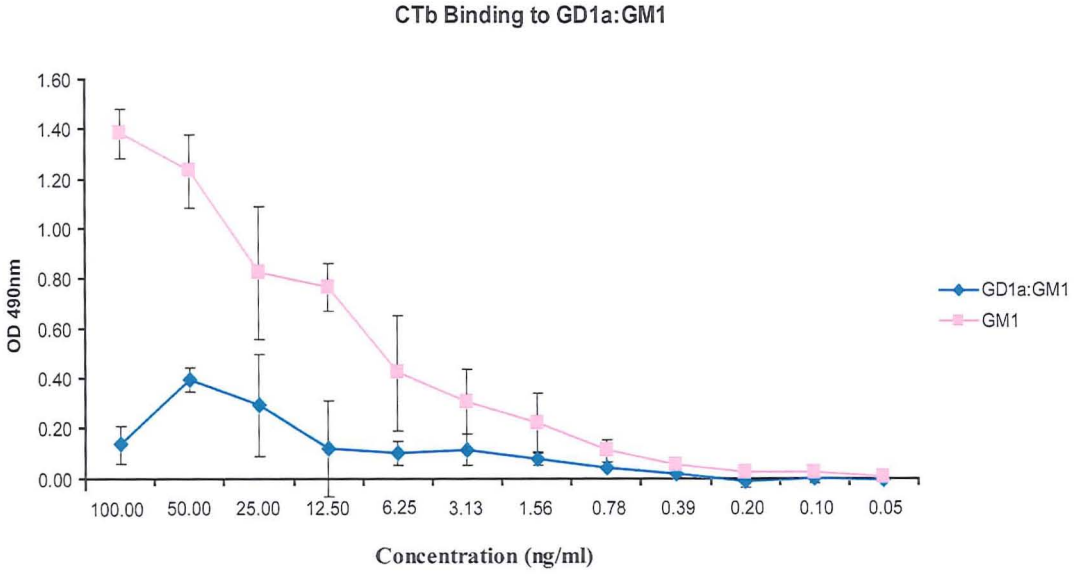

Fig 77 a) Comparison of CTb binding to GM1 alone, or GM1 mixed with GD1a. Neat sample of CTb is 100ng/ml.

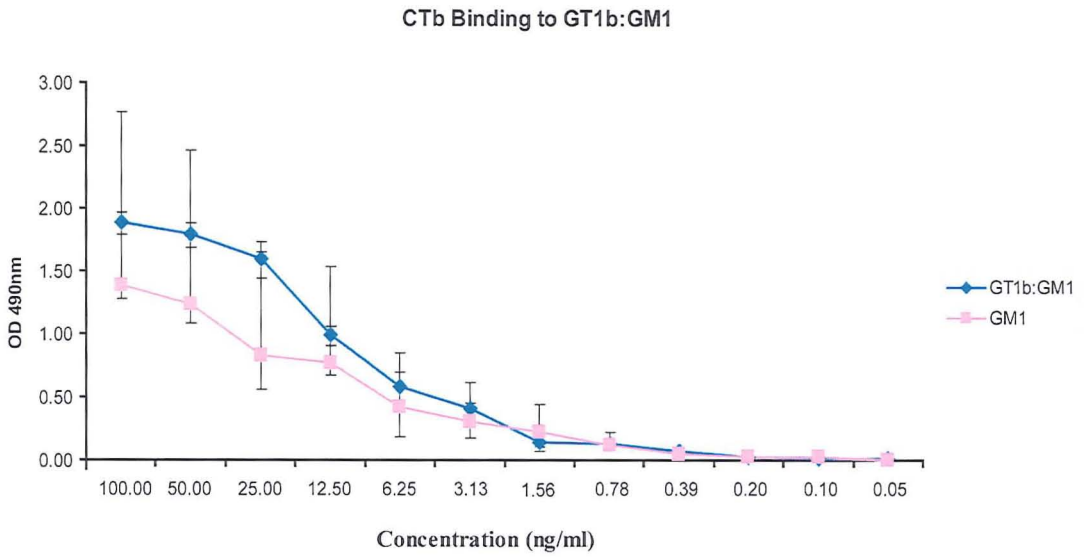

Fig 77 b) Comparison of CTb binding to GM1 alone, or GM1 mixed with GT1b.

Fig 77a) shows that GD1a is inhibiting CTb binding to GM1, and this is most obvious when CTb is applied to the wells at the starting concentration of 100ng/ml. GT1b has minimal inhibition on the binding of CTb to GM1. Therefore the results of the CTb binding experiment do not rule out the possibility that mixing GM1 and GD1a is artefactually interfering with the adsorption of GM1 to the plate.

6.2.4 *The Living Membrane*

From the ELISA studies it was not possible to confirm the inhibitory effect of GD1a. The next experimental approach was therefore to look directly at the living membrane.

6.2.4.1 *PC12 Cells: Removal of GD1a*

Neuraminidase (N'ase) is an enzyme which cleaves sialic acids from gangliosides and sialoglycoproteins (Cassidy *et al* 1965). Because only terminal sialic acids are

cleaved, ganglioside GM1 is resistant to neuraminidase, and removal of the terminal sialic acids from gangliosides such as GD1a will effectively transform them into GM1, as shown in Fig 78.

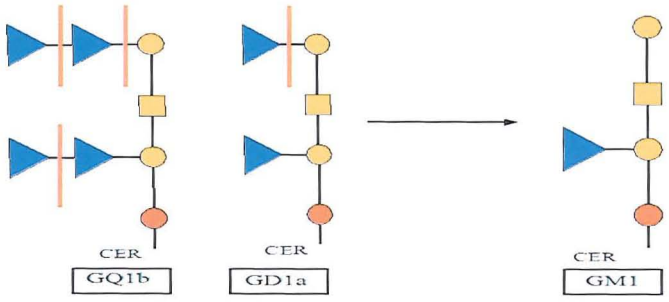

Fig 78. Heavy red lines show the sialic acid linkages which are sensitive to N'ase. The linkage of sialic acid to the internal galactose is resistant, meaning all complex gangliosides are reduced back to the structure of GM1 by N'ase, as shown in the schematic example.

Initially, N'ase treatment protocol was optimised using PC12 cells seeded onto coverslips, a convenient way of performing a dilution series, varying incubation times and viewing the results directly down the microscope. The aim of the experiment was to remove GD1a enzymatically without killing the cells, which would cause morphological alteration of the cell membrane. This would make it impossible to determine whether the observed increase in DG1 staining was due to removal of GD1a, or due to degradation of the membrane.

High doses of enzyme, prolonged exposure to the enzyme or dilution of the enzyme in PBS resulted in cell death as shown in the "Live/Dead" staining assay in Fig 79. Ethiduim homodimer-1(EthD-1) dye is excluded from live cells by the intact plasma membrane, but enters damaged membranes and binds to nucleic acids to give an intensely positive signal. Calcein green is indicative of vital cells as its fluorescence is induced by esterase activity of viable cells (Live/Dead Assay, Molecular Probes Inc.).

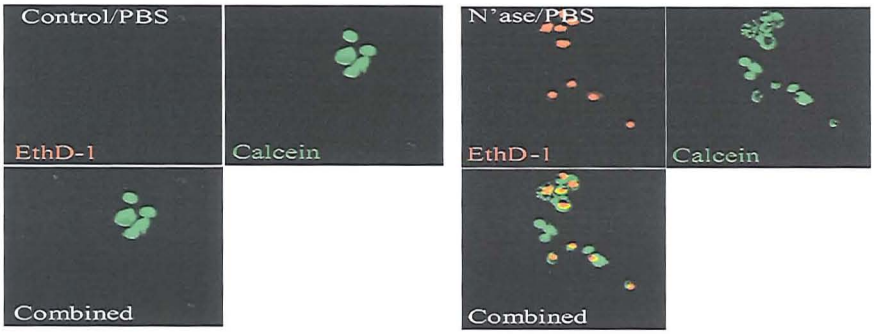

Fig 79 a) Left panel: cells incubated in PBS alone show no uptake of EthD-1, and are Calcein green positive. Right panel: incubation of cells in N'ase and PBS leads to leaching of the Calcein green and rapid EthD-1 uptake.

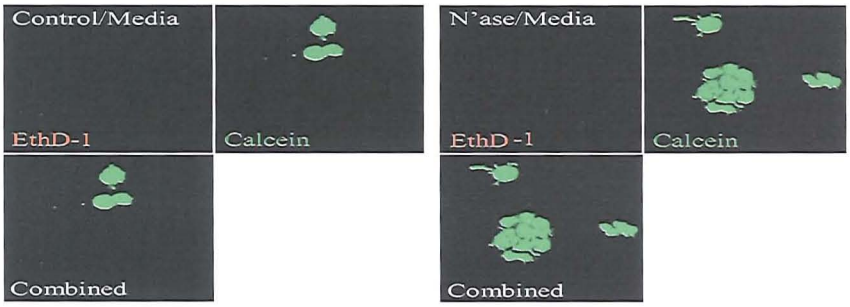

Fig 79 b) Left panel: cells incubated in serum free media (SFM) alone are Calcein green positive with no uptake of the EthD-1 dye. Right panel: N'ase treatment of cells in SFM does not lead to EthD-1 uptake and cells retain a strong Calcein green signal.

As shown, the optimal treatment of the cells was for no longer than 1.5hrs, using 2U of N'ase, in serum free DMEM at 37°C (Materials and Methods).

6.2.4.2 *Neuraminidase: FACS Analysis*

Cells were plated into 5ml tissue culture dishes, treated with enzyme (or control) and prepared for FACS analysis. A pilot study (n=1) revealed that a 1.5hr treatment of cells with 2U/ml resulted in a decrease in MOG 35 intensity with a concomitant increase in DG1 intensity (Fig 80,Fig 81 and Fig 82)

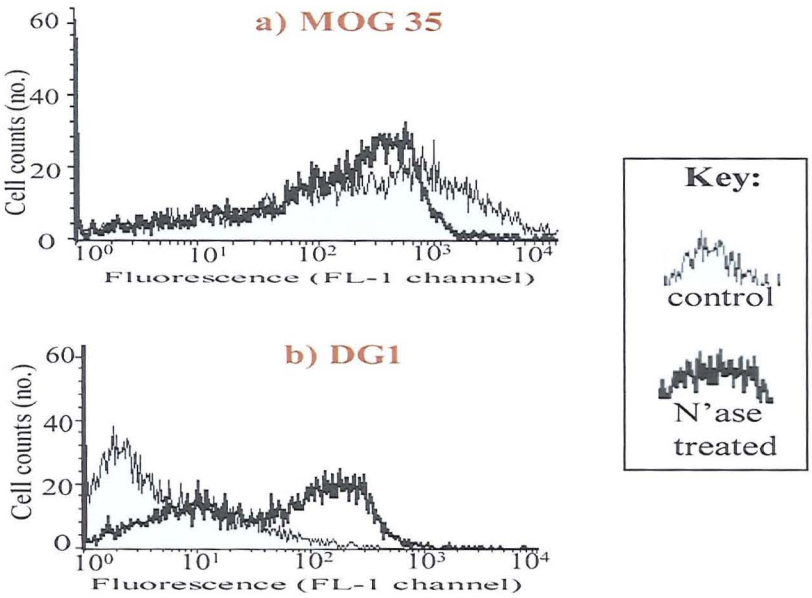

Fig 80. FACS histograms showing the shift in fluorescence of MOG 35 and DG1, before and after N'ase treatment.

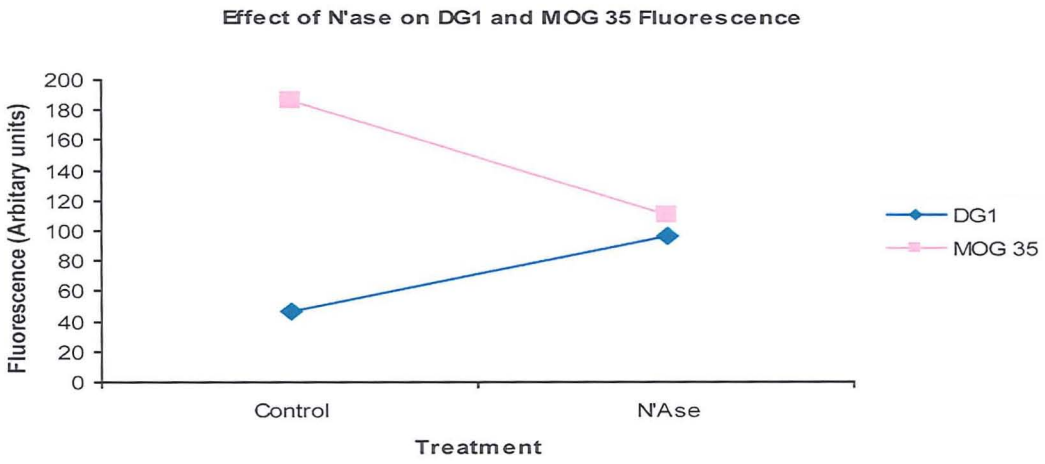

Fig 81. Effect of Neuraminidase treatment on MOG 35 and DG1 mean intensity, as determined by FACS analysis.

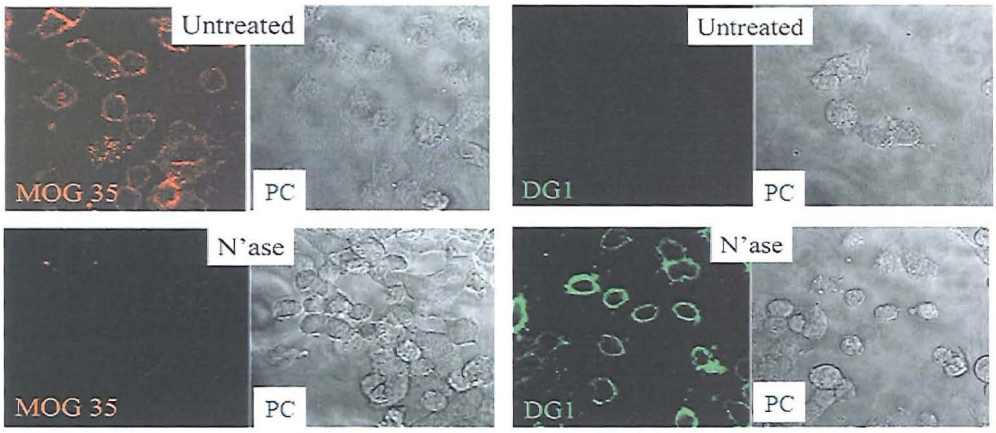

Fig 82: illustractive example of N'ase treatment on MOG 35 and DG1 intensity, as quantified by FACS analysis. PC= phase contrast.

Establishing that removal of GD1a correlates with an increase in the binding of DG1 led to the hypothesis that GD1a removal was "unmasking" GM1. Thus, reconstituting the cell membrane with GD1a following enzymatic removal (ie. adding back in exogenous GD1a) should result in a reduction of the DG1 signal. To test this hypothesis, a 3 day experimental procedure was designed:

Day 0: 7 dishes of cells (equal numbers) set up and left overnight in incubator.

Day 1: 5 dishes treated with N'Ase, and 2 with SFM to serve as controls.

Group a) FACS analysis performed on one dish of control and one dish of treated cells to confirm success of enzymatic treatment.

Group b) Exogenous ganglioside or placebo added to 3 enzymatically treated dishes and incubated overnight (Materials and Methods) along with one dish of untreated control cells.

Group c) Remaining dish (treated) was returned to serum-rich media to ensure "normal" ganglioside metabolism and incubated until day 3, to assess the effect of de-novo GD1a synthesis on DG1 binding.

Day 2: FACS analysis of *group b.*

Day 3: FACS analysis of *group c.*

Results:

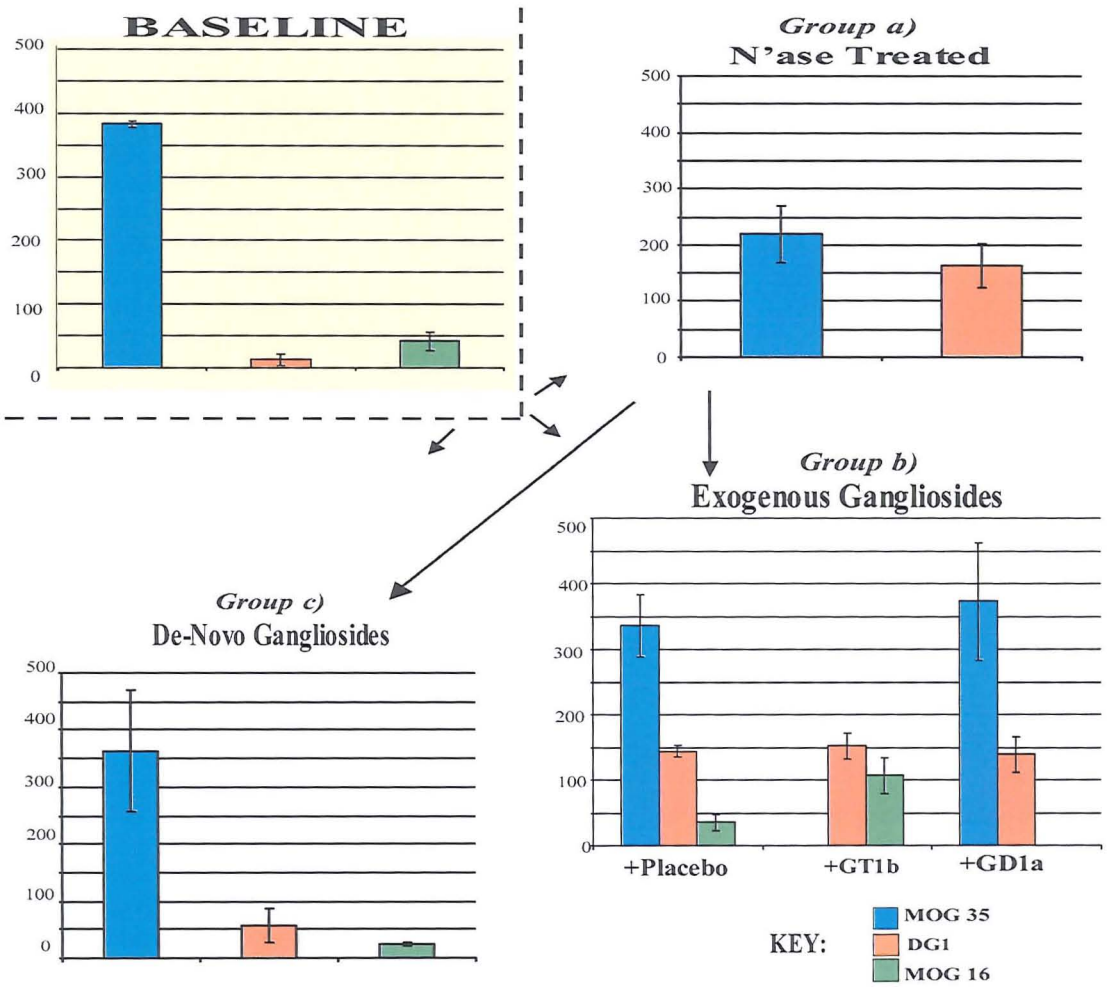

Fig 83. n=3 repeats, with all staining done in duplicate per experiment. Error bars indicate SEM. Baseline control is combined result of untreated cells analysed on Day 1(in *Group a*) and a further group of untreated cells analysed on day 2 (*in Group b*). Y scale represents fluorescence intensity (arbitary units).

Group a) Day 1: As expected, enzyme treatment resulted in a decrease in GD1a as shown by a decrease in MOG 35 intensity compared to control ($p<0.05$). DG1 intensity increased in treated cells compared to control ($p<0.05$), indicating there was an increase in accessible GM1.

Group b) Day 2: N'ase treated cells were reconstituted with GD1a, GT1b or placebo (ie. sonicated dH_2O added to the media). The resistance of exogenous GT1b to trypsinisation of the cells, and its increased detection with MOG 16 (anti-GT1b mAb) when compared to control cells ($p<0.05$) indicates that GT1b was successfully incorporated into the membrane. As predicted from earlier ELISA data, GT1b had negligible effect on DG1 binding when compared to the N'ase/placebo treated cells ($p>0.05$).

Insertion of exogenous GD1a to the membrane appeared less successful. Regarding MOG 16, there was an obvious increase in fluorescence when GT1b was added, compared to untreated or placebo treated cells ($p<0.05$). With MOG 35, exogenously added GD1a recovered the fluorescence to a level comparable with untreated cells ($p>0.05$). However it is possible that the recovery of fluorescence is due to a combination of de-novo GD1a synthesis and exogenous GD1a: it was predicted that placebo treated cells would retain a similar MOG 35 intensity to N'ase treated cells, however increased MOG 35 intensity in placebo treated cells indicates possible de-novo synthesis of GD1a. It is not known whether exogenous GD1a inserted into the membrane and "out-competed" de-novo GD1a, or whether the GD1a content of the reloaded cells was due to de-novo GD1a (perhaps supplemented by the exogenous GD1a). However, as the DG1 binding ability did not decrease compared to the N'ase

treated cells ($p<0.05$), the former theory is most likely, and it is probable that exogenous GD1a did enter the membrane but did not enter lipid rafts.

Addition of exogenous GT1b did not decrease the binding of DG1 compared to the N'ase treated cells ($p>0.05$), suggesting GT1b does not mask the GM1 epitope from DG1. Figure 84 shows a representation of the FACS histograms showing similar DG1 intensity for all 3 conditions (control, exogenous GD1a and exogenous GT1b).

Group c) Day 3: Restoration of the GD1a levels in the membrane by de-novo synthesis also reduced the binding of DG1 although not fully to the level of untreated control cells ($p>0.05$). Thus, de-novo synthesis of GD1a "re-masked" GM1, although incompletely. This further supports the observation that the GD1a in the membrane of the exogenously reloaded cells was not due to de-novo GD1a, as the DG1 signal did not decrease as shown for the decrease with de-novo synthesis.

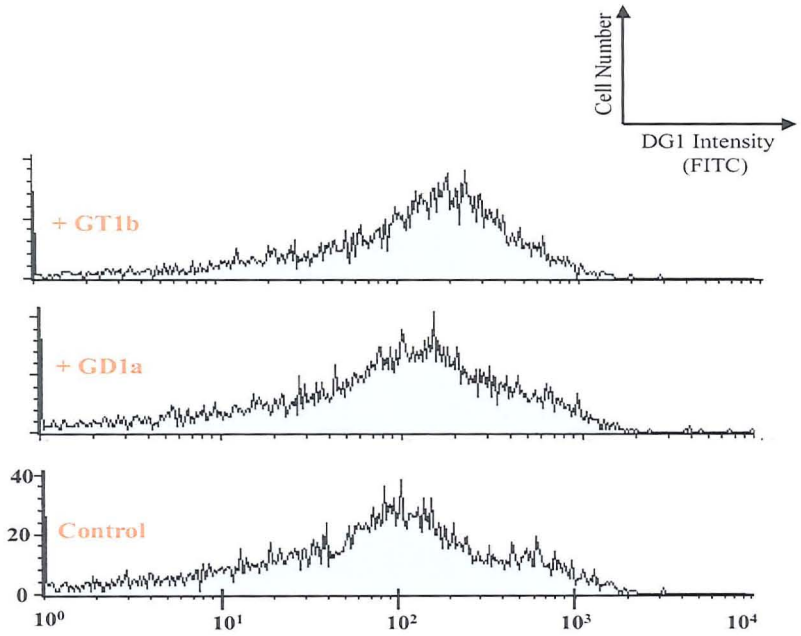

Fig 84. FACS histograms. Fluorescence intensity of DG1 did not show an obvious shift in the FACS profile when comparing control cells, cells with exogenous GD1a and cells with exogenous GT1b. Data illustrated here is shown quantitatively in Fig 83.

6.2.4.3 *GM1 and GD1a: Raft Fraction Analysis*

The failure of GD1a to decrease the binding of GM1 led to the hypothesis that the exogenous GD1a did not enter lipid rafts, where the interaction of GM1 and GD1a is likely to occur. Based on detergent insolubility in Triton-X100, and flotation on a sucrose gradient (Brown and Rose 1992), lipid raft fractions were prepared from untreated PC12 cells, N'ase treated PC12 cells and N'ase treated PC12 cells which had been "reloaded" with exogenous GD1a. Each fraction was then analysed by gel electrophoresis, allowing the presence of gangliosides and proteins in each fraction to be compared by Western Blotting. Using this technique, the distribution of GM1 and GD1a in raft versus non-raft fractions from each treatment were analysed, to determine the endogenous GD1a profile, and compare it to that of the GD1a profile after N'ase treatment and subsequent exogenous addition of GD1a.

Exposure times for blots were kept constant to ensure fair comparisons could be made regarding intensities, and results are shown in Fig 85a and Fig 85 b (shown together overleaf).

Figure 85a) shows that in untreated cells (top band), GD1a is distributed mainly in the raft fractions, with evidence also in the more dense membrane components in fractions 10, 11 and 12 (which contain dense core vesicles (Saegusa *et al* 2002)). In darker exposures (not shown as this led to over exposure of the fractions with exogenous GD1a), a faint smear of GD1a was also present in fractions 6-9. In the N'ase treated cells (middle band), the GD1a content of fractions is dramatically decreased compared to the control cells, proving the effect of the N'ase in removing GD1a. In the cells with exogenous GD1a added (bottom band), the ganglioside has recovered the MOG 35 signal in the raft fractions to a level comparable to control cells. However there is also evidence of more intense GD1a in all other fractions.

From this data it can be concluded that recovery of GD1a is in part due to de-novo GD1a synthesis (during the 18 hour incubation with the exogenous ganglioside) and exogenous GD1a, but the exogenous GD1a is likely to have inserted into other membrane fractions also.

Figure 85b shows the CTb signal for the raft fractions, and it is assumed that CTb is specific for GM1 in the fractions. Thus the distribution of GM1 shows an enrichment in the raft fractions 3, 4 and 5, but also a detectable signal in non-raft fractions. In N'ase treated cells GM1 becomes abundant in all fractions. This suggests that not all GD1a had been detected in Fig 85a), or that sialic acids from other glycolipids or proteins had contributed to the 'new' GM1 in the non-raft fractions. Addition of exogenous GD1a did not alter the profile of GM1 in the blots. Figs 85c and 85d prove the results obtained above are based on a valid raft preparation, using positive and negative controls for raft fractions. The transferrin receptor is not raft associated, but enriched in the greater membrane (Hering *et al* 2003, Eckert *et al* 2003). As shown in Fig 85c), there is enrichment of the transferrin receptor in non-raft fractions for all cell preparations. The structural protein flotillin is enriched in the raft fractions (Morrow and Parton 2005) and as shown in Fig 85d), in all raft preparations it is intense in fractions 3, 4 and 5.

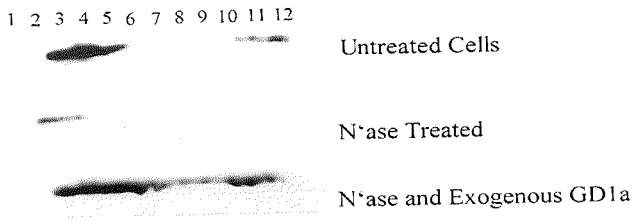

Fig 85a. Western Blot. Solubilised membrane fractions of PC12 separated and recovered from a sucrose gradient and each fraction electrophoresed. Blot shown was probed with MOG 35 showing GD1a distribution. Exposure times for each row were constant.

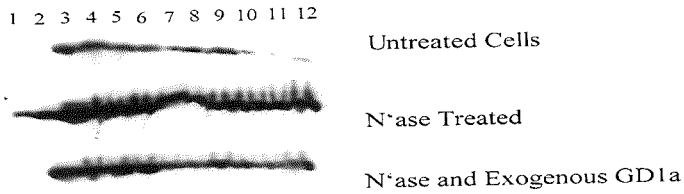

Fig 85b. Western Blot. As for Fig 85a), but probed with CTb (ie. GM1 distribution)

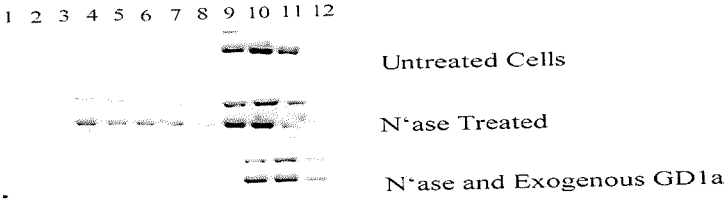

Fig 85c. Western Blot - Transferrin receptor (negative control, non raft associated protein). Top band represents the 180 kDa dimer with the 90kDa monomer below.

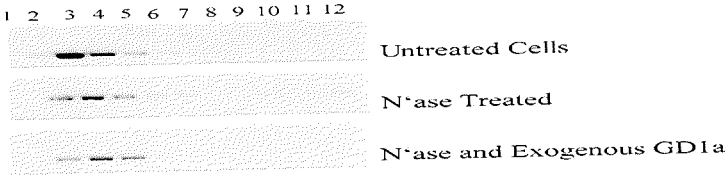

Fig 85d. Western Blot - flotillin (positive control, raft associated protein). 48 kDa protein.

6.2.4.2 *Summary of PC12 Data*

Treatment of PC12 cells resulted in the binding of DG1, owing to a population of available GM1. It was hypothesised that the re-addition of GD1a to the cells would assume the characteristics of endogenous GD1a, and interact with GM1 to mask it from DG1. This was shown not to be the case. However, after several days in culture, N'ase treated PC12 cells without the addition of exogenous GD1a were able to

express de-novo GD1a and concomitantly reduce the ability of DG1 to bind. Raft fraction analysis displayed that exogenously added GD1a was not specific for raft fractions. Taken together these data suggest that the exogenous GD1 did not interact with GM1 in a physiologically relevant way, and that de-novo synthesis of GD1a was required to interact with GM1.

6.2.5 *Translating the Data to the Mouse NMJ*

Investigating the presentation of GM1 in the membrane of a cultured cell line does not fully recapitulate the environment at the NMJ where DG1 does not bind, even weakly, in *ex-vivo* muscle preparations. The next logical progression in the epitope masking study was to move from the cell membrane to the more complex structural arrangement of the NMJ, using *ex-vivo* muscle preparations from the target disease model (the $GD3s^{-/-}$ mouse).

6.2.5.1 *Effect of N'ase on DG1 binding at the $GD3s^{-/-}$ NMJ*

N'ase was applied to TS preparations, and DG1 binding analysed in direct comparison to Ringer control tissue. For each comparison, microscope levels were kept constant.

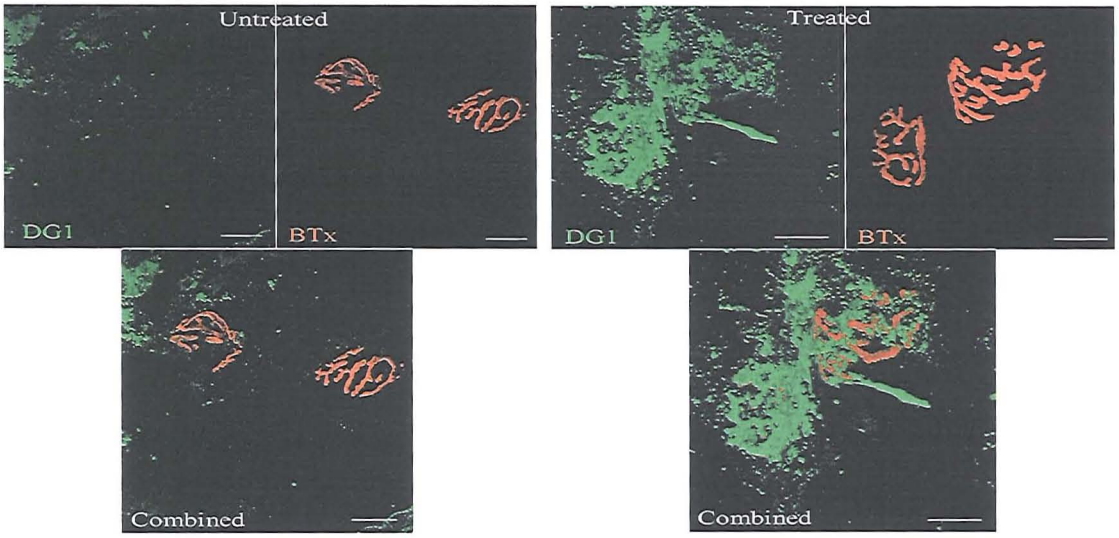

Fig 86. Effect of N'ase on DG1 binding in the GD3s$^{-/-}$ TS muscle (*ex-vivo* preparation). Negative control tissue (N'ase followed by secondary, showed no non-specific binding of the secondary to the tissue). Scalebar = 20μm

As shown in Fig 86, DG1 did not bind to control GD3s$^{-/-}$ tissue, however a strong IgG signal was detected following N'ase treatment. The antibody deposition appeared axonal. Fig 87 confirms that the antibody binding was functional, as complement activation was detected in a similar profile to the IgG deposition.

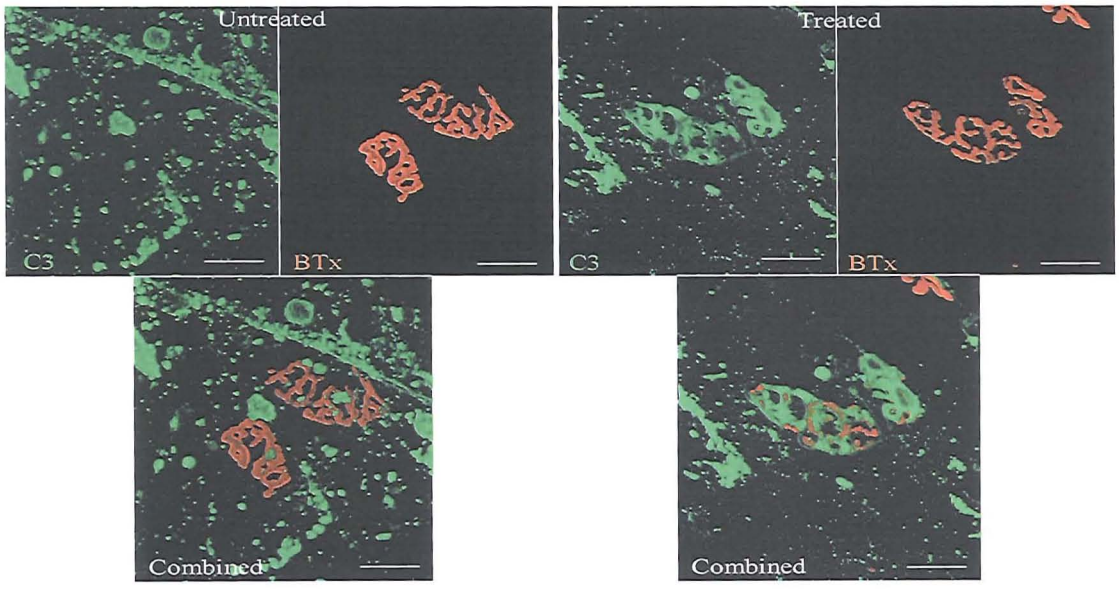

Fig 87. Ability of DG1 to activate complement in the GD3s$^{-/-}$ mouse. In N'ase treated tissue, C3 deposition is seen over the NMJ with a neuronal profile. Scalebar = 20μm

6.2.5.2 *Effect of N'ase on DG1 binding at the WT NMJ*

N'ase treatment of TS was repeated in the WT mouse, to confirm that the observed effects in the GD3s$^{-/-}$ are not unique to this genetically modified mouse.

The staining profile of DG1 in the N'ase treated tissue was axonal, and over the NMJ, although it did not appear to be as intense as shown in the GD3s$^{-/-}$mouse. DG1 did not bind to the control tissue.

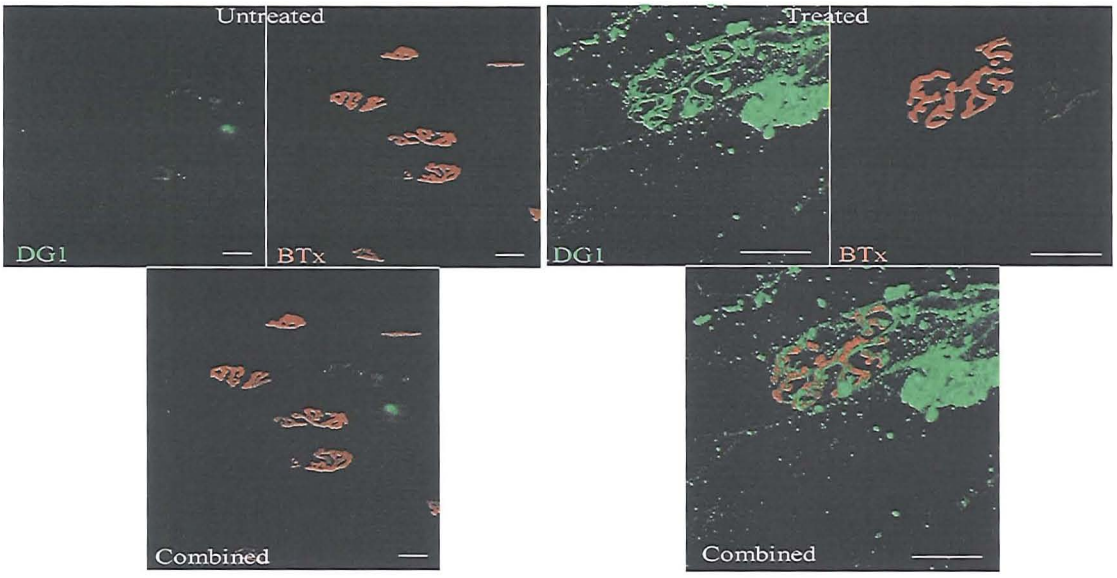

Fig 88. Effect of N'ase on DG1 binding in the WT TS muscle (*ex-vivo* preparation). N'ase results in deposition of DG1 over the NMJ. Scalebar = 20μm

6.2.5.3 *Effect of N'ase on Sm1 binding at the GD3s$^{-/-}$ NMJ*

The effect of N'ase in facilitating the binding of human antibodies was addressed, to illustrate that the N'ase protocol is effective in allowing both mouse antibodies, and those cloned from human neuropathy sera, to bind.

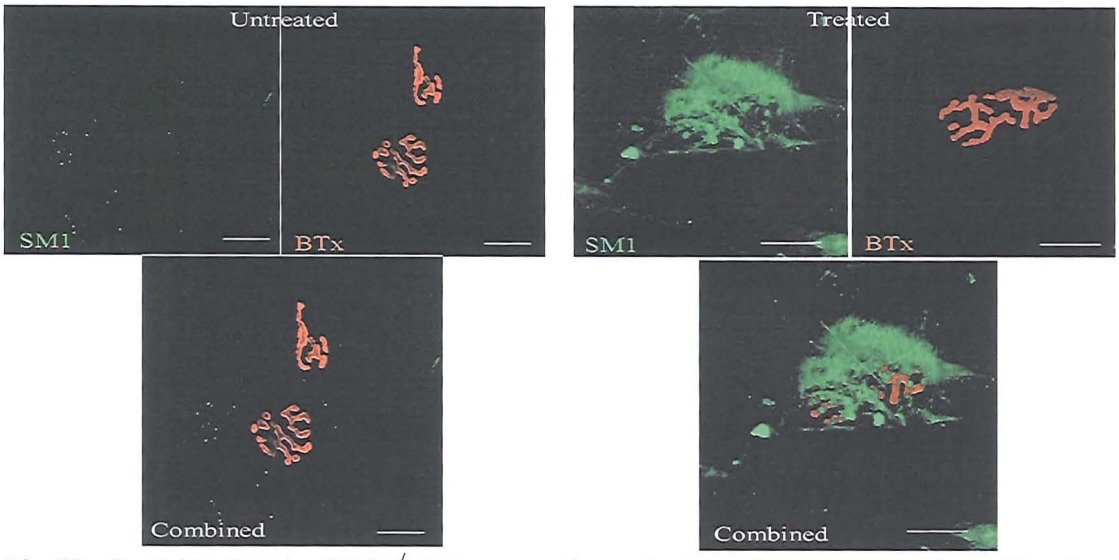

Fig 89. Sm1 binding in GD3s$^{-/-}$ TS preparation. Sm1 binds in a neuronal profile after N'ase treament, with evidence of PJF staining. Scalebar = 20μm

Fig 89 shows that Sm1 is only binding to the tissue in the GD3s$^{-/-}$ following enzymatic treatment. The antibody deposition appears concentrated over the NMJ and the profile looks axonal. However as shown, there is an additional staining blush over the endplate which may be evidence of PJF staining.

6.2.5.4 *N'ase Treated tissue: CTb Inhibition of DG1 Binding*

Thus far the data has assumed that DG1 is binding to GM1 following the N'ase treatment. To confirm that the epitope is GM1, the N'ase tissue was incubated in CTb prior to DG1 application. Any binding of DG1 following saturation of GM1 indicates that DG1 is binding to a different epitope. Results confirm that application of unlabelled CTb to N'ase treated tissue is able to inhibit the binding of DG1, both over the NMJ and in the axon (Fig 90).

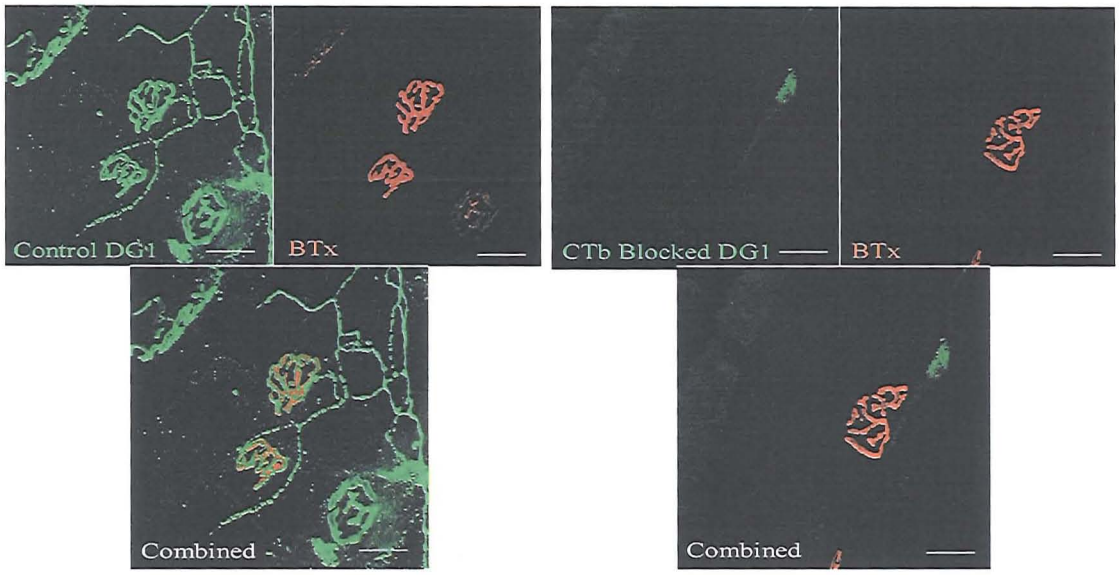

Fig 90. Effect of CTb on the ability of DG1 to bind in N'ase treated GD3s$^{-/-}$ TS preparation. N'ase treatment facilitates DG1 binding (left). N'ase followed by unlabelled CTb quenches GM1 and abolishes DG1 binding (right panel). Scalebar = 20μm

6.2.5.5 *N'ase Removal of GD1a*

The ability of N'ase to remove GD1a (as shown in PC12 cells) was confirmed at the NMJ by incubating both Ringer and N'ase treated tissue in MOG 35.

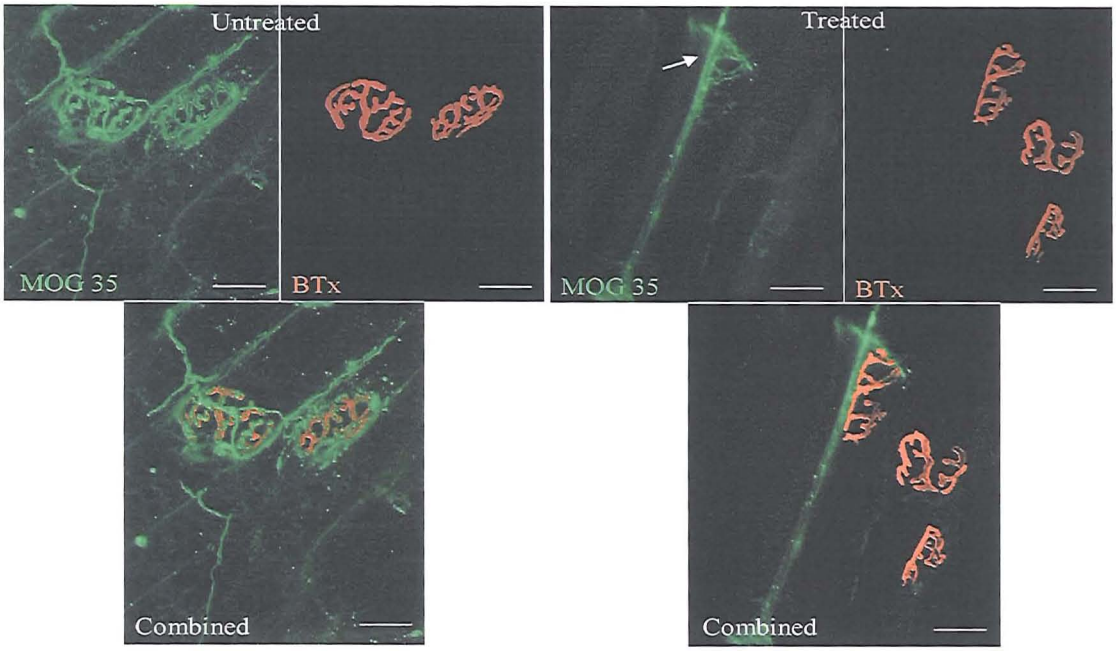

Fig 91. MOG 35 staining in N'ase treated GD3s$^{-/-}$ TS preparation, illustrating decreased staining when compared to untreated tissue. Arrow indicates persistence of GD1a in discrete areas, where MOG 35 is still able to bind. Scalebar = 20μm

In agreement with the previously characterised binding profile of this antibody (Goodfellow *et al* 2005), MOG 35 binds GD3s$^{-/-}$ tissue and has a strong axonal presence (Fig 91, left panel). Following treatment of the tissue with N'ase, the binding of MOG 35 is abolished, although as shown in Fig 91 (right panel), small but infrequent patches of staining remained (Fig 91, arrow), indicating these localised areas were not penetrated completely by the enzyme.

6.2.6 *N'ase Treatment in the Ex-Vivo Hemi Diaphragm*

The ability of DG1 to bind specifically to GM1, and activate complement, following N'ase treatment has been established. It is hypothesised that N'ase treatment followed by DG1 application and NHS will cause a complement mediated destruction of the motor nerve terminal.

6.2.6.1 *N'ase Dilution Series*

Owing to the fact the diaphragm is a thicker muscle that the TS, and to account for any possible differences in GD1a levels, a dilution series was performed to determine the optimal amount of enzyme needed to decrease GD1a in the diaphragm.

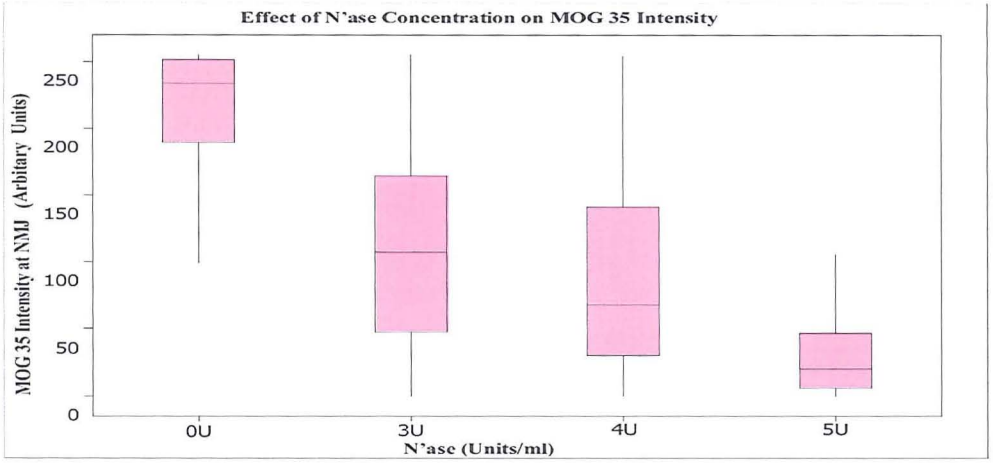

Fig 92. Dilution series performed in the GD3s$^{-/-}$ diaphragm to optimise the concentration of N'ase. N=1 animal, with a staining run of 3 slides from the beginning, middle and end of the cut series. Untreated tissue revealed no background staining.

As shown in the dilution series (Fig 92), MOG 35 binds strongly to PBS treated tissue (ie. 0 units of N'ase). For all concentrations of enzyme, a decrease in MOG 35 binding resulted when compared to the PBS control tissue ($p<0.0001$). The most significant decrease was at 5 units/ml, meaning this was selected as the optimal enzymatic concentration for removing GD1a.

6.2.6.1 *N'ase and DG1: IgG, C3, MAC, NF.*

Ex-vivo hemi-diaphragm muscle-nerve preparations were incubated in the following:

*Ringer followed by DG1 then NHS

*N'ase followed by DG1 then NHS

*N'ase followed by Ringer then NHS

Results were as shown in Fig 93:

IgG
Compared to DG1 application alone, N'ase treatment prior to DG1 leads to a significant increase ($p<0.0001$) in IgG deposition over the NMJ. There is no difference in IgG intensity between DG1 alone and N'ase alone treated tissue ($p=0.49$).

C3
C3 deposition is significantly increased in N'ase/DG1 treated tissue compared to DG1 alone ($p<0.0001$). There is no difference in C3 intensity between DG1 alone and N'ase alone treated tissue ($p=0.19$).

MAC
MAC intensity is greater in N'ase/DG1 treated tissue compared to DG1 application alone ($p<0.0001$). DG1 alone and N'ase alone led to no significant MAC deposition ($p=0.74$).

NF
N'ase application of the tissue caused a significant loss of NF coverage compared to DG1 alone treated tissue ($p<0.0001$). Application of N'ase/DG1 also caused a significant loss of NF in comparison to both DG1 alone ($p<0.0001$) and N'ase alone ($p<0.0001$).

Summary: Analysis of the control tissue, whereby N'ase was applied to the tissue and DG1 omitted before the addition of NHS demonstrates that N'ase treatment alone does not lead to C3 or MAC deposition, but causes NF loss. However NF loss in N'ase/DG1 treated tissue is significantly greater than in N'ase treated tissue

($p<0.0001$), indicating a significant proportion of this loss is attributable to the complement mediated destruction of the NF as a result of DG1 deposition.

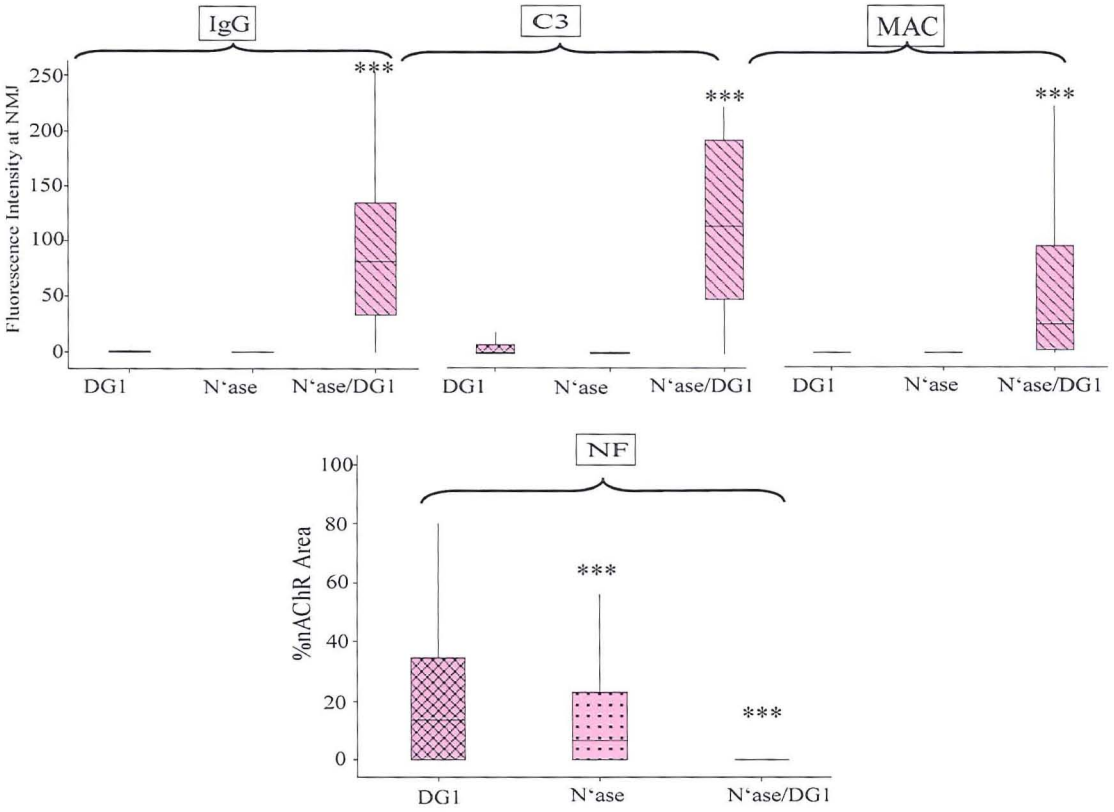

Fig 93. GD3s$^{-/-}$ hemi-diaphragm *ex-vivo* preparations. N'ase treatment leads to significant mAb, C3 and MAC deposition over the NMJ, and NF loss when compared to application of DG1 alone without prior N'ase treatment. Astrices indicate significance ($p<0.05$) when compared to DG1 alone treated tissue.

6.2.6.2. *Antibody Viabilty*

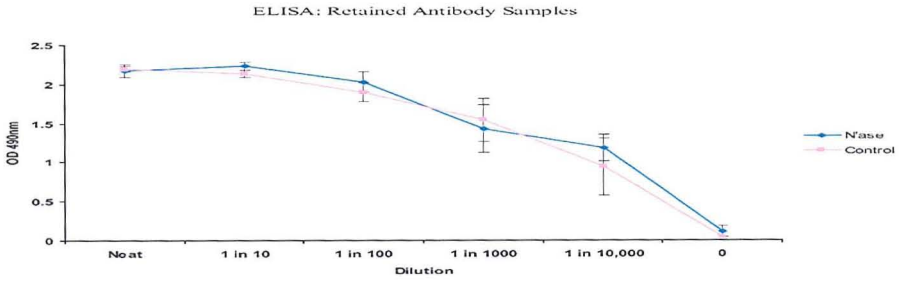

Fig 94: Retained antibody samples

6.2.6.3 *N'ase and Sm1*

The human antibody Sm1 was tested in the GD3s$^{-/-}$ hemi-diaphragm to look for pathological effect (Fig 95).

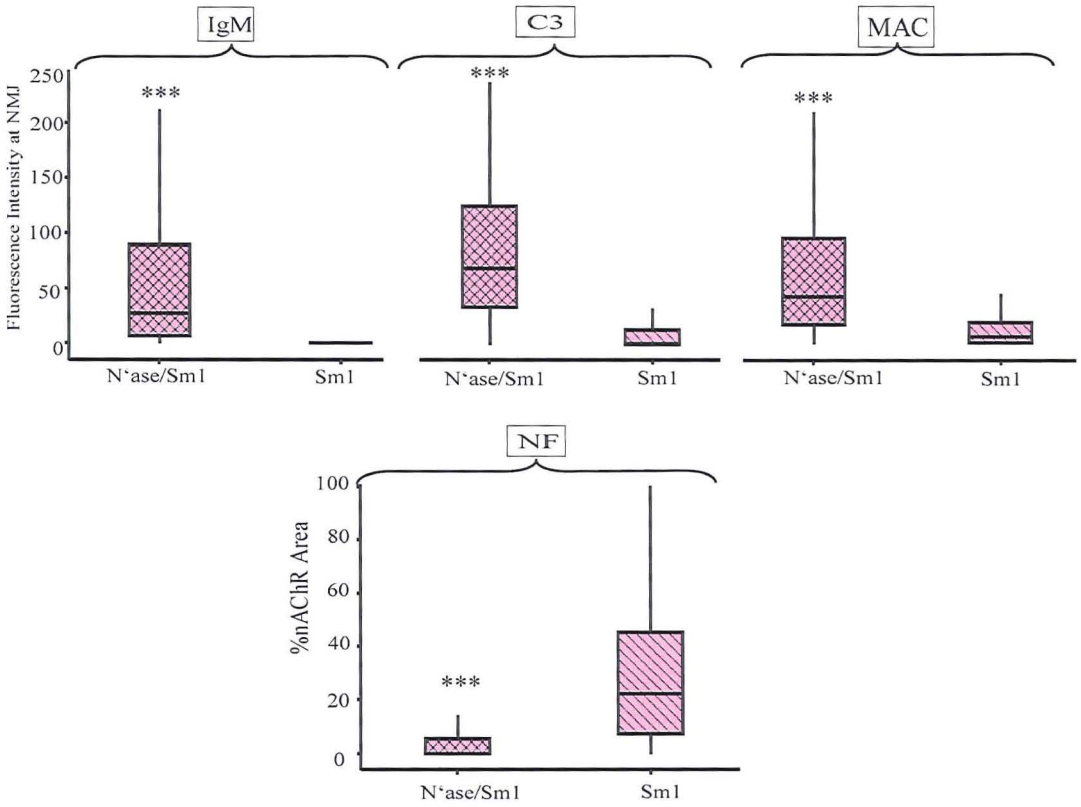

Fig 95. Sm1 in the GD3s$^{-/-}$ hemi-diaphragm. N'ase facilitates IgM deposition and a subsequent complement mediated lesion. Astrices indicate significance ($p<0.05$) when compared to tissue treated with Sm1 alone.

IgM
N'ase/Sm1 treatment of the tissue caused a significant increase in Sm1 (IgM) intensity over the NMJ compared to application of Sm1 alone ($p<0.0001$).

C3
N'ase/Sm1 treated tissue had more C3 activation over the NMJ than Sm1 alone treated tissue ($p<0.0001$).

MAC
There was a greater intensity of MAC in N'ase/Sm1 treated tissue compared to Sm1 treated tissue ($p<0.0001$).

NF
When compared to Sm1 alone, NF coverage over the NMJ was significantly reduced in N'ase/Sm1 treated tissue ($p<0.0001$).

Summary: N'ase allows Sm1 to bind over the endplate and cause a significant complement mediated lesion. Sm1 does not have this ability when applied to the tissue without prior N'ase treatment.

6.2.6.4 *N'ase and Do1*

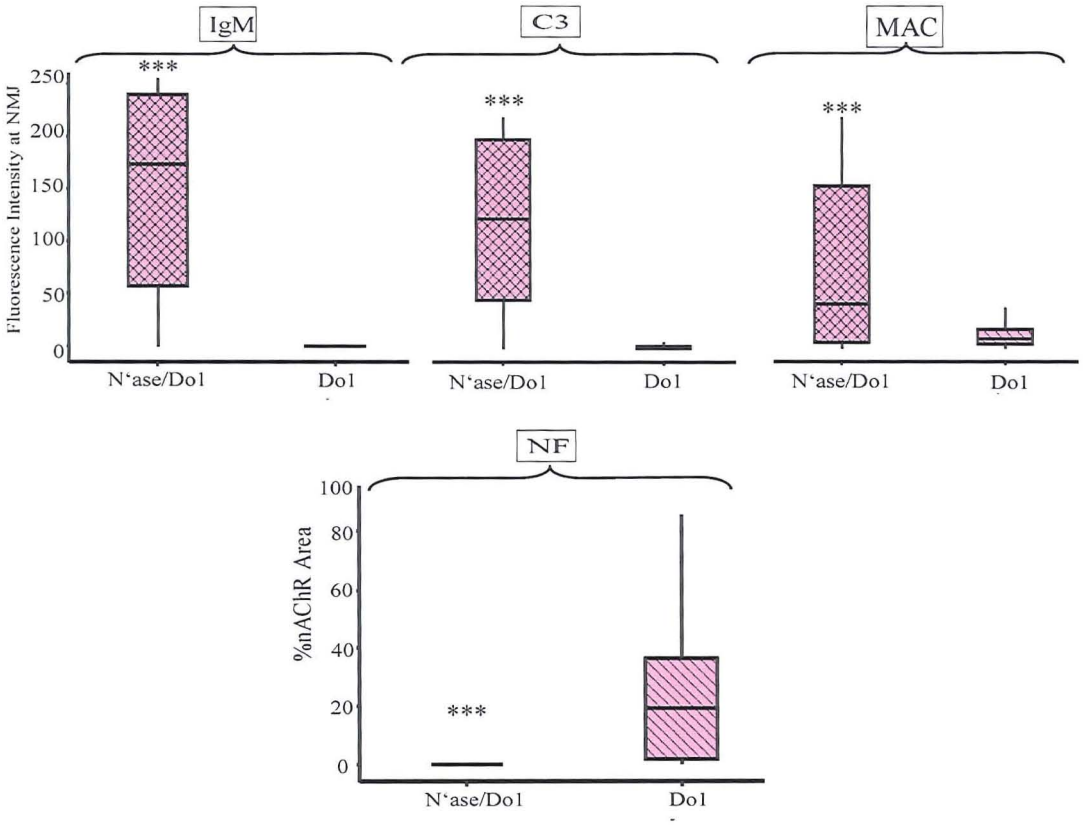

Fig 96. Do1 in the GD3s$^{-/-}$ hemi-diaphragm. Do1 is only pathogenic following N'ase treatment of the tissue. Astrices indicate significance ($p<0.05$) compared to Do1 alone.

IgM
IgM intensity over the NMJ was significantly increased in N'ase/Do1 treated tissue compared to tissue treated with Do1 alone ($p<0.0001$).

C3

Intensity of C3 deposition over the NMJ was significantly greater in N'ase/Do1 treated tissue compared to treatment with Do1 alone ($p<0.0001$).

MAC

N'ase/Do1 treated tissue had greater intensity of MAC over the NMJ when compared to Do1 treatment ($p<0.0001$).

NF

There was a significant reduction on NF when comparing N'ase/Do1 treated tissue to Do1 alone treated tissue ($p<0.0001$).

Summary: In a similar scenario to Sm1, Do1 is only able to bind, activate complement and lead to NF loss when the GD3s$^{-/-}$ hemi-diaphragm tissue has been pre-treated with N'ase.

6.2.7 *GM1 "Unmasked" versus "New" GM1*

One important question to address was whether the DG1 binding and subsequent lesion was due to DG1 binding to "unmasked" GM1, or simply whether DG1 was binding to the "newly created" GM1, generated from the enzyme treatment. In order to ascertain what population of GM1 the antibody was binding, an *ex-vivo* experiment was designed based on the hypothesis that application of a saturating dose of CTb should bind all native GM1, thus following N'ase treatment, the only GM1 available will be the "new" GM1 created by the enzymatic removal of sialic acid (shown schematically in Fig 97).

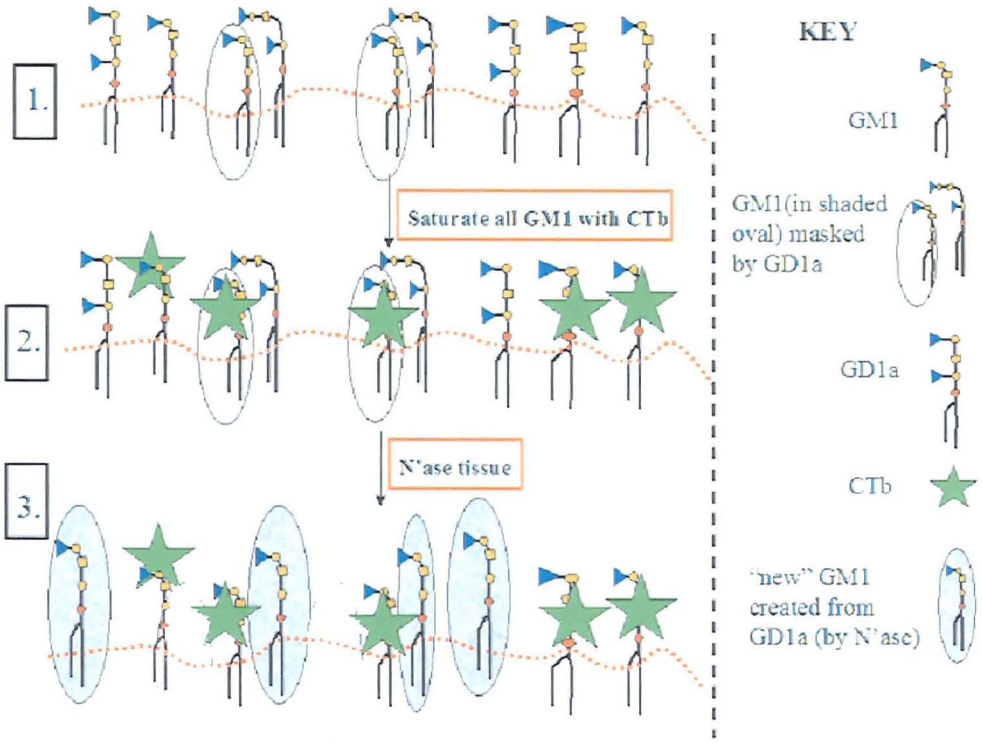

Fig 97. Schematic overview of experimental design. 1. Living membrane with GM1, GD1a and GM1 in grey oval represents the GM1 which is unavailable to DG1 due to masking by GD1a. 2. Saturating CTb applied to bind all endogenous GM1. 3. N'ase is applied, and removal of terminal sialic acid from GD1a results in creation of "new" GM1 (blue ovals) which is CTb free and thus available to mAbs.

As shown in Fig 98, DG1 bound strongly to Ringer-N'ase treated tissue, but the staining was dramatically reduced when compared to CTb-N'ase treated tissue ($p<0.0001$). For DG2, there was no significant difference in the signal intensity at the endplate when comparing Ringer-N'ase and CTb-N'ase treated tissue ($p=0.47$) (Fig 98).

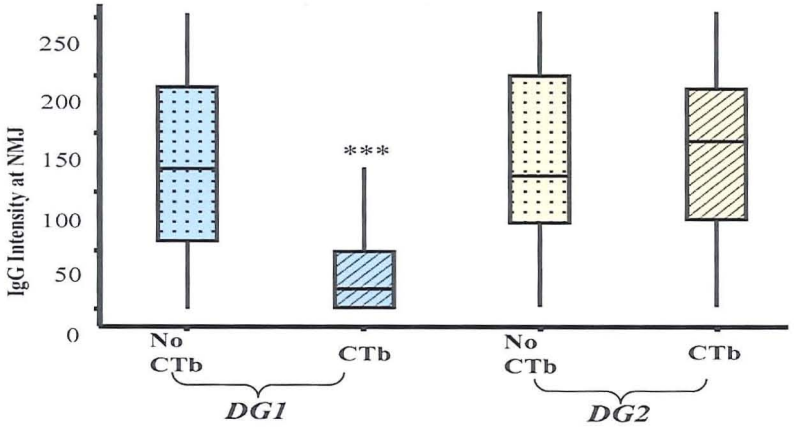

Fig 98. Effect of a saturating dose of CTb prior to N'ase treatment on the ability of DG1 and DG2 to bind to GM1. Astrices indicate significance ($p<0.05$) when comparing CTb blocked tissue to that without CTb for each antibody.

The interpretation of this data suggests that the ability of DG1 to bind following N'ase treatment relies on the presence of native GM1, which is being "unmasked", and the pre-saturation of this population with CTb is hindering the binding of DG1. DG2 binds to GM1 in the membrane under both treatment conditions (Ringer-N'ase and CTb-N'ase), suggesting that in the CTb blocked tissue, there is an abundant population of "new" GM1, which is available to DG2 binding. Fig 98a),b) provides an illustration of the binding profiles of DG1 and DG2 respectively.

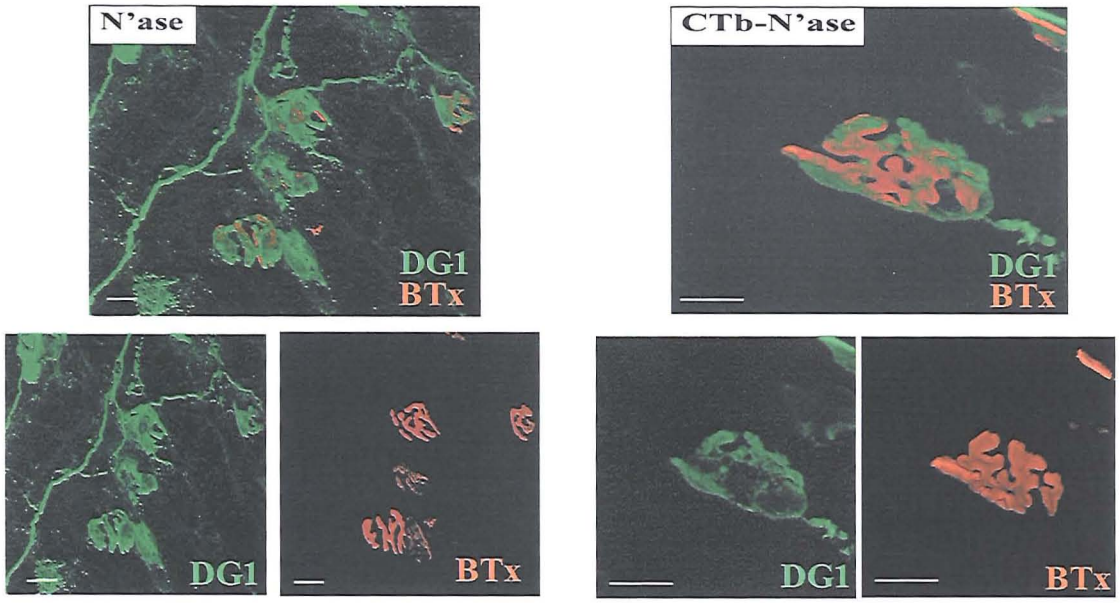

Fig 99 a) Left panel shows DG1 deposition after N'ase treatment. On the right, saturation of the tissue prior to N'ase treatment greatly reduces the ability of DG1 to bind. NMJ shown was chosen as an example as it displayed the strongest DG1 signal after the CTb block, and thus gives the best visualisation of the staining profile, which remains neuronal. Scalebar = 20μm

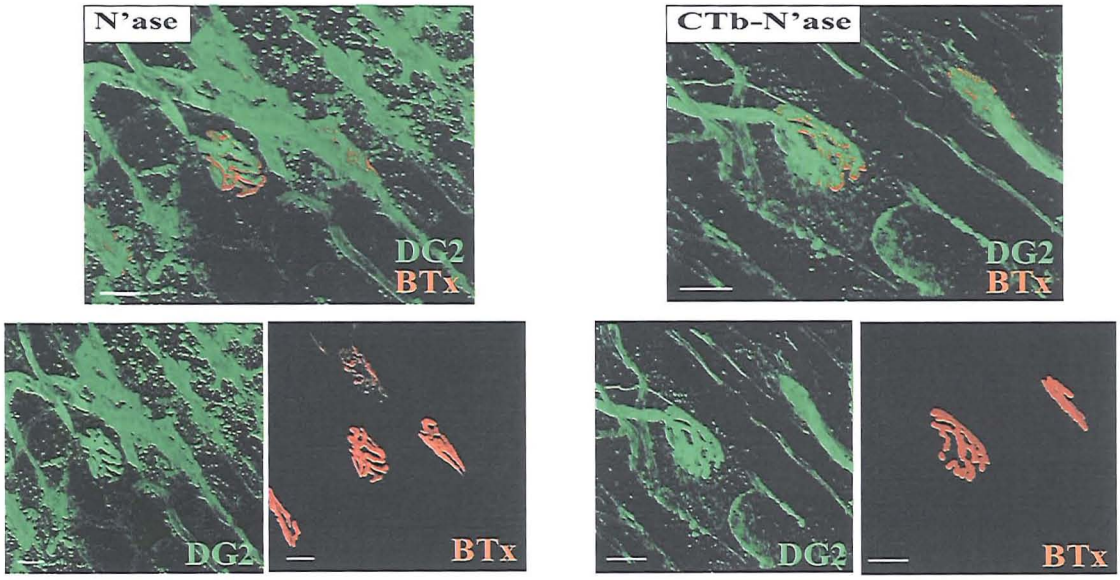

Fig 99b. As for Fig 99a, but with DG2. DG2 was still able to bind strongly over the NMJ after CTb saturation /N'ase treatment, although less intense staining of surrounding structures is seen. Scalebar = 20μm

From the illustrations, it is clear that in the Ringer-N'ase treated tissue (ie. no CTb block of GM1), there was more staining of other tissue structures, for example blood

vessels. However, as shown by the quantitative analysis (Fig 98), there was no significant change in signal intensity over the NMJ. This may be due to the fact that GD1a is strongly axonal, meaning the conversion of GD1a to GM1 by the enzyme is being bound by DG2 and the resultant signal is enough to compensate for the saturation of native GM1 over the endplate. In blood vessels however, there may be less GD1a and its conversion to GM1 is not enough to result in an intense DG2 signal.

6.2.8 *Discussion*

The use of ELISA is a powerful tool in determining antibody specificities for particular gangliosides. However the results displayed here indicate the use of ELISA to model complex antibody-antigen interactions is not ideal.

Certain "assumptions" will always cloud the data, for example the interaction of the ELISA plate and ganglioside may result in the epitope being presented to the mAb in a manner which would not occur in the membrane (Willison 2005).

On the same note, the interaction of 2 gangliosides on an ELISA plate and 2 gangliosides in the membrane may differ. On ELISA the gangliosides are brought together at a 50:50 ratio and have no other substrate (aside from the ELISA plate) to interact with. In the membrane, the presence of proteins and other lipids may influence the ganglioside-ganglioside interaction which would thus differ from the interaction represented in the ELISA experiment. Furthermore, membranes are fluid structures, with the presence of cholesterol facilitating the formation of transient and heterogenous lipid rafts which are not represented on a solid phase ELISA.

By ELISA, DG2 bound weakly to GD1b, so in order to determine the value of DG2 binding to GM1 alone in the mixed well, the binding of DG2 to GD1b alone was subtracted from the DG2 value obtained in the GM1:GD1b mixed well. This

methodology was also applied to the CTb results. What this has not accounted for, however, is the possibility that GM1 may actually have been inhibiting DG2 from binding to GD1b, and thus it is difficult to draw definitive conclusions from ganglioside mixing studies unless the mAb binds to GM1 alone. Even the use of CTb was not ideal, as CTb bound to other gangliosides on solid phase, a finding previously described (Kuziemko *et al* 1996). It is worthwhile also to note that the gangliosides used are only of 95% purity, and the addition of methanol to reconstitute means that every time a bottle is opened, evaporation occurs and this will eventually affect the overall concentration of the actual ganglioside. This is unavoidable within the laboratory environment where gangliosides are a common stock and routinely used. Thus, owing to the potential pitfalls of ELISA, this study was redesigned to focus on the interactions of gangliosides in the living membrane.

PC12 cells were chosen as these are an already characterised neuronal cell line that "provide an excellent model to study complex ganglioside expression" (Walton *et al* 1988). Ganglioside expression is maximal in cells grown at high density, although at more sparse densities expression decreases but the relative proportions of ganglioside species remain unaltered (Walton *et al* 1988).

N'ase treatment convincingly reduced the levels of GD1a and subsequentially increased the ability of DG1 to bind. The addition of exogenous GD1a to the cells was expected to interact with GM1 and again block the ability of DG1 to bind, however an immediate block of DG1 binding following GD1a application was not observed. Western blot data supports the theory that the exogenous GD1a did not specifically enter the raft fraction, as in N'ase treated and GD1a reloaded cells, there was an increased proportion of GD1a in the non-raft fractions when compared to the normal cells. The exogenous insertion of gangliosides to the bilayer is believed, in

certain systems, to disrupt the normal formation of the membrane and rafts. It has been shown that the exogenous application of gangliosides to MDCK cells inhibits cross linking of raft associated GPI anchored proteins, and increases their solubility (Simons *et al* 1999). It is proposed that the gangliosides disrupt attractive forces between such proteins allowing them to "escape" from the raft and presumably disorganising the architecture of the raft. Exogenous addition of gangliosides may also alter the architecture of the cell membrane, for example exogenous GM1 is thought to alter the dynamic properties of lipid rafts by excluding certain GPI anchored proteins (including Thy1), perhaps through competition between GM1 and the protein for raft occupancy (Crespo *et al* 2002). Interestingly, the same authors show that not all exogenously added GM1 becomes associated with detergent insoluble microdomains, unlike endogenous GM1. This indicates that exogenously added gangliosides may infer different functional properties to the cell membrane. Furthermore, GM1 has a large polar head group (Sonnino *et al* 2006) thus any alterations (eg. induced by N'ase) in the presentation of GM1 may cause exogenous GD1a to enter a neighbouring raft due to space limitation within the GM1 containing raft.

Using N'ase leads to the removal of sialic acid from gangliosides to increase the density of GM1 in the membrane. This would imply that, in the experiments within this chapter, enzymatic treatment is increasing the amount of GM1 and thus DG1 binding is dependent on the density of the epitope. As shown by the CTb saturation of tissue prior to N'ase treatment (Fig 98), DG1 binding decreased significantly suggesting its ability to bind after N'ase treatment depends on the unmasked endogenous GM1. However, it is not possible to discount the notion that the "new" GM1 is not at a high enough density for DG1 to bind, and that the binding observed

after N'ase treatment relies on a combination of unmasked GM1 and "new" GM1 to create an increased density of GM1 for DG1 to bind. This is difficult to address experimentally, but I favour the hypothesis that the increased availability of GM1 is due at least in part due to the exposure of "unmasked" GM1 (Ackerman *et al* 1980) based on the following rationale: N'ase treatment of the NMJ results in removal of a large proportion of GD1a from the membrane, as inferred from the decreased MOG 35 staining at the endplate when compared to untreated tissue. In line with the decrease in available GD1a, it is logical to assume that there is a parallel increase in the amount of GM1. Thus, one can use Fig 100 to rationalise what may be happening at the NMJ. For example, in the wild type (WT) mouse, it is highly likely that the GM1 band would increase to a more comparable level to the $GD3s^{-/-}$, and a concomitant decrease in wild type GD1a would be detected. In more simple terms, the N'ase treated WT NMJ should theoretically have a similar amount of GM1 as the $GD3s^{-/-}$ mouse. Therefore the ability of DG1 to bind in the N'ase treated WT mouse is not surprising. However, what is surprising is the inability of DG1 to bind to the membrane of the $GD3s^{-/-}$ mouse. Comparison of the N'ase treated WT mouse with the untreated $GD3s^{-/-}$ may reveal a similar level of GM1, however the levels of GD1a in the $GD3s^{-/-}$ mouse are greatly enriched when compared to the N'ase treated WT mouse. This observation supports the hypothesis that GD1a is cryptically masking GM1 in the membrane of the $GD3s^{-/-}$ mouse, and potentially also in the WT mouse where the GD1a removal is "unmasking" GM1. It is also possible that in the $GD3s^{-/-}$ mouse, the altered ganglioside profile may have a knock-on effect on the ganglioside content and presentation within lipid rafts; while this cannot be ruled out, it again supports the notion that while there is "enough" GM1 there, it cannot be seen by DG1.

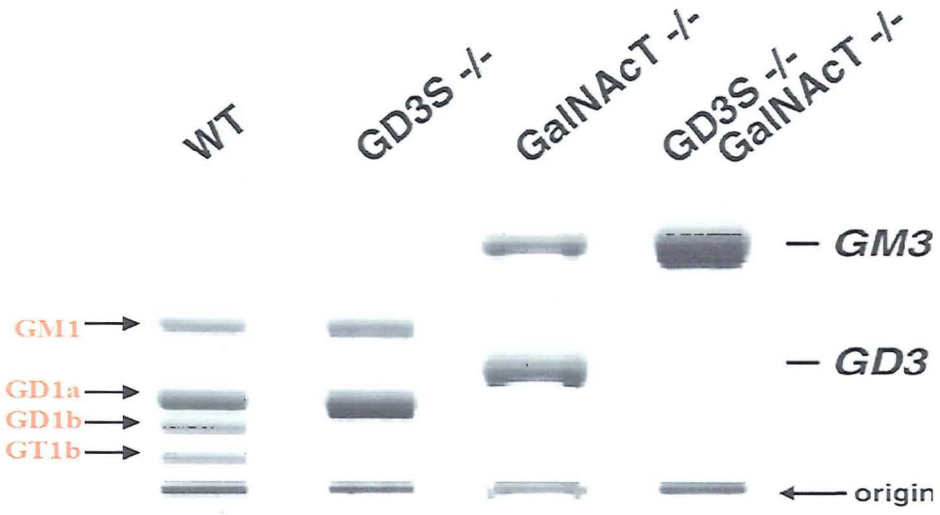

Fig 100. Modified from Kawai et al 2001. Comparison of GD3s$^{-/-}$ and WT ganglioside patterns.

Furthermore, the demonstration that saturation of endogenous GM1 with CTb prior to N'ase treatment leads to a significant increase in DG2 intensity but not DG1 intensity is evidence that the "new GM1" (created from GD1a) is not bound by DG1.

Chapter 7

7.1 Introduction

Results of the previous chapters are indicative that the removal of GD1a is allowing GM1 to become available to DG1. Gangliosides are raft associated (Brown and London 2000), and any such interaction between GM1 and GD1a is likely to occur within the domain of a lipid raft. This chapter investigates the spatial relationship between GM1 and GD1a, and also addresses the existence of rafts which contain both GD1a and GM1. Two approaches were used in this study: firstly, the colocalisation of GM1 and GD1a by microscopic analysis, and secondly, the association of GM1 and GD1a using biochemical techniques.

7.2 Microscopy

7.2.1 *Fluorescent Staining Profiles of GM1 and GD1a: NMJ*

Using MOG 35 and CTb to label GD1a and GM1 respectively, NMJs were stained in whole mount *ex-vivo* TS muscles. Images were rendered using "maximal intensity projection" (MIP), which is a flat projected z-stack in which the brightest pixel in each z-axis is displayed. This approach means any overlapping areas of FITC and TRITC staining will appear yellow, indicating overlap. As seen in Fig 101, there is considerable overlap of GM1 and GD1a staining over the endplate, with both gangliosides having a strong and overlapping axonal profile.

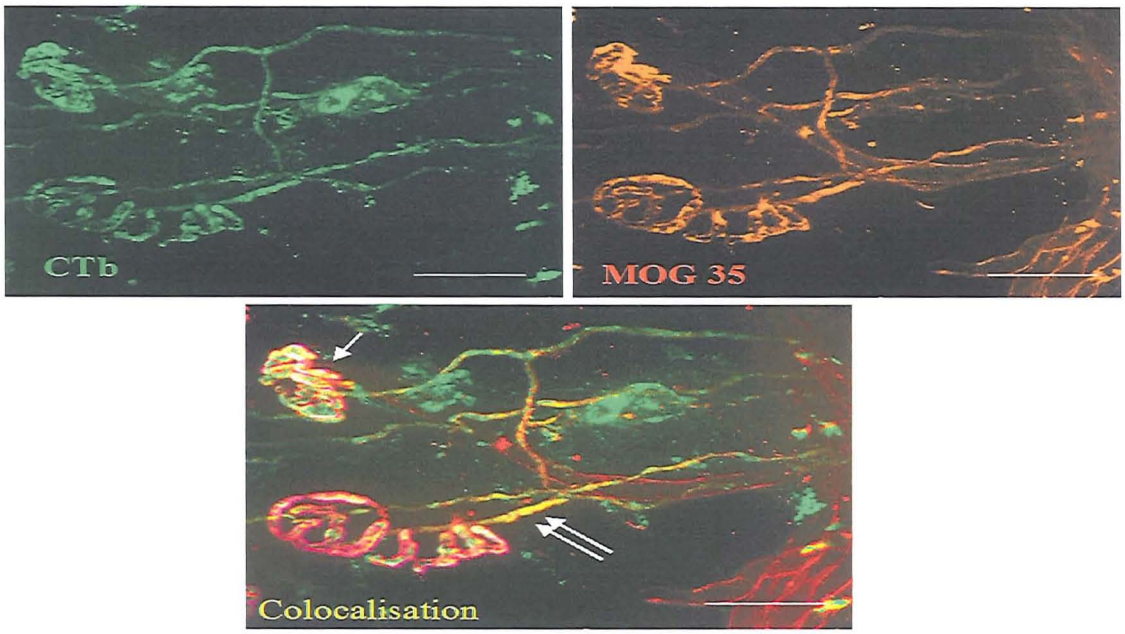

Fig 101: GD3s$^{-/-}$ *ex-vivo* TS preparations. CTb-FITC labels GM1, while the distribution of GD1a is shown by the binding of MOG 35 and secondary TRITC detection. On the combined image, overlapping areas of FITC and TRITC appear yellow, indicating colocalisation between GD1a and GM1. Arrow indicates an area of such colocalisation over the NMJ, and along the axon (double arrow). In the combined image, the BTx signal (pink) is shown to specifically define the NMJ. Scalebar = 20μm.

7.2.2 *Fluorescent Staining Profiles of GM1 and GD1a: PC12*

Because the NMJ is a complex structure, and discrete staining profiles are not easily imaged, the antibodies were applied to a more simple system, in this case PC12 cells. If a staining profile appears punctate, this is indicative that the epitope lies within defined regions of the membrane, as opposed to being diffusely distributed, and is therefore a useful, if indirect indicator of raft association. The appearance of domains with overlapping FITC and TRITC is evidence that within these defined regions, there is presence of both GM1 and GD1a.

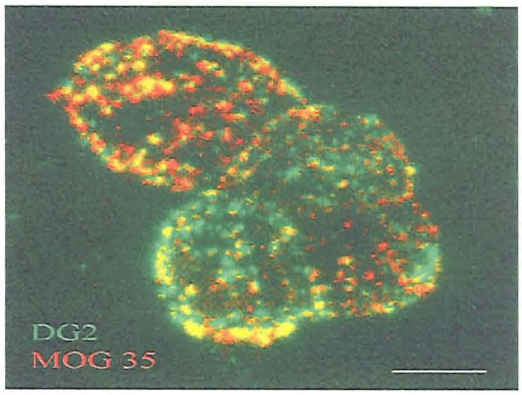

Fig 102. PC12 cells. MOG 35-TRITC and DG2-FITC labelling of GD1a and GM1 respectively, using unconjugated primary antibodies detected with sub-type specific fluorescent secondary antibodies. Image shows MIP of z-stack, where overlap of FITC and TRITC appears yellow. Non specific cross-reactivity between the secondary antibodies was ruled out by omission of either primary mAb and application of both secondaries. Scalebar = 15μm.

As shown in Fig 102, the staining profile of both GM1 (stained with DG2 and FITC conjugated secondary) and GD1a (stained with TRITC conjugated secondary) is not uniformly distributed over the cell surface, indicating that the gangliosides are located in discrete regions of the membrane. From the MIP image, it is apparent from the yellow colocalisation that there is overlap of the GM1 and GD1a associated signals. There are also areas of FITC or TRITC staining where no overlap is apparent, indicating GM1 and GD1a association is not obligatory. It is also possible that weak staining of either fluorophore was not detected by the microscope and therefore not represented on the MIP.

7.2.3 *MOG 35 and DG1 Staining: Primary Labelled mAbs*

Following removal of GD1a by N'ase, the profile of DG1 staining should indicate whether it is binding to raft or non-raft associated GM1. As both DG1 and MOG 35 are IgG2b subtypes, use of a secondary antibody would not distinguish DG1 and MOG 35

staining. The primary labelling of each antibody with different fluorophores overcame this problem. DG1 and MOG 35 were primary labelled using the *Zenon® Mouse IgG Labeling Kits* (Invitrogen, Paisley) following manufacturer's instructions.

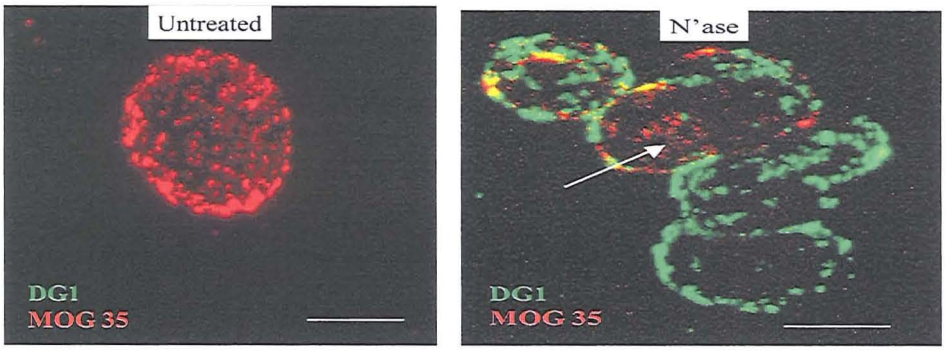

Fig 103. Untreated and N'ase treated PC12 cells. MOG 35 staining is mostly abolished upon treatment when compared to control cells. Note the intense DG1 staining in N'ase treated cells, except in the patches where MOG 35 staining persists (arrow). Scalebar = 15μm.

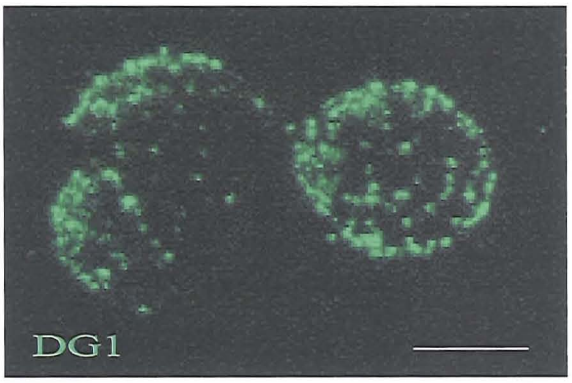

Fig 104. N'ase treated PC12 cells, stained with primary labelled DG1. Note the punctate non-uniform staining pattern of the cell surface. Scalebar = 15μm.

As can be seen in Fig 103, N'ase treatment resulted in an obvious removal of the MOG 35 signal, indicating GD1a levels were reduced, with a concomitant increase in DG1

staining. Fig 104 shows DG1 staining was non-random, and appeared in discrete patches on the membrane, again indicating a raft associated staining profile.

7.2.4 *GM1 and GD1a Pixel by Pixel Colocalisation*

Following the observation that GM1 and GD1a staining is non-uniform, a quantitative pixel by pixel analysis was performed on the stained cells in order to determine an overlap correlation coefficient (r^2) of GM1 and GD1a.

Cells were double stained in the following combinations:

GM1(FITC)		GD1a (TRITC)
CTb	+	MOG 35 then anti-mouse IgG2b
CTb	+	MOG 35 primary labelled
DG2 then anti-mouse IgG3	+	MOG 35 then anti-mouse IgG2b

In the last group, negative controls were performed by omiting MOG 35 and applying both secondaries, then omitting DG2 and applying both secondaries. This confirmed no cross reactivity of the secondary antibodies, and that they were subtype specific. Anti-mouse IgG2b was also confirmed not to bind to CTb.

Fig 105 displays an example of single cell fluorescent images, which were overlaid to give the combined colour image.

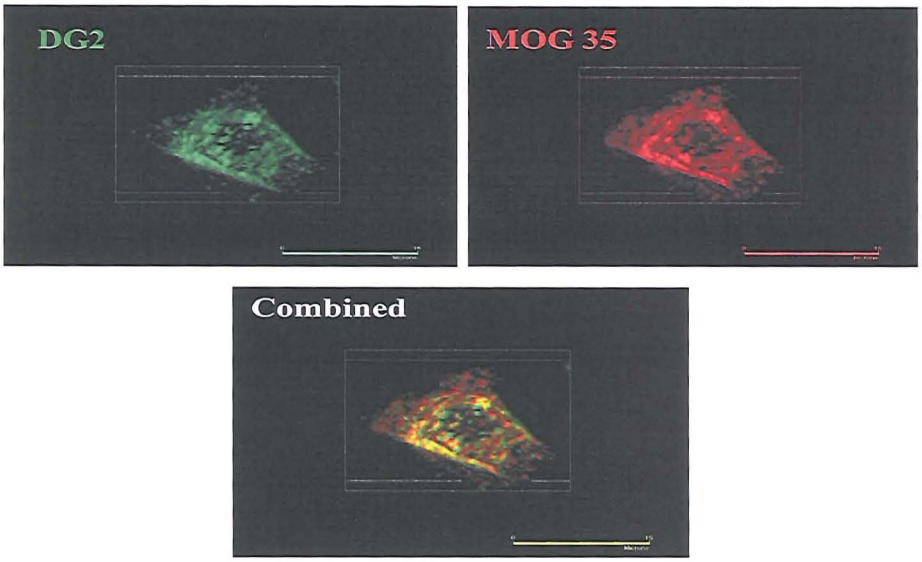

Fig 105. Z- stack reconstruction of images used for correlation analysis. Images were gathered using a Zeiss LSM 5 Pascal laser scanning confocal microscope (Carl Zeiss Inc., Welwyn Garden City, UK) with a x63 oil-immersion Plan Fluor Apochromat objective lens, numerical aperture 1.4. Scalebar = 15μm

The colour overlap was determined by selecting a region of zero fluorescence from an unstained (ie. background area) in both the FITC and the TRITC channel, and subtracting the respective level of background from each channel. Metamorph (version 6.3.3; Molecular Devices Corp., Downing, PA) correlation plot software was then used to compare the amounts of fluorescence in each pixel of the FITC and TRITC channels, where a perfect correlation would yield a coefficient of 1. Fig 106 illustrates this procedure for 1 cell. The colocalisation study (resultant data in Figs 105, 106 and 107) was done with the help of Dr John Pediani, University of Glasgow.

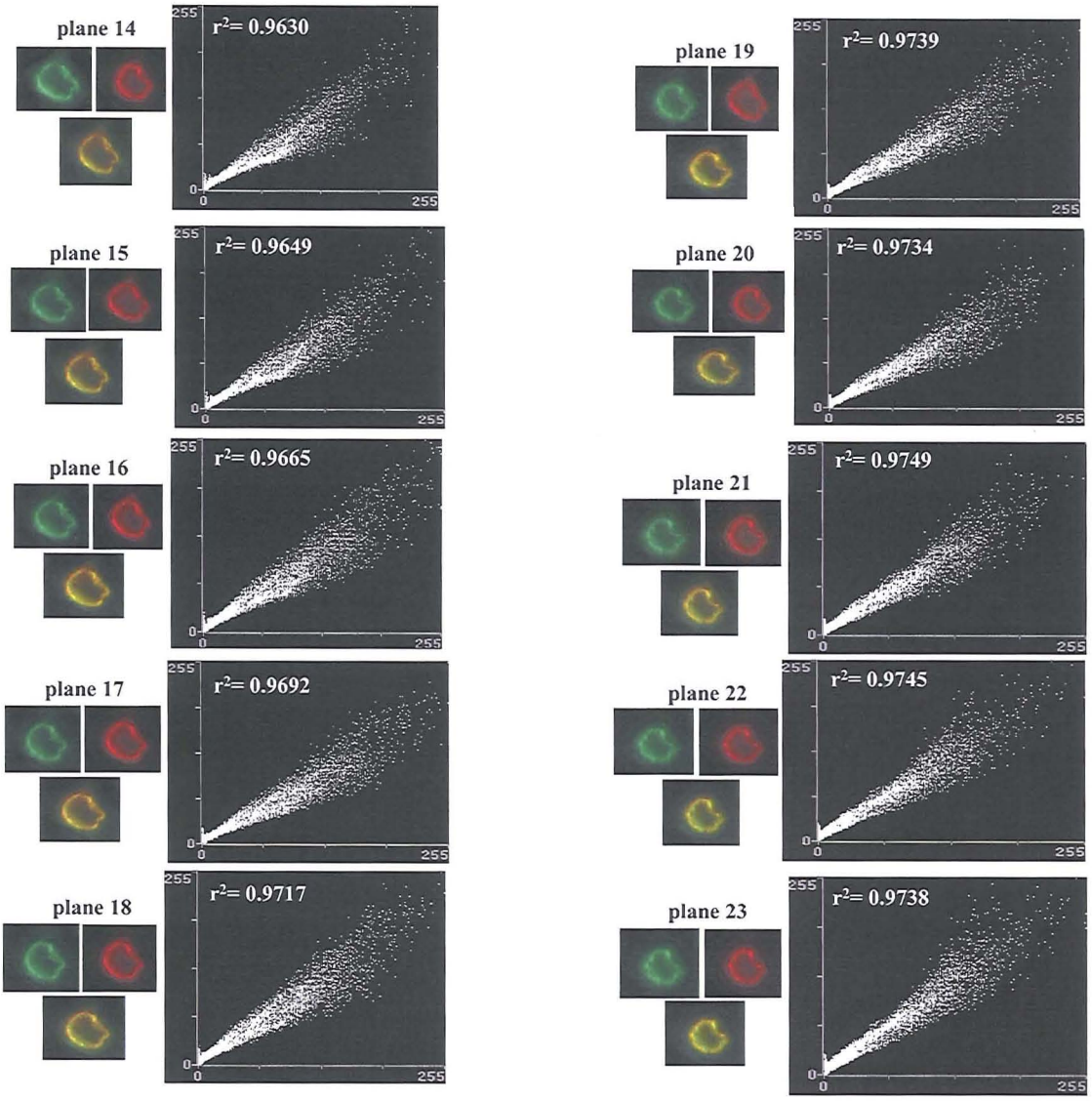

Fig 106. Plane by plane analysis of FITC and TRITC overlap for MOG 35 (primary labelled TRITC) and CTb (primary labelled FITC). Each plane is a 0.301μm step, meaning a depth of approximately 3 microns was analysed per cell to ensure an adequate sampling of the cell surface membrane. From the 10 planes, an average was calculated to give the correlation coefficient. This was repeated for 3 cells.

For each staining condition, a near perfect correlation coefficient was obtained, as shown in Fig 107.

Sample	Average r^2	S.E.M
A	0.96	0.02
B	0.96	0.01
C	0.95	0.01

Fig 107. Correlation coefficients for GD1a and GM1. SEM =standard error of the mean of 3 cells, with 10 planes per cell analysed as described for Fig X.
A= CTb FITC, MOG 35 primary labelled TRITC
B=CTb FITC, MOG 35 then anti-mouse IgG2b
C=DG2 and MOG 35 then anti-mouse IgG3 FITC and 2b TRITC respectively

This demonstrates that at the pixel level, GM1 and GD1a colocalise. The colocalisation obtained by primary labelled mAbs is similar to that of unconjugated mAbs which were detected using secondary fluorescence, which is indicative that the primary labelling is not altering the specificity or binding ability of the mAbs.

7.2.5 *GM1 and GD1a: Uncoupling with mAbs*

GD1a and GM1 colocalisation led to the hypothesis that the binding of MOG 35 to GD1a could be sufficient in altering the spatial relationship between GM1 and GD1a, and allow DG1 to bind to the unmasked GM1. The binding of GM1 in this scenario would indicate that there is a close interaction between GM1 and GD1a, which may be beyond that of the resolution obtained at the light microscope level.

As shown in Fig 108, when cells were incubated in primary labelled MOG 35, rinsed, and then incubated in primary labelled DG1, no DG1 binding could be detected. Assuming the primary labelling of the mAbs had not altered the specificity or binding dynamics, it can be concluded that antibodies against GD1a do not alter the orientation of GD1a in the membrane to expose GM1 in a way which allows DG1 to bind. Had the experiment

allowed DG1 to bind, this would have been strong evidence that GM1 and GD1a are in close spatial resolution beyond that of the resolution of the pixel by pixel analysis.

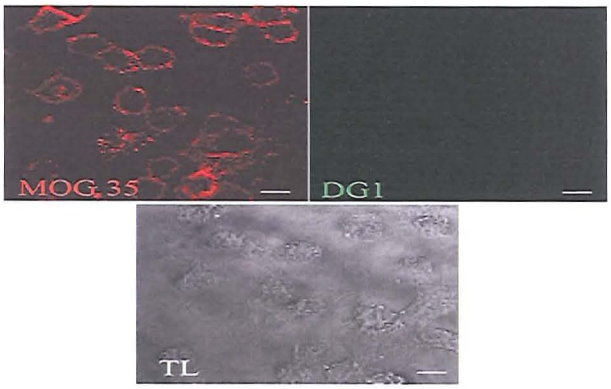

Fig 108. Pre-incubation of cells with MOG 35 (primary labelled TRITC) gave strong binding, however subsequent rinsing and application of DG1 (primary labelled FITC) did not result in any detectable binding. (TL=transmitted light).

7.2.6 *Fluorescence Resonance Energy Transfer (FRET)*

FRET is an established method for detecting clustered species in the membrane (Matko and Edidin 1997). The basis of FRET relies on labelling 2 membrane species with a different fluorophore, and upon excitation the energy absorbed by one fluorophore is transferred (resonantly) to the other. Thus, the 2 fluorophores are termed "Donor" and "Acceptor", and the choice of donor and acceptor must equal a functional "FRET pair". In other words, the emission spectra of the donor must overlap the absorbance of the acceptor, meaning that the acceptor is able to absorb the resonant energy emitted by the donor, to increase the acceptor fluorescence (Fig 109).

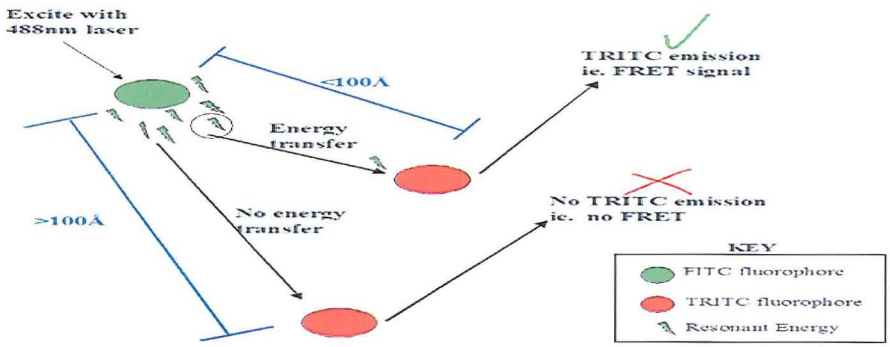

Fig 109. Simplified FRET overview. The FITC donor is excited at 488nm, and resonant energy transfers to a TRITC acceptor which lies within 10nm, and the excitation of the latter leads to an increase in its fluorescence. An acceptor located further than 10nm from the donor is not excited and thus does not get brighter.

The efficiency of this energy transfer depends crucially upon the distance between the 2 fluorophores (Garini *et al* 2005), and for efficient transfer to occur (ie. for FRET to be detected) the fluorphores should ideally lie within 100 Å (angstroms) (10 nanometers). So, a positive FRET signal infers that the 2 epitopes of interest lie within 100 Å. A pictorial overview of the FRET theory is shown in Fig 110.

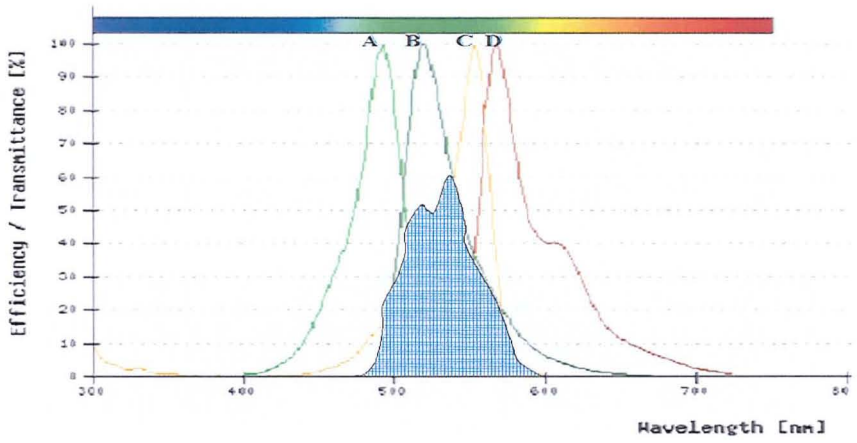

Fig 110. Modified from www.zeiss.co.uk. The overlap between the emission spectra of FITC and the absorption (excitation) spectra of TRITC is shown by the hatched area. **A**=FITC excitation, **B**=FITC emission, **C**=TRITC excitation, **D**=TRITC emmision.

2 common methods for detecting FRET are Photobleaching FRET and Sequential FRET, and these methods were used to optimise a method of detecting FRET for GM1 and GD1a. The accepted FRET pair of FITC and TRITC were chosen for this experiment. It should be noted, however, that where primary labelled mAbs were used, the fluorophores were either Alexa 488 or Alexa 555. These have been referred to as FITC and TRITC for ease of interpretation in this chapter, and do not alter the integrity of the FRET pair.

5.2.6.1 *Photobleaching FRET*

The acceptor photobleaching method measures the fluorescence of the donor both in the presence and photobleaching-induced absence of the acceptor (Kenworthy and Edidin 1998). By selecting a region of interest (ROI), the excitation of the donor in the presence of the acceptor can be measured. The acceptor is then photobleached in the ROI, and upon excitation of the donor, there should be a notable increase in donor signal intensity when compared to its signal when the acceptor was present. By bleaching out the acceptor, any emitted energy from the donor is not 'robbed' by the acceptor, and thus the donor fluorescence should increase.

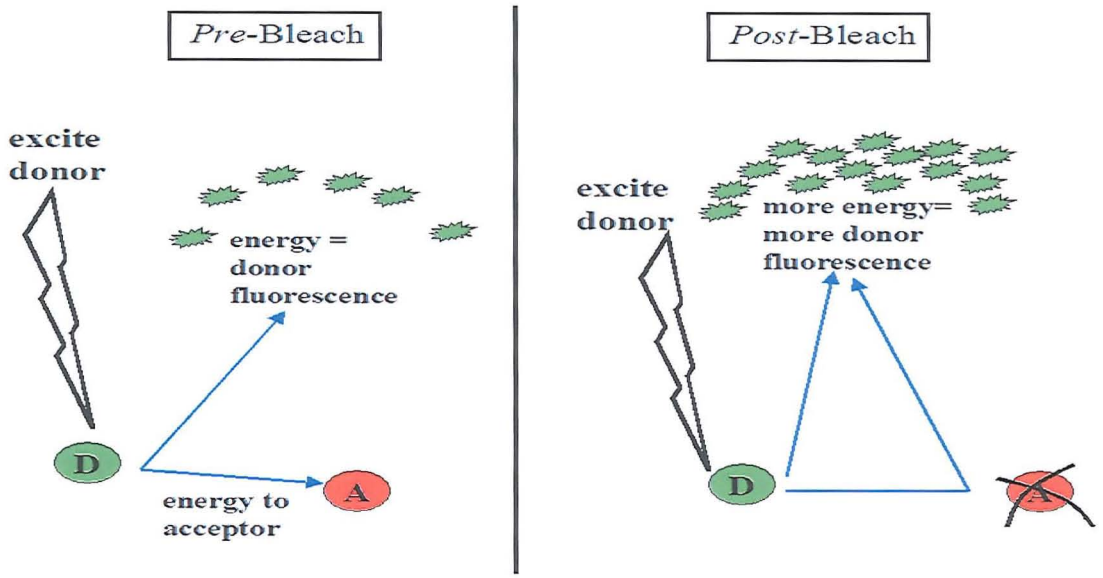

Fig 111. *Pre*-bleach: the donor is excited and energy transferred to the acceptor. This results in less fluorescence of the donor. *Post*-bleach: the donor is excited and all energy contributes to fluorescence as none is being 'sapped' by the acceptor (which is absent due to photobleaching).

PC12 cells were stained using probes conjugated to fluorescent dyes. GM1 was labelled with CTb-TRITC (Acceptor), and GD1a labelled with MOG 35-FITC (Donor), at dilutions of 1µg/ml and 12.5µg/ml respectively (following routine coverslip staining protocol in materials and methods).

Cells were stained with either: a) acceptor and donor

b) acceptor only, or

c) donor only.

In all cases, the pinhole of the microscope was opened.

An image was taken from a field of the donor and acceptor stained cells prior to any photobleaching, and these images designated "pre-bleach". An ROI was then defined within the field, and the region within the ROI was excited continually with the Helium-

Neon (HeNe) 543nm laser line until fluorescence had reduced to background levels (Fig 112a). Another image (using the same settings as the first acquisition) was then taken of the acceptor and donor, and these images termed "post-bleach". Using Image J, an area within the ROI was selected in the donor channel, and the average fluorescence intensity of this area measured in the pre and post bleach images. An area outwith the bleached ROI was measured in the same way (Fig 112b).

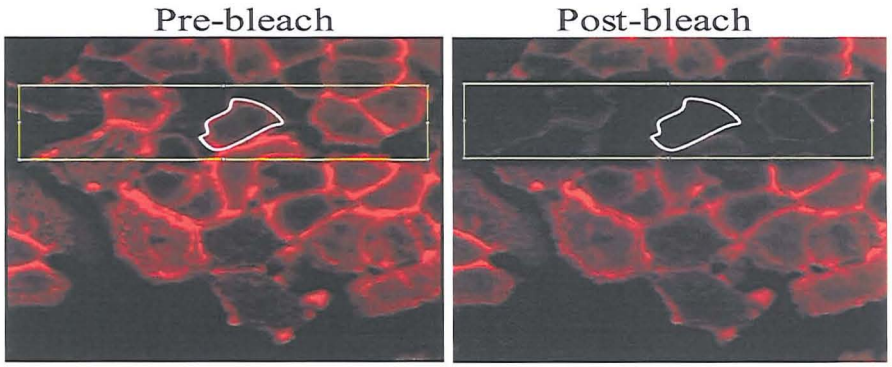

Fig 112a. **ACCEPTOR**: CTb (TRITC) fluorescence of PC12 cells. Pre-bleach image is shown on the left, with the area to be bleached designated by the ROI (yellow box). On the right, image of the same field after the ROI has been bleached. The white line depicts the selection of 1 area, where intensity pre and post bleach was compared.

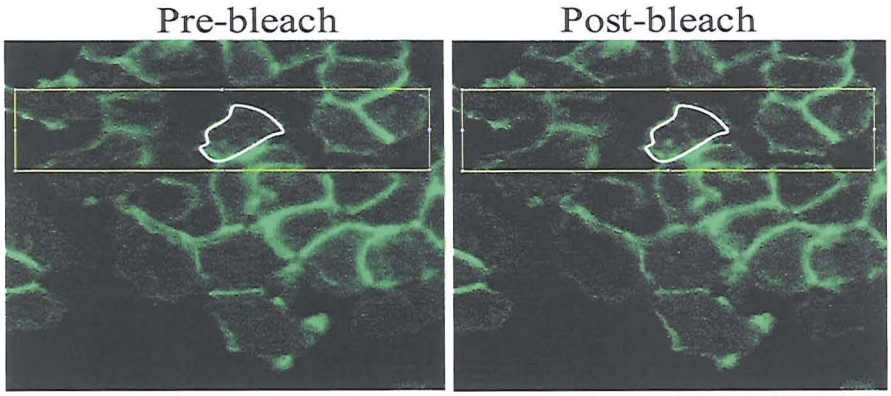

Fig 112b. **DONOR**: MOG 35 (FITC) fluorescence of PC12 cells. Pre-bleach image is shown on the left, with the ROI copied from the Acceptor channel, which will be bleached. Image on the right shows the same field following the bleaching of the Acceptor (TRITC). In a highly successful FRET experiment, the area within the ROI of

the donor post-bleach image may be noticeably brighter when compared to the ROI of the pre-bleach image.

The white line depicts the selection of 1 area, where intensity pre and post bleach was compared.

The results are shown in Fig 113:

Average Donor Intensity

ROI area		Control area	
Pre-bleach	Post-bleach	Pre-bleach	Post-bleach
36	34	62	60

Fig 113. Results shown are from the images in the above figure 112. Intensities are averages of 3 areas within the ROI, and 3 areas in the control region (ie. unbleached area outside the ROI).

From this experiment, it can be concluded that the photobleaching method is not ideal for detecting FRET in this system. In the ROI and surrounding (unbleached area) for the donor, there was evidence that the overall fluorescence had decreased. This is surprising, and indicates that the 543nm laser had caused an overall fading of the sample, and potentially negated the ability to detect FRET. Even in the control slides where cells were stained only with the donor, continual excitation with the 543nm laser line resulted in fading of the FITC signal. The HeNe 543nm laser of the microscope is not powerful enough to bleach the TRITC signal in under 30 minutes, and such prolonged exposure to high intensity light may explain why the overall fluorescence of the sample was compromised. On the same note, the lengthy bleaching duration meant when bleaching was complete, the sample had drifted considerably and the results of the experiment

relied on the correct realignment of the images manually using Image-J. Several attempts were made to rectify the problematic bleaching duration, such as mounting the cells in PBS (as opposed to an anti-fade mountant) to enhance the fluorophore bleaching, and reducing the intensity of the TRITC by applying a more dilute amount of CTb. However, none of these methods proved successful. Owing to the inherent problems with this technique, which could not be overcome with the current facilities, another FRET method was tested.

7.2.6.2 *Sequential FRET*

Sequential FRET relies on the theory that when the donor is excited at its specific wavelength, there will be a concomitant increase in the emission (fluorescence intensity) of the acceptor, as it is receiving energy from the laser excited donor (Gordon *et al* 1998).

Cells were labelled with CTb-FITC and MOG 35-TRITC and during image acquisition, the excitation levels were kept the same for the 488nm and 543nm lasers, and the detector settings for FITC and TRITC also kept the same.

The donor was excited using the FITC 488nm laser line, and detected between 505 and 530nm using the FITC detector, to prove that the settings are exciting FITC. The acceptor was then excited using the argon TRITC 543nm laser line, and detected on the TRITC detector between 560 and 615nm to ensure detectable presence of the acceptor. A third image was then gathered in the "FRET channel", where the FITC was excited using the 488nm laser line, but emission detected in the emission range of the TRITC (560-615nm). Thus, any evidence of fluorescence in the "FRET channel" is not due to the

TRITC being excited by the 543nm laser, but as a result of excitation from the transferred energy fron the excited donor. As shown in Fig 114, a strong FRET signal was detected in the FRET channel.

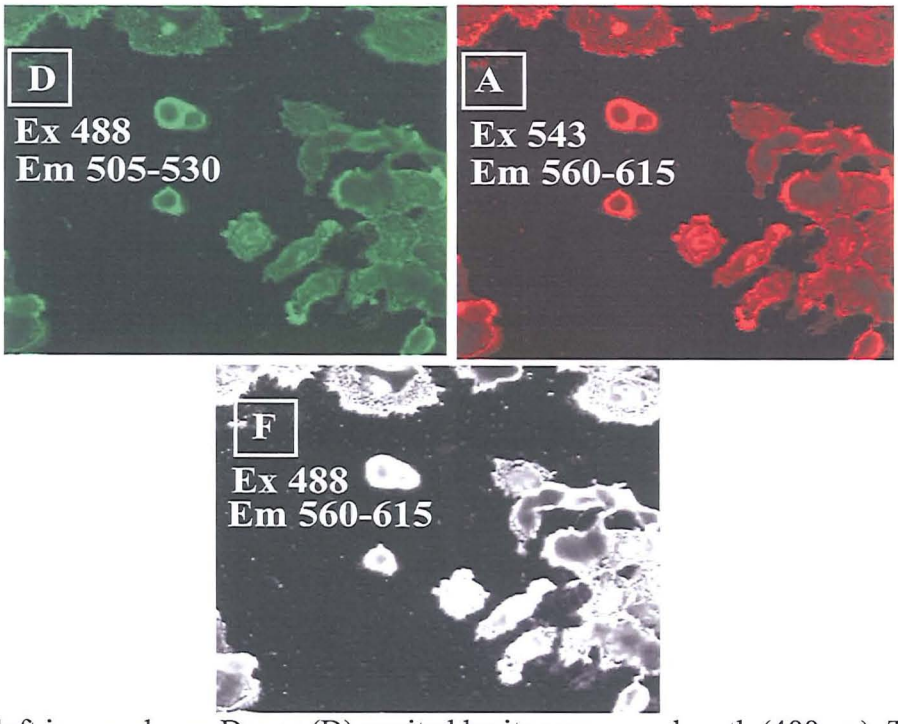

Fig 114. Top left image shows Donor (D) excited by its own wavelength (488nm). Top right shows acceptor (A) excited by its own wavelength (543nm). Bottom panel is the FRET image (F) showing fluorescence of the acceptor (which emits at 560-615nm) as a result of donor excitation (488nm). Excitation (Ex) and Emission (Em) wavelengths are in nanometers.

However, the integrity of this positive FRET signal was confounded by observations using the negative control. When samples were labelled using acceptor alone (ie. TRITC CTb), and the same sequential FRET procedure carried out, a strong "positive" FRET signal was detected (Fig 115).

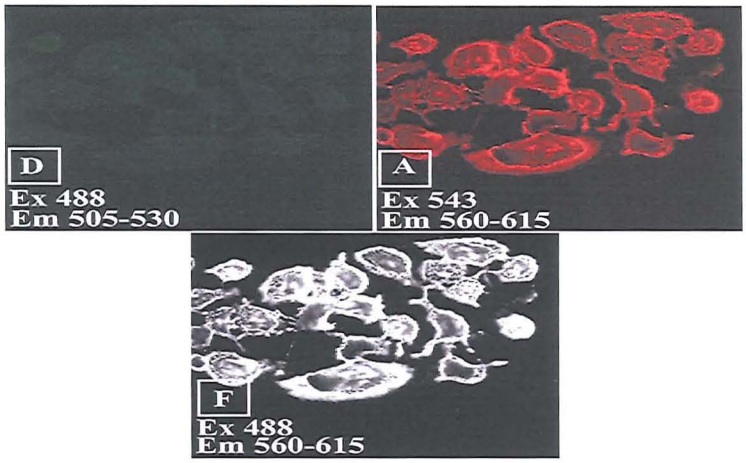

Fig 115. Acceptor only labelled cells. Top left shows absence of donor (D). Top right shows acceptor (A) excited by its own wavelength (543nm). Bottom panel is the FRET image (F) showing fluorescence of the acceptor (which emits at 560-615nm) as a result of donor excitation (488nm). Absence of the donor implies the signal is not due to FRET. Excitation (Ex) and Emission (Em) wavelengths are in nanometers.

The average fluorescence of the bleedthrough in the FRET channel of the negative control was subtracted from the average fluorescence of the FRET channel in the acceptor and donor labelled cells. A negative value was obtained indicating that none of the detected fluorescence in the FRET channel of the acceptor and donor labelled cells was due to FRET, and that it was all a result of bleedthrough.

The excitation of the acceptor cannot be from the donor (which is absent), so it is likely that the 488nm laser is exciting the TRITC (as shown in Fig 116).

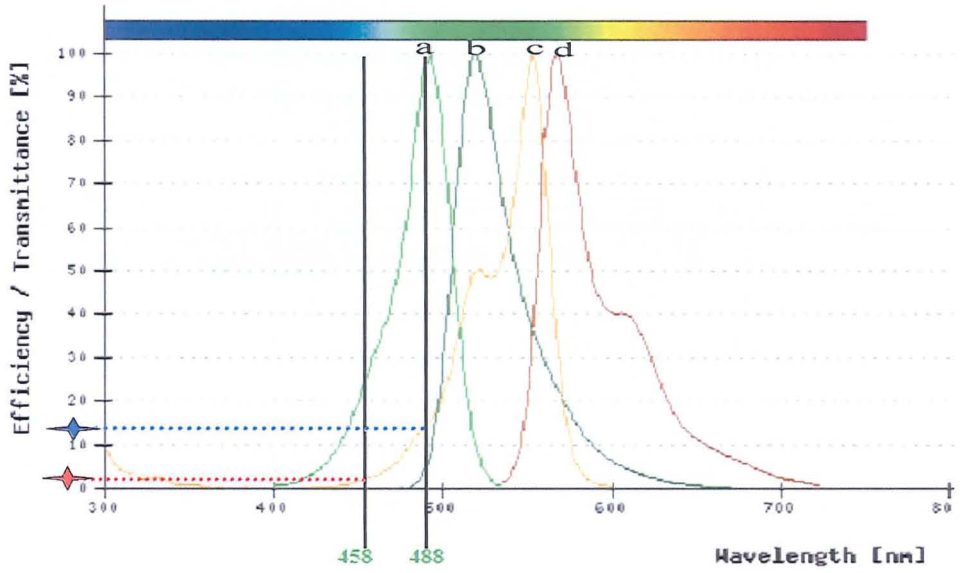

Fig 116. Modified from zeiss.co.uk. 488nm wavelength excites TRITC by 15% as shown by the blue line.458nm wavelength excites TRITC by less than 5%, as shown by the red line. **a**=FITC excitation, **b**=FITC emission, **c**=TRITC excitation, **d**=TRITC emission.

To overcome this problem, FITC excitation was attempted using the 458nm wavelength, which only marginally overlaps the lower end of the TRITC excitation spectrum (Fig 116). As shown in Fig 117, this alteration adequately excited the FITC, and the resultant FRET signal was negative.

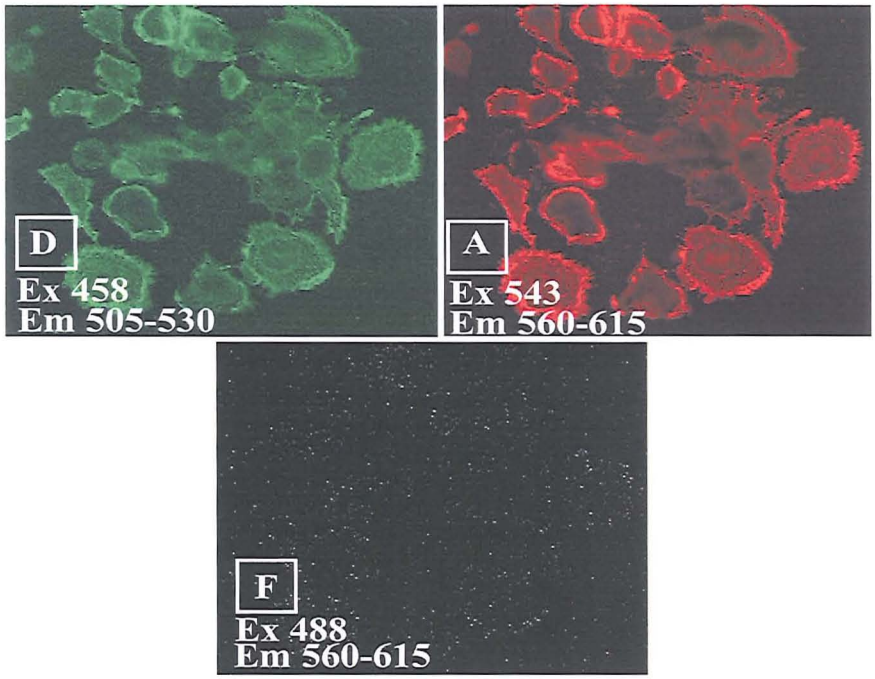

Fig 117. Top left shows donor (D) can be successfully excited with the 458nm wavelength. Top right shows acceptor (A) excited by its own wavelength (543nm). Bottom panel is the FRET image (F) showing fluorescence of the acceptor (detected between 560-615nm) as a result of donor excitation at 458nm. Absence of detectable FRET signal is shown in the bottom panel (F).

Both the 488nm and 458nm excitation protocols were repeated using other labelling conditions, such as labelling 2 different raft markers (Thy1 and GM1) or applying both FITC and TRITC CTb simultaneously, as the dual-colour labelling of a single raft associated molecule was considered an ideal positive control. A convincing FRET signal was not achieved.

7.3 Biochemistry

5.3.1 *Cholesterol Depletion*

Lipid raft integrity was disrupted using the cholesterol sequestering agent Methyl-β - cyclodextrin (Lang *et al* 2001) (Materials and Methods). This experiment was designed to test the hypothesis that upon physical dissolution of the raft, GM1 would no longer be cryptically hidden due to the dispersal of the raft associated proteins and lipids. Cells were analysed by flow cytometry and the fluorescence intensities of MOG 35, DG1 and CTb compared for treated and untreated cells.

Following treatment of the cells, cholesterol depletion was assayed using Infinity Cholesterol Reagent (Materials and Methods) and protein estimation was done using the BCA Protein Reagent Assay (Pierce Chemical Co., Rockford, IL,). Cholesterol was expressed as micrograms per milligram of protein for treated and control samples.

On average, cholesterol content of the control cells was 0.78μg of cholesterol per microgram of protein, and was reduced to 0.49μg of cholesterol per microgram of protein in treated cells (37% reduction from control cell levels). As shown in Fig 118, the FACS histograms do not show an increase in DG1 fluorescence in cholesterol depleted cells when compared to control.

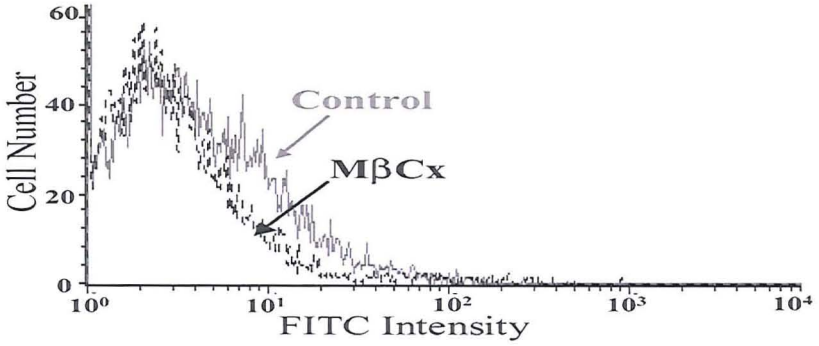

Fig 118. FACS histogram. Cholesterol depleted cells (MβCx treated) do not show an increase in DG1 fluorescence intensity compared to untreated cells.

Semi-quantification of the effect of cholesterol depletion is shown in Fig 119, where the fluorescence intensity of DG1 and CTb decreased, although this was not significant compared to controls ($p>0.05$). MOG 35 decreases significantly in MβCx treated cells when compared to control cells with normal cholesterol levels ($p<0.05$).

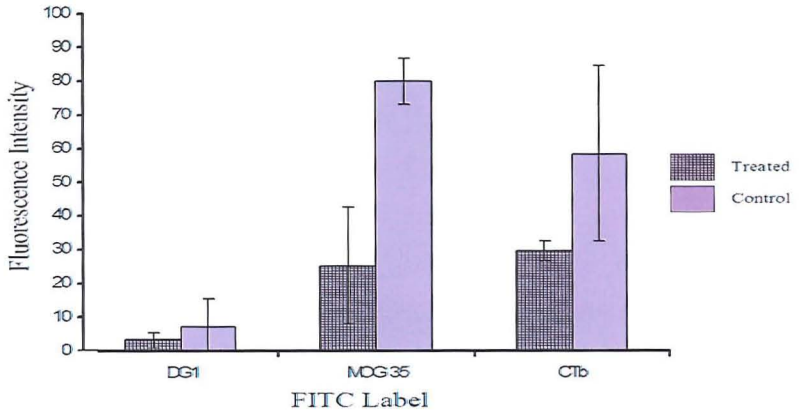

Fig 119. Effect of cholesterol depletion on the binding of DG1, CTb and MOG 35, as shown by fluorescence intensity.

7.3.2 *Raft Isolation and characterisation*

To test the hypothesis that GM1 and GD1a are contained within the same lipid raft, the lipid raft component of the cell membrane was isolated based on its detergent insolubility and light buoyant density (Brown and Rose 1992) when compared to the non-raft constituents of the membrane.

Evidence that GM1 and GD1a exist within the raft fraction is not enough to suggest they are contained within the same raft, as the isolated raft fraction comprises the entire pool of heterogenous rafts. Thus, individual rafts were isolated on the basis of GD1a content, and this GD1a positive subset were probed for the presence of GM1.

2 methods were tested for the isolation of the GD1a positive rafts, direct isolation and indirect isolation. (A detailed protocol for the raft isolation is in Materials and Methods). Rafts were prepared using the detergent Brij-96.

a) Indirect Isolation

Live cells were incubated in either MOG 35 (anti-GD1a) or EG1 (anti-GD3, GQ1b mAb, IgG), the latter as a control anti-ganglioside mAb which does not bind to PC12 cells. Raft fractions were then prepared and a sample retained as "starting material". Remaining rafts were incubated with anti-mouse IgG coated magnetic Dynabeads (Invitrogen). After incubation, the beads were applied to a magnet and the unbound raft fraction was removed and retained. Beads were resuspended and rinsed, before being boiled in SDS loading buffer to release the "bound" raft fractions from the beads, in order to analysed by electrophoresis on pre-cast gels. Gels were run for each set of beads to compare the

starting material, bound fraction and unbound fraction, where the bound fraction of the MOG 35 coated beads would be expected to have an enrichment of GD1a when compared to the unbound fraction.

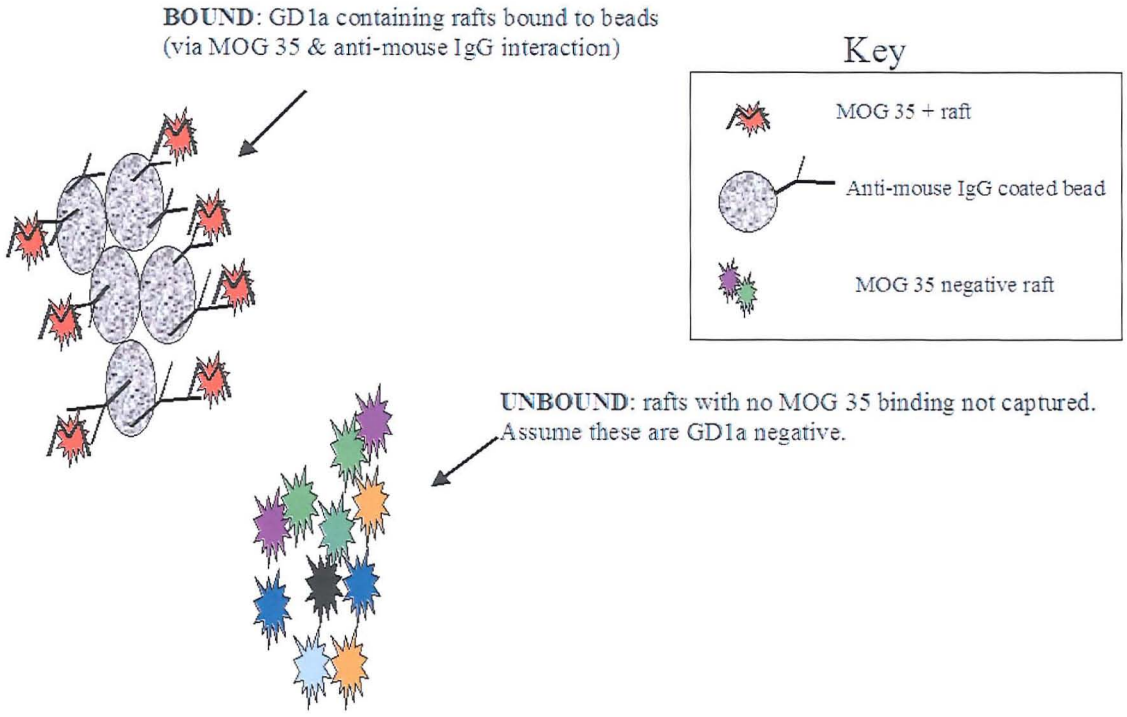

Fig 120. Schematic representation of the raft isolation procedure. Anti-mouse IgG coated beads are mixed with a heterogenous population of rafts. MOG 35 incubation of cells prior to preparation of raft fractions means MOG 35 will be associated with GD1a positive rafts. The anti-mouse IgG coated beads bind the MOG 35 and thus isolate the GD1a containing rafts. Rafts that did not bind(owing to no MOG 35 binding) are likely not to contain GD1a, do not bind to the beads and can be removed as the unbound fraction.

The retained starting material, unbound fraction and bound fraction from each condition were electrophoresed to ensure the bound fraction was GD1a positive, and to ensure no non-specific binding had occurred. In the EG1 incubated cells, no evidence was detected

of bound GD1a or GM1 positive raft samples, indicting that the GD1a positive rafts isolated from the MOG 35 positive isolated cells was due to a specific interaction of MOG 35 (bound to raft GD1a) and the anti-mouse IgG coated bead. Both the heavy and light chain of MOG 35 were detected, evidence of the antibody binding to GD1a. Isolated GD1a positive rafts were also positive for GM1 and flotillin. However they did not contain SNAP 25, another common raft protein (Chamberlain *et al* 2001) indicating the isolated GD1a positive rafts had retained their individual identity and had not coalesced with SNAP 25 containing rafts (Fig 121).

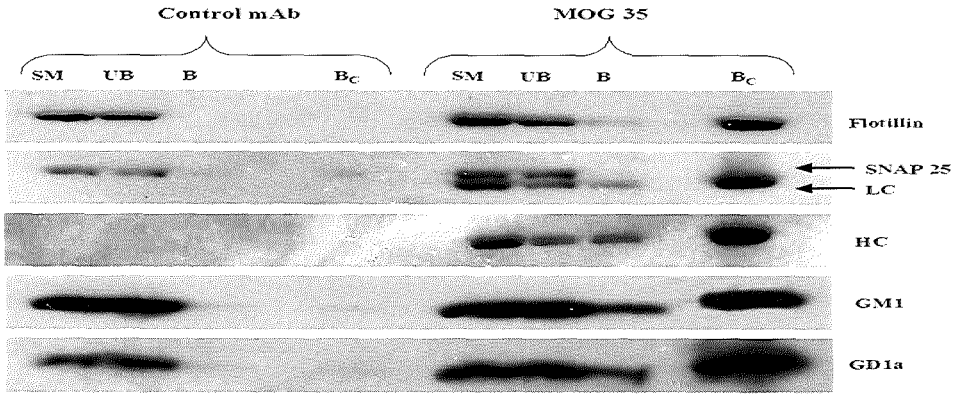

Fig 121. On the left, raft fractions of EGI (control mAb) incubated cells were mixed with anti-mouse IgG coated beads. Starting material (SM) and unbound material (UB) contained GM1, GD1a, SNAP 25 and flotillin. There was no evidence of antibody binding (no heavy (HC) or light chain (LC) detected) in the bound sample (B), and none of the sample bound to the beads, even after concentration of the sample to amplify any weak signal (Bc). On the right, raft fractions from MOG 35 incubated cells. Heavy and light chain of MOG 35 shows the mAb bound to raft GD1a in the live membrane, and the beads have isolated GD1a positive rafts which also have GM1 and flotillin. Note: this experiment was performed twice, with consistent results.

Confirmation that the raft fractionation procedure did not result in any contamination from the non-raft plasma membrane was obtained by running each membrane fraction on

a gel, and probing for proteins known to be either raft enriched (positive controls) or raft excluded (negative controls) (Fig 122)

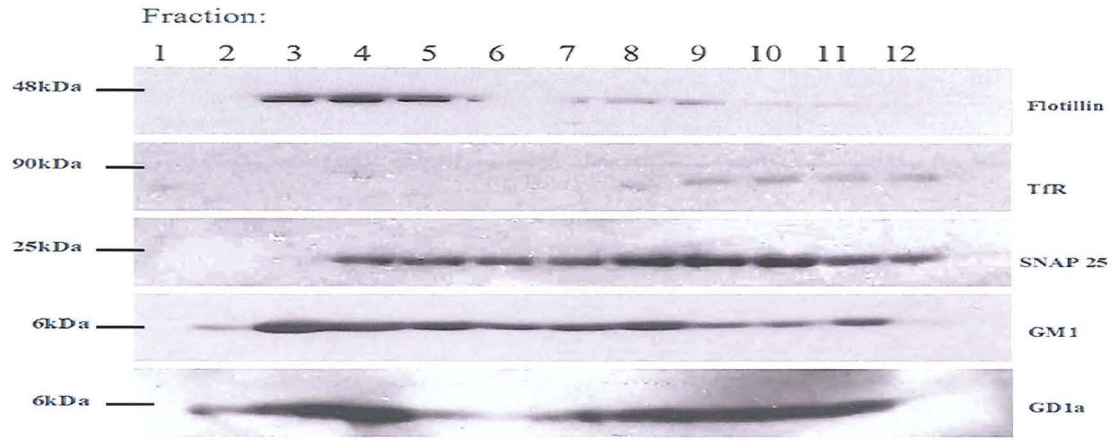

Fig 122. Flotillin is enriched in the raft fractions (Morrow and Parton 2005), while SNAP 25 is also in raft fractions. The transferrin receptor is not associated with the raft fractions (Herinig *et al* 2003, Eckert *et al* 2003). Note: in rafts prepared using Triton X-100, SNAP 25 is in all fractions, but enriched in the raft fractions (Chamberlain *et al* 2001). From the above results with Brij-96, SNAP 25 is strongly associated with fractions 3, 4 and 5 but not clearly enriched. GM1 and GD1a are present in raft and non raft fractions.

b) Direct Isolation

Anti-mouse IgG coated magnetic Dynabeads (Invitrogen) were incubated with MOG 35 or as a control, anti-mouse IgG (Sigma), and each set of beads mixed with a sample of the raft fraction from normal, untreated PC12 cells (a sample of the raft fraction was retained as "starting material"). Following incubation, the beads were applied to a magnet and the unbound rafts removed and retained. Beads were boiled as before, and the samples electrophoresed.

As the results show (Fig 123), the MOG 35 coated beads successfully isolated a subset of lipid rafts in which both GD1a and GM1 could be identified. However, the anti-mouse

IgG beads also isolated a proportion of rafts, which were positive for GD1a and GM1. The observation that the "random" anti-mouse IgG had isolated rafts is suggestive that there is non-specific binding of the raft fractions to the coated beads. It is therefore entirely possible that the rafts isolated by MOG 35 were not all GD1a positive, but were a random subset, some of which contained GD1a.

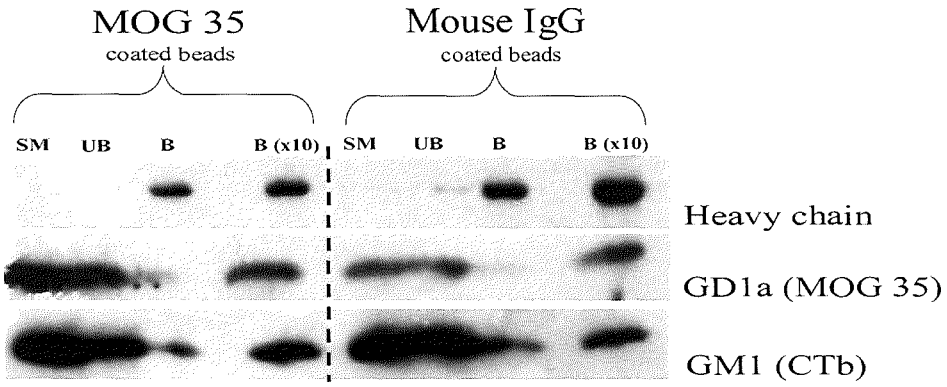

Fig 123. Isolation of GD1a positive rafts. For both sets of coated beads, starting material (SM) was GD1a positive, with GD1a also detected in the unbound fraction (UB). The bound fraction (B) contained a weak signal for GD1a, and upon concentration of this sample (B x10) the signal was intensified, proving presence of GD1a. Thus, both sets of beads had isolated raft fractions which were GD1a and GM1 positive. In the top line, presence of the antibody heavy chain in bound fractions proves the rafts were isolated based on interaction with the antibody.

7.4 Discussion

7.4.1 *Microscopy*

The colocalisation of GD1b and GM1 using MIP and pixel by pixel colocalisation studies is limited by the resolution of the light microscope (approximately 250nm, Hao and Maxfield 2001). To put this into perspective, if 2 widely spaced objects are observed from 100 miles away, then they may appear colocalised. The strongly positive results of the pixel-by-pixel colocalisation do, however, indicate that the advancement of the study using more refined techniques is worthwhile.

The technical problems encountered while trying to establish a successful method of detecting FRET demonstrated that the technique was unsuitable for generating reliable results. Availability of a microscope with a more powerful 543 He-Ne laser may have led to more success with the photobleaching method. However even using an ideal set up, the use of FRET to determine the colocalisation of 2 species is not always successful (Kenworthy and Edidin 1998).

Furthermore, the high intensity light during the bleaching can alter the characteristics of the FRET pair, for example their emission intensity (Sinnecker *at al* 2005) or wavelength may change (Ando *et al* 2002). This means the study design is of critical importance, with the effect of bleaching on donor only and acceptor only labelled cells being analysed to identify any such alterations which would invalidate the result of a possible FRET signal in the acceptor and donor labeled samples.

Results of sequential FRET show that exciting FITC with the 458nm laserline did not cause a detectable FRET signal. Although this wavelength was shown to excite the donor, the resultant energy increase (when compared to the ideal 488nm wavelength) may have been inadequate to provide sufficient energy to excite the acceptor to a detectable level. Ideally, maximal FRET intensities are achieved using a FRET pair which have a maximal spectral overlap (Berney and Danuser 2003). Obviously (and as shown with the 488nm excitation) this will mean the wavelength to excite the donor will also excite the acceptor. A series of complex indices can correct for the resultant 'crosstalk' and subtract any potential acceptor excitation from the true FRET signal to give a reliable result (Gordon *et al* 1998, Xia and Liu 2001). For the purpose of this experiment, a simple subraction of the bleedthrough in the FRET channel obtained in

donor only labelled cells from the signal detected in the FRET channel of the donor and acceptor labelled cells gave a negative value. This was taken as a good indication that even a weak FRET signal had not been detected above the level of the bleedthrough. Had the results given a more promising outcome, the technique could have been further optimised. For example, altering the donor:acceptor ratio may have resulted in generation of a better FRET signal (Kenworthy and Edidin1998). However owing to the complexity of generating reliable results using FRET indices, of which there is no universally accepted standard, and the timeframe available to this study, further investment of time and resources was not considered appropriate.

Even with optimal conditions in place, the ability to detect FRET is confounded by technical issues. One of the most relevant to this study is the use of fluorescently labelled antibodies and CTb in detecting gangliosides. The binding of antibody to ganglioside may occur in an orientation in which the fluorescent molecules are outwith the FRET distance of 100 Å , and the inability to detect FRET would falsely imply that the 2 gangliosides were outwith 100Å. The reverse scenario is also applicable, whereby the gangliosides may lie outwith 100 Å, but the binding of the fluorescent probes leads to the fluorescent labels being within 100 Å. The Y- shaped IgG molecule has a height of approximately 140 Å (14.5nm) (Silverton *et al* 1977), therefore the orientation of the fluorescently labelled MOG 35 could theoretically be 140 Å away from the CTb fluorescent tag, even if the gangliosides GD1a and GM1 are directly interacting (Fig 124)

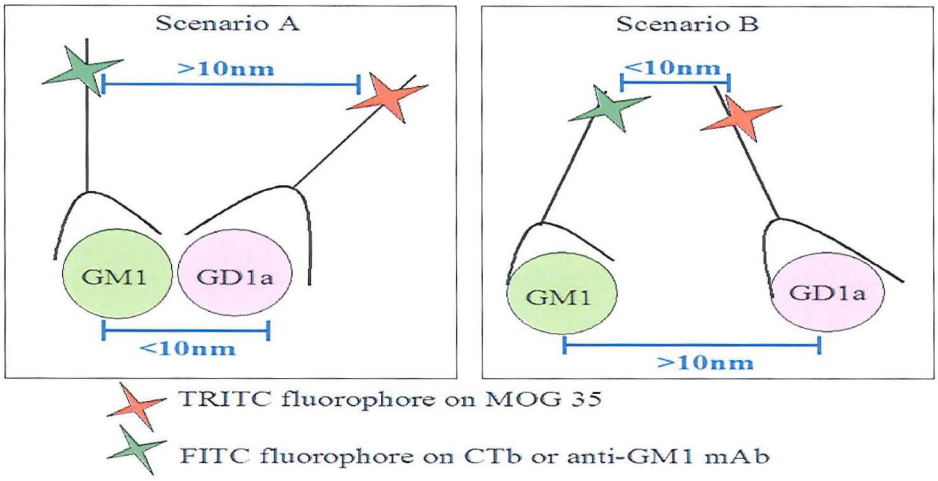

Fig 124. Scenario A: the 2 gangliosides are within 10nm, however the orientation of the probes leads to the donor and acceptor fluorophores lying outwith 10nm. Scenarion B: the gangliosides are not within 10nm of each other, but the donor and acceptor fluorophores are within the FRET efficiency range.

Furthermore, gangliosides are relatively tiny when compared to mAbs (approx 6 kDa and 65 kDa respectively). If GM1 and GD1a are tightly colocalised, the binding of CTb and MOG 35 may not be possible: the probes may be "large relative to the size of the microdomain, preventing simultaneous binding of probes to adjacent raft components" (Kenworthy *et al* 2000). On a similar note, in regions where GM1 and GM3 co-cluster, the intensty of the GM1 clustering is more discrete and intense when observed alone (ie. when GM1 alone was probed for). This indicates that in the co-labelling, anti GM1 and GM3 antibodies are binding overlapping epitopes and thus there is an element of steric hinderance interfering with their ability to access their respective epitopes (Fjita et al 2007). If GM1 and GD1a are tightly integrated, then once CTb has bound to GM1, MOG 35 binding to the associated GD1a may be hindered, and instead the mAb may bind GD1a in another region outwith the effective FRET range. Thus, no FRET would be detected due to epitope labelling problems. One way to address this would be to primary

label the ganglioside, but this may interfere with the spatial dynamics of the raft (Asuncion-Punzalan *et al* 1998) and remove the biological relevance of the system. Thus, biochemical techniques were utilised to study the interaction of the 2 gangliosides.

7.4.2 *Biochemistry*

Depletion of cellular cholesterol is known to perturb the integrity of lipid rafts (Lang *et al* 2001). By removing a significant proportion of cholesterol from the membrane, the liquid ordered state of the membrane is no longer under the mediation of cholesterol and thus becomes more liquid disordered, a state more in agreement with the Singer-Nicholson model in allowing random arrangement of the proteins and lipids (Singer and Nicholson 1972). Based on the observation that when the raft is disrupted, MOG 35, DG1 and CTb binding is decreased, it is concluded that the ganglioside epitopes become randomly associated in a way which increases their crypticity. For example, GM1 and GD1a may become hidden by proteins which are non raft associated, they may interact in a different spatial dynamic with raft proteins which have been released upon cholesterol depletion, or the gangliosides may not be physically hidden by another species, but instead may flip into an orientation whereby their antigenic site is buried in the bilayer. Furthermore, there is evidence that not all rafts are sensitive to methyl-β-cyclodextrin dependent cholesterol depletion, as treatment of Jurkat cells released a variety of raft proteins, but flotillin remained in the detergent resistant domains (Rajendran *et al* 2003).

A possible explanation for the differences in susceptibility of rafts to dissociation is the stabilisation of rafts by the cellular cytoskeleton (Fujiwara *et al* 2002). Thus, this support means upon cholesterol depletion there is incomplete dissolution of the raft (Fujita *et al* 2007) meaning *cis*-interactions between raft species are not disturbed. In this instance, the

GM1/GD1a complex would remain intact and the complex, as opposed to the individual gangliosides, would become orientated in one of the ways already described. From the results of this experiment, the *cis*-interaction of GM1 and GD1a remains hypothetical, and therefore further biochemical experiments were designed, based on detergent insolubility of lipid rafts as a tool to isolate them from the plasma membrane, as demonstrated in this chapter. There is evidence that during the isolation of the detergent resistant fraction, mixing of individual rafts can occur, a failure of the commonly used detergent Triton-X100 (Madore *et al* 1999). Extraction of rafts with Triton-X100 is believed to form lipid raft domains ranging from 15-20μm, which is suggestive that Triton-X100 leads to the association of smaller domains which existed prior to the detergent treatment (Giocondi *et al* 2000). However, Brij-96 was used in a similar application as applied in this chapter, and it was concluded that Brij-96 "fractionated the neuronal membrane such that the membrane of many individual rafts remained relatively intact and separate throughout all purification steps" (Brugger *et al* 2005). Taken together with the finding that GD1a positive rafts do not contain SNAP 25, this is highly suggestive that the colocalisation of GM1 and GD1a is not due to the coalescence of separate populations of rafts, and that individual GD1a containing rafts have been isolated.

The Dynabead isolation approach using antibodies bound to the whole cell represents the ideal system in which to analyse the ganglioside content of lipid rafts. In a model raft system, such as supported bilayers (Dietrich *et al* 2001) it may be possible to identify co-localisation of 2 gangliosides, but such static scenarios do not convincingly depict the situation in the living membrane, either of the PC12 cell or NMJ. For example, the

membrane associated cytoskeleton may play a role in regulating raft size and lateral position (Yu *et al* 1973, Jacobson and Dietrich 1999), so the cellular regulation of raft size and shape (Brown and London 1998) may mean "man made" rafts do not give the best representation of the *in-vivo* and thus clinically relevant scenario where anti-ganglioside antibodies bind the raft associated gangliosides. Coating the beads in antibody (ie direct isolation) was tested to eliminate the possibility that membrane bound MOG 35 may become bound to the raft associated ganglioside in such an orientation that the anti-mouse IgG cannot bind well and readily isolate it, and thus the direct isolation may result in an amplification of the bound rafts when compared to the previous indirect isolation. However the impracticality of this direct approach lies in the difficulty of finding an adequate negative control to compare to the anti-mouse IgG MOG 35 bound beads. A non-specific mouse IgG is theoretically an ideal control, however the fact that it bound to something in the raft fraction is suggestive that preparation of the isolated rafts had potentially exposed new epitopes which would not normally be seen. This theory is possible, as the mAb EG1 does not bind the PC12 cell, but when initially used as the control (before the anti-mouse IgG) it also bound to an epitope in the raft fraction, which indicates GD3 had been exposed during the raft preparation.

From the Western blots, the intensity of the GD1a band in the raft unbound fractions is strong: it was predicted that the procedure would isolate a higher proportion of rafts and lead to a more obvious depletion of the unbound fraction when compared to the starting material. The first possibility is that not enough MOG 35 was added to saturate the GD1a present on the cell surface, although this is unlikely because at this concentration, preparation of cells for immunofluorescence or FACS analysis gives an intense

fluorescent signal. The second, and perhaps more likely explanation is that MOG 35 is not able to see all GD1a contained in the membrane of the cell. This notion links to the observation that GM1 is invisible to DG1, and suggests that certain populations of GD1a may exist in domains where they are cryptically shielded. Overall, the isolation of GD1a positive rafts which also contain GM1 is evidence that both gangliosides exist within the same raft when extracted using Brij-96.

Chapter 8

8.1 Introduction

The binding ability of anti-GM1 monospecific antibody DG1 depends on the presentation of GM1 in the membrane, and in the GD3s$^{-/-}$ mouse relies, at least, on its *cis* interaction of GM1 and GD1a. DG1 was raised against the GM1 mimicking oligosaccharide (as described in Townson *et al* 2007 and references therein) isolated from *C. jejuni* and introduced to a mouse lacking gangliosides (to overcome immune tolerance). Thus, DG1 is specific for the GM1 mimicking oligosaccharide, but the antibody does not react with the ganglioside GM1 in mouse nervous tissue. In order to assess the significance of this, the ability of DG1 to bind to the GM1 mimicking oligosaccharide on the surface of intact *C.jejuni* was investigated. It was of interest to determine if DG1 would bind to the GM1 like oligosaccharide on live bacteria, or whether, akin to the live versus dead binding observed in earlier chapters, DG1 would only bind dead bacteria, where the membrane dynamics may alter the presentation of the oligosaccharide epitopes.

8.2 Live and Heat Inactivated *C.jejuni*

C.jejuni strain O:3 has no GM1 or GD1a mimicking oligosaccharide structures, and was included as a negative control, while strain O:19 has GM1 and GD1a like oligosaccharides (Bowes *et al* 2002) and was used to determine the ability of DG1 to bind to the GM1 like oligosaccharide in the presence of the GD1a like oligosaccharide. All bacteria and culture support was kindly provided by Mr J Guthrie (Department of Bacteriology, Southern General Hospital).

Bacteria of each strain were maintained in suspension in sterile PBS: half of each was removed and incubated at 60°C for 1 hour to heat inactivate (ie. kill) the bacteria, while the remainder was survived by maintaining at room temperature. Bacteria were pelleted and stained following the FACS staining protocol used for PC12 cells, as described in Materials and Methods. In deviation from this protocol, PBS was used instead of FACS buffer and bacteria were rinsed by pelleting at 13,000rpm for 3 minutes. Primary antibodies were used at 20μg/ml, and CTb-FITC (1μg/ml). Secondary antibodies (anti-mouse IgG-FITC) were used at 3.3μg/ml. In order to confirm heat inactivation had killed the bacteria, a sample was plated onto Skirrow (Skirrow 1977) agar medium (E & O Laboratories, Bonnybridge, UK) and maintained under microaerophilic (5% O_2, 10% CO_2, and 85% N_2) conditions along with a live sample (positive control). After 2 days at 42°C, colony formation from the live samples but not the heat inactivated was confirmed.

DG1, MOG 35 and CTb did not bind to strain O:3, either live or dead. Both antibodies and CTb bound to strain O:19, and as shown in the FACS histograms in Fig 125, the binding of MOG 35 and DG1 was greatly enhanced in heat inactivated strain O:19. The CTb binding intensity remained similar when comparing live and heat inactivated strain O:19.

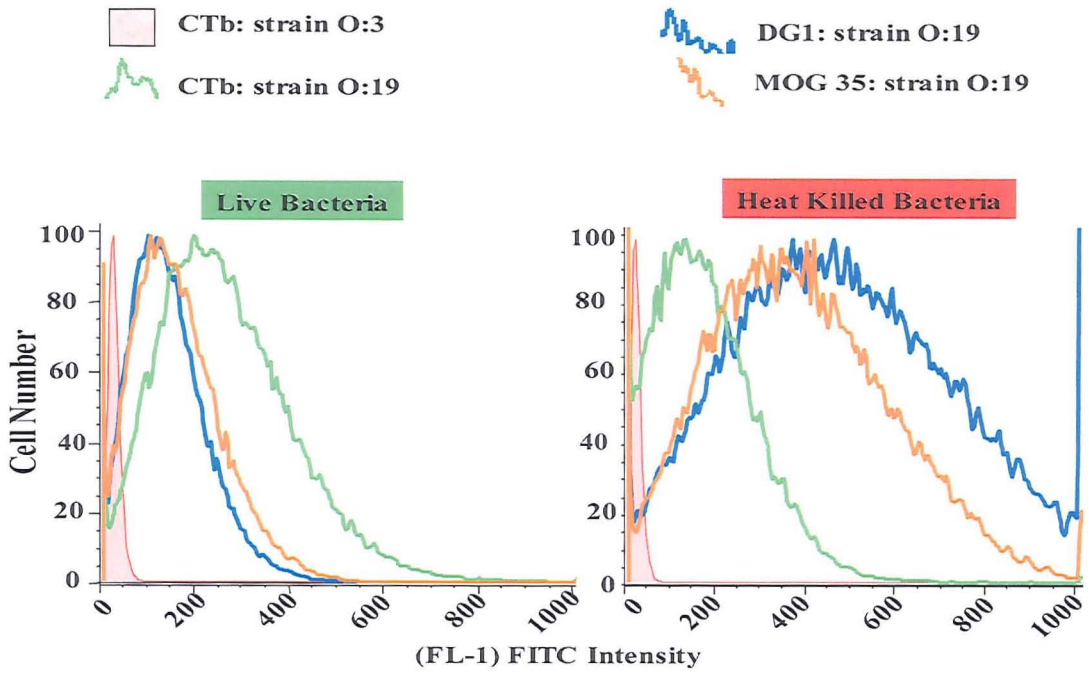

Fig 125. FACS histograms comparing the shift in fluorescence intensity when comparing DG1, MOG 35 and CTb binding to live and heat inactivated strain O:19 bacteria. Background fluorescence intensity is represented by the shaded curve, showing the negligible fluorescence of CTb binding strain O:3.

8.3 Live and Dead *C.jejuni*: UV and PFA inactivation

The heat inactivation of *C.jejuni* led to an increased ability of both mAbs to bind to the ganglioside like oligosaccharides. Heating of proteins leads to denaturation and it is therefore possible that the effect of heat on the oligosaccharide has altered the epitope and caused the increased antibody binding. Thus, different methods were used to kill the bacteria, and their effect on the binding of CTb and mAbs was again compared to live bacteria.

8.3.1 *Bacterial Inactivation Methods:*

* *PFA Fixation.* Bacteria were suspended in Eppendorfs containing 4% PFA for 25 minutes at room temperature, and rinsed by pelleting (13,000 rpm) and resuspending in PBS 3X.

* *UV Irradiation.* Bacteria were diluted in PBS and a thin film applied to the base of Petri dishes. These were placed (minus lids) in a UV crosslinker (XL-1000 UV Crosslinker, Spectronics Corp) for 30 minutes.

As already described, samples of live and dead bacteria were cultured to ensure efficiency of the treatment.

As a negative control, the ability of CTb to bind live, PFA fixed or UV irradiated strain O:3 was analysed. No binding was detected, as shown in the FACs histograms in Fig 126.

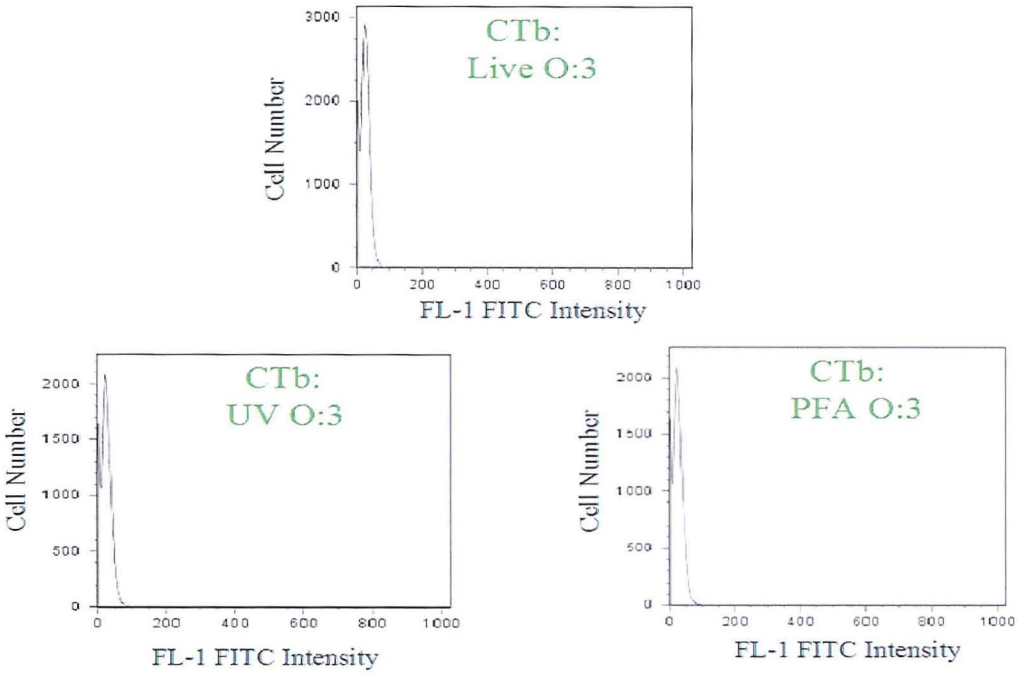

Fig 126. FACS histograms showing CTb fluorescence for live, PFA fixed and UV irradiated strain O:3 *C.jejuni.*

Fig 127 shows the FACS histograms of MOG 35 and DG1, with inset panels showing representative forward-scatter (FSc) and side-scatter (SSc) profiles. The gate position was set based on the live bacteria, and remained constant throughout the experiment to ensure that comparisons were drawn between morphologically similar

bacteria and any aggregations or fragmentation caused by the methods used to inactivate the bacteria did not bias the results. As can be seen in the fluorescence histograms (Fig 127), MOG 35 and DG1 fluorescence intensities remain comparable for all conditions.

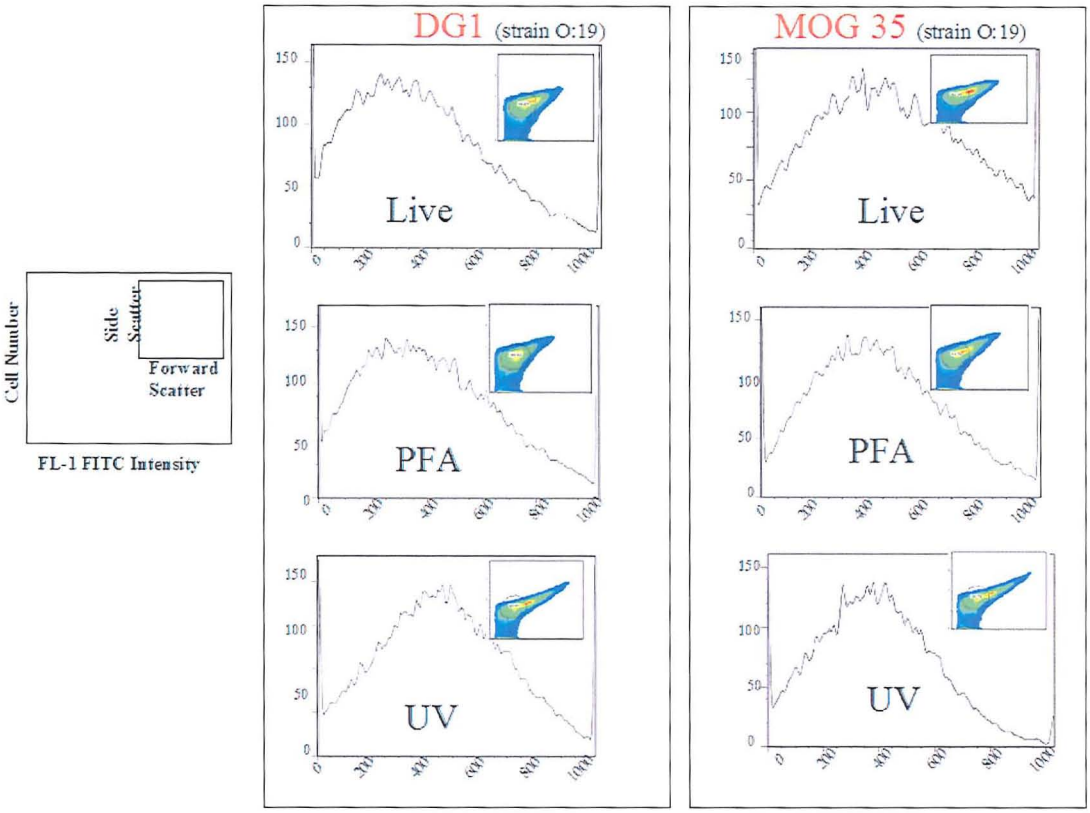

Fig 127. Flow cytometry histograms of DG1 and MOG 35 fluorescence in live and dead *C.jejuni* O:19. Inset panels show forward scatter (FSc) and side scatter (SSc) profiles.

Semi-quantification of this data is shown graphically in Fig 128, and from this it can be concluded that there is negligible difference between the binding of DG1, CTb and MOG 35 to bacteria which are live, UV irradiated or PFA fixed. Consistent with the results of section 8.2, the mAbs and CTb are able to bind the live bacteria. Statistical analysis was not appropriate: although all samples were analysed in duplicate, each experiment was performed once as a pilot study.

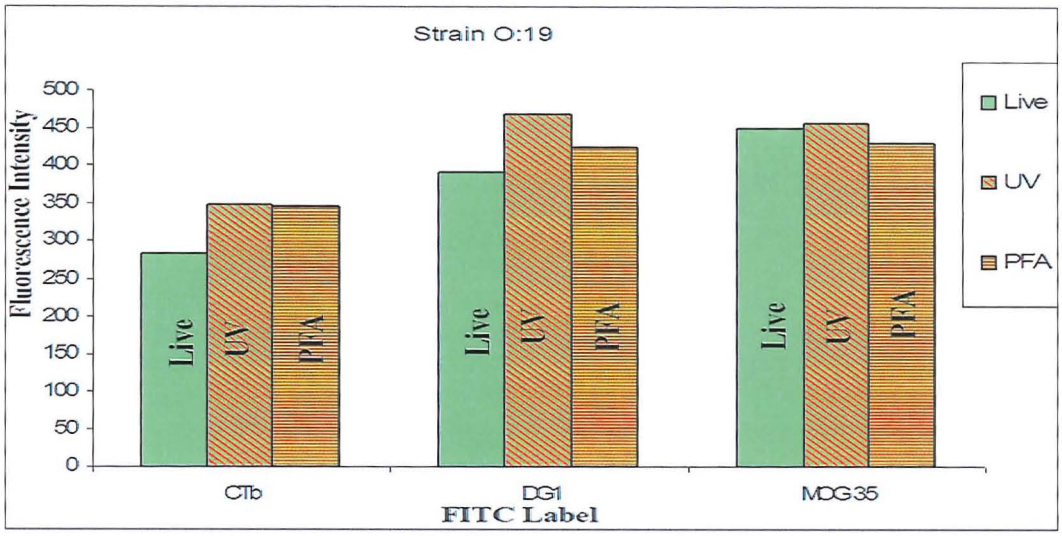

Figure 128. Fluorescence intensity of DG1, MOG 35 and CTb binding of live, PFA fixed and UV irradiated bacteria, as determined by flow cytometry.

8.4 Discussion

MOG 35 and CTb binding to *C.jejuni* O:19, but not the negative control *C.jejuni* O:3, show that GD1a and GM1 like oligosaccharides can reliably be detected in strain O:19. DG1 is also able to bind the GM1 like epitope on strain O:19. From the results, it is shown that heat inactivation of the *C.jejuni* O:19 greatly enhances the binding of MOG 35 and DG1, but this is not the case upon inactivation by UV exposure or PFA fixation. It can be concluded from this data that heating the oligosaccharide may be altering its conformation or presentation on the surface of the bacteria, and enhancing the ability of the antibodies to bind. CTb binding was not affected, perhaps implying that the CTb fluoresecence on live bacteria was maximal and thus no enhancement was detectable. It is surprising that the intensity of DG1 binding to the GM1 like oligosaccharide was greater than that of CTb. GM1 has a cross sectional diameter of less than 1nm, meaning the epitope is much smaller than pentameric CTb, and thus the surface density of GM1 is likely to be higher than that

of CTb (Wang *et al* 2001). The DG1 intensity implies that the antibody is smaller than CTb, meaning more DG1 is able to bind and result in a fluorescent signal which is more representative of the amount of epitope. The treatment of bacteria with UV irradiation caused a population of bacteria which appeared larger and more granular, as depicted by the population in the top right quadrant of the FSc and SSc plots (Fig 103). These bacteria are likely to be aggregates, or perhaps bacteria which have swelled owing to loss of function of the osmotic pumps induced by the inactivation. Only bacteria which were believed to be intact were included in analysis to ensure a fair comparison with live bacteria.

In summary, MOG 35, DG1 and CTb are able to bind both live and dead *C.jejuni* O:19, as determined by flow cytometry. This implies that the GM1 and GD1a mimicking oligosaccharides present on the surface of the bacteria do not *cis*-interact in a way which shields GM1 from DG1. This data highlights a fundamental difference from the presentation of ganglioside GM1 in neural membranes, where earlier chapters describe the potential *cis*- interaction of GD1a and GM1, leading to masking of GM1 from DG1. This data introduces the concept that DG1 like antibodies can opsonise potentially harmful pathogens bearing self-mimicking epitopes, but do so in a way which does induce an autoimmune reaction against the epitope expressed by self-tissue.

Chapter 9

9.1 Introduction

The ability of DG1 to bind to ganglioside GM1 when not in complex, as shown in the preceding chapters, is particularly novel in the evolving concept of GBS, where there is a growing emphasis on antibodies that can only bind to gangliosides when in complex.

Kaida and co-workers (Kaida *et al* 2004) pioneered the discovery of the GBS associated ganglioside complex hypothesis when they performed TLC immunostaining on a crude fraction of ganglioside from bovine brain using sera from a GBS patient. They noted that on the TLC overlay, a positive band was evident just below GD1a on the TLC overlay. Potentially this could have been a hithero undiscovered ganglioside, however the sera was also shown to react with a GD1a/GD1b complex, but not with the individual gangliosides (Fig 129). This study represents a milestone in the study of GBS antibodies, and is the first description of a GBS associated antibody which only reacts to ganglioside complexes as opposed to the individual species. The result was confirmed on ELISA, where the sera only bound to the gangliosides when coated to the plate as a mixture. Similar results were obtained for GD1a-GM1, GM1-GT1b and GD1b-GT1b complexes. This phenomenon has also been demonstrated for antibodies associated with MFS (Kaida *et al* 2006).

Evidence that such a serum is able to bind in the living membrane would prove that the phenomenon observed by Kaida and co-workers is relevant to the biological membrane (as opposed to solid phase assay), and would support the hypothesis generated in this thesis: GM1 and GD1a are able to *cis*-interact.

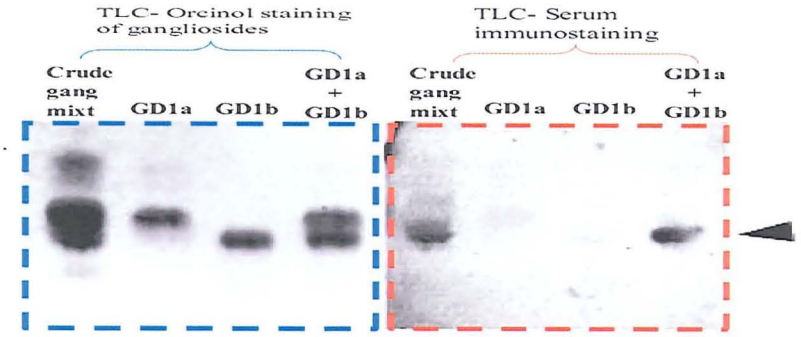

Fig 129. TLC studies, modified from Kaida *et al* 2004. Left TLC (blue outline) shows the position of the gangliosides in each lane. On the right (red outline), the position of the antibody binding. Binding in the crude ganglioside mixture lies just below the position of GD1a, and the arrowhead shows binding in the GD1a+GD1b lane, in a position overlapping the tail and head end of GD1a and GD1b respectively. This represents the area where the gangliosides were incompletely separated by the TLC.

9.2 Ability of Anti-GM1/GD1a complex Sera to Bind Living Tissue

Close to the completion of my PhD studies, I was fortunate to be provided with 4 aliquots of sera reactive to the GD1a-GM1 complex by Dr. S. Kusunoki (Kinki University School of Medicine, Japan). This allowed a pilot study to be undertaken, in which I investigated the ability of the sera to bind under physiological conditions. Less than 1ml of each sample was provided, and with such a small sample size the experimental approach was limited. I first decided to use a minimal amount of sera and characterize the binding ability of the anti-GM1/GD1a complex antibodies in the *ex-vivo* peripheral nerve of the GD3s$^{-/-}$, which has upregulated expression of gangliosides GM1 and GD1a, and no *b* series gangliosides. The GalNAc-T$^{-/-}$, which has no complex gangliosides, was used to confirm the antibody was specifically binding to the GM1/GD1a ganglioside complex.

The sera (diluted 50:50 with Ringer) was applied to the *ex-vivo* GD3s$^{-/-}$ TS preparation and in parallel, the GalNAc-T$^{-/-}$, following the same protocol as described

in Materials and Methods for antibody incubations in the TS preparation. As a control, NHS was applied to a parallel GD3s$^{-/-}$ preparation at the same ratio. Following incubation of anti-GD1a/GM1 complex sera or control sera, NHS was added as an additional source of complement to determine the pathogenic potential of the anti-complex antibodies.

9.2.1 *Preliminary Results*

Only one of the samples bound to GM1/GD1a complex and was able to activate the complement cascade. The preliminary results shown in Fig 130a show illustrations of the positive sera specifically binding the GD3s$^{-/-}$ nerve terminal and endplate, suggesting it is binding to the GM1-GD1a complex. As shown in Fig 130b, control sera did not bind to a detectable level. None of the sera bound to the GalNAc-T$^{-/-}$ (data not shown) indicating there was no cross-reactivity or non-specific binding to other epitopes, such as glycoproteins.

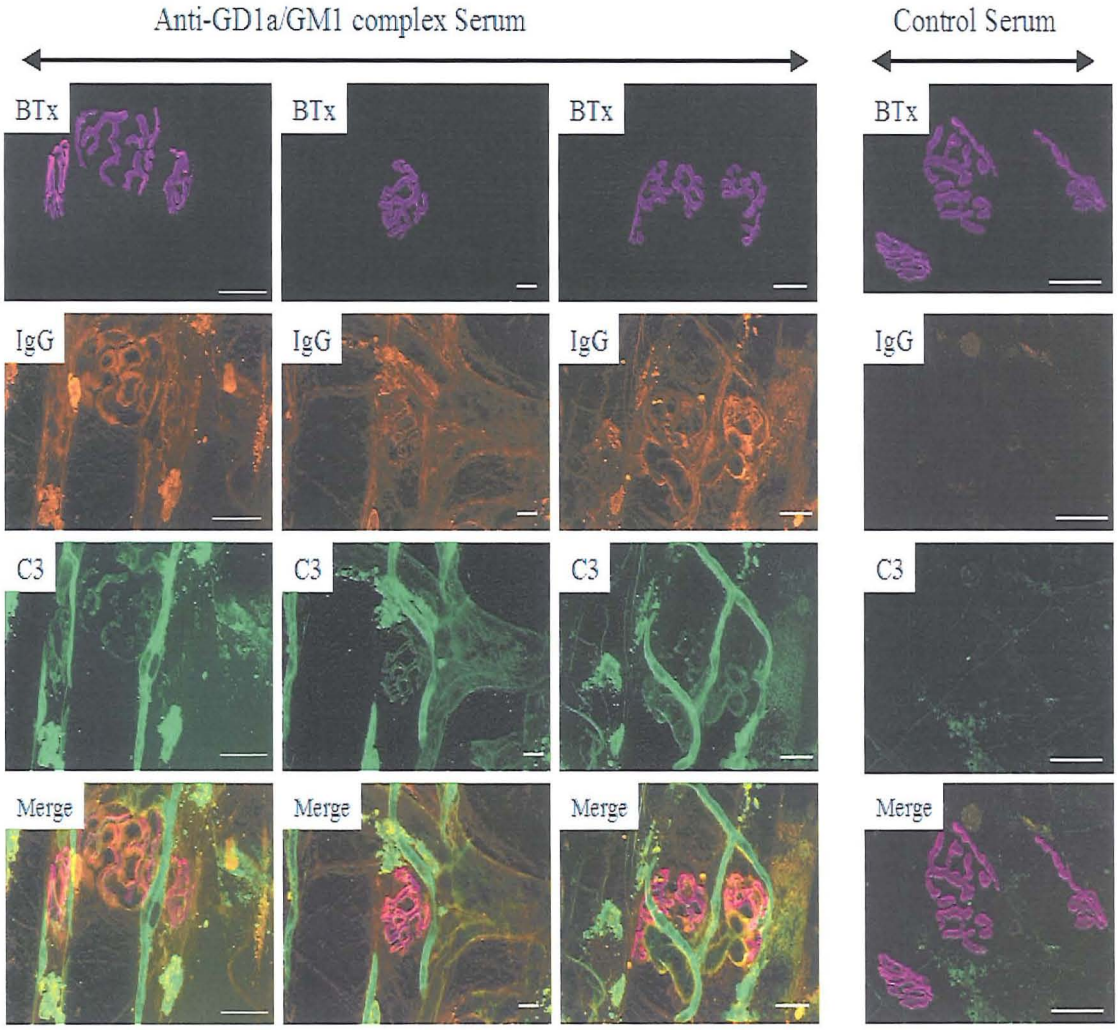

Fig 130a. Anti-GD1a/GM1 complex sera applied to the *ex-vivo* GD3s$^{-/-}$ TS preparation, followed by NHS. IgG and C3 deposition were detected over the endplate and distal nerves, as shown on the left group of images. On the right, control serum gave no IgG or C3 deposition. Scalebar = 20μm.

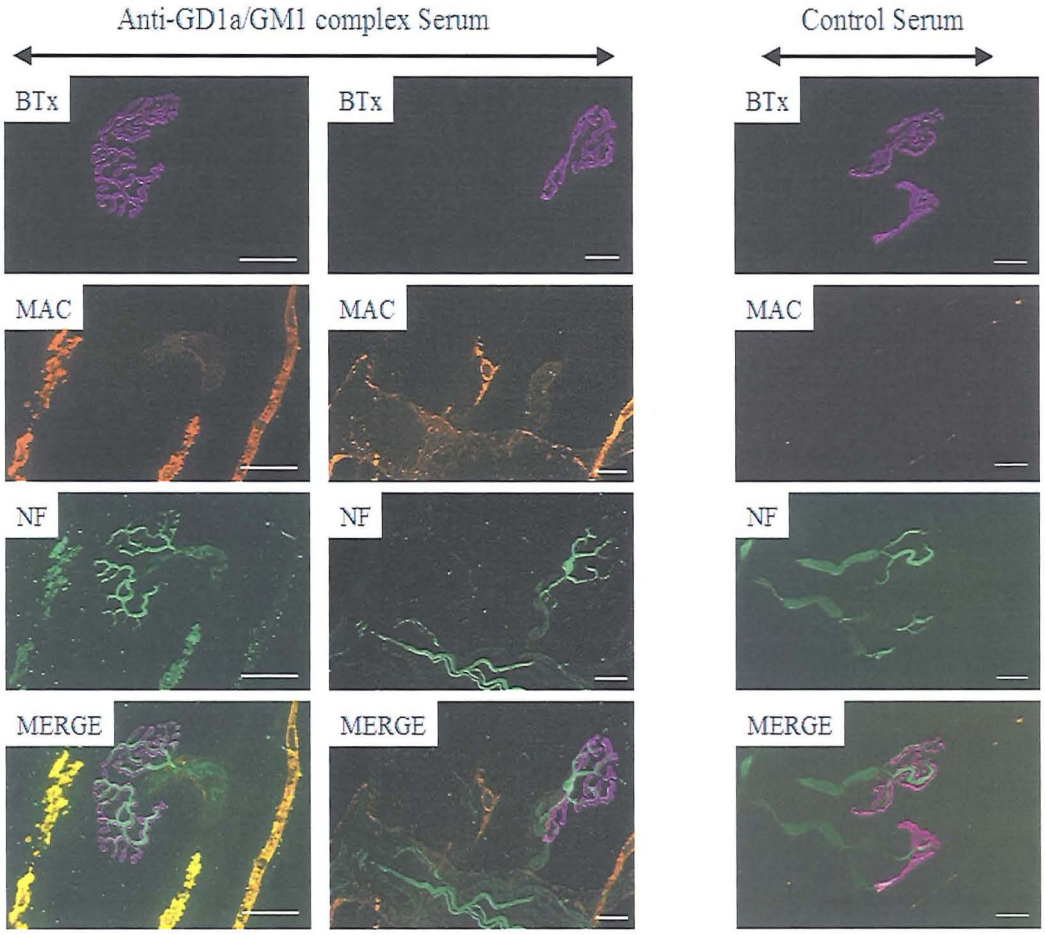

Fig 130b. As for Fig 131a), but showing MAC deposition and NF staining. MAC can be detected most strongly along the axon in the anti-complex treated preparation. NF appears normal over the endplate, and evidence of slight granulation is apparent upstream of the NMJ, where the complement deposition is strongest. Control treated muscles show no MAC deposition and NF is normal. Scalebar = 20μm.

9.3 Discussion

Although it is difficult to draw conclusions from such a limited study, the observation that a GBS associated antibody against the GM1/GD1a complexes is able to bind in the living membrane is perhaps one of the first illustrative examples that this antibody is specifically binding to the axon and is able to activate the complement cascade. No abnormalities were detected to the neurofilament of the axon. This observation is suggestive that the antibody is not causing an axonal lesion. However, it is my intention to send the remaining volume of the illustrated serum to our collaborators (J. Plomp, Leiden University, The Netherlands), where it will be applied to hemi-

diaphragm preparations (following the incubation protocol in Materials and Methods, but using a "strip-twitch" assay and thus a small volume of sera (Jacobs *et al* 2002), and electophysiological traces will be recorded. Any electrophysiological abnormalities induced by the serum will confirm that it is at least capable of inducing conduction block, perhaps severe enough to manifest as paralysis in the patient. Treated tissue from the Netherlands will be snap frozen following electrophysiology, and sent back to me, allowing it to be sectioned for quantification of antibody, C3 and MAC deposition (as done routinely for hemi-diaphragm analysis, protocols in Materials and Methods). NF analysis, however, may not be possible owing to the damage of the phrenic nerve during the assay procedure. The sera which was found to be unable to bind the nerve terminal will also be investigated in this manner; failure to detect antibody binding and complement activation does not rule out the possibility that even a very low level of antibody binding can cause altered nerve function. If electrophysiological abnormalities are detected, patients with GBS mediated by anti-complex antibodies (which behave similar to the provided samples) would be expected to recover rapidly as the axon is not damaged.

It would also be beneficial to test the ability of such sera to bind in WT mice, which have a normal ganglioside profile. Ability of the sera to bind in these mice would be more relevant to the human situation, as it would strongly suggest that in the peripheral nerve, and in the presence of other ganglioside species (a scenario not accounted for in the GD3s$^{-/-}$), GM1 and GD1a are able to *cis*-interact and thus represent a viable epitope to antibodies. Furthermore, provision of more sera samples would allow these to be screened, and more positive results such as that illustrated in this chapter would confirm that antibodies against ganglioside complexes are an

important future area of research, and should perhaps also be routinely screened for in GBS patients.

10.1 Discussion

The identification of GBS associated antibodies which are able to bind to epitopes presented on solid phase ELISA, but not in the living membrane, introduces a plethora of possibilities regarding the likely pathogenic mechanisms of such antibodies. This thesis demonstrated the concepts of epitope recognition using 2 in-house mouse anti-ganglioside antibodies (DG1 and DG2) which were produced by colleagues (as described in Townson *et al* 2007 a), and references therein). Both antibodies were raised in the GalNAc-$T^{-/-}$ mouse against GM1-like epitopes: DG1 was raised against GM1 like LOS isolated from *C.jejuni* strain O:19, and DG2 was raised against GM1 ganglioside containing liposomes. One of the most fundamental points which should be highlighted is that both DG1 and DG2 have similar heavy and light chain sequences, are structurally similar, and have similar binding affinities for GM1 (Townson *et al* 2007). In other words, comparing DG1 and DG2 is not like comparing "chalk and cheese", and the inability of DG1 to recognise GM1 in the living membrane suggests that the explanation relies on the availability of the epitope in the bilayer. On a similar note, both antibodies show strong binding to sulfatide by ELISA, yet neither were shown to bind it in tissue. The dichotomy in antibody binding abilities between ELISA bound epitopes and membrane bound epitopes underpins the emerging importance of "membranomics", whereby the pathogenicity of antibodies depends on the interactions of membrane proteins and lipids which regulate the availability of epitopes to antibodies. Crypticity of glycolipids is not a novel phenomenon, based on the inability of antigloboside antibodies to bind globoside in erythrocytes (Hakomori *et al* 1968) and more specific studies showing anti-ganglioside antibody binding to a given species is dependent on the coexpression

of other gangliosides in the membrane of melanoma cells (Lloyd *et al* 1992). The findings demonstrated in this thesis relate the phenomenon of crypticity directly to GBS, by demonstrating that the pathogenic potential of GBS-associated antibodies relies on the ganglioside presentation on the peripheral nerve. The crypticity of gangliosides is likely to be influenced largely by their presence in lipid rafts, which are transient structures in the living membrane (Dietrich *et al* 2002). The structure of the living membrane relies on energy (Morowitz 1968), and the existence of membrane proteins and lipids in their minimum energy states dictates their conformation. Thus, removal of energy from the membrane (for example, upon cell death) will deplete energy and may lead to conformational changes within rafts, as inferred from the ability of DG1 to bind only in dead tissue. The differential ability of antibodies to bind in tissue leads to many conceptual scenarios which may serve to enhance understanding of the pathogenesis of anti-glycolipid antibody mediated neuropathies and their treatment.

10.2 Molecular Masquarade: The Sulfatide System

The specificity of the mAbs DG1 and DG2 for sulfatide in addition to GM1 introduces the possibility of a new paradigm in autoimmunity, for which I have coined the term "molecular masquerade".

Sulfatide is a raft associated molecule, and is the sulfated derivative of GalC, both of which are synthesized by Schwann cells of the PNS (Taylor *et al* 2002). Sulfatide is a major surface determinant of myelin (Dupouey *et al* 1979), with an important role in its stability and function (Coetzee *et al* 1996.). Thus, any antibody mediated attack on sulfatide could lead to demyelination. Indeed, antibodies directed against sulfatide are implicated in demyelinating neuropathies, for example, antibodies to sulfatide

have been detected in the sera of Multiple Sclerosis (MS) patients (Ryberg 1978) and GBS patients (Willison and Veitch 1994, Ilyas *et al* 1991, Van den Berg 1993). The observation that antibodies specifically raised to a ganglioside structure are able to recognize sulfatide introduces the concept of molecular masquerade as a novel concept of autoimmunity. In other words, an antibody is raised against epitope "a" (i.e. the ganglioside like structure), but in tissue unwittingly reacts with an "imposter" epitope (i.e. sulfatide) to cause pathology. This hypothesis can be rejected by the observation that the mAbs which bind sulfatide on ELISA are not able to bind it in tissue, even in mice engineered to overexpress sulfatide, or following attempted epitope retrieval using EtOH or PFA, which have proven successful for other investigators (Quattrini *et al* 1992). There is much controversy surrounding the significance of anti-sulfatide antibodies in neuropathy. Because they are part of the natural immune repertoire, there is no consensus regarding the titre at which they are considered pathogenic, an issue further clouded by their different affinities, specificities and non-linearity in methods of detection (Terryberry *et al* 2005). Thus, the presence of anti-sulfatide antibodies in normal controls is an apparently benign situation as they do not react with PNS associated sulfatide, a scenario which is similar to the ability of DG1 and DG2 to bind sulfatide on ELISA but not in tissue. It would be of great interest to use these mAbs to determine the biological relevance of these anti-sulfatide antibodies. Sulfatide can be presented by CD1a cells to T-cells, leading to the activation of self-reactive T-cells (Shamshiev *et al* 2002). If anti-sulfatide antibodies which do not bind PNS myelin are able to recognize sulfatide when presented in this manner by CD1a cells, it is possible that by binding to the sulfatide they are able to interfere with the CD1a and T-cell receptor (TCR) interaction and limit the response of autoreactive T-cells.

What can be concluded from the observation that DG1 and DG2 can only bind sulfatide when it is coated to an ELISA plate is that sulfatide, when in the biological membrane of the PNS, is masked. It was surprising that use of tissue from a sulfatide over-expressing (CST) mouse and experimental conditions to enhance epitope exposure (such as cryosectioning and EtOH treatment) did not result in antibody binding. However, failure to expose sulfatide may be in part due to the size of the molecule, which is smaller than gangliosides. Taking this into consideration, it is highly likely that GPI anchored proteins and other gangliosides within the membrane lead to a deep cryptic domain from which sulfatide is not easily exposed and available as an epitope to the antibodies.

10.3 Anti-GM1 Antibodies: Pathogenesis Relies on Epitope Availability

The demonstration that WT and GD3s$^{-/-}$ mice have an abundance of ganglioside GM1 in their PNS (which is greatly enhanced in the latter strain) demonstrates that this site is vulnerable to attack by anti-GM1 antibodies. The ganglioside profile of the peripheral nerve was firstly demonstrated using CTb, which has one of the highest recognized protein-carbohydrate interactions (Schon and Freire 1989) and thus is reliable in demonstrating the distribution of GM1 throughout the tissue. The strong interaction of CTb for GM1 is due to the interaction of the pentameric toxin with 5 GM1 species, which increases the avidity from micromolar to nanomolar (Lauer *et al* 2002). The inability of the mAb DG1 to bind in living tissue in contrast to the success of DG2 binding shows that GM1 can be cryptic to certain ligands, in a manner which may vary between certain rafts or tissue types (such as the sensory motor system, which is spared in anti-GM1 antibody associated AMAN (Kaji and Kimura 1999)). Thus, the profiling of GM1 in the peripheral nerve relies critically on a ligand which

is likely to reveal all GM1, without failing to bind a proportion which may be masked. Again, this requirement is likely to be met by CTb, where the bivalent interaction of CTb and the GM1 oligosaccharide has been resolved to the Angsrom level and likened to a "two fingered grip" (Merritt *et al* 1994, Merritt *et al* 1998), enhanced by hydrogen bonding. Such a specific "grip", coupled with the high avidity, suggests CTb is highly likely to bind to GM1 regardless of the presentation of the epitope in the tissue. The results of DG2 show that anti-GM1 antibodies which rely on the Gal(β1-3)GalNAc epitope of GM1 are able to bind to GM1 in the mouse peripheral nerve, activate the complement cascade and cause calpain mediated destruction of the neurofilament via deposition of a MAC pore in the membrane (a similar mechanism to existing anti-ganglioside antibody mediated neuropathy models (Halstead *et al* 2004, Goodfellow *et al* 2005)). Gal(β1-3)GalNAc is a common epitope shared by GM1 and GD1b, meaning it is theoretically possible for DG2 to bind Gal(β1-3)GalNAc of GD1b (in a WT mouse), or indeed the Gal(β1-3)GalNAc epitope on glycoproteins. Demonstration that CTb can inhibit DG2 binding to WT tissue, but have no inhibitory effect on a specific anti-GD1b mAb has twofold implications: firstly, it demonstrates that CTb is specific for GM1 in the tissue, and that DG2 is specifically binding the Gal(β1-3)GalNAc epitope of GM1. Demonstration that the GalNAc-T$^{-/-}$ mouse has no DG2 binding confirms that DG2 is unlikely to be binding to Gal(β1-3)GalNAc in other structures, such as glycoproteins. The ability of DG2 to induce a lesion in both the WT and GD3s$^{-/-}$ is highly suggestive that it is binding the majority of PNS associated GM1, however it is possible that DG2 is binding an adequate population of GM1 to induce a lesion, but there may be underlying populations of GM1 which it does not bind. This possibility is difficult to address experimentally: DG2 gave a strong binding signal over the endplate on the WT and

GD3s$^{-/-}$ mouse indicating a saturating level of binding at the resolution of the light microscope. In order to define the microdistribution of DG2 binding, it would be interesting to compare the binding profile of DG2 and CTb at higher resolution (perhaps by electron microscopy using immunogold labeled ligands (Halstead *et al* 2004)) and to include an analysis of different tissue types and regions in such a study. Of particular interest would be a comparison of sensory and motor fibres, where it may be postulated that in sensory fibres, a significant proportion of GM1 is cryptically unavailable to DG2. This would fit with the observation that DG2 cannot bind GD1b via the common Gal(β1-3)GalNAc epitope, which implies that steric masking of Gal(β1-3)GalNAc is possible in a way which successfully restricts DG2. Any DG2 binding to available (i.e. non-cryptic) GM1 in sensory tissue may not be enough to manifest as a clinically defined lesion, perhaps due to not enough mAb binding, or due to mAb binding in rafts where GM1 is under more strict complement regulation and thus progression of the lesion is halted.

DG1, the monospecific anti-GM1 mAb was not able to bind GM1 in the live membrane of either the WT or GD3s$^{-/-}$ mice. This was surprising, as a monospecific anti-GM1 antibody was predicted to have an identical binding profile to CTb. The observation that DG1 cannot "see" GM1 proves that all GM1 detected by CTb is likely to be cryptic to DG1-like antibodies, a statement underlined by the inability of Sm1 and Do1 (antibodies cloned from patient sera) to bind the mouse peripheral nerve. Analysis of AMAN patient sera may reveal a high titre of an anti-GM1 antibody, which binds strongly to GM1 when presented on ELISA. However, akin to the DG1 scenario, this does not confirm that the antibody is able to bind GM1 in tissue and thus is not a reliable measure of pathogenicity.

The heterogenicity of lipid rafts mean that there may be several raft associated proteins and lipids which can interact with GM1. There may be region or tissue specific differences regarding the composition of lipid rafts, which may partly explain why GM1 is cryptic to anti-GM1 antibodies in sensory fibres but not motor. Treatment of cells with neuraminidase to deliberately increase GM1 content leads to significantly greater anti-ganglioside antibody induced cytotoxicity compared to cells with exogenously added GM1, taken as evidence that the exogenously added GM1 may partition into a "'lysis-resistant' membrane subdomain" (Zhang *et al* 2004). Conceptually, this can be related to the *in-vivo* situation in the nervous system: if different cell types and tissues have similar gangliosides, but these are partitioned into cell-type specific 'sub-domains', the implication is that not all cells may be equally susceptible to injury by anti-ganglioside antibodies. This finding may help clarify the susceptibility of the motor fibres in AMAN. However, what defines a true lysis resistant subdomain? For example, in the case of DG1, all native GM1 is in lysis resistant subdomains due to the fact that steric hindrance of GM1 from DG1 is enough to render GM1 lysis resistant . However in the presence of an antibody which is able to bind (eg. DG2), GM1 is likely to be accessible in domains rendered "inaccessible" by DG1. Thus, the pathogenic potential of a ganglioside critically depends on the specificity and affinity of the anti-ganglioside antibody. Furthermore, gangliosides are associated with lipid rafts, which are heterogenous (Schade and Levine 2002, Drobnik *et al* 2002) and thus likely to comprise of different protein species. This is relevant in the context of antibody induced complement activation. For example, an anti-GM1 antibody may bind, but the raft in which GM1 is situated may be under tight complement regulation. Thus, the antibody is unlikely to induce a complement mediated degradation of the peripheral nerve, but other, perhaps more subtle effects

may result. For example, the ability of anti-GM1 antibodies to cause conduction block could be due to the anti-GM1 antibody binding to GM1 in a raft enriched in complement regulators (which do not mask the GM1 from the antibody), and the binding alone may be enough to perturb function without causing actual cytolytic damage. This fits accordingly with the clinical course of anti-GM1 antibody mediated neuropathy, especially in cases where patients recover quickly (McKahnn *et al* 1993, Ho *et al* 1997). In such cases, complement activation and subsequent demyelination would not lend itself to a rapid reversal of symptoms, and furthermore, it has been shown that there is not necessarily a worsening of electrophysiological symptoms in conjunction with progressively worsening demyelination, suggesting conduction block is due to a "local anaesthetic" effect of antibodies at the node of Ranvier (Sumner *et al* 1982). Such a "local anaesthetic" effect can theoretically be illustrated by the conduction block induced by tetrodotoxin or saxitoxin, where electrophysiological readings return to normal within 5 days (Long *et al* 1990). There is evidence of similar recovery times in anti-GM1 antibody positive patients (Kuwabara *et al* 1998), and it can be proposed that the binding of an anti-GM1 antibody to a GM1 population under tight complement regulation may hinder the onset of demyelination, but allow the process of saltatory conduction to be impaired. For example, the disruption of sodium channels, known to cluster at the node of Ranvier (Shrager *et al* 1989), a situation which is also likely to be raft associated, may account for the observed conduction abnormalities.

It is also likely that GM1 exists in non-raft areas of the plasma membrane, as demonstrated from the ability of CTb to stain both raft and non-raft fractions of the plasma membrane in Chapter 7. This suggests that DG1 should bind to cells via non-raft associated GM1. However, the raft fractionation and Western blot data does not

quantify the relative amount of raft and non-raft GM1, and it is hypothesised that the GM1 in the non-raft areas of membrane is not of sufficient density to allow DG1 to bind. Alternatively, this non-raft GM1 may also be presented in an unfavourable way – for example the sialic acid of GM1 (on which DG1 binding relies) may be embedded in the bilayer of the membrane. However, the observation that gangliosides can exist both in and out of lipid rafts is interesting, and likely to be of significance owing to a similar scenario in the human intestine, which may yield clues into the selective pathology induced by anti-ganglioside antibodies in the nervous system. In human intestinal cells GD1a is not in rafts, whereas GM1 is (Fujinaga *et al* 2003). GD1a specific toxin (*E. coli* heat labile toxin type II, (LTIIb)) is unable to intoxicate intestinal cells due to the fact that intestinal GD1a is not in rafts, and it is concluded that only raft associated GD1a is able to internalise the toxin into the retrograde pathway which facilitates toxic action (Fujinaga *et al* 2003). Translating this to the nervous system, it is possible non-raft associated GM1 and raft associated GM1 are able to process bound antibodies in different ways. It has long been accepted that IgG antibodies are amenable to retrograde transport (Fabian 1990), and in the context of the current scenario, antibodies may bind to non-raft associated GM1 and remain associated with GM1 at the cell surface long enough to activate complement, whereas antibodies which bind raft GM1 are internalised and unable to activate complement. Of course, the reverse scenario may also be true. On a similar note, a specific anti-GD3 antibody (R24) binds GD3 at the cell surface of cultured ganglioside expressing cells, and the complex is endocytosed before being transported back to the plasma membrane (Iglesias-Bartolome *et al* 2006). What is most interesting is that R24 antibody, upon being recycled back to the membrane, was subsequentially detected in the cell culture medium. This suggests that *in-vivo*, an antibody-ganglioside complex

could be internalized, recycled back to the membrane and the anti-ganglioside antibody effectively ejected from the cell back into the extracellular compartment. It would be interesting to determine if the released antibody retained its ability to bind and activate complement. If not, the process of ejecting a non-functional antibody could be an efficient means of limiting pathogenesis, perhaps explaining the lack of anti-GM1 antibody mediated neuropathy in the sensory fibres.

As can be seen, there are various possibilities regarding antibody specificity, raft association, complement regulation based on raft constituents and the possibility of antibody internalization. This means that anti-GM1 antibody induced neuropathy represents an intertwined and probably incompletely characterized set of mechanisms which are perhaps impossible to resolve. However, one of the first steps in rationalizing the capricious nature of the GM1 epitope is to address what potential lipid raft associated structures could mask it. Before engaging in such discussion, it is worthwhile noting Fig 131, which depicts a bilayer containing GM1 and several leucocyte associated proteins. The most important point to glean from this diagram is that it is drawn to scale, and thus highlights to the reader that the overall membrane glycocalyx (which will include GPI anchored proteins) is central to the crypticity of gangliosides, which are a fraction of the size of the surrounding membrane proteins. Thus, in addition to the *cis*-interactions of gangliosides, there is a large influence of the glycocalyx in the availability of ganglioside epitopes.

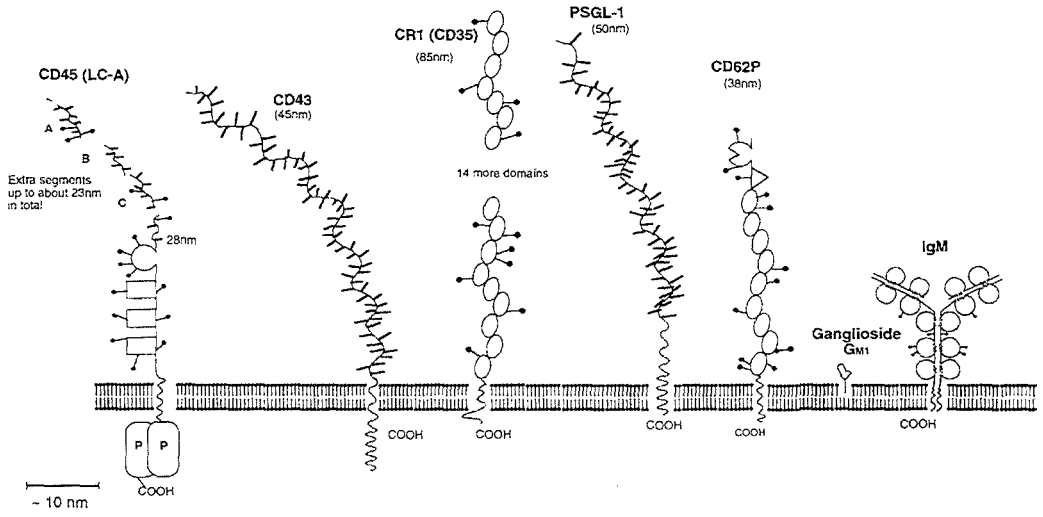

Fig 131. Exerted and modified from Barclay *et al*, 1997. The protein, ganglioside and immunoglobulin molecules are drawn to size and shape, with the height of the molecule from the cell surface also to scale. The most important feature of the diagram is the relative size of the ganglioside GM1 compared to the surrounding membrane proteins, meaning the membrane glycocalyx can be viewed as a canopy over the ganglioside and thus represents an important consideration in ganglioside crypticity. Also note the size of the ganglioside in comparison to the immunoglobulin molecule. Although sulfatide is not included in the diagram, it would be smaller the ganglioside.

10.4 GM1 and *cis*-interactions

Based on the binding characteristics of DG1 (i.e. the ability to bind dead tissue but not live) indicates that the crypticity of the ganglioside in live tissue is dependent on the inherent structure and fluidity of the living membrane. In Chapter 5 it was shown that removal of GPI anchored proteins from PC12 cells enhances the binding ability of DG2 and MOG 35 (anti-GM1 and anti-GD1a mAbs respectively). The association of GPI anchored proteins with lipid rafts (Sheets *et al* 1997), and their ability to restrict DG2 and MOG 35, is taken as evidence that gangliosides cluster within lipid rafts. Thus, in the living membrane, the lipid raft is likely to be the critical component in the masking of GM1.

The mAbs DG2 and MOG 35 were shown to bind to normal PC12 cells. If it is assumed that at least a proportion of this binding was to raft associated gangliosides,

then the observation that removal of GPI anchored proteins, such as Thy-1, can enhance their binding is indicative that in addition to the population of GM1 which was "non-cryptic", a new and previously cryptic population of GM1 and GD1a had been revealed. This provides evidence that lipid rafts are heterogenous and the masking of gangliosides relies on the constitution of the individual raft. What can also be gleaned from this experiment is that GPI anchored proteins are able to shield the Gal(β1-3)GalNAc epitope from DG2, but their removal does not allow DG1 to bind and therefore the sialic acid on which it relies must be masked by another raft associated species. The hypothesis that GM1 is masked from DG1 by GD1a was based on the observations in the $GD3s^{-/-}$ mouse. With an abundance of GM1, it is unlikely that the inability of DG1 to bind is due to the density of the epitope. However, the overexpression of GD1a and a lack of all *b* series gangliosides promote GD1a as the ganglioside which is most likely to interact with GM1 in the peripheral nerve.

The interaction of GM1 with other gangliosides and the subsequent effect on mAb binding was initially addressed using ELISA. Gangliosides GD1b and GT1b were each able to inhibit the ability of DG1 to bind GM1, but the inhibition was most significant with GD1a, which is in support of the initial hypothesis. The use of solid phase binding by ELISA provided a useful pilot study to specifically focus on the effects of individual gangliosides on masking GM1. However, interaction of a ganglioside with a plastic plate may interfere with the presentation of the glycolipid. When GM1, sulfatide or galactocerebroside are immunospotted on a TLC plate, they can be bound by the HIV glycoprotein gp120, however this binding is abolished when the glycolipids are presented on an ELISA plate or nitrocellulose membrane (McAlarney *et al* 1994). This indicates the lipid immobilization on the ELISA plate

alters the presentation of the headgroup, probably as a result of electrostatic interactions between the glycolipid and the plastic plate. With this in mind, the gangioside masking study was shifted to the interaction of GM1 and GD1a in the membrane. Treatment of the GD3s$^{-/-}$ and WT mouse with N'ase, to cleave the sialic acid from GD1a, resulted in the ability of DG1, Sm1 and Do1 antibodies to bind. In the GD3s$^{-/-}$, each proved successful in causing a complement mediated destruction of the peripheral nerve. The N'ase treatment of GD1a effectively causes it to become GM1, however as shown in Chapter 6 (Fig 98), blocking the cryptic GM1 with CTb, and testing the ability of DG1 to bind the "new" GM1 resulted in a weak signal, hence the strong DG1 signal in the N'ase treated tissue is largely due to it binding the "unmasked" GM1 (and to a much lesser extent some of the "new" GM1). This implies that the gangliosides GM1 and GD1a are able to *cis*-interact in such a way as to allow GD1a to mask the sialic acid of GM1. The inability of cholesterol depletion to disperse the complex, and the demonstration that binding of an anti-GD1a mAb to GD1a cannot alter the dynamics of the complex and allow DG1 to bind lead to the conclusion that the interaction of the 2 ganglioside species is strong.

As shown in Fig 132, ganglioside headgroups are able to interact with several ligands, including other glycosphingolipids. This alludes to the *trans* carbohydrate-carbohydrate interactions, for example, involved in processes such as cell recognition and adhesion between 2 interfacing cells (Kojima and Hakomori 1991).

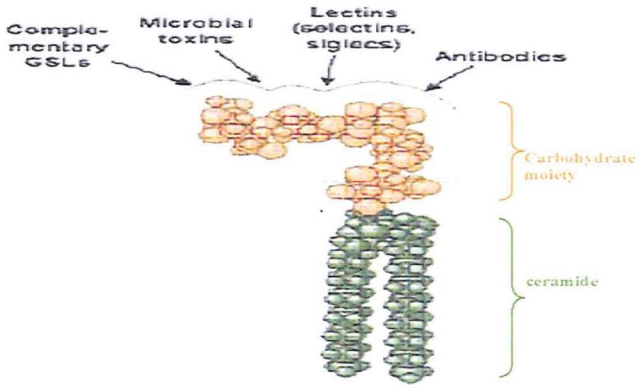

Fig 132. Modified from Hakomori 2001. The schematic diagram represents an example of a glycosphingolipid, which is held in the membrane in the minimal energy conformation. As shown, the carbohydrate portion (orange) is able to interact with antibodies, toxins, lectins, and most notably, other glycosphingolipids. The close interaction of 2 such carbohydrate headgoups could lead to the masking of epitopes on one species, or the creation of a complex which is targeted by anti-complex antibodies ("neo-epitope").

If glycosphingolipids can interact in such a "head on" (i.e. *trans*) fashion, then it is not unreasonable to assume that within the bilayer, if they are held in a suitable orientation, that they can also *cis*-interact. Indeed, and in agreement with the results of Chapter 7, it has been shown that cholesterol sequestering agents do not disrupt ganglioside clusters (in this case GD3) (Iwabuchi *et al* 1998). This indicates that ganglisodies are able to cluster in microdomains in a manner which does not necessarily depend on cholesterol, and is perhaps an intrinsic property of the interacting ganglioside species. This clustering ability may be due to the fact that glycosphingolipids contain hydroxyl groups which can act as hydrogen bond donors, and via this interaction are able to form side by side interactions in the microdomain (Hakomori 2001). However, the clustering ability alone does not provide evidence that the actual headgroups are able to closely *cis*-interact in a way which results in the masking of certain epitopes, such as the masking of the GM1 sialic acid by GD1a. One important consideration is that gangliosides in aggregate require a surrounding

area to host their oligosaccharide chain and its associated hydration water, meaning more complex headgroups such as GM1 and GD1a will have larger space requirements in the membrane (Sonnino *et al* 2006). However, in considering the small gangliosides (6kDa) and large mAbs (65kDa) (and again refer to Fig 131), the binding of the antibody to the gangliosides can be likened to "an elephant picking up a peanut". So, in appreciating the spatial dynamics of the antibody binding to the epitope, the presence of water surrounding the two neighbouring ganglioside headgroups is perhaps negligible, and there is sufficient side-side headgroup interaction to mask the sialic acid of GM1 from the antibody DG1. Furthermore, water may enhance the interaction between ganglioside monomers (Brocca *et al* 1998), and increasing the amount of ganglioside species within a microdomain may decrease the lateral mobility of the individual head group oligosaccharides, possibly due to intramolecular interactions between the headgorups (Sharom and Grant 1977). Figure 133 shows a simple schematic diagram of the possible interaction of GM1 and GD1a.

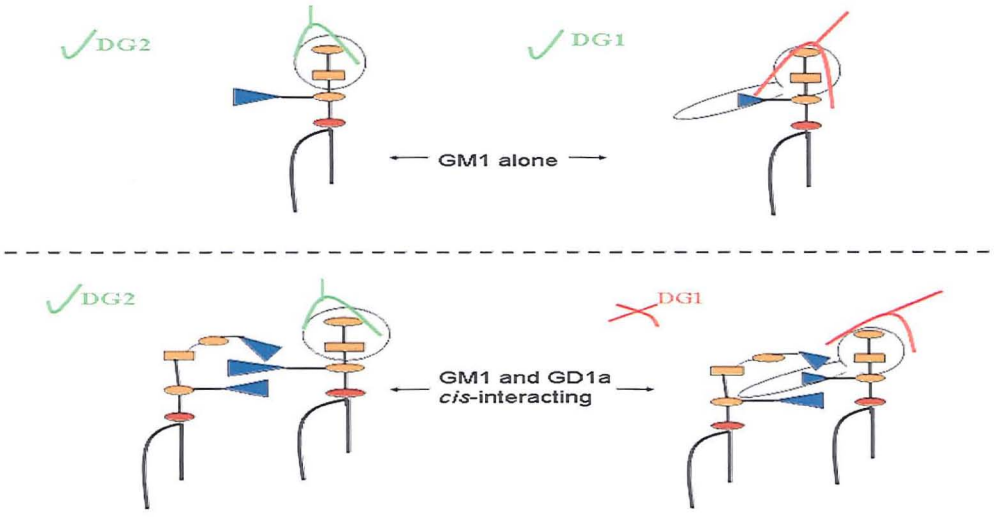

Fig 133. Above the line: GM1 alone can be bound by both DG2 and DG1. DG2 binds the Gal(β1-3)GalNAc epitope, while DG1 binds the Gal(β1-3)GalNAc epitope and the sialic acid of GM1. The epitopes are shown by the shaded ovals. Below the line is a schematic representation of the possible interaction between GM1 and GD1a. As shown, DG2 is still able to bind the Gal(β1-3)GalNAc epitope, but the sialic acid of

GM1 is hidden by GD1a, meaning DG1 is unable to bind. The position of the gangliosides is likely to be dictated by lateral mobility in the oligosaccharide head group which projects from the membrane. In addition to this, it is also worthwhile noting that variations in the length of the ceramide portion may influence the extent to which the headgroup sits above the membrane, and this may contribute to the ability of one ganglioside to "mask" another.

In summary, what can be concluded is that a set of anti-GM1 antibodies have been identified which are unable to bind GM1 when in complex with GD1a, and rely on the presentation of GM1 alone in the membrane. Although not explored in the context of the living membrane, it is feasible that other ganglioside species may exert a similar cryptic masking effect on GM1.

10.5 Ganglioside Complexes- Increasing Clinical Significance

While the studies of Kaida *et al*, as described in Chapter 9, show that antibodies to complexes exist in sera, the results of chapter 9 show that out of 4 samples, only one was able to bind to the target complex in the biological membrane. The screening of the sera (by Kaida and co-workers) was initially performed using paradigms which may not represent the epitope presentation in the biological membrane (i.e. TLC and ELISA as opposed to the phospholipid bilayer). This suggests that solid phase assays do not always faithfully represent the epitopes formed by interacting gangliosides, and it may be of more value to estimate the pathogenic potential of such antibodies by screening patient sera against cholesterol and ganglioside containing liposomes or model bilayers (which are more representative of the biological membrane).

It would be interesting to determine the effect of PI-PLC removal of GPI anchored proteins on the binding ability of the anti-complex antibodies. An increased ability to bind would suggest that the entire neoepitope (comprising the 2 gangliosides) can sit in a lipid raft and be masked by a GPI anchored protein. It would also be of interest

to repeat the experimental design of Chapter 8, and test the ability of the anti-complex antibodies to bind to both live and dead *C.jejuni*. *C.jejuni* strain O:19 was bound by DG1, taken as evidence that the ganglioside mimicking LOS do not *cis*-interact, and it would thus be predicted that the sera samples containing antibodies reactive to the GM1/GD1a complex would not be able to bind strain O:19.

The ability of 2 gangliosides to interact and form a new glycoepitope raises the possibility that the interacting gangliosides undergo a conformational change, which supports the idea that certain antibodies to the individual species are no longer able to bind (Kaida *et al* 2004). For example, a new glycoepitope formed by the interaction of GD1a and GM1 would be most likely to result in a conformation in which the Gal(β1-3)GalNAc of GM1 is available (as DG2 can bind), but the sialic acid (on which DG1 relies) is masked by the GD1a molecule. As MOG 35, the anti-GD1a mAb can bind well in tissue, it is likely that the orientation of GD1a does not lead to any part of the molecule becoming cryptic. The preference of antibodies for clusters of ganglioside is possibly for functional reasons. This idea is based on the homophilic binding observed for antibodies such as anti-GD3 antibody R24, which binds to itself or similar antibodies resulting in an increased avidity for GD3 (Chapman *et al* 1990, Dippold *et al* 1980, Pukel *et al* 1982). Carbohydrate-protein interactions are weak (in the micromolar range), compared to the nanomolar range of protein-protein interaction (Weis 1997, Wilson and Stanfield 1995, Thomas *et al* 2002), so binding of antibody (which is not capable of homophilic binding) to an epitope comprising two *cis*-interacting carbohydrate head groups may improve the strength of the interaction.

Another issue is the specificity of the anti-complex antibody. While it is hypothesized that the antibody is binding the "complex", this may not be the case. For example, a

patient may have a high titre of circulating anti-GD1a antibody, which does not bind GD1a alone in tissue, or on ELISA. However, when GD1a is in complex with GM1, a conformational change may alter the presentation of GD1a (perhaps by rotating the molecule in a certain manner, or inducing a curvature) and this allows the anti-GD1a antibody to bind. Thus, an alternative hypothesis is proposed for the binding of anti-complex antibodies. Anti-ganglioside antibodies are only able to bind to their target ganglioside when this is complexed with another species. In a similar system, as shown by the results presented within this thesis, the reverse scenario is also likely, where antibodies which are *unable* to bind gangliosides in complex exist.

It is likely that many GBS patients have these complex antibodies, but the traditional screening of sera against a panel of purified single species of gangliosides (Willison 2005) means that while the patients' sera may appear negative for anti-ganglioside antibodies, this may be because it is only able to react with complexes. Thus the discovery of ganglioside complexes may mean an evaluation of existing theories regarding serological and pathological relationships in GBS, where single species anti-ganglioside antibodies are focused on (Willison 2005).

10.6 Significance of DG1-like Antibodies in Health and Disease

In Health: Antibody Function

DG1 like antibodies which exist in the normal repertoire of healthy individuals are unlikely to be pathogenic. This is essentially owing to their inability to bind GM1 when the membrane is in its normal, physiological state. Only in situations which perturb the membrane and expose GM1 are DG1 like antibodies likely to become pathogenic, as will be discussed below. However, if the immune repertoire comprises of anti-GM1 antibodies that are not normally able to bind GM1, then what is the

purpose of having these antibodies? The observation that DG1 can bind to *C.jejuni* may partly explain this anomaly. Upon infection with *C.jejuni*, the molecular mimicry hypothesis states the immune response will raise antibodies to the ganglioside like structures on the bacterial surface, and instead of opsonising the bacteria, the antibodies unfortuitously bind to nerve associated gangliosides such as GM1 (Yuki *et al* 2004). This results in an immune response to self. If DG1 like antibodies were already present, then *C.jejuni* is likely to be immediately opsonised by these antibodies, meaning potentially self reactive antibodies would not be raised against the bacteria and lead to autoimmune nerve damage. DG1 would not bind to nerve associated GM1, and thus *C.jejuni* would be opsonised in a way in which nerve damage via molecular mimicry is impeded. *C.jejuni* strain O:19, which is strongly associated with AMAN, has both GM1 and GD1a like oligosaccharides on its coat (Yuki *et al* 1993, Aspinall *et al* 1994). The presentation of these epitopes clearly differs from the presentation of the gangliosides in the nerve membrane, where it is hypothesised that GM1 is masked by GD1a. This masking of self GM1 inhibits DG1 binding and is thus a highly significant feature in protecting the body from potential autoimmune attack. The *cis*-interaction of membrane associated GM1 and GD1a is unlikely to be replicated on the surface of *C.jejuni* strain O:19, based on DG1 binding ability. This may be explained by the lipid A region of the molecule, which anchors the molecule to the surface. In bacterial ganglioside mimics, the lipid A portion comprises of 4 chains, as opposed to the double chain of the ceramide which anchors a ganglisoide in the nerve membrane (Fig 134).

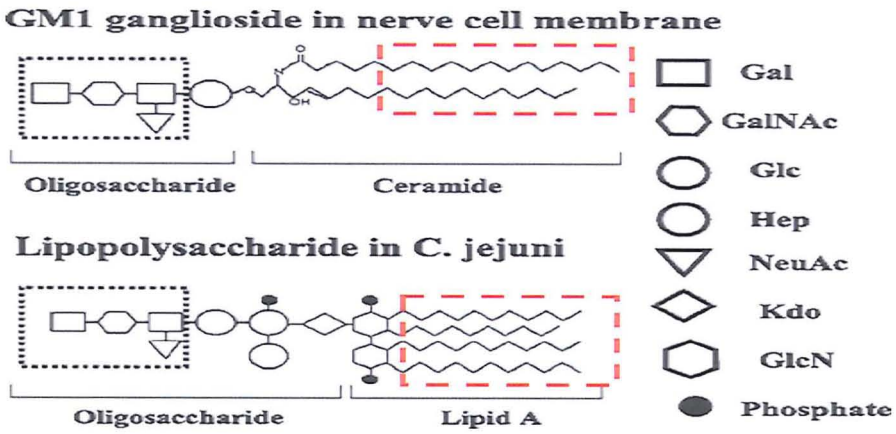

Fig 134. Modified from Yu *et al* 2006. The hatched red box shows the difference in structure of the anchoring lipid A and ceramide portions.

As shown in Fig 134, the oligosaccharide headgroups of the bacterial ganglioside mimics may be anchored outwith a distance by which they can physically interact, a statement which is likely to apply at least to *C.jejuni* strain O:19. The ability of nerve associated gangliosides to interact both with other gangliosides and GPI anchored proteins makes evolutionary sense. Firstly, it prevents nerve damage via molecular mimicry, and secondly, gangliosides are targeted by bacterial toxins (Willison and Kennedy 1993) meaning it is logical for them to be shielded.

GBS: The Initial Lesion

Like DG1, the human antibodies Sm1 and Do1 were unable to bind to GM1 when in complex, and required the removal of GD1a by N'ase. These human antibodies were cloned on the basis that they were of a high anti-GM1 titre in patients with acute neuropathy (Paterson *et al* 1995). From the observation that their epitope (GM1) is masked by GD1a in the living membrane, and therefore they cannot bind, the natural assumption is that these antibodies had no role in the patients' pathogenesis and were effectively "innocent". This theory may be overly simplistic. While, in the healthy membrane they would be inhibited from binding, there are a number of scenarios

which may arise to initiate irregularities in the membrane and lead to a situation where the antibodies can "see" GM1 and become pathogenic, as shall be discussed. Possible and novel insights into ganglioside expression and presentation by certain cells or tissues may be gained by looking at parallel example, such as the olfactory system. Olfactory ensheathing cells (OECs) are functionally similar to the Schwann cell of the PNS (Wewetzer *et al* 2002), and thus play a role in axonal support. It is believed that the expression of the glycolipid O4 by OECs is not due to actual synthesis of the glycolipid by the cell, but as a result of phagocytosing O4 positive axonal fragments (Wewetzer *et al* 2005). This theory can form the basis of a similar model in the PNS, involving anti-ganglioside antibodies. If the axon is damaged by a DG2-like anti-GM1, or anti-GD1a antibody, the Schwann cells may phagocytose the axonal fragments and subsequentially express gangliosides, including GM1. In this scenario, the newly acquired GM1 may be presented in a favourable way to DG1-like antibodies, and thus the lesion would progress to a second phase attack and further damage, in this case secondary demyelination.

Chapter 3 shows that the node of Ranvier has GM1 immunoreactivity, but the internodal regions of the Schwann membrane and also the pSC do not appear to have GM1. It is not easy to rationalise how or why the Schwann cell would limit and localise GM1 to these paranodal regions. The explanation may follow the theme of acquired gangliosides, whereby gangliosides may be shed (perhaps in exosomes) or flick from the axon into the Schwann cell at the paranodal region. DG1 was not able to bind this paranodal GM1, but it remains possible that it is displayed in a domain which makes it available to circulating anti-GM1 antibodies of other specificities. Such a mechanism may also occur in other tissues, and effectively sensitise them to anti-GM1 antibody mediated attack. If the "acquired" gangliosides are expressed in

different domains to those synthesised by the particular cell, then this may also partly explain the heterogenicity amongst lipid rafts, and also the observation that GM1 is in rafts but also non-raft areas of the membrane.

The clinical course of AMAN can be viewed as a two prong attack, as the initial lesion may begin as a purely axonal injury, but progress to a secondary attack on the myelin (Hadden and Hughes 2003). Again, DG1-like antibodies may play a role in this two stage process. If the initial disruption to the axon is initiated by either an anti-GM1 antibody (of a specificity which can bind axonal GM1) or perhaps an anti-GD1a antibody, the subsequent disruption may lead to a knock on disturbance of the myelin. Regardless of the cause, the structural disruption alone may be adequate in unmasking GM1 and allowing DG1-like antibodies to bind, thus initiating a second phase to the lesion. Interestingly, this disease model may be of relevance to other nerve disorders, such as multiple sclerosis (MS), where anti-ganglioside antibodies may play a role in axonal damage following the initial primary demyelinating lesion of MS. Fig 135 summarises the disease model in schematic form (Sadatipour *et al* 1998).

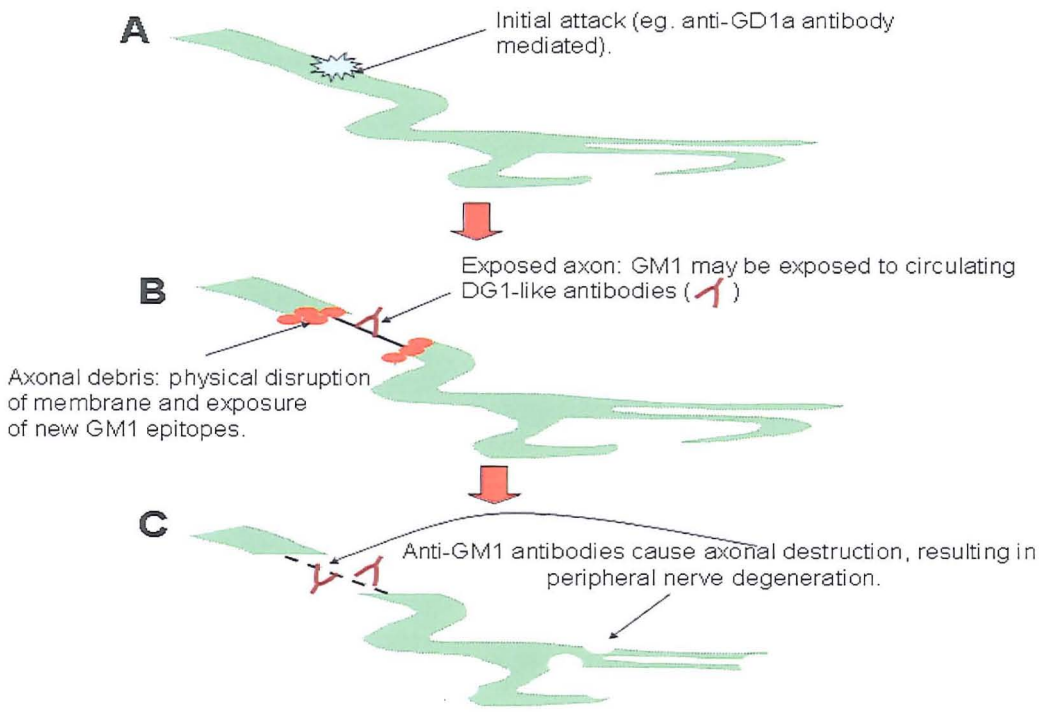

Fig 135 **A**. In the unlesioned peripheral nerve (shown in green), GM1 is not available to DG1-like antibodies. However, upon a primary lesion, cryptic GM1 is exposed and DG1 like antibodies can bind to induce the secondary phase of the lesion. The primary lesion could be an attack mediated against another ganglioside (e.g. GD1a,(Goodfellow et al 2005)) or the result of another disease process (e.g. multiple sclerosis (Sadatipour *et al* 1998)). **B**. Following exposure of GM1, DG1-like antibodies are able to bind and cause an anti-GM1 antibody mediated attack, to worsen the initial lesion. **C**. This secondary attack leads to anti-ganglioside mediated destruction of the peripheral nerve, and AMAN like pathology (eg. paralysis).

GBS: Recovery

The action of the sialidase N'ase was shown to enhance the binding of DG1 by exposing GM1 upon removal of GD1a. A parallel system may exist *in-vivo*, based on recent reports of plasma-membrane ganglioside sialidase activity in cultured hippocampal neurons (Rodriguez *et al* 2001). In this paradigm, the growth cone of the neurons has enhanced activity of this sialidase, probably to enhance the local levels of GM1, where its interaction with the TrK receptor (Duchemin *et al* 1998) would enhance growth of the axon tip. Assuming the neurons express GM1 and

GD1a in their undifferentiated state, a hypothesis can be generated, based on the *ex-vivo* observations with N'ase. Upon differentiation of the neurons, the expanding growth cones would have increased PMGS activity in direct correlation with a region specific decrease in GD1a and an increase in GM1. In such a differentiated cell, the soma would thus have the intrinsic expression of GM1 and GD1a, but in the growth cones there would only be GM1. If the "unmasking" hypothesis explored in this thesis hold true in this situation, then binding of DG1 to the PMGS rich growth cones would be possible, but the cell body would remain resistant to DG1, as the GM1 is not unmasked from GD1a by the PMGS. Relating this to the regeneration of the peripheral nerve in AMAN raises important considerations. Upon regeneration of the axon, PMGS activity would lead to an exposure of GM1 on the regenerating axon, which would be vulnerable to attack by DG1-like antibodies. The initial AMAN pathology may have been initiated by a different antibody, however only in the recovery phase would DG1-like antibodies become pathogenic. In order to validate this hypothesis, it would be interesting to perform some simple experiments on the hippocampal neurons. It can be predicted that the membrane of the cell body in the differentiating cells would be positive for MOG 35 (against GD1a), and also show CTb immunoreactivity against GM1. DG1 would not be expected to stain the cell body owing to the masking effect of GD1a. In the growth cone, areas of PMGS activity should directly colocalise with decreased MOG 35 staining and also with DG1 immunoreactivity (Fig 136). Indeed, samples of DG1 and MOG 35 were sent to Dr Rodriguez (Catholic University of Leuven and Flanders Interuniversitary Institute for Biotechnology Belgium) to address the above questions in PMGS expressing hippocampal neurons (Rodriguez *et al* 2001). However, experiments were not overseen by myself, and illustrative data sent to me was from an non-optimal

protocol; from this preliminary approach it was not able to reach a conclusion and this is an experiment which will be pursued.

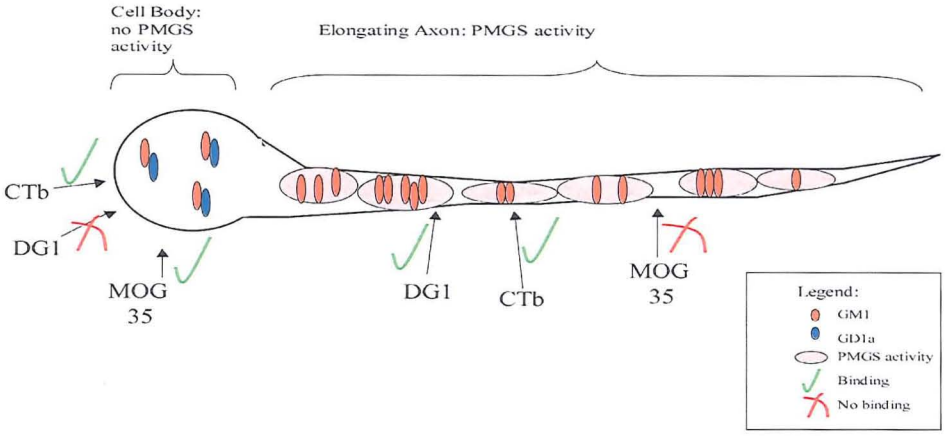

Fig 136. Schematic representation of hypothesis: cell body expresses GD1a and GM1, and DG1 cannot bind. Elongating axon has PMGS activity. Lack of MOG 35 binding proves PMGS is removing GD1a, and in these regions DG1 can bind.

The experimental approach described would conclusively prove that the removal of GD1a was facilitating the binding of DG1. But, this data alone does not entirely support the masking hypothesis, as binding may be due to an increased density from the conversion of GD1a to GM1.

However, the results of the DG1 studies in the GD3s$^{-/-}$ mouse are strongly suggestive that the phenomenon is due to masking, and taken together these data are strongly suggestive that this is the case in the differentiating axon. Proof that application of DG1 to the differentiating neurons can lead to antibody binding to the axon and subsequent inhibition of outgrowth would increase the feasibility of this system in the inhibition of regeneration of the peripheral nerve following AMAN. Specific delivery of sialidase to experimental PNS lesions in the rat is able to enhance axon outgrowth, thought to be as a result of increasing GM1 in the regenerating axons (Yang *et al* 2006). Furthermore, the authors of this study propose that sialidase activity acts to prevent the inhibition of regeneration by removal of complex gangliosides and thus

inability of myelin associated glycoprotein (MAG) to inhibit the outgrowth. MAG is an inhibitory protein which accumulates at injury sites in the nervous system and inhibits neurite outgrowth by binding complex gangliosides such as GT1a and GD1a (Vyas *et al* 2002). Thus, in AMAN, the regeneration of the peripheral nerve would be severely compromised in the presence of an antibody which specifically targets the GM1 expressed in the regenerating areas, but the situation is not entirely pessimistic owing to the continued inhibition of MAG. However, a recent study has demonstrated that passive transfer of anti-GD1a antibodies leads to IgG binding and clustering of GD1a in regenerating axons, which inhibit regeneration in a MAG independent process (Lehmann *et al* 2007). This suggests that anti-ganglioside antibodies can cluster gangliosides to inhibit regeneration. Thus, ability of DG1 like antibodies to bind sialidase rich growth cones could have catastrophic consequences to the regenerating nerve. Firstly, they could initiate a complement mediated attack, secondly, antibody binding to GM1 could induce functional impairment of GM1-TrK interaction, and thirdly, the clustering of GM1 by the antibodies could lead to inhibition of regeneration in a similar way to the anti-GD1a antibody example (Lehmann *et al* 2007).

These scenarios may explain the incomplete recovery demonstrated by some AMAN patients (Gregson *et al* 1991), and lead to the possibility of modified treatment regimens, such as prolonging the period of antibody clearance (Willison and Yuki 2002) to allow the axons to fully regenerated and assume the "normal" ganglioside profile as opposed the PMGS induced profile.

10.7 Future Work

Following the successful isolation of rafts containing both GM1 and GD1a, it would be worthwhile pursuing the detection of FRET between the species. The initial attempt to detect FRET was perhaps hindered greatly by the size of the antibodies and CTb compared to the small gangliosides. CTb and MOG 35 may have been too large to bind simultaneously to GD1a and GM1 in complex, or the location of the fluorescent conjugates on the probes may have led to them becoming too widely spaced to undergo FRET (as described in Chapter 7). A novel approach to the detection of FRET using antibodies may be to use smaller antibodies, such as that of the camel. Camel antibodies, unlike mouse and human antibodies, are more simple in structure as they lack light chains and consist only of the Y-shaped heavy chain (Hamers-Casteman *et al* 1993). This means they may be more amenable to binding gangliosides when in complex. The use of GM1 and GD1a specific antibodies of this strucure could be a very useful tool in the study of ganglioside interactions, with relevance not only to FRET, but also studies at the electron microscope level. The introduction of such an approach in the near future is unlikely, although continuing advances in antibody engineering mean it may become feasible.

Within this thesis, the study of antibody binding to complexes began by analysing antibody binding to ganglioside complexes coated to ELISA plates, and next progressed into the biological membrane. The *ex-vivo* study was possible due to the availability of a mouse which expresses only GM1 and GD1a, meaning the ideal biologically relevant model was available. However studies of other ganglioside complexes, such as GD1a and GD1b would require a different approach. In this case, it would be of interest to use cholesterol containing liposomes or model membranes to

determine the effect of ganglioside complexes on antibody binding. In such studies, the ability to vary the amount of cholesterol, and the ratios of gangliosides, may yield some insights into how ganglioside complexes form and are maintained within the membrane. More specific analysis of the antibody binding affinities could also be calculated, perhaps using the Biacore system and ganglioside containing liposomes (Erb *et al* 2000, Boffey *et al* 2005) to determine the affinity of (monovalent) antibody binding to ganglioside complexes.

The antibodies Do1 and Sm1 were cloned from human neuropathy sera on the basis that they were high titre, and bound well to GM1 on ELISA. However, in the mouse *ex-vivo* muscle nerve preparations, they did not bind to GM1 and were not pathogenic. This implies the patients may have had other antibodies, perhaps to ganglioside complexes, which were missed during routine screening. Although a daunting task, it would therefore interesting to re-screen GBS patient sera against single gangliosides and complex gangliosides, using cholesterol containing liposomes which bear more resemblance to the biological membrane than does an ELISA plate. This may yield an entirely new population of patients whose pathogenesis is mediated by antibody attack on ganglioside complexes, and lead to re-classification of the traditional clinical-serological relationships. On a similar note, during the production of the mouse monoclonal antibodies, when mice were inoculated with ganglioside mimicking oligosaccharides or ganglioside containing liposomes, sera were screened against single ganglioside species. This means the focus of research with mouse monoclonals has been on those which react with single ganglioside species. Sera which contained antibodies to complexes would have inadvertently been classed as negative and discarded. With our current understanding, it may be possible to identify

mouse antibodies which are reactive with complexes, which would be valuable tools for future research.

Aside from the aetiology of anti-complex antibodies, one of the most puzzling issues is how the antibodies to ganglioside complexes exist. It has already been demonstrated that DG1 cannot bind to GM1 when complexed with GD1a in the nerve membrane, but can bind to the GM1 oligosaccharide on *C.jejuni* in the presence of a GD1a like oligosaccharide. From this, it is unlikely that bacterial GD1a and GM1 like structures interact in a way which mimics the structure of the complex in the membrane. In other strains of *C.jejuni*, however, the presentation of the oligosaccharides may not resemble that of *C.jejuni* strain O:19. For example, the ratio or overall density of GM1 and GD1a like structures may differ, leading to an increased ability to interact. It is likely that certain strains of *C.jejuni* do bear oligosaccharides which give rise to anti-complex antibodies (Kuijf *et al* 2007), and this may be explained by genetic polymorphisms of *C.jejuni*, which influence the presentaion and strucure of the oligosaccharide (Godschalk *et al* 2004). This may be an evolutionary response of the bacteria to overcome opsonisation by antibodies which rely on singly presented epitopes, such as DG1. It is also hypothetically possible that the presentation of the oligosaccharides on certain *C.jejuni* strains could be altered post infection, an assumption based on the ability of trypanosomes to alter their sialic acid profiles. Trypanosomes are unable to synthesise sialic acid, and recently a form has been identified which can regulate the amount of sialic acid on its surface by modulating the expression of two different trans-sialidase enzymes, which transfer sialic acids from glycoconjugates present in host tissues to the trypanosome (Montagna *et al* 2006). If the sialic acids were removed from host gangliosides, this would lead to a new ganglioside profile in the tissue of the host, in addition to

modifying the surface coat of the trypanosome. Removal of the sialic acid from GD1a would result in the binding of DG1-like antibodies. Such a mechanism has not been demonstrated for *C.jejuni* infection, however it is feasible that sialidases present in the mucosal epithelia of the enteric tract may act on the sialylated epitopes of *C.jejuni* to change their structure and lead to the generation of antibodies with varying specificities. It would be of great interest to define the molecular structures of the epitopes present on *C.jejuni* isolated from individual patients and expand the current understanding of how anti-complex antibodies arise.

10.8 Conclusion

There is growing interest in the significance of GBS associated antibodies which are only able to bind ganglioside complexes, and the findings with DG1, Sm1 and Do1 add a new dimension to this by demonstrating existence of antibodies which are inhibited from binding by their target ganglioside being in a complex. Taken together, this points to the notion that the microarrangement of gangliosides in the membrane (which is likely to be raft associated) is important in determining the pathogenic potential of antibodies in GBS.

With specific regard to AMAN, the microheterogenicity of anti-GM1 antibodies underpins pathogenic potential, as demonstrated by DG1 and DG2, and the "membranomic" basis for these differences is largely due to *cis*-interacting gangliosides and to a lesser extent, the masking of epitopes by GPI anchored proteins. In addition to expanding the understanding of AMAN pathology, the observations in this thesis highlight the importance of epitope presentation in the context of antibody and sera screening, where the reliance on solid phase ELISA may hinder the discovery of antibodies to biologically determined complexes.

Appendix 1

A1.1 Introduction

Throughout this thesis, several transgenic mice have been used. This appendix provides a brief overview into the ganglioside profile of these mice. A diagram of the ganglioside biosynthetic pathway has already been shown in Chapter 1, and this is elaborated in Fig 137 to include the relevant enzymes involved in each step, and to include the synthesis of sulfatide. From this diagram, the relevant portions have been exerted and used to highlight the ganglioside profile of the transgenic strains where relevant.

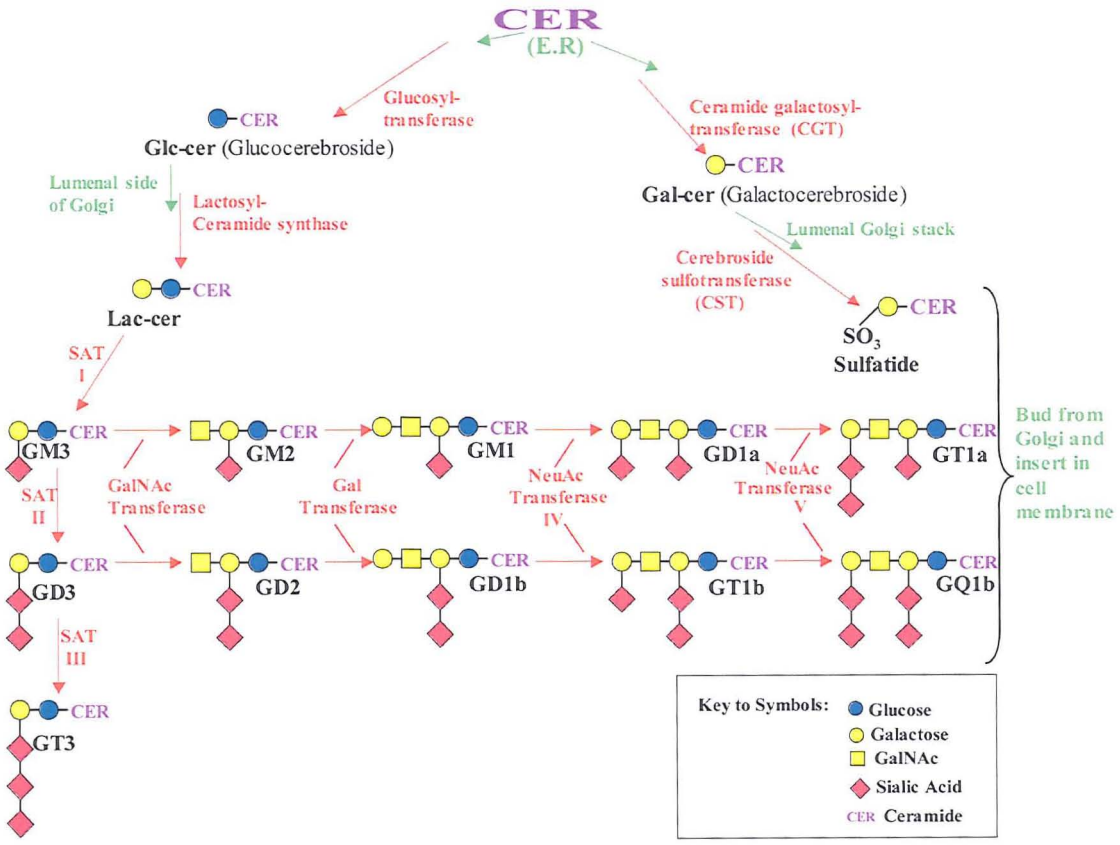

Fig 137. Simplified overview of the sulfatide and ganglioside biosynthesis pathways, with specific emphasis on the *a* and *b* series gangliosides (starting with GM3 and GD3 respectively). Diagram based on the review by Tettamanti 2004

A1.2 Ganglioside Lacking and Upregulating Mice

GD3s-/- This strain was obtained from Dr. K. Furukawa (Nagoya University, Japan, Okada *et al* 2002). As shown in Fig 138, this mouse only synthesises *a* series gangliosides, due to lack of the enzyme GD3 Synthase (Sat I). As GM3 is the substrate for this enzyme, the increased levels of GM3 mean the excess is utilised for *a* series, leading to an increased synthesis of the *a* series when compared to the WT mouse.

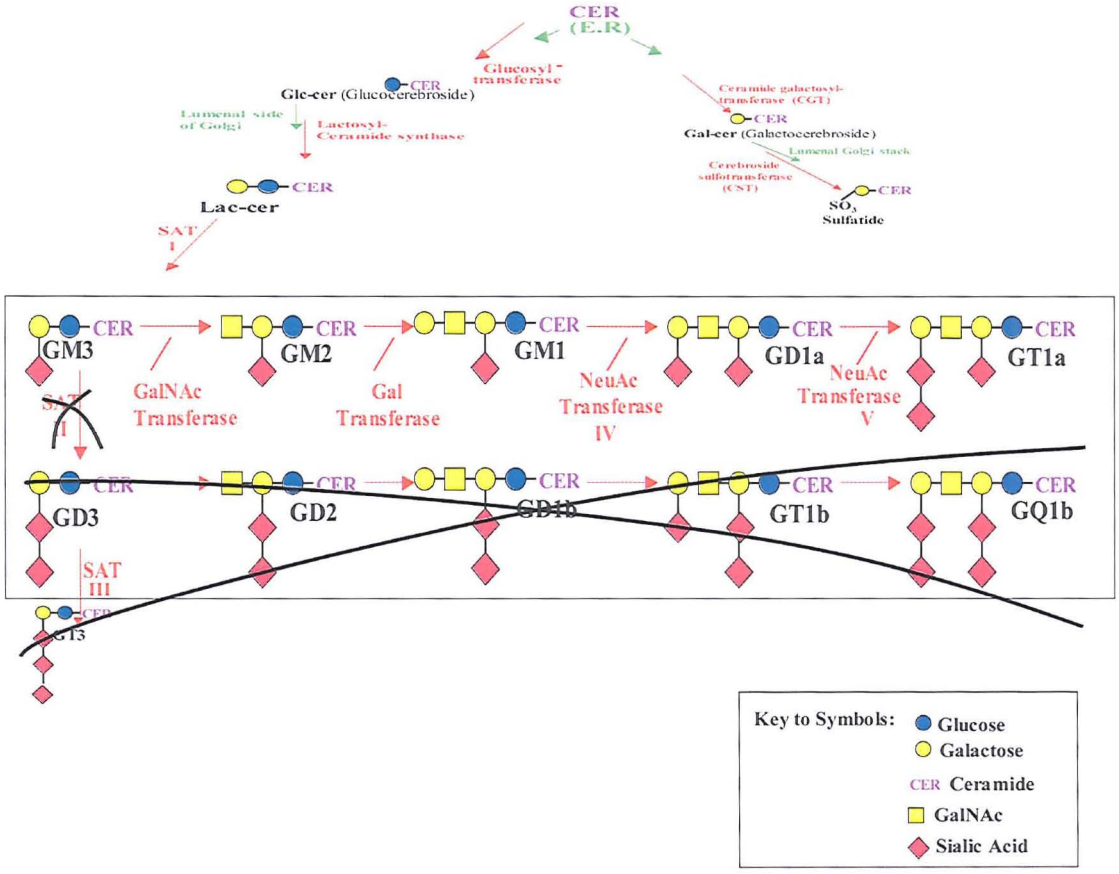

Fig 138. Diagram highlighting the ganglioside expression profile of the GD3s$^{-/-}$ mouse.

GalNAcT$^{-/-}$. This mouse was also obtained from Dr. K. Furukawa (Takamiya *et al* 1996). The GalNAcT$^{-/-}$ expresses only GM3, GD3 and GT3, meaning it has no complex gangliosides. This makes the GalNAcT$^{-/-}$ an ideal negative control for mAbs

to complex gangliosides. For example, positive binding in the GalNAcT$^{-/-}$ of a mAb which relies on the Gal(β1-3)GalNAc epitope suggests the mAb is binding the epitope on a glycoprotein, and this non-ganglioside associated binding should be accounted for in WT and GD3s$^{-/-}$ mice.

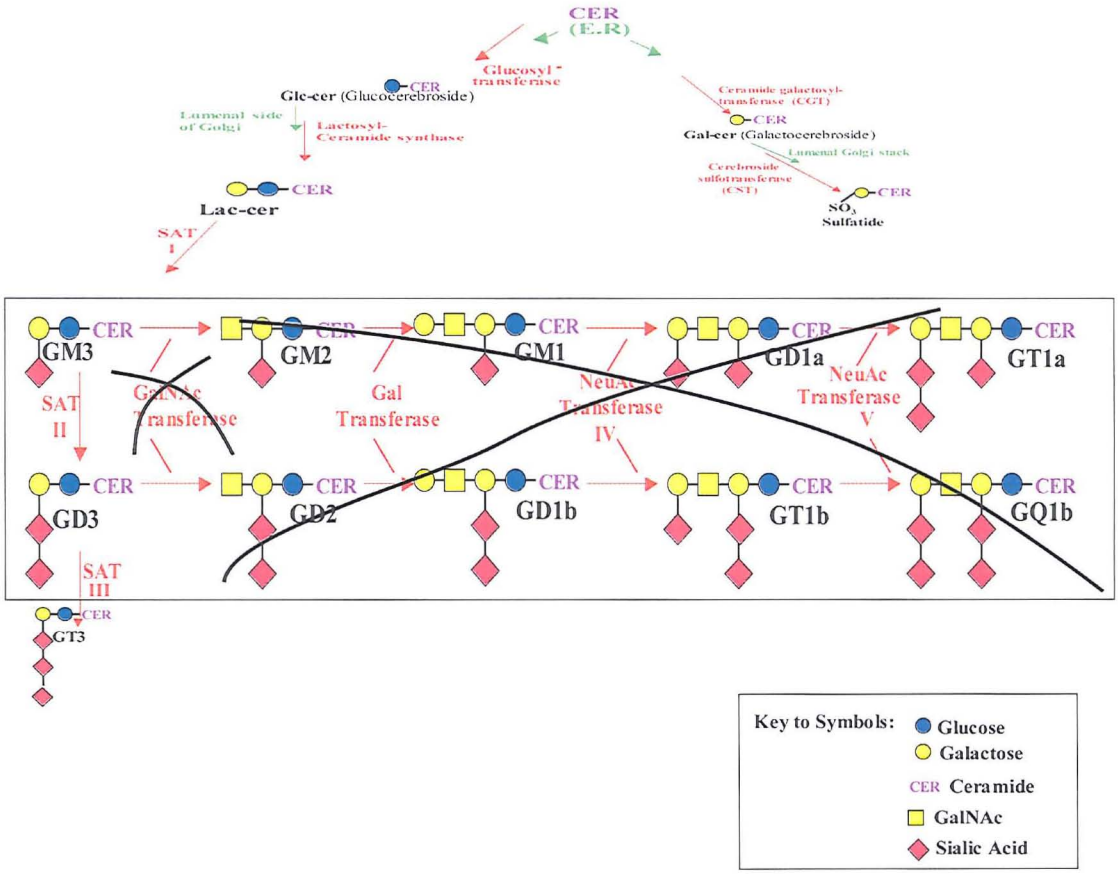

Fig 139. Diagram emphasising the ganglioside biosynthesis of the GalNAcT$^{-/-}$ mouse.

A1.3 Complement Regulator KO Mice:

CD59a$^{-/-}$: This mouse lacks the GPI anchored complement regulator protein CD59a, and has no known alteration in ganglioside expression. This strain was obtained from Dr BP Morgan (Cardiff University, Wales).

DAF1$^{-/-}$: The DAF1$^{-/-}$ mouse does not express the GPI anchored complement regulator DAF1, and has no known alteration on ganglioside expression. This mouse was obtained from Dr Feng Lin, Case Western Reserve University, Ohio, USA.

CD59a$^{-/-}$/DAF1$^{-/-}$: This double KO mouse was obtained by crossbreeding homozygous DAF1$^{-/-}$ and CD59a$^{-/-}$ parents, until doubly homozygous KO progeny were produced and maintained as a true breeding colony.

A1.4 "Triple KO" Mice

GD3$^{-/-}$/DAF1$^{-/-}$/CD59a$^{-/-}$. These mice have the same ganglioside repertoire as the GD3s$^{-/-}$ mouse, but also lack the complement regulator proteins DAF1 and CD59a. The GD3$^{-/-}$/DAF1$^{-/-}$/CD59a$^{-/-}$ mice were derived by crossbreeding the GD3s$^{-/-}$/DAF1$^{-/-}$ mice with CD59a$^{-/-}$/DAF1$^{-/-}$ mice. The breeding program used was the same as outlined for generating the double KO (CD59a$^{-/-}$/DAF1$^{-/-}$) already described, as both parent mice lack the DAF1 gene.

A1.5 Wild Type.

WT : WT mice have an unaltered ganglioside profile and are assumed normal. WT mice are C57BL/6 or C57BL/6-CBA background (Table 2).

Mouse	Phenotype	Background	True breeding?
GD3s$^{-/-}$	Lacks *b* series gangliosides. Increased levels of *a* series gangliosides (eg. GD1a, GM1).	C57BL/6-CBA	YES
GalNAc-T$^{-/-}$	Lacks complex gangliosides.	C57BL/6-CBA	NO
CD59a$^{-/-}$	Lacks CD59a complement regulator.	C57BL/6	YES
DAF1$^{-/-}$	Lacks DAF1 complement regulator.	C57BL/6	YES
CD59a$^{-/-}$/DAF1$^{-/-}$	Lacks CD59a and DAF1 complement regulators.	C57BL/6	YES
GD3s$^{-/-}$/CD59a$^{-/-}$/DAF$^{-/-}$	Lacks *b* series gangliosides, and complement regulators CD59a and DAF1. Over-expresses *a* series gangliosides.	C57BL/6	YES

Table 2. Overview of commonly used KO mice, listing the abbreviation, phenotype and whether the strain is true breeding. Note that the GalNAc-T$^{-/-}$ is not true breeding, as the males are sterile. Mice are all backcrossed onto the listed background, which is the strain which should be used for WT comparisons.

A1.6 Sulfatide Deficient and Accumulating Mice:

Tissue from these strains was provided by Dr Matthias Eckhardt, University of Bonn, Germany.

Sulfatide Accumulating
Arylsulfatase A-deficient/PLP-CST transgenic mice. Referred to in text as CST mice.

These mice over-express cerebroside sulfotransferase (CST), an enzyme located on the Golgi membrane and responsible for the sulfation of galactocerebroside, to form sulfatide. In addition to the increased conversion of galactocerebroside to sulfatide, sulfatide degradation is interrupted by the deficiency of Arylsulfase A, the specific enzyme involved in the catabolism of sulfatide. Together, these factors contribute to an accumulation of sulfatide in these mice.

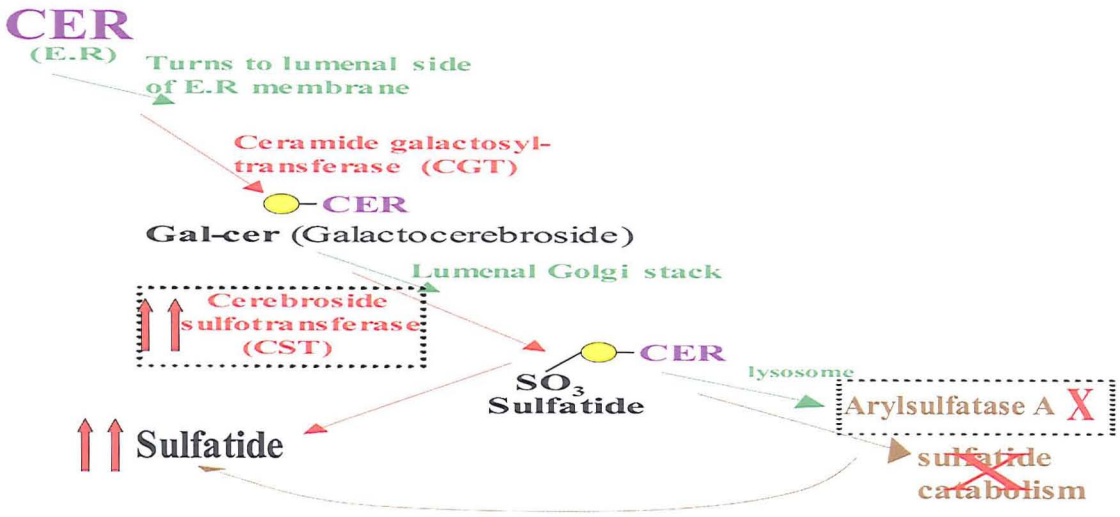

Fig 140. Sulfatide synthesis in the *Arylsulfatase A-deficient/PLP-CST transgenic mice.*

Sulfatide Deficient:

UDP-galactose:ceramide galactosyltransferase knock out ($CGT^{-/-}$) mice.

These mice lack UDP:galactose ceramide galactosyltransferase (Coetzee *et al* 1996), an enzyme located on the membrane of the ER and which functions to galactosylate ceramide. Thus, the lack of galactocerebroside means there is no substrate available for sulfation by CST, and the sulfatide biosynthetic pathway cannot continue. However, as ceramide is not entering the sulfatide synthesis pathway (due to a lack of CGT), this leaves an excess of ceramide which could theoretically enter the ganglioside biosynthetic pathway and lead to altered ganglioside expression.

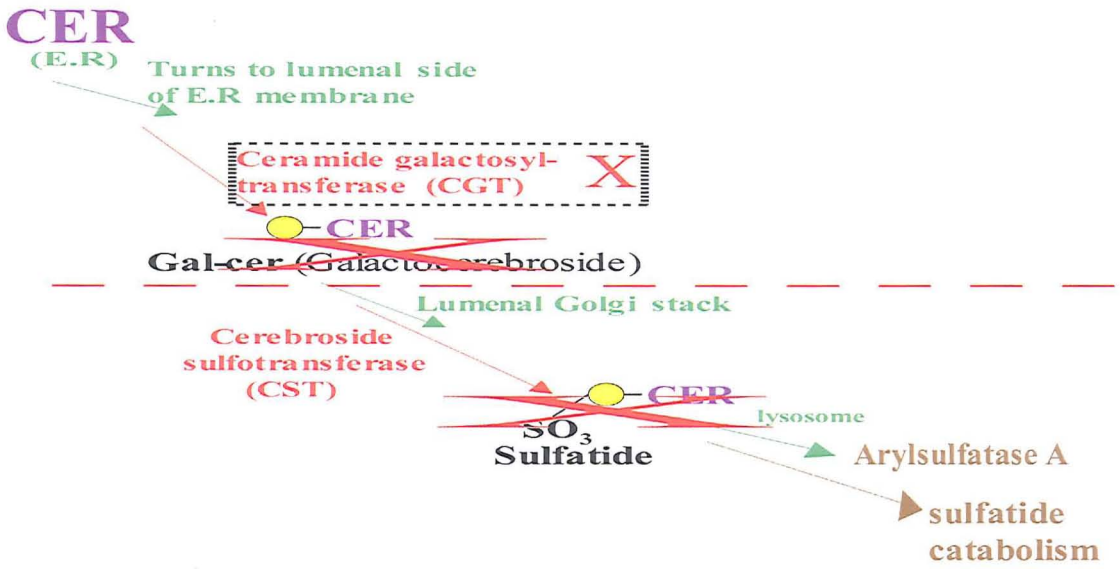

Fig 141. $CGT^{-/-}$ Pathway below the dotted red line is abolished, due to lack of Galactocerebroside substrate.

Appendix 2

A2.1 Introduction

This chapter contains detailed staining protocols which were developed during my PhD. However, they were not applied to the main body of work included in this thesis, and it was therefore not appropriate to include them amongst the routine techniques detailed in Materials and Methods. However, optimisation of these techniques was a significant achievement, and I therefore considered it worthwhile to include details of the staining protocols and images as an Appendix.

My aim was to develop a method of multi-colour staining which could be used to illustrate damage to the NMJ, induced by CGM3 (an anti-GD3, GQ1b and GT1b mouse IgM), and also the protective effects of Eculizumab, a C5 inhibitor.

CGM3 is an anti-disialosyl antibody which causes a complement mediated lesion to the NF and pSC in the mouse diaphragm (Halstead *et al* 2004). This effect was confirmed for the TS muscle. Lesion progression was monitored by dissecting out TS muscles from YFP mice, (which express YFP under the control of neuron-specific elements from the *thy1* gene (Feng *et al* 2000)) and imaging "real time". Muscles were pinned into Sylgard lined Petri-dishes, incubated in CGM3 (50μg/ml), and an initial picture taken showing the intact axon, as inferred by the normal YFP profile. After the addition of 40% NHS, further images were acquired. As seen in Fig 142, the profile of GFP becomes distorted, with evidence of axonal destruction over the NMJ and lysis of the pSC. This proves the rapid, complement mediated effects of CGM3 when applied to an *ex-vivo* TS preparation. These images were generated in collaboration with Dr R Ribchester, University of Edinburgh.

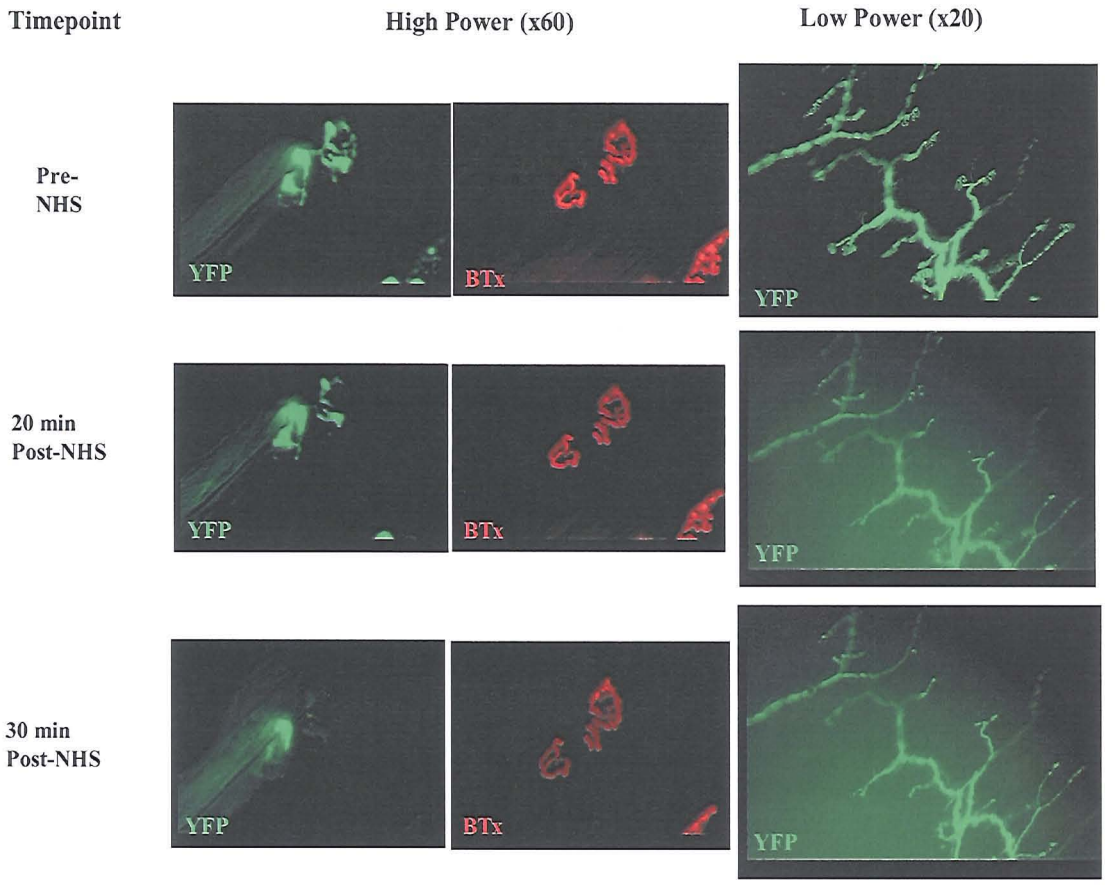

Fig 142. Real time images showing the complement mediated lesion induce by the mAb CGM3 in the *ex-vivo* TS preparation.

A2.2 *Ex-vivo* Protocols

TS muscles were dissected out and pinned into Sylgard lined wells as described in Materials and Methods section 2.2.1.1. Muscles were incubated in CGM3 (50µg/ml) plus BTx-Cy-5 (2µg/ml) followed by 40% NHS, with or without Eculizumab, as detailed in Halstead *et al* 2007 (manuscript currently in preparation). After incubation and 3X rinses in Ringer, the following staining protocols were developed:

A.2.2.1 MAC and C3

Tissue was incubated in anti-human C5-9b (363µg/ml) along with anti-C3-FITC (50 µg/ml) for 2 hours at RT. Following 3X rinses in Ringer, tissue was fixed in 4% PFA for 20 min at RT, rinsed in PBS and incubated in 0.1M glycine (in PBS) for 10 min at

RT. Overnight, a further incubation in anti-human C5-9b (concentration as before) was done, and after rinsing, anti-mouse IgG-TRITC applied (5 μg/ml in PBS) for at least 8 hours at 4°C. Tissue was rinsed 3X in PBS and mounted as before.

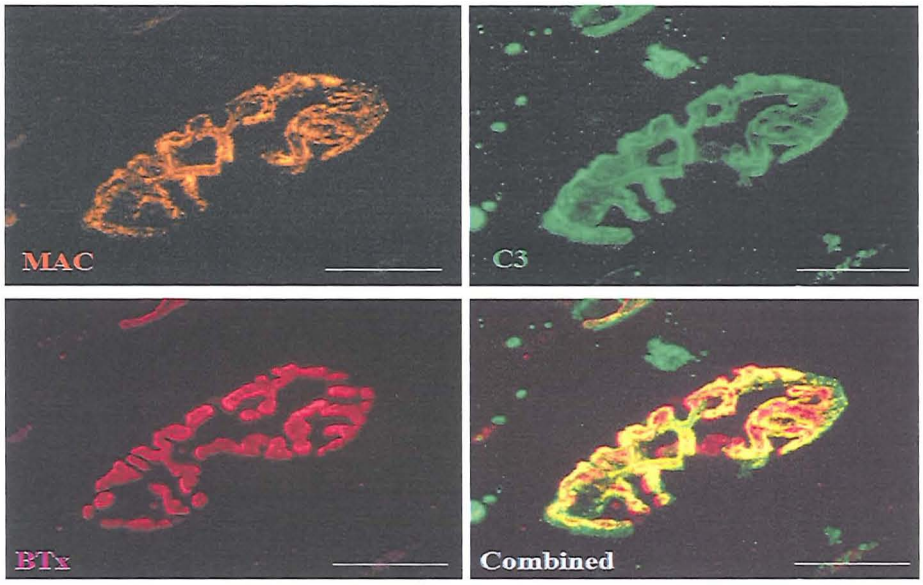

Fig 143 a). CGM3 + NHS and isotype control. MAC, C3 and BTx staining.

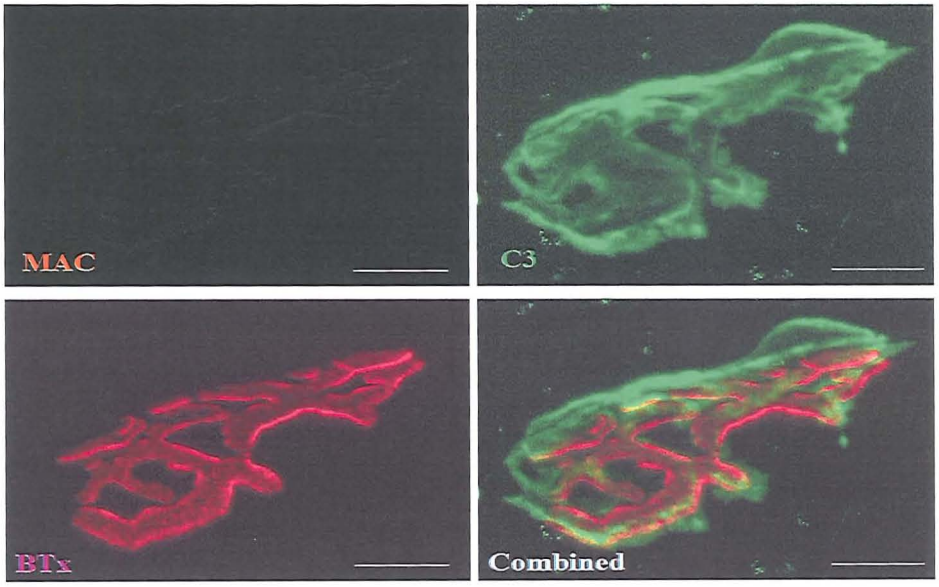

Fig 143 b). CGM3 + NHS and Eculizumab. MAC, C3 and BTx staining.

A2.2.2 MAC and EthD-1

Following 40% NHS, tissue was rinsed 3X in PBS and EthD-1 (2 μM/ml) and anti-human C5-9b (363 μg/ml) applied for 1 hour at RT, in Ringer. Tissue was rinsed 3X in Ringer and fixed as before. Anti-human C5-9b was applied overnight and detected as before.

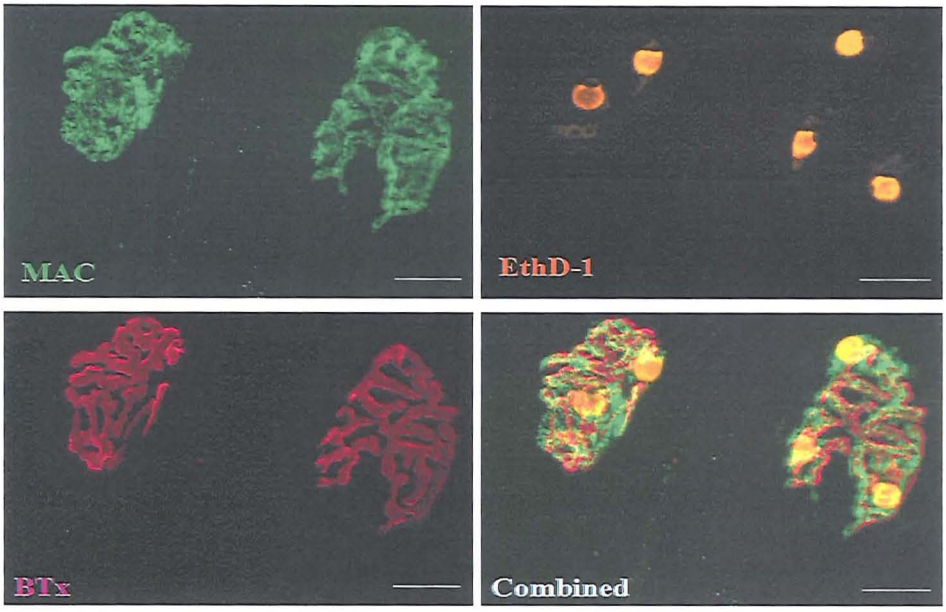

Fig 144 a) CGM3 + NHS and isotype control. MAC, EthD-1 and BTx staining.

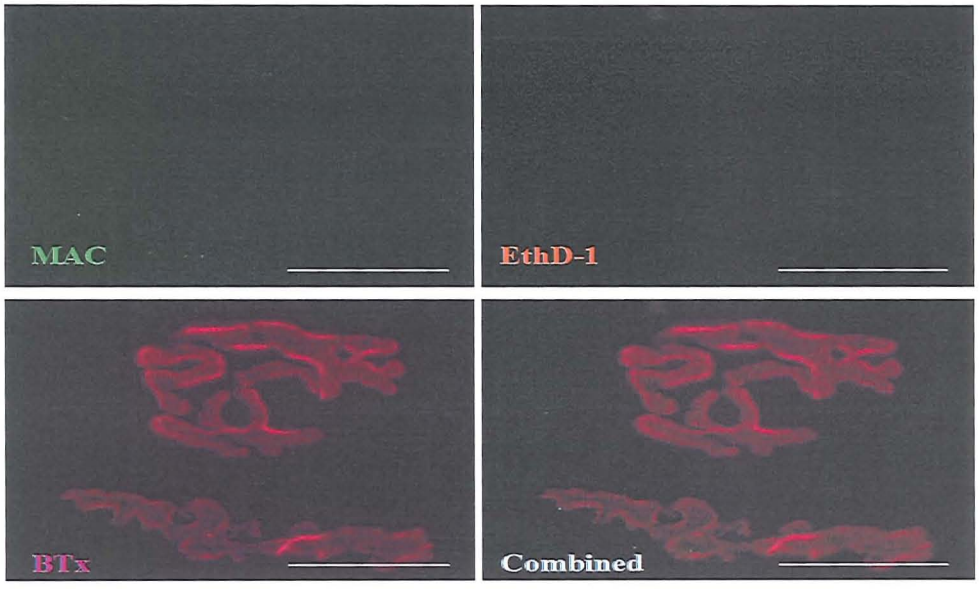

Fig 144 b) CGM3 + NHS and Eculizumab. MAC, EthD-1 and BTx staining.

A2.2.3 MAC and Neurofilament

Tissue was rinsed 3X in Ringer after 40% NHS, fixed in 2% PFA for 15 min at RT, rinsed in PBS and treated with 0.1M glycine for 10 min at RT. 0.5% Triton in PBS was added at RT for 1 hour to permeabilise the tissue, and anti-NF (anti-neurofilament 150 kD polyclonal antibody, Chemicon, diluted at 1 in 150) plus anti-human C5-9b (363µg/ml) applied overnight in 0.5% Triton/PBS at 4°C. Following 3X rinses in PBS, anti-rabbit IgG-FITC and anti-mouse-IgG-TRITC (5 µg/ml) applied for at least 8 hours at 4°C to detect NF and MAC respectively.

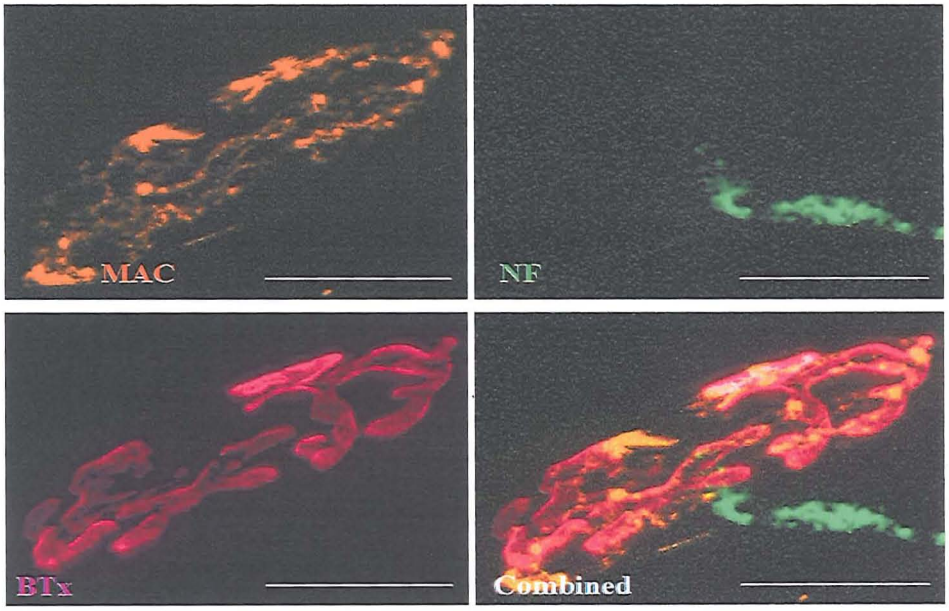

Fig 145 a) CGM3 + NHS and isotype control. MAC, NF and BTx staining.

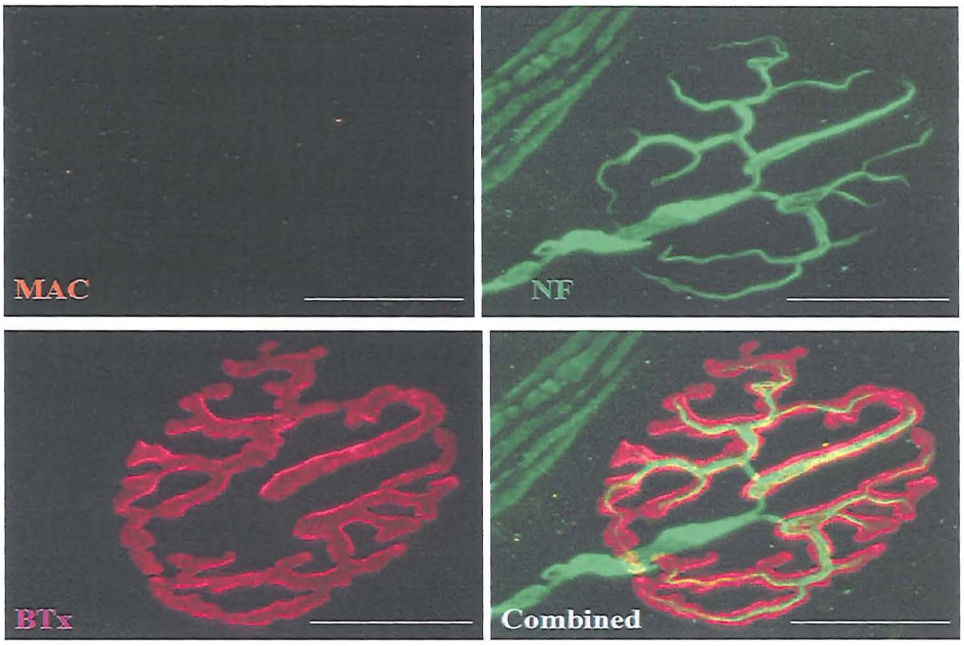

Fig 145 b) CGM3 + NHS and Eculizumab. MAC, NF and BTx staining.

A2.2.4 MAC and S100

Tissue was rinsed 3X in Ringer, fixed for 15 min in 2% PFA, rinsed in PBS and incubated for 10 min in 0.1M glycine. Anti-S100 (Dako) was diluted 22.5 µg/ml in 0.5% Triton in PBS, and to this solution anti-human C5-9b was added at 363 µg/ml. Tissue was incubated overnight at 4°C, rinsed 3X in PBS and anti-mouse IgG-TRITC and anti-rabbit IgG-FITC applied at 5 µg/ml in PBS for at least 8 hours (4°C) to detect MAC and S100 respectively.

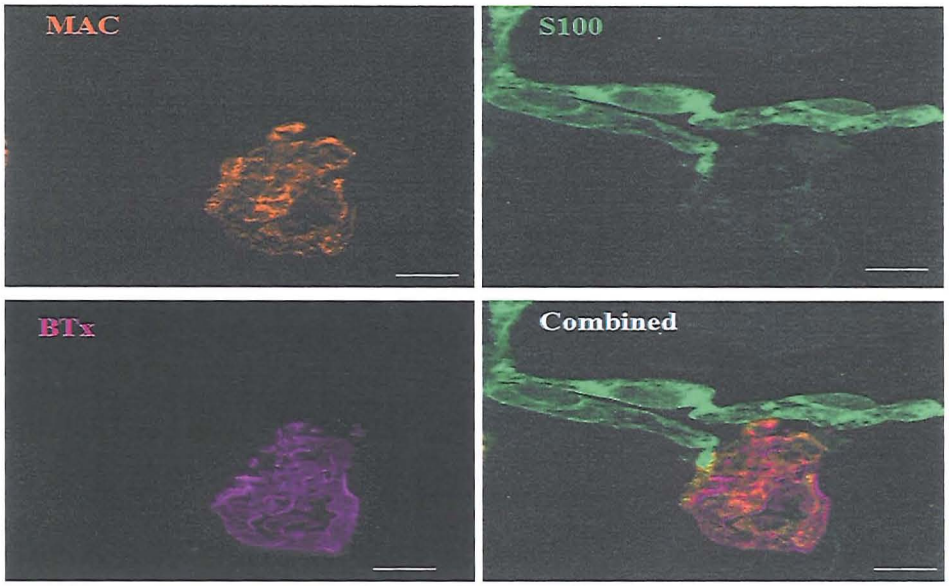

Fig 146 a) CGM3 + NHS and isotype control. MAC, S100 and BTx staining.

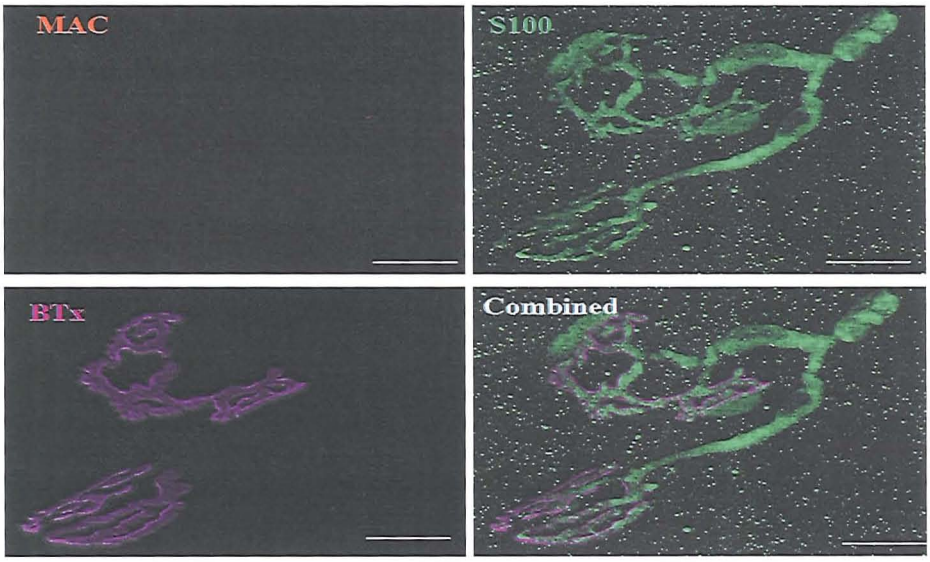

Fig 146b) CGM3 + NHS and Eculizumab. MAC, S100 and BTx staining.

A2.2.5 S100 and Ethidium

Following 3X rinses in Ringer, EthD-1 was applied for 1 hour as before. Tissue was rinsed 3X in Ringer, fixed for 15 min in 2% PFA, rinsed in PBS and incubated for 10 min in 0.1M glycine. Anti-S100 was diluted 22.5 µg/ml in 0.5% Triton in PBS and

applied overnight at 4°C. Tissue was rinsed 3X in PBS and anti-rabbit IgG-FITC applied (5 μg/ml) for at least 8 hours at 4°C.

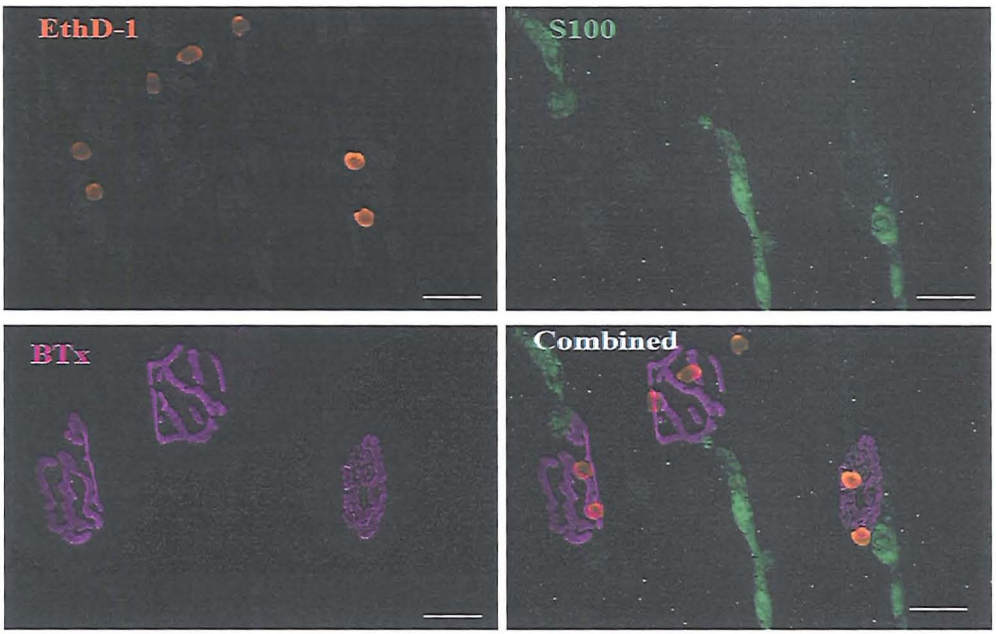

Fig 147 a) CGM3 + NHS and isotype control. EthD-1, S100 and BTx staining.

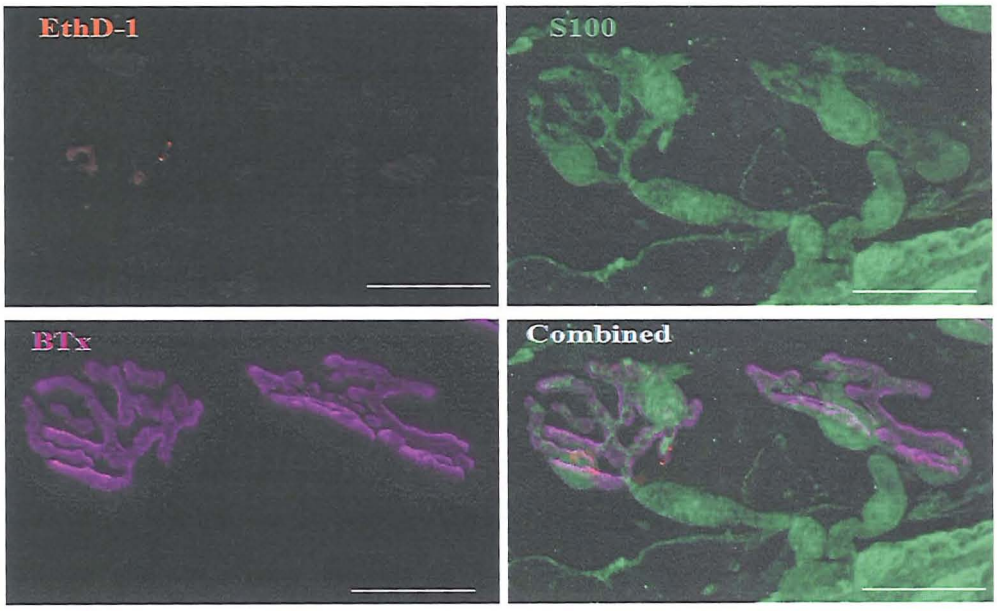

Fig 147 b) CGM3 + NHS and Eculizumab. EthD-1, S100 and BTx staining.

A2.3 *In-Vivo* Protocol

Proof of the viability of Eculizumab *in-vivo* was also determined, as outlined in Halstead *et al* 2007. To this end, the above staining procedures were repeated on TS muscles freshly dissected from the experimental animals (*in-vivo* passive transfers carried out by Dr S. Halstead, as detailed in Halstead *et al* 2007). Successful replication of the staining is shown, and the efficacy of Eculizumab *in-vivo* thus confirmed.

A.2.3.1 MAC and C3

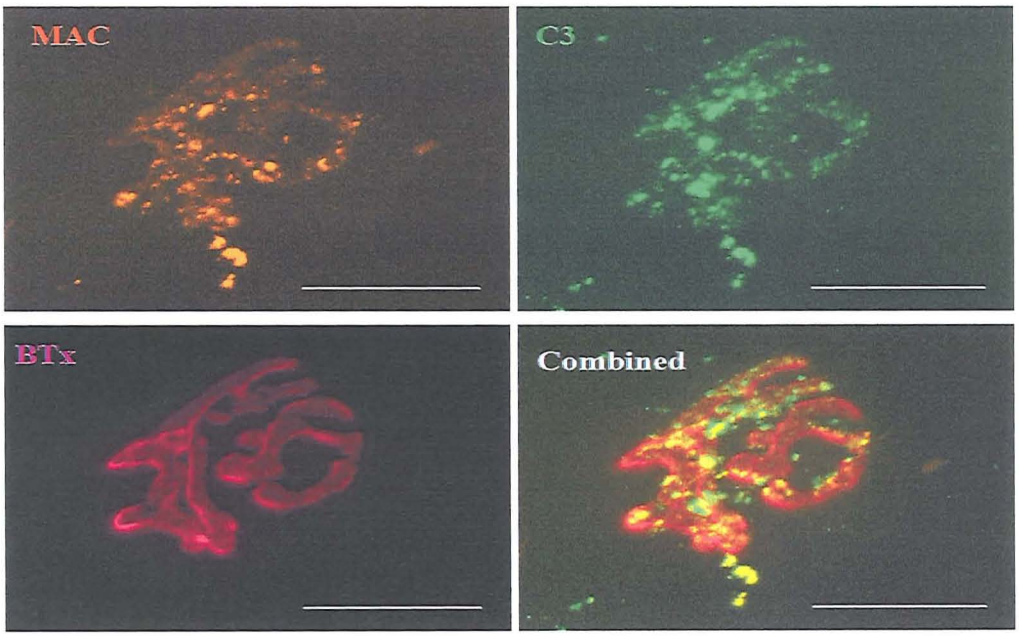

Fig 148 a). CGM3 + NHS and isotype control administered *in-vivo*. MAC, C3 and BTx staining.

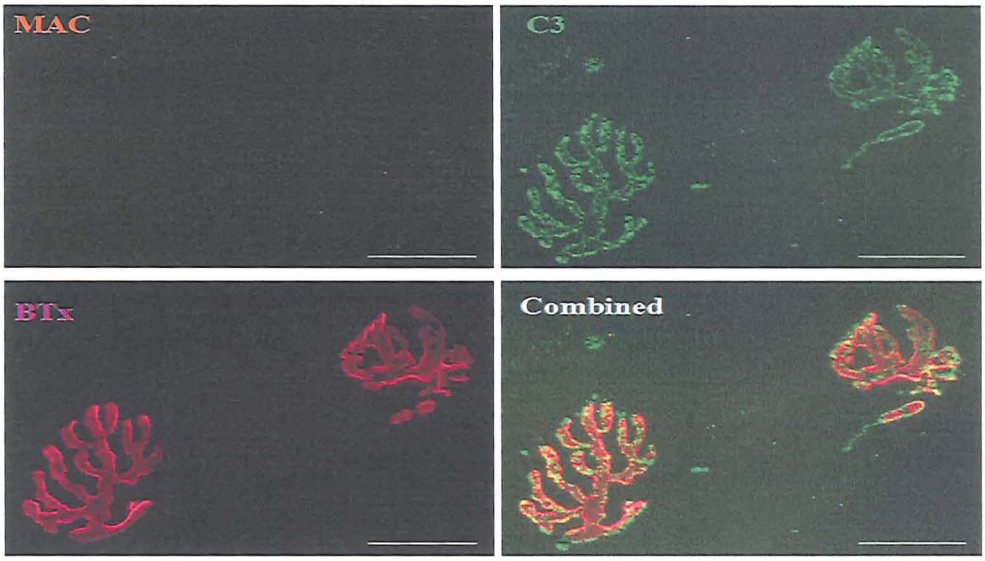

Fig 148 b). CGM3 + NHS and Eculizumab administered *in-vivo*. MAC, C3 and BTx staining.

A2.3.3 MAC and NF

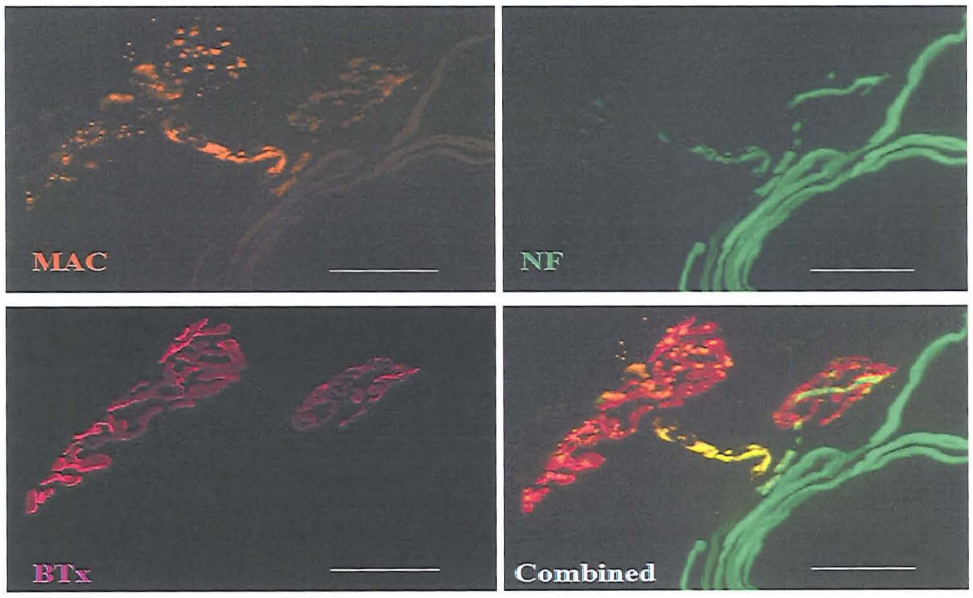

Fig 149 a). CGM3 + NHS and isotype control administered *in-vivo.* MAC, NF and BTx staining.

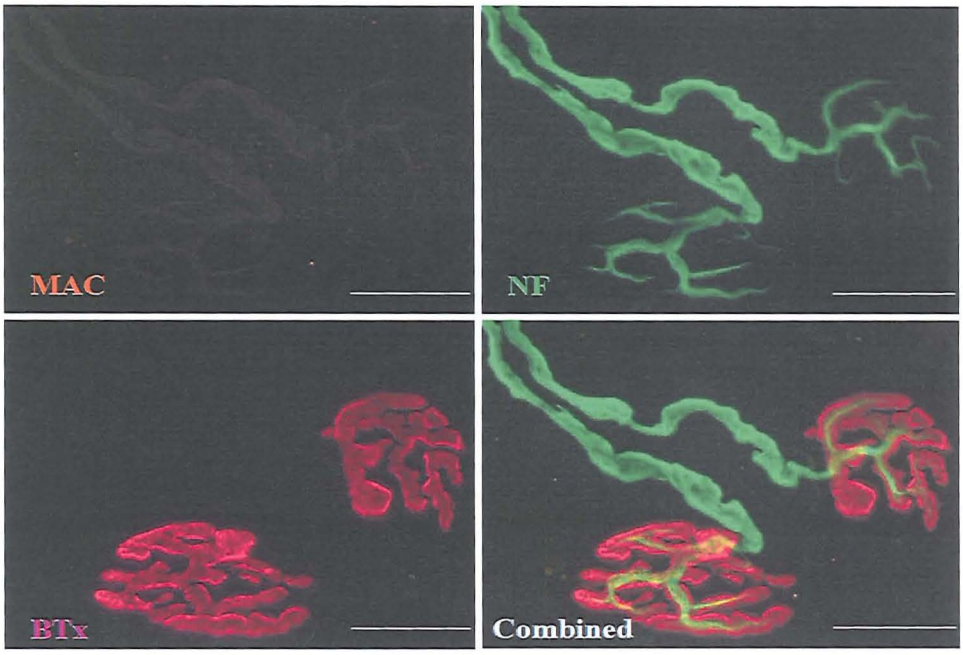

Fig 149 b). CGM3 + NHS and Eculizumab administered *in-vivo.* MAC, NF and BTx staining.

Appendix 3

A3.1 Introduction

Throughout this thesis, a number of anti-ganglioside mAbs have been referred to. Table 3 provides an overview the antibodies used, and is intended for use as an "at a glance" reference guide. It should be noted that sulfatide binding properties are specifically based on the abiltiy of the purified antibody to bind sulfatide (as it is thought there may be sulfatide binding epitopes in the tissue culture supernatant, which interfere with their ability, in the unpurified state, to bind sulfatide by ELISA). All documented mAb binding properties documented in Table 3 were generated by Ms Dawn Nichol, Southern General Hospital.

Strength of binding to the listed gangliosides is denoted by the symbols "**(+)**" and "**(-)**", which define the reactivity of the mAb for the ganglioside (or sulfatide) based on the OD_{490nm} by ELISA. The key to the symbols is as follows:

(-): OD ≤ 0.1

(+): OD $>0.1, \leq 0.5$

(+ +): OD $>0.5, \leq 1.0$

(+ + +): OD $>1.0, \leq 1.5$

(+ + + +): OD >1.5

mAb name	Isotype	Ganglioside Binding	Sulfatide Binding
EG1	IgG3	GT1a(++), GQ1b(++), GD3(++)	+++
DG1	IgG2b	GM1(++++)	+
DG2	IgG3	GM1(++++), GA1(+++), GD1b(+)	+++
MOG 16	IgG3	GD1a(+), GD1b(+++), GT1b(+++)	-
MOG 35	IgG2b	GD1a(++++)	+
CGM3	IgM	GT1a(++), GQ1b(+++), GD3(++)	++
MOM-1	IgG3	GM1(++++), GA1(++++), GD1b(++)	-

Table 3. Overview of the ganglioside species bound by the named mAbs. Ability to bind sulfatide was determined using the purified mAbs. Key to symbols: (-): OD ≤0.1 , (+): OD >0.1, ≤0.5, (+ +): OD >0.5, ≤1.0, (+ + +): OD >1.0, ≤1.5, (+ + + +): OD >1.5.
All data were obtained by ELISA, courtesy of Ms Dawn Nichol, Southern General Hospital.

References

Ackerman GA, Wolken KW, Gelder FB. Surface distribution of monosialoganglioside GM1 on human blood cells and the effect of exogenous GM1 and neuraminidase on cholera toxin surface labeling. A quantitative immunocytochemical study. J.Histochem.Cytochem. 1980; 28: 1100-1112.

Adams D, Kuntzer T, Burger D *et al.* Predictive value of anti-GM1 ganglioside antibodies in neuromuscular diseases: a study of 180 sera. J.Neuroimmunol. 1991; 32: 223-230.

Ahmed SN, Brown DA, London E. On the origin of sphingolipid/cholesterol-rich detergent-insoluble cell membranes: physiological concentrations of cholesterol and sphingolipid induce formation of a detergent-insoluble, liquid-ordered lipid phase in model membranes. Biochemistry 1997; 36: 10944-10953.

Albers JW, Donofrio PD, McGonagle TK. Sequential electrodiagnostic abnormalities in acute inflammatory demyelinating polyradiculoneuropathy. Muscle Nerve 1985; 8: 528-539.

Allen JA, Halverson-Tamboli RA, Rasenick MM. Lipid raft microdomains and neurotransmitter signalling. Nat.Rev.Neurosci. 2007; 8: 128-140.

Ando R, Hama H, Yamamoto-Hino M, Mizuno H, Miyawaki A. An optical marker based on the UV-induced green-to-red photoconversion of a fluorescent protein. Proc.Natl.Acad.Sci.U.S.A 2002; 99: 12651-12656.

Ando S, Tanaka Y, Waki H, Kon K, Iwamoto M, Fukui F. Gangliosides and sialylcholesterol as modulators of synaptic functions. Ann.N.Y.Acad.Sci. 1998; 845: 232-239.

Ang CW, Jacobs BC, Laman JD. The Guillain-Barre syndrome: a true case of molecular mimicry. Trends Immunol. 2004; 25: 61-66.

Angstrom J, Teneberg S, Karlsson KA. Delineation and comparison of ganglioside-binding epitopes for the toxins of Vibrio cholerae, Escherichia coli, and Clostridium tetani: evidence for overlapping epitopes. Proc.Natl.Acad.Sci.U.S.A 1994; 91: 11859-11863.

Apostolski S, Sadiq SA, Hays A *et al.* Identification of Gal(beta 1-3)GalNAc bearing glycoproteins at the nodes of Ranvier in peripheral nerve. J.Neurosci.Res. 1994; 38: 134-141.

Arasaki K, Kusunoki S, Kudo N, Kanazawa I. Acute conduction block in vitro following exposure to antiganglioside sera. Muscle Nerve 1993; 16: 587-593.

Archelos JJ, Roggenbuck K, Schneider-Schaulies J, Toyka KV, Hartung HP. Detection and quantification of antibodies to the extracellular domain of P0 during experimental allergic neuritis. J.Neurol.Sci. 1993; 117: 197-205.

Ariga T, Kohriyama T, Freddo L *et al.* Characterization of sulfated glucuronic acid containing glycolipids reacting with IgM M-proteins in patients with neuropathy. J.Biol.Chem. 1987; 262: 848-853.

Arnason BGW, Soliven B. Acute inflammatory demyelinating polyradiculoneuropathy. In Dyck PJ, Thomas PK, Griffin JW, Low PA, Podulso JF, eds. Peripheral neuropathy 3rd ed, Philadelphia: WB Saunders, 1993, 1437-1497

Arstila AU, Riekkinen PJ, Rinne UK, Pelliniemi TT, Nevalainen T. Guillan-Barre syndrome. Neurochemical and ultrastructural study. Eur.Neurol. 1971; 5: 257-269.

Asbury AK. Diagnostic considerations in Guillain-Barre syndrome. Ann.Neurol. 1981; 9 Suppl: 1-5.

Asbury AK, Arnason BG, Adams RD. The inflammatory lesion in idiopathic polyneuritis: its role in pathogenesis. Baltimore: Medicine, 1969; 8: 173-215

Asbury AK, Cornblath DR. Assessment of current diagnostic criteria for Guillain-Barre syndrome. Ann.Neurol. 1990; 27 Suppl: S21-S24.

Asbury AK. Gangliosides and peripheral neuropathies: an overview. Prog.Brain Res. 1994; 101: 279-287.

Aspinall GO, McDonald AG, Pang H, Kurjanczyk LA, Penner JL. Lipopolysaccharides of Campylobacter jejuni serotype O:19: structures of core oligosaccharide regions from the serostrain and two bacterial isolates from patients with the Guillain-Barre syndrome. Biochemistry 1994; 33: 241-249.

Astrom KE, Waksman BH. The passive transfer of experimental allergic encephalomyelitis and neuritis with living lymphoid cells. J.Pathol.Bacteriol. 1962; 83: 89-106.

Astrow SH, Qiang H, Ko CP. Perisynaptic Schwann cells at neuromuscular junctions revealed by a novel monoclonal antibody. J.Neurocytol. 1998; 27: 667-681.

Asuncion-Punzalan E, Kachel K, London E. Groups with polar characteristics can locate at both shallow and deep locations in membranes: the behavior of dansyl and related probes. Biochemistry 1998; 37: 4603-4611.

Auld DS, Robitaille R. Glial cells and neurotransmission: an inclusive view of synaptic function. Neuron 2003; 40: 389-400.

Auld DS, Colomar A, Belair EL *et al.* Modulation of neurotransmission by reciprocal synapse-glial interactions at the neuromuscular junction. J.Neurocytol. 2003; 32: 1003-1015.

Barclay AN, Brown MH, Law SKA, McKnight AJ, Tomlinson MG, van der Merwe PA. The Leucocyte Antigen FactsBook, 1997 (2nd ed.), Academic Press, San Diego

Barman S, Nayak DP. Analysis of the transmembrane domain of influenza virus neuraminidase, a type II transmembrane glycoprotein, for apical sorting and raft association. J.Virol. 2000; 74: 6538-6545.

Baron W, Decker L, Colognato H, ffrench-Constant C. Regulation of integrin growth factor interactions in oligodendrocytes by lipid raft microdomains. Curr.Biol. 2003; 13: 151-155.

Beghi E, Kurland LT, Mulder DW, Wiederholt WC. Guillain-Barre syndrome. Clinicoepidemiologic features and effect of influenza vaccine. Arch.Neurol. 1985; 42: 1053-1057.

Berney C, Danuser G. FRET or no FRET: a quantitative comparison. Biophys.J. 2003; 84: 3992-4010.

Berthold CH, Rydmark M. Electrophysiology and morphology of myelinated nerve fibers. VI. Anatomy of the paranode-node-paranode region in the cat. Experientia 1983; 39: 964-976.

Bieberich E, MacKinnon S, Silva J *et al.* Regulation of ganglioside biosynthesis by enzyme complex formation of glycosyltransferases. Biochemistry 2002; 41: 11479-11487.

Blank N, Schiller M, Krienke S, Wabnitz G, Ho AD, Lorenz HM. Cholera toxin binds to lipid rafts but has a limited specificity for ganglioside GM1. Immunol.Cell Biol. 2007; 85: 378-382.

Blaser MJ, Olivares A, Taylor DN, Cornblath DR, McKhann GM. Campylobacter serology in patients with Chinese paralytic syndrome. Lancet 1991; 338: 308.

Blom TS, Koivusalo M, Kuismanen E, Kostiainen R, Somerharju P, Ikonen E. Mass spectrometric analysis reveals an increase in plasma membrane polyunsaturated phospholipid species upon cellular cholesterol loading. Biochemistry 2001; 40: 14635-14644.

Boffey J, Odaka M, Nicoll D *et al.* Characterisation of the immunoglobulin variable region gene usage encoding the murine anti-ganglioside antibody repertoire. J.Neuroimmunol. 2005; 165: 92-103.

Boggs JM. Lipid intermolecular hydrogen bonding: influence on structural organization and membrane function. Biochim.Biophys.Acta 1987; 906: 353-404.

Boggs JM, Wang H, Gao W, Arvanitis DN, Gong Y, Min W. A glycosynapse in myelin? Glycoconj.J. 2004; 21: 97-110.

Boucquey D, Sindic CJ, Lamy M, Delmee M, Tomasi JP, Laterre EC. Clinical and serological studies in a series of 45 patients with Guillain-Barre syndrome. J.Neurol.Sci. 1991; 104: 56-63.

Bowes T, Wagner ER, Boffey J *et al.* Tolerance to self gangliosides is the major factor restricting the antibody response to lipopolysaccharide core oligosaccharides in

Campylobacter jejuni strains associated with Guillain-Barre syndrome. Infect.Immun. 2002; 70: 5008-5018.

Boyle ME, Berglund EO, Murai KK, Weber L, Peles E, Ranscht B. Contactin orchestrates assembly of the septate-like junctions at the paranode in myelinated peripheral nerve. Neuron 2001; 30: 385-397.

Bradshaw DY, Jones HR, Jr. Guillain-Barre syndrome in children: clinical course, electrodiagnosis, and prognosis. Muscle Nerve 1992; 15: 500-506.

Braun PE, Frail DE, Latov N. Myelin-associated glycoprotein is the antigen for a monoclonal IgM in polyneuropathy. J.Neurochem. 1982; 39: 1261-1265.

Brechenmacher C, Vital C, Deminiere C *et al.* Guillain-Barre syndrome: an ultrastructural study of peripheral nerve in 65 patients. Clin.Neuropathol. 1987; 6: 19-24.

Brocca,P., Berthault,P., and Sonnino,S. Conformation of the oligosaccharide chain of G(M1) ganglioside in a carbohydrate-enriched surface. Biophys. J. 1998 ; 74, 309-318.

Brosnan JV, Craggs RI, King RH, Thomas PK. Reduced susceptibility of T cell-deficient rats to induction of experimental allergic neuritis. J.Neuroimmunol. 1987; 14: 267-282.

Brown DA, Rose JK. Sorting of GPI-anchored proteins to glycolipid-enriched membrane subdomains during transport to the apical cell surface. Cell 1992; 68: 533-544.

Brown DA, London E. Structure and origin of ordered lipid domains in biological membranes. J.Membr.Biol. 1998; 164: 103-114.

Brown WF, Feasby TE. Conduction block and denervation in Guillain-Barre polyneuropathy. Brain 1984; 107 (Pt 1): 219-239.

Brugger B, Graham C, Leibrecht I *et al.* The membrane domains occupied by glycosylphosphatidylinositol-anchored prion protein and Thy-1 differ in lipid composition. J.Biol.Chem. 2004; 279: 7530-7536.

Brunetti M, Di Giamberardino L, Porcellati G, Droz B. Contribution of axonal transport to the renewal of myelin phospholipids in peripheral nerves. II. Biochemical study. Brain Res. 1981; 219: 73-84.

Buchwald B, Weishaupt A, Toyka KV, Dudel J. Pre- and postsynaptic blockade of neuromuscular transmission by Miller-Fisher syndrome IgG at mouse motor nerve terminals. Eur.J.Neurosci. 1998; 10: 281-290.

Buckley NE, Su Y, Milstien S, Spiegel S. The role of calcium influx in cellular proliferation induced by interaction of endogenous ganglioside GM1 with the B subunit of cholera toxin. Biochim.Biophys.Acta 1995; 1256: 275-283.

Bullens RW, O'Hanlon GM, Wagner E *et al.* Complex gangliosides at the neuromuscular junction are membrane receptors for autoantibodies and botulinum neurotoxin but redundant for normal synaptic function. J.Neurosci. 2002; 22: 6876-6884.

Burton DR. Immunoglobulin G: functional sites. Mol.Immunol. 1985; 22: 161-206.

Cajal RY Degeneration and Regeneration of the Nervous System. May RM (Ed). Oxford University Press, Oxford , 1928, p769

Campbell DG, Gagnon J, Reid KB, Williams AF. Rat brain Thy-1 glycoprotein. The amino acid sequence, disulphide bonds and an unusual hydrophobic region. Biochem.J. 1981; 195: 15-30.

Carpenter S. An ultrastructural study of an acute fatal case of the Guillain-Barre syndrome. J.Neurol.Sci. 1972; 15: 125-140.

Carpo M, Pedotti R, Lolli F *et al.* Clinical correlate and fine specificity of anti-GQ1b antibodies in peripheral neuropathy. J.Neurol.Sci. 1998; 155: 186-191.

Cassidy JT, Jourdian GW, Roseman S. The sialic acids. VI. Purification and properties of sialidase from Clostridium perfringens. J.Biol.Chem. 1965; 240: 3501-3506.

Celio MR. The Schmidt-Lantermann incisures of the myelin sheath of Mauthner axons: site of longitudinal myelin growth. Brain Res. 1976; 108: 221-235.

Chamberlain LH, Burgoyne RD, Gould GW. SNARE proteins are highly enriched in lipid rafts in PC12 cells: implications for the spatial control of exocytosis. Proc.Natl.Acad.Sci.U.S.A 2001; 98: 5619-5624.

Chandler DE. Comparison of quick-frozen and chemically fixed sea-urchin eggs: structural evidence that cortical granule exocytosis is preceded by a local increase in membrane mobility. J.Cell Sci. 1984; 72: 23-36.

Chapman PB, Yuasa H, Houghton AN. Homophilic binding of mouse monoclonal antibodies against GD3 ganglioside. J.Immunol. 1990; 145: 891-898.

Chiavegatto S, Sun J, Nelson RJ, Schnaar RL. A functional role for complex gangliosides: motor deficits in GM2/GD2 synthase knockout mice. Exp.Neurol. 2000; 166: 227-234.

Chiba A, Kusunoki S, Shimizu T, Kanazawa I. Serum IgG antibody to ganglioside GQ1b is a possible marker of Miller Fisher syndrome. Ann.Neurol. 1992; 31: 677-679.

Chiba A, Kusunoki S, Obata H, Machinami R, Kanazawa I. Serum anti-GQ1b IgG antibody is associated with ophthalmoplegia in Miller Fisher syndrome and Guillain-Barre syndrome: clinical and immunohistochemical studies. Neurology 1993; 43: 1911-1917.

Chiba A, Kusunoki S, Obata H, Machinami R, Kanazawa I. Ganglioside composition of the human cranial nerves, with special reference to pathophysiology of Miller Fisher syndrome. Brain Res. 1997; 745: 32-36.

Chiu SY, Ritchie JM, Rogart RB, Stagg D. A quantitative description of membrane currents in rabbit myelinated nerve. J.Physiol 1979; 292: 149-166.

Chomel AF, Journal Hebdomadaire de Médecine, 1828, 1: 333.

Chou DK, Ilyas AA, Evans JE, Costello C, Quarles RH, Jungalwala FB. Structure of sulfated glucuronyl glycolipids in the nervous system reacting with HNK-1 antibody and some IgM paraproteins in neuropathy. J.Biol.Chem. 1986; 261: 11717-11725.

Cinek T, Horejsi V. The nature of large noncovalent complexes containing glycosyl-phosphatidylinositol-anchored membrane glycoproteins and protein tyrosine kinases. J.Immunol. 1992; 149: 2262-2270.

Coetzee T, Fujita N, Dupree J *et al.* Myelination in the absence of galactocerebroside and sulfatide: normal structure with abnormal function and regional instability. Cell 1996; 86: 209-219.

Coetzee T, Li X, Fujita N *et al.* Molecular cloning, chromosomal mapping, and characterization of the mouse UDP-galactose:ceramide galactosyltransferase gene Genomics 1996; 35: 215-222.

Congia S, Melis M, Carboni MA. Epidemiologic and clinical features of the Guillain-Barre' syndrome in Sardinia in the 1961-1980 period. Acta Neurol.(Napoli) 1989; 11: 15-20.

Connor EA, McMahan UJ. Cell accumulation in the junctional region of denervated muscle. J.Cell Biol. 1987; 104: 109-120.

Corbo M, Quattrini A, Latov N, Hays AP. Localization of GM1 and Gal(beta 1-3)GalNAc antigenic determinants in peripheral nerve. Neurology 1993; 43: 809-814.

Cornblath DR, Sumner AJ, Daube J *et al.* Conduction block in clinical practice. Muscle Nerve 1991; 14: 869-871.

Court FA, Gillingwater TH, Melrose S *et al.* Identity, developmental restriction and reactivity of extralaminar cells capping mouse neuromuscular junctions. Manuscript in preparation

Couteaux R, Spacek J Specialization of the subsynaptic cytoplasm. Comparison of axospinous synapses and neuromuscular junctions. In: Cellular and molecular basis of synaptic transmission. Zimmerman H, ed., Berlin: Springer, 1988, pp 25–50

Craggs RI, King RH, Thomas PK. The effect of suppression of macrophage activity on the development of experimental allergic neuritis. Acta Neuropathol.(Berl) 1984; 62: 316-323.

Crespo PM, Zurita AR, Daniotti JL. Effect of gangliosides on the distribution of a glycosylphosphatidylinositol-anchored protein in plasma membrane from Chinese hamster ovary-K1 cells. J.Biol.Chem. 2002; 277: 44731-44739.

Damjanovich S, Vereb G, Schaper A *et al.* Structural hierarchy in the clustering of HLA class I molecules in the plasma membrane of human lymphoblastoid cells. Proc.Natl.Acad.Sci.U.S.A 1995; 92: 1122-1126.

Davis JQ, Lambert S, Bennett V. Molecular composition of the node of Ranvier: identification of ankyrin-binding cell adhesion molecules neurofascin (mucin+/third FNIII domain-) and NrCAM at nodal axon segments. J.Cell Biol. 1996; 135: 1355-1367.

De Angelis MV, Di Muzio A, Lupo S, Gambi D, Uncini A, Lugaresi A. Anti-GD1a antibodies from an acute motor axonal neuropathy patient selectively bind to motor nerve fiber nodes of Ranvier. J.Neuroimmunol. 2001; 121: 79-82.

Deinhardt K, Schiavo G. Endocytosis and retrograde axonal traffic in motor neurons. Biochem.Soc.Symp. 2005; 139-150.

Dietrich C, Volovyk ZN, Levi M, Thompson NL, Jacobson K. Partitioning of Thy-1, GM1, and cross-linked phospholipid analogs into lipid rafts reconstituted in supported model membrane monolayers. Proc.Natl.Acad.Sci.U.S.A 2001; 98: 10642-10647.

Dietrich C, Yang B, Fujiwara T, Kusumi A, Jacobson K. Relationship of lipid rafts to transient confinement zones detected by single particle tracking. Biophys.J. 2002; 82: 274-284.

Dippold WG, Lloyd KO, Li LT, Ikeda H, Oettgen HF, Old LJ. Cell surface antigens of human malignant melanoma: definition of six antigenic systems with mouse monoclonal antibodies. Proc.Natl.Acad.Sci.U.S.A 1980; 77: 6114-6118.

Dowling PC, Cook SD. Role of infection in Guillain-Barre syndrome: laboratory confirmation of herpesviruses in 41 cases. Ann.Neurol. 1981; 9 Suppl: 44-55.

Draganesco H, Claudian J. Sur un cas de radiculu-névrite curable (syndrome de Guillain-Barré) apparue au cours d'une ostéomyélite du bras. Revue neurologique, Paris, 1927, 2: 517-521.

Drobnik W, Borsukova H, Bottcher A *et al.* Apo AI/ABCA1-dependent and HDL3-mediated lipid efflux from compositionally distinct cholesterol-based microdomains. Traffic. 2002; 3: 268-278.

Duchemin AM, Neff NH, Hadjiconstantinou M. Induction of Trk phosphorylation in rat brain by GM1 ganglioside. Ann.N.Y.Acad.Sci. 1998; 845: 406.

Dupouey P, Zalc B, Lefroit-Joly M, Gomes D. Localization of galactosylceramide and sulfatide at the surface of the myelin sheath: an immunofluorescence study in liquid medium. Cell Mol.Biol.Incl.Cyto.Enzymol. 1979; 25: 269-272.

Dykstra M, Cherukuri A, Sohn HW, Tzeng SJ, Pierce SK. Location is everything: lipid rafts and immune cell signaling. Annu.Rev.Immunol. 2003; 21: 457-481.

Eckert GP, Igbavboa U, Muller WE, Wood WG. Lipid rafts of purified mouse brain synaptosomes prepared with or without detergent reveal different lipid and protein domains. Brain Res. 2003; 962: 144-150.

Edidin M, Zuniga MC, Sheetz MP. Truncation mutants define and locate cytoplasmic barriers to lateral mobility of membrane glycoproteins. Proc.Natl.Acad.Sci.U.S.A 1994; 91: 3378-3382.

Edidin M. The state of lipid rafts: from model membranes to cells. Annu.Rev.Biophys.Biomol.Struct. 2003; 32: 257-283.

Egorushkina NV, Ratushnyak AS, Egorushkin IV. The influence of exogenous gangliosides on the dynamics of the development of prolonged posttetanic potentiation. Neurosci.Behav.Physiol 1993; 23: 435-438.

Ehrlich P. Das sauerstoff-bedu¨rfnis des organismus: eine farbenanalytische studie. Habilitation thesis, Hirschwald, 1885

Einheber S, Zanazzi G, Ching W *et al.* The axonal membrane protein Caspr, a homologue of neurexin IV, is a component of the septate-like paranodal junctions that assemble during myelination. J.Cell Biol. 1997; 139: 1495-1506.

Ellisman MH, Levinson SR. Immunocytochemical localization of sodium channel distributions in the excitable membranes of Electrophorus electricus. Proc.Natl.Acad.Sci.U.S.A 1982; 79: 6707-6711.

Erb EM, Chen X, Allen S *et al.* Characterization of the surfaces generated by liposome binding to the modified dextran matrix of a surface plasmon resonance sensor chip. Anal.Biochem. 2000; 280: 29-35.

Exley AR, Smith N, Winer JB. Tumour necrosis factor-alpha and other cytokines in Guillain-Barre syndrome. J.Neurol.Neurosurg.Psychiatry 1994; 57: 1118-1120.

Fabian RH, Petroff G. Intraneuronal IgG in the central nervous system: uptake by retrograde axonal transport. Neurology 1987; 37: 1780-1784.

Fabian RH. Uptake of plasma IgG by CNS motoneurons: comparison of antineuronal and normal IgG. Neurology 1988; 38: 1775-1780.

Facci L, Leon A, Toffano G, Sonnino S, Ghidoni R, Tettamanti G. Promotion of neuritogenesis in mouse neuroblastoma cells by exogenous gangliosides. Relationship between the effect and the cell association of ganglioside GM1. J.Neurochem. 1984; 42: 299-305.

Facci L, Skaper SD, Favaron M, Leon A. A role for gangliosides in astroglial cell differentiation in vitro. J.Cell Biol. 1988; 106: 821-828.

Farbman AI. Olfactory neurogenesis: genetic or environmental controls? Trends Neurosci. 1990; 13: 362-365.

Favaron M, Manev H, Alho H *et al.* Gangliosides prevent glutamate and kainate neurotoxicity in primary neuronal cultures of neonatal rat cerebellum and cortex. Proc.Natl.Acad.Sci.U.S.A 1988; 85: 7351-7355.

Favoreel HW, Van de Walle GR, Nauwynck HJ, Pensaert MB. Virus complement evasion strategies. J.Gen.Virol. 2003; 84: 1-15.

Feasby TE, Gilbert JJ, Hahn AF, Neilson M. Complement depletion suppresses Lewis rat experimental allergic neuritis. Brain Res. 1987; 419: 97-103.

Feasby TE, Hahn AF, Brown WF, Bolton CF, Gilbert JJ, Koopman WJ. Severe axonal degeneration in acute Guillain-Barre syndrome: evidence of two different mechanisms? J.Neurol.Sci. 1993; 116: 185-192.

Feldman EL, Bromberg MB, Albers JW, Pestronk A. Immunosuppressive treatment in multifocal motor neuropathy. Ann.Neurol. 1991; 30: 397-401.

Feng G, Mellor RH, Bernstein M, Keller-Peck S, Nguyen QT, Wallace M, Nerbonne JM, Lichtman JW, Sanes JR. Imaging Neuronal Subsets in Transgenic Mice Expressing Multiple Spectral Variants of GFP. Neuron 2000; 28(1), 41–51

Fernandez SM, Berlin RD. Cell surface distribution of lectin receptors determined by resonance energy transfer. Nature 1976; 264: 411-415.

Figueras A, Morales-Olivas FJ, Capella D, Palop V, Laporte JR. Bovine gangliosides and acute motor polyneuropathy. BMJ 1992; 305: 1330-1331.

Finean JB. Phospholipid-cholesterol complex in the structure of myelin. Experientia 1953; 9: 17-19.

Fisher M. An unusual variant of acute idiopathic polyneuritis (syndrome of ophthalmoplegia, ataxia and areflexia). N.Engl.J.Med. 1956; 255: 57-65.

Fishman PS, Shy ME, Hart DE, Thompson PE, Cashman NR. Antibodies to the ganglioside GD1b in a patient with motor neuron disease and thyroid adenoma. Arch.Neurol. 1991; 48: 1188-1190.

Foster LJ, De Hoog CL, Mann M. Unbiased quantitative proteomics of lipid rafts reveals high specificity for signaling factors. Proc.Natl.Acad.Sci.U.S.A 2003; 100: 5813-5818.

Freddo L, Yu RK, Latov N *et al.* Gangliosides GM1 and GD1b are antigens for IgM M-protein in a patient with motor neuron disease. Neurology 1986; 36: 454-458.

Fridriksson EK, Shipkova PA, Sheets ED, Holowka D, Baird B, McLafferty FW. Quantitative analysis of phospholipids in functionally important membrane domains from RBL-2H3 mast cells using tandem high-resolution mass spectrometry. Biochemistry 1999; 38: 8056-8063.

Fujimoto S, Yuki N, Itoh T, Amako K. Specific serotype of Campylobacter jejuni associated with Guillain-Barre syndrome. J.Infect.Dis. 1992; 165: 183.

Fujinaga Y, Wolf AA, Rodighiero C *et al.* Gangliosides that associate with lipid rafts mediate transport of cholera and related toxins from the plasma membrane to endoplasmic reticulm. Mol.Biol.Cell 2003; 14: 4783-4793.

Fujita A, Cheng J, Hirakawa M, Furukawa K, Kusunoki S, Fujimoto T. Gangliosides GM1 and GM3 in the living cell membrane form clusters susceptible to cholesterol depletion and chilling. Mol.Biol.Cell 2007; 18: 2112-2122.

Fujiwara T, Ritchie K, Murakoshi H, Jacobson K, Kusumi A. Phospholipids undergo hop diffusion in compartmentalized cell membrane. J.Cell Biol. 2002; 157: 1071-1081.

Furuse H, Waki H, Kaneko K *et al.* Effect of the mono- and tetra-sialogangliosides, GM1 and GQ1b, on long-term potentiation in the CA1 hippocampal neurons of the guinea pig. Exp.Brain Res. 1998; 123: 307-314.

Ganser AL, Kirschner DA, Willinger M. Ganglioside localization on myelinated nerve fibres by cholera toxin binding. J.Neurocytol. 1983; 12: 921-938.

Garred P, Michaelsen TE, Aase A. The IgG subclass pattern of complement activation depends on epitope density and antibody and complement concentration. Scand.J.Immunol. 1989; 30: 379-382.

Gatchalian CL, Schachner M, Sanes JR. Fibroblasts that proliferate near denervated synaptic sites in skeletal muscle synthesize the adhesive molecules tenascin(J1), N-CAM, fibronectin, and a heparan sulfate proteoglycan. J.Cell Biol. 1989; 108: 1873-1890.

Gatto CL, Walker BJ, Lambert S. Local ERM activation and dynamic growth cones at Schwann cell tips implicated in efficient formation of nodes of Ranvier. J.Cell Biol. 2003; 162: 489-498.

Georgiou J, Charlton MP. Non-myelin-forming perisynaptic schwann cells express protein zero and myelin-associated glycoprotein. Glia 1999; 27: 101-109.

Ghabriel MN, Allt G. The role of Schmidt-Lanterman incisures in Wallerian degeneration. II. An electron microscopic study. Acta Neuropathol.(Berl) 1979; 48: 95-103.

Giocondi MC, Vie V, Lesniewska E, Goudonnet JP, Le Grimellec C. In situ imaging of detergent-resistant membranes by atomic force microscopy. J.Struct.Biol. 2000; 131: 38-43.

Girardi G, Berman J, Redecha P *et al.* Complement C5a receptors and neutrophils mediate fetal injury in the antiphospholipid syndrome
43. J.Clin.Invest 2003; 112: 1644-1654.

Giraudo CG, Daniotti JL, Maccioni HJ. Physical and functional association of glycolipid N-acetyl-galactosaminyl and galactosyl transferases in the Golgi apparatus. Proc.Natl.Acad.Sci.U.S.A 2001; 98: 1625-1630.

Giraudo CG, Maccioni HJ. Ganglioside glycosyltransferases organize in distinct multienzyme complexes in CHO-K1 cells. J.Biol.Chem. 2003; 278: 40262-40271.

Godschalk PC, Heikema AP, Gilbert M *et al.* The crucial role of Campylobacter jejuni genes in anti-ganglioside antibody induction in Guillain-Barre syndrome. J.Clin.Invest 2004; 114: 1659-1665.

Gong Y, Tagawa Y, Lunn MP *et al.* Localization of major gangliosides in the PNS: implications for immune neuropathies. Brain 2002; 125: 2491-2506.

Goodfellow JA, Bowes T, Sheikh K *et al.* Overexpression of GD1a ganglioside sensitizes motor nerve terminals to anti-GD1a antibody-mediated injury in a model of acute motor axonal neuropathy. J.Neurosci. 2005; 25: 1620-1628.

Goodyear CS, O'Hanlon GM, Plomp JJ *et al.* Monoclonal antibodies raised against Guillain-Barre syndrome-associated Campylobacter jejuni lipopolysaccharides react with neuronal gangliosides and paralyze muscle-nerve preparations. J.Clin.Invest 1999; 104: 697-708.

Gordon GW, Berry G, Liang XH, Levine B, Herman B. Quantitative fluorescence resonance energy transfer measurements using fluorescence microscopy. Biophys.J. 1998; 74: 2702-2713.

Gould RM, Byrd AL, Barbarese E. The number of Schmidt-Lanterman incisures is more than doubled in shiverer PNS myelin sheaths. J.Neurocytol. 1995; 24: 85-98.

Graves DT, Jiang Y. Chemokines, a family of chemotactic cytokines. Crit Rev.Oral Biol.Med. 1995; 6: 109-118.

Graziadei PP, Graziadei GA. Neurogenesis and neuron regeneration in the olfactory system of mammals. I. Morphological aspects of differentiation and structural organization of the olfactory sensory neurons. J.Neurocytol. 1979; 8: 1-18.

Griffin JW, Stoll G, Li CY, Tyor W, Cornblath DR. Macrophage responses in inflammatory demyelinating neuropathies. Ann.Neurol. 1990; 27 Suppl: S64-S68.

Griffin JW, Li CY, Ho TW *et al.* Guillain-Barre syndrome in northern China. The spectrum of neuropathological changes in clinically defined cases. Brain 1995; 118 (Pt 3): 577-595.

Griffin JW, Li CY, Macko C *et al.* Early nodal changes in the acute motor axonal neuropathy pattern of the Guillain-Barre syndrome. J.Neurocytol. 1996; 25: 33-51.

Guenard V, Gwynn LA, Wood PM. Astrocytes inhibit Schwann cell proliferation and myelination of dorsal root ganglion neurons in vitro. J.Neurosci. 1994; 14: 2980-2992.

Guillain G, Barre JA, Strohl A. Sur on syndrome de radiculoneurite avec hyperalbuminose sans reaction cellulaire: Remarques sur les caracteres cliniques et graphiques des reflexes tendineux. Bull Soc Med Hop Paris 1916;40:1462-1470

Guiloff RJ. Peripheral nerve conduction in Miller Fisher syndrome. J.Neurol.Neurosurg.Psychiatry 1977; 40: 801-807.

Guirland C, Suzuki S, Kojima M, Lu B, Zheng JQ. Lipid rafts mediate chemotropic guidance of nerve growth cones. Neuron 2004; 42: 51-62.

Haas KM, Hasegawa M, Steeber DA *et al.* Complement receptors CD21/35 link innate and protective immunity during Streptococcus pneumoniae infection by regulating IgG3 antibody responses. Immunity. 2002; 17: 713-723.

Hadden RD, Cornblath DR, Hughes RA *et al.* Electrophysiological classification of Guillain-Barre syndrome: clinical associations and outcome. Plasma Exchange/Sandoglobulin Guillain-Barre Syndrome Trial Group. Ann.Neurol. 1998; 44: 780-788.

Hadden RD, Hughes RA. Management of inflammatory neuropathies. J.Neurol.Neurosurg.Psychiatry 2003; 74 Suppl 2: ii9-ii14.

Hafer-Macko C, Hsieh ST, Li CY *et al.* Acute motor axonal neuropathy: an antibody-mediated attack on axolemma. Ann.Neurol. 1996; 40: 635-644.

Hafer-Macko CE, Sheikh KA, Li CY *et al.* Immune attack on the Schwann cell surface in acute inflammatory demyelinating polyneuropathy. Ann.Neurol. 1996; 39: 625-635.

Hakomori Si SI. Inaugural Article: The glycosynapse. Proc.Natl.Acad.Sci.U.S.A 2002; 99: 225-232.

Hakomori S. Bifunctional role of glycosphingolipids. Modulators for transmembrane signaling and mediators for cellular interactions. J.Biol.Chem. 1990; 265: 18713-18716.

Hakomori S. Glycosynapses: microdomains controlling carbohydrate-dependent cell adhesion and signaling. An.Acad.Bras.Cienc. 2004; 76: 553-572.

Hakomori SI, Teather C, Andrews H. Organizational difference of cell surface "hematoside" in normal and virally transformed cells. Biochem.Biophys.Res.Commun. 1968; 33: 563-568.

Hall SM, Williams PL. Studies on the 'Incisures' of Schmidt and Lanterman . J Cell Sci 1970; 6: 767-791.

Halstead SK, O'Hanlon GM, Humphreys PD *et al.* Anti-disialoside antibodies kill perisynaptic Schwann cells and damage motor nerve terminals via membrane attack complex in a murine model of neuropathy
4884. Brain 2004; 127: 2109-2123.

Halstead SK, Morrison I, O'Hanlon GM *et al.* Anti-disialosyl antibodies mediate selective neuronal or Schwann cell injury at mouse neuromuscular junctions. Glia 2005; 52: 177-189.

Hamers-Casterman C, Atarhouch T, Muyldermans S *et al.* Naturally occurring antibodies devoid of light chains. Nature 1993; 363: 446-448.

Hankey GJ. Guillain-Barre syndrome in Western Australia, 1980-1985. Med.J.Aust. 1987; 146: 130-133.

Harder T, Scheiffele P, Verkade P, Simons K. Lipid domain structure of the plasma membrane revealed by patching of membrane components. J.Cell Biol. 1998; 141: 929-942.

Harris CL, Abbott RJ, Smith RA, Morgan BP, Lea SM. Molecular dissection of interactions between components of the alternative pathway of complement and decay accelerating factor (CD55). J.Biol.Chem. 2004.

Hart DE, Rojas LA, Rosario JA, Recalde H, Roman GC. Childhood Guillain-Barre syndrome in Paraguay, 1990 to 1991. Ann.Neurol. 1994; 36: 859-863.

Hartung HP, Schafer B, Heininger K, Stoll G, Toyka KV. The role of macrophages and eicosanoids in the pathogenesis of experimental allergic neuritis. Serial clinical, electrophysiological, biochemical and morphological observations. Brain 1988; 111 (Pt 5): 1039-1059.

Hartung HP, Reiners K, Schmidt B, Stoll G, Toyka KV. Serum interleukin-2 concentrations in Guillain-Barre syndrome and chronic idiopathic demyelinating polyradiculoneuropathy: comparison with other neurological diseases of presumed immunopathogenesis. Ann.Neurol. 1991; 30: 48-53.

Hartung HP. Immune-mediated demyelination. Ann.Neurol. 1993; 33: 563-567.

Hartung HP, Pollard JD, Harvey GK, Toyka KV. Immunopathogenesis and treatment of the Guillain-Barre syndrome--Part II. Muscle Nerve 1995; 18: 154-164.

Hartung HP, Pollard JD, Harvey GK, Toyka KV. Immunopathogenesis and treatment of the Guillain-Barre syndrome--Part I. Muscle Nerve 1995; 18: 137-153.

Harvey GK, Toyka KV, Zielasek J, Kiefer R, Simonis C, Hartung HP. Failure of anti-GM1 IgG or IgM to induce conduction block following intraneural transfer. Muscle Nerve 1995; 18: 388-394.

Haymaker W, Kernohan JW The Landry-Guillain-Barre syndrome: A Clinopathologic report of fifty fatal cases and a critique of the literature. Medicine (Baltimore) 1949; 28, 59-141

Hays AP, Latov N, Takatsu M, Sherman WH. Experimental demyelination of nerve induced by serum of patients with neuropathy and an anti-MAG IgM M-protein. Neurology 1987; 37: 242-256.

Hays AP, Lee SS, Latov N. Immune reactive C3d on the surface of myelin sheaths in neuropathy. J.Neuroimmunol. 1988; 18: 231-244.

Heininger K, Schafer B, Hartung HP, Fierz W, Linington C, Toyka KV. The role of macrophages in experimental autoimmune neuritis induced by a P2-specific T-cell line. Ann.Neurol. 1988; 23: 326-331.

Hering H, Lin CC, Sheng M. Lipid rafts in the maintenance of synapses, dendritic spines, and surface AMPA receptor stability. J.Neurosci. 2003; 23: 3262-3271.

Herreros J, Ng T, Schiavo G. Lipid rafts act as specialized domains for tetanus toxin binding and internalization into neurons. Mol.Biol.Cell 2001; 12: 2947-2960.

Hesketh TR, Dourmashkin RR, Payne SN, Humphrey JH, Lachmann PJ. Lesions due to complement in lipid membranes. Nature 1971; 233: 620-623.

Ho TW, Mishu B, Li CY *et al.* Guillain-Barre syndrome in northern China. Relationship to Campylobacter jejuni infection and anti-glycolipid antibodies. Brain 1995; 118 (Pt 3): 597-605.

Ho TW, Li CY, Cornblath DR *et al.* Patterns of recovery in the Guillain-Barre syndromes. Neurology 1997; 48: 695-700.

Hoerr NL. Cytological studies by the altmann-gersh feezing drying method. III. The preexistance of neurofibrillae and their disposition in the nerve fiber. The Anatomical Record 2005; 66 (1): 81-90

Hoffken K, McLaughlin PJ, Price MR, Preston VE, Baldwin RW. Rat Clq: similarity to human Clq in functional and compositional properties. Immunochemistry. 1978; 15: 409-412.

Honavar M, Tharakan JK, Hughes RA, Leibowitz S, Winer JB. A clinicopathological study of the Guillain-Barre syndrome. Nine cases and literature review. Brain 1991; 114 (Pt 3): 1245-1269.

Hughes-Jones NC, Gorick BD, Howard JC. The mechanism of synergistic complement-mediated lysis of rat red cells by monoclonal IgG antibodies. Eur.J.Immunol. 1983; 13: 635-641.

Hughes R, Sanders E, Hall S, Atkinson P, Colchester A, Payan P. Subacute idiopathic demyelinating polyradiculoneuropathy. Arch.Neurol. 1992; 49: 612-616.

Hughes RA, Kadlubowski M, Gray IA, Leibowitz S. Immune responses in experimental allergic neuritis. J.Neurol.Neurosurg.Psychiatry 1981; 44: 565-569.

Iglesias-Bartolome R, Crespo PM, Gomez GA, Daniotti JL. The antibody to GD3 ganglioside, R24, is rapidly endocytosed and recycled to the plasma membrane via the endocytic recycling compartment. Inhibitory effect of brefeldin A and monensin. FEBS J. 2006; 273: 1744-1758.

Ilyas AA, Willison HJ, Dalakas MC, Whitaker JN, Quarles RH. Identification and characterization of gangliosides reacting with IgM paraproteins in three patients with neuropathy associated with biclonal gammopathy. J.Neurochem. 1988; 51: 851-858.

Ilyas AA, Li SC, Chou DK *et al.* Gangliosides GM2, IV4GalNAcGM1b, and IV4GalNAcGC1a as antigens for monoclonal immunoglobulin M in neuropathy associated with gammopathy. J.Biol.Chem. 1988; 263: 4369-4373.

Ilyas AA, Mithen FA, Dalakas MC *et al.* Antibodies to sulfated glycolipids in Guillain-Barre syndrome. J.Neurol.Sci. 1991; 105: 108-117.

Ilyas AA, Mithen FA, Dalakas MC, Chen ZW, Cook SD. Antibodies to acidic glycolipids in Guillain-Barre syndrome and chronic inflammatory demyelinating polyneuropathy. J.Neurol.Sci. 1992; 107: 111-121.

Inoue M, Fujii Y, Furukawa K *et al.* Refractory skin injury in complex knock-out mice expressing only the GM3 ganglioside. J.Biol.Chem. 2002; 277: 29881-29888.

Ipsen JH, Karlstrom G, Mouritsen OG, Wennerstrom H, Zuckermann MJ. Phase equilibria in the phosphatidylcholine-cholesterol system. Biochim.Biophys.Acta 1987; 905: 162-172.

Ishii N, Watanabe K. Aberrant expression of GM1 on lymph node cells of MRL/Mp-lpr/lpr mice: influences on the autoreactivities of anti-asialo GM1 antibodies. Autoimmunity 1992; 13: 107-116.

Itoh M, Fukumoto S, Iwamoto T *et al.* Specificity of carbohydrate structures of gangliosides in the activity to regenerate the rat axotomized hypoglossal nerve. Glycobiology 2001; 11: 125-130.

IUPAC-IUB Commission on Biochemical Nomenclature. The nomenclature of lipids. Hoppe-Seyler's Z. Physiol. Chem. 1977; 358**:** 617-63 1.

Iwabuchi,K., Handa,K., and Hakomori,S. Separation of "glycosphingolipid signaling domain" from caveolin-containing membrane fraction in mouse melanoma B16 cells and its role in cell adhesion coupled with signaling. J. Biol. Chem. 1998 ; 273, 33766-33773.

Jacobs BC, O'Hanlon GM, Bullens RW, Veitch J, Plomp JJ, Willison HJ. Immunoglobulins inhibit pathophysiological effects of anti-GQ1b-positive sera at motor nerve terminals through inhibition of antibody binding. Brain 2003; 126: 2220-2234.

Jacobs JM, Scadding JW. Morphological changes in IgM paraproteinaemic neuropathy. Acta Neuropathol.(Berl) 1990; 80: 77-84.

Jacobson K, Dietrich C. Looking at lipid rafts? Trends Cell Biol. 1999; 9: 87-91.

Jost P, Brooks UJ, Griffith OH. Fluidity of phospholipid bilayers and membranes after exposure to osmium tetroxide and gluteraldehyde. J.Mol.Biol. 1973; 76: 313-318.

Kadlubowski M, Hughes RA. Identification of the neuritogen for experimental allergic neuritis. Nature 1979; 277: 140-141.

Kaida K, Morita D, Kanzaki M *et al.* Ganglioside complexes as new target antigens in Guillain-Barre syndrome. Ann.Neurol. 2004; 56: 567-571.

Kaida K, Kanzaki M, Morita D *et al.* Anti-ganglioside complex antibodies in Miller Fisher syndrome. J.Neurol.Neurosurg.Psychiatry 2006; 77: 1043-1046.

Kaldor J, Speed BR. Guillain-Barre syndrome and Campylobacter jejuni: a serological study. Br.Med.J.(Clin.Res.Ed) 1984; 288: 1867-1870.

Kaminski MJ, MacKenzie CR, Mooibroek MJ *et al.* The role of homophilic binding in anti-tumor antibody R24 recognition of molecular surfaces. Demonstration of an intermolecular beta-sheet interaction between vh domains. J.Biol.Chem. 1999; 274: 5597-5604.

Kang H, Tian L, Thompson W. Terminal Schwann cells guide the reinnervation of muscle after nerve injury. J.Neurocytol. 2003; 32: 975-985.

Karpiak SE. Exogenous gangliosides enhance recovery from cns injury. Adv.Exp.Med.Biol. 1984; 174: 489-497.

Kawai H, Allende ML, Wada R *et al.* Mice expressing only monosialoganglioside GM3 exhibit lethal audiogenic seizures. J.Biol.Chem. 2001; 276: 6885-6888.

Kenworthy AK, Edidin M. Distribution of a glycosylphosphatidylinositol-anchored protein at the apical surface of MDCK cells examined at a resolution of <100 A using imaging fluorescence resonance energy transfer. J.Cell Biol. 1998; 142: 69-84.

Kenworthy AK, Petranova N, Edidin M. High-resolution FRET microscopy of cholera toxin B-subunit and GPI-anchored proteins in cell plasma membranes. Mol.Biol.Cell 2000; 11: 1645-1655.

Khalili-Shirazi A, Atkinson P, Gregson N, Hughes RA. Antibody responses to P0 and P2 myelin proteins in Guillain-Barre syndrome and chronic idiopathic demyelinating polyradiculoneuropathy. J.Neuroimmunol. 1993; 46: 245-251.

Kiernan JA, Barr ML. In Barr's The Human Nervous System: An anatomical viewpoint, 8th ed, Kiernan JA(eds). Philidelphia, Lippincott Williams and Wilkins. 2005, pp13-36.

Kiers L, Clouston P, Zuniga G, Cros D. Quantitative studies of F responses in Guillain-Barre syndrome and chronic inflammatory demyelinating polyneuropathy. Electroencephalogr.Clin.Neurophysiol. 1994; 93: 255-264.

Kieseier BC, Tani M, Mahad D *et al.* Chemokines and chemokine receptors in inflammatory demyelinating neuropathies: a central role for IP-10. Brain 2002; 125: 823-834.

Kitamura M, Takamiya K, Aizawa S, Furukawa K, Furukawa K. Gangliosides are the binding substances in neural cells for tetanus and botulinum toxins in mice. Biochim.Biophys.Acta 1999; 1441: 1-3.

Kojima,N. and Hakomori,S. Cell adhesion, spreading, and motility of GM3-expressing cells based on glycolipid-glycolipid interaction. J. Biol. Chem. 1991 ; 266, 17552-17558.

Kordeli E, Davis J, Trapp B, Bennett V. An isoform of ankyrin is localized at nodes of Ranvier in myelinated axons of central and peripheral nerves. J.Cell Biol. 1990; 110: 1341-1352.

Kordeli E, Bennett V. Distinct ankyrin isoforms at neuron cell bodies and nodes of Ranvier resolved using erythrocyte ankyrin-deficient mice. J.Cell Biol. 1991; 114: 1243-1259.

Koski CL, Sanders ME, Swoveland PT *et al.* Activation of terminal components of complement in patients with Guillain-Barre syndrome and other demyelinating neuropathies. J.Clin.Invest 1987; 80: 1492-1497.

Kuijf ML, Godschalk PC, Gilbert M *et al.* Origin of ganglioside complex antibodies in Guillain-Barre syndrome. J.Neuroimmunol. 2007; 188: 69-73.

Kukulansky T, Abramovitch S, Hollander N. Cleavage of the glycosylphosphatidylinositol anchor affects the reactivity of thy-1 with antibodies. J.Immunol. 1999; 162: 5993-5997.

Kuroki S, Saida T, Nukina M *et al.* Campylobacter jejuni strains from patients with Guillain-Barre syndrome belong mostly to Penner serogroup 19 and contain beta-N-acetylglucosamine residues. Ann.Neurol. 1993; 33: 243-247.

Kusunoki S, Chiba A, Tai T, Kanazawa I. Localization of GM1 and GD1b antigens in the human peripheral nervous system. Muscle Nerve 1993; 16: 752-756.

Kusunoki S, Shimizu J, Chiba A, Ugawa Y, Hitoshi S, Kanazawa I. Experimental sensory neuropathy induced by sensitization with ganglioside GD1b. Ann.Neurol. 1996; 39: 424-431.

Kusunoki S, Mashiko H, Mochizuki N *et al.* Binding of antibodies against GM1 and GD1b in human peripheral nerve. Muscle Nerve 1997; 20: 840-845.

Kusunoki S, Chiba A, Kanazawa I. Anti-GQ1b IgG antibody is associated with ataxia as well as ophthalmoplegia. Muscle Nerve 1999; 22: 1071-1074.

Kuwabara S, Yuki N, Koga M *et al.* IgG anti-GM1 antibody is associated with reversible conduction failure and axonal degeneration in Guillain-Barre syndrome. Ann.Neurol. 1998; 44: 202-208.

Kuwabara S, Ogawara K, Sung JY *et al.* Differences in membrane properties of axonal and demyelinating Guillain-Barre syndromes. Ann.Neurol. 2002; 52: 180-187.

Lainetti RD, Da Silva CF. Local addition of monosialoganglioside GM1 stimulates peripheral axon regeneration in vivo. Braz.J.Med.Biol.Res. 1993; 26: 841-845.

Lamb NL, Patten BM. Clinical correlations of anti-GM1 antibodies in amyotrophic lateral sclerosis and neuropathies. Muscle Nerve 1991; 14: 1021-1027.

Landry O. Note sur la paralyse ascendante aigue. Gaz Hebd Med Chir 1859; 6: 472-474, 468, 488

Lang T, Bruns D, Wenzel D *et al.* SNAREs are concentrated in cholesterol-dependent clusters that define docking and fusion sites for exocytosis. EMBO J. 2001; 20: 2202-2213.

Lange DJ, Trojaborg W, Latov N *et al.* Multifocal motor neuropathy with conduction block: is it a distinct clinical entity? Neurology 1992; 42: 497-505.

Lanterman AJ. Über den feineren Bau der markhaltigen Nervenfasern. Arch Mikrosk Anat Entw Mech 1877; 13:1–8

Lanzavecchia A, Lezzi G, Viola A. From TCR engagement to T cell activation: a kinetic view of T cell behavior. Cell 1999; 96: 1-4.

Larsson L, Edstrom L, Lindegren B, Gorza L, Schiaffino S. MHC composition and enzyme-histochemical and physiological properties of a novel fast-twitch motor unit type. Am.J.Physiol 1991; 261: C93-101.

Latov N, Hays AP, Donofrio PD *et al.* Monoclonal IgM with unique specificity to gangliosides GM1 and GD1b and to lacto-N-tetraose associated with human motor neuron disease. Neurology 1988; 38: 763-768.

Latov N. Antibodies to glycoconjugates in neuropathy and motor neuron disease. Prog.Brain Res. 1994; 101: 295-303.

Lauer S, Goldstein B, Nolan RL, Nolan JP. Analysis of cholera toxin-ganglioside interactions by flow cytometry. Biochemistry 2002; 41: 1742-1751.

Law SKA, Reid KBM. Complement 2nd Ed, D Male (ed), Oxford University Press, Oxford, 1995

Ledeen RW. Gangliosides of the neuron. Trends Neurosci 1985; 8:169-174.

Lehmann HC, Lopez PH, Zhang G *et al.* Passive immunization with anti-ganglioside antibodies directly inhibits axon regeneration in an animal model. J.Neurosci. 2007; 27: 27-34.

Lewis RA, Sumner AJ, Brown MJ, Asbury AK. Multifocal demyelinating neuropathy with persistent conduction block. Neurology 1982; 32: 958-964.

Li CY, Xue P, Tian WQ, Liu RC, Yang C. Experimental Campylobacter jejuni infection in the chicken: an animal model of axonal Guillain-Barre syndrome. J.Neurol.Neurosurg.Psychiatry 1996; 61: 279-284.

Lin S, Naim HY, Rodriguez AC, Roth MG. Mutations in the middle of the transmembrane domain reverse the polarity of transport of the influenza virus hemagglutinin in MDCK epithelial cells. J.Cell Biol. 1998; 142: 51-57.

Linington C, Wekerle H, Meyermann R. T lymphocyte autoimmunity in peripheral nervous system autoimmune disease. Agents Actions 1986; 19: 256-265.

Lloyd KO, Gordon CM, Thampoe IJ, DiBenedetto C. Cell surface accessibility of individual gangliosides in malignant melanoma cells to antibodies is influenced by the total ganglioside composition of the cells. Cancer Res. 1992; 52: 4948-4953.

Lloyd KO, Furukawa K. Biosynthesis and functions of gangliosides: recent advances. Glycoconj.J. 1998; 15: 627-636.

Loffel NB, Rossi LN, Mumenthaler M, Lutschg J, Ludin HP. The Landry-Guillain-barre syndrome. Complications, prognosis and natural history in 123 cases. J.Neurol.Sci. 1977; 33: 71-79.

Long RR, Sargent JC, Hammer K. Paralytic shellfish poisoning: a case report and serial electrophysiologic observations. Neurology 1990; 40: 1310-1312.

Lu P, Sharom FJ. Immunosuppression by YAC-1 lymphoma: role of shed gangliosides. Cell Immunol. 1996; 173: 22-32.

Luijten JA, Baart de la Faille-Kuyp. The occurrence of IgM and complement factors along myelin sheaths of peripheral nerves. An immunohistochemical study of the Guillain-Barre syndrome. Preliminary communication. J.Neurol.Sci. 1972; 15: 219-224.

Lukacik P, Roversi P, White J *et al.* Complement regulation at the molecular level: the structure of decay-accelerating factor. Proc.Natl.Acad.Sci.U.S.A 2004; 101: 1279-1284.

Lyons SF, Liebowitz DN. The roles of human viruses in the pathogenesis of lymphoma. Semin.Oncol. 1998; 25: 461-475.

Maccioni HJ, Daniotti JL, Martina JA. Organization of ganglioside synthesis in the Golgi apparatus. Biochim.Biophys.Acta 1999; 1437: 101-118.

Madore N, Smith KL, Graham CH *et al.* Functionally different GPI proteins are organized in different domains on the neuronal surface. EMBO J. 1999; 18: 6917-6926.

Marcus DM, Perry L, Gilbert S, Preud'homme JL, Kyle R. Human IgM monoclonal proteins that bind 3-fucosyllactosamine, asialo-GM1, and GM1. J.Immunol. 1989; 143: 2929-2932.

Marie P, Chatelin C. Note sur un syndrome de paralysie flasque plus ou moins généralisée avec abolition des reflexes, hyperalbuminose massive et xantochromie vers la guerison et de nature indéterminée. Revue neurologique, Paris, 1916, 30: 564-565.

Martini R, Schachner M, Faissner A. Enhanced expression of the extracellular matrix molecule J1/tenascin in the regenerating adult mouse sciatic nerve. J.Neurocytol. 1990; 19: 601-616.

Mayor S, Rao M. Rafts: scale-dependent, active lipid organization at the cell surface. Traffic. 2004; 5: 231-240.

Mayor S, Viola A, Stan RV, del Pozo MA. Flying kites on slippery slopes at Keystone. Symposium on Lipid Rafts and Cell Function. EMBO Rep. 2006; 7: 1089-1093.

McAlarney T, Apostolski S, Lederman S, Latov N. Characteristics of HIV-1 gp120 glycoprotein binding to glycolipids. J.Neurosci.Res. 1994; 37: 453-460.

McArdle JJ, Angaut-Petit D, Mallart A, Bournaud R, Faille L, Brigant JL. Advantages of the triangularis sterni muscle of the mouse for investigations of synaptic phenomena. J.Neurosci.Methods 1981; 4: 109-115.

McKhann GM, Cornblath DR, Ho T *et al.* Clinical and electrophysiological aspects of acute paralytic disease of children and young adults in northern China. Lancet 1991; 338: 593-597.

McKhann GM, Cornblath DR, Griffin JW *et al.* Acute motor axonal neuropathy: a frequent cause of acute flaccid paralysis in China. Ann.Neurol. 1993; 33: 333-342.

Melkonian KA, Ostermeyer AG, Chen JZ, Roth MG, Brown DA. Role of lipid modifications in targeting proteins to detergent-resistant membrane rafts. Many raft proteins are acylated, while few are prenylated. J.Biol.Chem. 1999; 274: 3910-3917.

Mendez-Otero R, Schlosshauer B, Barnstable CJ, Constantine-Paton M. A developmentally regulated antigen associated with neural cell and process migration. J.Neurosci. 1988; 8: 564-579.

Mendez-Otero R, Ramon-Cueto A. Expression of 9-O-acetylated gangliosides during development of the rat olfactory system. Neuroreport 1994; 5: 1755-1759.

Mendez-Otero R, Santiago MF. Functional role of a specific ganglioside in neuronal migration and neurite outgrowth. Braz.J.Med.Biol.Res. 2003; 36: 1003-1013.

Merelli E, Sola P, Faglioni P, Poggi M, Montorsi M, Torelli G. Newest human herpesvirus (HHV-6) in the Guillain-Barre syndrome and other neurological diseases. Acta Neurol.Scand. 1992; 85: 334-336.

Merritt EA, Sarfaty S, van den AF, L'Hoir C, Martial JA, Hol WG. Crystal structure of cholera toxin B-pentamer bound to receptor GM1 pentasaccharide. Protein Sci. 1994; 3: 166-175.

Merritt EA, Kuhn P, Sarfaty S, Erbe JL, Holmes RK, Hol WG. The 1.25 A resolution refinement of the cholera toxin B-pentamer: evidence of peptide backbone strain at the receptor-binding site. J.Mol.Biol. 1998; 282: 1043-1059.

Mishu B, Blaser MJ. Role of infection due to Campylobacter jejuni in the initiation of Guillain-Barre syndrome. Clin.Infect.Dis. 1993; 17: 104-108.

Mizuno M, Morgan BP. The possibilities and pitfalls for anti-complement therapies in inflammatory diseases. Curr.Drug Targets.Inflamm.Allergy 2004; 3: 87-96.

Mochizuki Y, Ojima K, Uezumi A, Masuda S, Yoshimura K, Takeda S. Participation of bone marrow-derived cells in fibrotic changes in denervated skeletal muscle. Am.J.Pathol. 2005; 166: 1721-1732.

Moffett S, Brown DA, Linder ME. Lipid-dependent targeting of G proteins into rafts. J.Biol.Chem. 2000; 275: 2191-2198.

Molander M, Berthold CH, Persson H, Andersson K, Fredman P. Monosialoganglioside (GM1) immunofluorescence in rat spinal roots studied with a monoclonal antibody. J.Neurocytol. 1997; 26: 101-111.

Monaco S, Bonetti B, Ferrari S *et al.* Complement-mediated demyelination in patients with IgM monoclonal gammopathy and polyneuropathy. N.Engl.J.Med. 1990; 322: 649-652.

Monaco S, Ferrari S, Bonetti B *et al.* Experimental induction of myelin changes by anti-MAG antibodies and terminal complement complex. J.Neuropathol.Exp.Neurol. 1995; 54: 96-104.

Montagna GN, Donelson JE, Frasch AC. Procyclic Trypanosoma brucei expresses separate sialidase and trans-sialidase enzymes on its surface membrane. J.Biol.Chem. 2006; 281: 33949-33958.

Moran AP, Prendergast MM, Appelmelk BJ. Molecular mimicry of host structures by bacterial lipopolysaccharides and its contribution to disease. FEMS Immunol.Med.Microbiol. 1996; 16: 105-115.

Moran AP. The role of lipopolysaccharide in Helicobacter pylori pathogenesis. Aliment.Pharmacol.Ther. 1996; 10 Suppl 1: 39-50.

Moreno-Altamirano MM, Aguilar-Carmona I, Sanchez-Garcia FJ. Expression of GM1, a marker of lipid rafts, defines two subsets of human monocytes with differential endocytic capacity and lipopolysaccharide responsiveness. Immunology 2007; 120: 536-543.

Morgan BP. Mechanisms of tissue damage by the membrane attack complex of complement. Complement Inflamm. 1989; 6: 104-111.

Morgan BP. The complement system: an overview. Methods Mol.Biol. 2000; 150: 1-13.

Morgan BP, Harris CL. Complement therapeutics; history and current progress. Mol.Immunol. 2003; 40: 159-170.

Mori K, Hattori N, Sugiura M *et al.* Chronic inflammatory demyelinating polyneuropathy presenting with features of GBS. Neurology 2002; 58: 979-982.

Morrow IC, Parton RG. Flotillins and the PHB domain protein family: rafts, worms and anaesthetics. Traffic. 2005; 6: 725-740.

Moss J, Vaughan M. Activation of adenylate cyclase by choleragen. Annu.Rev.Biochem. 1979; 48: 581-600.

Muller-Eberhard HJ. Molecular organization and function of the complement system. Annu.Rev.Biochem. 1988; 57: 321-347.

Munro S. An investigation of the role of transmembrane domains in Golgi protein retention. EMBO J. 1995; 14: 4695-4704.

Munro S. Lipid rafts: elusive or illusive? Cell 2003; 115: 377-388.

Murata M, Peranen J, Schreiner R, Wieland F, Kurzchalia TV, Simons K. VIP21/caveolin is a cholesterol-binding protein. Proc.Natl.Acad.Sci.U.S.A 1995; 92: 10339-10343.

Mutoh T, Tokuda A, Miyadai T, Hamaguchi M, Fujiki N. Ganglioside GM1 binds to the Trk protein and regulates receptor function. Proc.Natl.Acad.Sci.U.S.A 1995; 92: 5087-5091.

Nagai Y. Functional roles of gangliosides in bio-signaling. Behav.Brain Res. 1995; 66: 99-104.

Nagai *et al.* Ganglioside syndrome, a new autoimmune neurologic disorder, experimentally induced with brain gangliosides, Neurosci. Lett. 1976; 2: 107–111

Nardelli E, Steck AJ, Schluep M, Felgenhauer K, Jerusalem F. Neuropathy and monoclonal IgM M-protein with antibody activity against gangliosides. Ann.N.Y.Acad.Sci. 1988; 540: 378-380.

National Institute of Neurological and Communicative Disorders and Stroke. Ad Hoc Committee. Criteria for diagnosis of Guillain-Barre syndrome. Ann Neurol 1978;3:565-566

Nichols BJ, Kenworthy AK, Polishchuk RS *et al.* Rapid cycling of lipid raft markers between the cell surface and Golgi complex. J.Cell Biol. 2001; 153: 529-541.

Niu SL, Litman BJ. Determination of membrane cholesterol partition coefficient using a lipid vesicle-cyclodextrin binary system: effect of phospholipid acyl chain unsaturation and headgroup composition. Biophys.J. 2002; 83: 3408-3415.

Nobile-Orazio E, Carpo M, Legname G, Meucci N, Sonnino S, Scarlato G. Anti-GM1 IgM antibodies in motor neuron disease and neuropathy. Neurology 1990; 40: 1747-1750.

Nobile-Orazio E, Carpo M, Meucci N *et al.* Guillain-Barre syndrome associated with high titers of anti-GM1 antibodies. J.Neurol.Sci. 1992; 109: 200-206.

Norton WT. The Myelin Sheath. In: Scientific Approaches to clinical neurology, 1977

Nyland H, Matre R, Mork S. Immunological characterization of sural nerve biopsies from patients with Guillain-Barre syndrome. Ann.Neurol. 1981; 9 Suppl: 80-86.

O'Hanlon GM, Paterson GJ, Wilson G, Doyle D, McHardie P, Willison HJ. Anti-GM1 ganglioside antibodies cloned from autoimmune neuropathy patients show

diverse binding patterns in the rodent nervous system. J.Neuropathol.Exp.Neurol. 1996; 55: 184-195.

O'Hanlon GM, Plomp JJ, Chakrabarti M *et al.* Anti-GQ1b ganglioside antibodies mediate complement-dependent destruction of the motor nerve terminal. Brain 2001; 124: 893-906.

O'Hanlon GM, Humphreys PD, Goldman RS *et al.* Calpain inhibitors protect against axonal degeneration in a model of anti-ganglioside antibody-mediated motor nerve terminal injury. Brain 2003; 126: 2497-2509.

O'Malley JP, Waran MT, Balice-Gordon RJ. In vivo observations of terminal Schwann cells at normal, denervated, and reinnervated mouse neuromuscular junctions. J.Neurobiol. 1999; 38: 270-286.

Odaka M, Yuki N, Hirata K. Patients with chronic inflammatory demyelinating polyneuropathy initially diagnosed as Guillain-Barre syndrome. J.Neurol. 2003; 250: 913-916.

Ogawa-Goto K, Funamoto N, Abe T, Nagashima K. Different ceramide compositions of gangliosides between human motor and sensory nerves. J.Neurochem. 1990; 55: 1486-1493.

Ogawa-Goto K, Funamoto N, Ohta Y, Abe T, Nagashima K. Myelin gangliosides of human peripheral nervous system: an enrichment of GM1 in the motor nerve myelin isolated from cauda equina. J.Neurochem. 1992; 59: 1844-1849.

Oh SJ. Diagnostic usefulness and limitations of the sural nerve biopsy. Yonsei Med.J. 1990; 31: 1-26.

Oh SJ, Kurokawa K, de Almeida DF, Ryan HF, Jr., Claussen GC. Subacute inflammatory demyelinating polyneuropathy. Neurology 2003; 61: 1507-1512.

Okada M, Itoh MM, Haraguchi M *et al.* b-series Ganglioside deficiency exhibits no definite changes in the neurogenesis and the sensitivity to Fas-mediated apoptosis but impairs regeneration of the lesioned hypoglossal nerve. J.Biol.Chem. 2002; 277: 1633-1636.

Oliver JM, Ukena TE, Berlin RD. Effects of phagocytosis and colchicine on the distribution of lectin-binding sites on cell surfaces. Proc.Natl.Acad.Sci.U.S.A 1974; 71: 394-398.

Olney RK, Aminoff MJ. Electrodiagnostic features of the Guillain-Barre syndrome: the relative sensitivity of different techniques. Neurology 1990; 40: 471-475.

Olsson Y. Topographical differences in the vascular permeability of the peripheral nervous system. Acta Neuropathol.(Berl) 1968; 10: 26-33.

Osler W. The principles and practice of medicine, 1st edn. Appleton, New York, 1982

Pan CL, Yuki N, Koga M, Chiang MC, Hsieh ST. Acute sensory ataxic neuropathy associated with monospecific anti-GD1b IgG antibody. Neurology 2001; 57: 1316-1318.

Panasiewicz M, Domek H, Hoser G, Kawalec M, Pacuszka T. Structure of the ceramide moiety of GM1 ganglioside determines its occurrence in different detergent-resistant membrane domains in HL-60 cells. Biochemistry 2003; 42: 6608-6619.

Paradiso G, Tripoli J, Galicchio S, Fejerman N. Epidemiological, clinical, and electrodiagnostic findings in childhood Guillain-Barre syndrome: a reappraisal. Ann.Neurol. 1999; 46: 701-707.

Parry GJ, Sumner AJ. Multifocal motor neuropathy. Neurol.Clin. 1992; 10: 671-684.

Parton RG. Ultrastructural localization of gangliosides; GM1 is concentrated in caveolae. J.Histochem.Cytochem. 1994; 42: 155-166.

Parton RG, Joggerst B, Simons K. Regulated internalization of caveolae. J.Cell Biol. 1994; 127: 1199-1215.

Parton RG, Simons K. Digging into caveolae. Science 1995; 269: 1398-1399.

Parton RG, Richards AA. Lipid rafts and caveolae as portals for endocytosis: new insights and common mechanisms. Traffic. 2003; 4: 724-738.

Paterson G, Wilson G, Kennedy PG, Willison HJ. Analysis of anti-GM1 ganglioside IgM antibodies cloned from motor neuropathy patients demonstrates diverse V region gene usage with extensive somatic mutation. J.Immunol. 1995; 155: 3049-3059.

Pestronk A, Cornblath DR, Ilyas AA *et al.* A treatable multifocal motor neuropathy with antibodies to GM1 ganglioside. Ann.Neurol. 1988; 24: 73-78.

Pestronk A, Adams RN, Cornblath D, Kuncl RW, Drachman DB, Clawson L. Patterns of serum IgM antibodies to GM1 and GD1a gangliosides in amyotrophic lateral sclerosis. Ann.Neurol. 1989; 25: 98-102.

Pestronk A, Chaudhry V, Feldman EL *et al.* Lower motor neuron syndromes defined by patterns of weakness, nerve conduction abnormalities, and high titers of antiglycolipid antibodies. Ann.Neurol. 1990; 27: 316-326.

Pestronk A. Invited review: motor neuropathies, motor neuron disorders, and antiglycolipid antibodies. Muscle Nerve 1991; 14: 927-936.

Peterman AF, Daly DD, Dion FR, Keith HM. Infectious neuronitis (Guillain-Barre syndrome) in children. Neurology 1959; 9:533-38

Pfeiffer SE, Warrington AE, Bansal R. The oligodendrocyte and its many cellular processes. Trends Cell Biol. 1993; 3: 191-197.

Pike LJ, Han X, Gross RW. Epidermal growth factor receptors are localized to lipid rafts that contain a balance of inner and outer leaflet lipids: a shotgun lipidomics study. J.Biol.Chem. 2005; 280: 26796-26804.

Pike LJ. Rafts defined: a report on the Keystone Symposium on Lipid Rafts and Cell Function. J.Lipid Res. 2006; 47: 1597-1598.

Pillemer L, Schoenberg MD, Blum L, Wurz L. Properdin system and immunity. II. Interaction of the properdin system with polysaccharides. Science 1955; 122: 545-549.

Plomp JJ, Molenaar PC, O'Hanlon GM *et al.* Miller Fisher anti-GQ1b antibodies: alpha-latrotoxin-like effects on motor end plates. Ann.Neurol. 1999; 45: 189-199.

Poon PH, Phillips ML, Schumaker VN. Immunoglobulin M possesses two binding sites for complement subcomponent C1q, and soluble 1:1 and 2:1 complexes are formed in solution at reduced ionic strength. J.Biol.Chem. 1985; 260: 9357-9365.

Powell HC, Mizisin AP, Wiley CA, Morey MK, Hughes RA. Relationship of adjuvants and swine influenza vaccine to experimental neuropathy in rabbits. Acta Neuropathol.(Berl) 1987; 73: 12-18.

Prakash YS, Miller SM, Huang M, Sieck GC. Morphology of diaphragm neuromuscular junctions on different fibre types. J.Neurocytol. 1996; 25: 88-100.

Press R, Mata S, Lolli F, Zhu J, Andersson T, Link H. Temporal profile of anti-ganglioside antibodies and their relation to clinical parameters and treatment in Guillain-Barre syndrome. J.Neurol.Sci. 2001; 190: 41-47.

Prineas JW. Pathology of the Guillain-Barre syndrome. Ann.Neurol. 1981; 9 Suppl: 6-19.

Prinetti A, Chigorno V, Tettamanti G, Sonnino S. Sphingolipid-enriched membrane domains from rat cerebellar granule cells differentiated in culture. A compositional study. J.Biol.Chem. 2000; 275: 11658-11665.

Pritchard J, Hughes RA. Guillain-Barre syndrome. Lancet 2004; 363: 2186-2188.

Pukel CS, Lloyd KO, Travassos LR, Dippold WG, Oettgen HF, Old LJ. GD3, a prominent ganglioside of human melanoma. Detection and characterisation by mouse monoclonal antibody. J.Exp.Med. 1982; 155: 1133-1147.

Quattrini A, Corbo M, Dhaliwal SK *et al.* Anti-sulfatide antibodies in neurological disease: binding to rat dorsal root ganglia neurons. J.Neurol.Sci. 1992; 112: 152-159.

Rahmann H, Jonas U, Kappel T, Hilderbrandt H. Differential involvement of gangliosides versus phospholipids in the process of temperature adaptation in vertebrates. A comparative phenomenological and physicochemical study. Ann.N.Y.Acad.Sci. 1998; 845: 72-91.

Rajendran L, Masilamani M, Solomon S *et al.* Asymmetric localization of flotillins/reggies in preassembled platforms confers inherent polarity to hematopoietic cells. Proc.Natl.Acad.Sci.U.S.A 2003; 100: 8241-8246.

Ramirez OA, Gomez RA, Carrer HF. Gangliosides improve synaptic transmission in dentate gyrus of hippocampal rat slices. Brain Res. 1990; 506: 291-293.

Ranvier L, Traité technique d'histologie. 1 ed., Librairie F. Savy, Paris, 1875.

Raphael JC, Chevret S, Hughes RA, Annane D. Plasma exchange for Guillain-Barre syndrome. Cochrane.Database.Syst.Rev. 2001; CD001798.

Rasband MN, Trimmer JS, Schwarz TL *et al.* Potassium channel distribution, clustering, and function in remyelinating rat axons. J.Neurosci. 1998; 18: 36-47.

Ravi V, Taly AB, Shankar SK *et al.* Association of Japanese encephalitis virus infection with Guillain-Barre syndrome in endemic areas of south India. Acta Neurol.Scand. 1994; 90: 67-72.

Rees JH, Gregson NA, Hughes RA. Anti-ganglioside GM1 antibodies in Guillain-Barre syndrome and their relationship to Campylobacter jejuni infection. Ann.Neurol. 1995; 38: 809-816.

Rieger F, Daniloff JK, Pincon-Raymond M, Crossin KL, Grumet M, Edelman GM Neuronal cell adhesion molecules and cytotactin are colocalized at the node of Ranvier. J Cell Biol 1986;103: 379-391

Resh MD. Fatty acylation of proteins: new insights into membrane targeting of myristoylated and palmitoylated proteins. Biochim.Biophys.Acta 1999; 1451: 1-16.

Rhodes KM, Tattersfield AE. Guillain-Barre syndrome associated with Campylobacter infection. Br.Med.J.(Clin.Res.Ed) 1982; 285: 173-174.

Riboni L, Viani P, Bassi R, Prinetti A, Tettamanti G. The role of sphingolipids in the process of signal transduction. Prog.Lipid Res. 1997; 36: 153-195.

Rieger F, Daniloff JK, Pincon-Raymond M, Crossin KL, Grumet M, Edelman GM. Neuronal cell adhesion molecules and cytotactin are colocalized at the node of Ranvier. J.Cell Biol. 1986; 103: 379-391.

Riggott MJ, Matthew WD. Neurite outgrowth is enhanced by anti-idiotypic monoclonal antibodies to the ganglioside GM1. Exp.Neurol. 1997; 145: 278-287.

Ritchie JM, Rogart RB. The binding of saxitoxin and tetrodotoxin to excitable tissue. Rev.Physiol Biochem.Pharmacol. 1977; 79: 1-50.

Robertson JD. Structural alterations in nerve fibers produced by hypotonic and hypertonic solutions. J.Biophys.Biochem.Cytol. 1958; 4: 349-364.

Robertson JD, Preliminary Observations on the Ultrastructure of Nodes of Ranvier. Zeitschrift ffir Zellforschung 1959; 50, 553-560

Rochon D, Rousse I, Robitaille R. Synapse-glia interactions at the mammalian neuromuscular junction. J.Neurosci. 2001; 21: 3819-3829.

Rodriguez JA, Piddini E, Hasegawa T, Miyagi T, Dotti CG. Plasma membrane ganglioside sialidase regulates axonal growth and regeneration in hippocampal neurons in culture. J.Neurosci. 2001; 21: 8387-8395.

Roisen FJ, Spero DA, Held SJ, Yorke G, Bartfeld H. Ganglioside induced surface activity and neurite formation of Neuro-2a neuroblastoma cells. Adv.Exp.Med.Biol. 1984; 174: 499-511.

Roper J, Schwarz JR. Heterogeneous distribution of fast and slow potassium channels in myelinated rat nerve fibres. J.Physiol 1989; 416: 93-110.

Ropper AH, Wijdicks EF, Shahani BT. Electrodiagnostic abnormalities in 113 consecutive patients with Guillain-Barre syndrome. Arch.Neurol. 1990; 47: 881-887.

Ropper AH. The Guillain-Barre syndrome. N.Engl.J.Med. 1992; 326: 1130-1136.

Ropper AH. Miller Fisher syndrome and other acute variants of Guillain-Barre-syndrome. Baillieres Clin.Neurol. 1994; 3: 95-106.

Rose NR, Bona C. Defining criteria for autoimmune diseases (Witebsky's postulates revisited). Immunol.Today 1993; 14: 426-430.

Rosenbluth J. A brief history of myelinated nerve fibers: one hundred and fifty years of controversy. J.Neurocytol. 1999; 28: 251-262.

Rothberg KG, Ying YS, Kamen BA, Anderson RG. Cholesterol controls the clustering of the glycophospholipid-anchored membrane receptor for 5-methyltetrahydrofolate. J.Cell Biol. 1990; 111: 2931-2938.

Rothberg KG, Heuser JE, Donzell WC, Ying YS, Glenney JR, Anderson RG. Caveolin, a protein component of caveolae membrane coats. Cell 1992; 68: 673-682.

Roux A, Cuvelier D, Nassoy P, Prost J, Bassereau P, Goud B. Role of curvature and phase transition in lipid sorting and fission of membrane tubules. EMBO J. 2005; 24: 1537-1545.

Roux S, Colasante C, Saint CC *et al.* Internalization of a GFP-tetanus toxin C-terminal fragment fusion protein at mature mouse neuromuscular junctions. Mol.Cell Neurosci. 2005; 30: 79-89.

Rusnati M, Tanghetti E, Urbinati C *et al.* Interaction of fibroblast growth factor-2 (FGF-2) with free gangliosides: biochemical characterization and biological consequences in endothelial cell cultures. Mol.Biol.Cell 1999; 10: 313-327.

Rusnati M, Urbinati C, Tanghetti E, Dell'Era P, Lortat-Jacob H, Presta M. Cell membrane GM1 ganglioside is a functional coreceptor for fibroblast growth factor 2. Proc.Natl.Acad.Sci.U.S.A 2002; 99: 4367-4372.

Ryberg B. Multiple specificities of antibrain antibodies in multiple sclerosis and chronic myelopathy. J.Neurol.Sci. 1978; 38: 357-382.

Sabharanjak S, Sharma P, Parton RG, Mayor S. GPI-anchored proteins are delivered to recycling endosomes via a distinct cdc42-regulated, clathrin-independent pinocytic pathway. Dev.Cell 2002; 2: 411-423.

Sadatipour BT, Greer JM, Pender MP. Increased circulating antiganglioside antibodies in primary and secondary progressive multiple sclerosis. Ann Neurol 1998; 44: 980-983

Sadiq SA, Thomas FP, Kilidireas K *et al.* The spectrum of neurologic disease associated with anti-GM1 antibodies. Neurology 1990; 40: 1067-1072.

Saegusa C, Fukuda M, Mikoshiba K. Synaptotagmin V is targeted to dense-core vesicles that undergo calcium-dependent exocytosis in PC12 cells. J.Biol.Chem. 2002; 277: 24499-24505.

Saida K, Saida T, Brown MJ, Silberberg DH, Asbury AK. Antiserum-mediated demyelination in vivo: a sequential study using intraneural injection of experimental allergic neuritis serum. Lab Invest 1978; 39: 449-462.

Saida K, Saida T, Brown MJ, Silberberg DH. In vivo demyelination induced by intraneural injection of anti-galactocerebroside serum: a morphologic study. Am.J.Pathol. 1979; 95: 99-116.

Saida T, Saida K, Brown MJ, Silberberg DH. Peripheral nerve demyelination induced by intraneural injection of experimental allergic encephalomyelitis serum. J.Neuropathol.Exp.Neurol. 1979; 38: 498-518.

Saida T, Saida K, Silberberg DH, Brown MJ. Experimental allergic neuritis induced by galactocerebroside. Ann.Neurol. 1981; 9 Suppl: 87-101.

Saito F, Masaki T, Kamakura K *et al.* Characterization of the transmembrane molecular architecture of the dystroglycan complex in schwann cells. J.Biol.Chem. 1999; 274: 8240-8246.

Salazar-Grueso EF, Routbort MJ, Martin J, Dawson G, Roos RP. Polyclonal IgM anti-GM1 ganglioside antibody in patients with motor neuron disease and variants. Ann.Neurol. 1990; 27: 558-563.

Santoro M, Uncini A, Corbo M *et al.* Experimental conduction block induced by serum from a patient with anti-GM1 antibodies. Ann.Neurol. 1992; 31: 385-390.

Schade AE, Levine AD. Lipid raft heterogeneity in human peripheral blood T lymphoblasts: a mechanism for regulating the initiation of TCR signal transduction. J.Immunol. 2002; 168: 2233-2239.

Scherer SS, Xu T, Crino P, Arroyo EJ, Gutmann DH. Ezrin, radixin, and moesin are components of Schwann cell microvilli. J.Neurosci.Res. 2001; 65: 150-164.

Schmidt HD On the construction of the dark or double-bordered nerve fibre. Monogr Microsc J 1874; 11:200–221

Schnaar RL, Longo P, Yang LJ, Tai T. Distinctive ganglioside patterns revealed by anti-ganglioside antibody binding to differentiating CG-4 oligodendrocytes. Glycobiology 1996; 6: 257-263.

Schon A, Freire E. Thermodynamics of intersubunit interactions in cholera toxin upon binding to the oligosaccharide portion of its cell surface receptor, ganglioside GM1. Biochemistry 1989; 28: 5019-5024.

Schroder JM, Himmelmann F. Fine structural evaluation of altered Schmidt-Lanterman incisures in human sural nerve biopsies. Acta Neuropathol.(Berl) 1992; 83: 120-133.

Schroeder R, London E, Brown D. Interactions between saturated acyl chains confer detergent resistance on lipids and glycosylphosphatidylinositol (GPI)-anchored proteins: GPI-anchored proteins in liposomes and cells show similar behavior. Proc.Natl.Acad.Sci.U.S.A 1994; 91: 12130-12134.

Schwarz A, Futerman AH. Determination of the localization of gangliosides using anti-ganglioside antibodies: comparison of fixation methods. J.Histochem.Cytochem. 1997; 45: 611-618.

Sekar RB, Periasamy A. Fluorescence resonance energy transfer (FRET) microscopy imaging of live cell protein localizations. J.Cell Biol. 2003; 160: 629-633.

Seyfried TN, el Abbadi M, Ecsedy JA, Bai HW, Yohe HC. Influence of host cell infiltration on the glycolipid content of mouse brain tumors. J.Neurochem. 1996; 66: 2026-2033.

Sharom,F.J. and Grant,C.W. Glycosphingolipids in membrane architecture. J. Supramol. Struct. 1977 ; 6, 249-258.

Sheets ED, Lee GM, Simson R, Jacobson K. Transient confinement of a glycosylphosphatidylinositol-anchored protein in the plasma membrane. Biochemistry 1997; 36: 12449-12458.

Sheikh KA, Sun J, Liu Y *et al.* Mice lacking complex gangliosides develop Wallerian degeneration and myelination defects. Proc.Natl.Acad.Sci.U.S.A 1999; 96: 7532-7537.

Sheikh KA, Deerinck TJ, Ellisman MH, Griffin JW. The distribution of ganglioside-like moieties in peripheral nerves. Brain 1999; 122 (Pt 3): 449-460.

Shogomori H, Brown DA. Use of detergents to study membrane rafts: the good, the bad, and the ugly. Biol.Chem. 2003; 384: 1259-1263.

Shrager P. Sodium channels in single demyelinated mammalian axons. Brain Res. 1989; 483: 149-154.

Shy ME, Evans VA, Lublin FD *et al.* Antibodies to GM1 and GD1b in patients with motor neuron disease without plasma cell dyscrasia. Ann.Neurol. 1989; 25: 511-513.

Sieck GC, Fournier M, Enad JG. Fiber type composition of muscle units in the cat diaphragm. Neurosci.Lett. 1989; 97: 29-34.

Silverton EW, Navia MA, Davies DR. Three-dimensional structure of an intact human immunoglobulin. Proc.Natl.Acad.Sci.U.S.A 1977; 74: 5140-5144.

Sima AA. Diabetic neuropathy--the presence and future of a common but silent disorder. Mod.Pathol. 1993; 6: 399-401.

Simons K, Ikonen E. Functional rafts in cell membranes. Nature 1997; 387: 569-572.

Simpson MA, Cross H, Proukakis C *et al.* Infantile-onset symptomatic epilepsy syndrome caused by a homozygous loss-of-function mutation of GM3 synthase. Nat.Genet. 2004; 36: 1225-1229.

Simson R, Sheets ED, Jacobson K. Detection of temporary lateral confinement of membrane proteins using single-particle tracking analysis. Biophys.J. 1995; 69: 989-993.

Singer SJ, Nicolson GL. The fluid mosaic model of the structure of cell membranes. Science 1972; 175: 720-731.

Sinnecker D, Voigt P, Hellwig N, Schaefer M. Reversible photobleaching of enhanced green fluorescent proteins. Biochemistry 2005; 44: 7085-7094.

Skirrow MB. Campylobacter enteritis: a "new" disease. Br.Med.J. 1977; 2: 9-11.

Song KS, Sargiacomo M, Galbiati F, Parenti M, Lisanti MP. Targeting of a G alpha subunit (Gi1 alpha) and c-Src tyrosine kinase to caveolae membranes: clarifying the role of N-myristoylation. Cell Mol.Biol.(Noisy.-le-grand) 1997; 43: 293-303.

Sonnino S, Mauri L, Chigorno V, Prinetti A. Gangliosides as components of lipid membrane domains. Glycobiology 2007; 17: 1R-13R.

Sonnino S, Mauri L, Chigorno V, Prinetti A. Gangliosides as components of lipid membrane domains. Glycobiology 2007; 17: 1R-13R.

Sosinsky GE, Deerinck TJ, Greco R, Buitenhuys CH, Bartol TM, Ellisman MH. Development of a model for microphysiological simulations: small nodes of ranvier from peripheral nerves of mice reconstructed by electron tomography. Neuroinformatics. 2005; 3: 133-162.

Stoll G, Schmidt B, Jander S, Toyka KV, Hartung HP. Presence of the terminal complement complex (C5b-9) precedes myelin degradation in immune-mediated demyelination of the rat peripheral nervous system. Ann.Neurol. 1991; 30: 147-155.

Strigard K, Olsson T, Larsson P, Holmdahl R, Klareskog L. Modulation of experimental allergic neuritis in rats by in vivo treatment with monoclonal anti T cell antibodies. J.Neurol.Sci. 1988; 83: 283-291.

Stuart LM, Ezekowitz RA. Phagocytosis: elegant complexity. Immunity. 2005; 22: 539-550.

Sugimoto H, Wakata N, Kishi M *et al.* A case of Guillain-Barre syndrome associated with cerebellar ataxia and positive serum anti-GD1b IgG antibody. J.Neurol. 2002; 249: 346-347.

Sumner AJ, Saida K, Saida T, Silberberg DH, Asbury AK. Acute conduction block associated with experimental antiserum-mediated demyelination of peripheral nerve. Ann.Neurol. 1982; 11: 469-477.

Susuki K, Nishimoto Y, Yamada M *et al.* Acute motor axonal neuropathy rabbit model: immune attack on nerve root axons. Ann.Neurol. 2003; 54: 383-388.

Susuki K, Rasband MN, Tohyama K *et al.* Anti-GM1 antibodies cause complement-mediated disruption of sodium channel clusters in peripheral motor nerve fibers. J.Neurosci. 2007; 27: 3956-3967.

Svennerholm L. Composition of gangliosides from human brain. Nature 1956; 177: 524-525.

Svennerholm L, RAAL A. Composition of brain ganglio-sides. Biochim.Biophys.Acta 1961; 53: 422-424.

Svennerholm L. Chromatographic separation of human brain gangliosides. J.Neurochem. 1963; 10: 613-623.

Svennerholm L. Designation and schematic structure of gangliosides and allied glycosphingolipids. Prog.Brain Res. 1994; 101: XI-XIV.

Szymanska I, Ramwani J, Eylar EH. The passive transfer of severe allergic neuritis in Lewis rats with lymphoid cells preincubated with P2 protein. Cell Immunol. 1983; 82: 422-425.

Takamiya K, Yamamoto A, Furukawa K *et al.* Mice with disrupted GM2/GD2 synthase gene lack complex gangliosides but exhibit only subtle defects in their nervous system. Proc.Natl.Acad.Sci.U.S.A 1996; 93: 10662-10667.

Takigawa T, Yasuda H, Kikkawa R, Shigeta Y, Saida T, Kitasato H. Antibodies against GM1 ganglioside affect K+ and Na+ currents in isolated rat myelinated nerve fibers. Ann.Neurol. 1995; 37: 436-442.

Tanaka Y, Waki H, Kon K, Ando S. Gangliosides enhance KCl-induced Ca2+ influx and acetylcholine release in brain synaptosomes. Neuroreport 1997; 8: 2203-2207.

Tansey FA, Brosnan CF. Protection against experimental allergic neuritis with silica quartz dust. J.Neuroimmunol. 1982; 3: 169-179.

Tatum AH. Experimental paraprotein neuropathy, demyelination by passive transfer of human IgM anti-myelin-associated glycoprotein. Ann.Neurol. 1993; 33: 502-506.

Taylor CM, Coetzee T, Pfeiffer SE. Detergent-insoluble glycosphingolipid/cholesterol microdomains of the myelin membrane. J.Neurochem. 2002; 81: 993-1004.

Terryberry J, Sutjita M, Shoenfeld Y *et al.* Myelin- and microbe-specific antibodies in Guillain-Barre syndrome. J.Clin.Lab Anal. 1995; 9: 308-319.

Tettamanti G. Ganglioside/glycosphingolipid turnover: new concepts. Glycoconj.J. 2004; 20: 301-317.

Thomas FP, Trojaborg W, Nagy C *et al.* Experimental autoimmune neuropathy with anti-GM1 antibodies and immunoglobulin deposits at the nodes of Ranvier. Acta Neuropathol.(Berl) 1991; 82: 378-383.

Thomas PD, Brewer GJ. Gangliosides and synaptic transmission. Biochim.Biophys.Acta 1990; 1031: 277-289.

Thomas R, Patenaude SI, MacKenzie CR *et al.* Structure of an anti-blood group A Fv and improvement of its binding affinity without loss of specificity. J.Biol.Chem. 2002; 277: 2059-2064.

Townson K, Boffey J, Nicholl D, Veitch J, Bundle D, Zhang P, Samain E *et al.* Solid phase immunoadsorption for therapeutic and analytical studies on neuropathy-associated anti-GM1 antibodies. Glycobiology 2007 a); 17(3): 294-303

Townson K., Greenshields K., Veitch J., Nicholl D., Eckhardt M., Galanina O., Bovin N., Samain E., Antoine T., Bundle D., Zhang P., Ling C.C., and Willison H.J. Sulfatide binding properties of murine and human anti-ganglioside antibodies. Glycobiology 2007 b), ahead of publication.

Trojaborg W, Hays AP, van den BL, Younger DS, Latov N. Motor conduction parameters in neuropathies associated with anti-MAG antibodies and other types of demyelinating and axonal neuropathies. Muscle Nerve 1995; 18: 730-735.

Trowbridge HO, Emiling RC, Inflammation: A review of the process, 5th edition, Quintessence publishing co, inc, Chicago, IL, 1997

Tsuji S, Yamashita T, Tanaka M, Nagai Y. Synthetic sialyl compounds as well as natural gangliosides induce neuritogenesis in a mouse neuroblastoma cell line (Neuro2a). J.Neurochem. 1988; 50: 414-423.

Turnberg D, Botto M. The regulation of the complement system: insights from genetically-engineered mice. Mol.Immunol. 2003; 40: 145-153.

Turnbull WB, Precious BL, Homans SW. Dissecting the cholera toxin-ganglioside GM1 interaction by isothermal titration calorimetry. J.Am.Chem.Soc. 2004; 126: 1047-1054.

Urmacher C, Cordon-Cardo C, Houghton AN. Tissue distribution of GD3 ganglioside detected by mouse monoclonal antibody R24. Am.J.Dermatopathol. 1989; 11: 577-581.

Vabnick I, Trimmer JS, Schwarz TL, Levinson SR, Risal D, Shrager P. Dynamic potassium channel distributions during axonal development prevent aberrant firing patterns. J.Neurosci. 1999; 19: 747-758.

Vajsar J, Taylor MJ, MacMillan LJ, Murphy EG, Logan WJ. Somatosensory evoked potentials and nerve conduction studies in patients with Guillain-Barre syndrome. Brain Dev. 1992; 14: 315-318.

Vallat JM, Leboutet MJ, Jauberteau MO, Tabaraud F, Couratier P, Akani F. Widenings of the myelin lamellae in a typical Guillain-Barre syndrome. Muscle Nerve 1994; 17: 378-380.

van den Berg LH, Marrink J, de Jager AE *et al.* Anti-GM1 antibodies in patients with Guillain-Barre syndrome. J.Neurol.Neurosurg.Psychiatry 1992; 55: 8-11.

van den Berg LH, Lankamp CL, de Jager AE *et al.* Anti-sulphatide antibodies in peripheral neuropathy. J.Neurol.Neurosurg.Psychiatry 1993; 56: 1164-1168.

van Sorge NM, van den Berg LH, Geleijns K *et al* . Anti-GM1 IgG antibodies induce leukocyte effector functions via Fcgamma receptors. Ann.Neurol. 2003; 53: 570-579.

Visser LH, Schmitz PI, Meulstee J, van Doorn PA, van der Meche FG. Prognostic factors of Guillain-Barre syndrome after intravenous immunoglobulin or plasma exchange. Dutch Guillain-Barre Study Group. Neurology 1999; 53: 598-604.

Voet D, Voet JG. Lipid metabolism. In: Voet D, Voet JG, editors. Biochemistry. New York: John Wiley & Sons, Inc, 1995; 622-726

Vorup-Jensen T, Petersen SV, Hansen AG *et al.* Distinct pathways of mannan-binding lectin (MBL)- and C1-complex autoactivation revealed by reconstitution of MBL with recombinant MBL-associated serine protease-2. J.Immunol. 2000; 165: 2093-2100.

Vriesendorp FJ, Mishu B, Blaser MJ, Koski CL. Serum antibodies to GM1, GD1b, peripheral nerve myelin, and Campylobacter jejuni in patients with Guillain-Barre syndrome and controls: correlation and prognosis. Ann.Neurol. 1993; 34: 130-135.

Vyas AA, Patel HV, Fromholt SE *et al.* Gangliosides are functional nerve cell ligands for myelin-associated glycoprotein (MAG), an inhibitor of nerve regeneration. Proc.Natl.Acad.Sci.U.S.A 2002; 99: 8412-8417.

Waksman BH, Adams RD. Allergic neuritis: an experimental disease of rabbits induced by the injection of peripheral nervous tissue and adjuvants. J.Exp.Med. 1955; 102: 213-236.

Walsh FS, Cronin M, Koblar S *et al.* Association between glycoconjugate antibodies and Campylobacter infection in patients with Guillain-Barre syndrome. J.Neuroimmunol. 1991; 34: 43-51.

Wang H, Kunkel DD, Martin TM, Schwartzkroin PA, Tempel BL. Heteromultimeric K+ channels in terminal and juxtaparanodal regions of neurons. Nature 1993; 365: 75-79.

Wardrop J, Lancet, 1834.

Waugh MG, Lawson D, Hsuan JJ. Epidermal growth factor receptor activation is localized within low-buoyant density, non-caveolar membrane domains. Biochem.J. 1999; 337 (Pt 3): 591-597.

Weber F, Rudel R, Aulkemeyer P, Brinkmeier H. Anti-GM1 antibodies can block neuronal voltage-gated sodium channels. Muscle Nerve 2000; 23: 1414-1420.

Webster HF. The relationship between Schmidt-Lantermann incisures and myelin segmentation during Wallerian degeneration. Ann.N.Y.Acad.Sci. 1965; 122: 29-38.

Weis J, Fine SM, David C, Savarirayan S, Sanes JR. Integration site-dependent expression of a transgene reveals specialized features of cells associated with neuromuscular junctions. J.Cell Biol. 1991; 113: 1385-1397.

Weis WI. Cell-surface carbohydrate recognition by animal and viral lectins. Curr.Opin.Struct.Biol. 1997; 7: 624-630.

Weiss PA, Mayr R. Neuronal organelles in neuroplasmic ("axonal") flow. II. Neurotubules. Acta Neuropathol.(Berl) 1971; 5: Suppl-20.

Weng NP, Yu-Lee LY, Sanz I, Patten BM, Marcus DM. Structure and specificities of anti-ganglioside autoantibodies associated with motor neuropathies. J.Immunol. 1992; 149: 2518-2529.

Wessig C, Buchwald B, Toyka KV, Martini R. Miller Fisher syndrome: immunofluorescence and immunoelectron microscopic localization of IgG at the mouse neuromuscular junction. Acta Neuropathol.(Berl) 2001; 101: 239-244.

Wewetzer K, Verdu E, Angelov DN, Navarro X. Olfactory ensheathing glia and Schwann cells: two of a kind? Cell Tissue Res. 2002; 309: 337-345.

Wewetzer K, Kern N, Ebel C, Radtke C, Brandes G. Phagocytosis of O4+ axonal fragments in vitro by p75- neonatal rat olfactory ensheathing cells. Glia 2005; 49: 577-587.

Whitaker JN. The protein antigens of peripheral nerve myelin. Ann.Neurol. 1981; 9 Suppl: 56-64.

Wicklein EM, Pfeiffer G, Yuki N, Hartard C, Kunze K. Prominent sensory ataxia in Guillain-Barre syndrome associated with IgG anti-GD1b antibody. J.Neurol.Sci. 1997; 151: 227-229.

Wieraszko A, Seifert W. The role of monosialoganglioside GM1 in the synaptic plasticity: in vitro study on rat hippocampal slices. Brain Res. 1985; 345: 159-164.

Williams PL, Hall SM. Chronic Wallerian degeneration--an in vivo and ultrastructural study. J.Anat. 1971; 109: 487-503.

Willison HJ, Kennedy PG. Gangliosides and bacterial toxins in Guillain-Barre syndrome. J.Neuroimmunol. 1993; 46: 105-112.

Willison HJ, Veitch J. Immunoglobulin subclass distribution and binding characteristics of anti-GQ1b antibodies in Miller Fisher syndrome. J.Neuroimmunol. 1994; 50: 159-165.

Willison HJ, O'Hanlon GM, Paterson G *et al.* A somatically mutated human antiganglioside IgM antibody that induces experimental neuropathy in mice is encoded by the variable region heavy chain gene, V1-18. J.Clin.Invest 1996; 97: 1155-1164.

Willison HJ, O'Hanlon GM. The immunopathogenesis of Miller Fisher syndrome. J.Neuroimmunol. 1999; 100: 3-12.

Willison HJ. Ganglioside complexes: new autoantibody targets in Guillain-Barre syndromes. Nat.Clin.Pract.Neurol. 2005; 1: 2-3.

Wilson IA, Stanfield RL. A Trojan horse with a sweet tooth. Nat.Struct.Biol. 1995; 2: 433-436.

Winer JB, Hughes RA, Osmond C. A prospective study of acute idiopathic neuropathy. I. Clinical features and their prognostic value. J.Neurol.Neurosurg.Psychiatry 1988; 51: 605-612.

Winer JB, Hughes RA, Anderson MJ, Jones DM, Kangro H, Watkins RP. A prospective study of acute idiopathic neuropathy. II. Antecedent events. J.Neurol.Neurosurg.Psychiatry 1988; 51: 613-618.

Winner SJ, Evans JG. Guillain-Barre syndrome in Oxfordshire: clinical features in relation to age. Age Ageing 1993; 22: 164-170.

Witebsky, E., Rose, N. R., Terplan, K., Paine, J. R. & Egan, R. W. J. Amer. med. Ass. 1957; 164, 1439.

Wood SJ, Slater CR. Safety factor at the neuromuscular junction. Prog.Neurobiol. 2001; 64: 393-429.

Wu G, Xie X, Lu ZH, Ledeen RW. Cerebellar neurons lacking complex gangliosides degenerate in the presence of depolarizing levels of potassium. Proc.Natl.Acad.Sci.U.S.A 2001; 98: 307-312.

Xia Z, Liu Y. Reliable and global measurement of fluorescence resonance energy transfer using fluorescence microscopes. Biophys.J. 2001; 81: 2395-2402.

Yamakawa T, Nagai Y. . Glycolipids at the cell surface and their biological functions. Trends Inter.Biol. Sci.1978; 3: 128- 131.

Yamashita T, Hashiramoto A, Haluzik M *et al.* Enhanced insulin sensitivity in mice lacking ganglioside GM3. Proc.Natl.Acad.Sci.U.S.A 2003; 100: 3445-3449.

Yang JF, Cao G, Koirala S, Reddy LV, Ko CP. Schwann cells express active agrin and enhance aggregation of acetylcholine receptors on muscle fibers. J.Neurosci. 2001; 21: 9572-9584.

Yang LJ, Lorenzini I, Vajn K, Mountney A, Schramm LP, Schnaar RL. Sialidase enhances spinal axon outgrowth in vivo. Proc.Natl.Acad.Sci.U.S.A 2006; 103: 11057-11062.

J. Z. Young, 'Surface tension and the degeneration of nerve fibres', Nature, Lond., 1944, 154: 521-522.

Yu J, Fischman DA, Steck TL. Selective solubilization of proteins and phospholipids from red blood cell membranes by nonionic detergents. J.Supramol.Struct. 1973; 1: 233-248.

Yu RK, Usuki S, Ariga T. Ganglioside molecular mimicry and its pathological roles in Guillain-Barre syndrome and related diseases. Infect.Immun. 2006; 74: 6517-6527.

Yuan C, Johnston LJ. Atomic force microscopy studies of ganglioside GM1 domains in phosphatidylcholine and phosphatidylcholine/cholesterol bilayers. Biophys.J. 2001; 81: 1059-1069.

Yuki N, Sato S, Miyatake T, Sugiyama K, Katagiri T, Sasaki H. Motoneuron-disease-like disorder after ganglioside therapy. Lancet 1991; 337: 1109-1110.

Yuki N, Taki T, Inagaki F *et al.* A bacterium lipopolysaccharide that elicits Guillain-Barre syndrome has a GM1 ganglioside-like structure. J.Exp.Med. 1993; 178: 1771-1775.

Yuki N, Sato S, Tsuji S, Ohsawa T, Miyatake T. Frequent presence of anti-GQ1b antibody in Fisher's syndrome. Neurology 1993; 43: 414-417.

Yuki N, Yamada M, Sato S *et al.* Association of IgG anti-GD1a antibody with severe Guillain-Barre syndrome. Muscle Nerve 1993; 16: 642-647.

Yuki N, Kuwabara S, Koga M, Hirata K. Acute motor axonal neuropathy and acute motor-sensory axonal neuropathy share a common immunological profile. J.Neurol.Sci. 1999; 168: 121-126.

Yuki N, Yamada M, Koga M *et al.* Animal model of axonal Guillain-Barre syndrome induced by sensitization with GM1 ganglioside. Ann.Neurol. 2001; 49: 712-720.

Yuki N, Susuki K, Koga M *et al.* Carbohydrate mimicry between human ganglioside GM1 and Campylobacter jejuni lipooligosaccharide causes Guillain-Barre syndrome. Proc.Natl.Acad.Sci.U.S.A 2004; 101: 11404-11409.

Zacharias DA, Violin JD, Newton AC, Tsien RY. Partitioning of lipid-modified monomeric GFPs into membrane microdomains of live cells. Science 2002; 296: 913-916.

Zhang G, Lopez PH, Li CY *et al*. Anti-ganglioside antibody-mediated neuronal cytotoxicity and its protection by intravenous immunoglobulin: implications for immune neuropathies. Brain 2004; 127: 1085-1100.

Zhang J, Pekosz A, Lamb RA. Influenza virus assembly and lipid raft microdomains: a role for the cytoplasmic tails of the spike glycoproteins. J.Virol. 2000; 74: 4634-4644.

Zielasek J, Jung S, Schmidt B, Ritter G, Hartung HP, Toyka K. Effects of ganglioside administration on experimental autoimmune neuritis induced by peripheral nerve myelin or P2-specific T cell lines. J.Neuroimmunol. 1993; 43: 103-111.

List Of Publications

Papers

Sulfatide binding properties of murine and human anti-ganglioside antibodies, Townson K, Greenshields K, Veitch J, Nicholl D, Eckhardt M, Galanina O, Bovin N, Samian E, Antoine T, Bundle D, Zhang P, Ling CC, Willison HJ, Glycobiology, Sept 2007 (Ahead of print)

Identity, developmental restriction and reactivity of extralaminar cells capping mouse neuromuscular junctions, Court FA, Gillingwater TH, Melrose S, Sherman DL, Greenshields K, Morton AJ, Willison HJ, Brophy PJ, Ribchester RR. Manuscript in preparation.

Abstract

C5 inhibition protect motor nerve terminals from membrane attack complex mediated injury in murine Miller Fisher syndrome. Halstead SK, Humphreys PD, Greenshields K, Zitman FMP, Plomp JJ, Rother RP, Willison HJ. Molecular Immunology 44, 2007, 3909-3994.

Glycobiology vol. 17 no. 11 pp. 1156–1166, 2007
doi: 10.1093/glycob/cwm095
Advance Access publication on September 13, 2007

Sulfatide binding properties of murine and human antiganglioside antibodies

Kate Townson[1,2], Kay N Greenshields[2], Jean Veitch[2], Dawn Nicholl[2], Matthias Eckhardt[3], Oxana Galanina[4], Nicolai Bovin[4], Eric Samain[5], Tatiana Antoine[5], David Bundle[6], Ping Zhang[6], Chang Chun Ling[6], and Hugh J Willison[2]

[2]Division of Clinical Neurosciences, Glasgow Biomedical Research Centre, University of Glasgow, G12 8TA Scotland; [3]Institute of Physiological Chemistry, University of Bonn, Nussallee 11, D-53115 Bonn, Germany; [4]Laboratory of Carbohydrate Chemistry, Shemyakin & Ovchinnikov Institute of Bioorganic Chemistry, Miklukho-Maklaya 16/10, 117997 Moscow, Russia; [5]CERMAV-CNRS, BP53, F-38041, GRENOBLE, Cedex 9, France; and [6]Department of Chemistry, University of Alberta, Edmonton, Alberta, Canada T6G 2G2

Received on May 10, 2007; revised on August 28, 2007; accepted on September 3, 2007

Antiganglioside antibodies form an important component of the innate and adaptive B cell repertoire, where they provide antimicrobial activity through binding encapsulated bacterial glycans. In an aberrant role, they target peripheral nerve gangliosides to induce autoimmune nerve injury. An important characteristic of antiganglioside antibodies is their ability to selectively recognize highly defined glycan structures. Since sialylated and sulfated glycans often share lectin recognition patterns, we here explored the possibility that certain antiganglioside antibodies might also bind 3-*O*-sulfo-β-D-galactosylceramide (sulfatide), an abundant constituent of plasma and peripheral nerve myelin, that could thereby influence any immunoregulatory or autoimmune properties. Out of 25 antiganglioside antibodies screened in solid phase assays, 20 also bound sulfatide (10^{-5} to 10^{-6} M range) in addition to their favored ganglioside glycan epitope ($\sim 10^{-7}$ M range). Solution inhibition studies demonstrated competition between ganglioside and sulfatide, indicating close proximity or sharing of the antigen binding variable region domain. Sulfatide and 3-*O*-sulfo-β-D-galactose were unique in having this property amongst a wide range of sulfated glycans screened, including 4- and 6-*O*-sulfo-β-D-galactose analogues. Antiganglioside antibody binding to 3-*O*-sulfo-β-D-galactose was highly dependent upon the spatial presentation of the ligand, being completely inhibited by conjugation to protein or polyacrylamide (PAA) matrices. Binding was also absent when sulfatide was incorporated into plasma membranes, including myelin, under conditions in which antibody binding to ganglioside was retained. These data demonstrate that sulfatide binding is a common property of antiganglioside antibodies that may provide functional insights into, and consequences for this component of the innate immune repertoire.

Keywords: antibody/ganglioside/neuropathy/sulfatide

[1]To whom correspondence should be addressed: Tel: +44-141-330-8388; Fax: +44-141-330-4297; e-mail: k.townson@clinmed.gla.ac.uk

Introduction

Sulfated glycolipids frequently act as ligands for a diverse range of human and microbial glycan binding proteins including CD1 restricted T cell receptors (De Libero and Mori 2005), selectins (Aruffo et al. 1991), chemokines (Sandhoff et al. 2005), laminins (Talts et al. 1999), and toxins (Rousset et al. 1998; Wang et al. 2006). In particular, a wide range of studies have shown that immunglobulins react with sulfatide (3-*O*-sulfo-β-D-galactosylceramide) in both normal and disease states (Fredman et al. 1991; Avila et al. 1993; Dabby et al. 2000; Ilyas et al. 2003; Lopate et al. 2005) and many sulfatide-binding antisera and monoclonal antibodies (mAbs) have been isolated and studied (Hakomori 1974; Fredman et al. 1988; Kirschning et al. 1997; Wang et al. 2006).

Sulfatides are widely distributed throughout mammalian tissues, including serum, and are particularly prevalent in both neuronal and myelin membranes within the nervous system (Ishizuka 1997). As such, they have long been considered potential targets for autoimmune neurological disease pathogenesis. This cause and effect relationship has been studied in many model systems without a clear consensus, at least in part due to the likely diversity of the different antisulfatide antibodies studied. Nevertheless, it seems clear that antisulfatide antibodies are able to induce pathophysiological changes in the nervous system under certain experimental conditions (Petratos and Gonzales 2000; Rosenbluth and Moon 2003; Rosenbluth et al. 2003; Kanter et al. 2006; Wang et al. 2006).

One intriguing feature of certain classes of sulfatide-reactive antibodies is that in addition to binding sulfatide, they may more promiscuously bind other structurally similar (Eurelings et al. 2001) or even dissimilar ligands (Aotsuka et al. 1992). Conversely, antibodies raised against, and apparently specific for, a particular class of antigens may also bind sulfatide (Merten et al. 2003). Certain proteins, notably C-type lectins that bind sialyl oligosaccharides also bind sulfated structures (Galustian et al. 1997, 2004), both of which present a negative charge, and sulfation can strongly influence the binding of lectins, including siglecs, to their sialyl-glycans (Campanero-Rhodes et al. 2006). Since gangliosides are also sialylated, we have here analyzed the sulfated glycan binding properties of human and mouse antiganglioside antibodies to determine whether any dual specificity exists that may potentially contribute to their functional or pathophysiological properties.

Results

Binding of antiganglioside antibodies to sulfatide

Twenty mouse and five human antiganglioside mAbs with diverse specificities for neuropathy-associated ganglioside targets including GM1, GD1a, GD1b, GD3, and GQ1b were assessed in ELISA for binding to sulfatide. At a concentration

Table I. Binding specificities of a panel of antiganglioside mAbs, showing the relative strength of binding to sulfatide

Species	MAb	Subclass	Specificity	Sulfatide binding
Mouse	CGG1	IgG2b	GD3(++)	++
	DG1	IgG2b	GM1(+++)	++
	DG2	IgG3	GM1(+++),GA1(+++),GD1b(++)	++
	EG1	IgG3	GQ1b(++++),GD3(++++)	+++
	EG3	IgG1	GQ1b(++)	−
	MOG3	IgG3	GD1b(+++)	−
	MOG16	IgG3	GT1b(+++),GD1a(++),GD1b(+)	+
	MOG30	IgG3	GQ1b(++)	−
	MOG32	IgG2b	GD1a(+++),GT1b(+++),GD1b(+),GM1(+)	+
	MOG34	IgG2b	GD1a(+++),GT1b(++),GQ1b(+),GD1b(+)	+++
	MOG35	IgG2b	GD1a(+++)	++
	R24	IgG3	GD3(++++),GQ1b(+++)	++
	TBG3	IgG3	GD1a(++++),GT1b(++++)	++
	CGM2	IgM	GD3(+++)	+++
	CGM3	IgM	GQ1b(+++),GD3(++)	++
	EM1	IgM	GD3(++++),GQ1b(++++),GT1b(+++),GD1b(+++)	++
	EM4	IgM	GD1a(++++),GQ1b(+++),GD3(++)	+
	EM9	IgM	GD1a(+++),GT1b(++),GQ1b(+)	+
	MOM1	IgM	GM1(++++),GA1(++++),GD1b(++)	−
	MOM3	IgM	GM1(++++),GD1b(++++),GA1(++)	++
Human	BR	IgM	GM1(++)	++
	DO1	IgM	GM1(++),GA1(++),GD1b(+)	+
	HA1	IgM	GD3(+++),GQ1b(++),GT1b(++)	−
	SM1	IgM	GM1(++)	+
	WO1	IgM	GM1(+++),GA1(+++),GD1b(++)	+

$- = OD_{490nm} < 0.1$; $+ = 0.1 \leq 0.5$; $++ = 0.5 \leq 1$; $+++ = 1 \leq 1.5$; $++++ = > 1.5$.

of 10 μg/mL, 20/25 mAbs bound sulfatide in ELISA (Table I). No correlation was observed between the ganglioside binding profile of a mAb and its ability or inability to also bind sulfatide. Binding profiles for six mouse mAbs – 3 IgGs and 3 IgMs – representative of different ganglioside specificities (TBG3, GD1a; EG1, GD3/GQ1b; DG2, GM1; EM4, GD1a; EM1, GQ1b/GD3; MOM3, GM1/GD1b) and human anti-GM1 mAbs (SM1, BR1, WO1) were also assessed by titration analyses (Figure 1 and 2) and exhibited the sigmoid shaped curves typically seen for antibody–antigen interactions. In order to determine and compare the affinities of the mAb–sulfatide interaction with the mAb–ganglioside interaction, surface plasmon resonance was conducted using Fab fragments derived from the three representative mouse IgG mAbs, TBG3, EG1, and DG2, and the data are shown in Figure 3. The K_Ds for TBG3 and GD1a (9.5×10^{-7} M) (Boffey et al. 2005) and DG2 and GA1 (3×10^{-7} M) (Townson et al. 2007) have been previously reported. Whereas affinities for the preferred ganglioside were in the 10^{-7} M range for these three antibodies, affinities for sulfatide were on average 1 to 2 log lower – in the 10^{-5} to 10^{-6} M range.

Dependence of antibody binding on the sulfate and its position in the galactose ring

We next determined whether the antibody–sulfatide interaction depended upon the presence of sulfate, and its position in the galactose ring. Firstly, we established that galactocerebroside did not bind these antiganglioside antibodies (data shown for mAbs DG2, EM1, and BR1 – Figure 4B, D and F, lane 2). Secondly, we observed that cleavage of the sulfate from 3-*O*-sulfo-β-D-galactosylceramide by mild acid hydrolysis abolished binding, shown here by thin layer chromatography (TLC) overlay (Figure 4B, D and F, lanes 3, 4) and also by ELISA (Figure 4C, E and G). Thirdly, we determined the requirement for the sulfate to be positioned at the third carbon of the galactose ring by comparing the binding of DG2 to 3-sulfated galactose and to galactose with substitutions in the 4 and 6 positions. In solution inhibition studies, 3-sulfated galactose (in the form of ozonolyzed 3-*O*-sulfo-β-D-galactosylceramide, (sulph-OS)) was an effective inhibitor of solid phase mAb–sulfatide interaction, whereas D-Galactose-4-*O*-sulfate (Gal-4-sulfate) and D-Galactose-6-*O*-sulfate (Gal-6-sulfate) had no inhibitory activity (Figure 5, top panels). These data thus demonstrate both dependence of antibody binding on the sulfate and its location on the third carbon, as is found on sulfatide.

Occupancy of overlapping antigen-binding sites for ganglioside and sulfatide

The binding studies described above did not address whether sulfatide and ganglioside occupy the same position in the antigen-combining site or whether they bind to separate and distinct regions of the antibody molecule. To address this, we conducted solution inhibition studies to identify any competition for binding sites between ganglioside and sulfatide. Either ganglioside (GM1, GD1a, and GD3 for DG2, TBG3, and EG1, respectively) or sulfatide were immobilized, and the competing oligosaccharides introduced in solution. All antibodies were inhibited from binding solid phase ganglioside by the presence of solution phase sulfatide, and vice-versa, indicating that the antigen binding sites were competitively overlapping. Effective inhibition was thus observed irrespective of whether ganglioside or sulfatide were in the solid or solution phases (Figure 5).

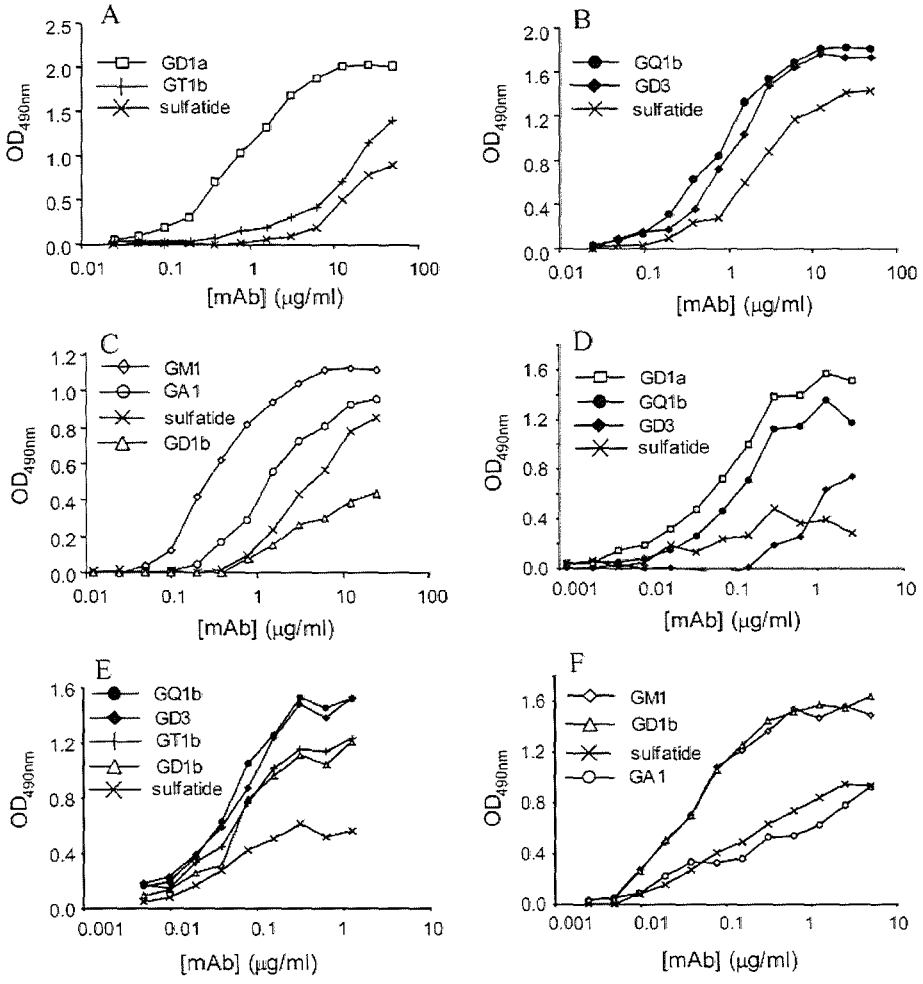

Fig. 1. ELISA titration curves of murine mAbs of different ganglioside specificities binding to their ganglioside and GA1 antigens and sulfatide. IgGs: (**A**) TBG3, (**B**) EG1, (**C**) DG2. IgMs: (**D**) EM4, (**E**) EM1, (**F**) MOM3.

Binding of antiganglioside mAbs to sulfated oligosaccharide conjugates

In order to investigate whether sulfatide recognition of these antiganglioside mAbs was specific for 3-sulfated galactose, or was actually a more promiscuous interaction with a range of sulfated oligosaccharides, we examined binding by ELISA of a selection of mAbs (CGG1, DG1, DG2, EG1, TBG3, MOG35, DO1, and BR1) to a panel of sulfated oligosaccharide–polyacrylamide (PAA) conjugates (Supplementary data, Table S). The only antibody–ligand pairing was DG2 and Galβ1-3GalNAcβ ($T_{\beta\beta}$), which is the terminal disaccharide of GM1, GA1, and GD1b. The other anti-GM1 mAbs require sialic acid for binding, except for DO1. The lack of binding of DO1 to $T_{\beta\beta}$ may be due to the more complex binding interactions of IgMs in comparison with IgGs. No binding was observed to any of the sulfated structures, including 3-*O*-Su-Galβ. It was therefore, not possible to establish the recognition patterns of the mAbs, as it appeared that the epitope may not have been presented on PAA in a way that could be recognized. Similarly, we observed that presentation of the epitope on bovine serum albumin (BSA) was also critical, as none of the sulfatide-binding mAbs were able to significantly bind 3-*O*-Su-Galβ-BSA (data not shown). Alternatively, this also raised the question as to whether the lipid component of sulfatide was necessary for binding.

Interaction of antiganglioside antibodies with sulfatide lacking one or both acyl chains

To examine in more detail the requirement for the lipid component of sulfatide for binding of these mAbs to the 3-*O*-Su-Galβ epitope, solution inhibition ELISAs were performed with sulph-OS, which lacks one acyl chain, and enzymatically cleaved sulfatide (ceramide glycanase treated 3-*O*-sulfo-β-D-galactosylceramide (sulph-CG)), which has both acyl chains removed. Binding of DG2 to solid phase GM1 and sulfatide was measured after mixing with the soluble sulfatide variants. DG2 interacted with both sulph-OS and sulph-CG, inhibiting binding to GM1 and sulfatide (Figure 6). Although not essential for binding, inhibition was greater when one of the acyl chains was present. This was most striking with GM1

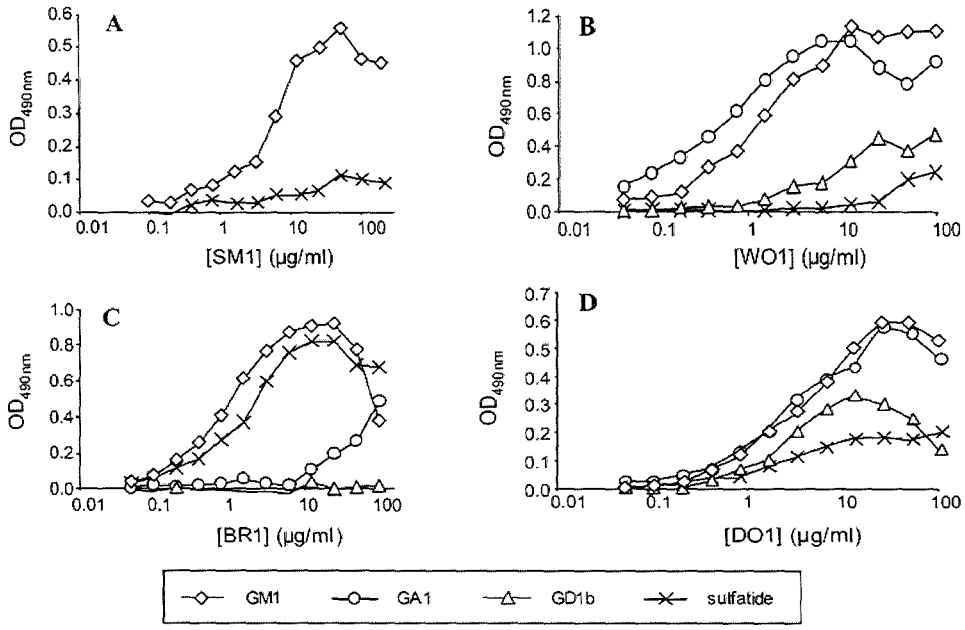

Fig. 2. ELISA titration curves of human mAbs, showing the relative binding to gangliosides, GA1, and sulfatide. (**A**) SM1, (**B**) WO1, (**C**) BR1, (**D**) DO1.

binding – 100% inhibition at 1 mM compared with 45% for sulph-CG.

Binding of antiganglioside antibodies to sulfatide in biological membranes

The binding of mAbs to sulfatide liposomes observed during the Biacore affinity measurements showed that antiganglioside mAbs are able to bind sulfatide effectively when incorporated into a membrane environment as well as when immobilized in pure form on ELISA polystyrene plates. We then determined whether antiganglioside mAbs were able to bind sulfatide in a more biologically relevant neural membrane environment. To achieve this, PC12 cells that do not naturally contain sulfatide (at least in the clone used for this study) were incubated with sulfatide, which become incorporated into the plasma membrane, and then GM1 epitopes on the cells were blocked by incubating with cholera toxin B subunit (CTB). The cells were then assessed for antiganglioside mAb binding by immunofluorescence microscopy and by FACS. The widely used mouse

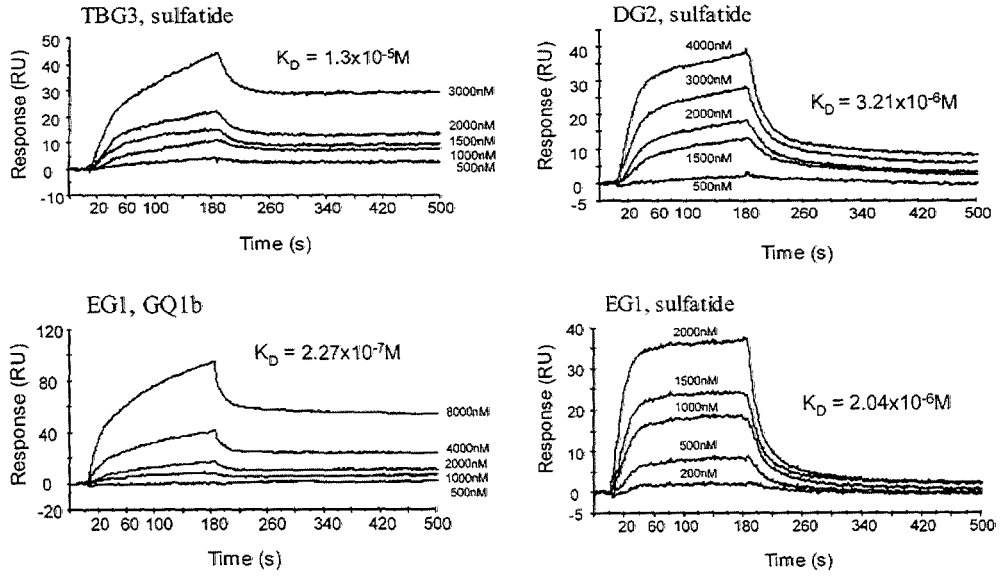

Fig. 3. Biacore sensorgrams of TBG3, DG2, and EG1 Fab fragments, at a series of concentrations, binding to immobilized sulfatide liposomes. EG1 Fab binding to GQ1b liposomes is also shown for comparison, whereas the binding of DG2 and TBG3 to ganglioside has been reported elsewhere. The K_D values for sulfatide binding were around 10-fold weaker than those for ganglioside binding.

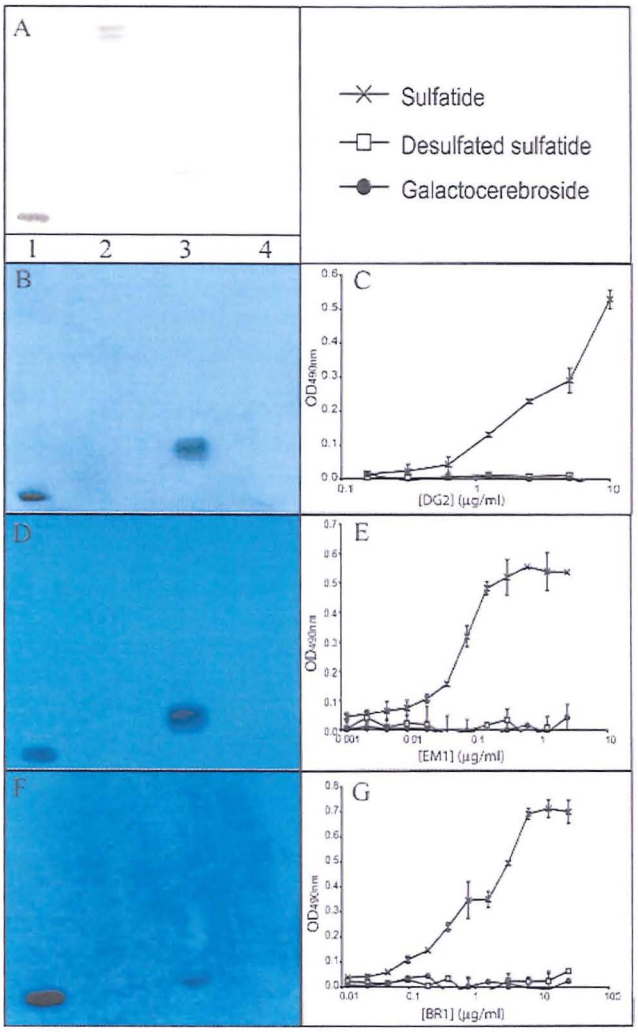

Fig. 4. Lack of binding of antiganglioside antibodies to sulfatide following mild acid hydrolysis to remove the sulfate group. GM1 or GD3 (lane 1), GalCer (lane 2), sulfatide (lane 3), and desulfated sulfatide (lane 4) were run on TLC and orcinol stained (**A**) TLC antibody overlays are also shown, alongside the corresponding ELISA binding curves: DG2 (**B** and **C**), EM1 (**D** and **E**), and BR1 (**F** and **G**). Error bars indicate SEM. Each of the mAbs binds sulfatide, but not GalCer or desulfated sulfatide.

IgM mAb, O4, which binds sulfatide in cells and tissues, was used as the indicator of membrane-associated sulfatide binding. EG3, which did not bind sulfatide in ELISA or Biacore, was used as a negative control mAb. PC12 cells incubated with sulfatide became primed to bind O4 (Figure 7, top panels, and Figure 8C), thereby demonstrating effective sulfatide incorporation into the plasma membrane. For antiganglioside antibody binding, PC12 cells remained negative or unchanged from baseline (Figure 7, lower panels, and Figure 8).

To address whether sulfatide-binding antiganglioside mAbs are able to bind sulfatide in peripheral nerve membranes, frozen sections from cerebroside sulfotransferase overexpressing, sulfatide accumulating (CST^{high}) and sulfatide deficient mice ($CGT^{-/-}$) were assessed for binding of O4, and the antiganglioside mAb, DG2, that binds both GM1 and sulfatide. As expected, O4 did not bind sulfatide deficient nerve, but bound sulfatide overexpressing nerve strongly (Figure 9, top panels). DG2 bound both sulfatide deficient and sulfatide overexpressing nerve strongly and equally well, by virtue of binding GM1 ganglioside (Figure 9, middle panels). When binding of DG2 to GM1 was blocked by preincubation of sections with CTB, DG2 binding was abolished in both sulfatide deficient and sulfatide overexpressing nerve sections (Figure 9, lower panels), indicating that DG2 cannot bind sulfatide in sulfatide rich nerve membranes. O4 staining intensity was unaffected by CTB preincubation, indicating that CTB is not masking sulfatide in nerve sections (not shown).

Discussion

These data demonstrate that a high proportion of both mouse and human antiganglioside antibodies used in this study are also able to bind sulfatide, independent of their specificity for the very highly defined glycan epitopes on the gangliosides or bacterial lipooligosaccharides against which they were raised and cloned. Thus antiganglioside antibodies that are specific for terminal Gal(β1-3)GalNAc disaccharides (e.g., DG2), terminal Neu5Ac(α2-3)Gal(β1-3)GalNAc trisaccharides (e.g., TBG3) or internal Neu5Ac(α2-8)Neu5Ac epitopes (e.g., EG1) may also bind 3-*O*-sulfo-β-D-galactosylceramide (i.e., sulfatide). The promiscuous binding of this class of antiglycan antibodies to sulfatide is therefore, not due to a general inability to discriminate between different glycan structures, as the ganglioside specificity is very discrete, and the sulfatide binding is entirely dependent on the sulfate being in the 3-position of the galactose. The antibodies may, however, be binding ganglioside and sulfatide at the same binding site, or at least at binding sites in close proximity, as binding to one ligand could inhibit binding to the other. Sulfatide binding is also not a universal feature of antiganglioside antibodies, since some antibodies of similar specificity to those identified above only bind sulfatide weakly or not at all, despite binding well to their ganglio-series glycan structure. We have previously shown that some antiganglioside antibodies are polyreactive, as defined by binding actin, thyroglobulin, tubulin or DNA (Boffey et al. 2004); however, this does not correlate closely with the ability to also bind sulfatide. For example, EG1 binds sulfatide strongly, but showed no binding to the above polyreactive antigens. By reviewing previously published mAb sequencing data, we have also examined the variable region gene usage of sulfatide binding antiganglioside antibodies in comparison with those that do not bind sulfatide and did not observe any distinctive patterns (data not shown).

It appears as though the interaction of these antiganglioside mAbs with sulfatide depends on the scaffold to which the monosaccharide is attached. Although the lipid moiety is not essential for binding, as mAbs interact well with sulph-CG that lacks this component, the presentation of the monosaccharide epitope in solid phase is important. This element of complexity is demonstrated by the lack of binding of the mAbs to 3-*O*-Su-Galβ presented on both PAA and BSA.

In general, the binding to sulfatide is at least a log lower affinity than binding to the dominant ganglioside glycan epitope, as assessed by both the affinity determinations in liposomal membranes using Biacore and the half-maximal binding data derived from ELISA. Nevertheless, this does not indicate insignificance of the sulfatide binding properties of these antibodies, since

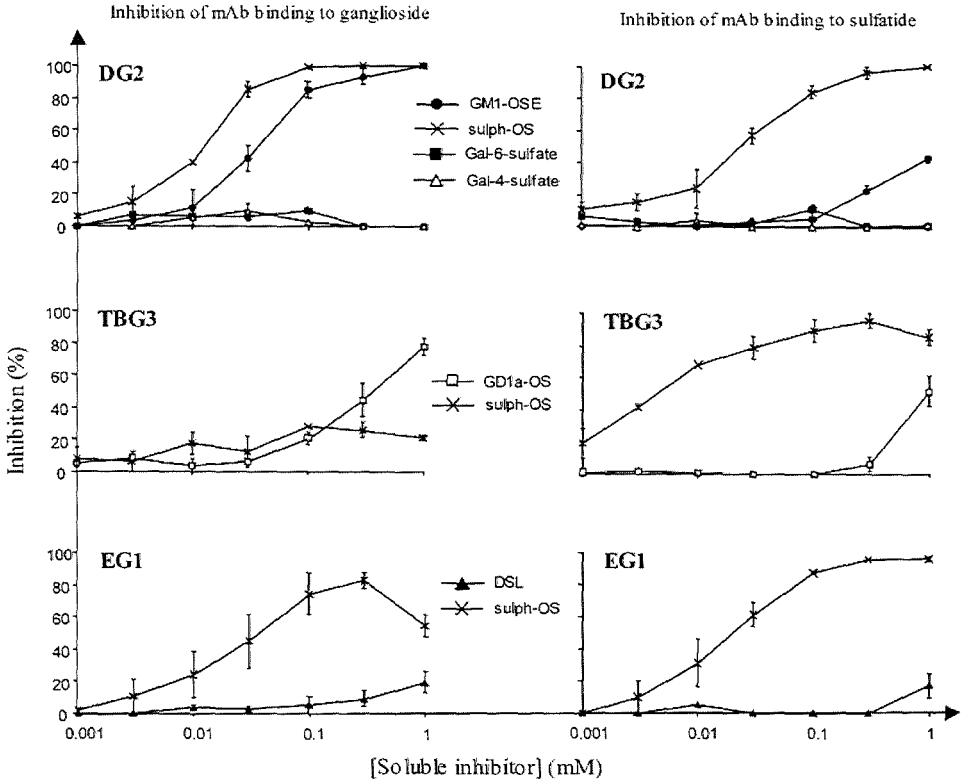

Fig. 5. Occupancy of overlapping binding sites for sulfatide and ganglioside was assessed by inhibition ELISA. MAbs were preincubated with soluble ganglioside oligosaccharide (EGM1-OS, GD1a-OS or DSL) or sulfatide monosaccharide (sulph-OS) and then binding to ganglioside and sulfatide was measured. Error bars show SEM from at least three repeats. Inhibition of binding indicated that ganglioside and sulfatide were sharing a common binding site. Gal-4-sulfate and Gal-6-sulfate were also tested with DG2. Inhibition was only achieved with the sulfate group at the third carbon position, indicating that the mAb-sulfatide interaction was specific for this saccharide.

at appropriate concentrations of sulfatide presented in the appropriate format (in micelles or a simple liposome membrane environment), interaction with sulfatide is observed.

The immunofluorescence evidence suggests that at least for the antiganglioside mAbs studied here, binding to sulfatide in normally organized myelin and neural membranes may be insignificant, and thus direct pathogenic effects of these antibody–sulfatide interactions are unlikely. Other antisulfatide antibodies, such as O4, that bind sulfatide in neural membranes may have the capability to drive direct pathogenic effects. However, there are other potentially important immunological, physiological or pathological actions for antibody–sulfatide interactions. Sulfatide is present in human plasma at a concentration of 0.6–0.7 nmol/mL and this concentration may vary in disease states (Buschard et al. 2005). In plasma, sulfatide may have antiatherosclerotic and anticoagulant activity (Kyogashima 2004) and it is possible that antisulfatide antibody might engage free or protein- bound circulating sulfatide and thereby modulate its biological effects. Antisulfatide antibodies may be able to bind the sulfatide saccharide presented by CD1 molecules and thereby modulate CD1-restricted sulfatide specific T cell interactions. Similarly, ganglioside and sulfatide binding B cell receptors may sense circulating sulfatide and thereby modulate B cell activation.

Apart from their association with disease states, many normal individuals have significant titres of "antisulfatide" antibodies. There is clearly considerable diversity amongst antisulfatide antibodies in terms of binding properties and functional effects, as demonstrated for modulation of insulin metabolism (Buschard et al. 2005). It is clear from this and other studies that these antibodies may have other more significant carbohydrate antigen recognition domains than sulfatide binding. Conversely, sulfatide reactivity could be viewed as a more general property of a wide range of carbohydrate binding antibodies and this characteristic may comprise a significant proportion of the innate antibody repertoire. The functional consequences of this are currently unknown. This study also demonstrates that identifying sulfatide reactivity in polyclonal sera, or in mAbs using solid phase assays, says little about sulfatide binding capacity in biological membranes. It also acts in a cautionary way to remind us that having identified sulfatide as a ligand for an antibody, this may represent one of the many possible ligands that could confound interpretation of subsequent studies unless it is identified. The advent of glycoarray screening would be one way through which such multiple ligand interactions could be easily identified.

Materials and methods

Purification and characterization of antiganglioside mAbs

Murine antiganglioside mAbs were cloned following immunization of HeN or GalNAc transferase knockout mice with

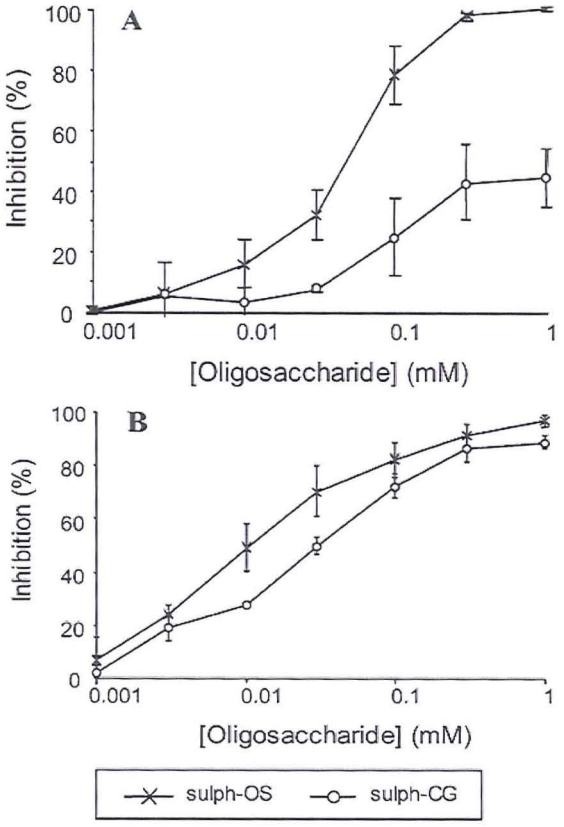

Fig. 6. Inhibition of binding of DG2 to GM1 (**A**) and sulfatide (**B**) by sulfatide that had been ozonolyzed, removing one acyl chain, or ceramide glycanase treated, to cleave both acyl chains of the lipid, was performed by soluble inhibition ELISA. DG2 bound less well, in solution, with its sulfated galactose epitope when both acyl chains were removed. Error bars indicate SEM.

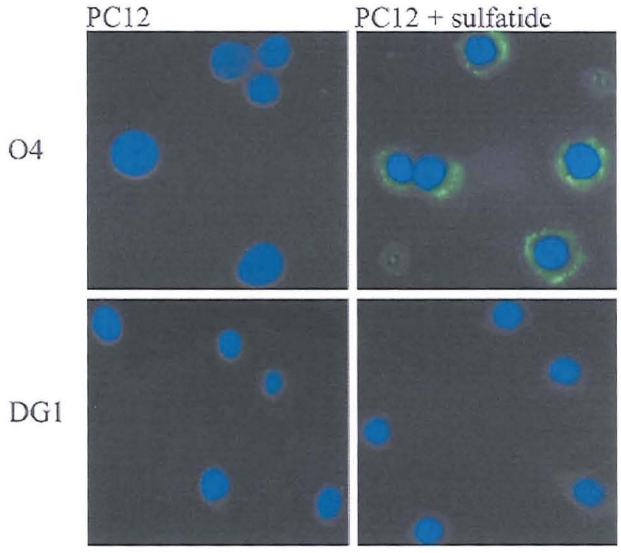

Fig. 7. Binding of mAbs to PC12 cells following incubation with exogenous sulfatide was measured using fluorescence microscopy with a FITC labeled anti-mouse IgG antibody. Cells incubated with O4 and DG1 mAbs, both before and after sulfatide incubation, are shown above. Any GM1 binding was blocked by CTB.

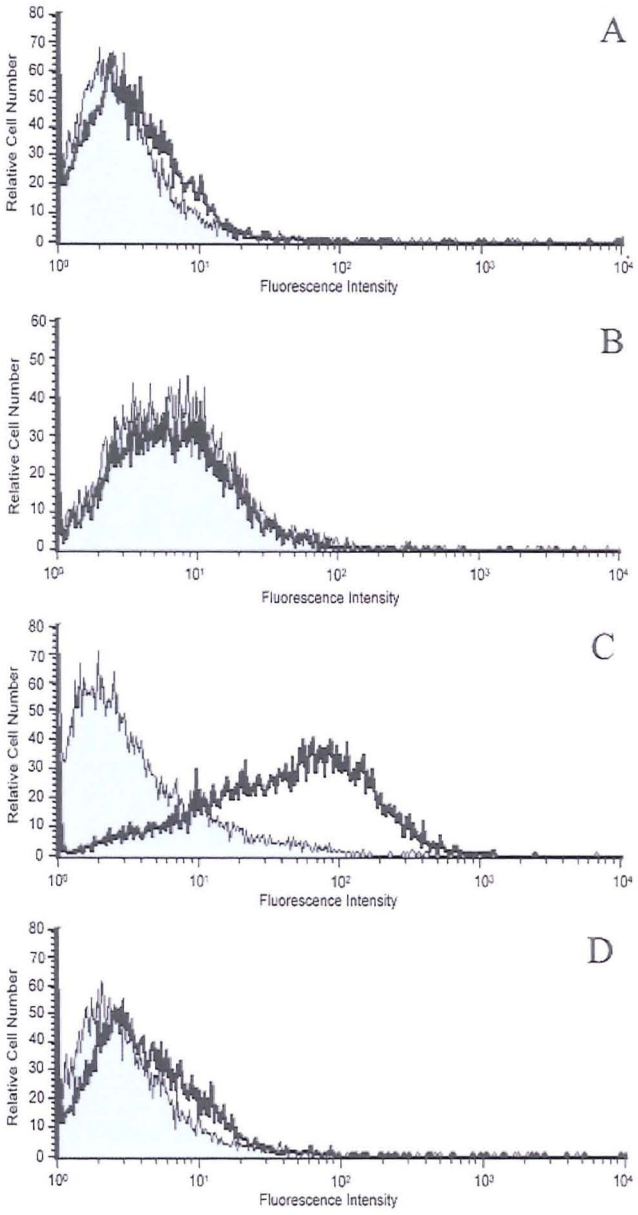

Fig. 8. Binding of mAbs to PC12 cells, before (shaded) and after sulfatide incorporation into the membrane, was analyzed by flow cytometry. No increase in binding of DG1 (**A**) and DG2 (**B**) to sulfatide-treated PC12s was observed. Binding of the antisulfatide mAb O4 (**C**), however, was clearly increased when sulfatide was incorporated into the membranes. A negative control sulfatide nonbinding mAb EG3 (**D**) was also analyzed. GM1 binding was blocked by CTB.

Campylobacter jejuni lipooligosaccharides or gangliosides in adjuvant as previously described (Goodyear et al. 1999; Bowes et al. 2002; Boffey et al. 2004, 2005). The anti-GD3 mAb, R24 (that also binds GQ1b) was obtained from American Type Culture Collection (Manassas, VA) (Dippold et al. 1980). Human mAbs were cloned from peripheral blood mononuclear cells isolated from patients with Guillian-Barré syndrome (DO1), multifocal motor neuropathy (WO1, BR1, and SM1) (Willison et al. 1994; Paterson et al. 1995; Goodyear et al. 1999) or ataxic

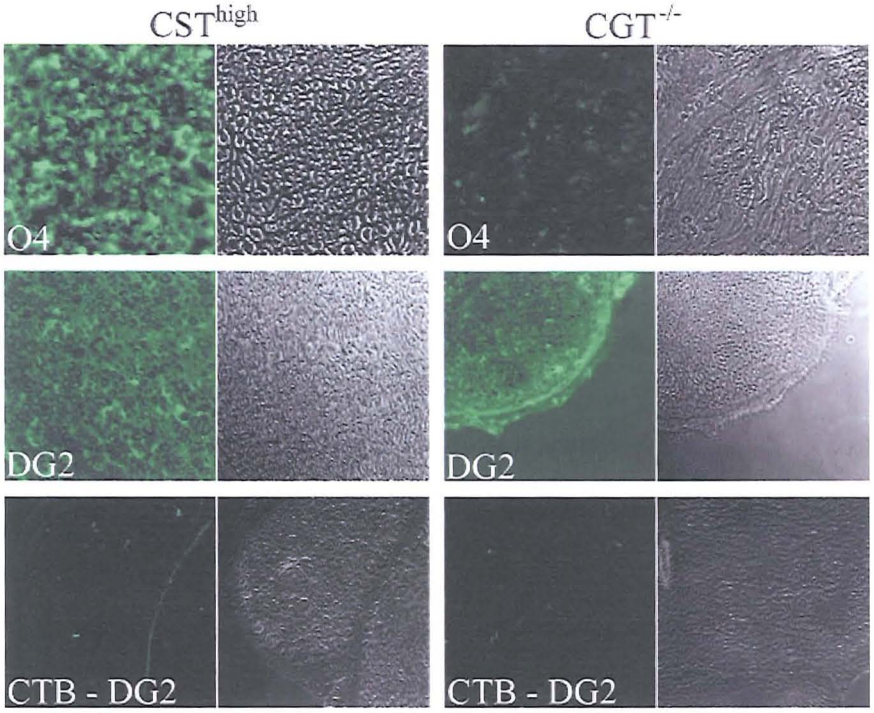

Fig. 9. Binding of mAbs DG2 and O4 to tissue from mice with upregulated (CST^{high}) and down-regulated ($CGT^{-/-}$) sulfatide levels. O4 binding was greatly increased in the CST^{high} tissue in comparison with $CGT^{-/-}$, whereas DG2 bound equally well to both. Blocking GM1 availability with cholera toxin virtually negated DG2 binding to both CST^{high} and $CGT^{-/-}$, suggesting that DG2 is unable to bind sulfatide (and GA1 and GD1b) in the tissue, despite the evidence of recognition from other binding assays.

neuropathy (HA1) (Willison et al. 1996). Murine IgGs were purified from tissue culture supernatants using HiTrap Protein A (IgG3) or Protein G (IgG1, IgG2b) affinity columns (Amersham Pharmacia Biotech, Buckinghamshire, UK). Human IgMs were purified by gel filtration using a Sepharose 6B column (Amersham Pharmacia Biotech).

Immunoassays and affinity determinations

Reactivity of mAbs with glycolipids was assessed by a standard ELISA using Immulon 2 microtitre plates (Dynatech Laboratories, Sussex, UK) coated with 200 ng of glycolipid per well and assays conducted at 4°C (Willison et al. 1999). Affinity analysis was performed on Fab fragments using surface plasmon resonance (Biacore 2000, Biacore AB, Uppsala, Sweden) as previously reported (Boffey et al. 2005). Briefly, ganglioside- or sulfatide-containing liposomes (0.2 mg/mL in phosphate buffered saline [PBS]) were prepared from 1,2-dimyristoyl-rac-glycero-3-phosphocholine (Calbiochem, Nottingham, UK) and ganglioside/sulfatide (Sigma, Poole, Dorset, UK) in a (w/w) ratio of 100:1, and resized to 50 nm. Approximately 5000 response units (RU) of liposomes were immobilized on an L1 pioneer sensor chip (Biacore AB) by injection at 2 μL/min. Fab fragments of Protein A/G purified mAbs were prepared by papain digestion (ImmunoPure Fab Preparation Kit, Pierce, Northumberland, UK) The liposome layer was regenerated with 100 mM NaOH. Measurements were carried out in PBS at 25°C. Kinetic analyses were performed using the BIA evaluation 3.1 package (Biacore AB).

Binding of antiganglioside mAb to desulfated sulfatide

The sulfate group of sulfatide was hydrolyzed using mild acid. Briefly, 5 mL of 50 mM HCl in methanol was incubated with 5 mg lyophilized sulfatide (Sigma) for 16 h at room temperature. Following this, 15 mL chloroform, 2.5 mL methanol, and 5.5 mL 0.2% Na_2CO_3 were added and the solution sonicated and centrifuged for 5 min at 1000 rpm. The upper phase was removed and the lower phase, containing the desulfated sulfatide, was washed with chloroform:methanol:KCl (3:48:47 v/v) and then chloroform:methanol:distilled H_2O (3:48:47 v/v). The extent of desulfation was assessed by TLC on silica gel high performance TLC plates (Merck, Nottingham, UK) with chloroform:methanol (2:1 v/v) running solvent and orcinol staining. Binding of murine IgG (DG2), IgM (EM1), and human IgM (BR1) mAbs to desulfated sulfatide and other glycolipids was assessed by TLC overlay as previously described (Willison et al. 1994). The glycolipids were separated by TLC, as above, and the plate blocked overnight with 2% (w/v) BSA. MAb, diluted to 10 μg/mL in 1% (w/v) BSA in PBS, was then applied to the plate and incubated for 1 h. Binding was detected using horse radish peroxidase (HRP)-conjugated anti-mouse IgG or IgM antibody (Sigma) or anti-human IgM antibody (DakoCytomation, Glostrup, Denmark), and developed using Super Signal West Pico enhanced chemiluminescence (Pierce).

Natural and synthetic oligosaccharides

Gangliosides, sulfatides, and the oligosaccharide of GD3 (disialyllactose, DSL) were purchased from Sigma. Gal-4-sulfate and

Gal-6-sulfate were from Dextra Laboratories (Reading, UK). The oligosaccharide of GM1 (EGM1-OS) was produced in *Escherichia coli* (Antoine et al. 2003; Townson et al. 2007). GD1a oligosaccharide (GD1a-OS) and sulph-OS were prepared by ozonolysis of GD1a and sulfatide respectively, which cleaves one of the acyl chains of ceramide and renders the oligosaccharides soluble. Briefly, GD1a and sulfatide were dissolved to 1 mg/mL in methanol and cooled in a dry ice/ethanol bath. Ozone was generated from oxygen using a bench top generator (Model OL80W, Ozone Services, Burton, BC, Canada). Ozone application time was optimized at 17 min by TLC monitoring of cleaved and uncleaved products. Ozone was then dispersed by passing oxygen through the sample, and dimethylsulfoxide (500 μL) added, stirred for 30 min on dry ice, then 90 min at room temperature. After drying under a stream of nitrogen, the cleaved long chain aldehyde was separated by adding 10 mL *n*-hexane, sonicating for 5 min and then centrifuging at 1400 rpm for 10 min. The *n*-hexane was then drawn off and the oligosaccharides dried under nitrogen.

Sulph-CG was prepared by enzymatic cleavage of both acyl chains by ceramide glycanase (Calbiochem). Sulfatide (5 mg) was dissolved by sonication in 40 mL 50 mM sodium acetate, pH 5.0, containing 1 mg/mL sodium cholate, and then 5 U of ceramide glycanase added and incubated, shaking for 64 h at 37°C. The sulph-CG was purified from the digestion mixture using Oasis HLB cartridges (Waters Ltd, Milford, MA) and then lyophilized. Purity was assessed by TLC.

Oligosaccharide inhibition ELISA

Inhibition of mAbs binding to solid phase gangliosides and sulfatide by their soluble counterparts was investigated by inhibition ELISA. MAbs were diluted in 0.1% (w/v) BSA in PBS and used at concentrations equivalent to half maximal binding, as determined by titration in ELISA. Stock solutions of oligosaccharides were prepared in distilled water to 5–10 mg/mL and further diluted in 0.1% (w/v) BSA in PBS. Equal volumes of mAb and oligosaccharide were mixed prior to application to a standard ganglioside ELISA (50 μL/well). Percentage inhibition was calculated by comparison to the binding of mAb/antisera alone (100%). All assays were performed in duplicate and repeated at least three times.

Binding of mAbs to a panel of sulfated oligosaccharide conjugates

Binding by ELISA of a selection of the mAbs in Table to a panel of sulfated oligosaccharide–PAA conjugates (Supplementary data, Table S) was measured. The ELISA protocol was optimized for oligosaccharide–PAA conjugates, rather than gangliosides, and consequently was slightly different from the ELISAs described above. ELISA 96-well plates (NUNC Maxisorp, Denmark) were coated with sugar–PAA conjugates (Lectinity Holding, Inc, Moscow, Russia) 10 μg/mL in 0.05 M Na-carbonate buffer, pH 9.6, for 1 h at 37°C. Plates were then blocked with 3% BSA in PBS (w/v) for 2 h at 4°C and washed three times with PBS containing 0.1% Tween-20 (washing buffer). MAbs were diluted to 50 μg/mL in 0.3% BSA/PBS and 100 μL added per well. The plates were then incubated for 2 h at 4°C. Plates were washed three times with washing buffer and incubated with anti-mouse Ig-HRP (Sigma) (1:1000 in 0.3% BSA/PBS) or anti-human Ig-HRP for 2 h at 4°C. After washing, the plates were developed as for the ganglioside ELISAs described above. Binding of DG2 to 3-*O*-Su-Galβ-BSA was also tested, following the ganglioside ELISA protocol, but coating with 10 μg/mL PBS overnight at 4°C and then washing prior to blocking.

Analysis of antiganglioside mAb binding to sulfatide in cell membranes

PC12 cells were cultured in poly-L-lysine (Sigma) coated tissue culture flasks with DMEM containing 7.5% foetal calf serum (FCS) and 7.5% horse serum (Sigma). After harvesting, the cells were coated onto coverslips overnight at 37°C (1.5×10^4 cells/coverslip). Sulfatide was reconstituted in a small volume of distilled H_2O by incubating at 37°C for 1 h with frequent vortexing and sonication. Serum-free DMEM was added to give a sulfatide concentration of 20 μg/mL. To allow sulfatide to insert into PC12 cell plasma membranes, coverslips were rinsed in serum-free DMEM and then incubated at 37°C for 18 h in serum-free DMEM with or without sulfatide. Coverslips were then washed in serum-free DMEM, and any GM1 on the cell surface was blocked by incubating with CTB (Sigma) (4 μg/mL in serum-free DMEM) for 1 h at 4°C. After washing, as before, antiganglioside mAb (DG1, DG2 or EG3) or antisulfatide positive control mAb O4 were diluted in serum-free DMEM (10 μg/mL) and added for 1 h at room temperature. All further washing steps and dilutions were performed in DMEM containing 7.5% FCS and 7.5% horse serum. After washing, FITC-labeled goat anti-mouse IgG (for DG1, DG2, and EG3) or IgM (for O4) (Southern Biotech, Birmingham, AL) diluted 1/300 (v/v) was added for 1 h, in the dark, at room temperature. Coverslips were then washed and fixed in methanol for 30 min at −20°C. Coverslips were mounted with vectashield containing DAPI (Vector Laboratories, Peterborough, UK). To check for nonspecific secondary antibody binding, sulfatide treated and untreated cells were stained as above, but without mAb.

Flow cytometry was performed on PC12 cells grown overnight in poly-L-lysine coated tissue culture dishes with DMEM containing 7.5% FCS and 7.5% horse serum. After washing with chilled, sterile PBS, sulfatide was added, reconstituted in serum-free medium as described above, and the cells incubated at 37°C for 18 h. All washes and dilutions were performed in PBS containing 2% FCS and all incubations were for 1 h at 4°C. Sulfatide-treated or untreated cells were harvested and aliquots of 1×10^5 cells incubated with CTB (4 μg/mL). The cells were then washed and incubated with antiganglioside mAb or antisulfatide control mAb (10 μg/mL), followed by FITC-labeled goat anti-mouse IgG or IgM. Binding was analyzed using a FACScan (Becton Dickinson, Oxford, UK). Only very low levels of nonspecific secondary antibody binding were observed, and these were subtracted.

Analysis of antiganglioside mAb binding to sulfatide in peripheral nerve sections

Sciatic nerves were removed from sulfatide accumulating and cerebroside sulfotransferase (CST) overexpressing (Arylsulfatase A-deficient/PLP-CST transgenic mice, 7 months) (H Ramakrishnan et al., in preparation) and sulfatide deficient (UDP-galactose:ceramide galactosyltransferase knock-out mouse ($CGT^{-/-}$), 3 weeks) mice (Coetzee et al. 1996), embedded immediately in semi-frozen OCT Embedding Matrix (CellPath, Hemel Hempstead, UK) and mounted onto a cryostat

chuck. Nerves were cryosectioned at 15 μm in the transverse plane onto L-lysine-coated (Sigma) glass slides. Sections were stained unfixed or fixed in ice-cold methanol or 4% paraformaldehyde. Slides were incubated with DG2 or O4 (10 μg/mL PBS) for 1 h at 4°C, followed by three rinses in PBS and incubation at 4°C for 2 h in FITC conjugated anti-mouse IgG and IgM, respectively (1/300 (v/v) PBS). In order to block DG2 binding to GM1, the nerves were pretreated with CTB (4 μg/mL PBS) for 1 h at 4°C, before rinsing and application of DG2. Substitution of primary antibody with PBS confirmed that in both control and CTB treated sections, there was no nonspecific binding of the secondary antibody. Nerves were mounted in Citifluor (Citifluor, Canterbury, UK) for imaging under identical settings with a Zeiss (Oberkochen, Germany) Pascal confocal microscope.

Supplementary data

Supplementary data for this article is available online at www.glycob.oxfordjournals.org.

Funding

This work was supported by grants to HJW from the Wellcome Trust (GR060349 and GR077041) and to DRB from the Canadian Institute of Health Research and Alberta Ingenuity.

Conflict of interest statement

None declared.

Abbreviations

BSA, bovine serum albumin; $CGT^{-/-}$, sulfatide deficient mice; CST^{high}, cerebroside sulfotransferase overexpressing, sulfatide accumulating mice; CTB, cholera toxin B subunit; DSL, disialyllactose; EGM1-OS, oligosaccharide of GM1; GD1a-OS, GD1a oligosaccharide; FCS, foetal calf serum; Gal-4-sulfate, D-galactose-4-*O*-sulfate; Gal-6-sulfate, D-galactose-6-*O*-sulfate; MAbs, monoclonal antibodies; PAA, polyacrylamide; PBS, phosphate buffered saline; Sulph-OS, ozonolyzed 3-*O*-sulfo-β-D-galactosylceramide; Sulph-CG, ceramide glycanase treated 3-*O*-sulfo-β-D-galactosylceramide; TLC, thin layer chromatography.

References

Antoine T, Priem B, Heyraud A, Greffe L, Gilbert M, Wakarchuk WW, Lam JS, Samain E. 2003. Large-scale in vivo synthesis of the carbohydrate moieties of gangliosides GM1 and GM2 by metabolically engineered *Escherichia coli*. Chembiochem. 4:406–412.

Aotsuka S, Okawa-Takatsuji M, Uwatoko S, Yokohari R, Ikeda Y, Toda G. 1992. Antibodies against sulphatide in sera from patients with autoimmune rheumatic diseases. Clin Exp Immunol. 87:438–443.

Aruffo A, Kolanus W, Walz G, Fredman P, Seed B. 1991. CD62/P-selectin recognition of myeloid and tumor cell sulfatides. Cell. 67:35–44.

Avila JL, Rojas M, Carrasco H. 1993. Elevated levels of antibodies against sulphatide are present in all chronic chagasic and dilated cardiomyopathy sera. Clin Exp Immunol. 92:460–465.

Boffey J, Nicholl D, Wagner ER, Townson K, Goodyear C, Furukawa K, Conner J, Willison HJ. 2004. Innate murine B cells produce anti-disialosyl antibodies reactive with *Campylobacter jejuni* LPS and gangliosides that are polyreactive and encoded by a restricted set of unmutated V genes. J Neuroimmunol. 152:98–111.

Boffey J, Odaka M, Nicholl D, Wagner ER, Townson K, Bowes T, Conner J, Furukawa K, Willison HJ. 2005. Characterisation of the immunoglobulin variable region gene usage encoding the murine anti-ganglioside antibody repertoire. J Neuroimmunol. 165:92–103.

Bowes T, Wagner ER, Boffey J, Nicholl D, Cochrane L, Benboubetra M, Conner J, Furukawa K, Willison HJ. 2002. Tolerance to self gangliosides is the major factor restricting the antibody response to lipopolysaccharide core oligosaccharides in *Campylobacter jejuni* strains associated with Guillain-Barré syndrome. Infect Immun. 70:5008–5018.

Buschard K, Blomqvist M, Osterbye T, Fredman P. 2005. Involvement of sulfatide in beta cells and type 1 and type 2 diabetes. Diabetologia. 48:1957–1962.

Buschard K, Fredman P, Bog-Hansen E, Blomqvist M, Hedner J, Rastam L, Lindblad U. 2005. Low serum concentration of sulfatide and presence of sulfated lactosylceramide are associated with Type 2 diabetes. The Skaraborg Project. Diabet Med. 22:1190–1198.

Campanero-Rhodes MA, Childs RA, Kiso M, Komba S, Le Narvor C, Warren J, Otto D, Crocker PR, Feizi T. 2006. Carbohydrate microarrays reveal sulphation as a modulator of siglec binding. Biochem Biophys Res Commun. 344:1141–1146.

Coetzee T, Fujita N, Dupree J, Shi R, Blight A, Suzuki K, Popko B. 1996. Myelination in the absence of galactocerebroside and sulfatide: normal structure with abnormal function and regional instability. Cell. 86:209–219.

Dabby R, Weimer LH, Hays AP, Olarte M, Latov N. 2000. Antisulfatide antibodies in neuropathy: clinical and electrophysiologic correlates. Neurology. 54:1448–1452.

De Libero G, Mori L. 2005. Recognition of lipid antigens by T cells. Nat Rev Immunol. 5:485–496.

Dippold WG, Lloyd KO, Li LT, Ikeda H, Oettgen HF, Old LJ. 1980. Cell surface antigens of human malignant melanoma: definition of six antigenic systems with mouse monoclonal antibodies. Proc Natl Acad Sci USA. 77:6114–6118.

Eurelings M, Moons KG, Notermans NC, Sasker LD, De Jager AE, Wintzen AR, Wokke JH, Van Den Berg LH. 2001. Neuropathy and IgM M-proteins: prognostic value of antibodies to MAG, SGPG, and sulfatide. Neurology. 56:228–233.

Fredman P, Mattsson L, Andersson K, Davidsson P, Ishizuka I, Jeansson S, Mansson JE, Svennerholm L. 1988. Characterization of the binding epitope of a monoclonal antibody to sulphatide. Biochem J. 251:17–22.

Fredman P, Vedeler CA, Nyland H, Aarli JA, Svennerholm L. 1991. Antibodies in sera from patients with inflammatory demyelinating polyradiculoneuropathy react with ganglioside LM1 and sulphatide of peripheral nerve myelin. J Neurol. 238:75–79.

Galustian C, Lawson AM, Komba S, Ishida H, Kiso M, Feizi T. 1997. Sialyl-Lewis(x) sequence 6-*O*-sulfated at *N*-acetylglucosamine rather than at galactose is the preferred ligand for L-selectin and de-N-acetylation of the sialic acid enhances the binding strength. Biochem Biophys Res Commun. 240:748–751.

Galustian C, Park CG, Chai W, Kiso M, Bruening SA, Kang YS, Steinman RM, Feizi T. 2004. High and low affinity carbohydrate ligands revealed for murine SIGN-R1 by carbohydrate array and cell binding approaches, and differing specificities for SIGN-R3 and langerin. Int Immunol. 16:853–866.

Goodyear CS, O'Hanlon GM, Plomp JJ, Wagner ER, Morrison I, Veitch J, Cochrane L, Bullens R, Molenaar PC, Conner J, Willison HJ. 1999. Monoclonal antibodies raised against Guillain-Barré syndrome-associated *Campylobacter jejuni* lipopolysaccharide react with neuronal gangliosides and paralyze muscle-nerve preparations. J Clin Invest. 104:697–708.

Hakomori S. 1974. Preparation and properties of anti-sulfatide serum. J Immunol. 112:424–426.

Ilyas AA, Chen ZW, Cook SD. 2003. Antibodies to sulfatide in cerebrospinal fluid of patients with multiple sclerosis. J Neuroimmunol. 139:76–80.

Ishizuka I. 1997. Chemistry and functional distribution of sulfoglycolipids. Prog Lipid Res. 36:245–319.

Kanter JL, Narayana S, Ho PP, Catz I, Warren KG, Sobel RA, Steinman L, Robinson WH. 2006. Lipid microarrays identify key mediators of autoimmune brain inflammation. Nat Med. 12:138–143.

Kirschning E, Rutter G, Huckhagel C, Ellhof I, Hohenberg H. 1997. A sulfatide-reactive monoclonal antibody derived from a patient with multiple sclerosis binds to myelin in situ. Ann N Y Acad Sci. 815:455–458.

Kyogashima M. 2004. The role of sulfatide in thrombogenesis and haemostasis. Arch Biochem Biophys. 426:157–162.

Lopate G, Pestronk A, Evans S, Li L, Clifford D. 2005. Anti-sulfatide antibodies in HIV-infected individuals with sensory neuropathy. Neurology. 64:1632–1634.

Merten M, Motamedy S, Ramamurthy S, Arnett FC, Thiagarajan P. 2003. Sulfatides: targets for anti-phospholipid antibodies. Circulation. 108:2082–2087.

Paterson G, Wilson G, Kennedy PG, Willison HJ. 1995. Analysis of anti-GM1 ganglioside IgM antibodies cloned from motor neuropathy patients demonstrates diverse V region gene usage with extensive somatic mutation. J Immunol. 155:3049–3059.

Petratos S, Gonzales ME. 2000. Can antiglycolipid antibodies present in HIV-infected individuals induce immune demyelination? Neuropathology. 20:257–272.

Rosenbluth J, Moon D. 2003. Dysmyelination induced in vitro by IgM antisulfatide and antigalactocerebroside monoclonal antibodies. J Neurosci Res. 71:104–109.

Rosenbluth J, Schiff R, Liang WL, Dou W. 2003. Antibody-mediated CNS demyelination II. Focal spinal cord lesions induced by implantation of an IgM antisulfatide-secreting hybridoma. J Neurocytol. 32:265–276.

Rousset E, Harel J, Dubreuil JD. 1998. Sulfatide from the pig jejunum brush border epithelial cell surface is involved in binding of *Escherichia coli* enterotoxin b. Infect Immun. 66:5650–5658.

Sandhoff R, Grieshaber H, Djafarzadeh R, Sijmonsma TP, Proudfoot AE, Handel TM, Wiegandt H, Nelson PJ, Grone HJ. 2005. Chemokines bind to sulfatides as revealed by surface plasmon resonance. Biochim Biophys Acta. 1687:52–63.

Talts JF, Andac Z, Gohring W, Brancaccio A, Timpl R. 1999. Binding of the G domains of laminin alpha1 and alpha2 chains and perlecan to heparin, sulfatides, alpha-dystroglycan and several extracellular matrix proteins. EMBO J. 18:863–870.

Townson K, Boffey J, Nicholl D, Veitch J, Bundle D, Zhang P, Samain E, Antoine T, Bernardi A, Arosio D, Sonnino S, Isaacs N, Willison HJ. 2007. Solid phase immunoadsorption for therapeutic and analytical studies on neuropathy-associated anti-GM1 antibodies. Glycobiology. 17:294–303.

Wang CH, Liu JH, Lee SC, Hsiao CD, Wu WG. 2006. Glycosphingolipid-facilitated membrane insertion and internalization of cobra cardiotoxin. The sulfatide.cardiotoxin complex structure in a membrane-like environment suggests a lipid-dependent cell-penetrating mechanism for membrane binding polypeptides. J Biol Chem. 281:656–667.

Willison HJ, O'Hanlon GM, Paterson G, Veitch J, Wilson G, Roberts M, Tang T, Vincent A. 1996. A somatically mutated human antiganglioside IgM antibody that induces experimental neuropathy in mice is encoded by the variable region heavy chain gene, V1-18. J Clin Invest. 97:1155–1164.

Willison HJ, Paterson G, Kennedy PG, Veitch J. 1994. Cloning of human anti-GM1 antibodies from motor neuropathy patients. Ann Neurol. 35:471–478.

Willison HJ, Veitch J, Swan AV, Baumann N, Comi G, Gregson NA, Llla I, Jacobs BC, Zielasek J, Hughes RAC. 1999. Inter-laboratory validation of an ELISA for the determination of serum anti-ganglioside antibodies. Eur J Neurol 6:71–77.